AD708621

AGARD-MAN-8-70

AGARD-MAN-8-70

AGARD

ADVISORY GROUP FOR AEROSPACE RESEARCH & DEVELOPMENT

7 RUE ANCELLE 92 NEUILLY SUR SEINE FRANCE

MANUAL ON FATIGUE OF STRUCTURES

Fundamental and Physical Aspects

by

W. G. Barrois

DDC
RECEIVED
JUL 20 1970
A

NORTH ATLANTIC TREATY ORGANIZATION

Reproduced by the
CLEARINGHOUSE
for Federal Scientific & Technical
Information Springfield Va. 22151

DISTRIBUTION AND AVAILABILITY
ON BACK COVER

This document has been approved
for public release and sale; its
distribution is unlimited

NORTH ATLANTIC TREATY ORGANIZATION

ADVISORY GROUP FOR AEROSPACE RESEARCH AND DEVELOPMENT

(ORGANISATION DU TRAITE DE L'ATLANTIQUE NORD)

MANUAL ON

FATIGUE OF STRUCTURES

FUNDAMENTAL AND PHYSICAL ASPECTS

by

William G. Barrois

Department Chief at the Société Nationale Industrielle Aérospatiale,
Paris, France

This Manual was prepared at the request of the Structures and Materials Panel of AGARD – NATO

Published June 1970

539.431

Printed by Technical Editing and Reproduction Ltd
Harford House, 7-9 Charlotte St, London. W1P 1HD

FOREWORD

The Structures and Materials Panel of the NATO Advisory Group for Aerospace Research and Development (AGARD) is constituted of engineers, scientists and technical administrators from industry, government and universities throughout the NATO nations. We are concerned with the advancement of aerospace research and development and the application of the results to the design and fabrication of the vehicles and equipment which NATO requires. The Panel provides a mechanism for the exchange of information, for conducting cooperative studies and experimental programmes and for the preparation and distribution of surveys and statements on the present state of knowledge in selected technical areas.

Many aspects of the fatigue of metal structures have received the attention of the Panel since its foundation in 1955. The nature and distribution of turbulence and other non-steady loadings, the response of structures to these loadings, resultant change at both macroscopic and microscopic scales and many detailed questions within each of these fields have been investigated by the structural analysts, metallurgists and metal physicists on the Panel and their colleagues throughout NATO. As a result, the Panel has been able to assist the better understanding and description of many fatigue phenomena at least amongst the specialists who are daily concerned with them. As part of this process, many data have been drawn together, analysed and evaluated. However, no matter how deep the understanding of these phenomena in the laboratory, the performance of aircraft, other vehicles and equipment can only be assured if this understanding is brought to bear during the processes of design and production.

During the lifetime of the Panel, the roles performed and the environment to which aircraft and equipment are subjected have undergone many changes. Unconventional loading spectra, new materials, the effects of heating and audio-frequency excitation are just some of the considerations which have had to be taken into account by design and production teams, often at short notice. Accordingly, the Panel decided that it should commission a Manual on the Fatigue of Structures presenting a synthesis of knowledge drawn from many specialist areas but primarily intended to provide design and production engineers with a proper appreciation of the many aspects of design against fatigue.

The Panel was fortunate in finding, from amongst its own membership, one who was equal to the task. Mr W. Barrois is one of the few engineers who combines the necessary specialist appreciation, engineering experience and design ability to undertake this work. In addition to these qualities Mr Barrois has demonstrated, during the course of preparing this Manual, a creditable humility in approaching others for comment and assistance.

The Panel is indebted to Mr Barrois for the tireless application of his many skills to the completion of this Manual and to those in several NATO nations who have assisted, as recorded in the author's Acknowledgements.

N. E. Promisel
Chairman
AGARD Structures & Materials Panel
Washington DC
1 March, 1970

Anthony J. Barrett
Vice Chairman
AGARD Structures & Materials Panel
London, England
1 March, 1970

ACKNOWLEDGEMENTS

This work would not exist without the encouragement received by the author and the interest shown by the Members of the Structures and Materials Panel, especially by

N.H. Mason, Ministry of Technology, former Chairman of the Panel,
R.V. Rhode, NASA, formerly Chairman of the Panel,
A. Barrett, Royal Aeronautical Society, former Chairman of the Structures Group,
G. Cooper, former Executive Secretary of the Panel,
and the late
F.J. Plantema, former Chairman of the Working Group on Fatigue, Secretary of the International Committee on Aircraft Fatigue (ICAF), and Head of the Structures Department at the N.L.R., Amsterdam.

The preparation of the English version from an initial French manuscript is the outcome of the work of G. Losson, former interpreter and technical translator at Nord-Aviation, and of numerous exchanges of views between the author and the following Members and Specialists of the AGARD Structures and Materials Panel, who checked the wording and some of the technical aspects:

P. Kuhn, Langley Research Center, NASA, USA,
A. Barrett, Royal Aeronautical Society, London,
E.R. Welbourne, Royal Aeronautical Society, London,
E.L. Ripley, Royal Aircraft Establishment, Farnborough,
J.R. Heath-Smith, Royal Aircraft Establishment, Farnborough,
J. Taylor, Royal Aircraft Establishment, Farnborough,
D.P. Rooke, Royal Aircraft Establishment, Farnborough,
N.H. Mason, Ministry of Technology, London,
J.I. Bluhm, Materials and Mechanics Research Center, US Army, Watertown,
D. Broek, National Aerospace Laboratory (NLR), Amsterdam,
W.B. Miller, Airframe Subsystem Engineering, AFSC, Wright-Patterson AFB,
F.R. Thurston, National Aeronautical Establishment, Ottawa,
A.H. Hall, National Aeronautical Establishment, Ottawa,
G. Cooper, Montreal.

The French version has been rewritten in order to take into account all the modifications that resulted from this team work. Although he assumes the responsability for all possible errors and questionable assertions, the author hesitates whether he should thank his colleagues for their constructive comments or consider them as being co-authors.

The Editorial Committee was composed of

B.P. Mullins, Head of the Structures Department, Royal Aircraft Establishment, Farnborough, England,
G.A. Leomand, Société Nationale Industrielle Aérospatiale, Châtillon-sous-Bagneux, France.

CONTENTS

CHAPTER I

STRENGTH OF STRUCTURES AND FATIGUE - GENERAL

W. Barrois: Fatigue of Structures, Vol. I
"Fundamental and Physical Aspects", AGARD, 1970

STRENGTH OF STRUCTURES AND FATIGUE - GENERAL

1.1 INTRODUCTION

The material of this work is partly derived from previous lectures held at the "Ecole Spéciale des Travaux Aéronautiques de Paris" from 1958 to 1962. In 1965 the "Association Française des Ingénieurs et Techniciens de l'Aéronautique et de l'Espace" (Toulouse Section) conducted a course of lectures on the fatigue strength of aircraft structures. On that occasion the writer made a general survey of the fatigue problem in structures and of the modern aspects of static strength and creep. The purpose of these lectures was to supplement the background knowledge of engineers engaged in aeronautical engineering by providing a state-of-the-art summary on the physical strength of structures, especially in fatigue, without excluding other types of failures and damage. The Structures and Materials Panel of the NATO Advisory Group for Aeronautical Research and Development (AGARD) expressed the desire to set up a Manual on Fatigue. The writer feels that such a synthesis can be accomplished by a working group only if several of its members have already started on it.

The present study might contribute to a more lasting work as a result of the confrontation of similar efforts. It is intended for design and production engineers in the aircraft industry and is therefore based on the problems and technology of aeronautics. However, the basic principles and a large number of specific data hold true for other fields of mechanical engineering where the same problems arise for different metals and different load statistics.

The documents referred to were obtained with the help of the French Aero-Space Documentation Service (SEDOCAR), AGARD Member Organizations such as NASA, Royal Aircraft Establishment (RAE), etc., and Members of the International Committee for Aircraft Fatigue (ICAF).

1.1.1 Representativeness of Fatigue Testing

Fatigue was encountered as a general problem when engineers were faced with difficulties such as failure of railway carriage axles or partial failure of mine cables under repeated loads of substantially lower magnitude than those inducing static failure. What occurred then was in fact structural fatigue.

The era of laboratory fatigue testing began in the 1860's when Wöhler[1] evolved the small-specimen rotating-bending fatigue test for assessing the relative merits in fatigue of steels used in the production of railway axles. On the basis of an idealized behaviour for mechanical components subject to a large number of loadings and for engineering steels, the experimental problem in those days was how to determine a fatigue limit, that is, a repeated load which could be sustained indefinitely.

Until about 1940 fatigue investigations included: some basic research into the physics of metals in an effort to discover its mechanism; systematic rotating-bending tests on smooth conical or waisted* specimens in order to qualify each metal by identifying its fatigue limit; finally, check tests on actual parts.

Between 1940 and 1945 it became obvious to most specialists that the rotating-bending test on smooth specimens was not representative of the behaviour of actual components and that the fatigue limit was not the only characteristic of interest. One improvement consisted in performing axial tension-compression tests on cylindrical specimens having a V-groove with a rounded root, the smooth specimen being replaced by a waisted one, with a very large radius of curvature, so that the heat induced by internal damping should no longer increase the temperature of the specimen and falsify the test results. It is now recognized that the purpose of fatigue testing is not to specify the fatigue limit, which is often hypothetical, but to provide the entire stress versus number of loadings curve from static strength, corresponding to one load application, up to a large number of cycles in laboratory tests of short duration. This number being large in comparison with the cycles sustained by the structure during its service life, testing must be speeded up as much as is practicable without distorting the results.

However, a factor of great importance in many service fatigue incidents was left out in the notched-specimen test: the contact alteration by friction due to very small relative displacements of the various parts of an assembly during the loading and unloading cycles. This phenomenon, known as "fretting", consists in the welding of asperities on the surfaces in contact and in the tearing-up of these microwelds; it is responsible for the initiation of fatigue cracks in assemblies and, in cases like the fitting of wheels on shafts or the bearing of bolts in lugs, it may reduce the fatigue life to a tenth of what it would otherwise be.

---

* In French this specimen is called "torique".

PRECEDING PAGE BLANK

An attempt was then made to evaluate metals and joining methods through tests on assembled parts. In most cases these tests are carried out in air-conditioned laboratories at frequencies ranging from 20 to 300 c/s. It was formerly assumed that the loading frequency had no effect on fatigue life. This assumption proves wrong if internal damping leads to considerable heating of the specimen, if the test duration is such that corrosion or creep plays a part, or if resonance of the specimen induces vibration modes and dynamic stresses whose distributions are unknown and are different from those of components in service.

Owing to the complexity of the loads used for simulating the mechanical history of flights in *complete airframe fatigue tests*, testing is very slow. The loading frequency for pressurized fuselages is about one five-minute cycle to represent one flight. Such tests often last over a year and take place in the open, with the fuselage immersed in a tank and filled with water to avoid all hazards which might be caused by bursting under air pressure. The fuselage and the water tank are drained once a day for fatigue damage crack inspection. Under these conditions, corrosion takes place in substantially the same way as in actual aircraft operation and some experiments suggest that the life of the specimen is reduced by half as compared with tests in a laboratory environment. Corrosion is possibly worse if galvanic action between fuselage and tank is not avoided by protective painting of the tank.

On the supersonic aircraft of the next generation, *kinetic heating* of the skin due to rapid compression of the accelerated air will produce temperatures likely to cause slight creep in small highly-stressed areas, such as stress concentrations at the edges of rivet holes or head-shank transitions in rivets. Technically speaking, the problem consists in designing the rivets so that no creep occurs and in selecting a material that is stable in the hot condition; in this way the problem is eliminated. To check this, combined long-time hot fatigue and creep tests have been conducted in real time (about 20 load cycles per hour). The second effect of kinetic heating is a non-uniform temperature distribution over the structure, which leads to different thermal expansions and produces heat-induced stresses in areas or components where thermal expansion is restrained. *Thermal stresses* are dependent on the temperature gradients, which attain their maximum values under transient conditions. For an aircraft flying at twice the speed of sound, with skin temperatures ranging from -30°C to 120°C during one flight, thermal stresses cannot be neglected in a fatigue test; simultation during testing should be carried out in real time for the transient flight phases, in climb and descent. The problem of thermal stresses also appears in other fields of mechanical structures and chemical installations (separation of radioactive isotopes, heating facilities, etc.).

For the present subsonic aircraft and, *a fortiori*, for supersonic aircraft and missiles, there is another problem related to the fatigue strength of skin panels under the effect of changes in pressure at *audio-frequencies* (acoustic fatigue). In the case of aircraft, excitation originates from engine noise during climb and from boundary layer turbulence of the aerodynamic flow during cruise. Thin skin panels bounded by the network of stiffeners respond to excitation according to their resonant frequencies, so the fatigue test must be performed on the actual complex structure and in real time, with the excitation having the same frequency spectrum as the actual excitation. Fatigue testing can only be shortened in duration by increasing the magnitude of excitation, which raises the problem of extrapolating the stress versus number of cycles curves for low stresses and very large number of cycles, between 10^9 and 10^{11}. Similar problems of extrapolation are met whenever the operational environment implies high-frequency vibrations (gear teeth, helicopter rotor blades, airscrew blades, turbine blades, etc.).

To conclude, it should be pointed out that the technical aspect of fatigue strength problems will necessitate tests of increasing complexity if the tests are to be representative. This also calls for a distinction between the small-specimen metal qualification tests, designed either to give a first rough comparative assessment or to serve as an acceptance check, and the technical development or verification tests in which design engineers are interested.

1.1.2 The Basic Aspects of the "Strength of Structures" Concept

The general problem of the service life of mechanical components or aircraft, helicopter and missile structures is associated with the interactions of damage causes which act separately in idealized laboratory tests and are classified into fatigue, creep, corrosion, etc. Fatigue problems cannot be isolated from those of strength as a whole. Among the specialists in the service behaviour of mechanical structures the idea is coming to the fore that any arbitrary dividing-up of the continuous spectrum of structural strength into various groups such as static strength, creep strength, stress corrosion strength, notch strength, fatigue strength, etc., should be rejected and that the time has come for collective concepts which integrate the knowledge concerning actual material properties, production defects, service environment, maintenance methods, and so on.

The "Strength of Materials" (or "Structural Mechanics"), as it is still being taught, is a "science" which includes a small amount of theory of elasticity, a great deal of statics and a lot of stressman's "know how" based on simplifying assumptions which have not been invalidated by experience. It has rendered valuable service and remains as the trunk upon which new grafts ought now to be made. For aircraft structures and other advanced complex structures the current tendency is to increase the contribution of the theory of elasticity either by computer-aided calculations with several thousands of redundant unknowns or by measurements on photoelastic models and actual components using photo-stress coating and electric strain gauges. Although this trend exhibits useful progress, the main problem does not lie in finding the stress state in the elastic range; what is important is the knowledge of the allowable stress values, taking into account the actual condition of the metal and of the environment.

The "Strength of Structures" would thus comprehend all the knowledge required for the service behaviour prediction of actual structures under actual operating conditions with regard to deflections and failure. The strength of actual structures depends on a large number of mostly unmeasurable parameters which define the material, its mechanical and thermal history (manufacturing, forging, heat treatment, mechanical treatment, machining, protective procedures), the shape of components as well as the environmental service conditions (loads applied, temperatures, corrosive environments, irradiation, etc.). Therefore, the "Strength of Structures" concept involves the theory of elasticity, static and dynamic mechanics, metallurgy, statistics, knowledge of the loads and service environments, the technology of fabrication, the methods of maintenance (damage detection and repair) and the testing procedures.

While the general concept is the same for all applications and requires analytical as well as overall knowledge in accordance with the needs of design engineers, it is, however, obvious that its contents vary to a certain extent for each individual engineering industry. This is the main reason why instruction is lacking in this field. Nevertheless, since the requirements and the ways of thinking in design offices remain fairly constant and differ from those prevailing in other specialties, due consideration should be given to this in the method of exposition. For example, structural designers apply the equilibrium-of-forces concept to a wide extent while some metal physicists consider things more as geometers and thermodynamicists than design engineers. Generally speaking, every specialty should be reviewed from the viewpoint of the design office, taking into account its links with other specialties, in order to meet the needs of the manufacturer, since the aim is to provide a general view and directions for the use of specialized documents. A clear understanding of the vocabularies used is also of great practical significance as we know of some accidents and many incidents caused by lack of understanding among specialists as a result of semantic difficulties.

Although structural deformation plays an important part, the main hazard evidently is failure by rupture. The various types of structural failure are as follows:

Static Failure. The component breaks as soon as an increasing load which is applied once reaches a sufficient value. The material is *ductile* if extensive permanent strain appears prior to failure; it is *brittle* in the opposite case. Brittleness of metals is more apparent on a component having a sharp geometrical notch or a crack (defect, fatigue or corrosion crack); the more brittle the material, the smaller the net rupture stress as compared to that of a smooth specimen. Brittleness depends on the absolute dimensions; thus a component of large thickness proves more brittle than a thin one. This point has become quite important in practice since it is not possible to avoid or detect all cracks from the start; it is desirable that the reduced static strength of components having a crack of safely detectable size should remain sufficiently high to make the probability of disaster negligible. At low temperatures certain steels become very brittle.

Creep Failure. Flow or creep of the material under constant loading causes a reduction in the cross-sectional area of components and a corresponding increase of the applied stress. Moreover, internal micro-cracks appear when a given value of elongation is obtained, and tend to lower the allowable stress value. Rupture occurs either through instability of the shape or through damage. Creep development and rupture are load-, time-, and temperature-dependent. The same phenomena are observed for an imposed elongation or load increasing with time. In rapid load applications, the creep test is again a static test. If failure takes place after a long period of time, fracture is usually intergranular.

Delayed Static Failure. Although permanent strain is small or unmeasurable, failure occurs suddenly after a certain period of time, which is short for high loads. The applied stress is constant but the allowable rupture stress decreases constantly. Some creep failures are of this type, since the term "creep" does not always imply a detectable elongation but merely the use of the conventional creep test apparatus. Brittle static failure is one specific case. This type of failure is also called *stress embrittlement* or *static fatigue*; it is found with glass, plastic materials and some ultra-high tensile steels. *Spontaneous failure* of certain quenched parts subject to internal stresses, with no external load applied, may be linked up with it, although stress corrosion could be responsible for the result. In steels this phenomenon is aggravated by the presence of *absorbed hydrogen*.

Stress-Corrosion Failure. This is failure caused by the simultaneous action of corrosion and stress producing intergranular or transgranular cracks. Local stresses are increased by corrosion cracks and the phenomenon develops in an exponential manner. All high-strength aluminium alloys may be sensitive to stress-corrosion, especially in the short transverse direction in the presence of steady assembly stresses (expansion pins, force fit pins, taper pins or bolts, expanded rivets, and so on). Some stainless steels and titanium alloys used at high temperatures show a certain sensitivity. In some cases one speaks of corrosionless stress-corrosion, which means that delayed static failure occurs with fracture features just as in the case of stress-corrosion.

Intergranular Corrosion. This may occur in the absence of any known load although the phenomenon can be aggravated by internal stresses or external loads. Quenching followed by slow cooling may sensitize certain naturally-ageing aluminium alloys of the Duralumin type (2014 or 2024). Intergranular corrosion is also found in heat-resisting alloys used for gas turbine blades. Some liquid metals such as hot cadmium can produce the equivalent of intergranular corrosion by reducing the cohesion between the grains of high-tensile steels.

Stress corrosion and intergranular corrosion often appear with cracking planes parallel to the forging or rolling plane and perpendicular to the direction of the thickness called "short transverse direction"; when using a material that is brittle or sensitive either to stress corrosion or to intergranular corrosion, the design office should avoid designing components liable to be subjected to steady tensile stress in the short transverse direction.

Fatigue Failure occurs with very small strains and transgranular fracture after applications of loads smaller than those which cause static failure. One speaks either of fatigue strength or of "fatigue life", and sometimes of "safe-life" or "endurance"; however, the term "endurance" is often used by engineers in connection with mechanical functional tests of components under low stresses, which permit the assessment of wear but not of fatigue strength. The *fatigue life* is *unlimited* if the number of loadings sustained by a structure is well above that required in service. This type of strength is necessary for mechanical engine components and machine-tools. For carbon steels and other metals showing a *fatigue limit*, the fatigue life is practically unlimited under stresses below the fatigue limit. The *fatigue life* is *finite* if a structure fails as a result of fatigue after a number of load cycles that is sufficient to guarantee the predicted life time. In the past, some laboratories were satisfied with tests that enabled them to specify the fatigue limit and they called "fatigue area" the range of stresses causing failure or no failure between 10^6 and 10^7 cycles in the case of steels; some specialists even considered that failure in less than 10^4 cycles was not fatigue. It is now recognized that the so-called low-cycle fatigue ranges from 2 to some thousands of cycles.

If the magnitude of the applied load varies periodically or at random (as with gust loads on aircraft lifting surfaces), crack initiation causes a reduction in static strength and final static failure occurs if the component is then subjected to a higher and therefore more seldom load. The operational time before fracture, hence the longest time before repair is necessary, depends upon the probability of occurrence of high loads, the ease of crack detection and the crack growth rate. This raises the very important question of the *residual static strength of a cracked component* as well as that of the *crack propagation rate*.

Failure caused by fatigue and creep or *hot fatigue* raises the problem of the "unit of life": cycle or second. At room temperature the duration of load application for engineering metals plays a negligible part in the development of failure; in fatigue the *load* magnitude and the numbers of cycles are overriding factors; the *unit of life is the loading cycle*. At *high temperatures* the load cycle exerts a negligible effect; the fatigue life depends on the total time of application for each load level; the *unit of life is the second*. There is an intermediate range of temperatures where the development of failure depends both on fatigue and creep and where the number of cycles and the frequency each have an important part to play.

Similarly, corrosion also introduces the "time" factor and eliminates the fatigue limit. As with intergranular corrosion and stress-corrosion, corrosion-fatigue tests in laboratories are merely of qualitative interest and give a poor representation of service behaviour in real time and in actual environment.

When fatigue loading includes a steady mean static load, *fatigue creep* is sometimes obtained: the test piece undergoes a progressive elongation and the permanent elongation tends towards a limit although the highest cycle load, when applied constantly, cannot produce any detectable creep elongation. This is a specific case of *fatigue softening* of initially work-hardened metals. Another result is a change in the static stress-strain curve due to fatigue which reduces the proportional limit stress and lowers the tangent modulus of elasticity $d\sigma/d\varepsilon$ in the slightly higher stress range. The practical implication that has been noticed in some aircraft is that the *compression buckling strength* may be reduced by fatigue and some components yield in flight under loads substantially below those attained during static tests on new structures. The compression buckling strength can also be time-dependent if the temperature is high enough. The foregoing shows to what extent classifications are arbitrary and that reality implies a number of interactions between the various types of failure.

1.1.3 The Case of Airframes

The term "airframe" covers all stressed aircraft components such as wings, fuselage, tail unit, ailerons, elevator, rudder, landing gear, flight controls.

The problem of fatigue in airframes was given some consideration as early as 1930 but remained a somewhat speculative matter in France till 1946. Before that, technological fatigue investigations were concerned with materials used in the construction of engines, propellors and helicopter rotor blades, and their aim was mainly to determine the fatigue limit.

During World War II the British and the Germans had encountered fatigue cracks on spar caps in bombers and transport aircraft. The Germans had undertaken an experimental investigation into the fatigue strength of spars. The spar cap failures were not the only troubles: wing skin cracks were reported on British bombers and landing gear cracks on US fighters.

On the other hand, German research workers had carried out an extensive test series on end fittings of tubular struts at the Deutsche Versuchsanstalt Luftfahrtforschung (DVL) in 1938.

After the war, fatigue failures on wing spars persuaded the British industry of the existence of a problem with wings. However, fatigue testing of prototype wings was restricted to the simulation of gust-induced alternating loads since the cruise equilibrium forces applied once per flight were supposed to exert a negligible effect similar to that of the pressurization loads with regard to the fuselage.

In France, the aircraft of that time had not yet had sufficient operating time to exhibit cracks that could be connected unquestionably with fatigue. Most of the engineers in the Aeronautical Industry and Government Services believed that designing airframes on the basis of specified static loads was enough to rule out any risk of fatigue failure as fatigue failure was considered to be due to a large number of load cycles. In short, one did not believe in the possibility of fatigue cracking occurring under a small number of cycles (100 to 1000), on account of the loads encountered in service. The appearance of fatigue failures in this range differs

but little from that of static ruptures and no discrimination could be made between them. Moreover, the only smooth-specimen fatigue tests that were available then did not show any significant lowering of strength from a single static load to a thousand repetitions of the load. Towards 1952 the French Aeronautical Research Services removed the matter from their working programme.

In Great Britain, although the problem was dealt with experimentally by the Royal Aircraft Establishment of Farnborough for military aircraft, Tye[2] could write in April 1952 that for the previous five years various learned bodies had been arguing whether fatigue was a serious problem or a joke in the case of aircraft structures, and that any further discussion had become useless the day when, in Autumn 1951, a British civil aircraft, believed to be free from any predisposition to fatigue, had a fatal accident.

The two accidents of the Comet I, due to fatigue failure of the fuselage under 3000 to 4000 pressurization cycles, as well as other accidents or incidents on military and civil aircraft made it clear, then, that the range in which fatigue causes failure or a severe reduction in static strength extends from a few score of cycles to several millions of cycles for the manoeuvre and gust load effects on the aircraft. Nowadays substantiation of the fatigue strength is an important part of civil certification prior to the introduction into service of new types of aircraft.

Since 1939 the problem has become more acute for several reasons:

(i) The design load factors for transport aircraft have been reduced, hence a relative greater importance of gust loads and a general decrease in the weight and strength of structures.

(ii) The daily operation time of transport aircraft (presently up to 12 hours) and their total lifetime (presently from 20,000 to more than 60,000 hours) have been increased.

(iii) Alloys with a high static strength but a moderate fatigue strength in the presence of notches are being used.

(iv) The duration of flights has been shortened, which implies a larger number of flights for the same period of time in hours.

(v) As far as military aircraft are concerned, there is an increase of the mean service load factors as a result of the use of anti-g clothing; high-speed flights in the most turbulent region of the atmosphere near the ground lead to a further increase of the number of high loads which are significant in fatigue.

It is considered that for military aircraft and missiles the fatigue problem begins at a few scores of load cycles. There are two further aspects of this problem at the present time:

(a) hot fatigue,

(b) audio-frequency vibrations (acoustic fatigue).

Let us return to the general aspect of the matter. It is desirable that no local fatigue failure should occur during the life of a structure. If the structure is to be a lightweight one, experience shows that some cracks which appear progressively during ground inspections on aircraft in service must necessarily be tolerated. Indeed, these inspections, which are carried out on a fairly extensive basis during general overhaul strippings, are restricted to vital components and to known sensitive points during the periodic checks. In practice, the development of repairable cracks is accepted on minor components. This leads to the following questions:

1. What extent of crack growth may be tolerated before a repair that requires aircraft grounding is carried out?

2. Should one repair a crack in order to stop its development, or check it frequently so as to determine its growth rate? This is important with respect to the preceding question.

3. What kind of laboratory test will allow a quantitative assessment of the repair?

4. What should be the time between inspections for checking known sensitive points?

When dealing with these problems of *maintenance*, due account must be taken of the technical data available from tests and from the behaviour of similar structures; in addition, the financial aspects of the operation and maintenance might be a reason to hasten or postpone repairs on non-vital components.

As far as the vital attachments are concerned, it is sometimes difficult to achieve a design of absolute safety because of weight or space restrictions; therefore the tendency is to increase the number of attachments and to diversify the possible stress paths so that a localized partial failure taking place between two inspections, which will surely permit detecting it, still leaves the aircraft with a sufficient probability of survival under the rare high loads encountered in service. The structure is then called *"fail-safe"*.

The term "fail-safe" is associated with a specific structure concept wherein the progress of damage remains confined to a small portion of a vital component or attachment during the time required for its detection. This period of time will be short for visible cracks in the outer skin and long for inner cracks hidden in assembled components; even in the case of hidden components the time required for detection may be shortened if a crack

is expected in a given area and if inspection means such as X-rays and ultrasonic waves are used in the area concerned, that is, if the existence and location of the crack may be assumed from information collected on other aircraft of the same type.

Parallel loading of several components does not suffice to obtain the fail-safe condition. If several identical components are subjected to an overall external load producing the same stresses in each one of them, failure of the first increases the stresses in its close neighbours and all components will break one after the other within a rather short time. At the beginning the "stand-by" components must be subjected only to low stresses in the areas where failure of the first component will transfer the load, while the other areas may be highly stressed by the primary functions of these components. The structure of uniform strength which is considered ideal by the stressman cannot be fail-safe.

Whenever introduction of the fail-safe concept does not result in an undue weight increase of the structure, it is advisable to resort to it. Many accidents have been avoided and many causes of failure determined thanks to the existence of several stress paths. It should also be pointed out that this concept provides protection against causes of local failure other than fatigue. Fail safe structures enable us to avoid a serious accident due to a local failure and permit the introduction of modifications to the structure concerned. This procedure will lead to a better design of structures with the same local characteristics. However, the importance of the concept implies that its application must not have just a formal appearance of making the structure fail safe: components which are completely hidden in an assembly do not contribute to safety if their failure cannot be suspected and detected; dividing a strong component into two elements of lower overall strength is a poor alternative.

We believe that it is necessary to improve and check the *quality* and that a detailed quality control can supplement the fail-safe condition or be substituted for it in cases where the fail-safe concept requires too much weight. When working out the design, setting up detail drawings and defining treatment and production processes, the engineer should give serious consideration to the problem of fatigue as well as to other causes of damage such as brittleness in the short transverse direction, stress-corrosion, intergranular corrosion, weld defects, residual tensile stresses due to grinding, machining defects, decarburization of treated steels, etc. Partial tests should be carried out so that a choice can be made between various shapes, methods of assembling, materials, fabrication processes and anti-corrosion treatments.

Sometimes quality involves no expenses: it only takes common sense to avoid sharp internal angles by using fillets, to blunt the edges of sharp external angles, to eliminate eccentricities in assemblies, to design the shapes of structural components with continuous cross-sectional development, etc. In other cases quality is expensive, so the resultant weight profit should be compared with its price; it is thus possible to cancel out detrimental implications of surface decarburization of steels by machining the entire component after it has been heat-treated or by using oversized rough-die-forged or rough-heat-treated areas.

Fabrication processes must be checked at every stage, from the production of material to the final dimensional inspection. At every stage the measurable parameters of each operation must remain constant (quality control). Furthermore, as visual inspection of the defects and dimensional measurements lead to rejections at every stage, it is most desirable that parts likely to be rejected at final inspection should be scrapped as soon as possible. In the case of mass production (propellor blades, helicopter rotor blades, turbine blades, etc.) a sample should be taken from time to time and subjected to destructive testing; *statistical control of the quality of fabrication* can be achieved by checking the constancy of the mean value and the scatter of the results. Quality control raises the question of the criteria to be considered for *concessions* from initial specifications.

When dealing with drawings, fabrication processes, quality control, final inspection or concessions, the engineer in charge must be aware of the final aim, of the interactions between the causes of defects, as well as of the effects of the means and remedies. The struggle for good fatigue strength is an art rather than a quantitative science. In this struggle the non-specialized engineer is bewildered by the whimsical appearance of experimental facts. He wants a guide for reasoning. Some qualitative explanations will therefore be given in the following chapters so that he should not feel confused any more when confronted with the problem.

First some aspects of the general problem should be emphasized. Proper designing of a structure with good static strength would be difficult if a thorough experience did not provide us with adequate simplifying assumptions and with allowable stress values calculated from test results on the basis of these assumptions. As soon as sufficient experience of fatigue behaviour from predictions and results is available, the engineer will have no more difficulties with repeated loads than with static loads. To gain this experience many test results on joints are needed and for this reason a large number of results will be quoted and commented on.

Certain parts may be judged adequate for fatigue on the basis of a rough comparison with known results. On conventional riveted or bolted structures this will be the case for finite life ($10^3 \leqslant N \leqslant 10^5$) with components that have low stress concentrations ($K_T \leqslant 3$) and can sustain a static load equal to five times the repeated load (a factor of 3 will often yield good results but this should be checked by tests on real parts).

From the experimental point of view the behaviour of components subjected to fatigue in service or in laboratory tests shows two embarrassing features: life to failure is very scattered, and cracking always starts at a stress concentration point where there is a defect due to the material or to marking, machining, etc. One could be tempted to link up the *scatter* with such defects and conclude that either all defects must be eliminated or that fatigue life cannot be predicted if these defects and their probability of existence are unknown.

In fact, defects often happen to be somewhat weaker points whereby the onset of cracking is located; in the absence of such defects detected by cracks, cracking would have begun a little later but final rupture would not have been delayed since the crack propagation rate is independent of the initial defects. Therefore, serious defects, e.g. unduly sharp geometrical notches, punched marks, segregation and inclusions in the planes perpendicular to tensile stresses, should be eliminated. Minor faults such as machining scratches can be tolerated and one should not be alarmed about them, provided a non-sensitive material is selected.

Scatter raises a psychological problem: is it possible for engineers to think in terms of probabilities? In the past, scatter was included in the margin of ignorance, which is what a *safety factor* really is. If the factor of safety must be reduced to save weight or increased as a result of new requirements, the scatter that still exists is sometimes the cause of unpredicted failures. Any repeated physical experiment yields a series of different measurements with a mean value and some scattered results below or above this mean value. Scientific prediction of the strength should include the probability of obtaining a stipulated result. The result will be satisfactory if the probability of failure is sufficiently low. A probability of accident of 10^{-8} will prevent none of us from occasionally going across the street outside the pedestrian crossings. Fatigue experiments with a dozen specimens show ratios of the highest to the smallest life that range from 2 to 10 for a given load. If the number of cycles could be imposed at will and the load level were obtained from the test, it would be seen that the scatter of the fatigue load is not much greater than that of the static rupture load, at least in the finite-life range ($10^3 \leqslant N \leqslant 10^5$) with regard to joints in aircraft structures. In laboratory tests, scatter is considerable for smooth specimens, moderate for notched specimens and joints, and small for assemblies with a large number of joints.

There is also *scatter in the loads* encountered in service; these loads should be given together with their probability of occurrence. In the static strength computations for aircraft structures this fact is masked by the application of design regulations where fixed values are specified for the loads. As the regulations are subject to revision, these fixed values vary in the course of time, due account being taken of the operational data concerning the frequency or rarity of service incidents which throw doubt on some of the regulatory provisions and the loads stipulated therein. In the future, fatigue loads may be defined on a fixed basis if recording of the vertical accelerations sustained by regular service aircraft provides some means of obtaining adequate *load statistics*.

The complexity of fatigue problems results as much from their specific nature as from the fact that they appear when practical reasons call for more accurate designing and less structural weight. Lightweight structures are compulsory when the margin for the aircraft operating range is small, since any increase in structural weight entails a corresponding increase in fuel weight. In the case of fighters, for which the operational safety depends on the manoeuvrability, an aircraft which is a little too light from the point of view of mechanical strength may prove safer. Certain weight and space requirements may lead to the use of *ultra-high tensile steels* treated to an ultimate tensile strength of 180 daN/mm^2 (260,000 lb/in^2)*. Now such steels offer the advantage of a high static strength in the presence of moderate geometrical notches (up to 300 daN/mm^2 for a notched cylindrical specimen having a circumferential groove with $K_T = 3$) but have the disadvantage of a very low strength in the presence of sharp notches or cracks. This has two implications:

First, one should avoid:

1. Sharp geometrical notches, including threads, unless special precautions are taken;
2. High residual tensile stresses, therefore no machining by grinding should take place and no electrolytically deposited protective coatings should be used unless shot peening is carried out before;
3. Internal notches in the form of inclusions, therefore vacuum casting and remelting should be used to prevent oxide inclusions;
4. Forging defects such as laps and surface decarburization, therefore the work should be completed by general machining. If treatment furnaces with infra-red vacuum heating for austenizing and cold argon quenching are used, the machining may be carried out prior to the treatment;
5. Generally speaking, all defects that may be tolerated for the same steel treated to 120 daN/mm^2 (174,000 lb/in^2).

An acceptable result will be obtained if quality control is exercised at every production stage of the metal - forging, rough machining (close to the final size), heat treatments, finish machining, anti-corrosive protection, assembly of parts - and if systematic checking is carried out in service. It is because of new problems of this kind that the overall project managers (both the design office and the production methods department) must check the work of each specialist and each sub-contractor.

Secondly, with high-tensile steels, the static test to failure will be less instructive than the fatigue test. For components with moderate design notches ($K_T \leqslant 3$), the ratios of net tensile strength to ultimate strength of smooth specimens will show similar values for, let us say, 4340 steel treated to $\sigma_{ult.} = 110$ daN/mm^2 (160,000 lb/in^2) or to 180 daN/mm^2 (270,000 lb/in^2); thus, the ratios of the static strength substantiated by tests on new components to the predicted strength will show comparable values in both cases. On the contrary, for

---

* In the new international system of metric units the Newton N gives an acceleration of 1 m/s^2 for a mass of 1 kg; 1 daN = 1.02 kg weight, 1 daN/mm^2 = 1.02 kg.w/mm^2 = 1450 lb/in^2.

service components with sharp surface scratches or small fatigue cracks, the net static strength of 110 daN/mm^2 steel will be reduced but little, while that of 180 daN/mm^2 steel will be seriously lessened. Therefore, in the case of 180 daN/mm^2 steel, static tests on new components will yield very poor information on their service behaviour.

All this is complicated by the fact that the loads likely to fatigue the structure in service are not always easy to predict and are sometimes only known after systematic and even statistical measurements have been carried out on a prototype aircraft or on the first production aircraft; this applies especially to the gust loads on the tail unit and to the taxying loads on the landing gear.

The design regulations, which specify the static loads that an aircraft must withstand, have so evolved that the regulatory limit loads correspond roughly to a mean frequency of occurrence of once in the life of the aircraft. The ultimate loads to be taken into consideration for static failure are obtained by multiplying the limit loads by 1.5; the probability of occurrence of these loads is extremely low. In fact, according to Taylor[3], the service loads may be related to two different types of statistics: on the one hand, statistics of loads of moderate levels and of large populations, responsible for causing fatigue damage, and, on the other hand, *statistics of rare and accidental* loads which dictate the static strength of the aircraft.

Similarly, as far as the allowable loads are concerned, there seems to be an ordinary scatter due to the statistics of large populations and, on the other hand, a much greater scatter due to very rare circumstances or to very detrimental fabrication defects that have not been detected during inspection. For instance, laboratory fatigue tests often show that ground high-tensile steel specimens have an excellent strength. There are, however, very rare cases where the strength is reduced by half for one batch of specimens; investigation after cross-sectioning thus reveals that the steel may be "burnt" by the grinding operation. Such defects are difficult to detect by current inspection means and the conclusion is that grinding of high-tensile steels must be avoided. Fatigue tests may yield excellent results for some batches, yet components of the other batches may well fail in service.

Because of these rare and severe statistical populations it is very difficult to make strength predictions and the problems encountered are more of a qualitative than of a quantitative nature. A good knowledge is required of all the factors governing the service strength, of the way they are linked with one another, and of their interactions and detrimental effects in each specific case. It is not enough that several specialists should each know some part of the problem; the design offices, the production engineering departments and the after-sales services must have an overall knowledge so that efficient general checking may be superimposed on the systematic survey of the work of each specialist.

1.1.4 Working Method and Mode of Writing

The foregoing general comment emphasizes the close interrelation of the various aspects of structural strength problems and the difficulty of classifying them in a coherent way. No definite choice can be made between the analytical and the synthetical method of presentation. Each of the following chapters deals with one subject but also mentions some topics that are discussed in detail in other chapters. Some subjects are examined several times so that every chapter may be read separately; the study of the details should not be dissociated from a comprehensive view: at no time should the investigation of a tree hide the forest.

In 1950 Dryden, Rhode and Kuhn[4] underlined the inability of the engineer to understand the physical nature of fatigue and to make a rational use of the large amount of published results. They insisted on the necessity of obtaining some practical data on the fatigue strength of airframes and also some guides for the interpretation of the results.

At that time the writer was engaged in a study of documents which resulted in a synthetical review on the plastic deformation and fatigue of metals[5], written at the Office National d'Etudes et de Recherches Aéronautiques de Paris (ONERA) in 1952 and circulated in 1963. In this work as well as in later work an attempt was made to formulate some assumptions that would account for all the known facts. Dealing with published information as raw material, a first set of documents was used to evolve some assumptions and other sets of documents to check or amend these assumptions. Our investigations always include a list of references for the facts and opinions selected from the scientific and technical literature. In some cases, however, our conclusions are different or less conservative than those of the authors quoted; sometimes we are led to make a choice between controversial views or to give our own opinion. This method of working is a little risky but it is justified by the necessity of providing the engineer with provisional rules as guides for immediate action or for the selection of solutions to be checked experimentally.

More recently the same practical necessities led us to a documentary survey on creep and corrosion. In the past, aluminium-copper-zinc alloys, for instance, were yielding good results in laboratory fatigue tests while showing a very poor behaviour in actual service. This situation resulted in a controversy between metallurgists and manufacturers, who were sometimes accused of not being able to design or construct; there was some truth in that opinion but it is now understood that the set-backs were partly due to the static properties of cracked components and above all to the interactions between fatigue and service corrosion. For the same alloy, short-duration stress-corrosion tests under laboratory conditions did not show a sensitivity differing from that of other alloys. However, long-duration tests in natural sea or industrial environment led to a change in the classification and showed that the laboratories were in the wrong although the users were referring to inappropriate reasons when giving up the alloy concerned. For the 7075 aluminium alloy (US) a tempering treatment, termed T73, is at present suggested by ALCOA; it solves the problem for forged parts but reduces the static strength by 10%.

If knowledge were conveyed only on the basis of unquestionable certainty, the physical science would never have progressed, as each generation gathers previous experimental data but changes the concepts of the preceding generation. Similarly, if only the ideas of the specialists were considered here and if only the points of general agreement were kept, the subject material left would sometimes be hardly usable for synthetical purposes. One could, of course, trust the specialists and neglect the apparent contradictions, the intermediate fields not covered by the various specialties, and the possible interactions. One could also restrict the survey to the natural history of the facts or do nothing.

So, if this work manages to assist people in getting a clearer understanding of the problem as a whole, despite the reservations it will give rise to, its aim will be achieved. It would be eventually agreeable to the writer to correct possible errors and thus supplement or amend his knowledge; this polishing may be accomplished by specialists if they are aware of the various problems facing the design engineers, for whom this work has been written.

The following parts of this chapter discuss the concepts required for complementing the present teaching of "Strength of Materials" with regard to fatigue and for laying the ground work for a subsequent study in greater depth.

Note: This work is partially a translation from previous French notes where figures in US or British units had been converted into metric units. Here the writer has retained international metric units and indicated figures in British units between brackets. In some cases the original British figures could not be traced back; hence some of the figures placed in brackets were computed through a double conversion which may have led to errors of about 2%.

1.2 FATIGUE NOTATIONS

The fatigue loading is defined by a number n^* of successive load applications and by the magnitude F, the nature (tension, shear, bending, torsion) and the variation (alternating or with a static component constantly applied) of the load. F is either a force or a set of forces and couples varying simultaneously. For a sinusoidal variation we may write:

$$F = F_{mean} + F_a \sin \omega t$$

where F_{mean} is the steady mean component and F_a the superimposed alternating component. For frequencies ranging from few cycles per minute to 12,000 cpm (200 Hz) it is assumed that the frequency exerts a negligible effect on the fatigue of engineering metals at room temperature. This assumption does not hold true in the case of high temperatures, corrosion, or very low and very high frequencies.

In the following we shall use the notation:

$$F = F_{mean} \pm F_a$$

and (see Figure 1.1)

$$F_{max} = F_{mean} + F_a , \qquad F_{min} = F_{mean} - F_a .$$

In order to retain only one variable for measuring the magnitude, F is sometimes defined by its greatest value, F_{max}, and by the ratio R:

$$R = \frac{F_{min}}{F_{max}} = \frac{F_{mean} - F_a}{F_{mean} + F_a} ,$$

hence

$$F_a = \frac{1 - R}{2} F_{max} , \qquad F_{mean} = \frac{1 + R}{2} F_{max} .$$

The mean load is sometimes taken as a reference and the ratio

$$A = \frac{F_a}{F_{mean}}$$

is used.

If the stresses can be calculated, we may also write

$$\sigma = \sigma_{mean} \pm \sigma_a , \qquad \tau = \tau_{mean} \pm \tau_a$$

where σ_{mean} is positive in tension.

---

* n denotes the applied number of cycles while N is the number of cycles to failure.

If carried out with a given strain as in Coffin's[6] tests, the loading will be defined by

$$\epsilon = \epsilon_{mean} \pm \epsilon_a , \quad \gamma = \gamma_{mean} \pm \gamma_a$$

depending on the type of strain (axial or shear), ϵ_{mean} being positive in the case of elongation.

In the finite-life range ($N < 10^5$) and in order to obtain dimensionless quantities for comparing the fatigue strengths of different components, we shall relate the fatigue strength to the static strength, as did Locati. If $F_{ult.}$ is the load that causes static fracture and F the fatigue failure load after N cycles, we may define a dimensionless coefficient as follows:

$$\Phi_N = \frac{F}{F_{ult.}} = \frac{F_{mean}}{F_{ult.}} \pm \frac{F_a}{F_{ult.}} = \Phi_{mean} \pm \Phi_a .$$

Φ_N is a function of the number of cycles N to failure. If F is not the load sustained but the load applied, we shall use the notation Φ_n. The symbol Φ_n denotes the load applied during n cycles and Φ_N the load to failure after N cycles. If the theoretical static strength defined by $\sigma_{ult.}$ is considered, we propose to take

$$\varphi_N = \frac{\sigma}{\sigma_{ult.}} .$$

However, it must be emphasized that Φ means no more than its two components F and $F_{ult.}$. It has only a full meaning in cases where the static rupture without buckling and the fatigue failure affect the same part subjected to stresses of the same type.

The following factors have also been used for a long time:

Stress Concentration Factor, K_T :

If σ, calculated in accordance with the theory of elasticity, is the largest stress at a notch and $\sigma_{nom.}$ the nominal stress in the notched cross-section, calculated by the elementary mechanics of materials, the stress concentration is defined by

$$K_T = \frac{\sigma}{\sigma_{nom.}} .$$

In Germany the notation used is α_k. In fact, K_T does not define the stress field in the neighbourhood of the largest stress and $\sigma_{nom.}$ remains rather subjective. The stress $\sigma_{nom.}$ must be clearly defined since researchers and this book refer $\sigma_{nom.}$ to the *net section area* while designers often work with a $\sigma_{nom.}$ referred to the *gross section area* where holes are disregarded. K_T is only well defined for simple specimens.

Fatigue Notch Factor, K_F :

K_F is the ratio of the fatigue rupture stress of a smooth specimen at N cycles to the nominal fatigue rupture stress of a notched component. This factor varies with N, with K_T, with the stress gradient, with the surface-hardened state at the root of the notch, and with the material and its mechanical and thermal history.

The notation for $K_F(N)$ in Germany is β_k.

Notch Sensitivity Factor q :

This factor is defined by

$$q = (K_F - 1)/(K_T - 1)$$

and its variation is $0 \leqslant q \leqslant 1$. It depends on the same parameters as K_F ; the notation for q in Germany is η.

Plastic adjustment of a material subjected to an increasing static load above the yield strength results in a levelling of the stress concentrations. Consequently, it has been possible to carry out static calculations by neglecting the stress concentrations which, according to the theory of elasticity, appear in the vicinity of discontinuities (holes, fillets, shoulder fillets, etc.) for stresses below the yield strength of the material. The existence of the plastic flow justifies most of the simplifying assumptions used by the engineers for static failure calculations.

With repeated or alternating fatigue loads the adjusting effect still exists but is too small to allow the usual simplifying assumptions. In the past it was hoped that the fatigue strength of notched components could be assessed by determining the maximum stresses in accordance with the theory of elasticity and comparing them with the allowable stresses derived from fatigue tests on smooth specimens.

---

* In the past we have used the symbol γ instead of Φ but we have now adopted Locati's notation so as to avoid confusion with the shear strain.

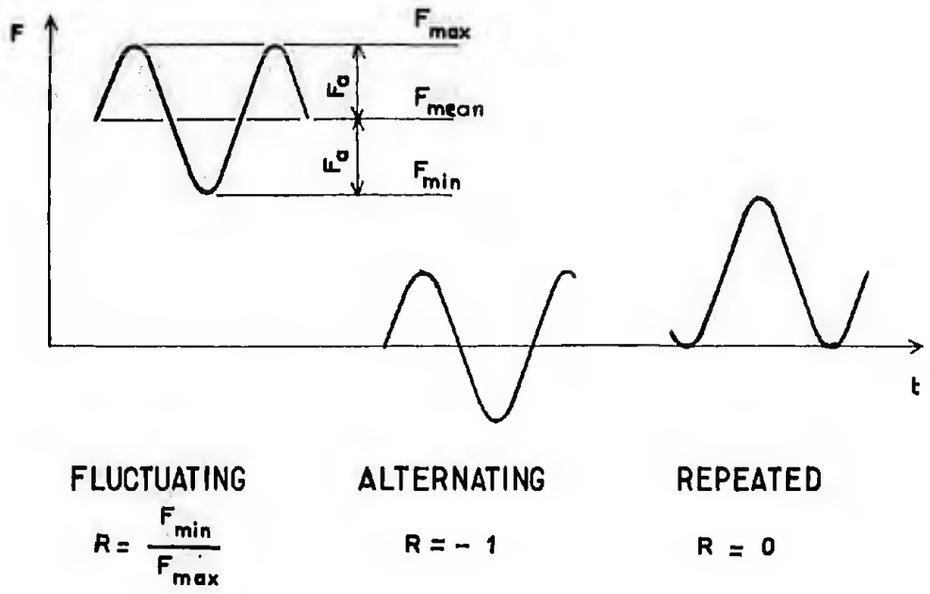

FLUCTUATING $R = \frac{F_{min}}{F_{max}}$ ALTERNATING $R = -1$ REPEATED $R = 0$

Figure 1.1

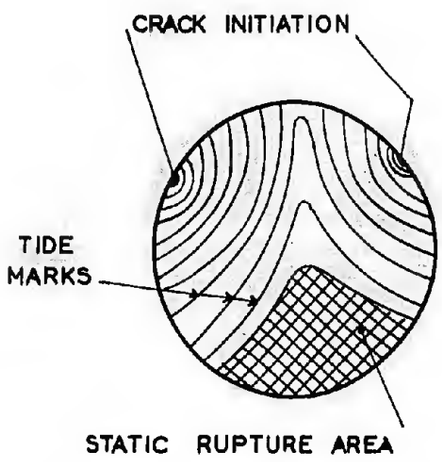

Fig. 1.2 Crack propagation in tension

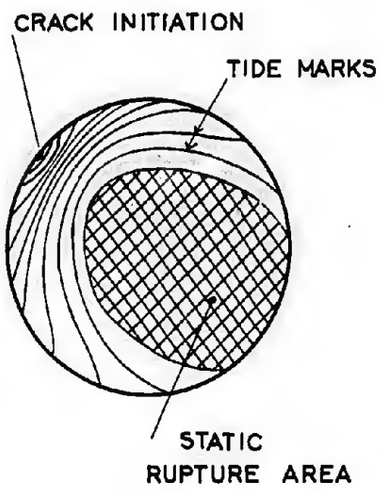

Fig. 1.3 Crack propagation in rotating-bending

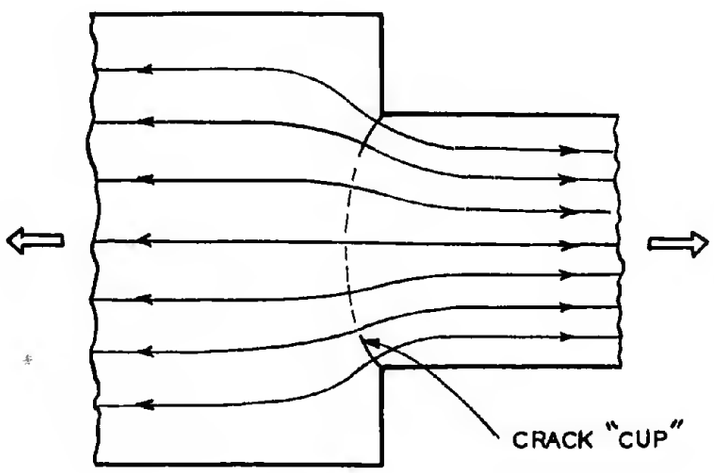

Figure 1.4

In fact, it appeared that the physical reality was between the two extremes of total adjustment assumed for certain static calculations and of perfect elasticity assumed for the second method of calculation. For a long time, however, the fatigue strength of the smooth specimen was still taken as a reference for the evaluation of the detrimental effect of notches. Numerous tests were thus performed on smooth specimens in the fallacious hope of establishing the fatigue strength of the materials used. Most of these tests were of the rotating-bending type.

In our opinion, the strength of smooth specimens is a poor reference for the design of notched components; rotating-bending tests on specimens of equal strength show that this reference is sometimes very bad. Indeed, certain steels subjected to alternating stress at a frequency as low as 25 Hz (Schenck pulsator) and certain light alloys tested at 150 Hz (Amsler Vibrophore) become hot as a result of internal damping. The test takes place at a temperature which depends on the balance between the heat added and the losses by conductivity. For smooth specimens of equal strength in which a large volume of material is stressed, the temperature is high enough to make the steels turn blue, whereby the result is seriously altered. On the contrary, in waisted and, *a fortiori*, notched specimens the small volume of material subject to high stress causes the heat to be increased only by a small amount which is easily dissipated; the test is performed at room temperature.

For this reason, and because the design offices are able to carry out static strength calculations fairly well, we shall, together with other modern authors, take the static strength of a component as a reference for the fatigue strength, thus replacing K_F by Φ_N, in the range $N \leqslant 10^5$.

The fatigue strength measured on smooth specimens is, however, still valuable since it corresponds to the limit which the strength of components with well-designed joints tends to approach. It should be pointed out that if the low fatigue strengths of some mechanical parts are sometimes due to errors in designs or drawings (e.g. sharp angles), the fact remains that joints will exhibit severe stress concentrations as long as no better fastening methods than rivets or bolts are used. A remedy to this consists in the use of locally oversized joints. For example, there are three possibilities for sheets with stringers:

(a) Increasing the thickness locally with bonded reinforcements; this solution is used on the Fokker Friendship aircraft and for grip-ends of specimens held in the jaws of testing machines;

(b) Leaving additional local thicknesses in the case of integral-stringer plates made by milling or chemical milling from thick plate material;

(c) Reinforcing the stringers locally.

1.3 ASPECT OF FATIGUE FRACTURES

On cylindrical parts in alternating tension-compressi . or in fluctuating tension, cracking originates on the outer surface from scratches or surface defects, except when severe internal flaws such as inclusions result in internal weak points. In this respect, *fatigue reveals defects which a cross-section made at random would be unlikely to detect.* In the absence of such defects, cracking starts at the surface.

We shall see that the development of fatigue before cracking is made possible or induced by microscopic plastic strains in metals. Plastic deformation of internal crystals is hindered by neighbouring crystals, while surface crystals have a free side and therefore yield more readily. If there are sharp edges on the contour of a specimen, the crystals located at the edges are even more subject to yielding and cracking will start from these edges; so it is advisable to blunt edges with a radius greater than the mean diameter of the grain (crystal) of the metal.

The fatigue crack grows from an initial point in width and depth as its front sweeps across the cross-section of the component, sometimes joining other fronts originating from other weak points. Finally the remaining section breaks statically during the last load cycle (Fig. 1.2).

If rupture occurs in service, the interruptions in the operation of the machine or equipment will result in tide marks corresponding with stationary positions of the crack front during crack propagation. In laboratory tests with continuous operation of the testing machine these marks are too fine to be always visible, but vaguely radiating ripples may show the crack initiation point or points.

In fatigue tests at low stress and with a large number of cycles, the texture of the fatigue cracking area is substantially different from that of the final static fractured area; it is thus possible to identify a fatigue fracture, to measure the statically fractured area, and to determine the static fracture stress of a component containing a fatigue crack.

With comparatively high stresses and a low number of load cycles, the plastic development in fatigue differs little from the plastic development prior to and during crack propagation in static tests and the appearances of the two fractured areas are very similar.

In some cases where the appearance of the fracture indicates static failure, caution is recommended since fracture might be caused either by static loading ($N = \frac{1}{2}$) or by fatigue loading at high stresses ($2 \leqslant N \leqslant 100$). If the investigation is not carried out by an experienced specialist, there may be uncertainty in the range $100 < N < 10^5$. One must then discuss the probabilities of loadings likely to cause either static or fatigue failure.

It should be noted that a slight necking (localized reduction in the cross-section area) does not prove that static rupture has occurred. Indeed, it is found that fluctuating tensile loading (with a mean static component) produces a *slight necking*. It will be seen later that alternating reversed stresses favour plastic flow in the direction of the static mean stress.

In *alternating bending* the front of the crack propagates in substantially the same way as in alternating tension.

In *rotating-bending* the maximum stress is always located at the intersection of the surface of the component or specimen with the crack front, as in the previous cases, but since the development of fatigue begins on the entire contour, the crack front will extend more rapidly over the surface than in depth and will tend to have a different curvature, assuming an elliptic shape around the final static rupture area. Peripheral propagation will be even faster if the component has a circumferential notch and if the static rupture area is internal; the crack front will be more concentric if the load is high (Fig. 1.3).

If a shaft loaded in rotating-bending contains a hole in the direction of its diameter, the edge of the hole is the seat of a stress concentration and its sharp angle will be a potential crack starter. Blunting the angle (chamfering) will delay the cracking.

In *alternating torsion* cracks are substantially perpendicular to the axis in ductile metals. In hard and brittle metals, however, they are inclined at 45° to the axis. If the shaft has a circumferential notch, the crack follows the root of the notch and extends in the direction of the cross-section; in hard and brittle metals it tends to incline in depth from several points and shows facets.

As will be explained in Chapter II, it is believed that the development of fatigue prior to cracking is governed by plastic shear strains which produce highly localized tensile stresses near the barriers to plastic slip. These heavily stressed areas are roughly aligned along the shear planes perpendicular or parallel to the axis. Rupture would then be conditioned by the localized tensile stresses, which are the sum of the mean principal stresses inclined at 45° on the axis and the previously mentioned stresses due to shear and induced by the plastic development in fatigue. Plastic development is considerable in ductile metals and much less in brittle metals, which accounts for the difference in behaviour.

In mechanical parts *the crack plane is often perpendicular to the lines of forces of the principal tensile stresses*. Thus, in the case of a shouldered shaft (Fig. 1.4) subjected to tension or rotating-bending, fracture exhibits a typical cup shape. For any component fractured or cracked in service, the direction of the principal tensile stresses can be inferred from the direction of cracking. Thus, in a wing-to-fuselage attachment fitting designed to absorb drag, the unusual direction of a crack as compared to the calculated stresses led to the conclusion that the attachment fitting also took up a certain amount of lift; since the lift is equal to about ten times the drag, the parasitic lift stresses were locally greater than the drag stresses: forces follow the path they can and do not necessarily travel along lines that are easy to calculate. In the case quoted, the phenomenon was checked by a static test including measurement of the local stresses. It should also be pointed out that *any investigation of cracks merely results in* presumptions that need to be checked. The study of fractures may be facilitated by a catalogue such as that issued by the RAE[7].

1.4 WOHLER $\sigma - N$ CURVE

A German mining engineer, Albert, two French engineers, Marcoux and Arnoux[8], and a British engineer, McDonnell, were the first to discover the "fatigue" phenomenon, thus termed by Poncelet. Wöhler carried out the first systematic laboratory experiments in the 1860s. A method of presenting test results was named after him; it consists in plotting the common logarithm of the number N of load applications to failure on the X-axis and the load F on the Y-axis. An F-N curve is thus obtained. Instead of the load F, one may also plot the alternating stress σ_a (Fig. 1.5). In the USA the σ-N curve is called "S-N curve" because the symbol S is widely used to denote nominal stress.

Figures 1.5 and 1.6, from a paper by Cazaud[9], give examples of this method of presentation. Points with an arrow indicate that the test concerned was stopped without failure of the specimen. Annealed mild steel has a fairly well defined fatigue limit at about 10^6 cycles. A specimen assuming the form of a body of revolution as illustrated in Figure 1.7 is termed *waisted specimen*.

Previous test results have shown that the strength is quite sensitive to the shape and to the surface conditions of the specimens. The waisted specimen, although containing a stress concentration, is more resistant than the cylindrical specimen.

It is our belief that this result, which seems paradoxical, is due to lesser heating of the waisted specimen since the volume of metal subjected to high stresses is comparatively smaller and the temperature of the metal during testing is more moderate. At a higher test rate (9,500 c/m) a change occurs towards 10^6 in the relative strengths of the cylindrical and waisted specimens. It seems that at high stresses the temperatures of both types of specimens, which are above the temperature of the test performed at 2,475 c/m, exceed the level that causes a great variation in strength (between 100° and 200°C), thus improving the behaviour of both specimens; on the contrary, the previously mentioned discrepancy remains at lower stresses. Although anomalies of this kind may be interpreted in other ways, it should be noted that tests conducted on specimens of equal strength sometimes have the disadvantage of heating effects such that actually the strength of the material is measured

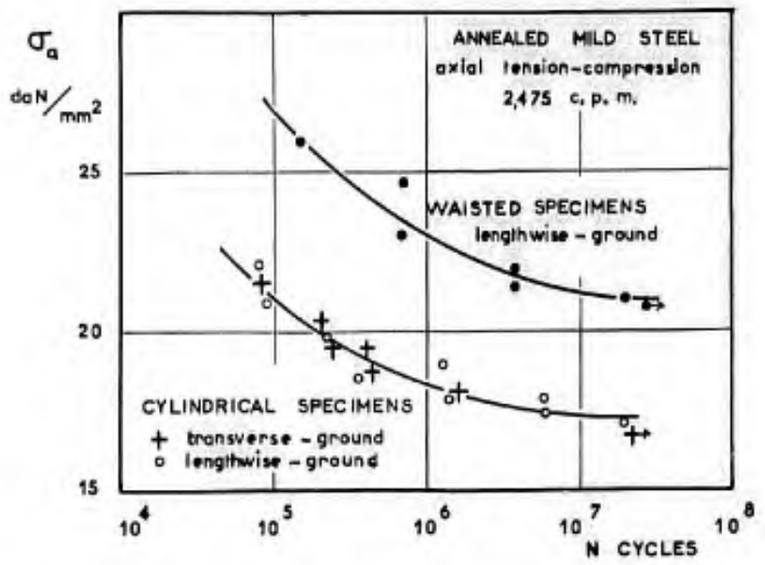

Figure 1.5

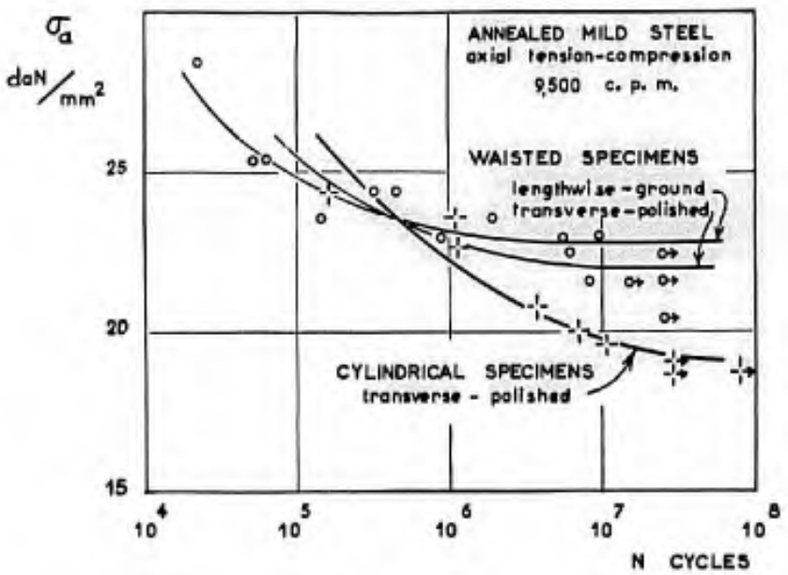

Figure 1.6

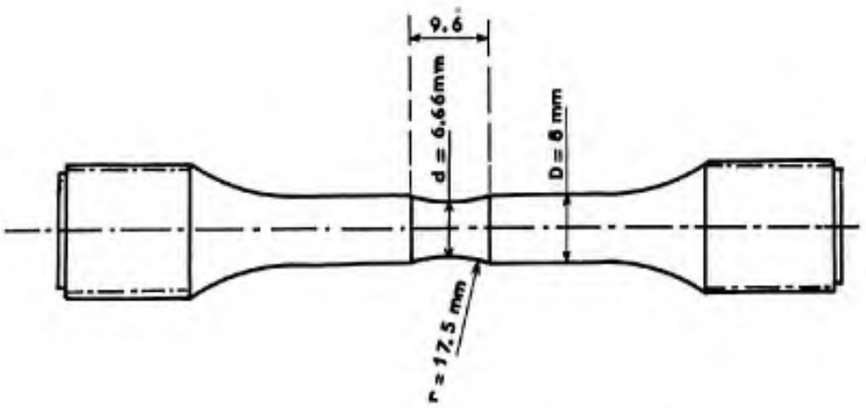

Fig. 1.7 Waisted specimen. K_T = 1.1 in axial tension-compression

at an unknown test temperature. The data obtained therefore cannot be used for designing mechanical components that are stressed under different conditions and they provide at best rough estimates that may be used as basis of discussion.

The *fatigue limit* is the stress below which no failure occurs, irrespective of the number of load applications. In the case of steel, it corresponds to N ranging from 10^6 to 10^7. For the American 75 S-T6 light alloy (Al + 5.5% Zn + 2.5% Mg + 1.5% Cu +..) Oberg[10] found the fatigue limit after 10^7 cycles and conducted certain tests up to 10^{10} cycles in order to check this point (Fig. 1.8). However, many laboratory people consider that aluminium alloys have no fatigue limit and they accept the arbitrary definition proposed by Templin: fatigue limit for light alloys is the stress to failure at 5×10^8 cycles. When prediction of a fatigue limit is not possible owing to the limited duration of the tests, the fatigue limit is to be assumed zero or to be reached at a very high value of N, which means the same in practice since all engineering structures have a limited life.

For very small values of N all σ-N curves contain an initial horizontal portion that goes through the point $N = \frac{1}{4}$ and $\sigma = \sigma_{ult.}$ corresponding to rupture under a static load. Then we have the finite-life range where the strength decreases more and more rapidly. Finally, the slope is less pronounced and the strength tends towards the fatigue limit σ_f, which may be zero. If only the portion of the curve near the fatigue limit and the slope of the curve in the finite life region are known, it may be helpful to interpolate between $\sigma_{ult.}$ and σ_f. However, the problem is to find functional scales of σ and N such that the curve becomes substantially a straight line and allows easy interpolation or slightly conservative extrapolation. Apart from the conventional σ – log N scales, one sometimes uses log σ – log N scales, for which a straight line corresponds to the equation $\sigma = a/N^b$; this change of scales is fairly useful for very large numbers of cycles when the fatigue limit is zero, but proves inefficient for small values of N.

In the finite-life range close to static rupture (here N = 1), one may consider the functions

$$\Phi = e^{-a(N-1)^b} \quad \text{or} \quad \log \log \frac{1}{\Phi} = \log(a \log e) + b \log(N-1)$$

$$\Phi = e^{-a(\log N)^b} \quad \text{or} \quad \log \log \frac{1}{\Phi} = \log(a \log e) + \log \log N$$

where $\Phi = \sigma/\sigma_{ult.}$ is a dimensionless relative stress; these functions have a maximum value equal to unity for N = 1 and tend towards zero when N tends towards infinity. If a metal has a fatigue limit σ_f, Φ may be substituted for $\Delta\Phi = (\sigma - \sigma_f)/(\sigma_{ult.} - \sigma_f)$.

The preceding figures give some examples of the conventional σ – log N presentation. A straight line is found only for a limited range of numbers of cycles. Figure 1.9 shows the log σ – log N scales; it illustrates the fatigue life of an outer ball-bearing ring under radial load[11]. Here the term "failure" applies to the detection of a change in the noise level by means of a stethoscope, which is confirmed by evidence of cracking or exfoliation on visual inspection after discontinuance of the test. No fatigue limit was found at 10^9 revolutions. This example shows considerable scatter of the fatigue life. For each load level the median line of results is plotted. The load is defined by the mean contact pressure (Hertz theory) measured in lb/in^2 ($0.69/1000$ daN/mm^2).

As a rule, Wöhler curves are found for rupture, crack initiation and the various detectable stages of the fatigue process. Figure 1.10 gives some alternating-tensile tests results for a steel joint located between an aircraft fuselage and a lower wing spar cap. Log log $1/\Psi$ and log log N scales are used. A first series of tests yielded the plain points through which a mean straight line was plotted for estimating the fatigue life at $\Phi_{max} = 0.563$, i.e. 5,400 cycles. The open points represent a second test series performed at $\Phi_{max} = 0.563$ to check the previous estimate.

Let us now consider the scatter in fatigue. If the form of the statistical distribution law of the number of cycles to failure were known, the probability of survival of a structure could be assessed from a small number of tests at an appropriate load level. Weibull[12] assumed a normal log N law; experimental results also permit the assumption of a normal log log N law in other cases. In fact, it appears that for a given value of N the load scatter is normal.

For a single load level and a normal log N law, Kennedy[13] presented a method of estimation with $x = \log N$ as the random variate, $\bar{X}$ and σ as the mean value and the root-mean-square deviation of x for an infinite population, $\bar{x}$ and s as the estimated values of $\bar{X}$ and σ from n observations, p as the probability of x smaller than $\bar{x} - ks$.

The statistical methods, assuming a normal distribution, permit the computation of k such that the estimated $\bar{x} - ks$, which is a function of the probability p, is smaller than or equal to the value of x of the same probability taken from the large population, and this with a given probability called *coefficient of confidence* and taken equal to 0.9 by Kennedy. If n is the number of available results,

$$s^2 = \frac{\Sigma x^2 - \frac{1}{n}(\Sigma x)^2}{n - 1};$$

k is given in Table 1.1.

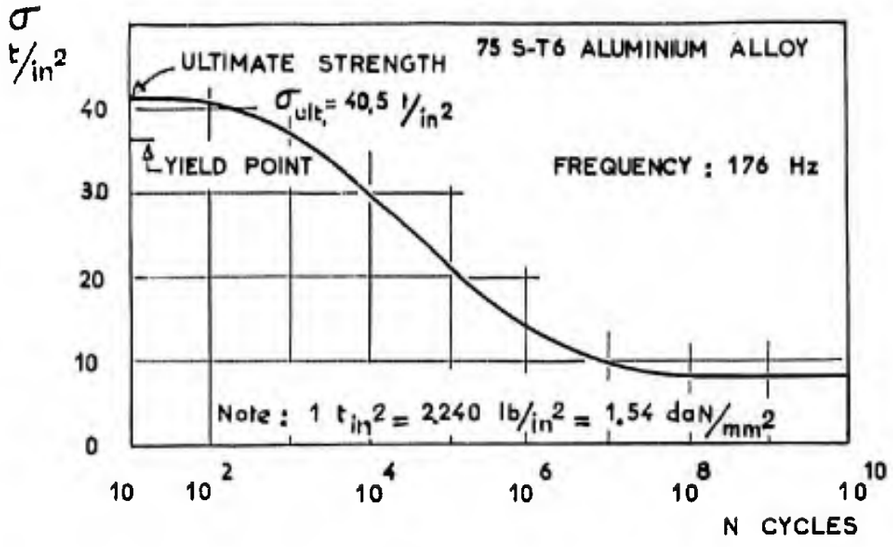

Figure 1.8

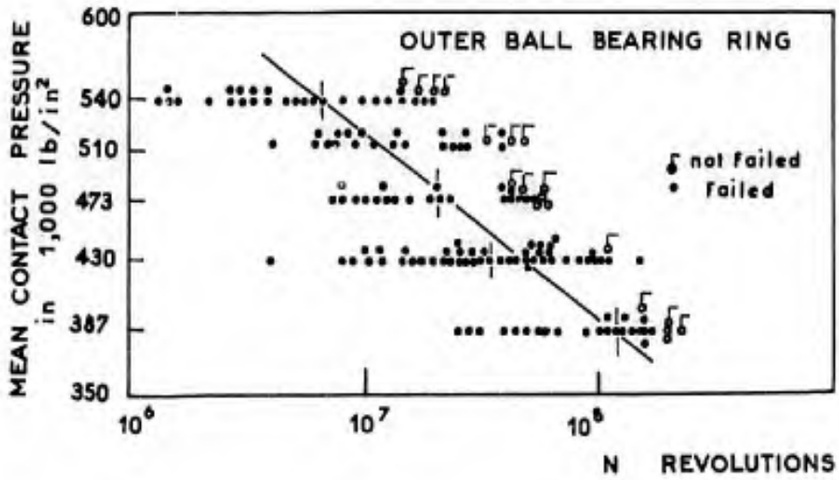

Figure 1.9

TABLE 1.1

Values of k in the estimate $\bar{x} - ks$ of x with a probability p for $x \leqslant \bar{x} - ks$ and with a coefficient of confidence of 0.9, after Kennedy

n \ p	0.5	0.1	0.01	0.002	0.001	0.0005
3	0.964	3.873	6.660	8.166	8.745	9.298
5	0.644	2.585	4.400	5.383	5.673	6.124
7	0.522	2.244	3.822	4.675	5.005	5.317
10	0.426	2.012	3.442	4.214	4.511	4.795
20	0.292	1.754	3.035	3.725	3.990	4.243
∞	0	1.282	2.326	2.878	3.090	3.291

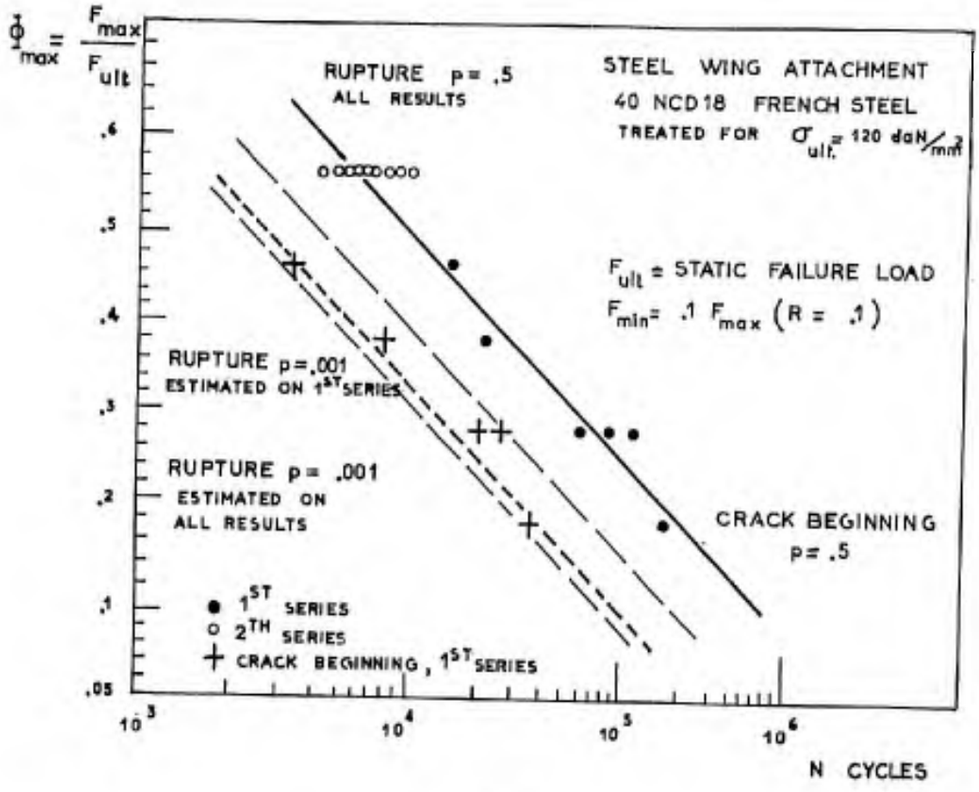

Figure 1.10

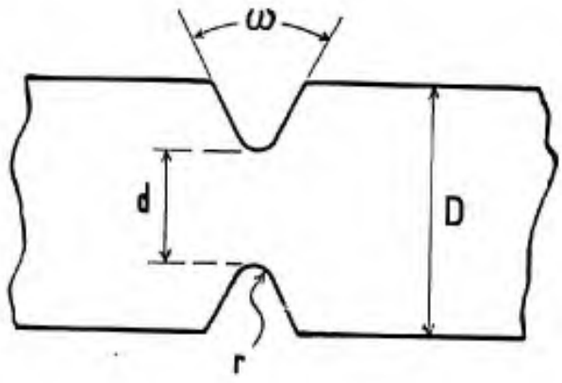

Figure 1.11

TABLE 1.2

Values of p and q for notched specimens

Type of loading	*Type of specimen*	p	q
Tension or compression	Flat	1.32	2
"	Cylindrical	1	2
Bending	Flat	0.825	2
"	Cylindrical	0.715	2
Torsion	Cylindrical	0.365	1

This table could be used directly if an adequate number of experimental points per load level were available. This is rarely the case; it is therefore necessary to use all the points known and, for this purpose, to assume that the dispersion in the X-direction on the Wöhler curve, here the log log N , is independent of the load. On the basis of this assumption, the mean line is plotted as well as possible across the m experimental points, then the mean s^2 of the sum of the squares of the deviation on the X-axis with respect to the straight line is calculated:

$$s^2 = \frac{\Sigma \epsilon^2}{m-2}$$

and we take $n = m - 1$ to use Table 1.1. If we refer to the black points in Figure 1.10, the root-mean-square deviation on the X-axis from the mean line is $s = l_1$* . For $n = 6 - 1 = 5$ and $p = 0.001$, the table gives $k = 5.67$, hence $ks = kl_1$. By shifting the mean line by kl_1 towards the low numbers of cycles, we obtain a dotted line such that the probability of encountering worse results because of scatter is reduced to 0.001, the second series of tests at the level $\Phi_{max} = 0.563$ resulted in a better knowledge of the resistance to high loads corresponding to the maximum service load of the aircraft. We shall see in a later chapter what practical conclusions can be drawn from such a calculation, which is of course a rough one.

Fatigue strength depends upon many factors. We shall first describe the effect of mechanical factors:

- stress concentrations
- mean static stress
- method of machining

for some materials used in the aircraft industry.

1.5 STRESS CONCENTRATIONS

The stress concentration factor K_T is the ratio between the largest stress due to a change in shape and the nominal stress calculated by the elementary mechanics of materials. It is interesting to know the orders of magnitude of K_T in joints and components:

Spot-welded sheet joints	$K_T \simeq 20$
Riveted sheet joints	10
Bolted lap joints	6 to 15
Lugs, pin-loaded holes	2 to 10
Plates with free holes	2 to 3
V-grooves with sharp roots	5 to 20
V-grooves with rounded roots	1.3 to 8
Screw threads not subjected to direct loading	3 to 6
Screw threads engaged in nuts	5 to 12
Fillets	1.1 to 4

The fatigue notch factor K_F may be about as large as the theoretical factor K_T ; on the other hand, it may be as small as 1/5 or 1/10 of K_T . For the same value of K_T and geometrically similar specimens, Kuhn[39] has pointed out that K_F decreases when the absolute size of the specimen increases.

Sometimes, one speaks of the "equivalent factor K_T" of a structure; for instance, an airframe is said to have a K_T-value of about 4. This means solely that its S-N curve, which is unknown, is about the same as that found for notched specimens with $K_T = 4$, taken as reference basis. The equivalent factor K_T is only useful if the reference basis is clearly defined. For a long time many specialists in airframe structures referred to test results obtained on small specimens by the Battelle Memorial Institute and published in the NACA Technical Notes Nos. 2324, 2389, 2390 and 2639. Such results should be considered only for interpolation in connection with test results found on actual components or structures.

In calculations of K_T such as carried out by Neuber[14], two extreme cases are often used for bracketing the real case: the "shallow notch" and the "deep notch". A circumferential V-groove on the surface of a cylindrical bar or two edge grooves on a flat specimen are defined by the dimensions d, D, r and ω of the Figure 1.11.

---

* l_1 is s plotted to the scale of Figure 1.10.

Neuber's formulae are rather complicated. Hottenrott[15] has proposed a good simplified approximation:

$$K_{Tp} = pK_p + 1 \quad \text{with} \quad K_p = \sqrt{\left(\frac{d}{2r} + 1\right)} - 1$$

for the deep notch and

$$K_{Tq} = qK_q + 1 \quad \text{with} \quad K_q = \sqrt{\left(\frac{D-d}{2r}\right)}$$

for the shallow notch; p and q are numerical factors which depend on the type of loading and on the stress state, the stress state being biaxial in flat specimens and triaxial in cylindrical specimens. The angle ω has little effect for $0 < \omega < 60^{\circ}$. The notch is shallow if D is close to d, and deep if the ratio D/d is large. Actual notches correspond to intermediate cases and K_T is obtained through Neuber's interpolation formulae*

$$K_T = 1 + \frac{1}{\sqrt{\left[\frac{1}{(K_{tp} - 1)^2} + \frac{1}{(K_{tq} - 1)^2}\right]}}$$

and

$$K_T = 1 + \frac{1}{\sqrt{\left\{1/p^2\left[\left(\frac{d}{2r} + 1\right) - 1\right]^2 + 1/q^2\left(\frac{D - d}{2r}\right)\right\}}}.$$

The factors p and q are given in Table 1.2.

Flat specimens having a hole are sometimes used. Howland[16] has studied the *circular hole* of diameter d drilled in a bar of width D, between d = 0 and d/D = 0.5; Weber[17] has found $K_T = 2$ for the limit case d = D. We have

d/d	0	0.1	0.2	0.3	0.4	0.5	1
K_T	3	2.7	2.5	2.35	2.25	2.17	2

The elliptic hole in an infinite plate subjected to tension allows the variation of K_T from 1 to a very high value:

$$K_T = 1 + \frac{2a}{b},$$

where a and b are the semi-axes of the ellipse, "a" being perpendicular to the load.

Scale Effect and Stress Gradient

We shall see later that for various reasons the state of the material at the surface and down to a certain depth is quite different from that of the material located at a great depth. In particular, the free surface causes the resistance to plastic strains at the surface to be lower for a material that has been work-hardened; the deeper grains exert a supporting effect which is large if the stress gradient in the direction of the depth is small. Surface hardening can produce the opposite effect. For these reasons the notch factor K_T does not suffice to define the stress state that is responsible for the development of fatigue before cracking. Furthermore we must also consider the gradient in depth of the largest tensile stress parallel to the free surface. For circular and elliptic holes as well as for Neuber's deep notches, calculation of the gradient with Neuber's expressions for the stresses yields

$$\Gamma = -\sigma_{nom.} \frac{K_T}{r} k,$$

where r is the local notch radius and k a factor having the following values:

Tension, circular hole $\quad k = 7/3$

Tension, elliptic hole $\quad k = \dfrac{3 + 4\sqrt{(a/r)}}{1 + 2\sqrt{(a/r)}}$

Tension, deep notch $\quad k = 1$

Bending, deep notch $\quad k = 2(1 + r/h)$,

h being the thickness at the root of the notch.

---

* Another interpolation is suggested by Dixon[38].

For a smooth specimen in bending

$$\Gamma = -\frac{2}{h}\sigma_{nom.}$$

where h is the depth of the beam.

It is seen that the smooth bend specimen cannot be compared with a smooth tension specimen. The use of the radius or of the half-thickness to define the stress gradient provides a first explanation of the scale effect.

For stresses above the fatigue limit the duration of cracking is approximately equal to half the life to failure and the crack may be considered equivalent to a very sharp notch. We shall show in another chapter that the stress distribution around the crack tip is also conditioned by the absolute size and exhibits a scale effect. Generally, the strength decreases with increasing size.

Some Results of Tests on Notched Specimens

As a rule, if we change over from smooth specimens to notched specimens, the Wöhler curve is lowered and moves to the left since the finite-life range begins earlier for notched specimens. Figure 1.12, relating to sheets made of aluminium-copper (24 S-T3) or aluminium-zinc (75 S-T6) alloys, is typical of airframes. On smooth specimens, the fatigue strength is reduced to half the static strength ($\Phi = 0.5$) for $N = 10^5$, whereas the same decrease is found on notched specimens for $N = 10^2$. At 10^7 we have $\Phi = 0.25$ for smooth specimens and $\Phi = 0.08$ for notched specimens.

For steels there is a fairly close correlation between the fatigue strength of smooth specimens and the ultimate static strength. The fatigue limit ($N \leqslant 10^6$) is between $0.4.\sigma_{ult.}$ and $0.5\,\sigma_{ult.}$. The solid curves in Figure 1.13 show that this correlation is also observed for small specimens in the finite-life range, so it is desirable to use high-tensile steels. The situation is somewhat different with notched specimens. For $N \geqslant 10^5$ the best steel in fatigue is the same as that which is considered best with regard to static strength. For $N = 10^3$, however, steel treated to 134 daN/mm^2 (190,000 lb/in^2) sustains 100 daN/mm^2 (143,000 lb/in^2) in fatigue while the same steel treated to 198 daN/mm^2 (280,000 lb/in^2) only sustains 86 daN/mm^2 (124,000 lb/in^2). In Figure 1.13 the fatigue strength is referred to the static strength; thus, the difference is even more apparent. This method of presentation is justified by the fact that high tensile steels are used to reduce the size of components. In addition, it should be noted that ultra-high tensile steels are very sensitive to embrittlement by absorbed hydrogen, especially after inappropriate cadmium-plating, and are thus liable to break spontaneously during machining or in service. They are also sensitive to nickel- or chromium-plating. They should be used with great care and a close check of the treatments and machining operations is recommended. Concerning the treatment of steels, the static strength should not exceed 120 daN/mm^2 (170,000 lb/in^2) if this is consistent with the objective of the design.

Figure 1.14, from Oberg and Trapp[21], illustrates the effect of the direction of loading compared to the direction of extrusion for extruded 14 S-T aluminium alloy sections. Roughly speaking, the fatigue strength varies in the same way as the static strength. In practice, if a component is sound, the fatigue strengths in the longitudinal and transverse directions are very similar. For components containing inclusions, however, the strength in the transverse direction may be rather low. In components made from thick plate material and subjected to tension in the direction of the thickness (short transverse direction) the fatigue strength may be very low, as may be the residual static strength after cracking.

In 1948 Russell, Jackson, Grover and Beaver[22] published a very comprehensive study on the strength of 24 S-T and 75 S-T sheets. The first tests on smooth specimens and small specimens with holes subjected to repeated tension showed (Fig. 1.15) the detrimental effect of cladding which is considerable for smooth specimens but negligible for specimens containing holes. For the latter, aluminium cladding is even beneficial if the number of cycles is less than 10^5. We believe that in actual joints where the notches are more severe cladding does not reduce much the fatigue strength obtained in laboratory tests. A fortiori, cladding is recommended for operational aircraft and structures subject to atmospheric corrosion since it delays corrosion and thus improves the fatigue strength. Besides, the same authors[23] showed that surface scratches, which are unavoidable on sheets, have a small effect on the fatigue strength provided the cladding layer is not broken.

The stress concentration factor K_T is only a rough reference for the notch sensitivity in fatigue. In effect, with simple geometric notches, $K_F (< K_T)$ varies with the number of cycles and can double if N is increased from 10^4 to 10^7 cycles. With pin-loaded holes, fretting (wear, contact alteration, corrosion) appears and, if $K_T = 3$, K_F may vary from 1.4 at 10^4 cycles to 8 at 10^7 cycles, the values at 10^7 cycles ranging from 4 to 8, according to tests on 2024 aluminium alloy (Ref. 24).

1.6 EFFECT OF STATIC MEAN STRESS AND RESIDUAL STRESSES

A steady mean stress is detrimental in tension and beneficial in compression. Very few data on repeated compression tests are available. Newmark and other authors[25] produce a Wöhler curve for repeated compression of waisted 24 S-T alloy specimens having the following properties:

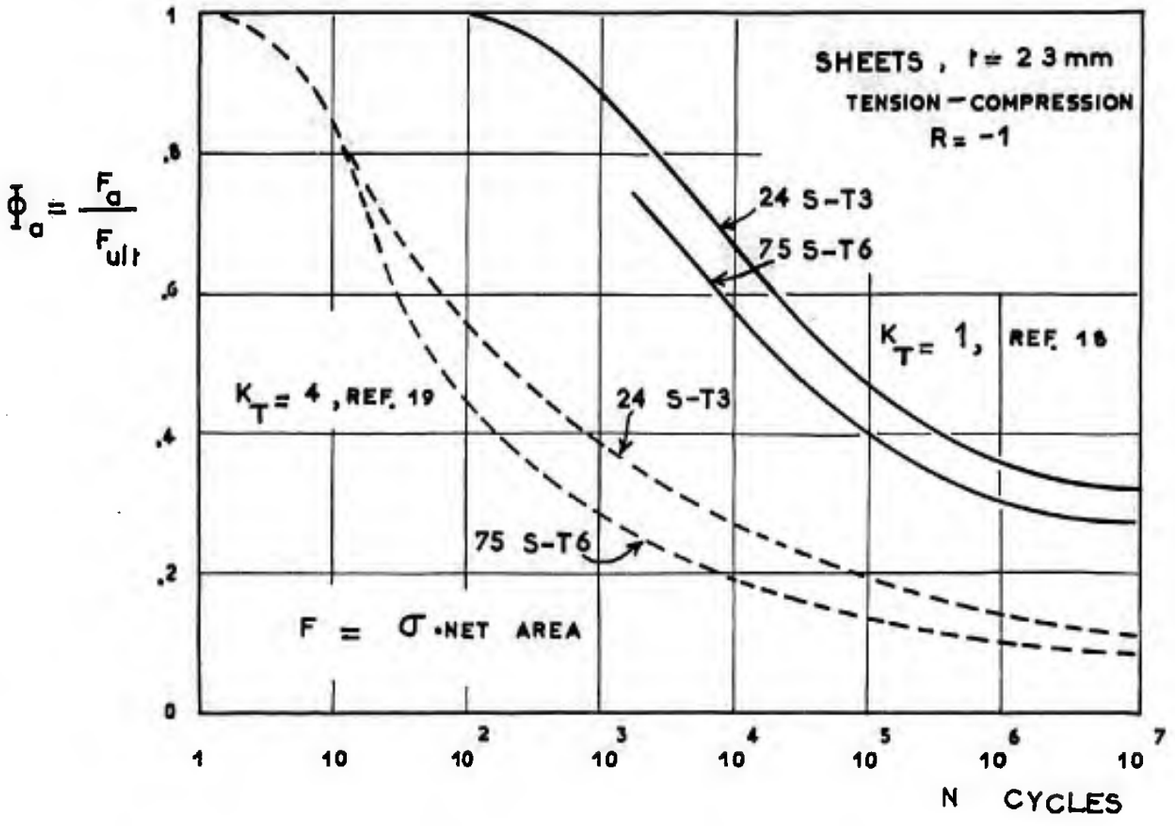

Figure 1.12

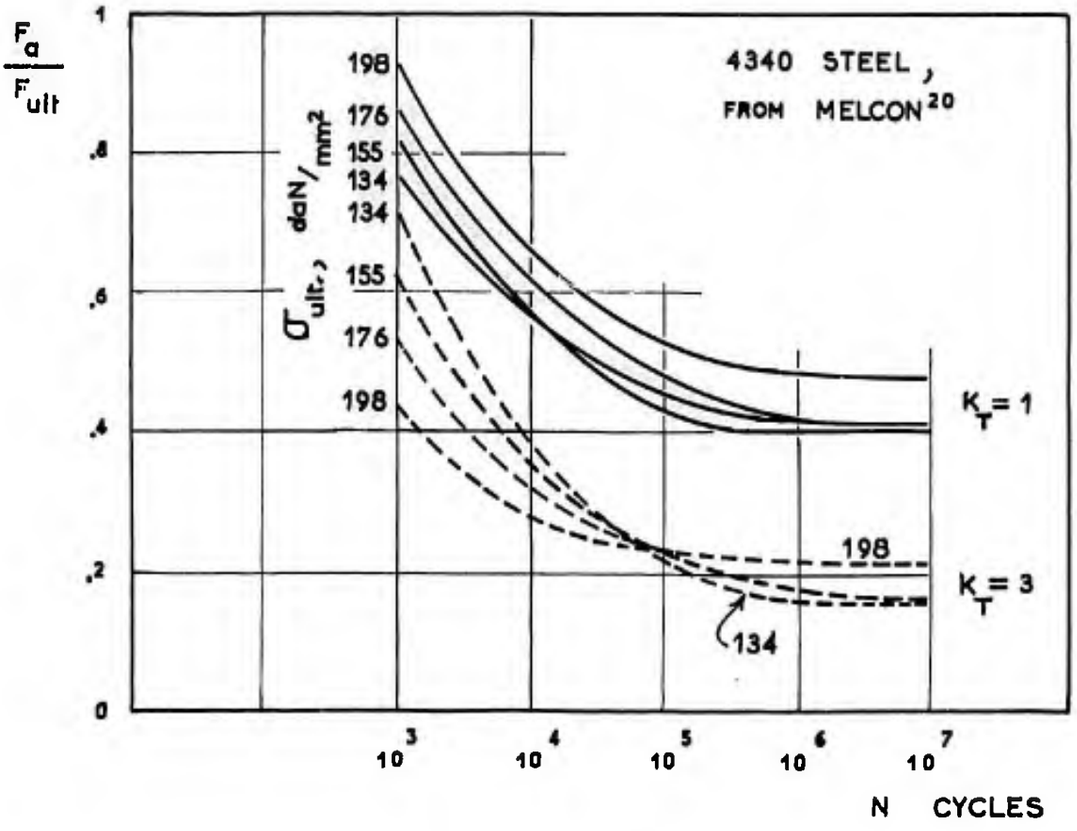

Figure 1.13

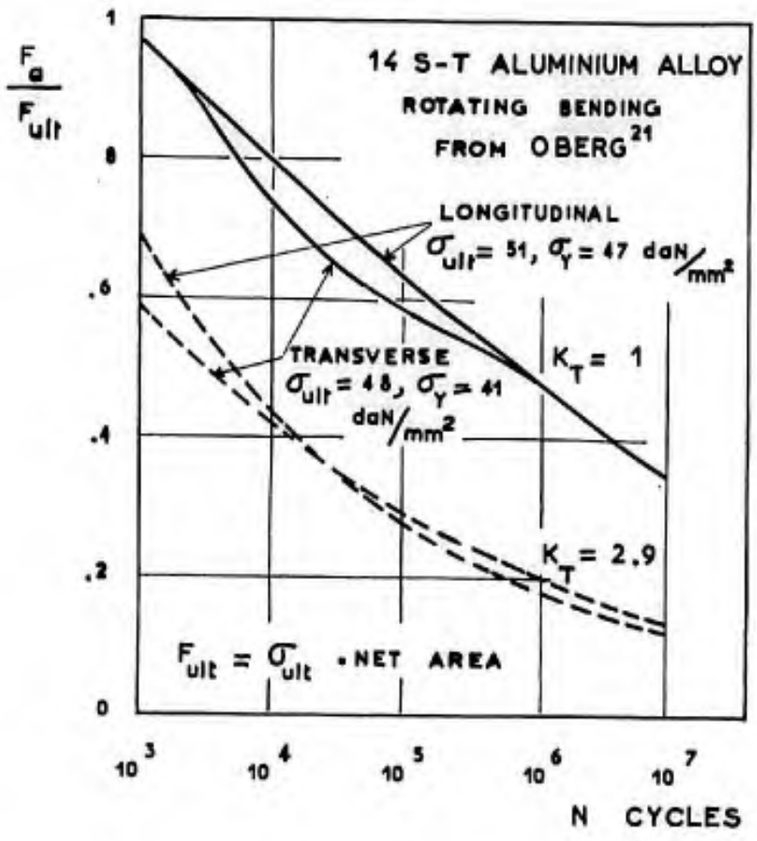

Figure 1.14

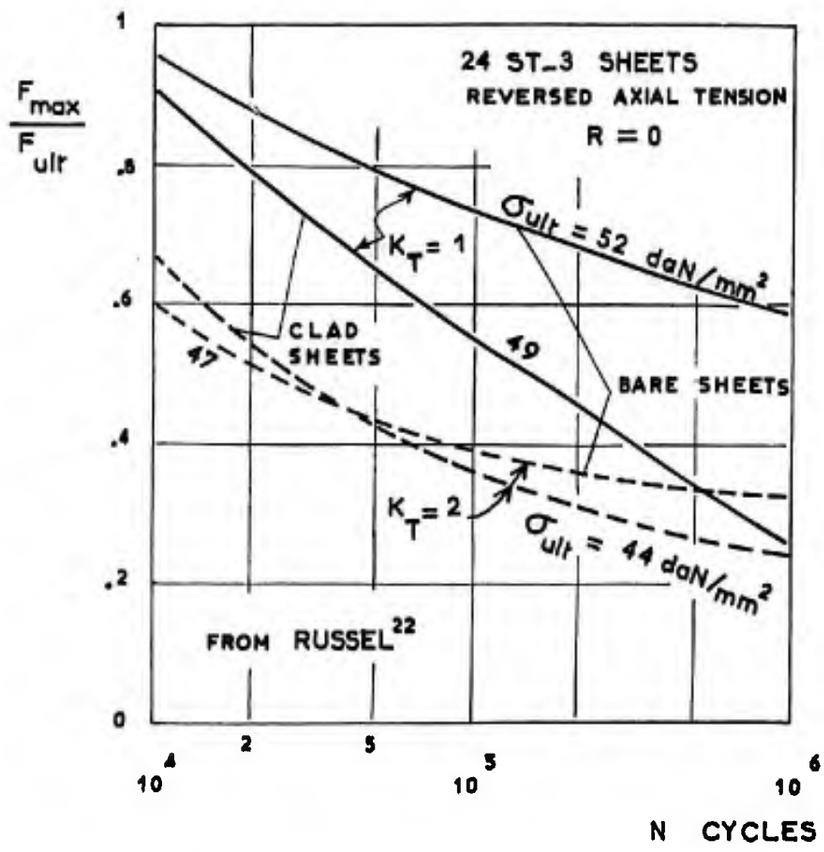

Figure 1.15

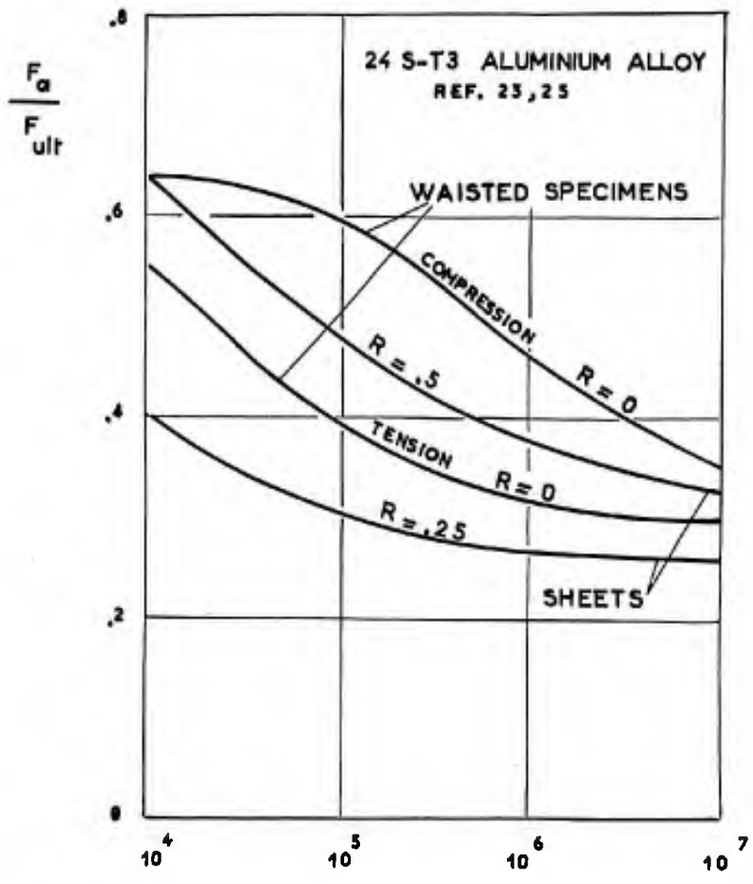

Figure 1.16

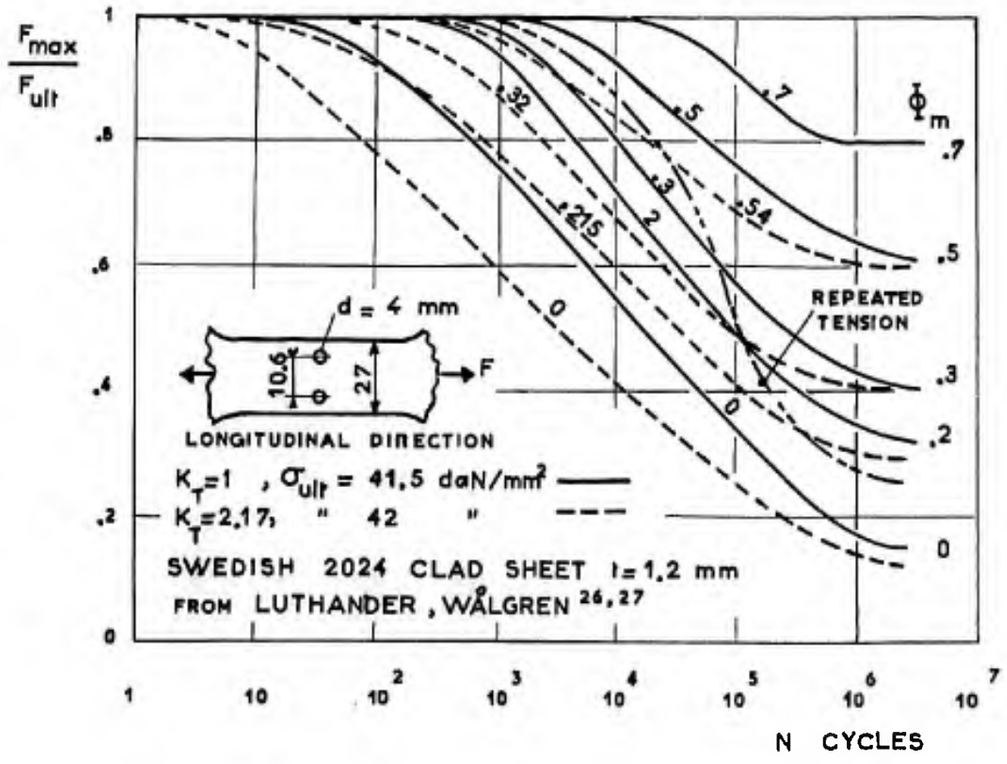

Figure 1.17

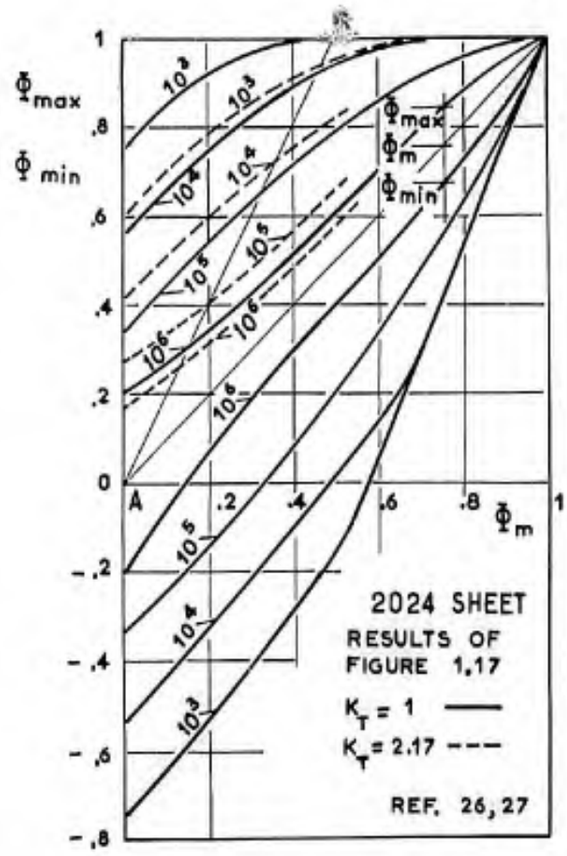

Fig. 1.18 Goodman diagram

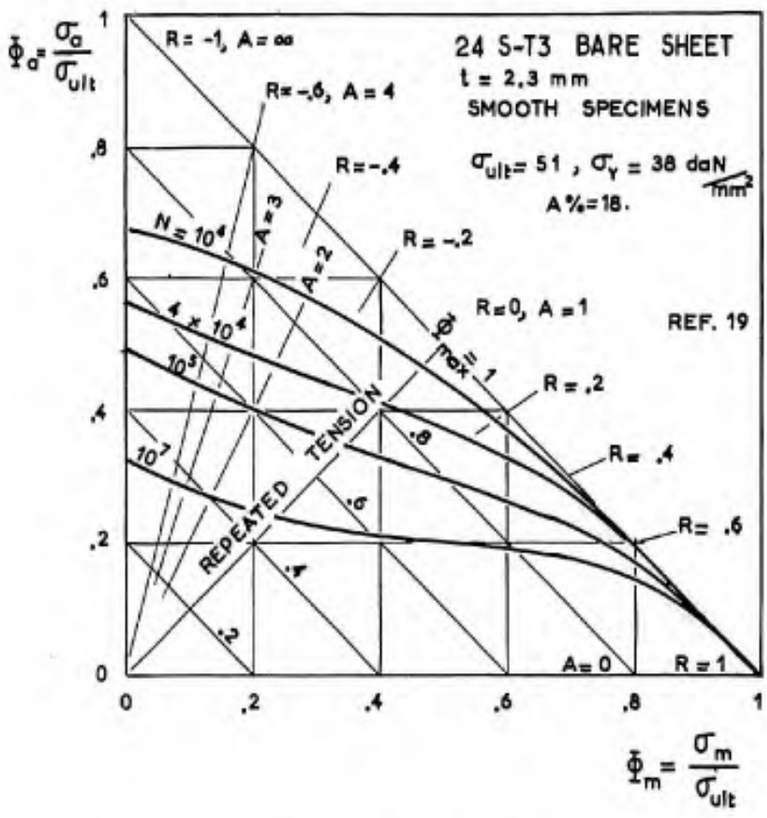

Fig. 1.19 Smith diagram

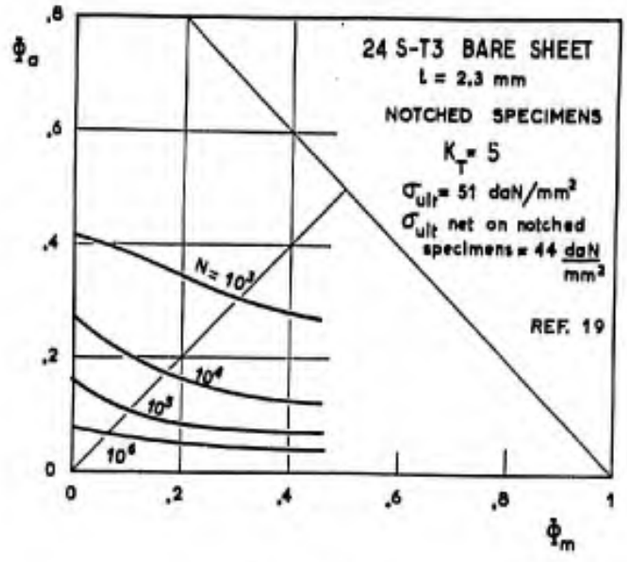

Figure 1.20

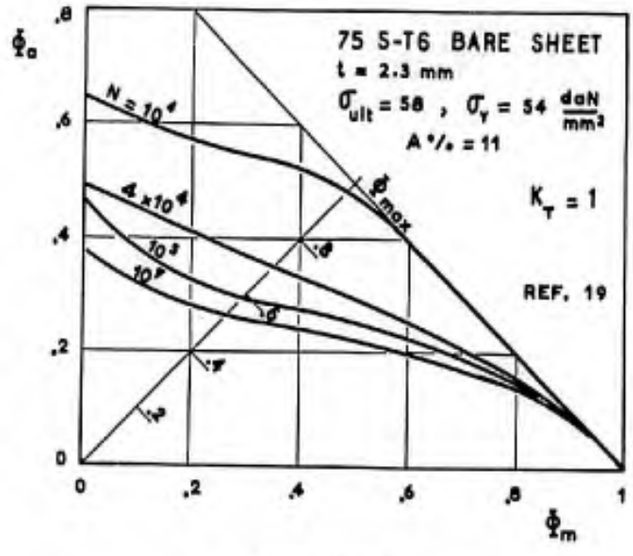

Figure 1.21

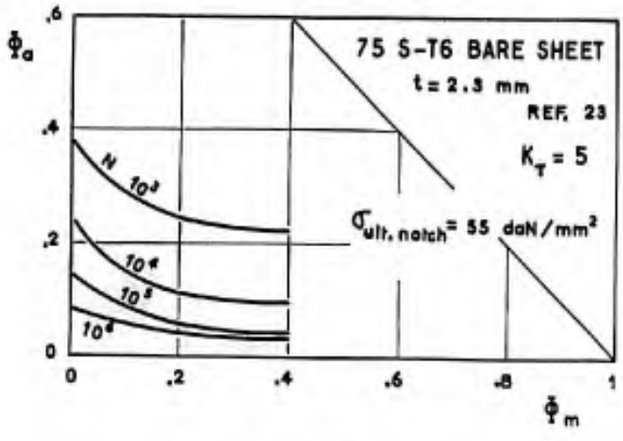

Figure 1.22

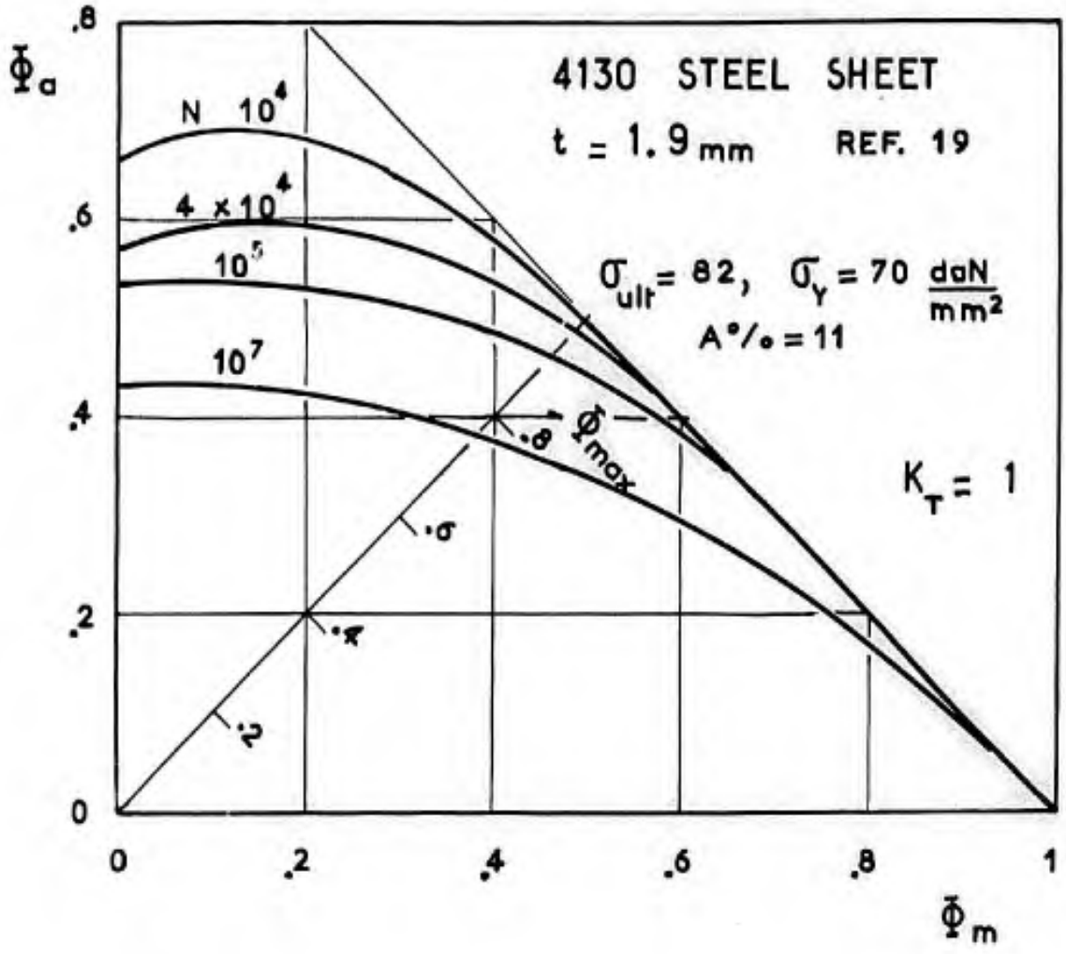

Figure 1.23

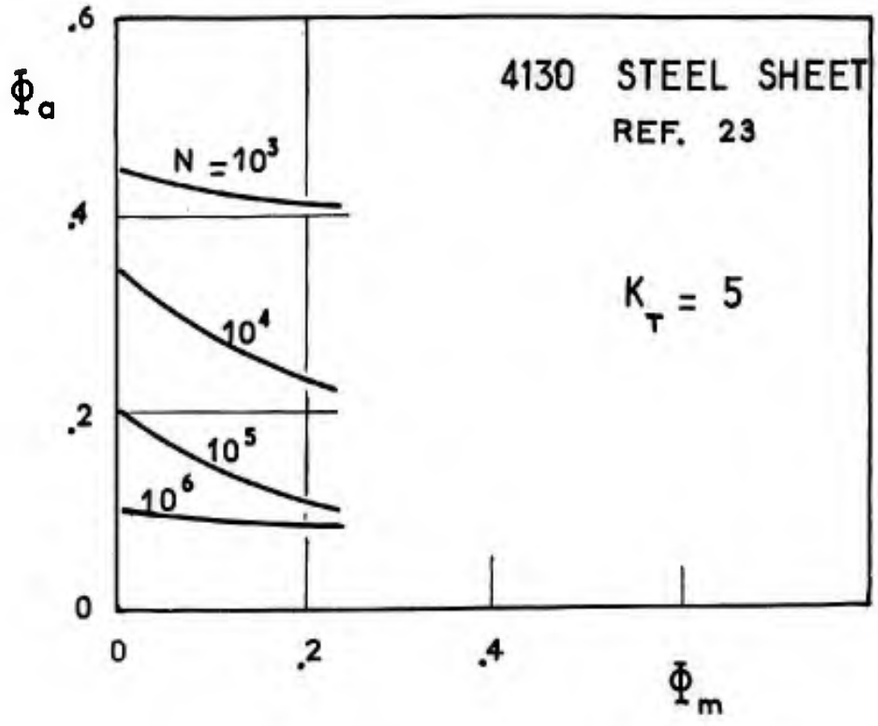

Figure 1.24

Compressive yield stress $\sigma_{0,1}$ = 34 daN/mm^2(48,500 lb/in^2)

Fatigue at 10^6 cycles:

repeated tension $\sigma_a = \sigma_m$ = 17 daN/mm^2 (24,250 lb/in^2)

tension-compression σ_m = 0, σ_a = 18 daN/mm^2 (25,500 lb/in^2)

repeated compression $\sigma_a = \sigma_m$ = 23 daN/mm^2 (32,600 lb/in^2) .

In Figure 1.16 these results are compared with those of Reference 23 for smooth specimens made from 24 S-T bare material and having substantially the same fatigue limit in repeated tension.

Figure 1.17 shows the Wöhler curves obtained by Luthander and Wallgren[26,27] for smooth specimens and specimens containing holes, made from clad 2024 aluminium alloy material, 1.2 mm (0.047 in.) thick. The results are also plotted in Figure 1.18 by means of the so-called *Goodman diagram* where the maximum cyclic load versus mean load is represented in dimensionless co-ordinates for a specified number of cycles to failure. The inclined line AB with a slope of 2 corresponds to $\Phi_{max} = 2\Phi_m$; its intersections with the curves for constant values of N indicate the points for repeated tension.

In Figures 1.19 to 1.24 further test results are given in the form of a *Smith diagram*, the alternating load being plotted on the Y-axis and the mean load on the X-axis. The maximum load corresponds to the 45°-line. From these figures it can be seen that there is a detrimental effect of the mean tension load on both smooth and notched specimens. However, for notched specimens, this effect remains constant above a certain value of the mean stress. This is due to the fact that the actual mean stress at the root of the notch decreases more rapidly in fatigue if it is large, as the alternating stress tends to favour localized flow under the effect of the mean stress. This detrimental effect is also found on smooth specimens since heterogeneous grains are equivalent to internal notches.

Although not easily detectable, *residual stresses* in a component not subjected to a load act like mean stresses produced by external loading. If a notched component is subjected to an external tensile load which causes plastic strain at the root of the notch while the rest of the material remains in the elastic range, reasoning and experience show that, after removal of the load, compressive residual stresses are found in a small volume of material at the notch, which are balanced by low tensile stresses in the rest of the material. As demonstrated by Kepert and Payne[28], static preloading up to 85% of the ultimate flight load can multiply by four the fatigue life of an aircraft structure. This beneficial effect is one reason why such methods of improvement as shot-peening, vapor-blast and rolling, which we shall examine later, are used.

Residual quenching stresses are due to contraction during cooling, to volumetric expansion during phase changes, or to a non-uniform temperature distribution during cooling. At the beginning of cooling, the surface of the component tends to be contracted and is subjected to tension while compressing the core hydrostatically. Since the core is not very compressible, the tension-loaded external surface yields as a result of plastic flow. With further cooling, the core contracts and compresses the hardened surface elastically. Finally, the surface is subjected to compression and the core to tension. If the material undergoes a crystalline phase change during cooling, this phase change may cause expansion, like the γ-α transformation of steels. The effect of expansion due to transformation is opposite to that of thermal contraction. The final result is, then, the difference of the two phenomena and depends on the rate of cooling, the temperature of the γ-α transformation, the soaking temperature and the temperature of the quenching bath. Generally, surface compression will be found in low-carbon steels and surface tension in high-carbon steels. During the quenching of aluminium alloys, thermal contraction produces compressive residual stresses at the surface.

Arc or torch welding produces tensile residual stresses in the neighbourhood of the weld line.

Cold-drawing produces compressive residual stresses if the reduction in area is small and tensile residual stresses if the reduction in area is significant (Bühler and Buchholtz[29]).

Grinding produces tensile residual stresses. Work-hardening by *rolling* or *shot-peening* gives surface compression. The same applies to *induction quenching, case-hardening* and *nitriding*.

Generally speaking, all fabrication processes, heat treatments, cold-working and machining operations produce residual stresses whose values are limited by plastic flow or rupture of the material. Details and figures are to be found in Horger's[30] survey. Residual quenching stresses may cause failure of the components during machining (if too much of the tension-loaded material is removed, the remainder may break under the thrust of the compression-loaded material) or during storage if the residual tensile stress approaches the ultimate stress. Large-size components should therefore be machined before quenching with only a small amount of material left for removal after quenching.

Metals are anisotropic crystalline grain structures with variable orientations from grain to grain. Owing to elastic and plastic anisotropy, mean stresses on the gross scale resolve, at the scale of the grain, into second-order stresses which are assumed to be uniform on each grain and varying from grain to grain. The elastic anisotropy of iron is such that the modulus of elasticity ranges from 29,000 daN/mm^2 (41.5 x 10^6 lb/in^2) to 13,500 daN/mm^2 (19.4 x 10^6 lb/in^2) depending on the direction of the load in the crystalline lattice. Even in the absence of stresses of the first order, the mechanism of plastic deformation followed by an elastic return

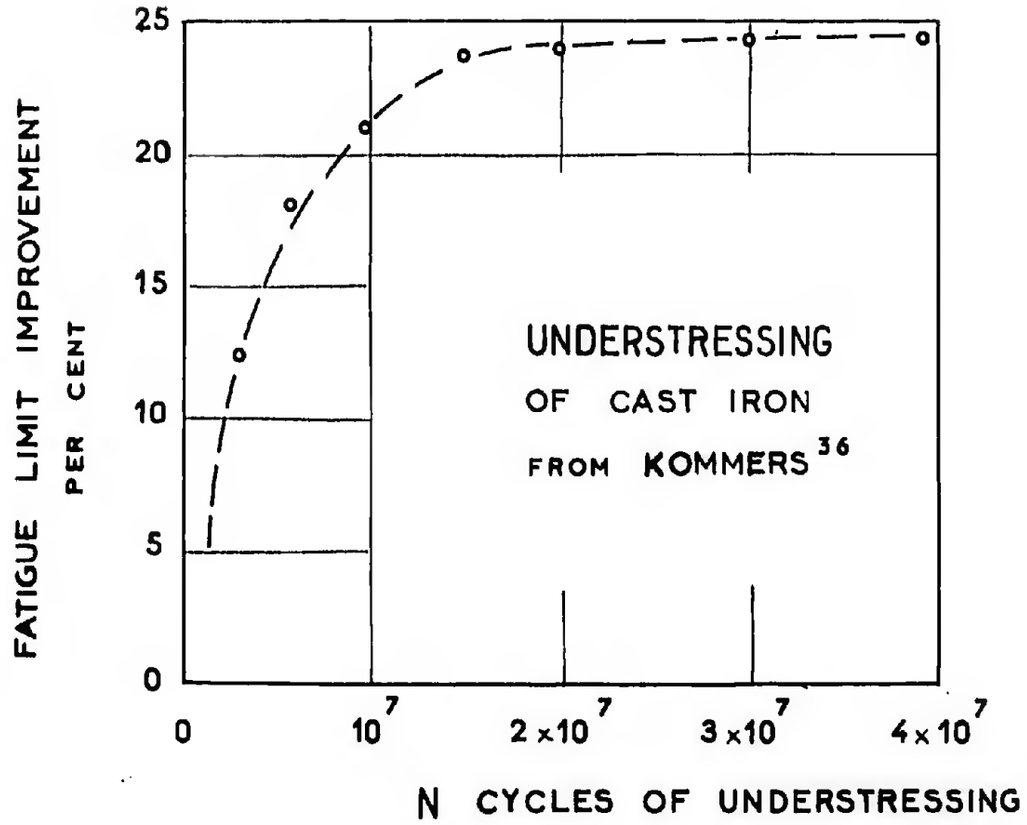

Figure 1.25

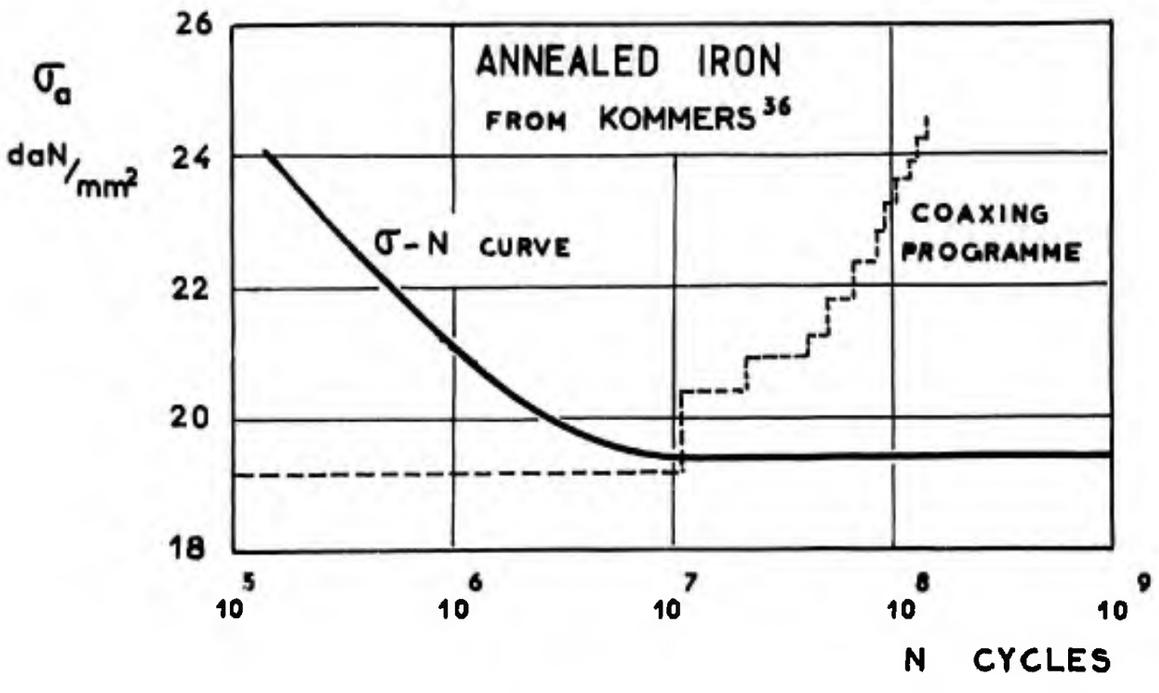

Figure 1.26

may leave residual stresses of the second order. Investigating residual stresses of the second order after extrusion through broadening of the X-ray diffraction rings, Megaw and Stokes[31] found for various metals:

	Fe	Ni	Cu	Ag	Al	Pb
$\sigma_{residual}$, daN/mm^2	58	53	23	22	3	0.7
$\sigma_{ult.}$, tension	30 - 80	35 - 120	23 - 47	28 - 36	6	1.2 - 2.1

In each grain there are slight variations in the crystalline orientation and structural defects in the lattice which induce stresses of the third order that cannot be measured, even indirectly.

Residual stresses change during fatigue. According to Rosenthal and Sines[32] for the 61 S-T aluminium alloy, static preloads equal to 80% of the conventional yield strength, i.e. 50% of the ultimate load, induce stresses that amount to 40% of the yield stress in notched (K_T = 2.5) specimens subjected to alternating-bending, whereby the fatigue limit is improved by 33% at 10^7 cycles. After fatigue loading these residual stresses are still equal to 34% of the yield stress. Moore[33] has studied the effect of fatigue on the residual stresses due to shot-peening and showed that these stresses decrease rapidly if the alternating stress is high. Studying the effect of rotating-bending at ±34 daN/mm^2 (48,500 lb/in^2) during 970,000 cycles on steel containing 0.36% of carbon and water-quenched at 600°C, Bühler and Buchholtz[34] found that the longitudinal residual compressive stress was lowered from 27 daN/mm^2 (38,500 lb/in^2) to practically zero. Schulz and Buchholtz[35] have reported that fatigue can generate residual compressive stresses in specimens that were originally free of such stresses.

The importance of residual stresses involves two consequences for fatigue testing:

1. Static tests under high loads must not be performed on structures that will be subjected to fatigue tests. The only exceptions are cases where the static preload is applied to actual components at the beginning of the operational life or during manufacture.

2. Since the residual stresses in actual components differ from those in specimens, the substantiation of a design can only be effected by direct fatigue testing on actual components. Tests on notched specimens or typical fittings are an idealization of tests on actual fittings and, consequently, they only permit interpolation or slight extrapolation on the basis of a limited number of tests on actual components.

From the point of view of manufacture, an effort should be made to reduce the residual tensile stresses, which are always detrimental. In the case of steel, stresses of the second order (on the scale of the grain) are lowered by prolonged heating at 100°C (212°F); stresses of the third order (on the scale of the precipitate), which are more stable, disappear at about 300°C (572°F), whilst stresses of the first order (on the gross scale) disappear only at high temperature. A relaxation treatment after tempering performed at the highest temperature consistent with the preservation of the as-tempered properties can be profitable. Stresses due to welding should be eliminated by a complete quenching and tempering heat treatment.

We shall later examine in detail all the methods of improvement which produce residual compressive stresses.

The development of residual stresses during fatigue probably accounts for the "understressing" and "coaxing" phenomena. *"Understressing"* is an increase of the fatigue limit through exposure of the specimen to alternating stress below the fatigue limit during a sufficiently high number of load cycles. The residual tensile and compressive stresses are reduced and, if the surface is subjected to tensile stress, subsequent fatigue loading above the previous fatigue limit may cause no failure. In Figure 1.25, from Kommers[36], the increase of the fatigue limit of cast iron under a stress slightly below the original fatigue limit is plotted against the number of cycles. We have drawn a dotted line to illustrate the assumed development of the residual stresses. For the cast iron tested, the improvement was independent of the understressing stress below 5.6 daN/mm^2. From 5.6 to 6.4 daN/mm^2 the improvement increased linearly from 16 to 31%.

The improvement is greater if the understessing stress approaches the fatigue limit. It is advisable to increase this understressing stress with the new fatigue limit. It is actually found that the fatigue limit can be raised by this process, called *coaxing*. Figure 1.26, after Kommers, shows a result for annealed iron. For carbon steel with a yield strength equal to 43 daN/mm^2 (62,000 lb/in^2), Bennett[37] managed to increase the fatigue limit from 35 to 42 daN/mm^2 by the coaxing method.

The term *"overstressing"* is used to define a decrease of the fatigue limit after initial fatigue loading at a higher level. We shall see later that on work-hardened engineering steels and notched components any loading at a high level produces an improvement over a small number of cycles but has, then, a damaging effect if the number of cycles is increased. A slight improvement by overstressing is sometimes observed in smooth specimens and some authors have stated that overstressing produces an effect of understressing! The analysis of damage caused by fatigue loading at various levels will be the subject of a later chapter.

REFERENCES

1. Wöhler, A. — Zeitschrift für Bauwesen, Vol. 8, pp. 1860-1870.
2. Tye, W. — The Aeroplane, April 1952.
3. Taylor, J. — *Manual of Aircraft Loads.* AGARD, Pergamon Press, 1965.
4. Dryden, H.L. et al. — *The Fatigue Problem in Aircraft Structures.* Paper 2, Fatigue and Fracture of Metals, 1950.
5. Barrois, W. — *Déformations Plastiques et Fatigue des Métaux,* 1952, Mémo Technique No. 27, ONERA, 1963; *Théorie de l'Evolution des Métaux Pendant la Fatigue.* Revue de Métallurgie, LV, No. 8, 1958.
6. Coffin, L.F., Jr. — *Low Cycle Fatigue: A Review.* Applied Materials Research, Vol. 1, No. 3, Oct. 1962, p. 129.
7. Longson, Jennifer — *A Photographic Study of the Origin and Development of Fatigue Fractures in Aircraft Structures.* Report Struct. 267, Royal Aircraft Establishment, Farnborough, March 1961.
8. Marcoux, -. Arnoux, -. — Quoted in Morin *Résistance des Matériaux.* Vol. II, 1862.
9. Cazaud, R. — Paper presented at VI° Convegno Nazionale A.I.M., Genoa, 1952.
10. Oberg, T.T. — Metal Progress Magazine, July 1951.
11. Styri, M — Proc. A.S.T.M., Vol. 51, 1951, p. 682.
12. Weibull, W. — *Symposium on Fatigue and Fracture of Metals.* A.S.M., 1950, p. 182.
13. Kennedy, A.P. — Journal of the Royal Aeronautical Society, Vol. 58, May 1954, p. 36.
14. Neuber, H. — Kerbspannungslehre, 2nd Ed. Springer, 1958.
15. Hottenrott, E. — La Recherche Aéronautique, No. 27, Paris 1952, p. 51.
16. Howland, -. — Phil. Trans. Roy. Soc., Series A, Vol. 229, 1930, p. 49.
17. Weber, C.
18. Hardrath, H.F. Illg, W. — NACA TN 3132.
19. Grover, H.J. et al. — NACA TN 2324.
20. Melcon, M.A. — Product Engineering, Oct. 1953.
21. Oberg, T.T. Trapp, W.J. — Product Engineering, Feb. 1951.
22. Russel, H.W. et al. — NACA TN 1485, 1948.
23. Grover, H.J. et al. — NACA TN 2389 and 2390.
24. Wållgren, G. Rudin, E. — F.F.A. Report NR HU - 281, Stockholm, May 1951.
25. Newmark, N.M. et al. — Proc. A.S.T.M., 1951, p. 792.
26. Luthander, S. Wållgren, G. — F.F.A. Report No. 5, Stockholm, 1948.
27. Wållgren, G. — F.F.A. Report No. 14, Stockholm, 1948.

28. Kepert, J.L.
Payne, A.O.
Report ARL/SM 207, Melbourne, Jan. 1955, and NACA TM 1397.

29. Bühler, H.
Buchholtz, H.
Archiv. für Eisenhüttenwesen, Vol.7, 1934, p.427.

30. Horger, O.J.
Residual Stresses. Chap.11 of "Handbook - Experimental Stress Analysis", Hetenyi, 1950.

31. Megaw, M.D.
Stokes, A.R.
In R.F. Mehl, *Recrystallisation.* Metals Handbook, 1948, p.259.

32. Rosenthal, D.
Sines, G.
Proc. A.S.T.M., 1951, p.593.

33. Moore, H.F.
Experimental Stress Analysis. Vol.2, No.1, p.170.

34. Bühler, H.
Buchholtz, H.
Mitt. Forschung Inst., Dortmund, Vol.3, No.8, Sept. 1933, p.235.

35. Schulz, E.H.
Buchholtz, H.
Inst. Verhand f. Materialprüfung Kongressbuch, Zurich, 1932, p.278.

36. Kommers, J.B.
Effect of Understressing and Overstressing in Fatigue. Proc. Soc. Exp. Stress Analysis, Vol.III, No.II, 1946, p.137.

37. Bennett, J.A.
A Study of the Damaging Effect of Fatigue Stressing on X 4130 Steel. A.S.T.M., Vol.46, 1946, p.693.

38. Dixon, J.R.
Stress Distribution Around a Central Crack in a Plate Loaded in Tension: Effect of Finite Width of Plate. Journal of the Royal Aeronautical Society, Vol.64, No.591, March 1960.

39. Kuhn, P.
Stockholm Colloquium on Fatigue, 1956. Published by Springer, Berlin, 1956.

CHAPTER II

PLASTIC STRAIN IN METALS

W. Barrois: Fatigue of Structures, Vol. I
"Fundamental and Physical Aspects", AGARD, 1970

PRECEDING PAGE BLANK

CHAPTER II

PLASTIC STRAIN IN METALS

Plasticity is the propensity of a deformable body to retain an imposed shape after the removal of the load that caused the deformation. At room temperature lead has very little elasticity and may be considered to be a plastic metal. *Elasticity* describes the immediate and complete return to the original shape after removal of the load. *Viscosity* measures the resistance to deformation the strain rate of which is proportional to the magnitude of the applied load. If a material includes viscous elements working in parallel with certain elastic elements, deformation decreases asymptotically with time after unloading. In *viscoelastic materials* such as nylon, this elastic after-effect may be significant with respect to the elastic deformation.

In metals, the application of loads at a high enough temperature first causes instantaneous elastic strain and a certain amount of plastic strain; at higher loads, continuous flow called *creep* is obtained. In some cases creep deformation has a small after-effect once the load is removed. Unlike metals, plastics are only plastic during manufacture; they are viscoelastic in the service condition and exhibit a large elastic after-effect resulting in *strain recovery*.

The material of this chapter is derived to a great extent from previous work[1,2]. Our basic approach includes one observation and one assumption. First, there are striking analogies for mechanical engineers in the mechanical behaviour, under appropriate conditions of temperature and time, of components made from such dissimilar materials as metals and plastics.

Among the analogies we find: the variation of the static stress-strain curve with test temperature and strain rate; the existence of a fatigue fracture mode and the improving effect of superimposed compressive stresses; the Bauschinger effect; the process of plastic flow and delayed elasticity (strain recovery); relaxation, etc. These macroscopic analogies between the behaviour of metals and that of plastics are not always apparent because certain effects are too small to be reported by the experimental means used and also because the loads may sometimes induce phase changes.

The occurrence of common phenomena on any scale of observation can only result from common elementary causes on a finer scale. Now the internal arrangements or structures of metals and plastics differ on each scale of observation. Metals are made up of crystallized grains in which the atomic array is a short-range and long-range pattern within a regular crystalline network; plastics exhibit statistical disorder on a microscopic scale, and an orderly local arrangement is suspected to exist over the range of neighbouring molecules. The types of atomic or molecular bonding in both cases are different.

The only points in common between metals and plastics are the existence of thermal agitation and metastable atomic or molecular configurations which may become unstable at high temperature or under external loads applied to a specimen for a long enough time.

We must therefore examine in what way external loads and heating can change the atomic or molecular arrangement and affect its stability.

Secondly, besides the conventional assumption regarding the plastic fracture of metals (increase of resistance to slip and decrease of resistance to cleavage as a result of the atomic disorder due to plastic deformation), we may formulate an additional hypothesis concerning a distribution mode of internal resistance to external loads over domains which decrease in size and number in the course of the deformation and during the time of loading. Consider the rupture of a stranded cable: the weakest wire breaks first; the load is then transferred to the other wires, of which each breaks in its turn, and so on until complete fracture occurs. We also assume that the diversification in stiffness and stability of metastable atomic or molecular configurations is increased by the load, which causes some areas to return to the original order (recovery) or to be arranged in a new order (polygonization and recrystallization of metals); thus the difference in state and hence in stress between the various areas is increased. This assumption is based on the known features of stress-strain loop adjustments and on the existence of the Bauschinger effect.

In simpler words, our assumption is that plastic development in metals before cracking causes a change in the relative plastic stiffnesses of neighbouring small regions, even though the average stiffness increases, which results in the transfer of a portion of the external loads to smaller areas likely to break.

PRECEDING PAGE BLANK

2.1 WORK-HARDENING AND RECOVERY

Cold-working of metals and the subsequent hardening effect are sometimes confused under the term "work-hardening". The term *"degree of work-hardening"* generally indicates a reduction in the cross-sectional area of drawn rods or a reduction in the thickness of cold-rolled sheets. In the following, we shall say that components are work-hardened by cold-working and that the resultant *work-hardening* may be represented by the *hardness* of the metal. Hardness is one of the measurable properties of work-hardening but it will be seen that the hardened condition is not completely defined by hardness. Furthermore we shall see that *straining of a cold-worked component can lower its hardness.*

Investigation of continuous straining at constant load, called creep, shows that deformation at constant speed may achieve a balance between the creation of new lattice distortions, which hardens the metal, and the partial recovery of an orderly lattice, which favours plastic flow.

It may therefore be assumed that straining has two simultaneous effects: the creation of obstacles to further strain and the disappearance of pre-existing obstacles.

2.1.1 Slip, Dislocations, Structural Defects

The structure of a machine describes the arrangement of its components; similarly, the structure of a metal, also called *texture*, covers the nature, size and orientation of the elementary crystals or *grains*, of which it is made up. In some cases, orderly domains of slightly differing orientation are observed in a grain; they are known as *mosaic domains* or *crystallites*. The structure of an elementary crystal, grain or crystallite, is typified by the relative arrangement of its atoms or molecules. This pattern exhibits an order which is responsible for the elastic properties under hydrostatic pressure and for the plastic flow under shear stress. Departures from a perfect order account for the resistance to plastic flow.

Crystals are characterized by a regular stacking of three-dimensional unit cells forming a space lattice, the corners, faces or centroids of which are occupied by atoms or molecules. Atoms are subject to vibrations of thermal agitation and their mean positions correspond to a state of equilibrium between the attractive and repulsive interatomic forces. If we consider two atoms which are a distance r apart, the mutual central force, f, varies with r as shown on the graph in Figure 2.1. This force is equal to zero at the equilibrium position, r_0, has a maximum value at M for a spacing r_d and then tends to zero if r tends to infinity. If the curve of $f(r)$ is replaced by its tangent at r_0, we obtain $f = k.(r - r_0)$, where k represents a modulus of elasticity. If the extension exceeds the critical value r_d, the force required to retain the equilibrium decreases and instability causes the separation or *decohesion* of the atoms. On the other hand, the fact that atoms approach one another implies repulsive forces which increase more rapidly than the distance decreases.

Cleavage or decohesion is the separation of two parts of a crystal through a displacement perpendicular to a plane of the crystalline lattice. Because of the yield phenomenon this type of fracture occurs in metals only on a microscopic scale and cannot be measured. Very rough assessment shows that cleavage stresses would be of the same order of magnitude as the modulus of elasticity, i.e. several thousands of decaNewtons per square millimeter. In fact, we know from practical experience that some fracture stresses are a hundred times lower after plastic deformation which may sometimes be considerable.

To explain this contradiction a theory due to Griffith[4] was first used. Griffith assumed the existence of microcracks which increased in size if the potential energy of the system was lessened by this increase. Beyond point M (Fig. 2.1), the force between atoms located on both sides of the crack decreases as their spacing increases; conversely, the forces between neighbouring atoms located on the same side of the crack increase with deformation. By equating to zero the variation of the sum of the surface energy and strain energy, we may obtain a relation between the applied stress and the critical crack size for which equilibrium is no longer possible and fracture occurs. This theory has been checked by Griffith for glass and by Joffe[5] for a large number of amorphous and brittle materials.

The first attempts to apply Griffith's theory to the fracture of metals were unsuccessful, due to the fact that yielding allows large local deformations to take place through a process in which the variation of the relative atomic spacing is not involved. It will be seen in a later chapter that by taking the yield phenomenon into account it becomes possible to extend Griffith's theory to fairly brittle metals.

Yielding in metals has been studied in single crystals by many researchers. The main experimental facts may be found in the work of Schmid and Boas[6] as well as in a paper by Gough[7]. To sum up, let us consider a crystal which, like magnesium, has only one family of parallel slip planes cutting a cylindrical bar into slices (Fig. 2.2). In axial tension the slices slip past each other in a direction contained in the slip plane, which allows an overall deformation of the bar without any significant disturbance of the atomic lattice. The mechanism of slip is illustrated in Figure 2.3: shear strain is first an elastic strain and corresponds to slight angular displacements; it ends with the atomic planes slipping past each other and a new stable equilibrium position, different from the initial position, is obtained. According to evaluations, the forces required for the relative overall slip of the two halves of a crystal would involve considerable stresses which are inconsistent with the very low slip stress values observed in single crystals.

This inconsistency disappears if we use the concept of *dislocations* of Prandtl and Dehlinger[8]. This concept was utilized by G. I. Taylor[9], Orowan[10] and Polanyi[11] to explain plastic strain in crystals. Its geometrical

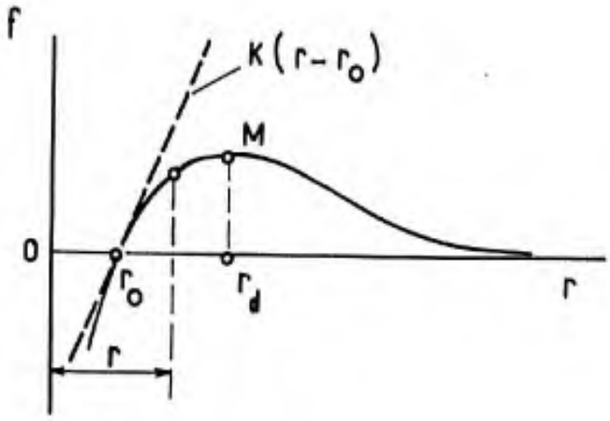

Fig. 2.1 Central force between neighbouring atoms against their mutual distance

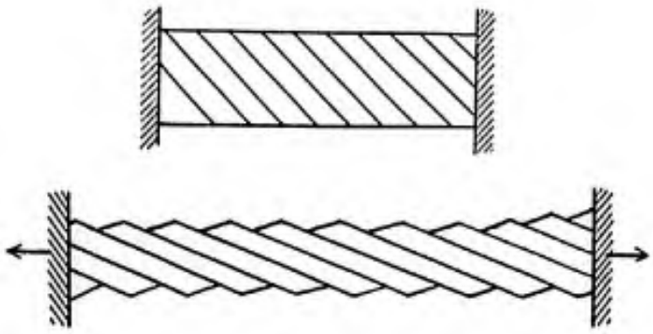

Fig. 2.2 Plastic elongation by slip

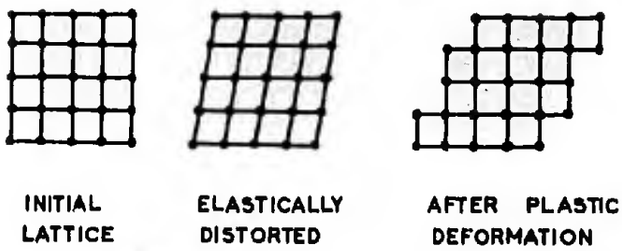

Fig. 2.3 Elastic and plastic deformations of crystal lattice

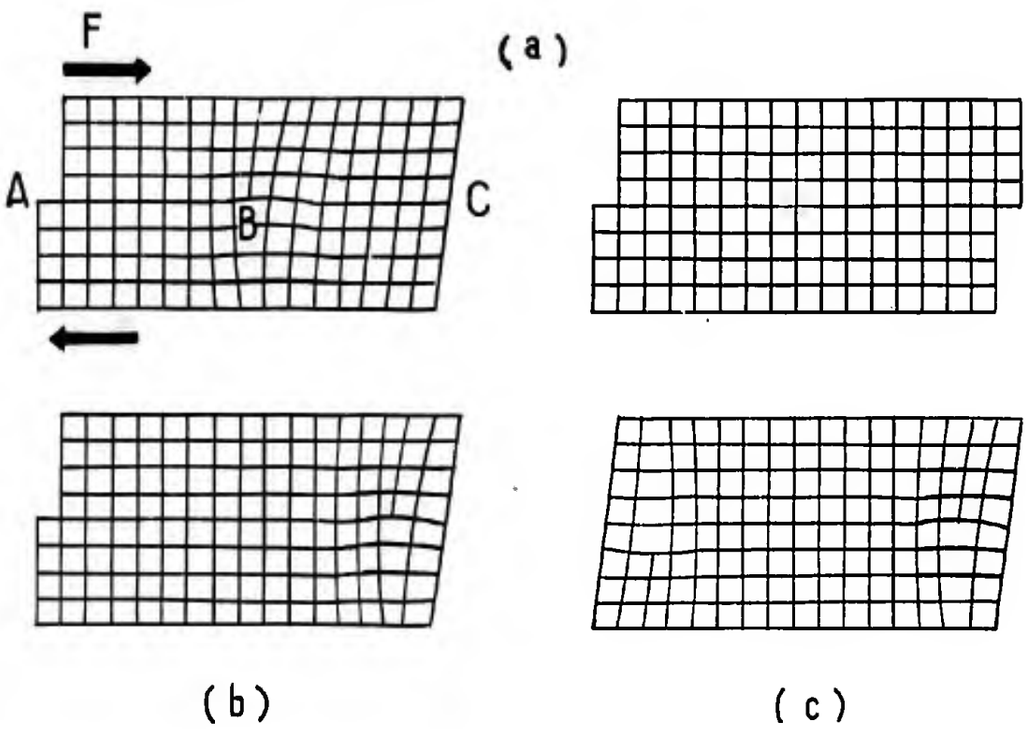

Fig. 2.4 Edge dislocations

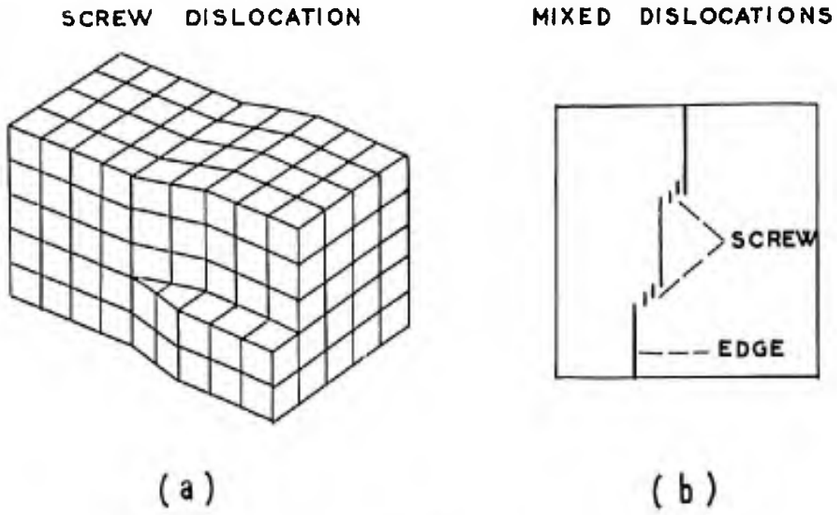

Figure 2.5

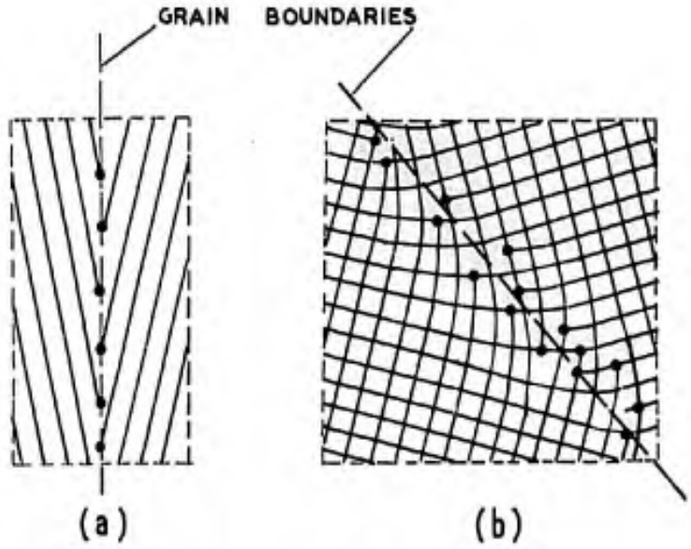

Fig. 2.6 Dislocations in grain boundaries

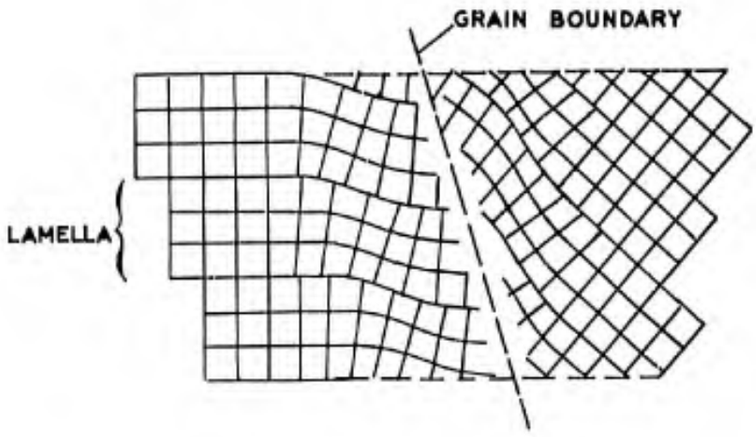

Fig. 2.7 Slip lamellae

description has been evolved by J.M.Burgers[12]. The edge dislocation (Burger's first type) is illustrated in Figure 2.4(a). At a point A of an initially perfect crystal the application of external shear forces F causes slip of one atomic distance. This slip is stopped in the vicinity of point B, i.e. the centre of the dislocation, where the upper half-plane of the figure contains one row of atoms more than the lower half-plane. Around B the atomic distances are modified and the crystal planes are curved, the upper half of the crystal being locally in compression whereas the lower half is subject to tension.

If at A and C the crystal lattice has two free edges, it remains perfect after passage of the dislocation, except for two misalignments at A and C. If C is located on a crystal boundary (Fig. 2.4(b)), the dislocation strikes this boundary. If A and C are crystal boundaries, two cases may be considered:

1. A dislocation already existed at one of the boundaries and it moves across the crystal to strike the other boundary.

2. Two dislocations of opposite sign (Fig. 2.4(c)) originate at the same point, between A and C; they propagate in opposite directions and strike the boundaries at A and C.

The second case is a simple and credible assumption on the formation of new dislocations in crystals. More complex assumptions have been formulated by Franck and Read[13]. In edge dislocations, the axis passing through B is perpendicular to the plane of the figure and all planes perpendicular to the axis show the same dislocations.

This is not the case with *screw dislocations* (Burger's second type) shown in perspective in Figure 2.5(a). This type of dislocation connects edge dislocations when propagation of the latter is impeded or in the case of non-uniform shear; *mixed dislocations* are thus obtained (Fig. 2.5(b)).

Dislocations are mobile along the slip planes and slip is caused by their displacement. In an initially regular crystal it appears as a first approximation that the variation of internal energy due to motion of a dislocation is equal to zero. In fact, the dislocation originates in an external force which is sufficiently great to force some atoms from one equilibrium position to another. Under higher loads, the dislocation traverses the crystal in an accelerated motion which is restrained only through dissipation of the vibration energy of atoms located on its trajectory and set in motion by its passage in the glide plane and the neighbouring planes.

Since motion of a dislocation takes place through relays of atomic vibrations, it can be deflected or reflected by insuperable obstacles or crystal boundaries, thus generating other dislocations on other planes or dislocations of a higher order on the same plane. It is assumed by Burgers[12] that grain boundaries comprise dislocations as illustrated on the diagrams of Figure 2.6.

If a pure or impure monocrystalline or polycrystalline metal is subjected to an imposed plastic deformation, it exerts a reaction force which increases with deformation up to a limit corresponding to flow under constant stress. To achieve large deformations high loads are required. This implies the existence of obstacles to the dislocation propagation. In polycrystalline materials grain boundaries are barriers which are hard to overcome; this also applies to inclusions of foreign bodies. In such cases there is a dislocation pile-up against every obstacle, which accounts for the resistance increasing with the imposed plastic deformation. Dislocations stopped by an obstacle cause elastic lattice distortions and bending of the crystalline planes in front of the obstacle (Fig. 2.7). With increasing number of dislocations, the curvature increases and induces elastic deformation of the lattice at larger distances from the obstacle while increasing the resistance to subsequent plastic strain. It creates slip lamellae which we shall examine in the next paragraph.

The formation of obstacles to the dislocation movement can be imagined even in initially perfect crystals. According to J.M.Burgers[12], if two dislocations of opposite sign move together on neighbouring parallel planes, their elastic interaction may impede the displacement (Fig. 2.8) and the dislocations will form a *knot* (Fig. 2.9) liable to result in localized lattice rotation.

The absence of one or more neighbouring atoms in the atomic lattice is referred to as a *vacancy*. Disturbance of the atomic lattice around a vacancy appears as an obstacle to the dislocation movement. Some vacancies are pre-existing in crystals while others result from dislocation displacements. Thus, if two dislocations of opposite sign travel on two neighbouring planes, the buttressing in Figure 2.8 can be replaced by a vacancy if point B lies below point A. Under the action of internal stresses and thermal agitation, the vacancies may be displaced by local diffusion atom by atom; self-diffusion is favoured by thermal agitation as well as by the disturbance due to the passage of dislocations.

Edge dislocations can avoid barriers through motion of the extra row of atoms perpendicular to the slip plane (*dislocation climb*). This shifting is promoted by tensile stresses parallel to the direction of slip and tending to separate the atoms above point B (Fig. 2.8); if the stress gradient is such that the atoms below B are in compression and those above B in tension, it is understood that point B can be moved upwards by single atomic steps while creating a vacancy in the atomic row.

Obstacles can also be bypassed by multiple slip along slip planes having the same slip direction. Finally, an edge dislocation can be shifted locally from one plane to another by means of two screw dislocations surrounding an obstacle; this is known as *cross-slip*.

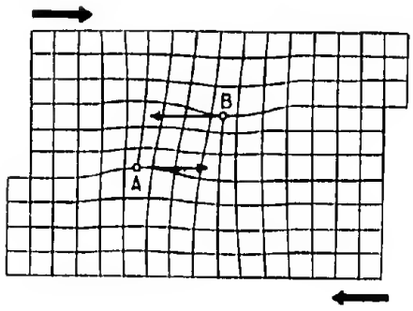

Fig. 2.8 Buttressing of two inverse dislocations on two neighbouring planes

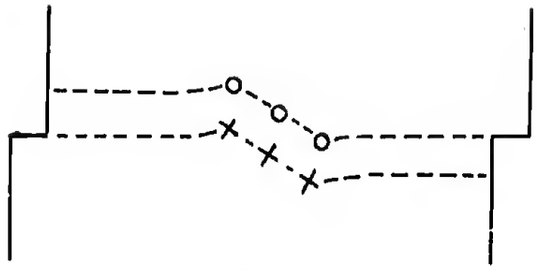

Fig. 2.9 Knot of dislocations, from J. M. Burgers[12]

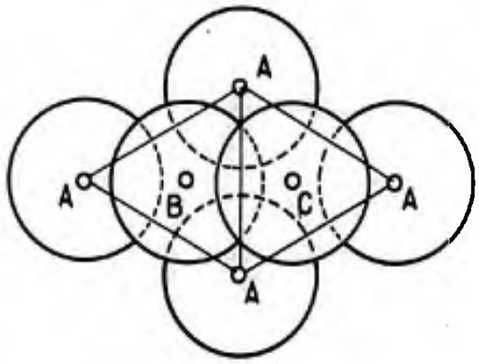

Fig. 2.10 Close-packed atoms. The three superimposed layers A.B.C. are drawn with the setting of the face centered cubic lattice, from Barrett[15]

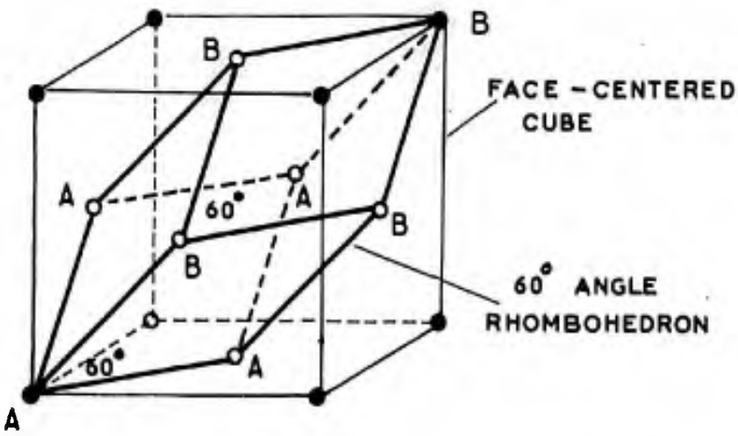

Fig. 2.11 Perspective of the 60° angle face-centered cubic lattice. From Mathieu[14]

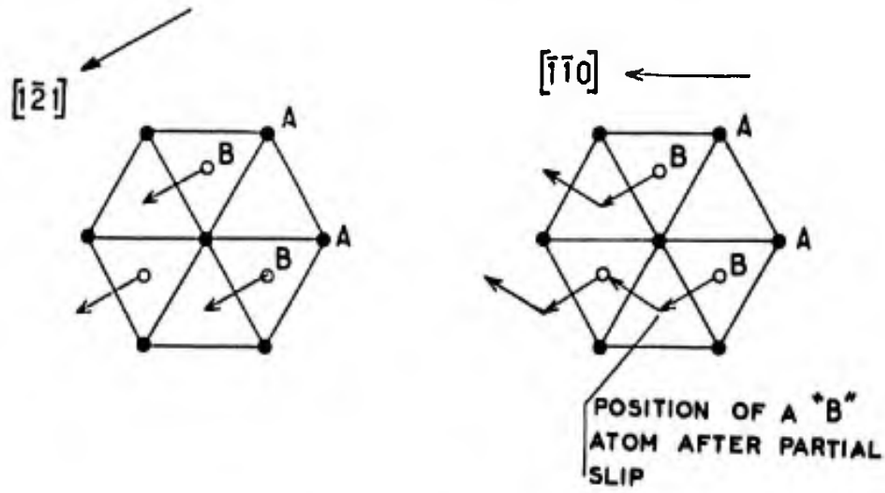

Fig. 2.12 Movements of compact layers in the face-centered cubic crystal. From Barrett[15]

Motion-pictures taken by P.B.Hirsch[14] with an electron microscope show the dislocation movement in various metals. A sheet 0.1 mm in thickness is reduced to 1000 Å (0.1 μm) by electro-polishing. Motion of the dislocations is obtained by local heating which generates high tensile stresses in the area observed (a few μm in diameter). Electrons are diffracted by the atoms of the lattice; the atoms near the dislocation are expelled from their regular equilibrium positions and produce an irregular diffraction involving a change in intensity of the electron picture, whereby observation becomes possible. Observation shows the existence of dislocations in grain boundaries and the displacement of dislocations by successive leaps. It also reveals the cancelling of two dislocations of opposite sign and the generation of dislocation knots. Today the dislocation is no longer a mere concept but a fact that can be observed.

The same method is used to observe dislocations that are locked in thin slices cut from specimens previously subjected to external forces or thermal stresses. The surface density of locked dislocations and its variation in the different crystal areas can also be measured this way. Similarly, the average density of dislocations and vacancies may be measured by the electrical resistivity, which increases linearly with this density.

According to Barrett[15], there are other faults resulting from deformation, such as *stacking faults* in close-packed crystal structures. In these structures the A atoms are closely grouped on one plane at the nodes of a plane hexagonal lattice, formed by equilateral triangles (Fig. 2.10). A similar layer B is stacked in half of the holes left by layer A. In the same way, a layer C is placed on layer B. If the C atoms are located just above the unoccupied holes of layer A, a *face-centered cubic structure* is obtained. If the B atoms are located just above the A atoms, a *hexagonal close-packed structure* is obtained (Figure 2.11 illustrates the 60°-angle rhombohedron in a face-centered cubic cell). Slip takes place through the relative displacement of two atomic layers. In Figure 2.12, the type of displacement required to achieve slip in the face-centered cubic system is shown. When slip ends, the atoms, returning to their equilibrium positions, will have the choice between two bedding systems in the holes of the lowest layer. If the position indicated in Figure 2.12(a) is used, the displacements will not preserve the structure continuity and will result in a stacking fault constituting a slip barrier on planes transverse to those which have just been operative.

Two crystals are said to be in a *twin* position if their orientations are different while their junction may be achieved without dislocations. This would be the case with the close-packed arrangement if a crystal with the sequence ABC, ABC,..., ABC was contiguous to a crystal BAC, BAC,..

Cottrell[17] has shown that the intersection of dislocations on several sets of slip planes in the face-centered cubic lattice can create stacking faults by which the dislocations are pinned down. This has been checked by Hirsch[14] with an electron microscope.

Inclusions of foreign bodies also offer impedance to dislocation propagation. Inclusions resulting from precipitation during the cooling of a supersturated solid solution are either coherent or incoherent with the matrix. The difference between an ordinary precipitate and a *coherent precipitate* is illustrated in Figures 2.13 and 2.14. According to Averbach[18], coherent precipitates disturb the matrix over a greater range and result in more efficient hardening than ordinary precipitates.

On a smaller scale, solute foreign atoms disturb the matrix and also impede dislocation movement. *Substituted atoms*, located at the lattice sites in place of some atoms of the matrix, are similar to coherent precipitates and very efficient if their positions correspond to an orderly array; *interstitial atoms*, located in the unit cells of the matrix, are also more efficient if they are suitably arranged and occupy comparable positions in neighbouring unit cells: a regular arrangement makes the atomic positions in the lattice more stable.

The preceding pages are based on a review of documents published before 1953. In 1956, Friedel[97] issued a detailed monograph on dislocations. Reference to more recent investigations will be found in the work of McLean[87] and Kennedy[89]. The present trend of specialists is to evolve a quantitative theory associating the stress state with dislocation movement, vacancy migration, microcracks generation and stability of microcracks in stress fields. The final objective is to attain a quantitative theory of strain and rupture in metals. This objective is not yet in view; consequently we shall restrict ourselves to a simplified qualitative statement of well-known facts solely with the aim of showing their general link-up. However, theories based on statistical mechanics and involving elementary facts for which the probabilities of occurrence are assumed to be statistically independent have proved fairly successful for creep strain or diffusion studies where mean effects are involved.

2.1.2 Slip Planes, Lamellae and Slip Bands

In cubic metals a slip plane is defined by its intercepts on the three rectangular axes of the cube, the numbers being enclosed in parentheses; for example, the plane xOy will be designated by (110). The slip direction is specified by the direction indices, the numbers being placed in brackets; for example, one of the largest diagonals of the cube will be [111].

Slip in crystals has been studied by Joffe[5] for rocksalt, by Schmid and Boas[6] for single crystals, by Gough[7] for metals, by Nye[19] for silver chloride, and by many other researchers. The transparency and birefringence of silver chloride have permitted photoelastic investigation of the slip phenomenon. The slip planes in opaque metal crystals are identified by the markings they leave on the surface of the test specimen. Such markings are revealed by etching with a selective reagent which removes the distorted areas of the lattice. Examination with an optical microscope shows thick lines called *slip bands*; in grazing illumination they look like steps.

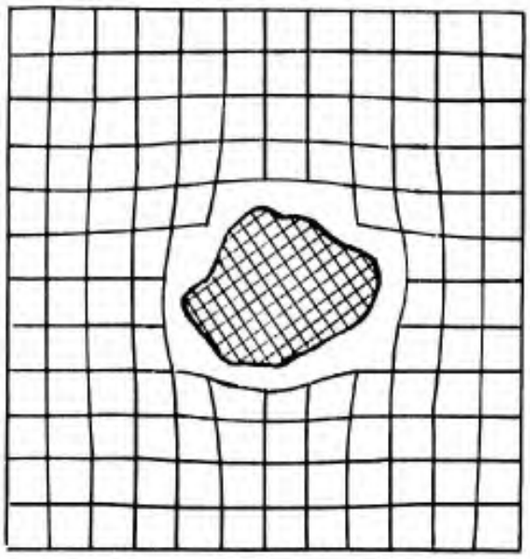

Fig. 2.13 Inclusion

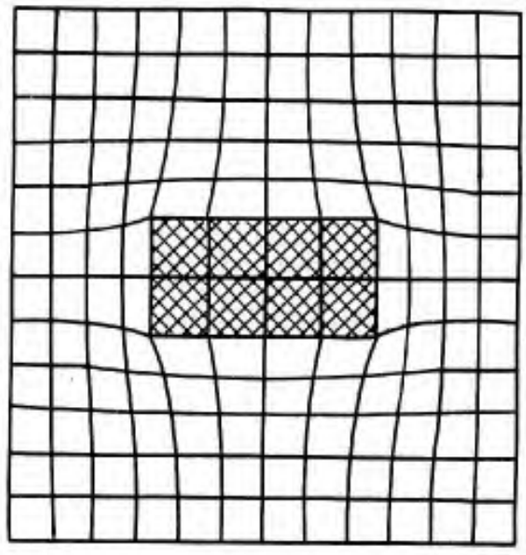

Fig. 2.14 Coherent precipitate

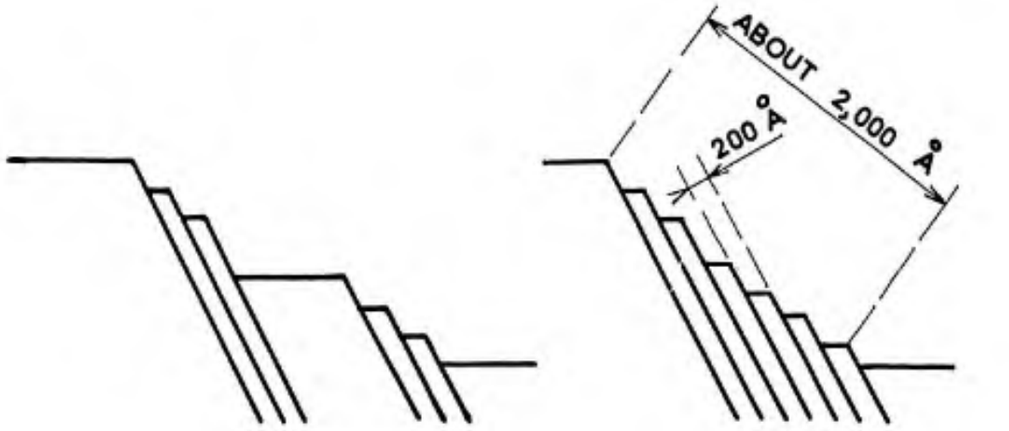

Fig. 2.15 Slip bands

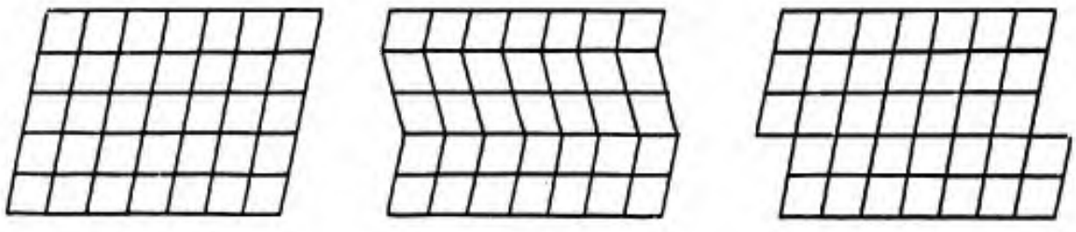

Fig. 2.16 Deformation by twinning or slip

Investigating a replica from an aluminium specimen with an electron microscope, Heidenreich and Shockley[20] showed that each slip band, of about 2,000 Å in width (1 Å = 10^{-8}cm), could be resolved into smaller steps, i.e. *slip lamellae*, of 200 Å, as illustrated in Figure 2.15.

Slip is evidenced by the occurrence of slip bands and *twins*, the lattice of which is still regular although distorted. Twins are local symmetrical reversals of the lattice (see Figure 2.16). Like the various grains of a metal, they are detected by a change in the reflective power of the surface which depends on the orientation of the lattice and on the angle of the grazing light beam.

In 1963, Gough[7] made a survey of the physical research work carried out on slip and twinning under static and fatigue loads. Permanent deformation in metal crystals is due to slip in a direction that always coincides with one of the crystallographic axes of maximum atomic density. The slip plane is always close to a plane of high atomic density but not necessarily to that of the highest density. Slip occurs when the shear stress component in the slip direction reaches a limiting value, which varies with the different crystallographic planes. Slip planes and crystal orientations are identified by the position of the Laue spots on the X-ray reflection diagrams.

Simultaneous slip is often found on different planes. In the body-centered cubic lattice of iron, for example, the slip planes (110), (112) and (113) contribute to slip in one of the [111] directions. The slip lines are rectilinear in the [111] direction and wavy in a transverse direction, as reported by Taylor and Elam[21]. Cahn's[22] view is that the face-centered cubic lattice of aluminium exhibits simultaneous slip on the $(\bar{1}11)$ and (111) planes in the same [110] direction. It may be recalled that a dash over a number designates a negative value: $\bar{1} = -1$.

When two or three slip directions are subject to neighbouring shear stresses, simultaneous slip may be found in several directions. The slip lines will then form a regular array. Slip is a local phenomenon; in torsion, a single crystal can show slip along different planes at different points without disruption of the crystal coherence. Slip generates lattice distortions liable to impede subsequent slip along the same slip plane or along another set of planes, whereby a general hardening of the crystal is obtained.

The density of slip lines increases during deformation. To explain the shape of the stress-strain curve, reference has been made (see Volley[23]) to a statistical distribution of the resistance to slip on the different planes. This assumption does not account for the experimental periodicity between slip bands. We have made a basic assumption which we shall use in later chapters: "Slip on a plane creates lattice distortions in this plane and diminishes pre-existing distortions in neighbouring planes."

The first part of the proposition is obvious, since the word "plane" does not designate one single plane but a set of very close planes where dislocation knots may be created according to the mechanism suggested by Burgers[12]. The second part of the proposition is based on the nature of the dislocation movement, which is propagated by local changes of the average atomic positions; this propagation takes place by leaps, from one atom to the next, each leap being equivalent to an impact energizing the neighbouring atoms. Passage of a dislocation results in the thermal agitation being increased locally. The heat produced is diffused on each side of the slip plane and favours slip on more remote planes which are unaffected by the geometrical disturbance caused by slip along the first plane.

Figure 2.17 illustrates this point and offers an explanation for the formation and periodicity of slip lamellae, the periodicity being imposed by the radius of action of localized distortions along a slip plane. Experience shows that the number of lamellae per slip band is limited and that the width and spacing of slip bands do not exhibit the statistical scatter required if slip is to be considered as restricted to initially weak planes. Some interdependence must therefore be assumed between slip planes. We have seen that slip causes bending of the lamellae; this bending is impeded by the elastic resistance of the neighbouring lattice and induces resistance to plastic deformation. The next slip band will form at a weak point so far from the first band that the induced resistance is negligible. These concepts are in conformity with the work of Yamaguchi[24] and with Brown's theory[25].

In single crystals, slip along a set of parallel planes starts at a given initial value of the *resolved shear stress* along these planes; slip generates lattice distortions opposing subsequent slip which can only take place with greater stress values. The number of active planes decreases constantly and the stress required to initiate slip is raised: this corresponds to Stage I, for which the σ-ϵ curve is concave towards the σ-axis; the rate of hardening $d\sigma/d\epsilon$ increases with ϵ. Sometimes slip becomes easier on planes initially more resistant to slip or less favourably oriented than the first set of planes; multiple slip is then encountered along several sets of planes with a common direction. With increasing load the hardening rate tends towards a maximum and the σ-ϵ curve exhibits a point of inflexion (Stage II). If the test is carried out under still higher loads, the various sets of slip planes are pinned down at certain points but there remains the possibility of bypassing these points by means of screw dislocations, allowing shifts from one plane to a parallel one; this operation is known as *cross-slip*. The hardening rate $d\sigma/d\epsilon$ is reduced (Stage III) until the maximum rupture stress is reached.

Multiple slip and cross-slip are common in single crystals of crystallized body-centered cubic metals such as α-iron (ferrite), molybdenum, tungsten and tantalum. In polycrystals of such metals, Stage I only exists for those grains with a privileged orientation. In single crystals of face-centered cubic metals such as γ-iron (austenite), aluminium and nickel, cross-slip is difficult and Stages I and II are encountered. Only hexagonal metals have an easy glide plane and little cross-slip is found: in polycrystals, Stage III corresponds mainly with the formation of twins at the grain boundaries.

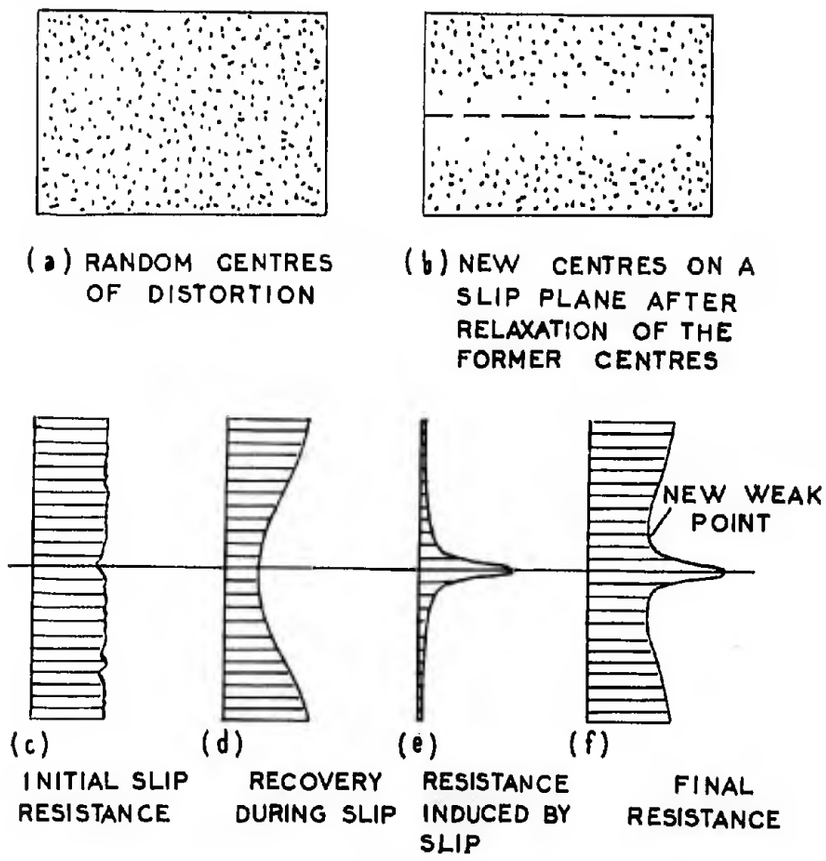

Fig. 2.17 Hardening and recovery

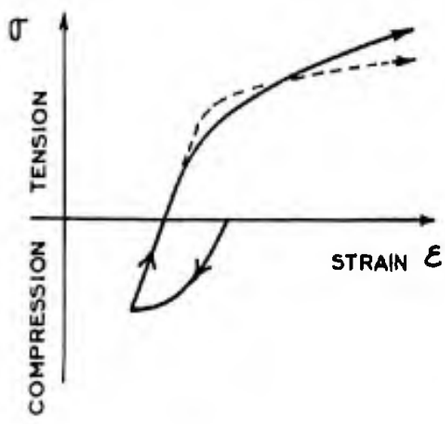

Fig. 2.18 Bauschinger effect, from Kuntze and Sachs[27]

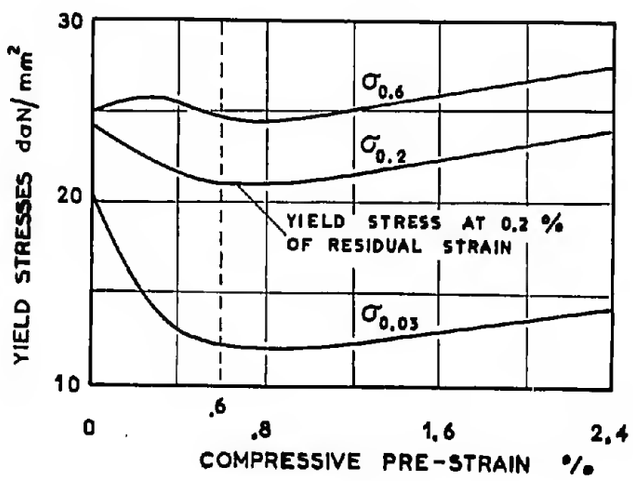

Fig. 2.19 Pre-compression effect on the yield stresses of aluminium alloy in tensile test. From Kuntze and Sachs[27]

In engineering alloys with fine precipitates scattered in a matrix, cross-slip and dislocation climb are the common ways of achieving large deformation at elevated temperatures.

2.1.3 The Bauschinger Effect and Similar Processes

Bauschinger[26] was the first to show that the tensile yield stress is decreased as a result of previous compressive loading and that under alternating loading the loop varies with repeated loading and unloading.

The first aspect has been studied more recently by Kuntze and Sachs[27] (Figures 2.18 and 2.19).

In Figure 2.18, the dotted-line curve represents the result of a tensile test without compressive pre-straining. With previous compression the slip resistance is lower for low loads and higher for high loads. This is in agreement with the assumptions made in the preceding paragraph: compressive plastic deformation occurs by slip along certain planes and the heat diffused reduces some distortions on neighbouring planes. Under subsequent tension slip becomes easier along these planes, which accounts for the lowering of the proportional limit. With increasing deformation new distortions are created which add to these existing that were stable enough to resist recovery during compression. The average stability of distortions thus is greater than in the tensile test without precompression and the metal will yield less under high stresses. In the case of large previous compression, the weak slip planes are less numerous and the *Bauschinger effect* is less evident. In technical literature, the term "Bauschinger effect" only implies a change in the yield strength at 0.2% permanent strain and does not imply any increase in plastic stiffness in the case of large deformations. In Figure 2.19, a maximum effect is shown for aluminium alloy subjected to 0.6% pre-compression.

Karpof[28] has carried out compression tests on copper at strain rates V_1 of 0.02, 1 and 2,000% per sec., followed by a compression test at a rate V_2 of 1% per sec. Figure 2.20 illustrates the results of the second test. The explanation of the shape of the strain-stress curves is based on the existence of a recovery process. Under the first high-rate loading the recovery effect is small and unable to relieve some metastable distortions which will increase the resistance to strain at the beginning of the second test; during the second test, performed at a lower rate, recovery takes place and the strain-stress curves approach a common limit.

These facts as well as others reported by Bolchanina[28] suggest that plastic strain-hardening is the result of a competition between simultaneous hardening and recovery.

In 1910, Bairstow[29] studied the strain-stress cycle variation of steel under fatigue in tests performed at a rate slow enough to allow continuous strain measurements by means of a Martens extensometer with a mirror. The variation in width of the σ-ϵ loop with the number of cycles N for several successive levels of alternating stress is shown in Figure 2.21. From the first tension-compression stress level $\sigma = \pm 25.8$ daN/mm^2(37.000 lb/in^2) in the initially elastic range, it can be seen that plastic work, at first negligible, increases constantly and tends towards a limit which depends on the load level. A sufficiently high stress brings about an almost immediate increase in plastic work per cycle, followed by an asymptotic reduction: first the pre-existing plastic distortions are relieved, then the dislocation movement creates further distortions liable to cause hardening after initial softening. On the other hand, plastic work is the main part of *damping* under fatigue loading in the low-frequency range.

Figure 2.22, from Bairstow, shows how, for the same steel, permanent elongation increases slowly at first, then more rapidly with repeated loading; the pre-existing distortions disappear and the metal becomes softer. The permanent elongation approaches a limit while deformation creates new distortions which are more stable under repeated stress; the metal becomes harder again and its new yield strength is close to 36 daN/mm^2. Flow is due to alternating stress; indeed, if the maximum stress of 36 daN/mm^2 is maintained and if the mean stress value is reduced, flow starts again although the duration of high loading decreases. This is *fatigue creep*, for which the unit of time is the cycle and not the second.

From these facts we have drawn the following conclusion: *Static or alternating loads tend to reduce previous strain-hardening associated with the past history of the metal and to substitute a new strain-hardened state typical of the new loading. The alternating stress superimposed on a static stress partly destroys the hardening resulting from the latter and is likely to favour plastic flow and creep.*

At the same time, Polakowski[30] measured the Hertzian hardness changes in metals during tensile loading. His aim was to establish a correlation between the following phenomena:

(a) The recrystallization temperature of a metal usually decreases with increasing cold-work but a reversal of the direction of deformation causes an increase of the recrystallization temperature over that at the end of the first straining (after Ludwik[31] and Kochendorfer[32]).

(b) Deep-drawing practice in the manufacture of cartridges has shown that *reversed drawing*, in which the preformed cup is turned over like a glove finger, facilitates deeper draws without interstage annealing than the unidirectional method (after Morgan[33] and Grainger[34]).

Unidirectionally rolled sheets are harder than those whose direction of rolling or type of rolling is altered after each pass (after Feitknecht[35], Bowles and Boas[36]).

(c) The slope of the hardness-deformation curve is low or even negative in the early stages of deformation in carbon- and low-alloy steels heat-treated to over 300 HV (after Gross and Brenner[37]).

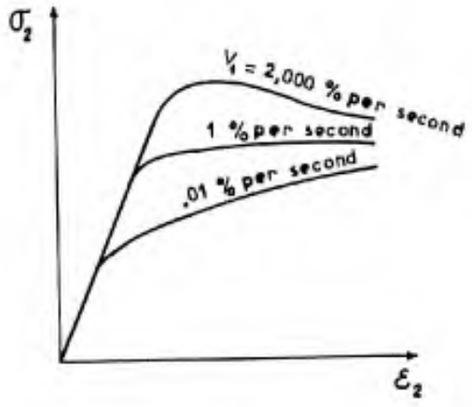

Fig. 2.20 Compressive $\sigma_2 - \varepsilon_2$ curve of copper after pre-compression at different rates V_1 in per cent per second and loaded at the rate V_2 = 1%/sec.

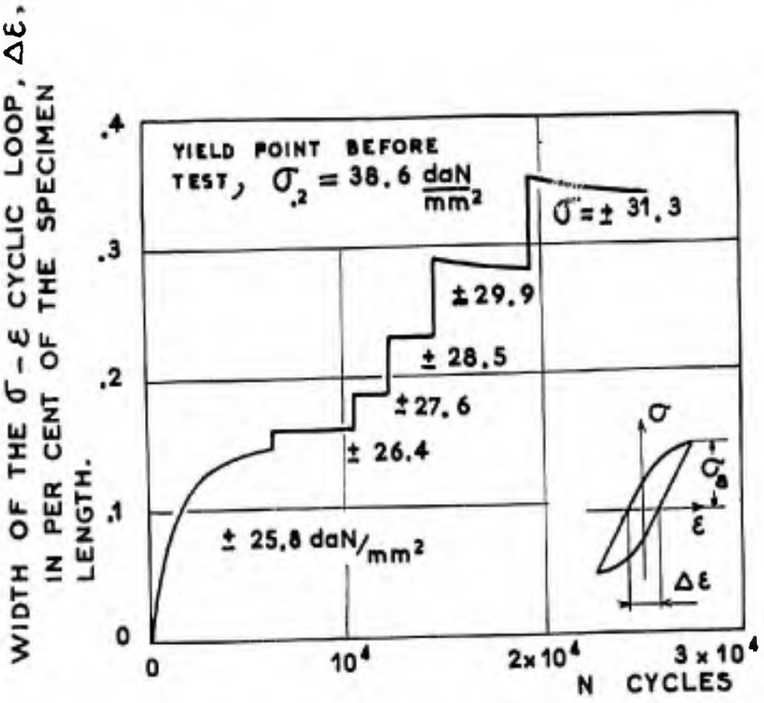

Fig. 2.21 Damping variation during the fatigue of steel

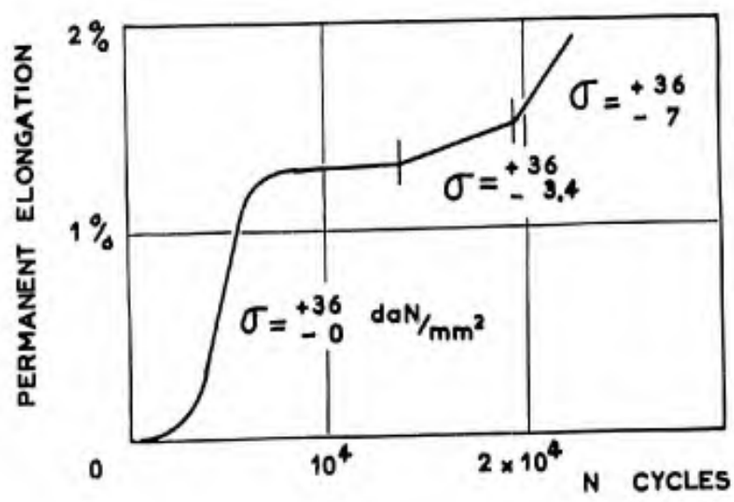

Fig. 2.22 Permanent elongation of steel under fluctuating loading

Polakowski's tests were carried out on steels of various carbon contents, Monel metal, annealed copper and commercial aluminium. Briefly, his conclusions were as follows:

1. Strengthening of a metal either by cold-working or by quenching induces in it systems of internal stresses which differ according to the method of treatment applied.

2. The application of an external force, which tends to produce new internal stresses, causes "work-softening" in the first instance as is demonstrated by the lowered indentation hardness, raised recrystallization temperature[36,37], and elongation value, as well as by relevant changes in X-ray patterns.

3. The energy which is released reduces the amount of deformation energy required to start and maintain plastic flow.

4. Cold-working tends to produce in a steel a system of internal stress more or less different from that caused by a quenching treatment. Therefore, cold-working after quenching may lower the stress value at which such a steel exhibits a permanent set.

5. Since work-softening appears irrespective of the method of cold-working, it involves development of internal stresses that are different from those resulting from the previous treatment, whether that treatment was mechanical or heat treatment.

More recently, in 1954, the same author[38] published results of *hardness tests carried out during alternating fatigue of metals* and came to the same conclusion: "It is now postulated that stress cycles of a given type and amplitude should tend to produce a specific strain-hardened condition irrespective of the initial work-hardened condition of the metal". In the discussion of this paper, Coffin indicated that the mechanism of the phenomenon may be as follows: "The agitation supplied to the structure by cyclic strain is here thought to be the motivating factor in reducing those regions of high energy by permitting adjustments in the structure to lower energy level".

In conclusion, the general law of such phenomena is as follows:

There is a specific statistical distribution of geometries and stabilities of atomic lattice distortions for a given metal and a given mechanical and thermal history. Any further mechanical loading or heat treatment tends to relieve the less stable pre-existing distortions by substituting new distortions, more stable under the action of the new load and heat conditions.

We shall find further evidence for this postulate in the study of creep.

2.2 STABILITY OF ATOMIC LATTICE DISTORTIONS

2.2.1 Energy Barriers, Deformation Bands

Slip line micrographs and measurements of crystalline lattice disorientation by broadening of the Laue spots or the Debye-Scherrer rings in the X-ray diffraction or reflection diagrams show that removal of the load still leaves some lattice distortions: the regions subject to compression or tension are unable to relax completely by means of a reversed motion of the dislocations.

Taylor[9] introduced the concept of *energy barriers* created by lattice irregularities (vacancies, impurities, etc.) which offer impedance to dislocation movement. Each obstacle can be bypassed only by providing potential energy with a sufficient stress level. For example, the mutual buttressing of two dislocations of opposite sign operating on two neighbouring planes (Fig. 2.8) can be overcome only if the potential and kinetic energy of both dislocations is sufficient to cause cross-slip of the extra atoms through compression of the metal between both slip planes, due consideration being given to the heat-induced vibration energy losses. The energy required for dislocation propagation by one unit of length at each point may be imagined along a slip plane. Consider a dislocation moving in the AE direction in Figure 2.23. Between A and B the resistance is increased while the velocity of the dislocation first increases, then decreases. It is equal to zero at B if the energy provided is just high enough to overcome the obstacle. Between B and C the velocity increases, the kinetic energy of the dislocation being the difference between the amount of work due to external loads and the sum of the losses caused by thermal diffusion and by the passage of the intermediate obstacle F.

At C the dislocation strikes obstacle D after a few oscillations; its kinetic energy is transformed into potential energy with a loss due to thermal diffusion which shifts the point to C′. On removal of the external loads, the potential energy repels the dislocation and is transformed into kinetic energy. The loss through thermal diffusion brings the energy level to C″ on the barrier B and the dislocation is captured between the obstacles B and D while exerting on obstacle B a pressure which represents a residual stress.

This dislocation-blocking phenomenon is an explanation of the work-hardening process of metals by deformation: most of the distortions caused by plastic deformation remain after unloading and prevent any significant subsequent deformation under a load that is smaller than the preceding one.

Burger's concept of dislocation knots has an experimental connection with *deformation bands*. The circumstances under which deformation bands appear have been defined by Cahn[22]. Cahn studied plastic strain in single crystals of pure aluminium (99.99%), stretched at a rate of 1% per sec. and subjected to total strains ranging from 5 to

Best possible scan

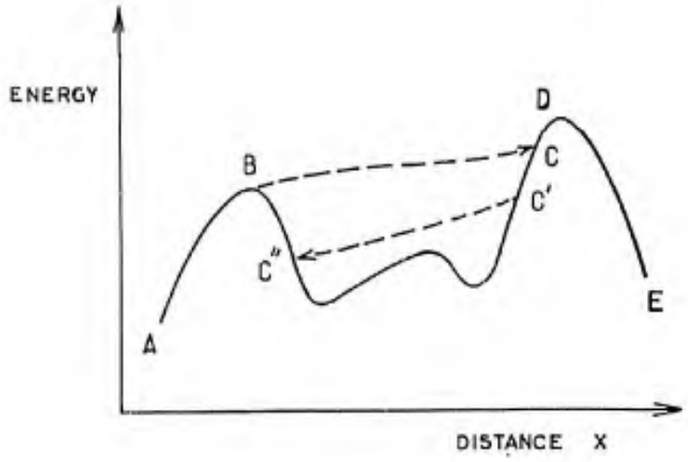

Fig. 2.23 Energy barriers

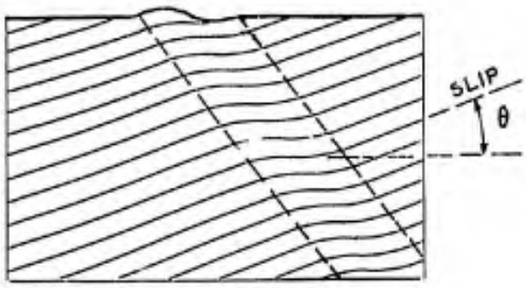

Fig. 2.24 Undulation of the surface by a deformation band

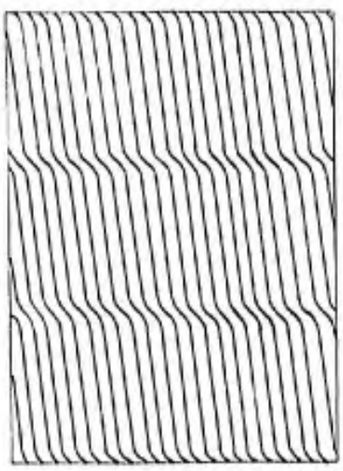

Fig. 2.25 Undulated slip lines, sketch from Fig. 76 in Laurent[43]

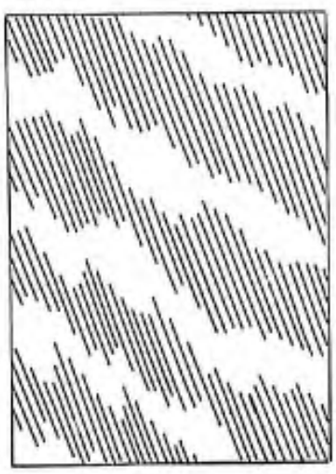

Fig. 2.26 Band lines, sketch from Fig. 99 in Laurent[43]

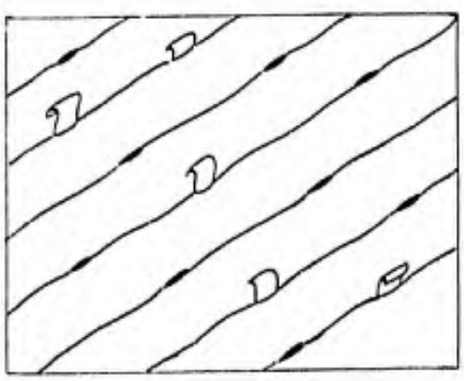

Fig. 2.27 Sketch from Forsyth[46]. Soft points and "extrusions" along slip lines for Al-4% Cu alloy in metastable solution

30%, i.e. large strains similar to those attained in static rupture tests. For deformations of the order of 7%, the slip lines were rectilinear in the [110] direction of slip. For larger deformations, between 15 and 20%, the slip lines exhibited *waves* in the slip direction.

Such waves, as shown schematically in Figure 2.24, line up along surfaces which are parallel to the (110) plane. Traces left by these surfaces on the surface of the specimen are revealed by superficial waves which are the most apparent aspect of deformation bands. The lattice in deformation bands rotates by an angle θ increasing with the extension of the specimen. The spacing of the deformation bands remains unchanged as the extension increases, except for the very rare occurrence of new bands between the main bands.

Deformation bands are substantially rectilinear in the case of small extensions but become more irregular for extensions of about 20%. They appear at room temperature and up to 400°C. Discussing the results, Cahn gives this explanation for the increase of curvature in deformation bands: "Once well started, the band acts as a highly efficient dislocation trap, as may be appreciated from the fact that many of the slip lines in a band are discontinuous. The efficiency of a band in this respect increases with its curvature; this is probably why a few bands develop strongly, while the majority remain very weak". Deformation bands correspond to slip which may originate in a heterogeneous distribution of impurities or of fine mosaic lamellae suspected by Crussard and Guinier[42] in all metals. The planes of such lamellae are parallel to the (100) plane for cubic metals, the lamellae being thus cut by the slip plane.

For still larger extensions, between 25 and 30%, Cahn observed cross-slip in deformation bands which he associates with *polygonization* resulting in the creation of crystallites by arrangement of the dislocations along surfaces that confine regular domains with a new lattice orientation. Annealing at 450°C produces observable crystallites in deformation bands.

In his thesis, Laurent[43], studying fatigue in aluminium, found specific features which we can compare with the phenomena observed by Cahn in static strain ($d\epsilon/dt$ = 1% per sec.) and by Wilms and Wood[44] in creep. The latter had developed a cellular appearance in the specimen surface by slow deformation of 10% at 250°C, the cellular structure corresponding to a fairly advanced polygonization of deformation bands (XCIV plate, Figure 2 of 44). Laurent conducted alternating torsion tests at 100 c/s on specimens of refined aluminium that had been rolled to final thickness, machined and then annealed for 12 hours at 600°C.

The fatigue test was carried out with an imposed strain so that, owing to work-hardening, the stress increased with the number of cycles until crack initiation and then decreased during the final stage. The result of these conditions was an increase in the duration of crack development. The specimens were electro-polished before the fatigue test and microscopic examination during fatigue was made without preliminary etching.

Assuming perfect elasticity, the imposed strains were converted by calculation into fictitious shear stresses. The following results, where τ is the torsion shearing stress expressed in daN/mm²*, were obtained:

With $\tau = \pm 0.44$, 0.53 or 0.63 daN/mm² for 3.10^6 cycles, no slip lines were observed.

With $\tau = \pm 0.73$ daN/mm², a few parallel slip lines which did not cross the grain boundaries were obtained.

With $\tau = \pm 1.06$ daN/mm², the grain boundaries were revealed by numerous slip bands; some crystals had undergone slip along two sets of planes.

With $\tau = \pm 5$ daN/mm², surface changes were observed during fatigue. A large number of slip bands appeared at 5,500 cycles. After 45,000 cycles some grains had been partially dislodged as a result of changes in level at the grain boundaries (the specimen used had only one grain in the direction of the thickness). Some grooves also appeared inside the grains. The dislodging process and some surface undulations developed as the number of cycles increased. After 280,000 cycles, a large number of transgranular cracks showing no apparent connection with undulations or grain dislodging were observed.

With $\tau = \pm 12.2$ daN/mm² and after 18,000 cycles, the surface undulations were more dense and exhibited a cellular structure (Figure 60 from Laurent) which we can compare with that obtained by Wilms and Wood under slow creep straining at 250°C (Figure 2, plate XCIV of 44). It is believed that the surface undulations observed in fatigue by Laurent are similar to Cahn's static deformation bands and that the cellular appearance and the dislodging of grains correspond respectively to polygonization and to micro-slip of grain boundaries as observed by Garrod, Suiter and Wood[45] – a subject which will be examined later.

2.2.2 Diversification of Plastic Stiffness on Slip Planes

For annealed aluminium, Laurent [43] found an interesting feature. At the beginning of the tests, slip lines were always rectilinear. With increasing number of cycles, they exhibited a wavy appearance (see Figure 2.25) as in Cahn's static tests, which implies surface changes in level. This was followed by development of marked undulations typical of deformation bands. Figure 2.26, corresponding to low alternating bending stress, shows the first visible stage of slip line formation leading to the creation of deformation bands; regions of higher slip density are apparent along the slip lines. This seems to suggest the existence of lattice recovery due to alternating dislocation movement at some points on a slip plane and of lattice hardening at others.

* 1 daN = 10/9.8 kg-weight, 1 daN/mm² = 1450 lb/in², 1000 lb/in² = 0.69 daN/mm².

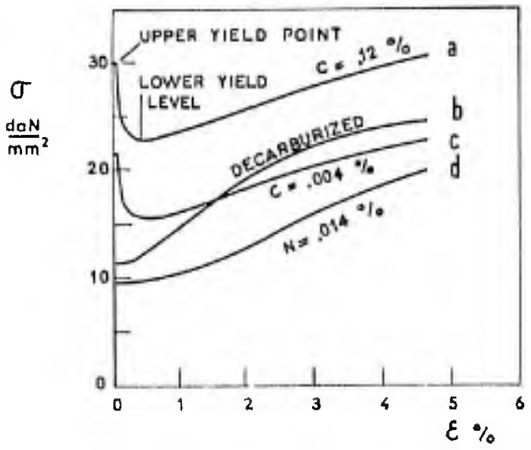

Fig. 2.28 Effect of C and N impurities on the σ-ϵ curve of steel

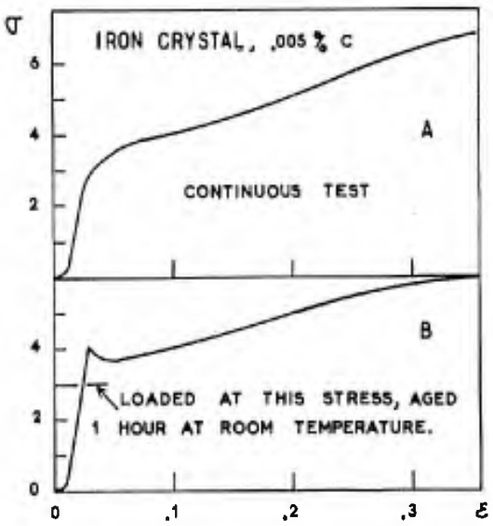

Fig. 2.29 Tensile tests on two similar single crystals of iron; (A) continuous test; (B) aged one hour under load; from Holden and Kunz[51]

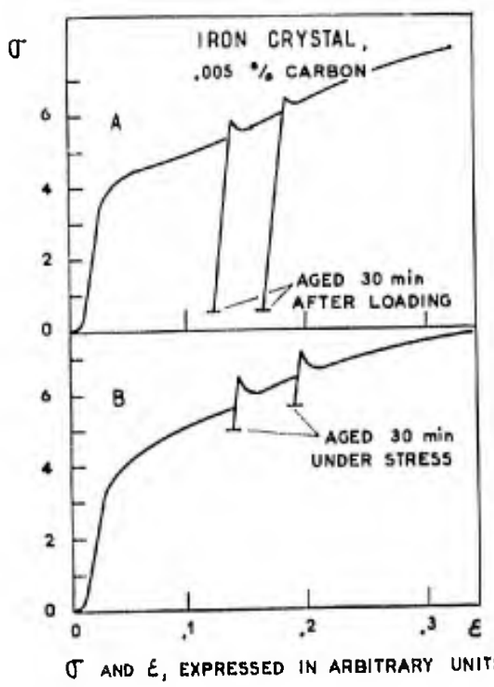

Fig. 2.30 Tensile tests on two similar single crystals of iron; effect of ageing: (A) after unloading; (B) under load; from Holden and Kunz[51]

This interpretation is supported by a report of Forsyth and Stubbington[46]. In an aluminium alloy containing 4% of copper in metastable solution, these authors obtained cracks along slip lines with surface defects which an electron microscope examination identified as "extrusions" of fairly soft metal through the surface under the effect of pressure exerted by the surrounding harder metal. Such extrusions occur from place to place along slip lines and seem to correspond to an alternation of areas softened by recovery and hardened areas. As Forsyth puts it, "the process by which soft points can be generated under cyclic stress appears to be the fundamental cause of fatigue". A sketch derived from a photograph by Forsyth is given in Figure 2.27.

According to McLean[87], cold-worked metals exhibit cellular arrangements of dislocations with a high density inside the walls of the cells, which implies that some regions are more rigid than others.

These observations permit the following assumptions:

Recovery during loading and the simultaneous hardening process lead to a selection of the more stable atomic lattice distortions and may cause greater diversification in the geometrical distribution of the stability of slip barriers.

Certain distorted areas are thus overstressed by the applied stresses, either because their stiffness has been increased by hardening or because less stable distortions have been cancelled elsewhere by recovery.

2.2.3 The Cottrell Effect, Stabilization by Impurities

Very pure metals are soft and the hardening produced by strain disappears within a short time. Thus, very pure (99.9986%) aluminium recovers spontaneously at room temperature through recrystallization immediately after deformation. According to Hutchison[47], deformation should take place at the temperature of liquid air and be maintained at this temperature if a lasting work-hardening effect is to be obtained. Conversely, recovery of less pure aluminium after work-hardening requires higher temperatures: 100°C for 99.997% aluminium and 200°C for 99.995% and 99.99% aluminium.

In the case of iron, low solute carbon and nitrogen contents of the order of 0.001% have a considerable stabilizing effect; solute carbon contents above 0.005% are responsible for the typical upper and lower yield points in the stress-strain curve of iron and low-carbon steels[48]. In Figure 2.28, from Wood and Clark[48], the stress-strain curves are plotted: (a) for annealed steel containing 0.12% of carbon; (b) for the same steel decarburized by exposure for one hour to wet hydrogen at 930°C; (c) for decarburized 0.004% carbon steel; and (d), for nitrided 0.014% nitrogen steel.

It is well-known that grain boundaries and operative slip planes contain more solute atoms than the rest of the metal. During cooling of a solid solution, precipitates appear first in these regions. Lacombe[49] has shown that after recrystallization of aluminium the boundaries of the pre-existing grains are still apparent in the new ones, which suggests the presence of impurities in the former boundaries.

Cottrell[50] assumed the existence of a cloud of solute atoms around each dislocation centre and the sweeping along of this cloud during the dislocation movement. We have seen that each dislocation comprises a region subject to tension and another subject to compression. Deformation promotes interstitial migration of solute atoms – originally distributed throughout the metal – to vacancies in the lattice; interstitial diffusion is also supposed to be responsible for the drift of solute atoms caused by dislocation movements.

In plastic strain, slip lines pass grain boundaries with difficulty. The boundaries, which are quite stable in impure metals, show less stability in purified metals, which results in a lower resistance to slip.

We consider that the stability of lattice distortions as slip barriers is increased by solute foreign atoms settling in their vacancies as a result of dislocation movements.

During dislocation propagation, local thermal agitation caused in every atom by the passage of the dislocation produces, of course, the same effect as an increase in temperature, since it favours the displacement of foreign atoms carried along by the dislocation movement ("drainage"). When a dislocation with its cloud of foreign atoms strikes a barrier, the migration of foreign atoms to vacancies in the barrier is caused by the action of mechanical and thermal agitation and is more complete if the dislocation remains longer on the barrier.

This seems to be confirmed by an experiment conducted by Holden and Kunz[51] on a single iron crystal containing approximately 0.005% of carbon in solid solution. Under small loads the σ-ϵ curve is at first concave towards the positive values of σ, which shows that at the beginning the hardening effect develops more rapidly than recovery. This trend vanishes at higher stress. If the test is discontinued and the metal allowed to rest (Fig. 2.29), the solute carbon atoms "drained" by the dislocations and anchored in the vicinity of the lattice distortions have the time to diffuse into the vacancies in a more stable arrangement, which results in the obtaining of the upper yield point as well as the horizontal line typical of the σ-ϵ curves for low carbon steels.

This interpretation is supported by another result obtained by the same authors, illustrated in Figure 2.30. For a given time of ageing after deformation, hardening due to the carbon arrangement in slip barriers is greater when ageing takes place under stress, that is, when the dislocations with their clouds of foreign atoms remain anchored in the immediate neighbourhood of slip barriers for a longer time.

At moderately elevated temperatures, for which thermal agitation proves less efficient than mechanical agitation due to the passage of dislocations, the time-dependence of the "drainage" of foreign atoms by dislocations is comparatively less significant. The rate of propagation of dislocations by successive leaps from one obstacle to another varies with the stress but depends little on the rate of plastic strain, $d\varepsilon/dt$, as long as it is of moderately high value. This explains why fatigue strength at room temperature is little affected by the rate of loading but is governed by the number of cycles, i.e., by the forward and backward motion of dislocations. Thermal agitation only compares with mechanical agitation at elevated temperatures, the units of time being the cycle at low and normal temperatures, the cycle and the second at intermediate temperatures, and only the second at elevated temperatures, at which fatigue is supplanted by creep.

In conclusion, *the stabilization of slip barriers by the settlement of solution atoms "drained" by dislocation movements depends but little on thermal agitation; it is essentially influenced by dislocation movements under the action of external loads.*

2.2.4 Residual Stresses and Strains

When a metal is so hard that plastic strain becomes impossible, the resistance to strain originates in the forces existing between neighbouring atoms. On an observation field of size above the atomic, stress is described as the quotient of the resultant of interatomic forces applied to a facet and the surface area of this facet. The conventional stress concept vanishes on a small observation field, leaving only interatomic forces. Technically speaking, stress is determined by applying a known force to a part of appropriate shape and of known cross-sectional area, and by computing the force/cross-section quotient.

On a smaller scale and for a cross-section of complex shape, Hooke's proportional stress-strain relation is assumed to be true and strain is measured on a standard length at the surface of the component. X-rays on the scale of the crystalline grain are used to measure the mean variation of the unit cell, i.e., the spacing of the lattice planes, and, hence, the mean strain from which the mean stress considered by the stressman is derived by means of Hooke's law.

Since stress can never be measured, the concept could be eliminated from the mechanics involved. However, stresses are forces and are governed by the simple conditions of static equilibrium in mechanics and easy computation is therefore possible. The term "stress" is often used when the quantities observed are in fact strains.

Applied stresses are those which are necessary and sufficient to counterbalance external loads; they are distinguished here from self-balanced *residual stresses* which exist in the absence of external loads. The formation of precipitates or local changes in the metallurgical phase may cause expansion or contraction inducing residual stresses. The anchoring of dislocations after plastic deformation leaves stresses near the slip barriers.

On the scale of mechanical parts, non-homogeneous cooling produces residual stresses. The mechanism of this process was studied by Portevin[52] as early as 1918. At the onset of cooling, the surface of a component tends to contract and is subjected to tension while compressing the core slightly. Since the core is not very compressible, the external surface subjected to tension yields by plastic flow. At lower temperatures the core shrinks in its turn while compressing the hardened, now elastic surface layer. Finally, the surface is in compression and the core in tension.

In the case of metals undergoing a crystal transformation during cooling, the phase change may cause expansion as with the γ-α transition of steels. The reverse effect of thermal contraction follows and the final result represents the difference between the two effects. This result depends on the rate of cooling, the γ-α transformation point, the temperature before quenching and the quenching bath temperature. In general, the surface stresses are found to be compressive for low carbon steels and tensile for high carbon steels, since martensite forms at a lower temperature.

Surface stress has been the subject of numerous investigations, the earliest and most important of which are reviewed by Horger[53]. Loading of ductile metals and alloys above the yield point, assuming a non-uniform stress distribution, gives rise to *residual stresses of the first order* due to elastic return during unloading.

Metals are assemblies of anisotropic crystalline grains with orientations varying from one grain to the next. Because of elastic and plastic anisotropy, stresses of the first order, i.e., stresses observed on the scale of components in metals that are supposed to be homogeneous and isotropic, resolve themselves – on the scale of the grain – into *stresses of the second order* which are considered uniform in a given grain and variable from one grain to the next. Anisotropy exists even in crystals of the cubic system. For instance, the elastic modulus of iron is 20,000 daN/mm^2 in the [111] direction, i.e., a diagonal of the cube, and 13,500 daN/mm^2 in the [100] direction of the cube edge. Even in the absence of mean stresses of the first order, there are residual stresses of the second order due to a plastic strain process which is followed by an elastic return, as mentioned previously.

Wood and Dewsnap[54] have studied specimens of 99.99% aluminium, pure iron and commercial iron of various grain sizes, using X-rays. The residual stresses measured in each grain showed considerable scatter and were sometimes of the order of magnitude of the applied stresses. According to Wilson[55], residual stresses in grains reach the yield point in the case of steel. Rosenthal[56] suggests a Gaussian distribution of such stresses. It is suggested by Paterson and Orowan[57], along with Hutchison[47] and the abovementioned authors, that broadening of

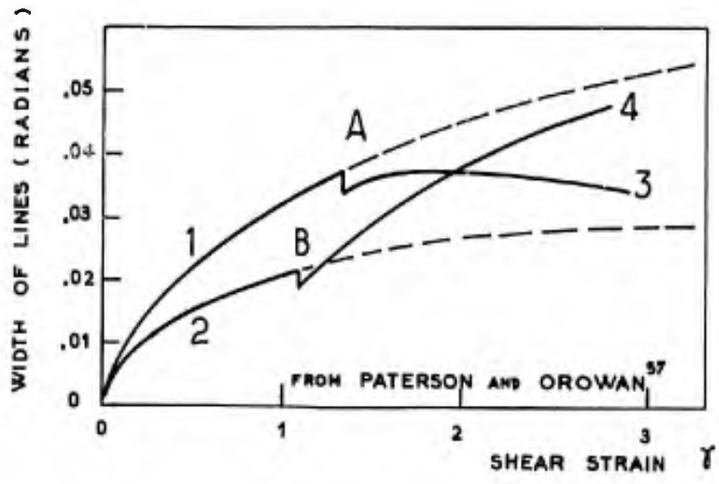

Fig. 2.31 Curves of broadening of X-ray diffraction rings against strain for copper

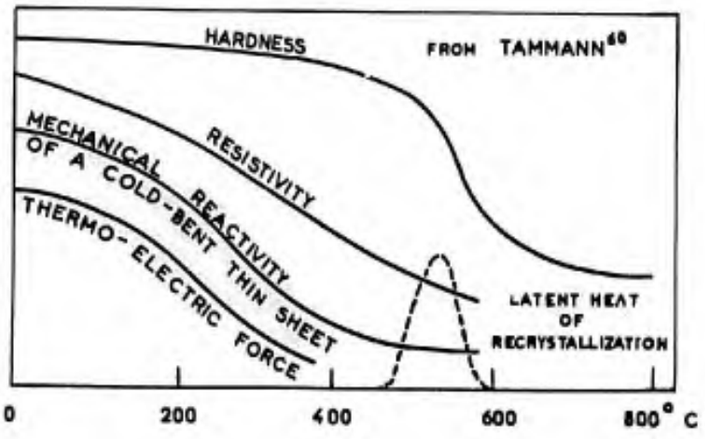

Fig. 2.32 Recovery and recrystallization of a thin sheet cold-rolled to 95%, annealed 1 hour

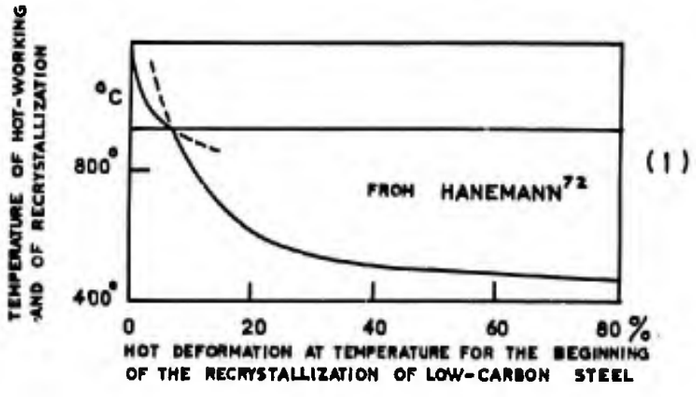

Fig. 2.33(1) Influence of temperature and degree of deformation at temperature on curve of initial recrystallization of low-carbon steel (Hanemann)

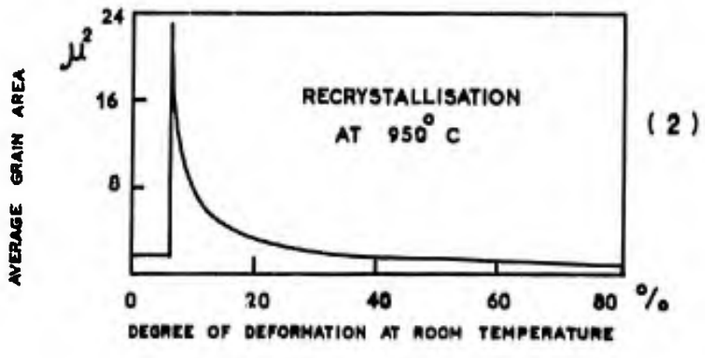

Fig. 2.33(2) Influence of degree of cold-deformation on grain size developed at 950°C in low-carbon steel (Hanemann)

the rings in the X-ray diagrams is caused by residual stresses on the scale of the grain. In Figure 2.31, the variation in width of the 74°30′ ring as a function of strain is plotted for copper at two test temperatures. The line width does not tend towards a constant value and the curves simply flatten with increasing deformation, as stress-strain curves do. In the case of a temperature change during deformation, the system approaches a state corresponding to the new temperature, which is another substantiation of the conclusions stated in paragraph 2.1.3.

Megaw and Stokes[59], investigating draw-induced residual stresses in various materials by means of the broadening of the X-ray rings, have obtained the following results:

Metal	*Fe*	*Ni*	*Cu*	*Ag*	*Al*	*Pb*
Stress calculated from width of rings, in daN/mm²*	58	53	23	22	3	0.7
Tensile strength, in daN/mm²*	30-80	35-120	23-47	28-36		2-2.1

On the whole, the residual stresses of the second order on the scale of the grain are comparable in magnitude to the applied stresses of the first order on the geometrical scale.

We have no knowledge about stresses of the third order on a scale ranging from a few atomic distances to the size of mosaic domains. Paterson and Orowan[57] believe that such stresses contribute but little to the ring broadening. First, the total volume of regions around the dislocations is small compared with that of the specimen; moreover, coherent regions subject to such stresses extend only over a few atomic distances. High "stresses" around dislocations would only contribute to the background density of X-ray diagrams. If other factors, such as impurities and thermal agitation, could be eliminated, the background density would be a measure of the dislocation density in the metal. More recently, a method of measuring the dislocation density with an electron microscope has been evolved and it appears that plastic strain is proportional to the density of dislocations (see References 94 and 95).

2.3 HOT RECOVERY AND RECRYSTALLIZATION

The cold-worked state of metals is unstable and residual stresses tend to decrease. Work-hardening causes a change in the physical properties of metals: hardness, yield strength and ultimate tensile strength are increased; electrical conductivity and density are decreased; thermal expansion and compressibility are increased, and corrosion sensitivity is modified. Heating of work-hardened metals reduces the lattice distortions as it changes the physical properties, leading to *recovery* of the characteristics that existed prior to work-hardening. Along with Mehl[60], we distinguish three possible processes during annealing:

1. *Recovery* with no change in the grain structure.
2. *Recrystallization:* formation and growth of new grains extending throughout the work-hardened structure.
3. Further *growth of new grains* after complete recrystallization.

These processes depend also on the amount of and the stability of lattice distortions. The stability of work-hardening can be measured by the time and temperature of recovery. Recovery is the return to the condition that existed before work-hardening; it may be described as follows[1]:

After cold-rolling, the grains of the hardened metal present small distorted regions which correspond to very high stresses or atomic forces; large regions such as grains or sub-grains undergo elastic deformation and are subject to mean residual stresses which can only be reduced by plastic slip or by the formation of a new crystalline network. Displacements by which a new configuration of lowest potential energy can be obtained are slowed down or impeded by solute impurities and inclusions which have a stabilizing effect on distortions.

At appropriate temperatures, thermal agitation eliminates certain small and unstable distortions such as dislocations of opposite sign distributed on the slip planes. The remaining distortions are then overstressed by unrelieved residual stresses which lessen their stability. Some of the overstressed distortions start yielding and a sudden motion of the released dislocations takes place, causing a portion of the potential energy to be transformed into vibration energy.

This additional atomic agitation favours the disappearance of other distortions which yield in their turn while reducing the mean thrust due to residual stresses. Local thrusts decrease with the mean thrust but increase as the number of plastic slip barriers decrease. This process ceases as soon as the local thrusts are too low to overcome the stability of the remaining slip barriers; it is promoted by residual stresses and initiated by thermal agitation.

* 1 decaNewton = 10/9.8 kg-weight, 1 daN/mm² = 1450 lb/in².

Grain boundaries are the most stable barriers and can only be overcome by rearrangements of the lattice under action both of high residual stresses and elevated temperatures which reduce the stability of grain boundaries and allow them to move (recrystallization). With moderate work-hardening and temperature, recovery without recrystallization can be obtained.

Sudden displacements or *avalanches of dislocations* have been demonstrated by Rusch[61], repeating Kaiser's[62] experiments for steel. He detected and measured by means of a microphone the intensity and frequency of sounds which were produced by internal movements in the metal during the tensile test. The main results are as follows:

1. The intensity of the noise is some orders of magnitude below the lower limit of audibility but the frequencies lie beyond the upper limit.
2. The frequencies and amplitudes increase with the applied stress.
3. The intensity of the noise is higher under a first loading.
4. Under further loading, it remains low as long as the previously applied stress is not exceeded. (This was used by Rusch to determine the largest previous loading applied to mild steel bars from reinforced concrete structures.)

In a review of recrystallization studies, W.G.Burgers[63] wonders whether recovery and recrystallization are two different and successive phenomena or whether recovery is recrystallization on such a fine scale that there is no longer any reason to discriminate between them.

Averbach[64] has stated that recovery is similar to recrystallization in that it already implies the formation of small orderly domains. Kuhlman, Masing and Raffelsieper[65] have studied recovery in crystals subject to shear and demonstrated that it is favoured by shear stresses. Cahn[22] has found that very low stresses applied during annealing of aluminium promote the formation of crystallites in polygonized deformation bands. *Polygonization* is a process of transformation of a crystalline lattice, bent by distributed dislocations, into a polygonal structure in which regular lattice regions are separated by domains of high dislocation concentration. Crussard[66] considers that this phenomenon corresponds to an *"in-situ recrystallization"*. Polygonization would be the intermediate stage between recovery and recrystallization.

We may now sum up the essential features of the known facts about *recrystallization*. After cold-work followed by prolonged heating at a high enough temperature, nuclei of new grains appear in the distorted lattice regions, i.e., at grain boundaries, on slip lines, in deformation bands and on planes of twinning. Mehl[60], Van Arkel[57] and Van Liempt[68] stated around 1930 that the growth of a lattice region takes place at the expense of its neighbourhood if the region concerned is more stable, that is, less deformed than neighbouring regions, and they supposed that initially deformed blocks constituting potential nuclei are relieved by heat treatment which changes them into real nuclei likely to grow.

After complete recrystallization, subsequent overdevelopment of one of the new grains is sometimes observed at the expense of others, as has been reported by Mehl[60], Calvet, Buckles and Changarnier[69]. In 1952, Beck[70] suggested that conventional recrystallization results from overdevelopment of one of the crystal sub-grains, these being obtained by in-situ recrystallization or polygonization. Recovery would first correspond to an orderly array of distortions inside the sub-grains and then to their growth. This process would eliminate the old concept of recrystallization originating in mysterious nuclei and Beck asked the question: do metals recrystallize?

It seems difficult to distinguish very different mechanisms here. Recovery, which leaves sub-grains while destroying finer structures, Crussard's in-situ recrystallization, which destroys some sub-grains while respecting the grain structure, conventional recrystallization, where sub-grains grow to such an extent that the former grain structure disappears, and the overdevelopment of grains into new recrystallized structures, all these processes exhibit similar characteristics. We believe that the mechanism is the same and that it is the order of magnitude that is different. We think that the mechanism is controlled by the relative stability of lattice distortions and that atom movements are generated at various temperatures and rates, depending on the case. From the preceding, the *recovery and recrystallization process* may be imagined as follows:

After cold-work, the metal presents the following lattice imperfections, in a decreasing order of stability and size: grain boundaries, deformation bands producing a cellular structure in grains, slip bands creating a finer structure, slip lamellae and distributed dislocations.

As soon as work-hardening is completed, some distributed dislocations migrate as a result of thermal agitation and cancel out in pairs if they are of opposite sign. This first recovery cannot cause any change in the mechanical properties that could be measured by plastic strain, as plastic strain recreates in its first stage all the destroyed dislocations. It can be inferred from an increased electrical conductivity[60,96] (see Figure 2.32).

The cancelling of dislocations that can be neutralized results in dislocation clusters or very slightly curved deformation bands being overstressed by mean residual stresses in the grains and diminishes the relative stability of such slip barriers. Some of these yield through an avalanche reaction and localized mechanical shocks favour the migration of dislocations to more stable obstacles. The fine cellular structure of slip lamellae is thus eliminated and the remaining structure is that defined by the deformation bands.

During the next stage, the deformation bands are overstressed and disappear if they are of low stability, the dislocations being rearranged by polygonization into small regular domains; if they exhibit greater stability, crystallites form in less stable regions inside the bands. Stresses are then considerably reduced as shown by the overall strain of a thin sheet initially rolled on a mandrel (Fig. 2.32); the mechanical properties are still unaffected since the more stable obstacles, i.e., grain and sub-grain boundaries, remain up to that moment and hence nothing is visible in the optical microscope. This process may be termed *recrystallization incubation*.

Hardness varies but little, as shown in Figure 2.32 for iron, as long as recrystallization is not initiated; indeed, the large deformation achieved in the hardness test re-creates many distortions eliminated by annealing. *Resistivity* implies the existence of distortions irrespective of their stability and decreases continuously with the annealing temperature (see Chapter V, Section 5.1.5). The mechanical recovery of cold-bent thin sheets implies overall elastic strains due to the relaxation of mean stresses in the hardest outer fibres of the specimen.

If the temperature is high enough for recrystallization to occur, the residual stresses are low but increased thermal agitation causes their effect on stability to be significant. According to Rathenau and Custers[71], residual stresses that persist in non-recrystallized regions may strain and further work-harden the new grains; the grains formed towards the end are less deformed and are likely to grow at the expense of others.

The temperature of recrystallization depends on the degree of work-hardening. If the temperature is raised, the general stability of slip barriers decreases, the potential energy threshold for the appearance of nuclei (onset of local polygonization) drops and recrystallization becomes easier. The temperature of recrystallization increases with the stability of the distortions, which explains why pure metals recrystallize at moderately elevated temperatures.

For hot-worked low-carbon steel, Figure 2.33(a) shows the degree of deformation at the temperature of hot-working necessary for recrystallization to start at this temperature. According to Mehl[60], diagrams for deformation at room temperature and recrystallization at elevated temperature differ only in degree and have the same general form for all metals and alloys. On the left and below these curves no recrystallization occurs but only recovery.

For mild steel samples cold-deformed then heated at 950°C, Figure 2.33(b) illustrates the sharp onset of recrystallization for a *critical degree of cold-working* corresponding to a sudden grow of grains of a large size; below this threshold of deformation, recrystallization does not take place.

Except for crystal phase changes, a temperature may be found at which the former sub-grains that have recovered will be in the situation of sub-grains formed by previous work-hardening; the critical degree of work-hardening will be low since the recrystallization nuclei are probably regular lattice regions which grow at the expense of more distorted neighbouring regions. The number of nuclei increases with the degree of work-hardening: new grains will be scarcer, and therefore larger, as the degree of critical work-hardening is approached, as long as secondary recrystallization does not occur.

According to Mehl[60], the tendency to recrystallize is reduced *if straining has been successive, i.e., the result of loadings of different types or of successive stress reversals.*

In the first case, i.e., successive static loadings of different types, for example torsion followed by tension, different slip planes are involved, this resulting in the creation of a network of anchored dislocations along each set of planes, and leading to more efficient hardening. Dislocations are more stable, therefore recovery and polygonization will be slower. In the case of alternating loading, the stability of distortions increases through the progressive elimination of less stable distortions and the creation of new distortions which are more stable.

Impurities in solid solution and *finely divided non-miscible impurities* slow down the slip and impede the preliminary process of recovery and nucleation (or polygonization). After nucleation, according to Mehl, solute impurities have little effect on the growth of grains whereas non-miscible impurities exert a marked influence. We assume that stabilization of the dislocations by solute foreign atoms decelerates the rapid movements that give rise to nuclei, but that slow dislocation diffusion allows the new grains to grow slowly. Conversely, non-miscible impurities cannot diffuse and constitute blocks which slow down both recovery and recrystallization.

2.4 DEFORMATION AND METALLURGICAL TRANSFORMATIONS

The preceding statements on questions related to the physics of metals involve concepts which are likely to be easily understood by mechanical engineers although they are more familiar to metallurgists. We must now consider the metallurgical transformations brought about by heat treatment, in association with the effect of deformations occurring during fabrication and service.

2.4.1 Precipitation, Ageing, Structural Hardening

Some alloys are prepared for use by a heat treatment that gives high strength by precipitation of one or more constituents. The treatment includes heating to a sufficiently elevated temperature to enable one of the constituents to go into solid solution; for example, 500°C for aluminium alloy containing 4% Cu, 0.5% Mn, 0.3% Si.

Water-quenching then produces a solid solution in a metastable state. Owing to thermal agitation the copper atoms distributed in the aluminium matrix diffuse and are arranged along (100) planes; these clusters are likely to grow during subsequent tempering.

According to Guinier[73] and Preston[74], one of the first phases of this process is the formation of a precipitate, as a result of quenching stresses, in the form of very thin platelets at the grain boundaries and along the slip planes. The precipitate, θ', which cannot be observed with the optical microscope but which is revealed by X-ray patterns, is coherent with the matrix. In other words, it subjects the unit cell of the matrix to such strains that the transition from the lattice of the matrix to that of the precipitate is continuous, as shown in Figure 2.14. This implies that precipitates must be of small size, as their growth is conducive to matrix deformations capable of generating vacancies, with a resulting loss of coherency between the lattice of the matrix and that of the precipitates. Beyond a certain critical size the conditions are favourable for the formation of stable Cu Al_2 precipitates at the expense of coherent precipitates, the diffusion being promoted by a local opening of the matrix cells[18]. Hardening of aluminium alloy after quenching corresponds to the formation of invisible transition precipitates; it is favoured by tempering at 100°C. Tempering at 150°C produces softening due to the loss of coherency and to the formation of Cu Al_2 precipitate.

The same type of transformation is encountered in Al-Mg-Si alloys, where Mg_2 Si is the constituent responsible for *structural hardening*. After quenching, the solute atoms diffuse and gather in rows likely to be developed by tempering in the range of 200°C to 250°C. The Mg_2 Si precipitate forms at 300°C. Many binary and ternary alloys exhibit the same characteristics.

Aluminium alloys containing 4% Cu, such as 2014 and 2024, are used in the quenched and aged condition. After quenching, the metal is very soft and can withstand large shaping, stamping or drawing deformations in fabrication. The alloys then harden by *natural ageing* at room temperature. The 7075 aluminium alloy, which contains zinc, and the preceding aluminium alloys may be subjected to a quenching heat treatment followed by tempering in the range of 150°C to 200°C: this is called *artificial ageing*.

Work-hardening after quenching exerts a considerable influence on ageing. Ageing is accelerated and the ductility may suffer. Cold-work may favour subsequent recrystallization during service at elevated temperature. It may also promote the appearance of large precipitates through loss of coherency and through the coalescence of transition precipitates (overageing) with a consequent softening of the matrix. If deformation is required it should be applied immediately after quenching and carefully controlled. Overageing can occur at elevated temperature with or without simultaneous external loading. The following may then be assumed.

Dislocation movements during deformation under load or during recovery favour the interstitial diffusion of solute foreign atoms to slip planes and, within the slip planes, to slip barriers.

In addition, dynamic shocks due to disturbance of the equilibrium of certain slip barriers under the thrust exerted by the applied or residual stresses may cause a *brief local increase in temperature* in these supersaturated regions, thus promoting a new atomic arrangement. The steps in the stress-strain curves of commercial aluminium and aluminium alloys tested at appropriate temperatures have been attributed by Kawai[76] to an alteration of structural hardening and slip. Hanstock[77] has studied the structural hardening of British RR 56-2% Cu alloy under vibration and fatigue conditions. He concluded as follows: "The preliminary effect of vibration on solution heat-treated and quenched alloy is shown to be equivalent to an acceleration of the process of natural ageing. Prolonged vibration causes the precipitation process to continue. Thus, if the alloy is brought to a condition in which it has high strength by vibration, natural ageing or elevated-temperature ageing, further vibration causes growth and coalescence of precipitation centres, leading to an increase of the strain-concentration factor and consequently a decrease in strength." In fatigue tests at a constant stress amplitude, deformation first decreases during structural hardening, goes through a minimum and then increases, unlike Al-Mg alloys containing 5% and 11% Mg, in which case the metal is continuously hardened by fatigue.

Whenever a new alloy or a known alloy in a new temperature range is used, an experimental investigation of the influence of fabrication deformation on the mechanical behaviour should be carried out.

2.4.2 Martensitic Transformation

In *carbon steel*, *martensite* is a needle-shaped constituent which forms during low-temperature transformation of the solid solution of carbon in γ-iron, called *austenite*, into α-iron, called *ferrite*. In austenite, the solute carbon takes up interstitial positions in the face-centered cubic lattice. With slow cooling, precipitates of iron carbide called *cementite*, are obtained, which are embedded in an α-iron matrix crystallized in the body-centered cubic system and still containing some traces of dissolved carbon. The rhombohedral cementite unit cell contains 4 carbon atoms for 12 iron atoms, which corresponds to the chemical formula $(Fe_3C)_4$.

Figure 2.34 shows the conventional diagram for the slow transformation of iron with various carbon contents. For a C_1 concentration, austenite is slowly transformed into ferrite by cooling to a temperature T_1, the carbon content of the remaining austenite being increased. At 700°C, the carbon solubility in ferrite is approximately 0.025% compared with 10^{-7}% at room temperature. The transformation point T_1 drops with an increasing carbon content of austenite and, by cooling, the point (T,C) on the diagram is shifted towards point E, corresponding to a possible simultaneous existence of austenite, ferrite and cementite. For *eutectoid steel*, with $c = 0.87\%$, transformation may take place at constant temperature at point E. For hyper-eutectoid steel, with $c > 0.87\%$, cementite forms and reduces the carbon content of austenite; ferrite forms rapidly at the temperature of point E.

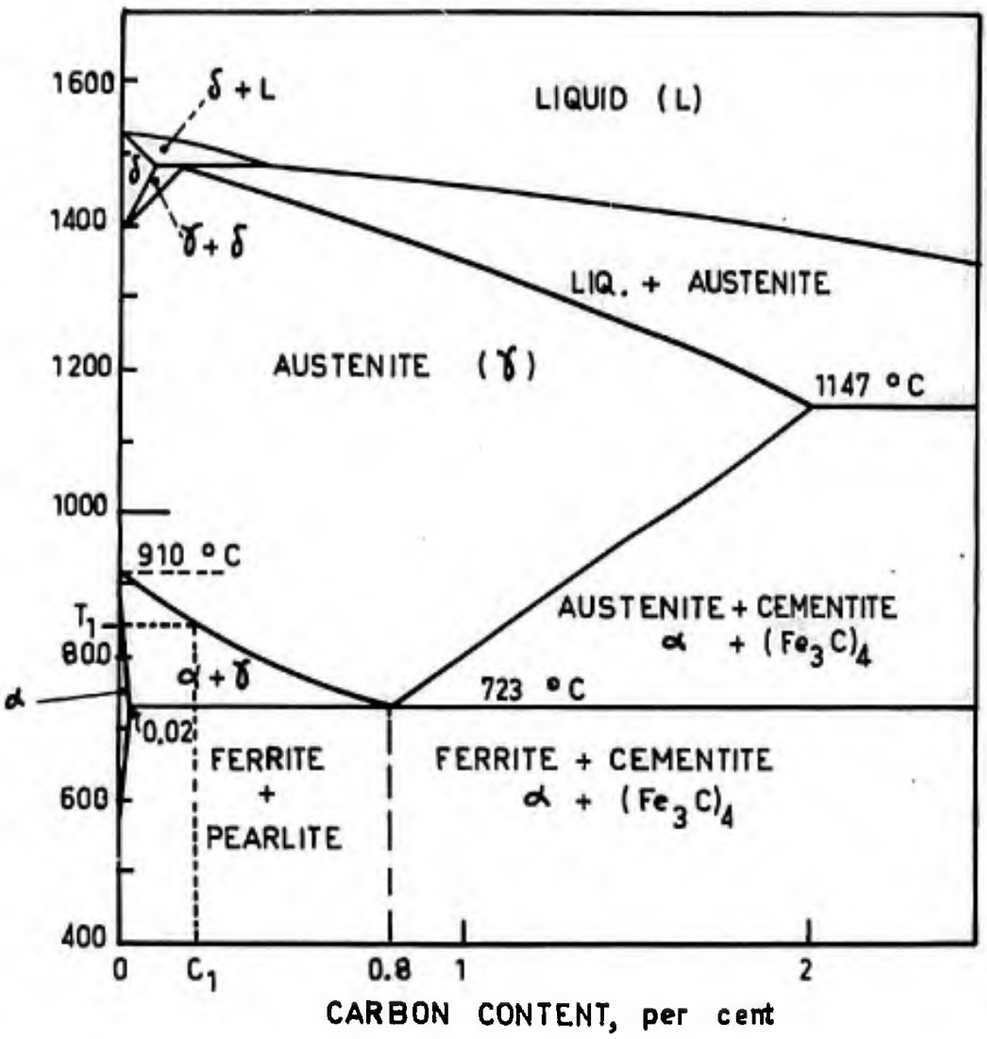

Fig.2.34 Diagram of slow transformations in steels

For eutectoid steel, an aggregate of alternating ferrite and cementite lamellae, called *pearlite*, is found in each crystal when cooling has occurred at a moderately high rate. Cementite first forms in the distorted regions of austenite. According to Delbart and Ravery[78], the stresses induced in austenite during cementite formation create new nuclei. The rate of nucleation and the rate of growth increase with decreasing temperature, the increase of the former being more rapid than that of the latter. Consequently, we believe that the formation of nuclei is partially due to the action of stresses while their growth is caused by carbon diffusion. At lower temperature, the stresses increase but the possible strains are smaller since stabilization is improved by lower thermal agitation.

In effect, low thermal agitation allows diffusion of the carbon to vacancies whereas excessive thermal agitation tends to produce a uniform distribution of the dissolved carbon. Owing to this, the cementite lamellae which constitute pearlite are small if transformation takes place at low temperature. If cooling is sufficiently quick, the atomic migration hysteresis shifts the transformation lines of the diagram towards the lower temperatures. With a suitable cooling rate, carbon is unable to migrate to the grain boundaries in time and cementite forms in some crystalline planes while generating *lamellar pearlite*.

If the temperature is kept below or near point E, lamellar pearlite coalesces and the cementite lamellae become globules; the metal is then in the softest state. More rapid cooling produces cementite crystals which cannot be resolved by the optical microscope and *sorbite* is obtained. "Soft" quenching results in even finer pearlite. During "hard" quenching, e.g. in water, cementite has no time to form and a metastable solid solution of carbon in α-iron, called *martensite*, is obtained. Ultra-rapid quenching, or hyperquenching, would maintain more of the initial solid solution of carbon in γ-iron, i.e. austenite.

As the γ-α transformation and cementite precipitation both depend on the residual stresses and strains resulting from cooling, traces of residual austenite and of cementite are obtained by a treatment that produces lamellar pearlite. The variations in microstructure from one point to another are caused by the heterogeneity of stresses due to heat treatment and cooling strains.

The purpose of treatments is to modify an unfavourable structure and produce better mechanical properties. For instance, let us consider the normalizing treatment given to steel castings. Provided the amount of carbon present is sufficient, the properties may be improved by heating to an appropriate temperature in order to achieve a uniform distribution of the dissolved carbon; by quenching, to maintain the divided state of carbon; and by reheating to a moderately elevated temperature, called tempering, so as to produce the desired pearlitic structure. Small grains and a very fine carbide distribution are desired.

According to Andrew[79], transformation of the γ solid solution in hyper-eutectoid steel is initiated by the formation of Fe_3C aggregates of martensitic structure, the volume expansion of the γ-α transformation being of the same order as that resulting from quenching which produces martensite. Quenching delays the formation of $(Fe_3C)_4$ cementite and preserves a substantial portion of austenite. Ageing at 100°C increases the martensite content at the expense of the residual austenite. Annealing at increasing temperatures up to 300°C promotes both the formation of martensite from austenite and the formation of cementite from martensite.

The tempering process in steels is described as follows by Ballufi, Cohen and Averbach[80]:

(a) After quenching, the matrix consists of martensite containing residual austenite. By heating to 205°C, a high-carbon transition product which precipitates in martensite is obtained; the martensite contracts.

(b) Between 205°C and 315°C, the residual austenite decomposes into *bainite* and the volume of steel increases.

(c) Above 205°C, the first transition precipitate turns into cementite with an increase in volume.

(d) Above 540°C, complex carbides form at the expense of cementite in certain alloy steels.

The transformation of residual austenite to martensite is a very rapid phenomenon. Troiano and Greninger[81], together with McReynolds[82], indicate the following characteristics for the martensitic transformation of steel:

1. No diffusion, no change in the chemical composition.
2. Transformation begins at a given temperature, M_S, and does not develop at constant temperature; small volumes of the initial solid solution suddenly undergo a change in their crystalline structure and martensite plates appear.
3. The amount transformed depends little on the cooling rate, but mainly on the chemical composition and the grain structure.
4. Transformation is favoured by shear.
5. Martensite is a metastable transition between the initial γ solid solution, which is supersaturated and unstable, and the final phase, during which precipitates appear.
6. Martensite forms in plates parallel to some crystallographic planes of the lattice and hardens the lattice.

Many alloys and even pure metal such as lithium exhibit a transformation of the martensitic type: Cu-*Al* alloys[83], Fe-Ni alloys[84], Cu-Zn alloys[85], etc.

McReynolds[82] stated: "Many studies of the lattice orientation relationship of martensite to austenite have been made on iron-carbon and iron-nickel alloys. Although they differ in detail, the proposed relations all lie rather close together and all were explained on the basis of single or double homogeneous shears of the lattice followed by dimensional readjustment. Recently, Barrett proposed that the lattice change could also be effected by a heterogeneous shear, possibly by passage of a group of dislocations along adjacent planes causing small shears of successive layers in various directions." This would imply a relationship between slip deformation and martensitic transformation.

McReynolds concluded: "On the whole the present results do not support the hypotheses that transformation is a homogeneous shear or that it is effected by the action of shearing forces on a mechanically unstable lattice. It appears that slip and transformation are not alternative ways of yielding but are closely connected, since thermal transformation (by cooling) leads to yielding, and on the other hand deformation by stress results in isothermal transformation. If the lattice is violently deranged by slip, however, the displaced atoms fall into the more stable martensite structure. Furthermore, it is possible that these forcibly deformed regions are large enough to serve as nuclei which spread into larger martensite plates."

During rapid cooling, austenite transforms spontaneously into martensite below the M_S temperature. Residual stresses increase during cooling and tend to relax by sudden plastic slip which favours the transformation. The M_S point would be determined by the residual stresses, by their stability and by the atomic equilibrium between regions where the austenitic lattice is the least stable. Plastic deformation achieved at a temperature above M_S lowers the M_S point through stabilization of the slip barriers.

Scheil[84] found a dependence of the M_S temperature on the grain size and suggested that the limitations imposed by the grain boundaries on the growth of martensite plates partly determines M_S and also that the formation of the first plates subdivides the grains, whereby a further decrease in temperature is required to form additional plates.

Plastic deformation under external loads promotes martensitic transformation. Tests carried out by McReynolds yielded the following results:

1. "The yield stress (for 0.02% plastic yield) begins to increase markedly with decreasing temperature and is at a maximum just above M_S. As the temperature is decreased from just above M_S to just below M_s, the yield stress changes discontinuously from a maximum to a very low value." It may be assumed that with complete transformation the solid solution is replaced by large precipitates which harden the lattice only little; on the other hand, incomplete transformation leaves coherent and finely divided transition precipitates.

2. "Plastic deformation, at any temperature from below the M_S point to above the M_d point (such that plastic strain occurs only by slip above M_d), has a stabilizing effect on the remaining austenite such that the beginning of subsequent transformation by cooling is depressed as much as 20°C and the temperature range over which transformation occurs is spread out."

French[86], in 1933, studied the *influence of quenching on the fatigue strength of steels*. He pointed out the *accelerating effect of alternating deformation on the transformation of residual austenite into martensite* and the beneficial influence of this transformation on the fatigue strength of steels: "It seems probable that the retention of austenite can operate through alteration in the stresses arising from martensitization, so as to reduce or eliminate real or pseudo cracks and so to improve the mechanical properties and especially the resistance to fatigue of the steel..."

From the foregoing facts we may draw the following conclusions:

(a) The martensitic transformation occurs at low temperature by cooling of a supersaturated solid solution; it takes place without diffusion and is favoured by plastic strain and shear stresses. It is found in many alloys, such as carbon steels, aluminium bronzes, tin bronzes, brasses, etc.

(b) After quenching and re-heating at increasing temperatures, transition precipitates which are coherent with the matrix are first formed, visible precipitation then occurs and finally – if the soluble element content is below the saturation limit – the precipitates are dissolved.

(c) The quite distinctive effect of plastic strain and shear may be explained on the basis of the following assumptions:

The martensitic transformation under load takes place in the neighbourhood of slip barriers in overstressed regions, these slip barriers being stable with respect to slip but unstable with respect to shear strain which causes lattice change. Residual stresses due to cooling and those due to previous work-hardening play the same role as external loads; their action is consistent with the assumptions laid down earlier in this chapter.

(d) Ageing after quenching and after deformation is caused by the combined action of residual stresses and recovery which completes the transformation at the overstressed but stable points and produces local annealing at the overstressed but unstable points, where disturbance of the equilibrium generates localized mechanical shocks. This allows the following statement:

Alternating fatigue loading aids the martensitic transformation, which may modify the distribution of hard regions, concurrently with recovery and work-hardening. The volume expansion that accompanies the transformation may induce local compressive and tensile stresses.

2.5 COMMON FEATURES AND DIFFERENCES IN STATIC AND FATIGUE FAILURES

The quantitative technical aspect of the various types of failure will be dealt with later. Here an attempt is made to show how identical processes of plastic deformation can lead to qualitative differences in the behaviour of metals with respect to the various types of failure, i.e. static failure, creep failure, and fatigue failure.

2.5.1 Static Failure

On a cylindrical *tension* specimen, the presence of a free surface makes plastic deformation easier in peripheral regions, where tensile stresses are reduced and hardening slowed down, which implies that the stress concentrations around slip barriers are lower in those regions than in the core of the test piece.

Consequently, damage before cracking is more advanced in the core of the specimen. If the test is continued, the microscopic cracks in the core join to produce a central crack (see Bluhm and Morissey[75]) in the necked-down portion of the specimen corresponding to a *reduction in area*, the cylindrical form of specimen being unstable. The front of the central crack is subject to a high stress concentration; the latter relaxes shear on facets at 45° to the crack plane and at the same time generates microcracks which are developed by a further increase of the load; the same phenomenon is repeated on another facet perpendicular to the first and at 45° to the mean plane of the crack which remains perpendicular to the tensile axis. From a given crack size, the tensile stress increases sufficiently by diminution of the area in tension to cause almost instantaneous crack propagation and final fracture.

High stresses favour a greater width of the last crack extension at 45° to the mean plane and result in a conical appearance of the fracture although the surface condition is still rough on a small scale. The *conventional cup and cone fracture of ductile metals* results. The cone shape may also be attributed to rapid *adiabatic shear* failure with a local increase in temperature. Indeed, Zener and Hollomon[88] have shown that in impact punching of steel plates the deformation is localized on a thin cylinder where the existence of martensite proves that there has been a significant increase in temperature followed by rapid cooling. Bevelled fracture may, however, appear in slow failure, as is sometimes the case before final fatigue fracture in thin sheets.

Failure in *torsion* originates at the surface on a transverse plane perpendicular to the tensile axis and results from microcracks created by plastic shear strain. McLean[87] explains this by the fact that during torsion the deformation of crystals causes their slip planes to be swept by the longitudinal plane of the specimen whereas the transverse plane remains stationary with respect to the grains. Another possible reason is that the screw deformations of the generating lines of the specimen induce longitudinal elastic tensile stresses which are proportional to the square of the elastic shear strains and are balanced by compression of the core.

Hydrostatic pressure, according to Bridgman[58], enables large shearing strains to be obtained even with brittle materials such as marble and increases the amount of strain necessary to cause rupture of the metals; the initiation and joining of microcracks require greater plastic deformation leading to higher microscopic stress concentrations.

Hydrostatic tension is very difficult to achieve; a condition which is close to it is the state of triple tensile stress in the core of specimens severely notched by deep annular grooves. However, the detrimental effect of tension is opposed by and often cancelled out by the reduction in shear. If the metal is not very ductile, fracture may begin at the root of the notch, where shear is significant. This question will be examined in more detail at the beginning of Chapter IV.

Brittle fracture is not easy to define. For specialists in metallography, it means fracture with lack of cohesion perpendicular to a cleavage plane or to a grain boundary. On the scale of the specimen, it is fracture perpendicular to the direction of tensile stress, which involves no necking or 45° facets and originates at a surface defect or a surface stress concentration. In torsion, brittle fracture tends to be of helical form.

Some authors state that brittle fracture is aided by the existence of an excessively small margin between the offset yield strength and the static rupture strength of metals. This assertion is questionable for most of the engineering alloys, as we shall see in the following chapters. In fact, *ductility*, which is the property in contradistinction to *brittleness*, is measured by the elongation prior to failure or by the reduction in area defined as $\Sigma = 1 - A/A_0$, where A/A_0 is the ratio of the fractured area to the initial cross-sectional area of the specimen. Brittleness is characterized by a small reduction in area and by a fracture propagated from a surface defect along a plane perpendicular to tensile stress.

2.5.2 Creep and Activation Energy

Creep deformation under constant stress increases with time; the static test is one specific case of creep under high stress increasing over a very short period of time. At moderately elevated temperatures and during the first stage of creep at decreasing rate (*primary creep*), the mechanisms of deformation are the same for creep as for static testing: lattice distortions which relax by dislocation migration to the boundaries of sub-grains (polygonization) are initially created by slip; at any moment the deformation involves new dislocations which generate slip barriers, relieved by thermal agitation. If the strain rate is constant, as in *secondary* or *steady-state creep*, the creation of new slip barriers balances exactly the relaxation of those formed earlier. The resulting sub-structure remains fairly constant through readjustment of its boundaries. A fine sub-structure forms at the grain boundaries and may exhibit apparent slip along these boundaries.

Under large deformations some grain boundaries are displaced by atomic diffusion, atom by atom; hence the shape of such grains is preserved despite large overall deformations. This second mechanism may prevail at elevated temperatures.

When the strain rate, $d\epsilon/dt$, increases before final rupture during the so-called *tertiary creep stage*, cavities are found at the grain boundaries. Such cavities may join to form cracks under the influence of tensile stresses and final fracture is often *intergranular*. Depending on the metals and their initial condition, failure of a specimen is the result of large elongation with a significant reduction in the cross-sectional area (ductile fracture) or the result of small elongation after formation of intergranular cavities by coalescence of vacancies.

The balance achieved during secondary creep between the creation of slip barriers and their disappearance by thermal agitation justifies the attempts made to characterize the stability of such obstacles to slip with respect to the effect of temperature. Dorn[98] and other authors have shown that creep tests on metals such as aluminium alloys and copper obey the law

$$\epsilon = f(te^{-Q/RT}) ,$$

where the activation energy Q is calculated to give the best adjustment if the absolute temperature T varies, ϵ being the elongation per original unit length and t the time.

However, some imperfections in the crystal lattice, such as solute foreign atoms, vacancies, anchored dislocations, and so on, exhibit a temperature-dependent equilibrium concentration. If complete statistical disorder in the space distribution of imperfections and statistical independence of the variations are assumed, Boltzmann's statistical mechanics allow the expression of the equilibrium concentration c to be written as follows:

$$c = Ae^{-U/kT} ,$$

where c is the mean concentration per atom of the lattice,
U expressed in terms of electron volts, is the free formation energy of an imperfection,
$k = 1.371.10^{-16}$ erg/Kelvin degree, is the Boltzmann's constant,
T the absolute temperature,
A a coefficient close to unity, after Friedel[97].

The number of all imperfections contained in a molecule-gram, also referred to as mole, is

$$C = ALe^{-Q/RT} ,$$

where the thermal activation energy Q is expressed in cal.-g per mole,
$L = 6.06.10^{23}$ is Avogadro's number (atoms per mole),
$R = kL = 1.98$ cal.-g/degree, is the gas constant (1,000 cal.-g per mole = 0.1135 eV/atom).

In diffusion processes, if N is the number of particles per unit volume and $\partial N/\partial t$ the flow per unit surface along an x-direction, we have

$$\frac{\partial N}{\partial t} = D \frac{\partial^2 N}{\partial x^2} ,$$

where the diffusion factor D is defined by

$$D = Be^{-Q/RT} ,$$

B being independent of T and Q representing the diffusion activation energy.

Kennedy[89] suggests that the dislocation movement in aluminium crystals with no other defects involves $Q = 3.4$ kg-cal/mole. The formation of dislocation clusters by multiple slip corresponds to $Q = 12$ kg-cal/mole; we have 23 kg-cal/mole for transverse slip, 27.9 kg-cal/mole for self-diffusion and 31 kg-cal/mole for recrystallization. All these processes occur by atomic steps and are comparable to diffusion but with different activation energy values. It is sometimes concluded that a mechanism of deformation may be operative when its activation energy is compared with that of the macroscopic effect, e.g. elongation.

The activation energy for creep at high temperatures is close to that of self-diffusion but, according to Kennedy, this can be explained as much by grain boundary migration as by dislocation climb with vacancy diffusion. At moderately elevated temperatures, other mechanisms take place in work-hardened engineering alloys since it is hardly likely that only one activation energy is involved.

On the other hand, activation energy only measures the stability under thermal agitation. For mechanical deformation in general and creep in particular, stress plays a predominating part; the activation energy often decreases with increasing stress. Now stress varies from one crystal to another in polycrystalline metals. If one grain yields under high stress over an appropriate period of time at a temperature T, the load will be transferred to the neighbouring grains where the stress will increase, thus reducing the time required for these grains to yield in their turn as their activation energy is diminished. This phenomenon is apparent in carbon steel owing to stabilization by the carbon atom arrangement and it accounts for the almost instantaneous formation of *Lüders lines* caused by ar avalanche disappearance of slip barriers on all the grains.

The same phenomenon takes place on a microscopic scale: some deformation barriers are stressed in parallel and deformation can only become significant when incubation by thermal agitation has reduced some of them by overstressing the others, thus decreasing their activation energy. This may also be expressed in the following terms:

The assumption of statistical independence for similar occurrences has not been substantiated and Boltzmann's statistics do not apply.

The diffusion theories for creep are successful with metals of simple structure since the stability of deformation barriers becomes more homogeneous by the selective action of stress and deformation. They fail, however, with engineering alloys because of the heterogeneous stability of structure defects.

To establish a quantitative theory, statistical distributions of the position and stability of slip barriers under the action of stress and thermal agitation should be assumed and measured. Moreover, statistical mechanics should be developed with more complex assumptions than Boltzmann's with respect to the probability of a given occurrence if a similar occurrence has taken place in the vicinity. The present work is confined to a qualitative description of the phenomena and to the statement of qualitative laws.

2.5.3 Fatigue

Fatigue loading is essentially characterized by the periodic reversal of stress. As under steady static loads, deformation conducive to damage results from plastic slip and microcracks form on the slip planes of grains. However, alternating dislocation motion has two consequences:

(a) Obstacles created by slip are partially eliminated during each half-cycle;

(b) Foreign atoms "drained" to slip barriers by the dislocation movement increase the stability of slip barriers that do not disappear at the beginning of fatigue.

Reversal of the stress destroys obstacles of low stability and, by causing more diversification in the geometrical distribution of the plastic stiffness (hardening rate) of crystalline lattice distortions, it concentrates the stress on small domains.

Development before crack initiation is governed by plastic deformation, hence by shear. Slip, which in work-hardened engineering metals is small during the first cycles, increases at the beginning while destroying slip barriers on neighbouring planes. For stresses below the fatigue limit, the number of effective slip planes approaches a limit, as stated by Gough[7]. Large distortions are localized in the immediate vicinity of the fracture area. Plastic development in fatigue is rapid if the slip deformation due to shear is large; it governs the crack growth before each propagation of the crack front.

Pre-cracking damage is associated with the plastic deformation of favourably oriented surface grains which exhibit a lower hardening rate, $d\tau/d\gamma$. In addition, the surface includes geometrical irregularities resulting in stress concentrations. Thus cracking originates at the surface, unless there are large internal defects.

Direct observations of the initiation of surface cracking have been carried out chiefly on pure metals or simple alloys specially manufactured for laboratory tests purposes. The publications of Gough[7], Laurent[43], Forsyth[90] and Craig[91] emphasize that cracks appear in slip bands and that slip bands contain regions of unequal resistance to plastic deformation.

Forsyth's most recent investigation shows that, apart from crevices, there are other surface features such as extrusions, which suggests local irregularities in the resistance to glide at the surface of the grains. Wood[92] has made the assumption that reverse slip is responsible for these surface undulations. Alternating shear stresses applied to a pack of cards would give a similar effect if friction between the cards was variable. It is possible that local tensile and compressive stresses are responsible for the formation of crevices and extrusions where the metal is softened by some plastic deformation mechanism.

Forsyth[93] has observed two stages in the development of cracks. During stage I, the cracks form at the surface on those crystallographic slip planes that are closest to the maximum shear planes and they extend

inwards in the slip direction. This type of propagation often terminates at grain boundaries. Stage I is favoured by low stresses with slow crack propagation, and by corrosion. It follows on as a continuous process from the initiation stage, and is governed by shear stresses.

During stage II, crack propagation occurs along a mean plane perpendicular to the highest tensile stress. Fracture reveals ridges or small parallel plateaus ploughed by grooves in the direction of propagation and by striations perpendicular to this direction. Each striation indicates a stop of the crack front and each growth increment comprises a double deviation of the crack in relation to its mean plane. Progress prior to the passage of the crack front and in the immediate neighbourhood of the latter is governed by local shear. The propagation itself is controlled by the tensile stresses which are composed of the stresses on the geometrical scale and of local stress variations resulting from heterogeneous shear. The effect of geometrical stresses is significant if the metal is brittle and if cleavage fracture predominates. Stage II may be delayed by surface compressive stresses and favoured by mean tensile stresses as well as by high alternating stress levels. It is the common form of fatigue cracking observed in component failures.

Final static fracture occurs when the cross-sectional area of the specimen is sufficiently reduced by the crack.

If fatigue corresponds to an increasing diversification in plastic resistance to slip, or to a diminution of the entropy, the action of heat must eliminate the influence of the load cycle as soon as thermal agitation is sufficiently high to prevent stabilization of the deformation barriers. There is a range of high temperatures for each metal in which the unit time for damage is no longer the cycle but the second. Creep behaviour under fluctuating stress with a permanent component is then obtained.

2.5.4 Conclusion

The aim was to highlight all aspects of the phenomena under review, and in particular to explore interactions. An attempt was then made to determine whether the qualitative relationships so obtained were confirmed or invalidated by other phenomena which take place more rarely. The method is an overall investigation of statistical qualitative nature of a large number of related phenomena, rather than the more usual study of a particular phenomenon. It involves, of necessity, assumptions that may sometimes seem questionable to specialized researchers.

In this field an engineer is faced with dispersed and occasionally contradictory statements of specialists, and with the scatter and apparent contradiction of the experimental fact. In the present state of the art, few valid predictions can be made by formal computation because of the lack of scientific quantitative laws, and much progress might be made if the engineer could rid himself momentarily of every intellectual inhibition in connection with the physical mechanics of metals and related sciences or techniques. If he is convinced that formal rational fatigue analysis of structures cannot be achieved in the foreseable future, he must envisage technical testing with the best possible representation of those environmental parameters that qualitative analysis has indicated as significant.

REFERENCES

1. Barrois, W. — *Déformations Plastiques et Fatigue des Métaux*. ONERA, Mémo Technique No. 27, 1963, Manuscript, October, 1952.
2. Barrois, W. — *Théorie de l'Evolution des Métaux Pendant la Fatigue*. Revue de Métallurgie, LV, No. 8, 1958.
3. Barrois, W. — *Le Fluage des Métaux dans les Cellules d'Avions*. DOC - AIR-ESPACE, No. 84, January, 1964.
4. Griffith, A.A. — *The Phenomena of Rupture and Flow in Solids*. Phys. Trans. Roy. Soc., Vol. 221, 1920, p. 163.
5. Joffe, - — *The Physics of Crystals*, 1928.
6. Schmid, E.S. Boas, W. — *Kristalplastizität*. Springer, 1935.
7. Gough, H.F. — *Crystalline Structure in Relation to Failure of Metals, Especially by Fatigue*. Proc. A.S.T.M., Vol. 33, 1963.
8. Dehlinger, U. — Ann. Physik, Vol. 5, 1929, p. 2.
9. Taylor, G.I. — Proc. Roy. Soc., Vol. A 145, 1934, p. 362.
10. Orowan, E. — Z. Physik, Vol. 89, 1934, p. 634.

11. Polanyi, M. — Z. Physik, Vol. 89, 1934, p. 660.

12. Burgers, J.M. — Proc. Kon. Ned. Akad. Wet., Vol. 42, 1939, pp. 293 and 378.

13. Frank, F.C.; Read, W.I. — Phys. Rev., Vol. 79, 1950, p. 722.

14. Hirsch, P.B. — *Observations et Cinématographie au Microscope Electronique de l'Arrangement et du Mouvement des Dislocations dans les Métaux.* Conference held Feb. 20, 1958. Société de Metallurgie, Paris.

15. Barrett, C.S. — *The Crystallographic Mechanisms of Translation, Twinning and Banding.* In *Cold-working of Metals.* Published by A.S.M., 1949.

16. Mathieu, J.P. — *Spectres de Vibration et Symétrie des Molécules et des Cristaux.* Paris, 1945.

17. Cottrell, A.H. — *The Formation of Immobile Dislocations during Slip.* Phil. Mag., Vol. 43, June, 1952, p. 643.

18. Averbach, B.L. — *The Effect of Plastic Deformation on Solid Reactions.* Part I: Diffusion, reactions. In *Cold-working of Metals.* A.S.M., 1949, p. 262.

19. Nye, J.F. — *Mise en Evidence des Tensions Internes et des Dislocations dans les Métaux par le Comportement Photo-Elastique du Chlorure d'Argent.* Revue de Métallurgie, Paris, June 1949, p. 371; Proc. Roy. Soc., Vol. A 198, 1949, p. 190, Vol. A 200, p. 48.

20. Heidenreich, R.D.; Shockley, W. — *Study of Slips in Aluminium Crystals by Electron Microscope and Electron Diffraction Methods.* Report on Strength of Solids, Phys. Soc., 1947.

21. Taylor, G.I.; Elam, C.F. — Proc. Roy. Soc., Vol. A 112, 1926, p. 337.

22. Cahn, R.W. — *Slip and Polygonization in Aluminium.* Journal Institute of Metals, Vol. 79, May 1951, p. 129.

23. Volley, R.L. — *Work-hardening in Polycrystalline Pure Metals.* Phys. Soc. Report on Strength of Solids, London, 1948.

24. Yamaguchi, K. — Sci. Papers Inst. Phys. Chem. Research, Tokyo, Vol. 8, 1928, p. 289.

25. Brown, A.F. — *Slip Bands and Hardening Processes in Aluminium.* The Journal of the Institute of Metals, Publication No. 1331, Nov. 1951, (3), p. 115.

26. Bauschinger, J. — *Changes in Yield Limits Under Cyclically Varying Stress* (in German). Civil Ingenieur, 1881.

27. Kuntze, W.; Sachs, G. — *Der Fliessbeginn bei wechselnder Zug-Druckbeanspruchung.* Mitt. der Materialprufungsanstalten, Vol. 14, 1930, p. 77.

28. Karpof; quoted in: Bolchanina, M.A. — *Hardening and Relaxation, Basic Phenomena in Plastic Deformation* (in Russian). Science Acad., U.R.S.S., Series Physics, tome XIV, No. 2, 1950, p. 223. This paper is a review on works by several Russian researchers.

29. Bairstow, L. — *The Elastic Limits of Iron and Steel under Cyclical Stress Variations.* Phil. Trans. Roy. Soc. A, P. 210, 1910.

30. Polakowski, N.H. — *Magnetic Properties, Internal Strains and the Bauschinger Effect in Metals.* Nature, Vol. 168, Nov. 1951, p. 838; *Softening of Metals During Cold-Working.* Journal of the Iron and Steel Institute, Vol. 169, Dec. 1951, London, p. 337.

31. Ludwik, P. — Z.f. Metallkunde, Vol. 11, 1919, p. 157.

32. Kochendörfer, - — *Plastische Eigenschaften von kristallen und metallischen Werkstoffen.* Berlin, 1941.

33. Morgan, H.E. — *Cold-pressing of Steel.* Institution of Automobile Engineers, Report No. 8601 B, Class. 81, 1936, p. 51.

34. Grainger, J.A. — Sheet Metal Industries, Vol. 23, 1946, pp. 1568 and 1923.

35. Feitknecht, W. — Journ. Inst. Metals, Vol. 35, 1926, pp. 131, 165.

36. Bowles, J.S.; Boas, W. — Journ. Inst. Metals, Vol. 74, 1948, pp. 501, 519.

37. Goss, N.P. Bronner, W. — Trans. A.S.M., Vol.30, 1942, pp.936, 945.

38. Czochralski, J. — Z., Metallkunde, Vol.17, 1925, p.1.

39. van Arkel, A.F. van Bruggen, M.G. — Z.f. Physik, Vol.80, 1933, p.804.

40. Polakowski, N.H. Palchouduri, A. — *Softening of Certain Cold-worked Metals under the Action of Fatigue Loads.* Proc. A.S.T.M., 1954, p.701.

41. Coffin, L.F., Jr. — *The Problem of Thermal Stress Fatigue in Austenitic Steels at Elevated Temperatures.* Publication A.S.T.M., S.T.P. No.165, 1954, p.31.

42. Crussard, C. Guinier, A. — Revue de Métallurgie, Vol.46, 1949, p.61.

43. Laurent, P. — Publication Scientifique No.256 du Ministére de l'Air, Thèse 10 Janvier 1951, Paris.

44. Wilms, G.R. Wood, W.A. — *Mechanism of Creep in Metals.* Journ. Inst. of Metals, Vol.75, 1949, p.693.

45. Garrod, R.I. et al. — *An Electron Microscope Study of the Effect of Temperature and Strain-Rate on the Mechanism of Deformation of Aluminium.* Phil. Mag., Vol.43, June 1952, p.677.

46. Forsyth, P.J.E. Stubbington, C.A. — *The Slip Band Extrusion Effect Observed in Some Aluminium Alloys Subjected to Cyclic Stresses.* R.A.E., Farnborough, Report Met.78, Jan. 1952.

47. Hutchison, T.S. — *Cold-working of Aluminium at Low Temperatures.* Nature, Vol.162, 1948, p.374.

48. Woods, D.S. Clark, D.S. — *Delayed Yield in Annealed Steels of Very Low Carbon and Nitrogen Content.* Trans. A.S.M., Vol.44, 1952, p.726.

49. Lacombe, P. — *Sub-Boundary and Boundary Structures in High Purity Aluminium.* Phys. Soc., Report on Strength of Solids, 1948.

50. Cottrell, A.H. — *Theory of Dislocations.* Progress in Metals Physics, London, 1948.

51. Holden, A.N. Kunz, F.W. — *Note on the Strain-Ageing of Iron Single Crystals.* Journal Appl. Physics, Vol.23, July 1952, p.799.

52. Portevin, M. — C.R. Acad. Sc. Vol.167, 1918, p.531; Vol.169, 1919, p.955; Vol.175, 1922, p.959; Vol.186, 1928, p.939.

53. Horger, O.J. — *Residual Stresses.* Chap.11 of *Handbook of Experimental Stress Analysis.* Hetenyi, 1950.

54. Wood, W.A. Dewsnap, N. — Journ. Inst. Metals. Publication No.1241, March 1950, p.65.

55. Wilson, D.W. — Nature, Vol.167, 1951, p.899.

56. Rosenthal, D. — Journal Applied Physics, Vol.20, Dec. 1949, p.1257.

57. Paterson, M.S. Orowan, E. — Nature, Vol.162, 25 Dec. 1948, p.991.

58. Bridgman, P.W. — Journal Applied Physics, Vol.20, Dec. 1949, p.1241.

59. Megaw, H.D. Stokes, A.R. — In Mehl, Ref. 60.

60. Mehl, R.F. — *Recrystallization.* Metals Handbook, 1948, p.259.

61. Rusch, V.D.I. — Annual Meeting; Festigkeits Kolloquium, Stuttgart, May 29, 1952.

62. Kaiser, - — Archiv. Eisenhüttenwesen, Vol.24, (1/2), 1953, p.43.

63. Burgers, W.G. — Conférence au IX Congrès SOLVAY, Bruxelles, 24-29 Sept. 1951.

64. Averbach, B.L. — Metals Trans., Vol.185, 1949, p.491.

65. Kuhlman, D. et al. — Z. Metallkunde, Vol.40, 1949, p.241.

66. Crussard, C. — Conférence aux Journées de Physique des Métaux, Paris, 1952.

67. van Arkel, - — Revue de Métallurgie, Vol. 33, 1936, p. 197.

68. van Liempt, J.A.M. — Z. Anorg. Allg. Chem., Vol. 195, 1931, p. 366.

69. Calvet, J. et al. — La Recherche Aéronautique, No. 26, 1952, p. 47.

70. Beck, P.A. — *The Formation of Recrystallization Nuclei.* Jour. Appl. Physics, Vol. 20, June 1945, p. 633. *Do Metals Recrystallize?* Journ. of Metals (USA), Sept. 1952, p. 979.

71. Rathenau, G.W. Custers, J.F.H. — Philips Res. Rep., Vol. 4, 1949, p. 241.

72. Hanemann, - — In Mehl (Ref. 60).

73. Guinier, A. — C.R., Vol. 208, 1938, p. 1011; Annales de Physique, Vol. 12, 1939, p. 192.

74. Preston, - — Proc. Roy. Soc., Vol. A 167, 1938, p. 526.

75. Bluhm, J.I. Morissey, R.J. — *Fracture in a Tensile Specimen.* Proc. First International Conference on Fracture, Vol. 3, 1965, pp. 1739-1780.

76. Kawai, T. — Science Report, Tonoku University, 1st Series, Japan, Vol. 22, 1933, p. 354.

77. Hanstock, R.F. — Journ. Inst. of Metals, May 1948, p. 469.

78. Delbart, G. Ravery, M. — Revue de Métallurgie, June 1949.

79. Andrew, J.H. — Revue de Métallurgie, April 1949, p. 238.

80. Ballufi, R.W. et al. — Trans. A.S.M. Vol. 43, 1950, p. 497.

81. Troiano, A.R. Greninger, A.B. — *The Martensite Transformation.* Metals Handbook, 1948, p. 263.

82. McReynolds, A.W. — Journ. Applied Physics, Vol. 20, Oct. 1949, p. 896.

83. Greninger, A.B. — Trans. A.I.M.E., Vol. 133, 1939, p. 204.

84. Scheil, E. — Z.f. anorg. u. allg. Chemie, Vol. 207, 1932, p. 21.

85. Greninger, A.B. Mooradian, V.G. — Trans. A.I.M.E., Vol. 128, 1938, p. 337.

86. French, H.J. — Trans. Am. Soc. Steel Treatment, Vol. 21, 1933, pp. 899, 946.

87. McLean, D. — *Mechanical Properties of Metals.* Wiley and Sons, 1942.

88. Zener, C. Hollomon, J.H. — *Effects of Strain Rate upon Plastic Flow of Steel.* J. Applied Physics, Vol. 15, 1944, p. 22.

89. Kennedy, A.J. — *Processes of Creep and Fatigue in Metals.* Oliver and Boyd, 1962.

90. Forsyth, P.J.E. — *Some Metallographic Observations on the Fatigue of Metals.* J. Inst. Metals, London, Vol. 80 (4), Dec. 1951.

91. Craig, W.J. — Technical Report No. 27, Urbana, Illinois, Feb. 1952.

92. Wood, W.A. — *Symposium on Basic Mechanisms in Fatigue.* A.S.T.M., 1959, p. 110.

93. Forsyth, P.J.E. — *A Two Stage Process of Fatigue Crack Growth.* Crack Propagation Symposium, Cranfield, 1961.

94. Keh, A.S. — *Work Hardening and Deformation Sub-Structure in Iron Single Crystals Deformed in Tension at 298°K.* Phil. Mag., Vol. 12, No. 115, July 1965, pp. 9-20.

95. Gilbert, A. et al. — *The Effect of Strain Rate on Dislocation Multiplication in Polycrystalline Molybdenum.* Phil. Mag., Vol. 12, No. 117, Sept. 1965, pp. 649-653.

96. Cuddy, L.J. *An Electrical Resistivity Study of Deformation of Iron at Low Temperature.* Phil. Mag., Vol.12, No.118, Oct. 1965, pp.855-865.

97. Friedel, J. *Les Dislocations.* Gauthier-Villars, Paris, 1956.

98. Dorn, J.E. Journal Res. Phys. Solids, Vol.3, 1955, p.85.

CHAPTER III

STATIC TESTS OF SPECIMENS - CREEP

STATIC TESTS OF SPECIMENS - CREEP

Having studied in detail the mechanism of development towards failure in metals subjected to stresses inducing plastic strains, we shall now consider the mechanical behaviour of metals from a point of view that is closer to the technology of mechanical tests. We shall sometimes use the laws and assumptions set forth in Chapter II. We shall keep in mind the profound unity they reveal in the mechanical and thermal behaviour of metals. The classification of the type of loadings under headings such as static tests, creep tests, fatigue tests, is rather arbitrary. It will be seen that the study of fatigue strength at room temperature requires some knowledge of the specific features of static tests and that the study of hot fatigue must be preceded by a study of creep.

3.1 TENSILE TESTS, HARDNESS TESTS, NOTCH-IMPACT TESTS

The deformation and tensile rupture test can be carried out in two different ways. If it is performed with a test duration ranging from one second to one minute, and if the strain rate remains fairly constant, it is called a *static tensile test*, which yields a stress σ-**strain** ϵ **curve.** If the load is kept constant and if the test duration is expressed in hours, it is a *creep test*, the result of which is a strain ϵ-time t curve. At constant test temperature the resistance to plastic strain depends on the strain ϵ, the strain rate $\dot{\epsilon} = d\epsilon/dt$ and the time t, owing to strain-hardening and recovery as well as to various metallurgical transformations (recrystallization, precipitation, martensitic transformation) which have been examined in Chapter II. Thus we have

$$\sigma = f(\epsilon, \dot{\epsilon}, t, T) ,$$

where T is the temperature of the specimen.

Static tension corresponds to $\dot{\epsilon}$ = constant and T = constant while creep implies σ = constant. The $\sigma(\epsilon)$ and $\epsilon(t)$ curves represent two complementary aspects of the same physical phenomenon and their characteristics result from the same elementary processes, except for the specific orders of magnitude of the temperature and strain rate of each test. Certain features of the curves are not typical and are due to the method of testing. This applies to the maximum of the stress-strain curves (Figures 3.1 and 3.2). In conventional tests the variation in length of a specimen between two reference marks is recorded as a function of the applied load. The maximum of the load values corresponds substantially to the preferential development of plastic flow in a given section of the specimen length where the cross-sectional area decreases rapidly to form a *neck*. The maximum is not apparent if the true stress, $\sigma^* = P/A$, is plotted (Fig. 3.2) against the true strain, ϵ^*, such that

$$\epsilon^* = \int_{l_0}^{l} \frac{dl}{l} = \log_e(l/l_0) .$$

Assuming that the volume does not change during plastic deformation, we have

$$Al = A_0 l_0 \quad \text{and} \quad \epsilon^* = \log_e(A_0/A) ,$$

where A is the cross-sectional area of the specimen at the neck and A_0 the initial value prior to the test.

Acceptance test specifications use the following symbols to define the tensile test results:

σ_Y *yield strength* at 0.2 offset (which corresponds to a stress leaving a 0.2% strain after unloading);

σ_n *yield stress* at n% residual strain (in France, n = 0.05%, 0.1% and 0.2% for metal qualification tests);

$\sigma_{ult.}$ *ultimate strength*, P_{max}/A_0 ;

A% *permanent elongation* after fracture, measured between two reference marks which are $k\sqrt{A_0}$ apart from one another, k being specified by standards and ranging from 4 to 10, depending on the country and the product (8.16 in France for metals);

$Z\% = 100(1 - A/A_0)$, *reduction in area* at the neck after fracture.

PRECEDING PAGE BLANK

BLANK PAGE

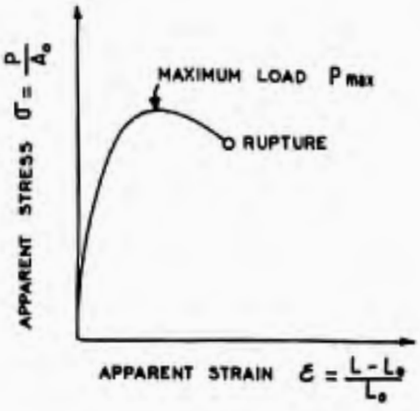

Fig. 3.1 Apparent σ–ϵ curve

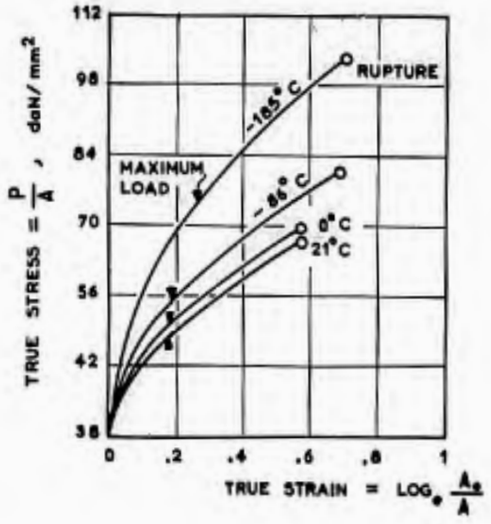

Fig. 3.2 True σ–ϵ curves of brass at different temperatures. From MacGregor[1]

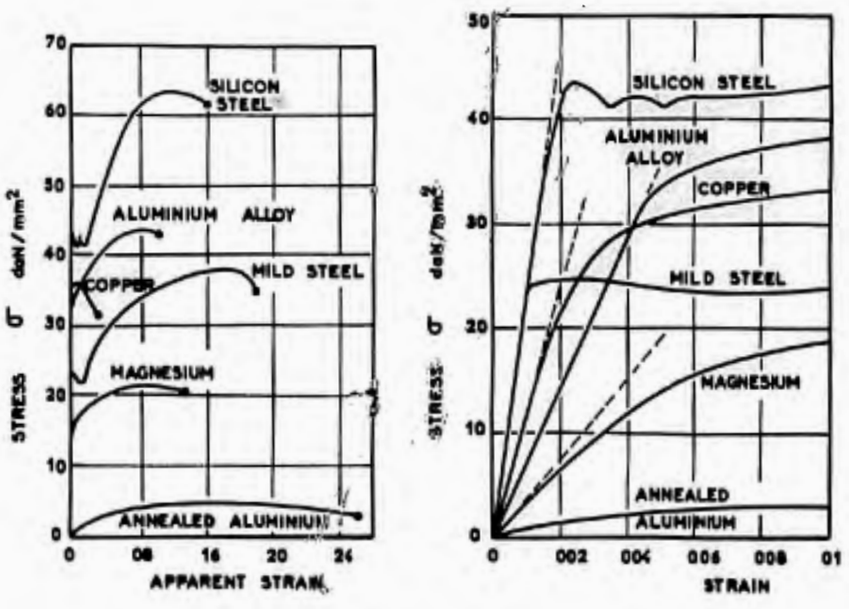

Fig. 3.3 σ–ϵ curves of common engineering metals at two different scales, from Templin and Sturm[2]

TABLE 3.1

Strength Properties of 30 NCD 16 Steel for Several Tempering Temperatures

Composition, per cent: 0.28 C, 3.85 Ni, 1.17 Cr, 0.28 Mo, 0.24 Mn, 0.26 Si. Oil-quenched at 875°C								
	Tempering temperatures							
	without	*200°C*	*300°C*	*400°C*	*500°C*	*550°C*	*600°C*	*650°C*
Rc hardness	49	49	46	44	41	40	36	31
$\sigma_{ult.}$	117	170.5	155.5	157	142.5	123	110	101 daN/mm²
$\sigma_{0.2}$	113.5	125.5	125.5	127	122	111	101.5	85 "
$\sigma_{0.1}$	96.5	113.5	119	120	117	107.5	97.5	78.5 "
$\sigma_{0.05}$	78	100	113	112	113	104	94	72 "
$\sigma_{prop.}$	49	70	100	96	100	92	84	57 "
A%	10	11	10	10.5	9.5	12.5	14.5	17 %
Fatigue, σ_f	90	90	76	72	66	70	68	64 daN/mm²
$\frac{\sigma_{ult.} - \sigma_{0.2}}{\sigma_{ult.}}$	0.31	0.26	0.13	0.18	0.14	0.10	0.08	0.16 "
$\sigma_f/\sigma_{ult.}$	0.51	0.53	0.49	0.48	0.46	0.57	0.62	0.63 "

The relation between true fracture strain and Σ is:

$$\epsilon^*_{ult.} = \log_e[1/(1-\Sigma)] \approx \Sigma + \frac{1}{2}\Sigma^2 + \frac{1}{3}\Sigma^3 + \ldots ,$$

so that $\Sigma \leqslant \epsilon^*_{ult.}$ serves as a measure of the true fracture strain.

Engineers are primarily interested in the deformation under maximum load which may contribute to plastic adjustment before necking. Σ is a measure of the ductility of the metal, which is of importance in cold-working and affects the residual static strength of cracked components. The yield stresses at 0.05%, 0.1% and 0.2% residual strain allow the bend of the stress-strain curve to be defined more accurately and provide a useful basis of comparison for buckling in the plastic range.

Figure 3.3 shows some $\sigma - \epsilon$ curves for engineering metals. At the left, the curves for mild steel and silicon steel exhibit one or two local maximums followed by typical *level* portions. As seen in Section 2.2.3, this phenomenon results from the arrangement of solute carbon atoms in the crystalline lattice vacancies.

The curves for steel and aluminium alloys start with a substantially linear section, the slope of which represents the *modulus of elasticity*, also called Young's modulus. The *proportional limit* is the stress at which the curve starts to deviate from linearity. The *true elastic limit* is the highest stress for which there is no permanent residual deformation after removal of the load. Both limits are somewhat subjective since their values decrease as the accuracy of the measurements increases.

In the case of steel, the first maximum represents the *upper yield point*, variable with the elasticity of the test set-up. The level defines the *lower yield point*, which constitutes a better physical constant although it is affected by the test rate (see Section 3.1.1); this yield point often approaches quite closely the yield strength at 0.2% offset.

Roberts, Carruthers and Averbach[3] have measured the residual plastic strain in various irons and steels as a function of the applied compressive stress. Measuring the permanent strain with an accuracy of 2×10^{-6}, they found a net elastic limit varying from 2/3 to 4/5 of the upper yield point. For pure iron or steel specimens containing free ferrite, the curve gradually rounds off between the elastic limit and the upper yield point. On the other hand, pearlitic steel test pieces exhibit steps in the same portion of the curve (Fig. 3.4); no noticeable aftereffect has been found during checks. The heterogeneous structure of pearlite is revealed by the steps. In *ferritic steels*, previous deformation raises the upper yield point but lowers slightly the true elastic limit (similar to the Bauschinger effect).

The proportional limit varies with the treatment and can be lower for quenched steel with no tempering than for quenched steel "softened" by tempering. Table 3.1 shows how the properties of a weldable alloy steel change with the tempering temperature[4]. The following comment can be made:

1. There is no clear relation between the plastic strain properties of steel during static testing, and the fatigue limit.
2. The material can be simultaneously hard for high stress (Rc hardness) and soft for low stress (small proportional limit).
3. The fatigue limit can lie far above or below the proportional limit $\sigma_{prop.}$
4. There is normally a loose correlation between the static strength $\sigma_{ult.}$ and the fatigue limit σ_f.

3.1.1 The Effect of the Test Rate

The effect of the test rate on the $\sigma - \epsilon$ curve varies to some extent with the material. It can affect the recovery of distributed dislocations, the polygonization of slip bands, recrystallization, the arrangement of solute foreign atoms, precipitation and martensitic transformation: Test rate influences temperature-dependent phenomena and its effect therefore changes with temperature. Figure 3.5 shows that the strain rate at room temperature and at the temperature of liquid air has little influence on the σ-ϵ curve for values which are close to the range of the usual tensile test rates and for commercial US 2S-O aluminium[5].

A significant effect of the test rate is found for temperatures at which creep occurs, as with SAE-1090 steel at 540°C (Fig. 3.6), and for very high strain rate, as with annealed carbon steel (Fig. 3.7). Steel is "harder" in rapid tests since it takes some time for the solute carbon atoms to be expelled by strain from the orderly positions they occupy in the iron lattice. Clark and Wood[7] report comparable effects for SAE-4130 steel (0.13% C, 0.62% Mn, 0.47% Si, 0.81% Cr, 0.16% Mo), oil-quenched at 850°C and tempered 45 minutes at 350°C; the effect is quite distinct if the test duration is less than one-hundredth of a second. Stainless AISI-302 steel (0.15% C, 18% Cr, 8% Ni) exhibits a clearer effect ($\sigma_{0.2}$ increases by 20% for a loading period of less than five-hundredths of a second); this is partially due to the transformation of some austenite into martensite. On the other hand, no significant strain-rate effect is observed in 24 S-T and 75 S-T aluminium alloys for loading periods of more than 1/100 of a second. However, Heimerl and Manning[105] have shown for 2024-T3 aluminium alloy a $\sigma_{ult.} = 70{,}000$ lb/in^2 at conventional speed, 74,000 lb/in^2 for about 0.1 sec. and 80,000 lb/in^2 for a 0.05 sec. test.

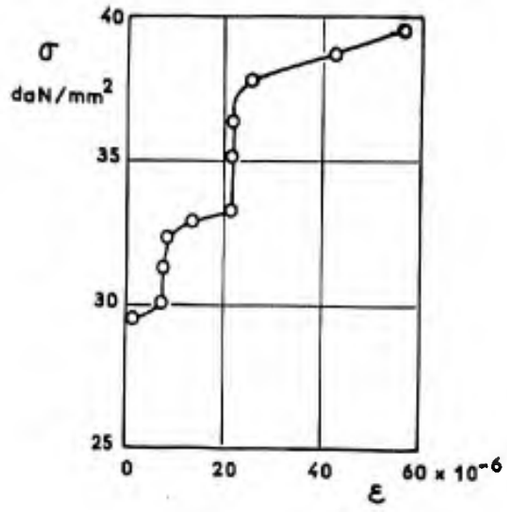

Fig.3.4 Compression of 1.06% carbon pearlitic steel[3]. Permanent discontinuous strain

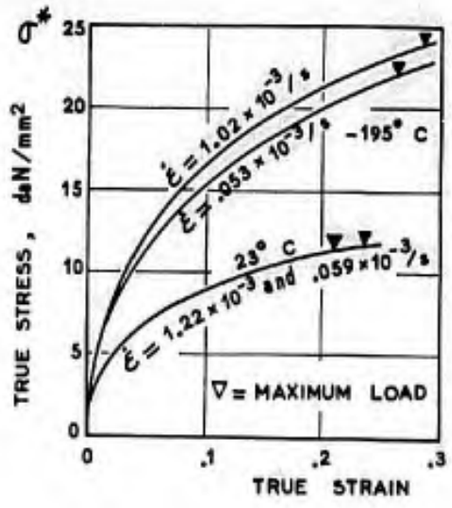

Fig.3.5 Strain rate effect on permanent strain for 2S-O aluminium alloy, from Tietz and Dorn[5]

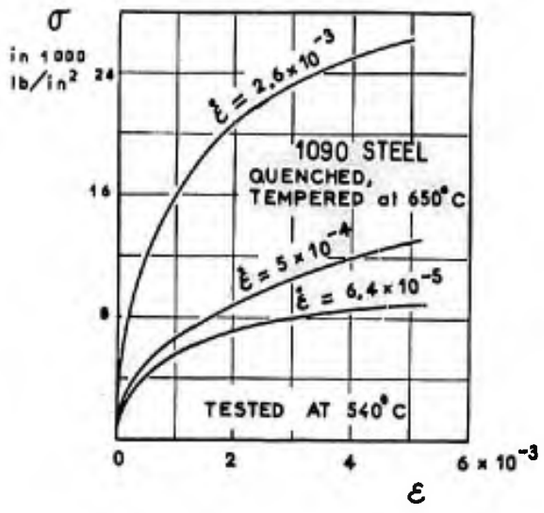

Fig.3.6 Stress-strain curves of 1090 steel at 540°C for various strain rates, from Nadai and Manjoine[6]

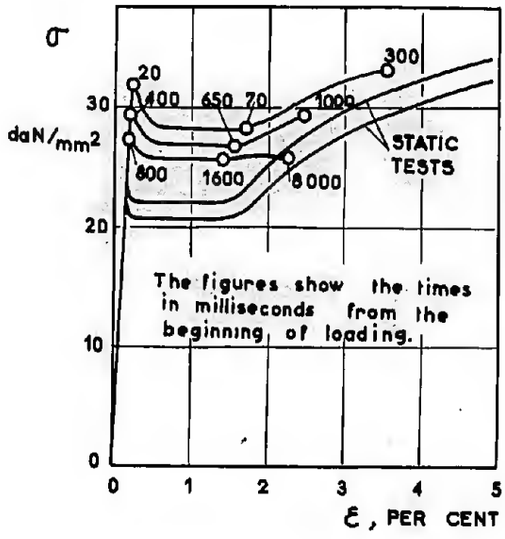

Fig.3.7 σ–ϵ curves of annealed carbon steel subjected to fast loadings, from Clark and Wood[7]

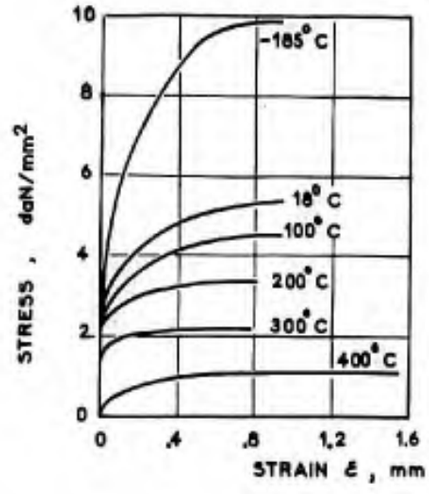

Fig.3.8 Temperature effect on aluminium crystals, from Boas and Schmid[8]

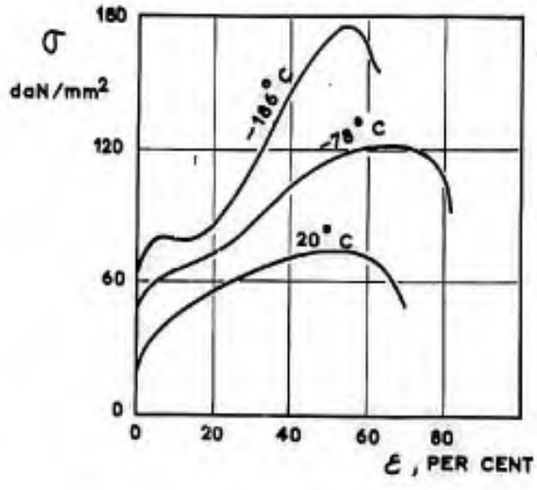

Fig.3.9 Annealed austenitic stainless steel (18 Cr-9 Ni)

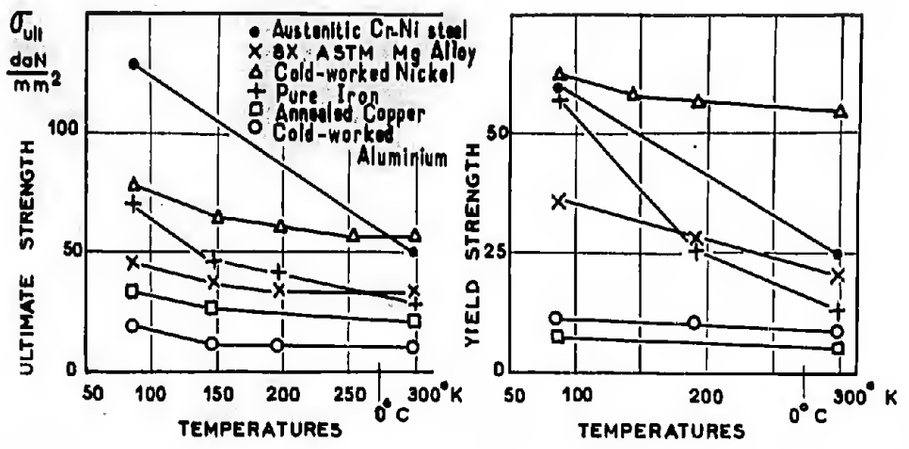

Fig. 3.10 Ultimate and yield tensile strengths at low temperatures, from Seigle and Brick[10]

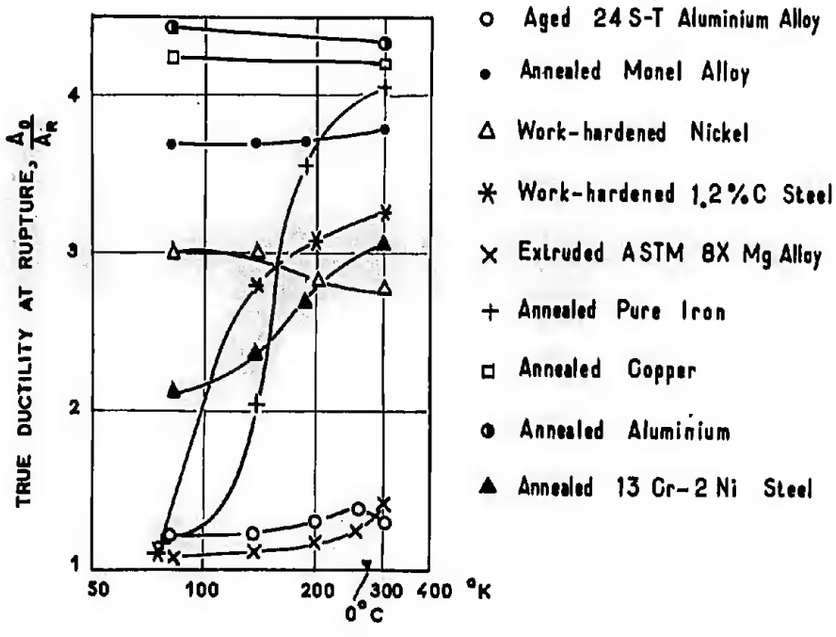

Fig. 3.11 Ductility at low temperatures, from McAdam et al.[9]

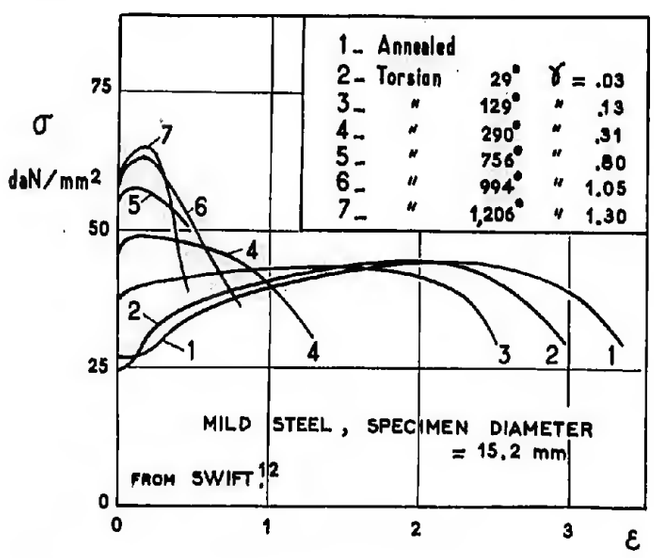

Fig. 3.12 Effect of pre-strain in torsion on the tensile σ-ε curve of mild steel

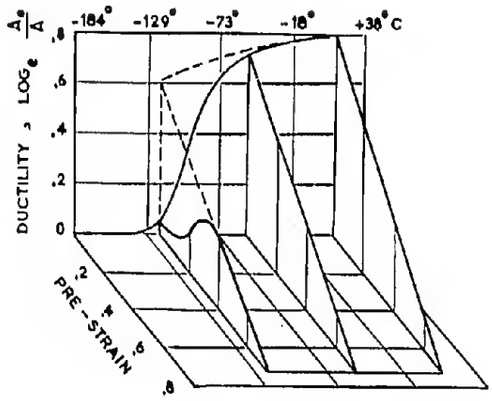

Fig.3.13 Effect of tensile pre-strain at 21°C on ductility, from Ripling and Baldwing[13]

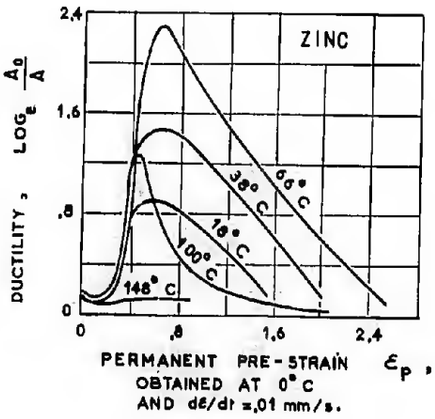

Fig.3.14 Predeformation effect at several test temperatures on the ductility of zinc, from Ref.13

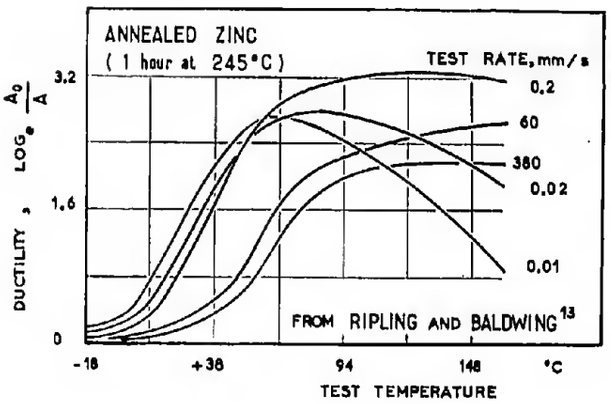

Fig.3.15 Effects of temperature and test rate on the ductility of annealed zinc

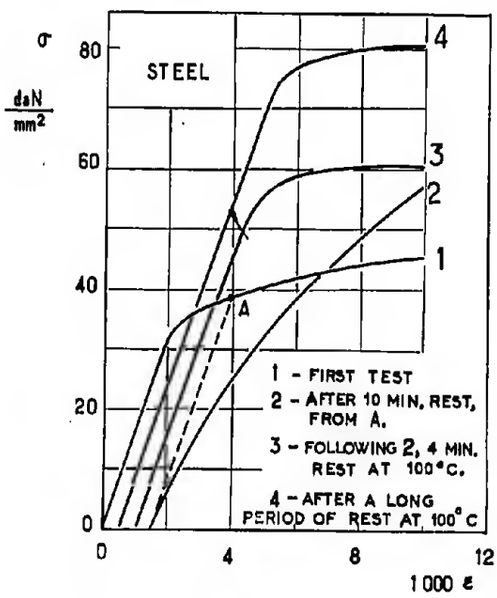

Fig.3.16 Effects of pre-strain and ageing on carbon steel, from Ewing[14]

3.1.2 The Effect of Temperature

Figure 3.8, from Boas and Schmid[8], illustrates the effect of temperature on the stress-strain curve of single aluminium crystals; it is representative of the behaviour of metals having a stable and homogeneous structure.

Figure 3.9 shows the effect of martensitic transformation on the shape of stress-strain curves for stainless austenitic steel, unstable at low temperature[9].

Seigle and Brick[10] have gathered data on the behaviour of engineering metals at low temperatures. The variation of the fracture strength and of the 0.2% offset yield strength is plotted in Figure 3.10.

Figure 3.11 shows the variation of ductility for engineering metals subject to low temperatures. Ductility is defined here as the ratio $A_o/A_{ult.}$ of the initial cross-sectional area to that of the neck after fracture.

All three ferrous metals exhibit a large decrease in ductility below -50°C. Carbon steels are very sensitive to low temperatures while the alloy steels used on aircraft structures behave well.

Kalish and Dunkerley[11] have demonstrated that β-tin, of body-centered tetragonal structure, and tin-lead alloys with a low lead content are brittle below -120°C; at -200°C the strength and the reduction in area are low ($\sigma_{ult.} = 3.6$ daN/mm^2; $\Sigma = 6\%$); around -140°C, the strength passes through a maximum ($\sigma_{ult.} = 10$ daN/mm^2), which corresponds to a sudden increase of the reduction in area, up to $\Sigma = 100\%$. The reduction in area then remains constant and the strength decreases regularly to $\sigma_{ult.} = 1.2$ daN/mm^2 at +40°C. This phenomenon is attenuated if the lead content rises from 5 to 50%. Note that lead crystallizes in the face-centered cubic system like aluminium, copper, nickel, and alloys which are not very brittle in the cold condition, such as austenitic steels.

In the case of iron, the increase in ductility with rising temperature may be explained by the arrangement of foreign atoms in the lattice distortions. Diffusion at very low temperatures is too weak for the solute atoms to be "drained" by the dislocations but the arrangement of such atoms in the distortions is impeded by thermal agitation, so that instability reaches a maximum.

3.1.3 The Pre-Straining Effect

A systematic study of the effect of previous torsion on the tensile test of annealed mild steel has been made by Swift[12]. Previous torsion increases both the ultimate strength (Fig. 3.12) and the yield strength. The true fracture stress and the reduction in area change very little. The effect of torsion appears to be due to lattice distortions occurring on slip planes that are different from those involved in torsion. The true σ^*–ϵ^* curves are parallel; previous torsion seems to raise the stability of plastic strain barriers without modifying the number and relative stability of the obstacles by which fracture is governed. Figure 3.13, from Ripling and Baldwing[13], illustrates the effect of tensile pre-straining on the ductility of steel. At low temperatures, the ductility goes through a maximum if pre-straining reaches a critical value which is higher than the strain in the cold tensile test. At temperatures close to room temperature, the sum of pre-strain and fracture strain is, of course, constant.

The existence of a critical pre-strain is more distinct for zinc, of hexagonal close-packed crystal structure. Ripling and Baldwing have studied the effect of test rate, temperature and pre-straining on the ductility of zinc (Figures 3.14 and 3.15). There is a critical pre-strain value below which ductility is not improved in the high temperature test; the temperature range for which ductility improves is shown to be small for large pre-strains. We believe that this phenomenon is associated with some recrystallization or polygonization process (see Chapter II) and that the material remains brittle if no local recrystallization takes place or if it takes place too early in the tensile test.

Ewing[14] has investigated the effect of rest and ageing at 100°C on carbon steel. If, after a first loading and removal of the load, a tensile test 1, interrupted at A (Fig. 3.16), is resumed immediately, the material is substantially elastic until the stress returns to that of point A (dotted curve). After a 10 minutes' rest at room temperature, curve 2 is obtained: the metal has become softer under low stress and harder under high stress. This is equivalent to the Bauschinger effect of the second order mentioned in Section 2.1.3 for aluminium alloy; indeed, the first loading eliminates some obstacles to plastic strain while creating others that are more stable if the test is continued immediately; during the period of rest there is a recovery process which causes most of the new obstacles to disappear. If the metal is loaded again (curve 2), it exhibits less plastic stiffness and the deformations give rise to a large number of new slip barriers with lower internal stresses. A rest at 100°C enables the carbon atoms to settle in the remaining obstacles, which become more stable. In this way, a harder metal is obtained (curve 3) until the stress is high enough to overcome the new slip barriers, the stability of which is more uniform. Curve 4 was obtained after further stressing and exposure to 100°C. This straining and recovery may be continued until the specimen exhibits brittle fracture for a stress value considerably in excess of the standard ultimate strength of the metal.

The effect of cold-rolling and ageing after rolling on the σ–ϵ curve of mild steel is illustrated in Figures 3.17 and 3.18.

After deformation at temperatures between 150°C and 300°C or after heating in the range of 150°C to 300°C, the impact strength decreases at room temperature. Between 200°C and 300°C, the ductility is reduced (Fig. 3.19). This phenomenon is called *blue brittleness* and can be encountered at lower temperatures after longer periods of heating. Ripling[18] reports that titanium containing hydrogen exhibits a somewhat similar feature. We believe

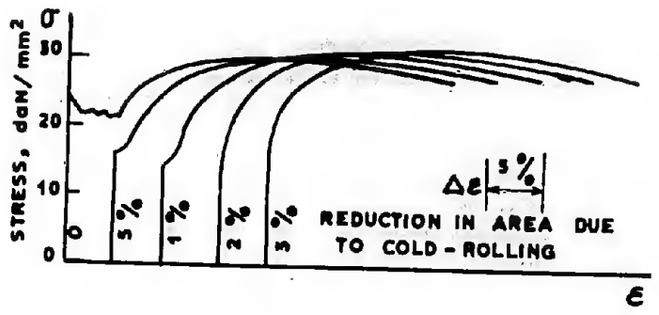

Fig.3.17 Mild steel - effect of cold-rolling on σ-ϵ curves

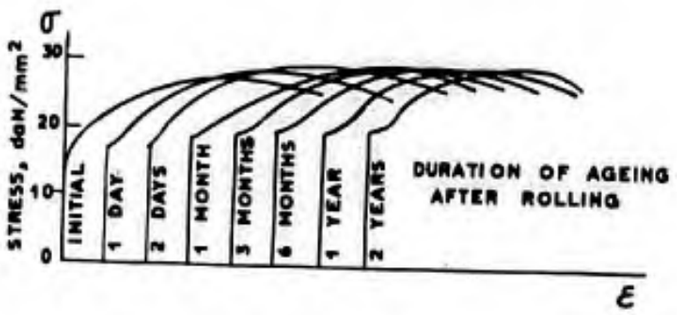

Fig.3.18 Mild steel - ageing

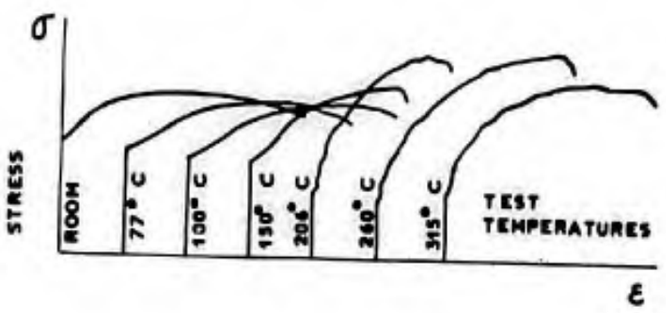

Fig.3.19 Mild steel - blue brittleness

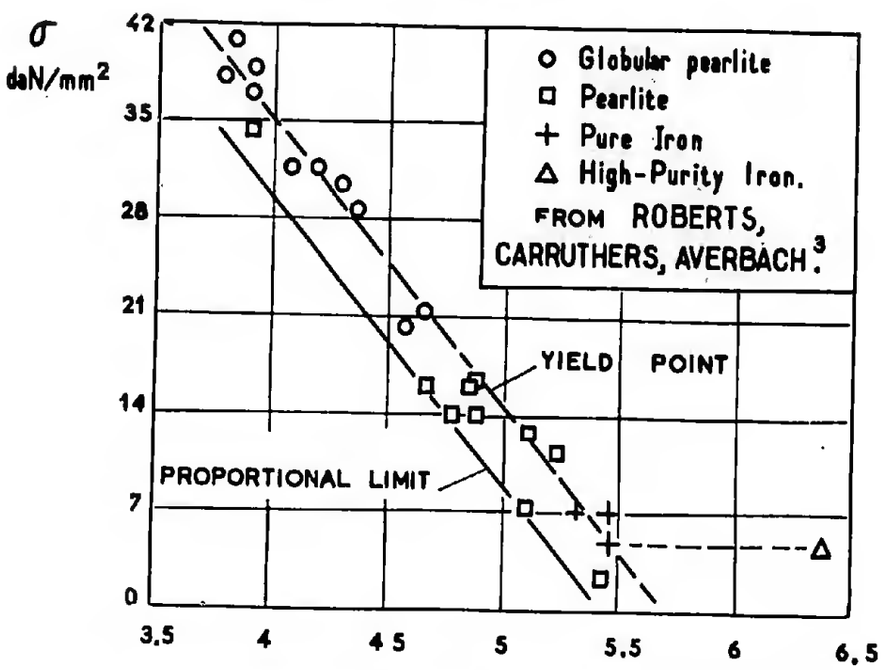

Fig.3.20 Log_e of the mean length of dislocation paths in ferrite ($1\text{Å} = 10^{-8}$ cm)

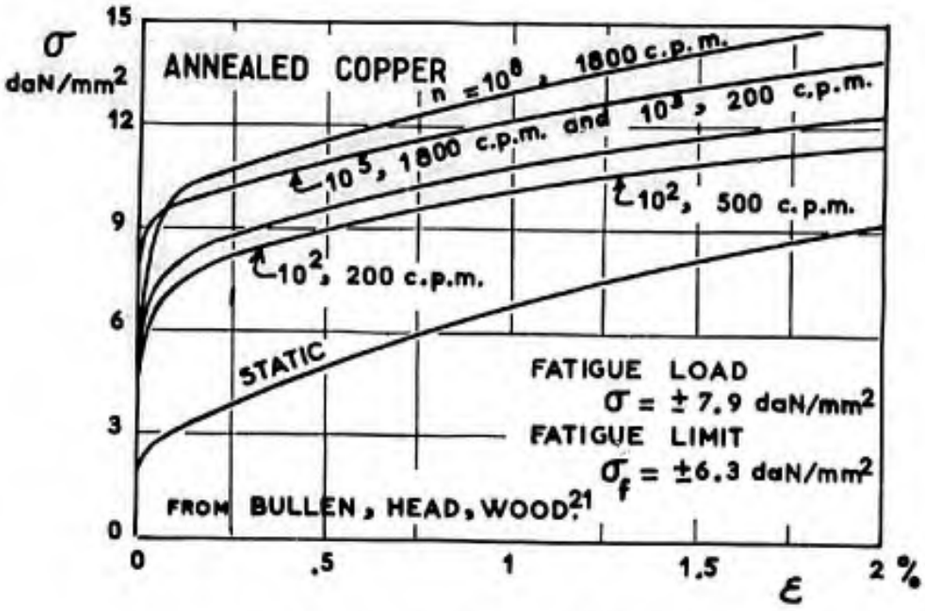

Fig. 3.21 Fatigue effect on σ-ε curve

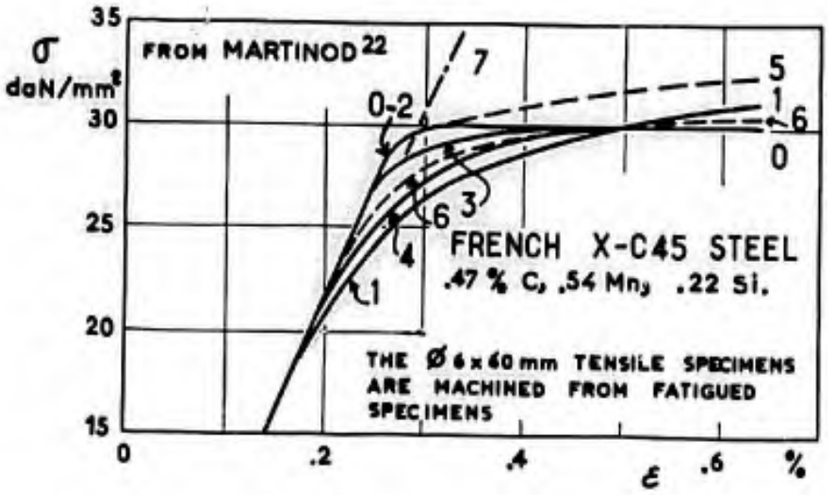

No	INITIAL FATIGUE		TENSILE PROPERTIES			
	± σ	n	σ_{prop}	$\sigma_{.2}$	$\sigma_{ult.}$	A %
0	0	0	27	30.7	58.2	26.2
1	22	24×10^6	18.2	31	61.1	23.9
2	23	200,000	28.9	32.6	60.4	23.8
3	23	666,000	26.4	32	61.5	14.6
4	23	932,000 +	23.2	32	61.5	18.8
5	27	39,000	30.1	34.5	61.7	18.5
6	27	188,000 +*	19	30		
7	22	48×10^6	32	48	70.3	13.8

NOTE: + SPECIMENS FRACTURED IN FATIGUE;
* UNCOOLED SPECIMEN;
THE OTHER SPECIMENS WERE COOLED;
STRESSES ARE IN daN/mm².

Fig. 3.22 Effect of previous fatigue on the tensile properties of carbon steel

that it is yet another process involving selection in the stability and in the number of slip barriers: the number decreases and the stability rises, producing higher local stresses in regions where microcracks appear prior to rupture.

Polakowski[19] assumes that the effect of cold-work varies with the type of steel and the type of deformation (tension, torsion, drawing, rolling).

The existence of a correlation between the yield strength and the free mean path of dislocations in ferrite has been demonstrated for annealed steel by Roberts, Carruthers and Averbach[3] (Fig. 3.20). The free path would be defined in globular structure as the distance between precipitates, in pearlite as the average distance between pearlite particles, in ferrite as the average distance between inclusions and grain boundaries, measured by the method of Howard and Cohen[20]. This correlation does not hold for pure iron, in which inclusions are too scarce.

The characteristics observed during the tensile test are modified by fatigue. Bullen, Head and Wood[21] have studied the behaviour of pure annealed copper. The results are reproduced in Figure 3.21. It is seen that initially annealed copper is strain-hardened by fatigue.

The variations of hardness and σ–ϵ curves in tension during axial tension-compression fatigue testing have been examined by Martinod[22] on rolled 40mm diameter bars of XC 45 steel containing 0.47% C, 0.54% Mn and 0.22% Si, in the as delivered condition. The σ–ϵ curves for 6mm diameter × 60mm length specimens machined from 14mm diameter × 140mm length specimens subjected to fatigue are plotted in Figure 3.22. If the fatigue specimens are cooled during the fatigue test, the yield strength and ultimate strength vary but little while the proportional limit, the bend of the σ–ϵ curve and the length of its horizontal section are modified. If the specimens are not cooled, the temperature may reach 200°C and the static properties are considerably modified.

Let us now consider the metallurgical effects of deformation. Apart from the obvious purpose of shaping a metal, *hot-work* is used to alter the *structure*, i.e., the size of grains and sub-grains, and the *texture*, i.e., the elongation, flatness and orientation of grains. Crystal lattice distortions generated by hot-work are more stable in the cold condition than those obtained by cold-work. In alloys, the structure obtained by hot forging remains to some extent even after application of the heat treatment designed to dissolve the foreign atoms before quenching. Hot-work by "kneading" in the three directions produces good tensile properties with a texture that is less oriented, therefore less brittle in the short transverse direction. The improvement is also due to compression which tends to close the microscopic voids, as is shown by Dixon's and Foley's[23] comparative tests on the forging of carbon steel through rolling, conventional die forging or closed-die forging with final hydrostatic compression of the metal. In France, a good percent elongation at rupture in the direction of thickness was obtained on plates of A-U4SG alloy (similar to American 2014) by kneading before final shaping and quenching. Cold-working of light alloys prior to solution treatment and quenching plays a role which is comparable to that of forging in the case of steels. It is sometimes used to initiate the forming operation, which is then continued after quenching and before artificial ageing.

Cold-working of aluminium light alloys between quenching and artificial ageing leads to a preferential formation of precipitates in dislocations and thereby increases the number of small stable precipitates which impede subsequent plastic slip.

The *American notations*, commonly used in Western Europe *for the treatment of light alloys* are as follows:

T 3	Solution treatment,	quenching,	1% drawing.
T 4	"	"	"	natural ageing at room temperature.
T 6	"	"	"	artificial hot ageing.
T 81	"	"	"	1% drawing and hot ageing.
T 86	"	"	"	6% " " " "

The effect of treatment on the first portion of the σ–ϵ curve for American 2024 alloy is indicated in Figure 3.23, from tests conducted by the supplier (ALCOA) on sheets.

3.1.4 Hardness

Hardness is a measure of the resistance opposed to the pressure of a rigid indenter. The latter has various shapes: a ball in the Brinell and Rockwell tests, a pyramid shape in the Vickers test. As for other plastic deformation processes, the rate of testing exerts an influence on the results; the time of loading is restricted to a few seconds in order to avoid creep. Consider the case of a spherical indenter. For a low value of the load P, the elastic strain is given by the Hertz formulae[24]. Under a high enough load, a permanent impression is obtained after unloading. With increasing loads, the material forced outward from the indentation tends to produce a growing ridge around the impression. In Figure 3.24, f is the indentation under load and f_1 the elastic reduction of the indentation after removal of the load. The elastic variation in diameter of the indentation is negligible[25], so that radius a can be measured and used as reference for hardness.

The Meyer hardness[26] is defined as the ratio

$$H_M = P/\pi a^2 .$$

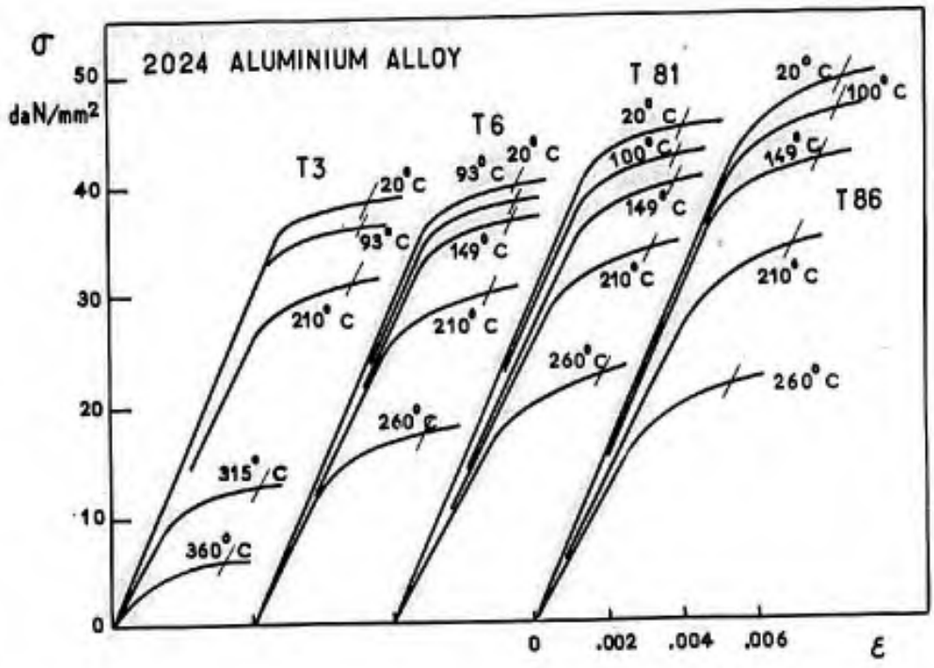

Fig. 3.23 Effect of heat treatment on the yield strength of 2024 aluminium alloy, from ALCOA .

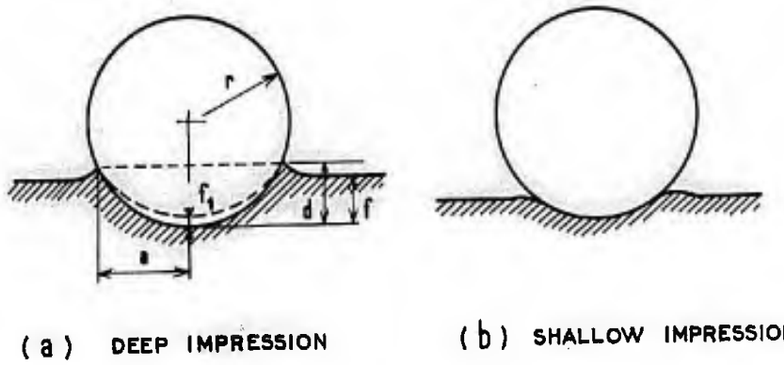

Fig. 3.24 Hardness test impression

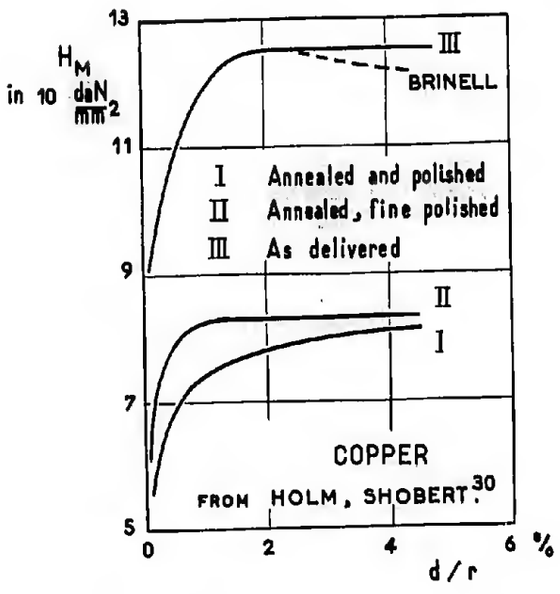

Fig. 3.25 Effect of cold-work on the Meyer hardness

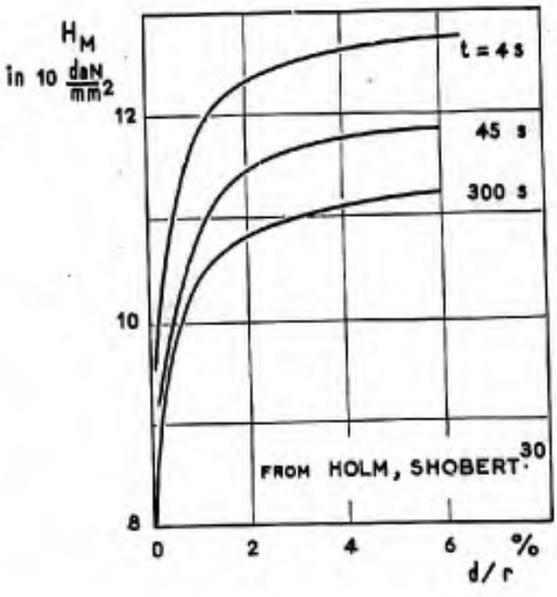

Fig. 3.26 Effect of the time of loading on the hardness of copper

Radius a is a function of P and of the material. It is found that with increasing value of P , H_M passes through a maximum and we have

$$H_M = H_U(a/r)^{n-2} ,$$

H_U and n being independent of the radius r of the ball[27]. H_M is equivalent to stress and a/r to plastic strain. There is some correlation between the Meyer hardness and the σ-ϵ curve. Tabor[28] has demonstrated that if the σ_{true}-ϵ_{true} curve is represented by the equation

$$\sigma = k\epsilon^m ,$$

then the Meyer hardness can be expressed by

$$H_M = ck(0.2\ a/r)^m ,$$

c being a constant. Consequently plastic strain may be defined by H_U and by n as well as by k and m .

Brinell[29] measured hardness in dividing P by the curved area of the impression; the pressure reaches a maximum with an increasing value of P ; Brinell selected the load and diameter of the ball so as to obtain a point near the maximum. A pyramid impression is used in the Vickers test. In the Rockwell test, the depth of the impression, d , is measured by means of a dial gauge.

According to Holm and Shobert[30], the Meyer hardness is associated with the depth, d , through the relation

$$H_M = K(d/r)^p .$$

For annealed copper, we have K = 112 daN/mm^2 and p = 0.085 . Some hardness curves for various conditions of copper are plotted in Figure 3.25 and 3.26; the latter also shows the influence of the time of loading.

Provided that the duration of loading and the rate of penetration remain within close limits, hardness tests provide as good an indication of surface plasticity as do tensile tests for the bulk of the material. Hardness tests are non-destructive and may be repeated at neighbouring points.

From conversion tables of the Metals Handbook[28], approximate values for the ultimate strength of steel may be obtained by multiplying the Brinell number by 500 to express the strength in lb/in^2 or by 0.35 to express it in daN/mm^2.

Späth[106] reports after Kürth[107] that there is a linear relationship between hardness and yield-strength variations in the case of a specimen cold-strained in tension.

Several authors[31,32,33,34] have tried to measure the *surface residual stresses* through their effects on the *Hertzian limit of elasticity*. The latter is defined as the largest value of contact pressure under which permanent deformation does not yet take place. If P is the corresponding load and r the radius of the ball, the compressive stress is given by a Hertz formula:

$$p = \frac{1}{\pi}\sqrt[3]{\left[\frac{3}{2}\left(\frac{E}{1-\nu^2}\right)^2 \frac{P}{r^2}\right]} ,$$

where ν is the Poisson's ratio.

If there are equiaxial surface residual stresses $\sigma_2 = \sigma_3$, the stress state will be the sum of a hydrostatic compression tensor (σ,σ,σ) , producing no plastic strain, and fictitious surface compression $p-\sigma$, which must reach the limiting value p to allow the initiation of plastic strain. The Hertzian limit of elasticity will therefore be increased by the value of the equiaxial compressive stresses. Uniaxial surface residual compression does not modify the Hertzian limit of elasticity since slip can produce yielding in the perpendicular direction. On the contrary, uniaxial tension favours yielding in its own direction and lowers the Hertzian limit of elasticity.

Hausseguy and Martinod[34] have carried out tests to substantiate these assumptions. Measuring the depth of the residual ball penetration under increasing loads P to within 1/100, they obtained the following results for various surface conditions of XC 45 steel (French steel containing 0.45% C) with a yield strength value of 25 daN/mm^2 (36,000 lb/in^2):

Lathe-machining followed by 0000 polishing	p = 125 daN/mm^2 .
Lathe-machining, then electro-polishing	p = 102 daN/mm^2 .
Thorough electro-polishing	p = 97 daN/mm^2 .

On annealed XC 18 steel (similar to 1020 American steel) with a yield strength value of 17.5 daN/mm^2 (25,300 lb/in^2), which had been lathe-machined and then 0000 polished, they found p = 97 daN/mm^2 . For this steel, which was free of residual stresses, hardness varied with external axial loading, as illustrated by the results of Figure 3.27. The Hertzian limit of elasticity remains invariable under external axial compressive

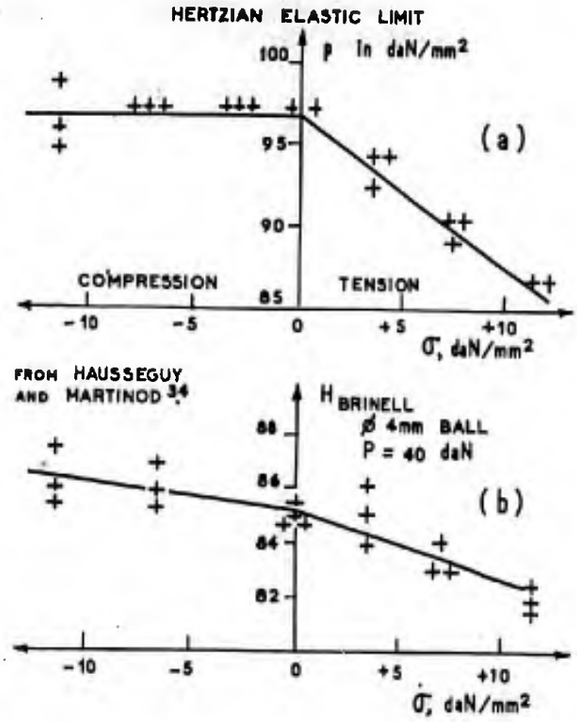

Fig.3.27 Effect of an applied axial load on the Hertzian elastic limit and Brinell hardness

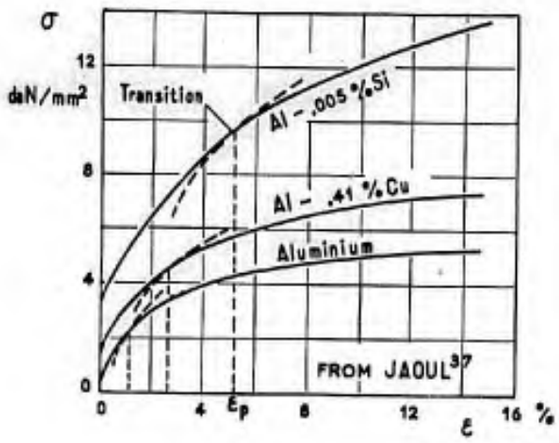

Fig.3.28 Effect of soluble impurities in aluminium on σ–ϵ curves

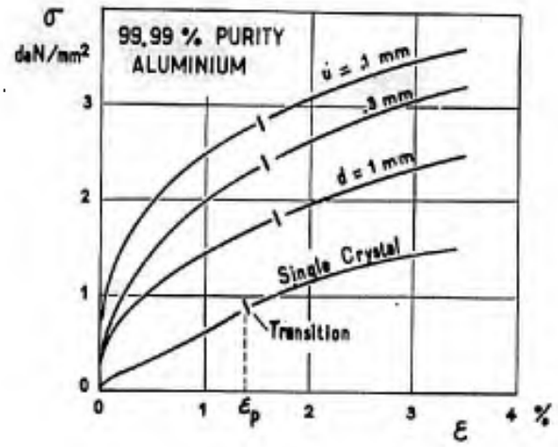

Fig.3.29 σ–ϵ curves of 99.99% purity aluminium for several magnitudes of grains, from Crussard and Jaoul [36]

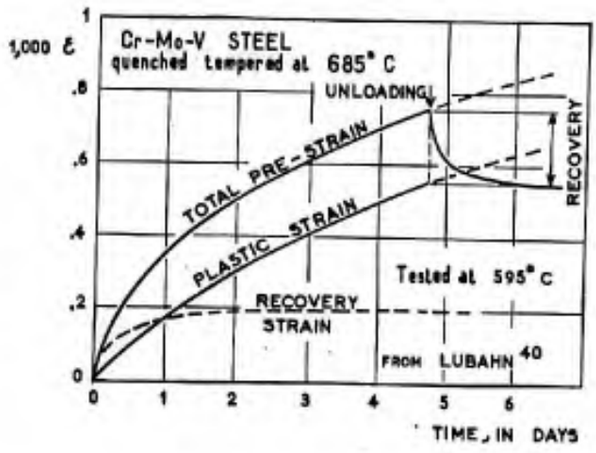

Fig.3.30 Creep and recovery of Cr-Mo-V steel

loading and is diminished under axial tensile stress by the exact value of the applied stress. Brinell hardness measurements yield results that are not as clear.

It should also be noted that the Hertzian limit of elasticity is determined by point measurements. Because of the high accuracy required, such tests are of no practical value. One of the previous methods[32,33] may therefore be used, for example the variation of the electrical contact resistance between the ball and the bar considered[33].

3.1.5 Notch Impact Strength

This property is measured by the energy loss of a pendular mass which strikes a notched bar and causes its rupture. The energy required for the impact fracture includes three components: (a) the energy due to plastic strain before cracking (which is influenced by the impact velocity, depending on the response of the material); (b) the energy due to friction on the supports (which varies with the bend of the bar before cracking); (c) the brittle fracture energy.

In France, the impact energy value of the Mesnager specimen, ρ_M, has been measured under standard experimental conditions. There is no distinct correlation between the impact value and such useful properties as σ_Y, $\sigma_{ult.}$, A%, $\Sigma\%$, the fatigue limit σ_f and the residual static strength of fatigue-cracked specimens. At best the impact value measures the impact strength in the quite specific case of the test machine.

After numerous attempts to compare test results for various shapes of specimens, the tendency is now to consider the impact energy value as a characteristic of little interest to the designer.

Even as a means of selecting the heat treatment for a given material, the use of notch impact specimens with a geometrical notch prolonged by a fatigue crack approximates to measuring the residual static strength of fatigue-cracked specimens. Such test bars are more brittle, their bend prior to fracture is smaller, and mainly brittle energy is measured. However, this type of measurement is only valuable if there is some correlation with the residual static strength of the cracked specimen.

3.1.6 Notch Effect

Geometrical notches with a moderately high concentration factor, K_T, increase the net ultimate strength of a specimen, whereas very sharp notches may reduce it. Circumferential notches are likely to result in an improvement of up to 50%. The improvement is smaller and the weakening greater on thin sheets. This subject will be discussed in more detail at the beginning of Chapter IV.

3.2 CREEP

Creep occurs when the strains and strengths under constant static loading are time-dependent. Deformation before fracture is liable to impair the use of the material or fracture may occur without appreciable deformation, depending on the material and the temperature; *ductile creep* or *brittle creep* is therefore possible.

The problem of creep first appeared on aircraft structures in refractory steel gas turbine blades and light alloy compressor blades. Recently, kinetic heating of supersonic transport aircraft skin panels has raised the same problem but with very small permissible deformations (less than 0,1%). In such cases, creep is associated with alternating loads with a steady component, and the actual problem of creep and hot fatigue implies comparatively low allowable stresses if only creep is considered[35].

Slow static testing is a particular case of creep in which elongation always attains the limit value corresponding to the instantaneous stress value before any significant increase of the stress takes place; on the contrary, with high-rate testing (see Figure 3.35), elongation is delayed in relation to the limit value obtained in conventional testing. We shall first examine the aspects of plastic deformation common to both static testing and creep, and the apparent differences due to the time and temperature ranges considered.

3.2.1 Straining in Crystals

Crussard and Jaoul[36], carrying out static tests on aluminium, iron, copper, zinc and magnesium, demonstrated the existence of two distinct ranges in the stress-plastic strain curve, which are governed by different equations:

$$\sigma = \sigma_0 + A\epsilon^m \quad \text{up to the } \epsilon_p \text{ transition}$$

and

$$\sigma = \sigma_0' + B\epsilon^m \quad \text{beyond } \epsilon_p .$$

The transition is believed to be due to polygonization (dislocation arrangement generating sub-grains). Up to the transition, deformation is caused by slip with a dislocation pile-up against the grain boundaries. In Figure 3.28 some σ–ϵ curves and the transition points are plotted. Figure 3.29 indicates that the plastic stiffness of high-purity 99,99% aluminium increases with the grain fineness while the transition elongation depends little on it. Jaoul[37] has shown that this elongation is governed by the relation $\epsilon_p = kx^{1/3}$, where x is the proportion of solute foreign atoms.

Gensamer[38], studying steels, found a good correlation between σ_{20} (i.e., the stress for 20% strain) and the exponent m in the relation

$$\sigma = \sigma_{20}(\epsilon/0.2)^m .$$

From his results we obtain the expression

$$1/m = 1.4 + \sigma_{20} \Big/ \left(17 \frac{daN}{mm^2}\right).$$

σ_{20} is a function that increases with the density of carbide precipitates. The effect of soluble addition elements such as nickel and chromium is that a greater carbide dispersion is introduced, the respective effects being additive: 1% Cr produces an effect similar to that of 0.22% Ni.

Garrod, Suiter and Wood[39] have shown by an electron-microscope study that there are three processes of plastic deformation for 99.99% aluminium. With 12% strain at room temperature, conventional lamellar slip which terminates at the grain boundaries is obtained. The second process takes place only at a higher temperature (300°C) and with a lower strain rate (0.17% per hour). It includes polygonization by which the grain is divided into cells. The third process begins at a still higher temperature (390°C) with a rate of 8% over 72 hours and exhibits slip substantially parallel to the grain boundaries. If the strain rate is very high (12% in 20 sec.) at the same temperature (390°C), conventional intragranular slip is found again.

At a sufficiently elevated temperature the slip barriers inside the grains disappear and plastic stiffness is provided by the disturbed regions of the grain boundaries. According to Lubahn[40], Hanson and Wheeler have encountered slip in grains and at grain boundaries during the same creep test, the slip at the boundaries occurring in the mid-period of the test during slow deformation and allowing spontaneous recovery of the strain-hardening inside the grains.

Creep strength varies with the grain size. Above an "equi-cohesion" temperature, coarse grains are more resistant than fine grains (for a given strain rate). Similarly, for a given temperature, there is a transition strain rate below which coarse grains have greater strength[41,42]. At low temperatures and high strain rates, recrystallization or polygonization does not occur very much and fine grains show the advantage of a greater density of boundaries which constitute slip barriers. At elevated temperatures and low strain rates, by which recrystallization is initiated, coarse grains are more resistant because intracrystalline hardening is more stable and less dense, thereby delaying recrystallization. Besides, previous work-hardening above the critical recrystallization level promotes recrystallization during creep and thus softens the material for subsequent creep strain[42]. Recrystallization, or at least polygonization, occurs during the creep of most metals and makes the effect of temperature, test rate and grain size more complex.

For instance, coarse grains withstand creep fairly well if intracrystalline hardening is stable. This result may be obtained by creating lattice distortions through rolling, by then eliminating the less stable distortions through fast annealing under controlled temperature and time conditions, and by finally creating new ones through another cold-rolling operation. On light aluminium alloy of the A-U2GN type (French alloy similar to English RR 58) such a process has produced grains that were three times larger with intermediate annealing than without it; the strength at 150°C for an elongation of 0.1% over 1,000 hours was found to be equal to 19 daN/mm² with annealing but to only 12 daN/mm² without annealing. If, however, sheets with fine grains or grains controlled by rolling and annealing are subjected to cold-work between the quenching and artificial ageing operations, the reduction in creep strength is more significant for fine grains. Thus, according to results from Sud-Aviation[78], the stresses in A-U2GN required to obtain a 0.1% elongation over 100 hours at 175°C are as follows, expressed in daN/mm²:

	Quenching + Hot ageing	*6% drawing + Quenching and Hot ageing*	*Quenching + 6% drawing + Hot ageing*
Fine grains of 27μ	16.5	16.5	11.5
Controlled grains of 50μ	21	16.5	11.5

It is seen that the creep strength is not dependent on the grain size alone.

For pure aluminium subjected to fatigue at a temperature of 250°C and a rate of 1440 c/m, Daniels and Dorn[76] showed that fine grains (50 per mm²) and coarse grains (1 per mm²) had the same sub-grain size and fatigue strength at 10^5 cycles. This seems to give evidence that, in the hot condition, sub-grain boundaries are the most stable obstacles to plastic strain, whereas grain boundaries are unstable.

For stainless steel and Inconel exposed to high temperatures, Robinson and Dorn[77] observed that the creep strength depends little on the grain size but much on the annealing treatment; the grain size plays no part in hot fatigue. In the hot condition, the low plastic stability of grain boundaries implies transcrystalline fractures, except at the junction of three grains.

loading and is diminished under axial tensile stress by the exact value of the applied stress. Brinell hardness measurements yield results that are not as clear.

It should also be noted that the Hertzian limit of elasticity is determined by point measurements. Because of the high accuracy required, such tests are of no practical value. One of the previous methods[32,33] may therefore be used, for example the variation of the electrical contact resistance between the ball and the bar considered[33].

3.1.5 Notch Impact Strength

This property is measured by the energy loss of a pendular mass which strikes a notched bar and causes its rupture. The energy required for the impact fracture includes three components: (a) the energy due to plastic strain before cracking (which is influenced by the impact velocity, depending on the response of the material); (b) the energy due to friction on the supports (which varies with the bend of the bar before cracking); (c) the brittle fracture energy.

In France, the impact energy value of the Mesnager specimen, ρ_M, has been measured under standard experimental conditions. There is no distinct correlation between the impact value and such useful properties as σ_Y, $\sigma_{ult.}$, A%, $\Sigma\%$, the fatigue limit σ_f and the residual static strength of fatigue-cracked specimens. At best the impact value measures the impact strength in the quite specific case of the test machine.

After numerous attempts to compare test results for various shapes of specimens, the tendency is now to consider the impact energy value as a characteristic of little interest to the designer.

Even as a means of selecting the heat treatment for a given material, the use of notch impact specimens with a geometrical notch prolonged by a fatigue crack approximates to measuring the residual static strength of fatigue-cracked specimens. Such test bars are more brittle, their bend prior to fracture is smaller, and mainly brittle energy is measured. However, this type of measurement is only valuable if there is some correlation with the residual static strength of the cracked specimen.

3.1.6 Notch Effect

Geometrical notches with a moderately high concentration factor, K_T, increase the net ultimate strength of a specimen, whereas very sharp notches may reduce it. Circumferential notches are likely to result in an improvement of up to 50%. The improvement is smaller and the weakening greater on thin sheets. This subject will be discussed in more detail at the beginning of Chapter IV.

3.2 CREEP

Creep occurs when the strains and strengths under constant static loading are time-dependent. Deformation before fracture is liable to impair the use of the material or fracture may occur without appreciable deformation, depending on the material and the temperature; *ductile creep* or *brittle creep* is therefore possible.

The problem of creep first appeared on aircraft structures in refractory steel gas turbine blades and light alloy compressor blades. Recently, kinetic heating of supersonic transport aircraft skin panels has raised the same problem but with very small permissible deformations (less than 0.1%). In such cases, creep is associated with alternating loads with a steady component, and the actual problem of creep and hot fatigue implies comparatively low allowable stresses if only creep is considered[35].

Slow static testing is a particular case of creep in which elongation always attains the limit value corresponding to the instantaneous stress value before any significant increase of the stress takes place; on the contrary, with high-rate testing (see Figure 3.35), elongation is delayed in relation to the limit value obtained in conventional testing. We shall first examine the aspects of plastic deformation common to both static testing and creep, and the apparent differences due to the time and temperature ranges considered.

3.2.1 Straining in Crystals

Crussard and Jaoul[36], carrying out static tests on aluminium, iron, copper, zinc and magnesium, demonstrated the existence of two distinct ranges in the stress-plastic strain curve, which are governed by different equations:

$$\sigma = \sigma_0 + A\epsilon^m \quad \text{up to the } \epsilon_p \text{ transition}$$

and

$$\sigma = \sigma_0' + B\epsilon^m \quad \text{beyond } \epsilon_p .$$

The transition is believed to be due to polygonization (dislocation arrangement generating sub-grains). Up to the transition, deformation is caused by slip with a dislocation pile-up against the grain boundaries. In Figure 3.28 some σ–ϵ curves and the transition points are plotted. Figure 3.29 indicates that the plastic stiffness of high-purity 99.99% aluminium increases with the grain fineness while the transition elongation depends little on it. Jaoul[37] has shown that this elongation is governed by the relation $\epsilon_p = kx^{1/3}$, where x is the proportion of solute foreign atoms.

Gensamer[38], studying steels, found a good correlation between σ_{20} (i.e., the stress for 20% strain) and the exponent m in the relation

$$\sigma = \sigma_{20}(\epsilon/0.2)^m .$$

From his results we obtain the expression

$$1/m = 1.4 + \sigma_{20} \Big/ \left(17 \frac{daN}{mm^2}\right).$$

σ_{20} is a function that increases with the density of carbide precipitates. The effect of soluble addition elements such as nickel and chromium is that a greater carbide dispersion is introduced, the respective effects being additive: 1% Cr produces an effect similar to that of 0.22% Ni.

Garrod, Suiter and Wood[39] have shown by an electron-microscope study that there are three processes of plastic deformation for 99.99% aluminium. With 12% strain at room temperature, conventional lamellar slip which terminates at the grain boundaries is obtained. The second process takes place only at a higher temperature (300°C) and with a lower strain rate (0.1% per hour). It includes polygonization by which the grain is divided into cells. The third process begins at a still higher temperature (390°C) with a rate of 8% over 72 hours and exhibits slip substantially parallel to the grain boundaries. If the strain rate is very high (12% in 20 sec.) at the same temperature (390°C), conventional intragranular slip is found again.

At a sufficiently elevated temperature the slip barriers inside the grains disappear and plastic stiffness is provided by the disturbed regions of the grain boundaries. According to Lubahn[40], Hanson and Wheeler have encountered slip in grains and at grain boundaries during the same creep test, the slip at the boundaries occurring in the mid-period of the test during slow deformation and allowing spontaneous recovery of the strain-hardening inside the grains.

Creep strength varies with the grain size. Above an "equi-cohesion" temperature, coarse grains are more resistant than fine grains (for a given strain rate). Similarly, for a given temperature, there is a transition strain rate below which coarse grains have greater strength[41,42]. At low temperatures and high strain rates, recrystallization or polygonization does not occur very much and fine grains show the advantage of a greater density of boundaries which constitute slip barriers. At elevated temperatures and low strain rates, by which recrystallization is initiated, coarse grains are more resistant because intracrystalline hardening is more stable and less dense, thereby delaying recrystallization. Besides, previous work-hardening above the critical recrystallization level promotes recrystallization during creep and thus softens the material for subsequent creep strain[42]. Recrystallization, or at least polygonization, occurs during the creep of most metals and makes the effect of temperature, test rate and grain size more complex.

For instance, coarse grains withstand creep fairly well if intracrystalline hardening is stable. This result may be obtained by creating lattice distortions through rolling, by then eliminating the less stable distortions through fast annealing under controlled temperature and time conditions, and by finally creating new ones through another cold-rolling operation. On light aluminium alloy of the A-U2GN type (French alloy similar to English RR 58) such a process has produced grains that were three times larger with intermediate annealing than without it; the strength at 150°C for an elongation of 0.1% over 1,000 hours was found to be equal to 19 daN/mm² with annealing but to only 12 daN/mm² without annealing. If, however, sheets with fine grains or grains controlled by rolling and annealing are subjected to cold-work between the quenching and artificial ageing operations, the reduction in creep strength is more significant for fine grains. Thus, according to results from Sud-Aviation[78], the stresses in A-U2GN required to obtain a 0.1% elongation over 100 hours at 175°C are as follows, expressed in daN/mm²:

	Quenching + Hot ageing	*6% drawing + Quenching and Hot ageing*	*Quenching + 6% drawing + Hot ageing*
Fine grains of 27μ	16.5	16.5	11.5
Controlled grains of 50μ	21	16.5	11.5

It is seen that the creep strength is not dependent on the grain size alone.

For pure aluminium subjected to fatigue at a temperature of 250°C and a rate of 1440 c/m, Daniels and Dorn[76] showed that fine grains (50 per mm²) and coarse grains (1 per mm²) had the same sub-grain size and fatigue strength at 10^5 cycles. This seems to give evidence that, in the hot condition, sub-grain boundaries are the most stable obstacles to plastic strain, whereas grain boundaries are unstable.

For stainless steel and Inconel exposed to high temperatures, Robinson and Dorn[77] observed that the creep strength depends little on the grain size but much on the annealing treatment; the grain size plays no part in hot fatigue. In the hot condition, the low plastic stability of grain boundaries implies transcrystalline fractures, except at the junction of three grains.

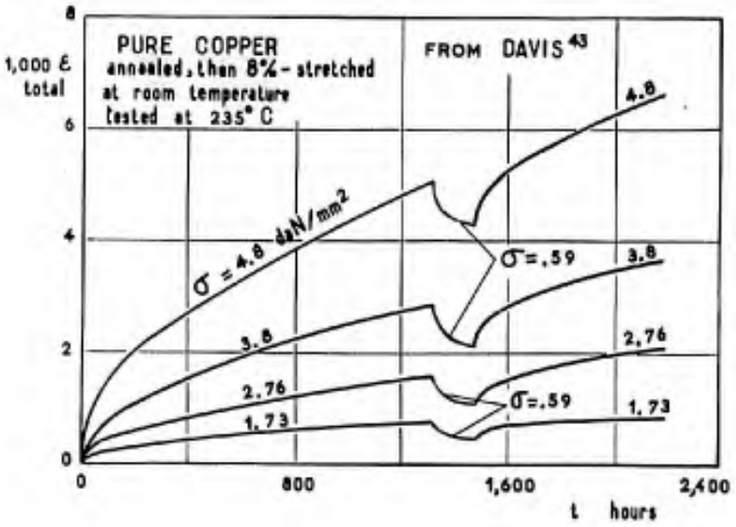

Fig. 3.31 Creep and recovery of copper

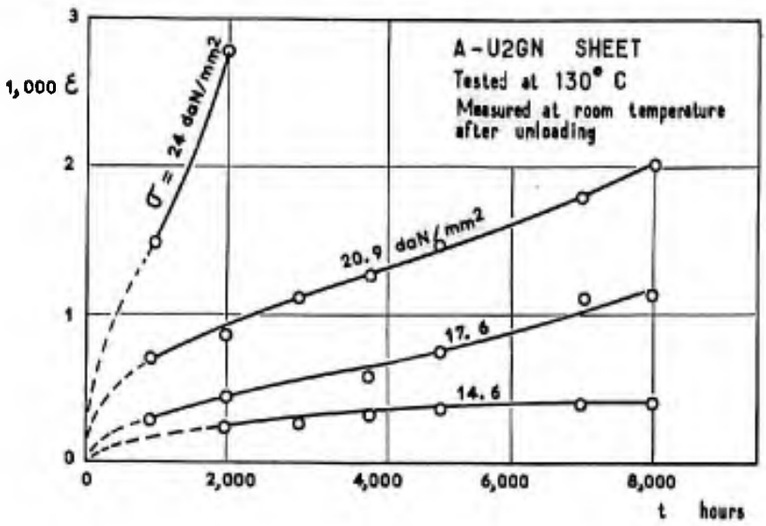

Fig. 3.32 Creep of A-U2GN aluminium alloy

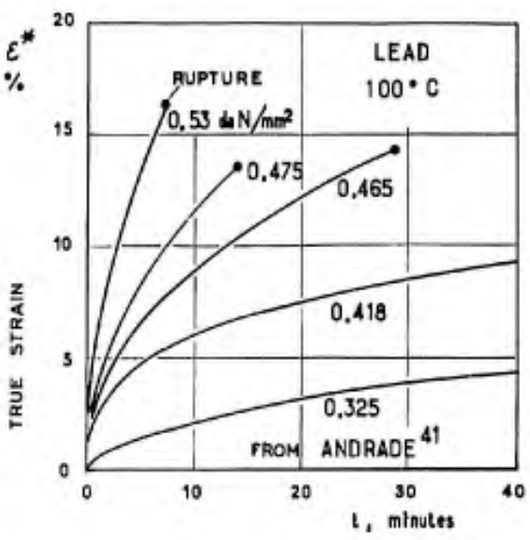

Fig. 3.33 Creep of lead

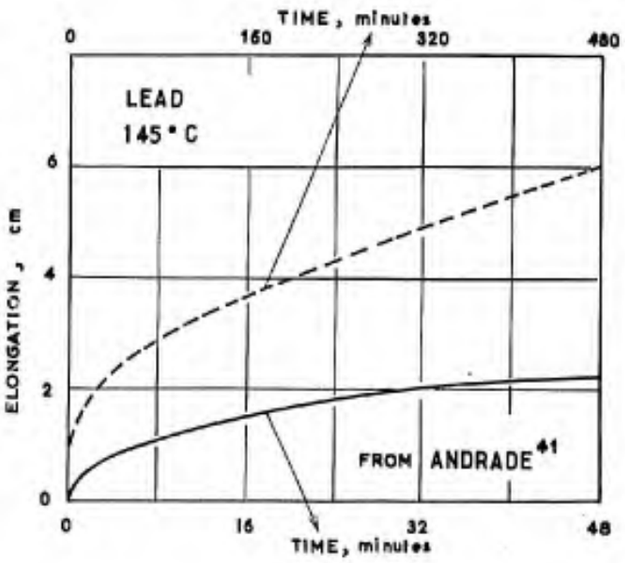

Fig. 3.34 Creep of lead on two different time scales

Plastic flow in creep and under small strains is also affected by *delayed elasticity*, or *elastic after-effect*. In Figure 3.30, the nature of this effect is illustrated after results obtained by Lubahn[40] for the creep of quenched and tempered (685°C) Cr-Mo-V steel tested at 595°C. Upon removal of the load, deformation decreases slowly towards a limit. This phenomenon corresponds apparently to partial recovery which allows reversed slip to occur under the action of residual stresses. Figure 3.31, from Davis[43], gives another example of elastic after-effect by unloading during the creep of pure annealed and 8%-drawn copper at room temperature. Elastic after-effect occurs frequently in creep tests and complicates the measurement of elongation, this being carried out with high accuracy after dismounting the specimen or with high sensitivity by means of continuous recording.

3.2.2 Description of Creep

When a tension specimen is subjected to a load which is held constant, the following can be observed in measuring the elongation:

(a) Up to a certain value of the load, elongation occurs upon loading and the residual elongation after unloading remains constant.

(b) Under higher loads, up to a given value, permanent elongation increases with time and then reaches asymptotically a constant limiting value: creep is then *transient and limited*.

(c) Under still higher loads, the elongation ϵ still increases with time but the rate of flow $u = d\epsilon/dt$ gradually decreases toward a minimum value $u_{min} = (d\epsilon/dt)_{min}$. Considering the entire process, it may be said that creep comprises a *transient* part, during which the creep rate diminishes regularly, and a *steady-state* part, of constant creep rate. As long as the transient component predominates, the creep obtained is called *primary creep*. It is followed by *secondary creep*, of constant rate. If the load is decreased to keep the stress constant on account of the reduction in cross-sectional area of the specimen, secondary creep often ends by fracture with no modification of the characteristic shape of its ϵ–t curve.

(d) Under still higher loads which are held constant, the true stress increases owing to the cross-sectional reduction, and the creep rate increases again after reaching a minimum; fracture is caused by necking. *Tertiary creep* is then obtained; it corresponds to mechanical instability or, in some fairly rare cases, to structural instability of the material.

(e) Finally, under still higher loads, when creep occurs during the time-under-stress to failure, there is no difference between a creep test and a more or less rapid static test.

In the case of A-U2GN aluminium alloy sheets, for which the creep test results[44] at 130°C are reproduced in Figure 3.32, the test points show secondary creep and the onset of tertiary creep. The scatter of the measurements makes it difficult to decide whether the rate of steady-state creep is zero in the test with $\sigma = 14.6$ daN/mm^2. It is likely that no secondary creep and, a fortiori, no tertiary creep would take place in the stress range 5 daN/mm^2 $< \sigma <$ 8 daN/mm^2, which is typical of the cruise flight of supersonic Mach-2 aircraft. In such cases, apart from a test designed to check this at 20,000 hours under the highest steady stress typical of cruise flight, all other tests should be stopped as soon as the creep rate is zero or impossible to measure. These tests would be used to investigate transient primary creep alone and could only be conducted by increasing the accuracy of measurement and by reducing the causes of scatter.

An accuracy of 0.01% over a gauge length of 100 mm corresponds to an accuracy of measurement of 0.01 mm; it is difficult to obtain a better result with successive measurements requiring dismounting of the specimen. Provided the temperature is controlled to within ±0.5°C, one could even measure to one micron and hence obtain an accuracy of 0.001% (10^{-5}). We may recall that under the stresses likely to occur during cruise on supersonic Mach-2 aircraft, the elastic strains are of the order of 10^{-3}; plastic strains of the order of 10^{-4} are negligible. However, to extrapolate a short-time test up to 20,000 hours, a good knowledge of the creep rate is required; with 1,000 hr-tests an accuracy of 10^{-5} is probably sufficient for extrapolation if some long-time tests have shown that extrapolation is allowed.

Ripley[45] considers that the scatter in creep tests is mainly due to temperature variations and to non-axial loads; if the temperature variation does not exceed ±0.2°C, an accuracy of 10^{-5} is reached with automatic continuous recording of the elongation.

A distinction must be made between accuracy and sensitivity. Both are involved in measurements effected after dismounting of the specimen. In continuous measurements, sensitivity may be good with very poor accuracy; in this case, it is at least possible to determine the shape of the curve and hence to estimate by extrapolation whether the strains remain negligible over 20,000 hours.

In order to reduce the scatter and improve the absolute accuracy, we suggest that three creep tests be performed under supposedly identical conditions and that the mean curve be taken into account.

The fast increase of strain in tertiary creep is often caused by an increase of true stress as a result of the reduction in cross-sectional area. If an apparatus is available for measuring the cross-section and setting the load so that stress be held constant, then tertiary creep disappears sometimes and curves of the type illustrated in Figure 3.33 are obtained. The use of a relation between true strain, true stress and time permits more accurate computations in the case of variable stress values.

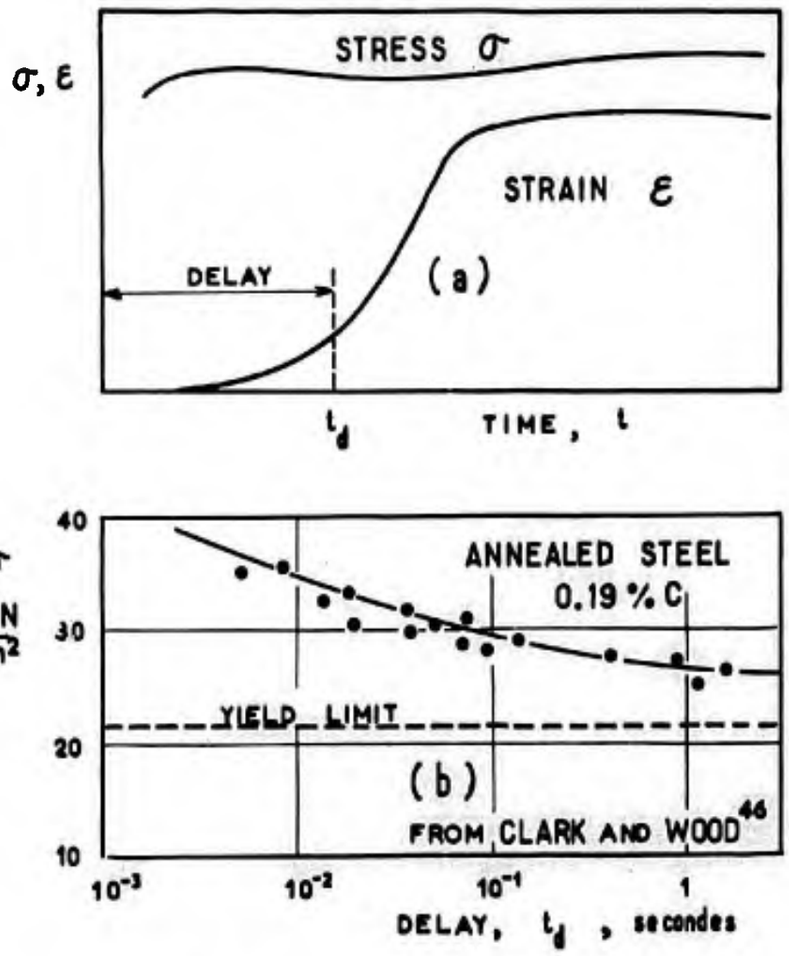

Fig.3.35 Delayed fast creep in static test

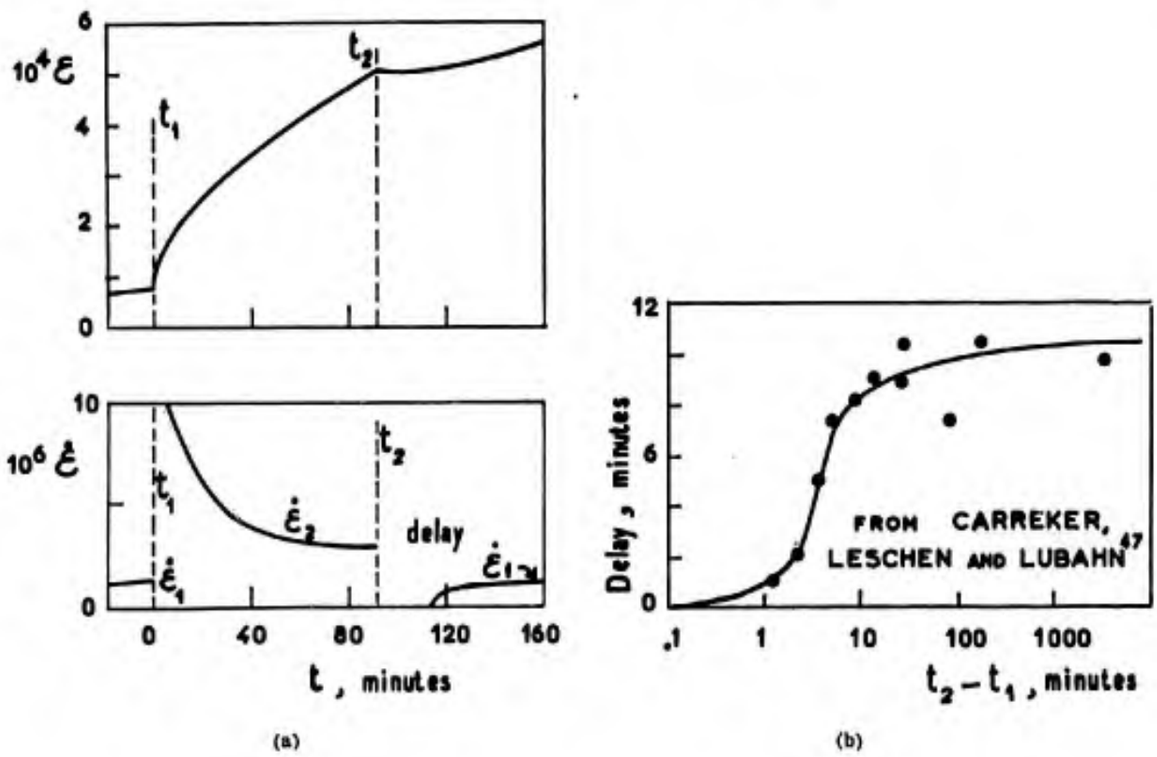

Fig.3.36 Transient creep of lead

Primary creep is rather difficult to define, as shown in Figure 3.34, where the creep of lead is represented on two different time scales; the definition of secondary creep by an almost rectilinear curve is also a very subjective one.

Secondary creep has been studied quite extensively for certain applications such as centrifugal compressor discs and blades, which are subjected to the maximum allowable stresses consistent with no-failure conditions and with deformation conditions which permit reliable operation. For such applications creep limiting stresses have been fixed which correspond to strains of 0.1% and 0.2%. On airframes, the conditions of secondary creep would exist in notches if plastic flow itself did not set limits to the stresses by reducing the stress concentrations and by introducing residual stresses after removal of the load (these conditions are favourable from the point of view of fatigue). In this case, secondary creep will only occur in joints and will be related to the shear of rivets and the corresponding bearing stresses in sheets.

Let us return to the description of creep. Primary creep is sometimes preceded by a period of very low creep representing a kind of delay in the establishment of primary creep. This *delayed creep* is illustrated in Figures 3.35(a) and (b) for annealed 0.19% carbon steel, from Wood and Clark[46].

In the case of carbon steel this phenomenon is attributed to the arrangement of solute carbon atoms in the iron lattice. The same authors have observed a delay in decarburized iron. ($C \leqslant 0.001\%$) . As to other materials (18-8 stainless steel, 7075 aluminium alloy), tests do not exhibit any delay, either because it is non-existent or because it is too small to be measured.

Carreker, Leschen and Lubahn[47] have studied delayed creep in lead, copper and 61 S-T aluminium alloy. Their results for lead are illustrated by Figures 3.36(a) and (b).

An increase in stress causes a sharp increase in the creep rate which then rises asymtotically to a new substantially constant value, somewhat higher than the first. A return to the first value of stress entails a delay in creep; the creep rate then increases slowly to reach its first value. This has also been observed by Sherby, Trozera and Dorn[48] (Figures 12 and 13 from the authors) in pure aluminium; they found a creep delay in 2.1% magnesium aluminium alloy at a temperature of 327°C and under stresses ranging from 0.35 to 2.45 daN/mm^2 (Figures 12 and 13 from the authors). Delayed creep was also found by Shahinian and Achter[49] in Cr-19.1% Al-3.6% nickel alloy at 816°C under a stress of 5.6 daN/mm^2; the creep rate, at first very low, passes through a maximum (Fig.3.37). The rate may reach a maximum several times during the same creep test, as is the case (Fig.3.37) with nickel at 816°C under 1.82 daN/mm^2 with a 6.35 mm diameter specimen whereas another 9 mm diameter specimen breaks when reaching the second maximum. In the cases mentioned previously, delayed creep seems to occur at temperatures well above the recrystallization temperature (lead recrystallizes at room temperature), except for steel, where the phenomenon is caused by the arrangement of solute atoms. We see, then, that a point of inflection in the creep curve $\epsilon = f(t)$ does not necessarily originate from an undetected error of measurement.

It is very difficult to predict the localized shape of a creep curve for lack of elongation measurements at very short intervals. Thus, the acceleration of the creep rate at about 80 hr on curve II of Figure 3.37 would pass undetected with measurements carried out every 100 hr; we prefer continuously recorded measurements. Similarly, Figure 3.38, from Shahinian and Achter[49], contains creep curves on two different time scales. With measurements every 100 hr, the initial elongation proportional to time would not be apparent and a very high initial rate could be assumed, as is sometimes encountered (almost instantaneous plastic elongation upon loading).

3.2.3 Graphic Representations and Mathematical Approximations of Creep, Extrapolations

If measurements were very accurate, the graphic representation of creep would only be a matter of convenience. But they exhibit scatter and even errors and, since the range of measurements often happens to be rather restricted, the way of plotting the creep results often suggests a particular mean line and a kind of mathematical relationship leading to a method of extrapolation.

The creep phenomena are associated with a relation

$$\epsilon = f(\sigma, t, T) \qquad (1)$$

between four physical quantities: ϵ = permanent elongation; σ = applied stress; t = time; T = absolute temperature.

Two quantities can be plotted along the coordinate axes and an additional quantity on level curves. Instead of direct quantities, we may consider functions of these quantities, for example:

$$\log \epsilon , \quad \log \sigma , \quad \log t , \quad 1/T .$$

We may also consider groups of quantities as parameters, for example:

$$\Phi(t,T) = \begin{cases} t.e^{-k/T} \\ T(\log t + C) \\ t.T^{b} . \end{cases}$$

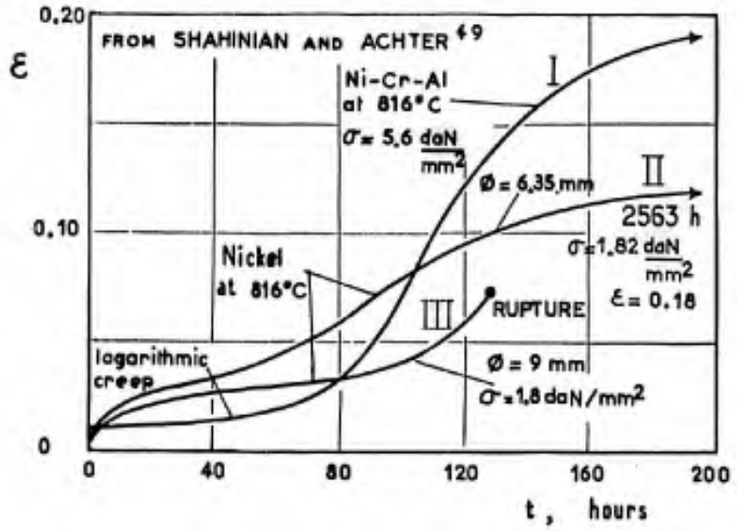

Fig. 3.37 Creep of nickel and nickel alloys

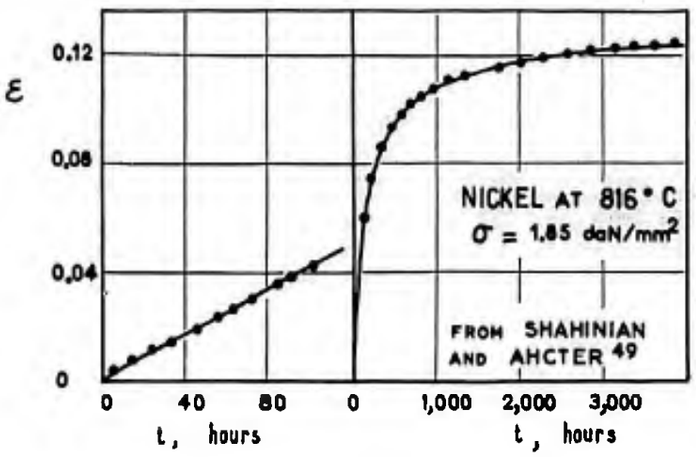

Fig. 3.38 Creep of nickel represented on two time scales

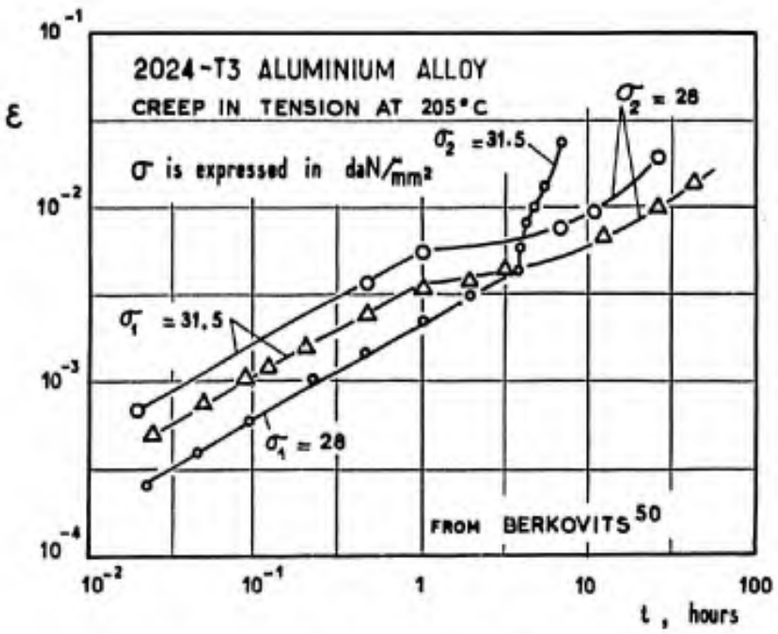

Fig. 3.39 Two-stress-level creep of 2024-T3 aluminium alloy

One or two quantities can be held constant during the test and for its graphic representation. We may have, for instance:

$$
\begin{array}{lllll}
T \text{ constant} & \sigma \text{ constant} & \epsilon = f(t) & \text{creep} & \epsilon,\ t \ ;\ \epsilon,\ \log t \ ;\ \log \epsilon,\ \log t \\
 & t \text{ "constant"} & \epsilon = f(\sigma) & \text{stress-strain curve} & \sigma,\ \epsilon \ ;\ \log \sigma,\ \log \epsilon \ ;\ \sigma,\ \log \epsilon \\
 & \epsilon \text{ constant} & \sigma = f(t) & \text{relaxation} & \sigma,\ t \ ;\ \sigma,\ \log t \\
\epsilon \text{ given :} & \sigma \text{ constant} & t = f(T) & \text{time-temperature correspondence} & \log t,\ T \ ;\ \log t,\ 1/T
\end{array}
$$

$$\Phi(t, T) = f(\sigma) ,$$

For constant temperature and stress, Andrade[41] proposes in the case of lead

$$l = l_0(1 + \beta t^{1/3})e^{kt} , \tag{2}$$

which corresponds to primary creep for $k = 0$ or for a small value of t and to steady-state creep for $\beta = 0$. The author assumes that β and k are related to two different creep processes, β being determined by plastic slip in the grains of the metal and k by relative displacements of the grains.

For primary creep the $\log \epsilon - \log t$ representation is often used. Figure 3.39 shows the results of Berkovits[50] for 3 mm thick 2024-T3 aluminium alloy sheet at 205°C, subjected to tension at two successive stress levels, σ_1 and σ_2. For $\sigma_1 > \sigma_2$, delayed creep, as mentioned previously, is found under σ_2. The first rectilinear portion of the curves is expressed by

$$\epsilon = A.t^k , \tag{3}$$

where $k = 0.5$. In Figure 3.40, from the same author, the creep curves are plotted for the same material under various tensile stresses. Some scatter can be observed. For small elongations, $\epsilon = A\sqrt{t}$ is verified by the rectilinear portion with a slope of 0.5. When the slope exceeds 1, creep is certainly in the tertiary stage.

The elongation at fracture ϵ_{ult} does not depend on the stress but exhibits some scatter. To define the influence of stress σ, Berkovits proposes the law

$$\epsilon = A.t^k \operatorname{Sh}(\sigma/\sigma_0) , \tag{4}$$

where $A = 6.8 \cdot 10^{-5}$, $k = 0.5$, $\sigma_0 = 6.5$ daN/mm^2.

Note that for $\sigma = 45{,}000$ lb/in^2 (31 daN/mm^2) and 20,000 lb/in^2 (13.8 daN/mm^2) the curves are in poor agreement with $\epsilon = A\sqrt{t}$; for $\sigma = 20{,}000$ lb/in^2 we would have $\epsilon = At$ in the case of small strains.

We return to the ϵ-t representation with the work of Davis[43] on pure copper, annealed for 1 hr at 500°C and 8%-stretched at room temperature under 23,000 lb/in^2 (16 daN/mm^2) prior to testing (see Figure 3.31 of Section 3.2.1). The creep rate, $u = d\epsilon/dt$, diminishes with time and tends asymptotically toward the minimum value of secondary creep, u_{min}, for which Davis gives the expression

$$u_{min} = u_1 e^{\sigma/\sigma_0} . \tag{5}$$

This law is suggested by straight lines on a $\sigma - \log u_{min}$ representation for various temperatures. It is inconsistent since it exhibits a creep rate at zero stress. For this reason Davis then uses the law

$$u_{min} = 2\, u_1 \operatorname{sh}(\sigma/\sigma_0) , \tag{6}$$

which is more suitable for the results of tests performed at 235°C. The quantities σ_0 and u_1 are constants which vary with the test temperature:

$$\sigma_0 = 11{,}020 - 15.8\ T, \text{ expressed in lb/in}^2 \tag{7}$$

$$u_1 = 0.054\ e^{-6282/T} . \tag{8}$$

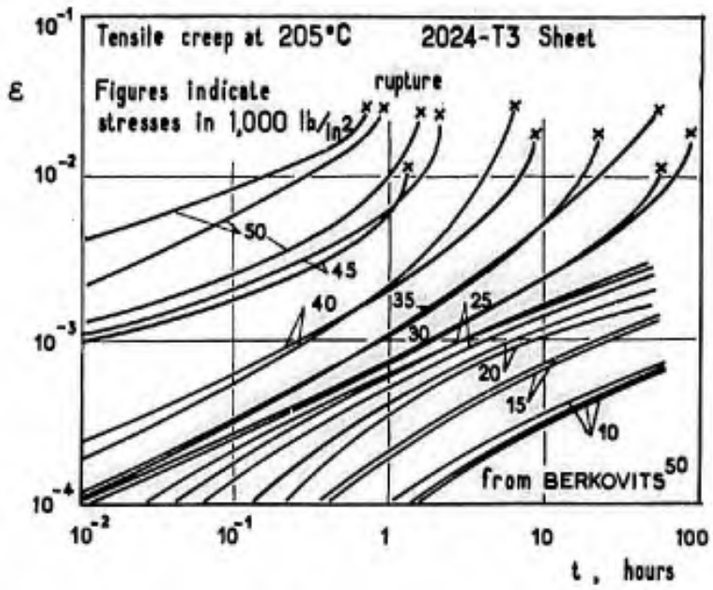

Fig 3.40 Tensile creep of 2024-T3 aluminium alloy sheets at 205°C

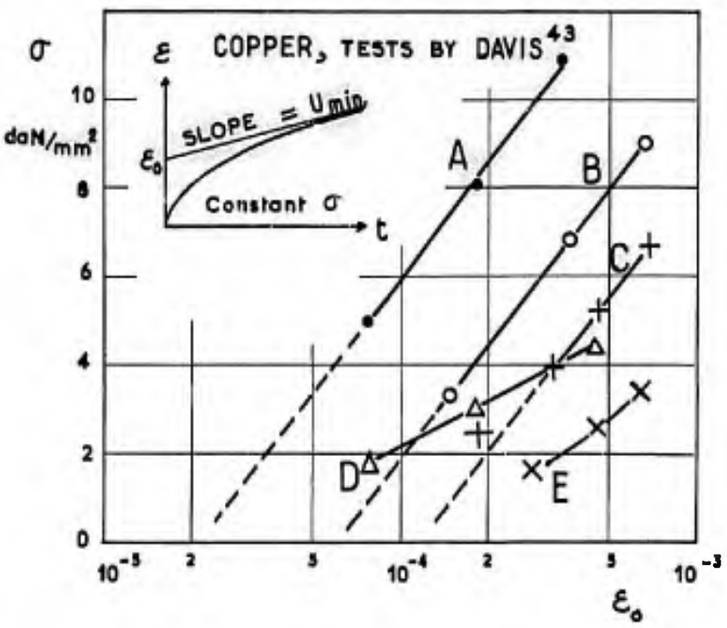

Fig. 3.41 Creep of copper

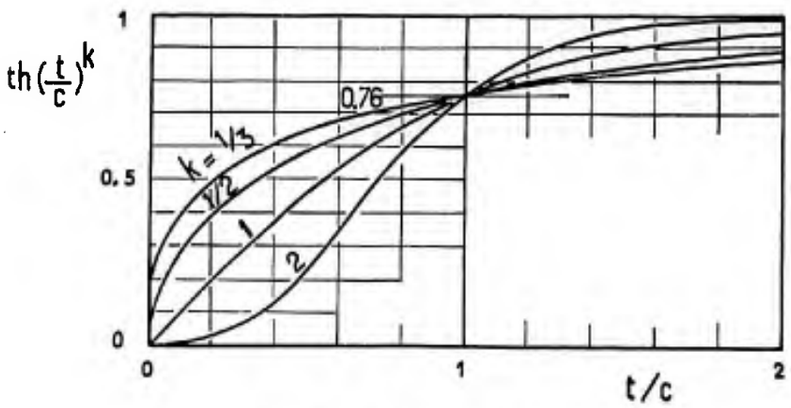

Fig. 3.42 Functions to represent transient creep

As set forth in Chapter II, Section 2.5.2, the general form of the relation (8) has been proposed by many authors on the analogy of the rate u of chemical reactions:

$$u = Ae^{Q/RT} , \tag{9}$$

where the activation energy Q is expressed in calories per mole and R denotes the perfect-gas constant (see Chapter II for numerical values). It is plotted by a straight line on a log u–1/T diagram.

This law is encountered in the physics of metals whenever the process of the phenomenon is controlled by self-diffusion of the atoms of the matrix or by diffusion of foreign atoms and if only one type of diffusion takes place. We have seen that three main types of processes occur in plastic strain: slip in grains, rearrangement of grain boundaries and recrystallization. The first involves the diffusion of impurities which stabilize the slip barriers while the two others also include the diffusion of the atoms of the matrix from grain to grain. The law (8) is actually verified for secondary creep in Davis's tests.

We shall now check whether a similar law fits primary creep by using, after Davis, the values of ϵ_o, i.e., the intersection of the asymptotes of the creep curves with the ϵ-axis at zero time; ϵ_o represents fairly well the whole process of transient creep (Fig. 3.41). The expression

$$\epsilon_o = 10^4 \, e^{-3,000/T} \, e^{/5,750} \tag{10}$$

provides a good representation of the curves A, B, C and E in Figure 3.41 for temperatures of 80, 130, 165 and 235°C, while curve D is an aberration. In comparing the expressions (8) and (10), it is seen that the activation energy of primary creep is half that of secondary creep. We may conclude that *a single temperature law cannot account for the whole process of transient and steady-state creep and a law based on steady-state creep does not hold for transient creep.*

For the empirical analysis of transient creep, Davis has proposed

$$\sigma = K\epsilon^m (d/dt)^m , \tag{11}$$

hence

$$\epsilon = Bt^{n/(m+n)} , \tag{12}$$

with $m = 0.71$, $n = 0.15$ and $K = 9.3 \cdot 10^7$ for copper, t being expressed in hours and σ in lb/in^2.

This formula, where $n/(m+n) = 0.175$, is to be compared with Andrade's, where the exponent of t is 1/3. An expression such as (11) can be useful for creep buckling calculations.

To cover both creep ranges, Davis has tried the formula suggested by Soderberg[51]:

$$u = 2 u_1 \, sh(\sigma/\sigma_o) \left[\frac{1}{th(\alpha t + \beta)}\right], \tag{13}$$

hence

$$\epsilon = \frac{u_{min}}{\alpha} \log_e \left[\frac{sh(\alpha t + \beta)}{sh \beta}\right], \tag{14}$$

with $\alpha = 1.12 \cdot 10^{-3}$ and $\beta = 0.035$, t being expressed in hours. This function has been utilized by Davis for relaxation calculations which have been substantiated fairly well by tests.

For the primary creep of 2024-T3 at 205°C, Berkovits[50] has applied the law

$$\epsilon = \frac{\sigma}{E} + A \, t^k \, sh(\sigma/\sigma_o) , \tag{15}$$

where $A = 6.8 \cdot 10^5$, $k = 0.5$, t being expressed in hours.

We propose the use of a rather general expression for both primary and secondary creep, considering merely the influence of time:

$$\epsilon = u_{min} t + \epsilon_o \, th(t/c)^k , \tag{16}$$

with $k > 0$, u_{min} and ϵ_o as functions of stress and temperature. The first term corresponds to steady-state creep and the second to transient creep. For a small value of t, the second term becomes $\epsilon_o (t/c)^k$, which is the most common expression for primary creep. In Figure 3.42 the forms of the function are plotted against several values of k; 1/3 is suitable for lead, 0.5 for 2024-T3, 1 for nickel in Figure 3.38, and $k > 2$ for the delayed creep on curve I in Figure 3.37.

Instead of discriminating between transient and steady-state creep, it may be assumed, after Graham[52], that creep strain is the sum of strains due to various processes, the contribution of each being represented by expressions of the same algebraical form:

$$\epsilon = \sum_{i=1}^{i=n} C_i . \sigma^{n_i} . t^{k_i} \quad (17)$$

The effect of temperature is introduced by substituting for t

$$\Phi = t(T_i' - T)^{-A_i} , \quad (18)$$

T_i' and A_i being constants. Graham takes:

$$k_1 = 1/3 , \quad k_2 = 1 , \quad k_3 = k_4 = 3 ,$$

with only one value for T_i' and A_i, which leads to the expression

$$\epsilon = C_1\sigma^{n_1}\Phi^{1/3} + C_2\sigma^{n_2}\Phi + \left[C_3\sigma^{n_3} + C_4\sigma^{n_4}\right]\Phi^3 , \quad (19)$$

where $\Phi = t(T' - T)^{-A}$.

This expression includes ten arbitrary constants: the term with $\Phi^{1/3}$ corresponds to Andrade's primary creep, the term with Φ to secondary creep, the term with Φ^3 to tertiary creep. If the experimental points are plotted on a $\log \epsilon - \log \Phi$ diagram, the expression which provides the best fit to the test results will yield a polygonal line with three rectilinear segments united by transition curves, the slopes of the segments being equal to 1/3, 1 and 3. Walles and Graham[53] have applied these formulae to the creep of steels and Nimonic 100.

The parameter Φ in the expression (19) provides the first example of a time-temperature relationship. For Nimonic 100, Walles and Graham[53] indicate $A = 20$ but with $T' > T$, corresponding to T–log t curves at constant σ which are convex toward the log t axis. For concave curves, they suggest

$$\Phi = t(T - T')^{20} , \quad (20)$$

with $T' < T$.

Dorn[54] has used the theoretical parameter of diffusion (see Equation (9))

$$\Phi = t.e^{-Q/RT} , \quad (21)$$

hence $$\log t - (Q/RT).\log e = \text{constant}$$

and $$T(\log t + D) = \text{constant} , \quad (22)$$

where D depends on the metal. This law has been proposed by Hollomon and Jaffe[56] for the tempering of steel and later by Larson and Miller[57] for creep.

Manson and Haferd[55] assume

$$\Phi = (T - T_a)/(\log t - \log t_a) , \quad (23)$$

where T_a and t_a are constants in tests at σ constant, but dependent on σ.

Sud-Aviation[58] have taken

$$t\,T^b = \text{constant} . \quad (24)$$

All these expressions, except (21), are empirical ones and should only be used to interpolate between test data or to provide orders of magnitude for designing the test and measuring means. The expression (21) only holds if the creep range considered is controlled by a single diffusion process.

We have just reviewed a number of mathematical expressions suitable to describing the time, stress and temperature effect on permanent creep elongation. If test data are available for specific temperatures, times, stresses, metallurgical states and mechanical histories of a material, several expressions may often be found to provide curves that cross the scattered experimental points reasonably well. The selected expression may depend on the kind of representation used. An expression is sometimes chosen as reference and the deviations are supposed to result from a "structural" change of the material.

Using the law

$$\epsilon = f(\sigma, \Phi) , \quad \Phi = \int_0^t e^{-(\Delta H/RT)}dt \quad (25)$$

and $$\Phi = te^{-(\Delta H/RT)} \quad \text{if} \quad T = \text{Constant},$$

hence $$(\partial f/\partial \Phi) = (d\epsilon/dt)e^{(\Delta H/RT)} = F(\sigma,\epsilon) \quad \text{if} \quad \sigma = \text{Constant},$$

Sherby, Trozera and Dorn[48] have obtained a good correlation for the secondary creep of pure aluminium, aluminium alloy containing 0.1% of copper atoms, and aluminium alloy containing 2.1% of magnesium atoms. For high stresses, they find

$$F(\sigma,\epsilon) = S''(\epsilon).\sigma^B \tag{26}$$

and state that the function $S''(\epsilon)$ characterizes the structural change during creep. For lower stresses

$$F(\sigma,\epsilon) = S'(\epsilon)\sigma^n, \tag{27}$$

their conclusion is still that $S'(\epsilon)$ represents an almost constant structural parameter. Apparently, the proposed expressions are not quite appropriate to represent primary creep.

We believe that, even in the case of materials which are simple and "stable", i.e., such that simple exposure to the test temperature does not affect the results, and which are manufactured for the purpose of laboratory tests, the actual laws are too complex for a simple mathematical expression to cover the whole range of times, stresses and temperatures. This would probably be possible with a complex mathematical expression containing many arbitrary constants, as long as tests at constant stress and temperature are considered, especially as scatter justifies the ruling out of certain results which are not in accordance with the selected expression, this being unduly attributed to mere chance. Even if it is correct, such an expression will not be very useful since we are investigating loadings at variable stress and temperature in the low stress region where transient primary creep is prevailing and remains small enough to raise great difficulties of measurement.

Mathematical expressions should only be used to interpolate on temperatures or to extrapolate on times over a temperature and stress range for which the extrapolation is justified by measurement. A distinction must, however, be made between extrapolation for data utilization, which is always hazardous, and legitimate extrapolation for defining a new test range or a material acceptance test. In the latter case, for example, it has been suggested that the creep test designed to determine the stress for 0.1% creep elongation over 10,000 hours at 130°C should be replaced by a 100-hr acceptance test at 175°C for RR-58 and A-U2GN aluminium alloys. This test is justified since its sole purpose is to check that the fabrication process is identical with that used for a similar batch of material delivered previously. It is relevant if the 0.1% elongation constitutes an adequate criterion or if a different value of elongation is conditioned in the same way by the fabrication parameters.

Depending on the problems to be solved, three types of extrapolations may be considered:

(a) Predicting the elongation over a period of time $t_2 > t_1$ at constant stress σ and temperature T, the curve $\epsilon = f(t)$ being known for time t_1. This extrapolation is permissible if instant t_1 lies well within the constant-rate steady-state creep range. It is valid if long-duration tests at higher stress or temperature show that tertiary creep has not yet started.

(b) Predicting the elongation over a given time t at constant temperature T and under a stress $\sigma < \sigma_1$, the elongation being known for stresses equal to and above σ_1 over the same period of time. This extrapolation is less conservative than the former, but the strain may be estimated conservatively, using the empirical law with $e^{(\sigma/\sigma_0)}$, if applicable. On the contrary, extrapolation to higher stresses is never safe.

(c) Predicting the elongation for $T < T_1$ and $t > t_1$ under a known stress σ, the elongation being known for T_1 and t_1. This extrapolation is the most useful one since accelerated tests may be carried out on this basis. Yet, it is also the most questionable one and should only be used after some checks which would provide a measure of interpolation. The checks need not necessarily include a large number of stress values; it is only necessary to cover the range of variation of σ.

In more complex cases of stresses and temperatures varying cyclically with time, extrapolations to the general stress and temperature level are even more risky and a check of the empirical laws at the boundaries of the investigated range is always recommended.

3.2.4 Creep Life

The creep rupture life of ductile materials exhibits considerable scatter and is of little practical interest in view of the very large strains occurring prior to rupture; consideration is usually paid to the time to reach a specified value of strain. An example is given for thick A-U2GN (English RR-58) aluminium alloy plates, water-quenched at 538°C and aged for 24 hrs at 200°C, in Figure 3.43, from Sud-Aviation[58], where the creep strengths with 0.2% strain are plotted for temperatures of 130°C, 150°C, 175°C and 200°C.

Between 150°C and 200°C, the activation energy is 37,000 cal.-g per mole, while it amounts to 45,000 cal.-g in the range of 130°C to 150°C. Thus, the diffusion process differs at moderately elevated temperatures and at high temperatures.

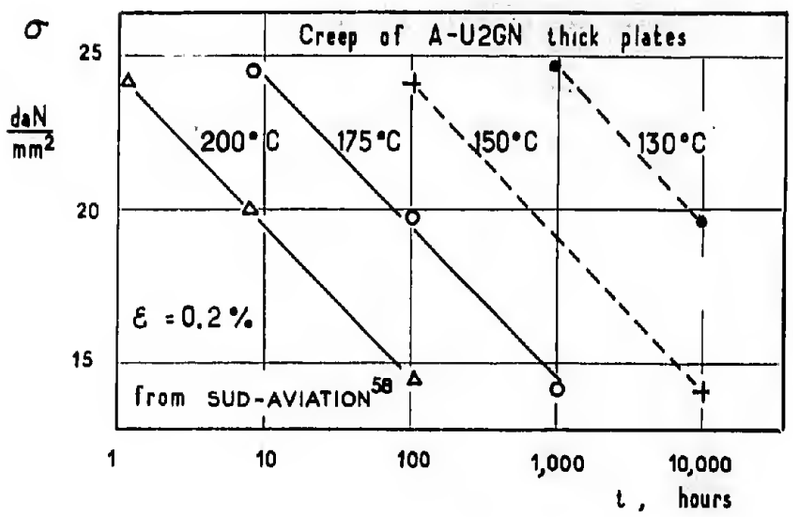

Fig. 3.43 Stresses for 0.2% creep elongation at various temperatures

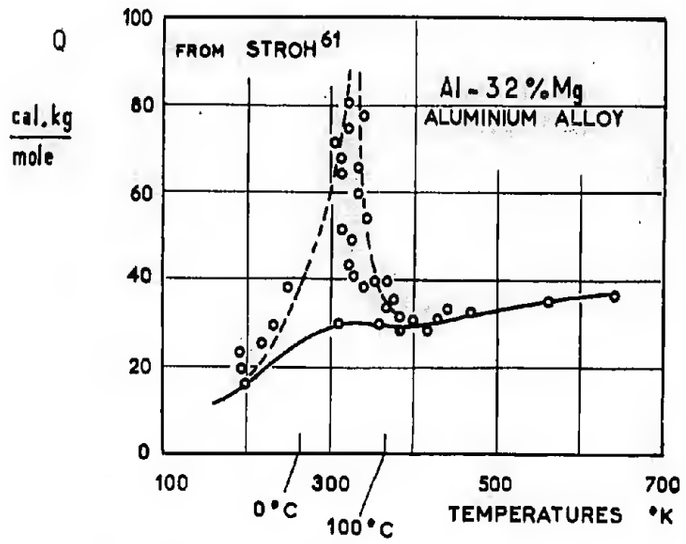

Fig. 3.44 Activation energy in creep

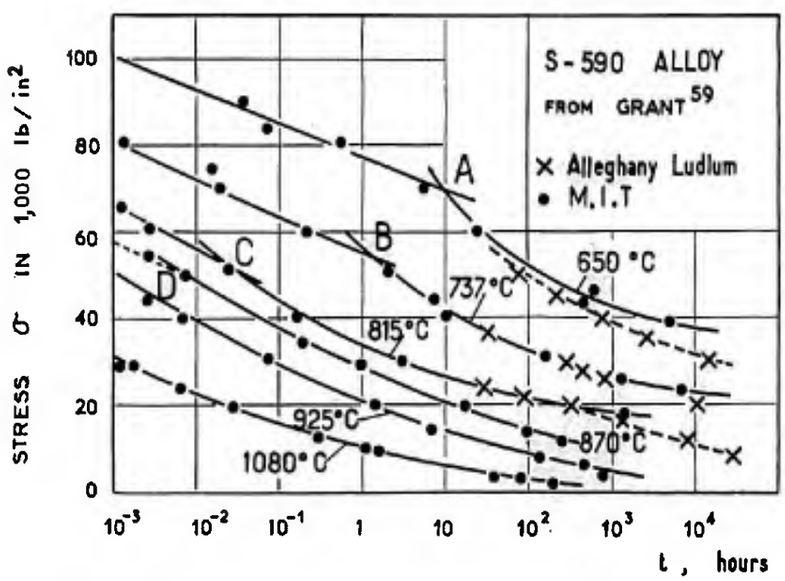

Fig. 3.45 Static life before failure of S-590 alloy at elevated temperatures

In Figure 3.44, after Stroh[61], the variation of creep activation energy is plotted against temperature for aluminium alloy containing 3.2% of magnesium. The deviation and scatter may be attributed to dislocations being anchored by solute Mg atoms. This is associated with the existence of a level portion on the σ–ϵ curve of the alloy. At very low temperatures the dislocations do not drain the solute atoms, the diffusion being too weak, whereas the diffusion at very high temperatures is such that the atoms may leave the dislocations. From these examples it follows that extrapolation is difficult and that a long-time test at moderately elevated temperatures cannot be replaced by an accelerated test at high temperatures.

Returning to A-U2GN and Figure 3.43, we may sum up the results by writing

$$\epsilon = f[te^{-Q(T)/RT}e^{\sigma/\sigma_0}] , \qquad (28)$$

where $\sigma_0 = 5$ daN/mm^2 . In view of the increase of $Q(T)$ in the temperature range between 150°C and 130°C, it is to be feared that lower values will be found toward 100°C, whereas a law assuming

$$\epsilon = F[tT^b e^{\sigma/\sigma_0}]$$

would yield larger stress values; extrapolation must therefore be carried out carefully.

On more brittle materials the *time to fracture* may be assessed; it is a function of stress and is low for high stresses and high temperatures. In Figure 3.45, after Grant[59], the times to fracture are given for S-590 refractory alloy of the following percent composition: 20 Cr, 20 Ni, 20 Co, 4 W, 4 Mo, 4 Cb, 0.5 C, remainder Fe.

Points A, B C and D divide two different types of strain and rupture. To the left, deformation occurs by plastic slip as in the cold condition and fracture is transcrystalline. To the right, deformation corresponds to grain boundary displacements and fracture is intercrystalline, typical of creep rupture. For a given test period, say 0.01 hour, there is an *equicohesion temperature* above which deformation and fracture corresponding to the behaviour at high temperature are obtained.

The strengths of some plastic materials and of glass under static loads depend upon the time of loading. Figure 3.46, from Hsiao and Sauer[60], is relative to polystyrene. Here, the influence of time is explained by the viscosity effect which allows progressive relaxation of some molecular chains, whereby others are overstressed.

3.2.5 The Effect of Pre-Strain

Owing to its utilization for jet engine turbine blades, the American N-155 refractory alloy has been investigated quite comprehensively at elevated temperatures. Frey, Freeman and White[62], then Ewing and Freeman[106] have studied the dependence of hot creep properties on the temperature and degree of rolling. Cold rolling is the term employed for rolling at temperatures below recrystallization temperature. The material under review had the following composition: 0.13 C, 3.05 Mo, 1.5 Tu, 0.98 Cb, 0.14 N, remainder iron (about 33%). The treatment applied was: rolling of a square 33 cm ingot to a square 22 mm bar at a temperature between 1130°C and 1040°C, solution treatment for 1 hour at 1200°C, and water-quenching. The rolling operation was as follows: 127 mm diameter rollers; at room temperature, 8 alternate runs on each side pair; in the hot condition, heating to 11°C above the desired temperature for ½ hr, 15% reduction.

In the above tests, recrystallization during hot rolling occurred at 1200°C and had not yet started at 1120°C. In Figure 3.47(a) the effect of rolling at room temperature is plotted against the minimum rate of secondary creep. A reduction in area of 40% produces a hardening effect which is greater than critical hardening and favours recrystallization at 650°C. At the same test temperature, a reduction in area of 15% by hot rolling above 700°C promotes recrystallization under a stress of 35 daN/mm^2 (Fig. 3.47(b)).

The authors have studied the effect of annealing for 1, 10, 100 and 1,000 hours after rolling. Annealing has no influence if the temperature is below recrystallization temperature.

In light alloy aircraft structures, hardening due to cold forming usually takes place after quenching and before artificial ageing. Strain must be restricted if hot recrystallization is to be avoided. In some cases, pre-forming is carried out upon annealing, followed by less heavy additional forming between quenching and artificial ageing, in order to obtain more stable distortions in the crystal lattice.

In Figure 3.48, concerning A-U2GN plates at the four following conditions:

A – Quenched from 538°C, aged 4 hr at 200°C,

B – Quenched, 1.5% stretched, aged,

C – " 6% " "

D – " 6% " aged, 1.5% stretched,

the creep elongations are indicated for 1,000 hours at 130°C.

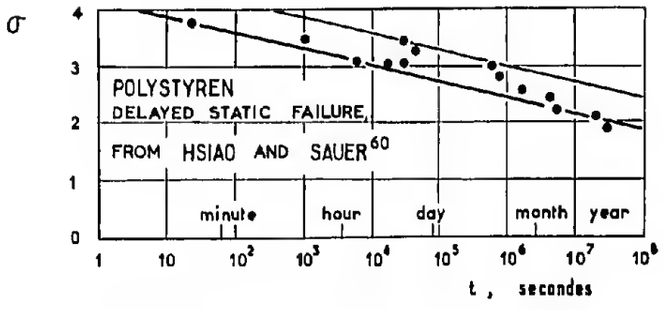

Fig. 3.46 Delayed static failure of plastics

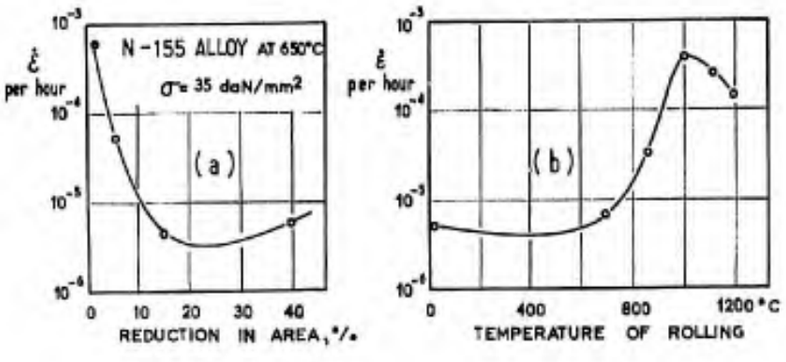

Fig. 3.47 Steady-state creep of N-155 alloy

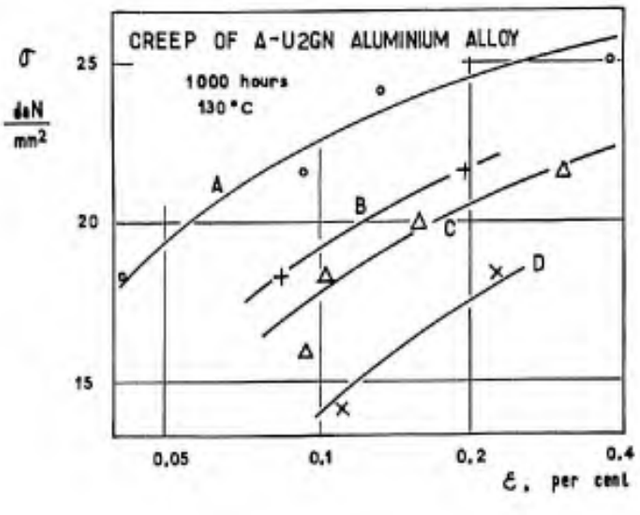

Fig. 3.48 Effect of drawing between quenching and ageing on the creep of A-U2GN aluminium alloy

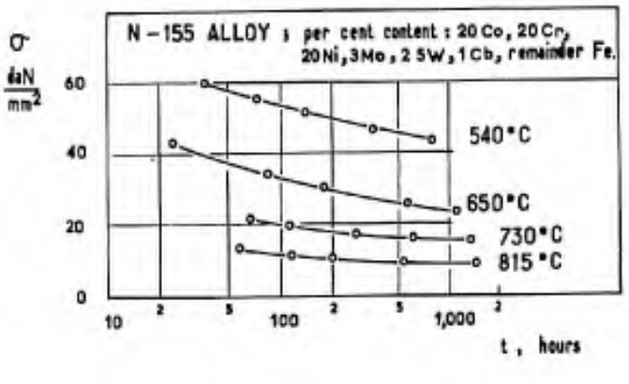

Fig. 3.49 Creep life of N-155 alloy

Here, an adverse effect of cold-stretching before or after artificial ageing is observed on the creep strength. By contrast, cold-stretching improves the yield strength and ultimate strength in rapid cold static tests; in the case of A-U2GN, σ_{ult} increases from 42 daN/mm^2 (60,500 lb/in^2) to 46 daN/mm^2 and $\sigma_{0,2\%}$ from 35 to 39 daN/mm^2 with 6% stretching performed between quenching and ageing[64]. Stretching decreases the residual quenching stresses and causes the precipitates to grow faster in dislocations which are anchored on the multiple slip planes of heavily deformed grains, thus increasing the low-temperature strength. At high temperature and during creep, the precipitates continue to grow, the smaller ones coalesce and overageing takes place, reducing plastic stiffness.

The above phenomenon is common to artificially aged alloys and to alloys hardened by ageing, as is the case with 2.2% beryllium copper alloy, the 0.2% yield strength of which increases from 23 daN/mm^2 after quenching to 110 daN/mm^2 after quenching and ageing and to 127 daN/mm^2 (184,000 lb/in^2) if cold-stretching is inserted between quenching and ageing[65]; cold stretching causes the proportional limit to increase from 35 daN/mm^2 to 70 daN/mm^2 (100,000 lb/in^2).

3.2.6 Intermittent Creep

Under repeated or fluctuating tensile stress, creep occurs if the elongation is only dependent on time, while fatigue occurs if the elongation is only dependent on the number of cycles.

In 1955, NACA[67] published a very comprehensive study of the correlation of the static, creep and fatigue properties of N-155 alloy at elevated temperatures. The static properties were as follows:

Stresses are expressed in daN/mm^2 (1 daN/mm^2 = 1450 lb/in^2)					
Temperature	σ_{ult}	σ_{prop}	$\sigma_{0.2\%}$	A%	Σ%
540°C	93	32	37	44	41
815°C	44	27	36	22	14

Creep rupture is illustrated by the curves in Figure 3.49. Ultimate elongation was approximately 20% and did not depend on temperature; it tended to decrease under low stresses and over great lengths of time.

If stress includes an alternating component, ultimate strength becomes smaller (10%). Creep strength based on mean stress decreases as the alternating stress increases, but it is less affected if the temperature is high and the time to rupture considerable. The impact on strain over a specified period of time is even less important. Apparently, load cycling causes no change in the development of creep. The strength under alternating stress decreases less rapidly with temperature than the static strength or creep strength. Between 1,500 and 3,600 c/m, the rate of fatigue loading has no effect on the strength obtained under alternating loading (the process involved is therefore fatigue) or on the creep life expressed in hours (thus, fatigue only occurs with a zero mean component). The ratio time-to-cracking/total time-to-fracture for notched specimens subjected to alternating fatigue is larger at high temperature. In alternating fatigue, the influence of the surface condition is governed by the residual stresses and not by roughness. Heating, although prolonged, hardly changes the residual stresses which, however, disappear during the development of fatigue or creep and do not modify the strength at high temperature.

The situation is less complex for aluminium alloys in the hot condition. One may imagine an on-off variation of temperature within two limits (step variation). Tests conducted at the University of California and the Cornell Laboratory have led to the following findings[68,69]:

(a) The creep strain and time-to-rupture of aluminium alloys are not affected by intermittent temperature application when compared with tests under constant load and temperature conditions, considering the net time-under-stress at elevated temperature.

(b) Creep is accelerated and fracture occurs more rapidly under intermittent stressing at constant temperature.

(c) In the case of 2024-T3 below 235°C, the time-under-stress is the predominant factor in constant-temperature tests. Between 235°C and 315°C, recovery intervenes during every off-load period, whereby the strain is increased and the time to fracture reduced. Furthermore, overageing increases the recovery effect and at 600°C its influence is more significant on cyclically stressed specimens than on specimens subjected to constant stress.

(d) In the case of 7075-T6 at 150°C, the off-load periods accelerate the development of creep (net time-under-stress) if the stress is high (33 daN/mm^2 = 47,000 lb/in^2). At 315°C, creep is increased under low stresses and over great lengths of time (effect of time at high temperature).

It should also be noted[68] that, when cyclic stressing reduces the ductility owing to its effect on a given phase change, the result is premature failure (as with N-155 steel at 730°C).

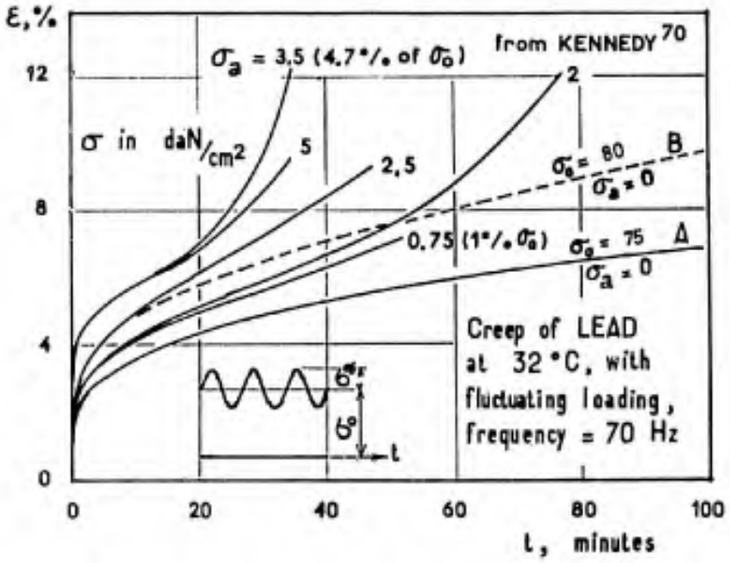

Fig. 3.50 Creep of lead under steady or fluctuating loading

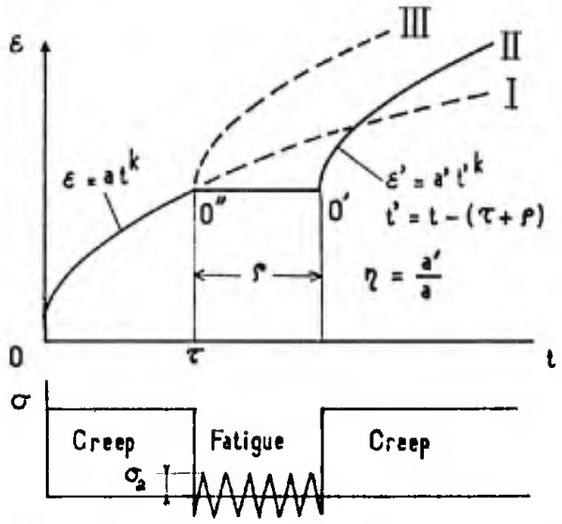

Fig. 3.51 Effect of rest and fatigue on the creep of lead, from Kennedy[70]

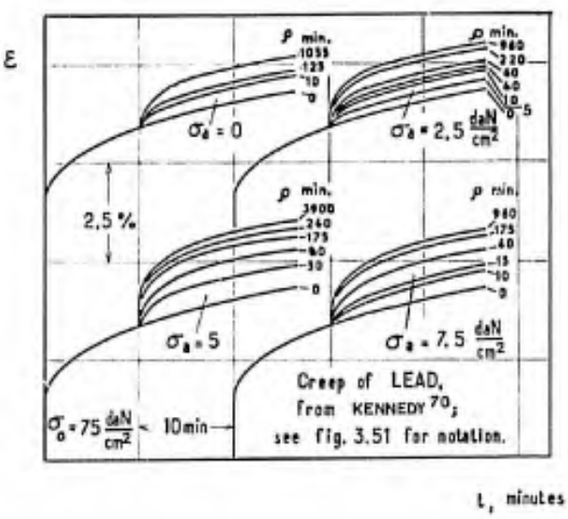

Figure 3.52

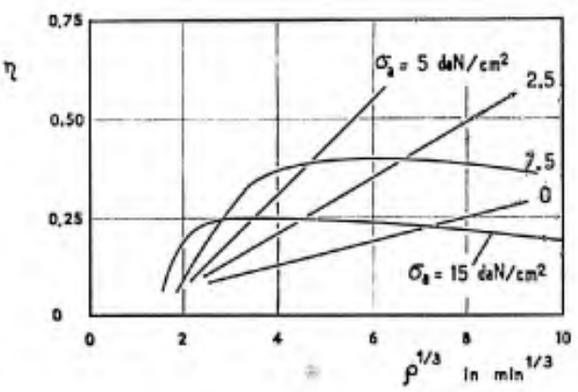

Fig. 3.53 Creep of lead, effect of rest and fatigue, from Kennedy[70]

Total elongation under intermittent stressing is predicted by means of the equivalent-life-fraction expression:

$$L = \sum \frac{t_i}{t_{F,i}} , \tag{29}$$

where t_i = time under σ_i at the temperature T_i, $t_{F,i}$ = time under σ_i at T_i to attain a given deformation ϵ or failure, in a creep test at constant stress σ and constant temperature T.

The prediction would be accurate if $L = 1$ was obtained. In fact, the assessment is often a rough one, except for materials which are stable under the effect of temperature in the absence of stress.

For lead subjected to fluctuating stress $\sigma = \sigma_0 + \sigma_a \sin\omega t$ at 300 c/s, Kennedy[70] has found the results plotted in Figure 3.50. The creep of lead is faster under $\sigma = 75 \pm 2.5$ daN/cm^2 than under $\sigma_0 = 80$ daN/cm^2 and the time to fracture much shorter. With $\sigma = 75 \pm 3.5$ daN/cm^2 the strain rate passes through a maximum and elongation at fracture becomes quite significant. The strain rate and the elongation at fracture decrease if $\sigma = 75 \pm 5$ daN/cm^2. Such circumstances make creep prediction impossible.

In fact, for certain materials, load interruption or over-stressing can involve a considerable change in the behaviour which may be predicted on the basis of the above cumulative rule.

In the fatigue of steel (Figure 2.21, after Bairstow), we have seen the net effect of alternating stress which favours the elongation due to mean stress. It therefore appears necessary to investigate the effect of vibration on creep strain, which depends on time, and on steady fatigue strain, which depends on the number of cycles.

For 4% - copper aluminium alloy (Simmons and Cross[72]) subjected to repeated stress of 17.4 daN/mm^2 = 25,000 lb/in^2 (1 minute under stress, 1 minute off-stress), the creep rate was $0.5 \cdot 10^{-3}$% per hour, that is, 10^{-3} per hour of stressing instead of $0.65 \cdot 10^{-3}$ per hour under a constantly applied stress.

In other cases quoted by Kennedy[71], various sequences of loading and resting either accelerate or delay creep: e.g. Al-Zn-Mg[73], Inconel[74], steels, aluminium alloys, magnesium alloys, titanium alloys[75]. The conclusion is that tests must be carried out for each specific case to determine the effect of load interruption or alternating load on creep.

Kennedy's[71] studies on lead are of little technical interest but, being systematic investigations, they have a great scientific significance. Their main purpose was to study the effect of periods of rest or of fatigue on creep. Figure 3.51 illustrates the loading sequence and some results are plotted in Figures 3.52 and 3.53.

At the beginning of the test under constant load, curve I applies until the instant $t = \tau$ according to the relation

$$\epsilon = at^{1/3} . \tag{30}$$

After an off-load period $\rho(\sigma = 0)$ with or without vibration $(\sigma = \sigma_a \sin\omega t)$, the test is resumed at the time

$$t = \tau + \rho \quad \text{or} \quad t' = 0 .$$

Creep then follows the law

$$\epsilon' = a' t'^{1/3} .$$

The metal becomes soft again, although less than at the beginning, and the degree of *recovery* is measured by

$$\eta = a'/a .$$

Prior to initial creep stressing, resting at room temperature has no relieving influence on the strain hardening due to fabrication. After creep initiation, the action of resting, that is, of thermal agitation alone, and the action of low alternating stressing are of the same nature. The degree of recovery η increases regularly with time:

$$\eta \simeq 0.1 + 0.01(1 + 2\sigma_a)(\rho^{1/3} - 0.2^{1/3})$$

where σ_a is expressed in daN/cm^2 and ρ in minutes.

If, according to our assumption (Chapter II, Section 2.3), recovery consists in the progressive elimination of the less stable atomic lattice distortions under the joint action of residual stresses and thermal agitation as well as under mechanical fatigue shaking, it cannot be complete. If the time of resting is sufficiently long, η will approach an asymptotic maximum. As long as the alternating stresses σ_a are low enough to create no new stable lattice distortions under the effect of the creep stress σ, the tendency should remain the same. Figure 3.53 shows that, with $\sigma_a \geq 7.5$ daN/mm^2, η passes through a maximum over a length of time ρ_1 and then fatigue generates hardening. Here we find an equivalent of the phenomenon examined in Section 2.1.3: thermal agitation due to fatigue destroys the less stable distortions induced by previous work-hardening

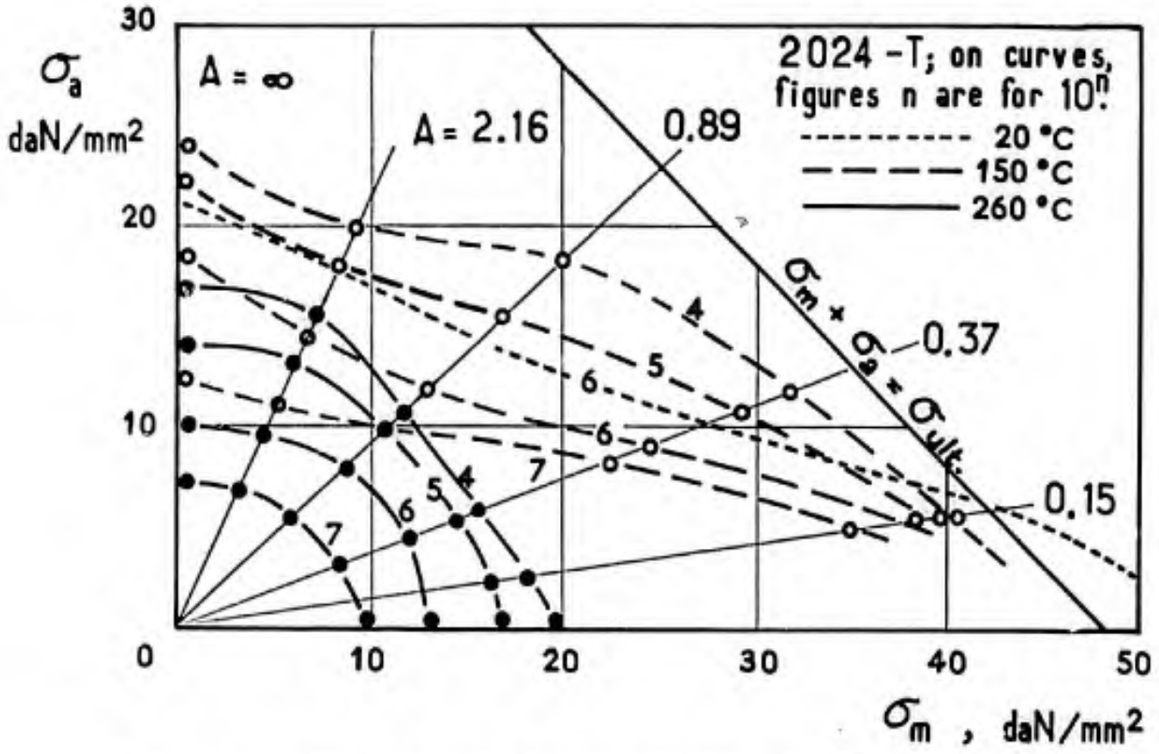

Fig. 3.54 Life of 2024 aluminium alloy in cold and hot fatigue, from de Mocy and Lazan[82]

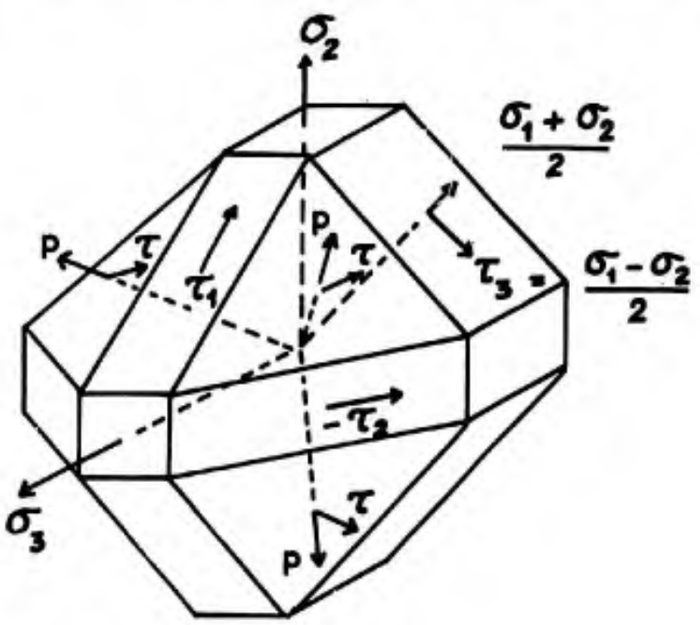

σ_1 , σ_2 , σ_3 : principal stresses

τ_1 , τ_2 , τ_3 : principal shears

$p = (\sigma_1 + \sigma_2 + \sigma_3)/3$: hydrostatic pressure

$\tau = \frac{2}{3}\sqrt{\tau_1^2 + \tau_2^2 + \tau_3^2}$: octahedral shear stresses

Fig. 3.55 Octahedral stresses

in order to replace them by new distortions, the result being a softening effect followed by hardening. This phenomenon belongs to the same group as the Brinell hardness variation during static or fatigue tests obtained by Polakowski[II.30, II.40] on work-hardened engineering metals.

In the same tests, Kennedy also investigated the variation of recovery as a function of the time τ of the first creep, assuming a constant time of interruption $\rho = 70$ min and various alternating stresses. The maximum recovery as well as the alternating stress from which it originates are increased if the duration of the first creep is reduced. This supports our opinion that creep reinforces the stability of those lattice distortions which it has not eliminated in the initial stage. Recovery develops with the number of vibration cycles, hence with frequency. It mainly concerns transient creep and stresses close to the yield strength of the metal.

With 14 S-T aluminium alloy (similar to French A-U4SG) heated to 905°C, Manjoine[79] has found that under 19.4 daN/mm^2 rupture corresponds to $\epsilon_{ult} = 3.4\%$ and $t_{ult} = 65$ hours, and under 19.5 ± 1.95 daN/mm^2 to $\epsilon_{ult} = 4.2\%$ and $t_{ult} = 29$ hours.

On A-U2GN aluminium alloy at 175°C, tests conducted by Sud-Aviation[80] show no difference over 100 hours between static creep under $\sigma = 15.5$ daN/mm^2 and creep with vibration (f = 330 Hz) under $\sigma = 15.5 \pm 1.5$ daN/mm^2. This does not prove that the phenomenon will be absent at lower temperatures and higher stresses.

The same alloy has been used to test formula (26) in order to determine the effect of creep under 16 daN/mm^2 with a cyclic temperature variation between 40°C and 175°C. The durations found were somewhat shorter than predicted (70%), but scatter was considerable owing to an inaccurate temperature control.

On 2024-T3 alloy exposed to 150°C, Shepard, Starr, Wiseman and Dorn[81] have registered a considerable increase of creep under 32.5 daN/mm^2 when introducing an half-an-hour's rest every two hours. Under a stress as low as 4 daN/mm^2 (5,600 lb/in^2) the effect was still such that a load interruption of one hour every two hours produced the same deformation for the same total length of time. This effect is much smaller for 7075-T6 aluminium alloy subjected to 33 daN/mm^2. Formula (29) may result in the time-to-failure being overestimated by a factor of 2 to 5 for 2024-T3 and 1.5 for 7075-T6 when stress or temperature are cycled.

De Money and Lazan[82] have studied the axial fatigue and creep strength of 24 S-T rolled bars at three temperatures, 20°C, 150°C and 262°C, the frequency of the alternating stress being 60 c/s. In Figure 3.54 it is shown that the effect of mean stress is of the same nature at 20°C and 150°C; the process involved is hot fatigue. At 260°C, the $\sigma_a - \sigma_m$ plot for a specified value of N is typical of creep. It is relevant to recall that $A = \sigma_a/\sigma_m$. For $0 < A \leq 0.37$, ultimate elongation is approximately 20%, typical of creep. With $A = 0.89$ and 2.16, it is substantially lower, being in the range of 0.01 to 0.1. At 150°C and 260°C, the study of the elongation progress with the number of cycles shows that the relative elongation ϵ/ϵ_{ult} at the beginning of the test is large if the alternating stress is well above the mean stress; the effect of alternating stress on primary creep is observed again here.

From the foregoing it appears clearly that the prediction of the time to a given strain or to fracture in creep or fatigue-creep under complex load and temperature conditions can only result from interpolation on direct tests. Instead of the law (29), we may use the equivalent-time concept with the Larson-Miller parameter (Eq. (22)), which varies with stress and is substantially representative of the activation energy:

$$Q = 1.98T(\log t + D) \text{ cal.g/mole} .$$

3.3 SIMULTANEOUS STRESSES - YIELDING

From the point of view of strength under applied stresses, the design of mechanical components is conditioned by two requirements: on the one hand, permanent deformation under the highest service loads must remain within limits consistent with the geometrical operating conditions; on the other hand, uncertainties regarding the effective stresses, the adequacy of the design analysis and the actual properties of the materials must be offset by a proper *safety margin* between the predicted stresses and those liable to cause failure of the components.

The elastic limit implies the absence of permanent deformation. This is a rather subjective concept and its magnitude decreases with increasing accuracy of measurement. We are therefore led to take as reference for the allowable permanent deformation the *offset yield strength*, which is defined as the highest tensile stress producing a residual strain equal to a given threshold (0.2% for example).

In the case of combined axial and shear loadings, it is useful to anticipate the stress value at which the yield strength will be reached. It might also be useful to assess the stress distribution in the plastic range and the stresses for localized fracture.

3.3.1 Simplifying Assumptions of Plastic Yielding Theories

We have already discussed the complexity of the plastic behaviour of metals; computation is only possible by resorting to a simplified representation. The following assumptions are used wholly or partly in various theories:

1. Hydrostatic compression or tension causes no plastic slip.
2. Conversely, plastic slip develops under constant-volume conditions.
3. Metals are statistically isotropic and isotropy remains after plastic deformation.
4. There are identical strain-hardening states for different stress states around a point; in other words, the strain and distortion condition of a metal may be defined for subsequent loading as a scalar quantity with regard to the stress-strain relations on a microscopic scale.

Using axial compression, Bridgman[II, 58] has demonstrated that steel increases in volume above the yield stress although the theory of elasticity predicts a reduction in volume. Practically, the assumptions 1 and 2 seem to hold in the vicinity of the yield point.

Statistical isotropy means that the stress-strain curves are independent of the orientation of the external load. Bars and sheets subjected to heavy drawing or rolling exhibit the following characteristics:

(a) There is a tendency toward a privileged mean orientation of the crystalline grain planes.

(b) Grains undergo an overall elongation or flattening process.

(c) The slip planes which appear in each grain prove more rigid in relation to subsequent sliding under further loading.

(d) Prior plastic strain due to fabrication induces residual stresses whose location and mean orientation typify the work-hardening effect.

Grain orientation anisotropy, (a), has some considerable implications on recrystallization but is unimportant in the mechanical range owing to the large number of slip directions in cubic lattice metals such as iron and aluminium.

Grain shape anisotropy, (b), plays a greater part because grain boundaries constitute very stable slip barriers and hardness is conditioned by their average distance.

Anisotropies (c) and (d), which cannot be separated, represent mechanical anisotropy.

Klinger and Sachs[82] have conducted tensile and compressive tests in the longitudinal and transverse directions - relative to the direction of rolling - on sheets of 24 S-T and 24 SR-T (24 S-T work-hardened by heavy cold-rolling). In each case the ultimate strengths in both directions were identical whereas the tensile yield strength was lower by 15% and the compressive yield strength higher by 12% in the transverse direction, this corresponding to a Bauschinger effect. In the course of plastic deformation the tension or compression curves for both directions tended to join. Sachs[83] has shown that ageing at 150-180°C reduces the difference between transverse and longitudinal directions. Consequently, the anisotropy of rolling, like that of static tension, appears to be related to the Bauschinger effect, hence to the stability of slip barriers, and is more associated with the residual stresses and the microscopic distribution of the applied stresses than with a preferential orientation. Large strains cancel the effect of previous anisotropy and may restore a certain amount of isotropy at the onset of polygonization (see Section 2.3).

We have previously supposed that plastic deformation is governed by shear, and is not affected by hydrostatic pressure; while fracture depends on the local tensile stresses which are the sum of hydrostatic tension and stresses resulting from the transformation of mean shear stress to tensile (and compressive) stresses on the slip barriers.

3.3.2 Invariants of the State of Stress and of the State of Strain

State of Stress

The state of stress around a point is defined by the three principal stresses $\sigma_1, \sigma_2, \sigma_3$ and by the directions of the corresponding principal axes. In a reference system aligned with the principal axes, the stress tensor is represented by a matrix T :

$$T = \begin{bmatrix} \sigma_1 & 0 & 0 \\ 0 & \sigma_2 & 0 \\ 0 & 0 & \sigma_3 \end{bmatrix} = \begin{bmatrix} p & & \\ & p & \\ & & p \end{bmatrix} + \begin{bmatrix} s_1 & & \\ & s_2 & \\ & & s_3 \end{bmatrix},$$

which may be separated into a diagonal scalar matrix p representing the hydrostatic pressure tensor

$$p = 1/3(\sigma_1 + \sigma_2 + \sigma_3)$$

and a matrix s representing a deviator, such that

$$s_1 = \sigma_1 - p, \quad s_2 = \sigma_2 - p, \quad s_3 = \sigma_3 - p.$$

The tensor T is dependent on the invariants k_1, k_2 and k_3,

$$k_1 = -(\sigma_1 + \sigma_2 + \sigma_3) ,$$

$$k_2 = (\sigma_1\sigma_2 + \sigma_2\sigma_3 + \sigma_3\sigma_1) ,$$

$$k_3 = -(\sigma_1\sigma_2\sigma_3) ,$$

and satisfies the equation

$$T^3 + k_1T^2 + k_2T + k_3 = 0 .$$

With $S = T - p$ and $k_1 = -3p$, the deviator S satisfies the equation

$$S^3 + (k_2 - k_1^{2/3})S + \frac{2}{27} k_1^3 - k_1k_2/3 + k_3 = 0 .$$

The deviator includes only two invariants:

$$J_2 = k_1^2/3 - k_2 , \quad J_3 = k_1k_2/3 - \frac{2}{27} k_1^3 - k_3 ,$$

such that

$$S^3 = J_2S + J_3 .$$

Computation yields

$$J_2 = \frac{2}{3}(\sigma_1 - \sigma_2)^2/4 + (\sigma_2 - \sigma_3)^2/4 + (\sigma_3 - \sigma_1)^2/4 , \tag{31}$$

where the quantities in parentheses are the maximum shear stresses

$$\tau_3 = (\sigma_1 - \sigma_2)/2 , \quad \tau_2 = (\sigma_2 - \sigma_3)/2 , \quad \tau_1 = (\sigma_3 - \sigma_1)/2 ,$$

whence

$$J_2 = \frac{2}{3}(\tau_1^2 + \tau_2^2 + \tau_3^2) ,$$

with

$$\tau_1 + \tau_2 + \tau_3 = 0 .$$

It is easy to give a simple geometrical interpretation of J_2 and p by means of the components of the stress applied to a unit facet of 111-direction, the normal unit vector of which has the following column of components*:

$$X = \frac{1}{\sqrt{3}} \begin{bmatrix} 1 \\ 1 \\ 1 \end{bmatrix} .$$

The components of the force exerted on the facet are given by the column $F = TX$, the projection of which on X is $X\bar{X}F/\bar{X}X$ and on the plane of the facet $(1 - X\bar{X}/\bar{X}X)F = t$.

The square of the tangential stress magnitude is

$$\bar{t}t = \frac{2}{9}(\sigma_1^2 + \sigma_2^2 + \sigma_3^2 - \sigma_1\sigma_2 - \sigma_2\sigma_3 - \sigma_3\sigma_1) = \tau_{oct.}^2 \tag{32}$$

The square of the normal stress magnitude is $n^2 = p^2$.

The tangential stress on the facet is called *octahedral shear stress* because the facets of normal 111 form an octahedron (Fig. 3.55); it is expressed by

$$\tau_{oct.} = \frac{2}{3}\sqrt{(\tau_1^2 + \tau_2^2 + \tau_3^2)} ,$$

hence

$$J_2 = \frac{3}{2} \tau_{oct.}^2$$

---

* With the notations used here, if X is a matrix-column, $\bar{X}$ is the matrix-row which has the same elements, being the transposed matrix-row of the matrix-column; $\bar{X}X$ is a scalar, $X\bar{X}$ a square matrix and T the square matrix of the stress tensor[101].

In writing the invariant $J_3 = s_1 s_2 s_3$, we obtain

$$J_3 = \frac{8}{27}(\tau_1 - \tau_3)(\tau_2 - \tau_1)(\tau_3 - \tau_2)$$

$$= \frac{1}{27}(2\sigma_1 - \sigma_3 - \sigma_2)(2\sigma_2 - \sigma_1 - \sigma_3)(2\sigma_3 - \sigma_2 - \sigma_1) . \qquad (33)$$

Since $\tau_1 + \tau_2 + \tau_3 = 0$, J_2 and J_3 are functions of τ_1 and τ_3.

Taking $\tau_1 + \tau_3 = A$ and $\tau_1 - \tau_3 = B$, it follows that

$$J_2 = 2A^2 + \frac{2}{3}B^2 , \qquad J_3 = -\frac{2}{27}B(9A^2 - B^2) .$$

If we put

$$\mu = \frac{B}{A} = \frac{\tau_1 - \tau_3}{\tau_1 + \tau_3} = \frac{2\sigma_2 - (\sigma_1 + \sigma_3)}{\sigma_1 - \sigma_3} ,$$

with $A = (\sigma_1 - \sigma_2)/2$, we have

$$J_2 = \frac{1}{4}(\sigma_1 - \sigma_3)^2\left(1 + \frac{\mu^2}{3}\right), \qquad J_3 = -\frac{1}{108}(\sigma_1 - \sigma_3)^3\mu(9 - \mu^2) .$$

It can be demonstrated that the components of $\tau_{oct.}$ are

$$(2\sigma_1 - \sigma_2 - \sigma_3)/3\sqrt{3} , \quad (2\sigma_2 - \sigma_3 - \sigma_1)/3\sqrt{3} , \quad \text{and} \quad (2\sigma_3 - \sigma_1 - \sigma_2)/3\sqrt{3} ,$$

so that μ is related to the direction of vector $\tau_{oct.}$ in the octahedral plane. Finally, J_2 characterizes the magnitude of the resulting mean shear stress and J_3 defines the direction thereof.

State of Strain

The state of strain is defined by the principal directions, which may differ from those of stress and by the three principal dilatations ϵ_1, ϵ_2 and ϵ_3. The strain tensor is represented on the principal axes by the matrix

$$D = \begin{bmatrix} 1 & & \\ & 2 & \\ & & 3 \end{bmatrix} = e + d = \begin{bmatrix} e & & \\ & e & \\ & & e \end{bmatrix} + \begin{bmatrix} d_1 & & \\ & d_2 & \\ & & d_3 \end{bmatrix},$$

where $e = (1/3)(\epsilon_1 + \epsilon_2 + \epsilon_3)$ is the unit volume expansion and d_1, d_2 and d_3 the components of the deviator d which depends only on the shearing strains. This deviator is dependent on the two invariants

$$I_2 = -(d_1 d_2 + d_2 d_3 + d_3 d_1)$$

and

$$I_3 = d_1 d_2 d_3 .$$

Computation shows that the dilatation perpendicular to an octahedral facet is $e = (1/3)(\epsilon_1 + \epsilon_2 + \epsilon_3)$. The largest shearing strain on the octahedral facet is

$$\gamma_{oct.} = \frac{2}{3}\sqrt{[(\epsilon_1 - \epsilon_2)^2 + (\epsilon_2 - \epsilon_3)^2 + (\epsilon_3 - \epsilon_1)^2]} \qquad (34)$$

in a plane identified by the normal and a vector having the components

$$\frac{2\epsilon_1 - \epsilon_2 - \epsilon_3}{C} , \quad \frac{2\epsilon_2 - \epsilon_3 - \epsilon_1}{C} , \quad \frac{2\epsilon_3 - \epsilon_1 - \epsilon_2}{C} ,$$

where

$$C = \frac{3\sqrt{3}}{2}\gamma_{oct.} .$$

Then we have

$$\gamma_{oct.}^2 = \frac{8}{3}I_2 .$$

Further we obtain

$$I_3 = \frac{1}{27C^3}(2\epsilon_1 - \epsilon_2 - \epsilon_3)(2\epsilon_2 - \epsilon_3 - \epsilon_1)(2\epsilon_3 - \epsilon_1 - \epsilon_2) .$$

Given $\epsilon_1 - \epsilon_3$, ϵ_2 is defined by

$$\nu' = \frac{\gamma_3 - \gamma_1}{\gamma_2} = \frac{2\epsilon_2 - \epsilon_3 - \epsilon_1}{\epsilon_1 - \epsilon_3}$$

and it follows that

$$I_2 = \frac{1}{4}(\epsilon_1 - \epsilon_3)^2\left(1 + \frac{\nu'^2}{3}\right), \quad I_3 = -\frac{1}{108}(\epsilon_1 - \epsilon_3)^2\nu'(9 - \nu'^2) . \tag{35}$$

Stress-strain Relations

In the elastic range we have

$$E\epsilon_1 = \sigma_1 - \nu(\sigma_2 + \sigma_3)$$

$$E\epsilon_2 = \sigma_2 - \nu(\sigma_3 + \sigma_1)$$

$$E\epsilon_3 = \sigma_3 - \nu(\sigma_1 + \sigma_2) ,$$

whence

$$Ee = p(1 - 2\nu) , \quad E\gamma_{oct.} = 2(1 + \nu)\tau_{oct.} \tag{36}$$

and, with $G = E/2(1 + \nu)$, $G\gamma_{oct.} = \tau_{oct.}$; the Lode coefficients μ and ν' are equal.

In the plastic range, if the metal is and remains isotropic, various conditions are used to define attainment of the yield stress.

The Tresca condition reads as follows:

$$\sigma_1 > \sigma_2 > \sigma_3 , \quad \left(\frac{\sigma_1 - \sigma_3}{2}\right)^2 = k^2 ;$$

the maximum shearing stress reaches a certain limit value k .

The von Mises condition is expressed by $J_2 = k^2$, where k is the yield point in pure shear; it is also given by

$$\tau^2 = \frac{4}{9}(\tau_1^2 + \tau_2^2 + \tau_3^2) = \tau_{oct.}^2 = \frac{2}{3}k^2 \tag{37}$$

or

$$k^2 = \frac{2}{3}\left[\left(\frac{\sigma_1 - \sigma_2}{2}\right)^2 + \left(\frac{\sigma_2 - \sigma_3}{2}\right)^2 + \left(\frac{\sigma_3 - \sigma_1}{2}\right)^2\right] .$$

Instead of $\tau_{oct.}$ and $\gamma_{oct.}$, some authors use the so-called *effective values* of τ and γ which reduce to tensile stress and axial strain in standard tests designed to determine the strength and ductility of materials. With $\sigma_1 = \bar{\sigma}$, $\sigma_2 = \sigma_3 = 0$, $\epsilon_2 = \epsilon_3 = -\nu\bar{\epsilon}$, we obtain

$$\tau_{oct.} = \frac{1}{3}\sqrt{[\Sigma(\sigma_i - \sigma_j)^2]} = \frac{\sqrt{2}}{3}\bar{\sigma} ,$$

$$\gamma_{oct.} = \frac{2}{3}\sqrt{[\Sigma(\epsilon_i - \epsilon_j)^2]} = \frac{2\sqrt{2}}{3}(1 + \nu)\bar{\epsilon} ,$$

whence

$$\bar{\sigma} = \frac{3}{\sqrt{2}}\tau_{oct.} = \frac{1}{\sqrt{2}}\sqrt{[\Sigma(\sigma_i - \sigma_j)^2]} , \tag{38}$$

$$\bar{\epsilon} = \frac{3}{2\sqrt{2}(1 + \nu)}\gamma_{oct.} = \frac{1}{\sqrt{2}(1 + \nu)}\sqrt{[\Sigma(\epsilon_i - \epsilon_j)^2]} . \tag{39}$$

With $\nu = 0.5$ (case of plasticity), we obtain

$$\bar{\epsilon} \simeq \frac{\sqrt{2}}{3}\sqrt{[\Sigma(\epsilon_i - \epsilon_j)^2]} \tag{40}$$

This is the expression used by several authors such as Davis and Parker[84], Coffin[102] and Steele[103].

Several researchers have carried out tests on tubes subjected to biaxial stresses through combined axial tension, pressure or torsion. For mild annealed steel, tests conducted by Davis and Parker[84] at room temperature and at -94°C on isotropic metals have shown good agreement of the $\bar{\sigma}$-$\bar{\epsilon}$ curves, except for true ultimate elongation and the corresponding stress, $\sigma_{ult.}$ varying from 73 to 94 daN/mm^2. Previously, the agreement of the $\bar{\sigma}$-$\bar{\epsilon}$ curves was found to be very good by Davis[104] for copper, except near fracture, in which case ϵ_{ult} is equal to 0.68 lengthwise and to 0.27 circumferentially. Swift[12] obtained fairly comparable curves for mild steel in tension and in torsion.

The fact that a lower ultimate elongation is attained in the *short transverse direction* on a large number of engineering metals does not imply that the yield properties are poorer but that fracture occurs at a smaller elongation, the $\bar{\sigma}$-$\bar{\epsilon}$ curve being, up to that point, close to the curve obtained in the longitudinal direction. In such cases, ultimate elongation is restricted by an internal notch effect.

In creep, whether transient or secondary, there is also a relation

$$\bar{\sigma} = f(\bar{\epsilon}, t, T) . \tag{41}$$

It is verified fairly well if the directions and ratios of the principal stresses vary little during straining. Wu[85] using the stress-plastic strain relations

$$\epsilon_1 + \epsilon_2 + \epsilon_3 = 0 ,$$

$$\frac{\sigma_1 - \sigma_2}{\epsilon_1 - \epsilon_2} = \frac{\sigma_2 - \sigma_3}{\epsilon_2 - \epsilon_3} = \frac{\sigma_3 - \sigma_1}{\epsilon_3 - \epsilon_1} ,$$

$$\tau_{oct.} = F(\gamma_{oct.}) ,$$

was thus able to solve a number of problems of revolution (spherical membranes, rotating discs).

Strain Energy

It has been suggested that the octahedral stress be considered as a measure of the elastic shear energy. The total elastic energy in the unit volume of material is

$$\frac{1}{2E}[\sigma_1^2 + \sigma_2^2 + \sigma_3^2 - 2\nu(\sigma_1\sigma_2 + \sigma_2\sigma_3 + \sigma_3\sigma_1)] ;$$

the hydrostatic compression energy is

$$\frac{1 - 2\nu}{E} \cdot \frac{3}{2}\left(\frac{\sigma_1 + \sigma_2 + \sigma_3}{3}\right)^2 = \frac{3}{2} p^2 \cdot \frac{1 - 2\nu}{E} .$$

Subtracting, we obtain the elastic shear energy

$$U = \frac{1 + \nu}{E}[\sigma_1^2 + \sigma_2^2 + \sigma_3^2 - \sigma_1\sigma_2 - \sigma_2\sigma_3 - \sigma_3\sigma_1] , \tag{42}$$

whence

$$U = \frac{1 + \nu}{6E}\Sigma(\sigma_i - \sigma_j)^2 = \frac{3}{2} \cdot \frac{1 + \nu}{E} \cdot \tau_{oct.}^2 .$$

On the other hand, with

$$\gamma_{oct.} = \frac{2(1 + \nu)}{E} \cdot \tau_{oct.} ,$$

we may write

$$\int_0^{\gamma_{oct.}} \tau_{oct.} d\gamma_{oct.} = \frac{1 + \nu}{E} \tau_{oct.}^2 .$$

and $$U = \frac{3}{2}\int_0^{\gamma_{oct.}} \tau_{oct.}\, d\gamma_{oct.} = \frac{2}{3}(1+\nu)\int \sigma_{eff.}\, d\epsilon_{eff.} \quad (43)$$

In the plastic range, this expression will be retained, as are

$$\int \tau\, d\gamma \quad \text{and} \quad \int \sigma\, d\epsilon\,,$$

corresponding to simple shear and tension, respectively.

3.4 BUCKLING DURING OR AFTER FATIGUE AND CREEP

The *buckling* or instability of shape of compressed components includes a region of unstable elastic equilibrium which has been known since Euler for columns and has been extended to more complex components (see Timoshenko[86]). Under high stresses the process involved is yielding with regard to strength at room temperature and creep with regard to strength at elevated temperature.

At room temperature, buckling in the plastic range is governed by the stress-compressive strain curve above the proportional limit. The buckling load may be predicted by replacing the modulus of elasticity, E, in the theoretical relations of the elastic range by one of the fictitious moduli of elasticity:

(i) the tangent modulus, $E_\sigma = d\sigma/d\epsilon$,

(ii) the secant modulus, $E_s = \sigma/\epsilon$,

(iii) the reduced Kármán modulus[87], E_r, which is obtained by assuming that the metal deforms according to the σ–ϵ curve under increasing stress and remains elastic with the modulus E under decreasing stress. For I-sections with concentrated flanges and webs of small thickness,

$$E_r/E = \frac{2\,E_\sigma/E}{1 + E_\sigma/E}\,; \quad (44)$$

for solid rectangular sections,

$$E_r/E = \frac{4\,E_\sigma/E}{[1+\sqrt{(E_\sigma/E)}]^2}\,; \quad (45)$$

we also have approximately

$$E_r/E = k\,\frac{E_\sigma/E}{[1 + (\sqrt{k}-1)\sqrt{(E_\sigma/E)}]^2} \quad (46)$$

with $k = 3.6$ for thin tubular sections[88] and $k = 3.8$ for solid circular sections.

As shown by Shanley[89], the buckling load calculated with E_r represents the upper limit of the load that is actually held by a rectilinear column whereas the tangent modulus E_σ defines the lower limit. Furthermore, owing to slight eccentricities likely to occur in practice, computation with the secant modulus or the tangent modulus are better verified by the facts.

In the case of an initial eccentricity of the load or initial lateral deflection the column is stressed in bending-compression. If elasticity is assumed, there is an equilibrium deflection curve for each value of the load. In the plastic range above the proportional limit, there are two equilibrium deflection curves, a stable one and an unstable one, for each value of the load below the critical value[92]. At the critical load, the two deflection curves coincide and consequently stable equilibrium proves impossible. The critical load is a function of the initial eccentricity or lateral deflection and, conversely, for a given load there is a critical value of the initial eccentricity or deflection.

At elevated temperature, the metal subjected to constant stress creeps and the deflection or eccentricity increases constantly until equilibrium becomes impossible. In 1952, Shanley and Higgins[89] presented an excellent discussion of the problem. More recently, Freijs de Veubeke[90] pointed out that the main effect of creep is to increase the initial eccentricities or deflections and that rapid buckling takes place when the deflection curve resulting from creep reaches a critical magnitude corresponding to instability under the applied load. This analysis of the problem remains an academic one if creep and final failure occur under the same load and temperature conditions.

One may, however, consider the case where creep occurs at high temperature under small loads, thereby increasing the initial imperfections without buckling taking place, buckling occurring later at a lower temperature under very high loads. Creep thus causes some damage which reduces the subsequent buckling load.

We believe that the three causes of damage liable to lower the buckling strength of a structure are as follows: creep modifying the initial imperfections depending on steady loading, temperature and time; continuous fatigue deformation depending on alternating loading, steady loading and number of cycles; finally, the action of creep and fatigue reducing the previous work-hardening of the metal and modifying the σ-ϵ compression curve which governs rapid buckling. The general problem of predicting the buckling load or the *critical time to buckling* after creep or fatigue may be divided into three distinct items:

1. Determination of the static compression σ-ϵ curves at the temperature T of rapid buckling, after creep and/or fatigue. This is a matter for experiment.

2. From these curves, computation of the *critical buckling load* for a given initial deflection or, conversely, computation of the *critical initial deflection* corresponding to the applied stress.

3. Prediction of the critical time before the initial deflection increases sufficiently to cause rapid buckling at the critical deflection. Stresses vary during bending-compression creep; algebraic calculation in accordance with the relation $\epsilon = f(\sigma, t)$ or digital computation assuming a constant stress value over a fairly short time interval may then be effected. Calculations of this kind are to be found in the work of Higgins[89], Chapman, Erickson and Hoff[99], and Fraijs de Veubeke[90].

With regard to creep and final buckling computation, the assumption that buckling does not decrease stress proves conservative and sufficiently accurate. In the case of rapid buckling of rectilinear bars, this amounts to applying the tangent modulus theory. With advanced means of digital computation more complex cases than bars of constant cross-section with hinged ends, as investigated in the foregoing references, may be dealt with by this method.

Supersonic aircraft structures raise a more complicated problem because the creep loads and temperatures involved vary in flight and the high loads capable of causing buckling are random quantities, thus increasing the scattering of the critical time.

Another difficulty lies in the establishment of a safe upper limit for defects in straightness and eccentricities. These can easily be measured on simple parts such as bars. But measurements or predictions are hardly feasible for complex components masked in an assembly. *In the case of cold aircraft where no creep occurs, the purpose of static tests of aircraft structures to ultimate loads is to reveal the implications of eccentricities and unavoidable defects.* For supersonic aircraft exposed to high temperatures at cruising speed, fatigue and creep tests could be performed under load and temperature conditions designed to simulate the service conditions over a period of time equal to two or three times the operating life so as to take account of scatter; they might be followed by a static rupture test for determination of the existing margins of buckling strength after the initial geometrical defects have been increased by fatigue and creep.

On the other hand, if the usual safety factor of 1.5 between the highest design loads, of very rare occurrence in service, and the ultimate loads is retained, even quite visible faults can be tolerated. Tests performed in 1943 on steel tubes[92] of slenderness $\lambda = L/r = 30$ showed that the critical stress was 51 daN/mm^2 with a relative initial deflection $a/L = 1/1,000$ and 41 daN/mm^2 with $a/L = 7/1,000$. If $L = 200$ mm, 0.2 mm deflections are not apparent but 1.4 mm deflections can hardly remain undetected in detailed inspection. The ratio of strengths is $51/41 = 1.25$; although smaller than 1.5, this ratio is large enough for safety if inspections permit reliable detection of the growth of geometrical defects.

If deflection variations are not very fast, this problem may be dealt with by maintenance inspections, the lower value of the safety factor being offset by frequent inspections.

3.4.1 Eccentric Buckling in the Plastic Range

The following results are derived from an unpublished theoretical and experimental investigation carried out by the "Service Technique Aéronautique" and the "Etablissement Aéronautique de Toulouse" in 1943.

Tubes are simulated by I-section bars having concentrated flanges and webs of negligible thickness. Figure 3.56 represents the cross-section of such an I-bar having an area A and a depth h. If σ_1 and σ_2 are the compressive stresses in each flange, P the compressive load eccentric by a distance e from the centre of the section, L the length of the bar with hinged ends, y the lateral deflection of the neutral axis from its initial rectilinear position, and ρ the radius of curvature, the mean compressive stress is

$$\sigma_0 = P/A ,$$

the bending moment

$$M = P(e + y) = A(\sigma_2 - \sigma_0)h/2 ,$$

and the radius of curvature satisfies

$$1/\rho = \frac{\Delta}{h} = -y'' ,$$

where $\Delta = \epsilon_2 - \epsilon_1$ is equal to the difference in deformation of the two flanges. Simplifying, we may write

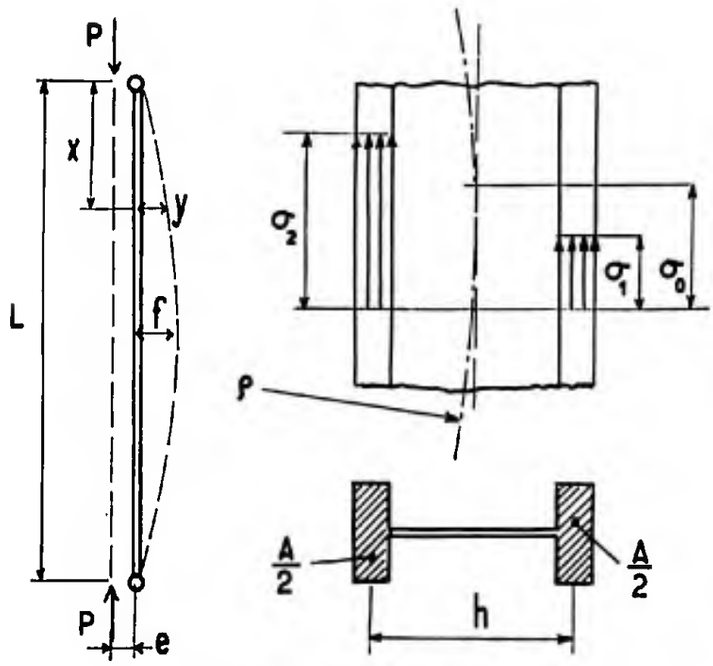

Fig. 3.56 Eccentrically loaded column

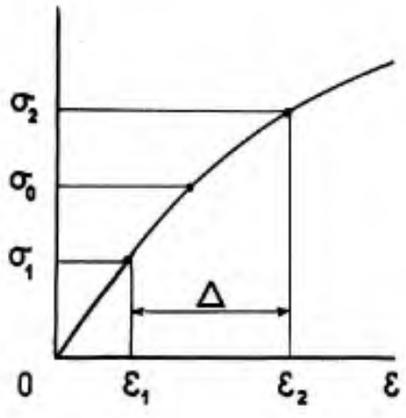

Figure 3.57

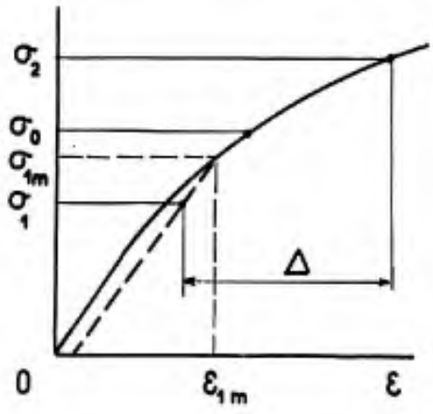

Figure 3.58

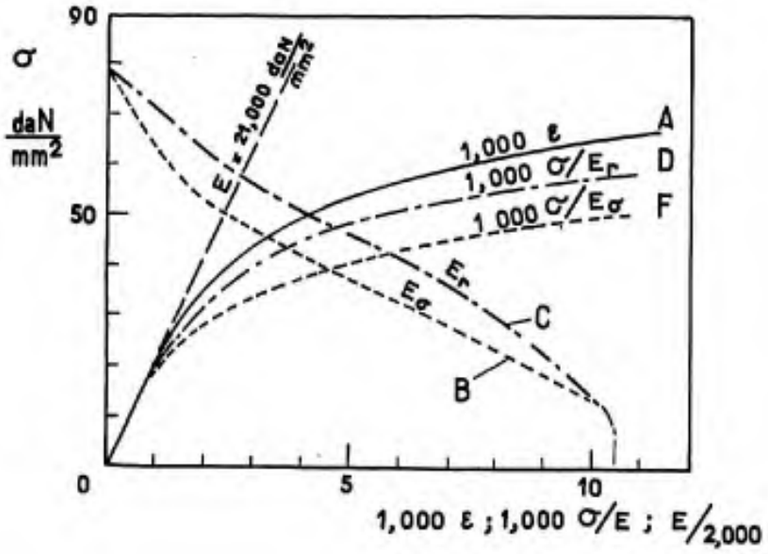

Fig. 3.59 Stress-strain properties of Cr-Mo steel tubes in compression

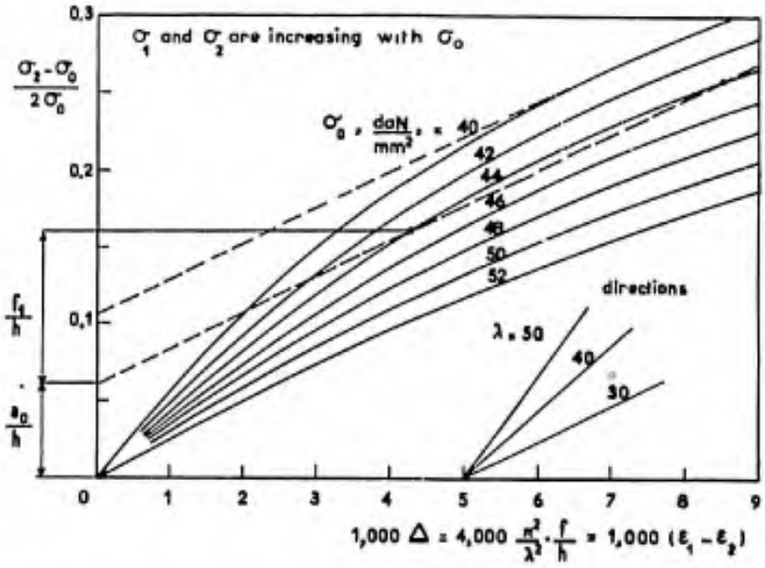

Fig. 3.60 Dimensionless bending moment-curvature curves, computed from data represented in Figure 3.59.

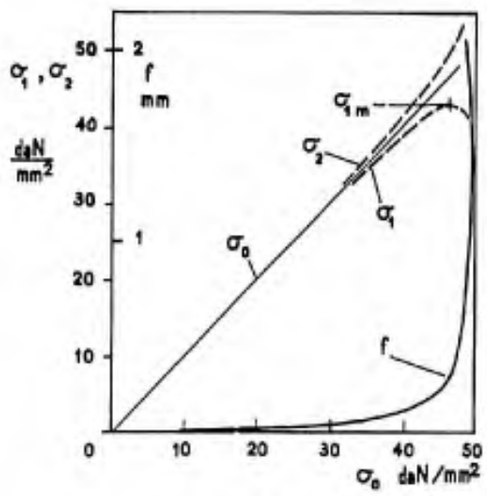

Figure 3.61

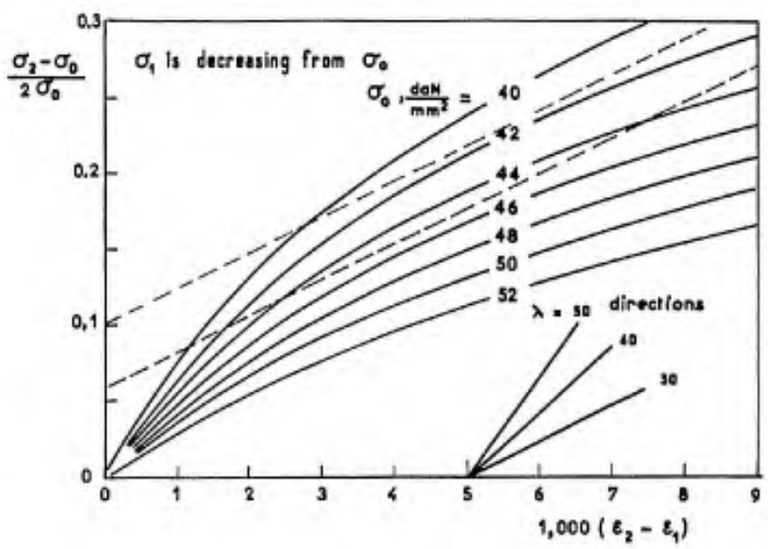

Figure 3.62

$$M/Ph = (\sigma_2 - \sigma_0)/2\sigma_0 = (e + y)/h \qquad (47)$$

$$\Delta = \epsilon_2 - \epsilon_1 = -hy'' . \qquad (48)$$

Considering the small load eccentricities encountered in practice $(1/500 > e/L > 1/1000)$, the bending stresses, $\sigma_2 - \sigma_0 = \sigma_0 - \sigma_1$, remain negligible in relation to σ_0 until σ_0 increases. Up to a certain value of σ_0, σ_1 and σ_2 are increasing; their figurative points, (σ_1, ϵ_1) and (σ_2, ϵ_2), are located on the compression σ-ϵ curve (Fig. 3.57). Then the least stress σ_1 goes through a maximum σ_{1m} which corresponds to the value σ_{0m} of σ_0. For $\sigma_0 > \sigma_{0m}$, the point (σ_1, ϵ_1) moves along a secant passing through $(\sigma_{1m}, \epsilon_{1m})$ and having a slope equal to the modulus of elasticity E (Fig. 3.58).

From the assumption of Figure 3.57 and a σ-ϵ curve of the metal (Fig. 3.59), dimensionless bending moment – curvature curves may be calculated for each value of Δ (Fig. 3.60):

$$\frac{\sigma_2 - \sigma_0}{2\sigma_0} = F(\sigma_0, \Delta) .$$

We shall first use a method of approximate numerical integration and successive iterations suitable for the most complex cases of variable cross-section and built-in conditions. Consider a bar with hinged ends of length L (Fig. 3.56), compressed by a load $P = A\sigma_0$ of relative eccentricity $e/L = 0.6/1000$. We shall assume a slenderness $\lambda = 2L/h = 30$ and, for numerical computation, L = 200 mm, e = 0.12 mm.

Let us begin with $\sigma_0 = 40$ daN/mm^2. In the elastic range the lateral deflection in the middle of the length of the bar is $f = e(1 - \cos u)/\cos u$, with $u = \frac{1}{2}\sqrt{(\sigma_0\lambda^2/E)}$. We obtain $f = 0.031$ mm and assume a parabolic deflection curve y_0:

x =	0	20	40	60	80	100 mm
y_0 =	0	0.0012	0.0050	0.0112	0.0200	0.0310 mm .

The bending moment is proportional to $e + y$:

$$e + y_0 = 0.120 \quad 0.121 \quad 0.125 \quad 0.131 \quad 0.140 \quad 0.151 \text{ mm} ;$$

here $h = 13.33$ mm and $(\sigma_2 - \sigma_0)/2\sigma_0 = (e + y)/13.33$:

$$\frac{(\sigma_2 - \sigma_0)}{2\sigma_0} = 0.0090 \quad 0.0091 \quad 0.0094 \quad 0.0098 \quad 0.0106 \quad 0.0114 .$$

Owing to the very small values of $(\sigma_2 - \sigma_0)/2\sigma_0$, we shall not use Figure 3.60 to calculate Δ, but the limit relation for σ_2 close to σ_0:

$$\Delta = -hy'' = -\frac{2(\sigma_2 - \sigma_0)}{d\sigma/d\epsilon} = -\frac{4\sigma_0}{E}\cdot\frac{\sigma_2 - \sigma_0}{2\sigma_0} .$$

If $\sigma_0 = 40$ daN/mm^2, Figure 3.59 gives $\sigma_0/E_\sigma = 4.5\cdot10^{-3}$, hence $10^3\, y'' = 1.35(\sigma_2 - \sigma_0)/2\sigma_0$. It follows that

$$10^6 y_1'' = 12.1 \quad 12.2 \quad 12.6 \quad 13.2 \quad 14.3 \quad 15.4 .$$

Taking into account the boundary conditions, $y' = 0$ at $x = L/2$ and $y = 0$ at $x = 0$, approximate integration by the trapeze method yields

$10^6 y_1'$ =	1319	1076	828	572	297	0
$10^6 y_1$ =	0	23950	42990	56990	65480	68450
y_1 =	0	0.024	0.043	0.057	0.065	0.068

By iteration, y_6 and y_7 differ by less than 1/100 and we have

$$y = 0 \quad 0.035 \quad 0.064 \quad 0.085 \quad 0.098 \quad 0.103 \text{ mm} .$$

This deflection curve is of near-sinus form. The stresses in the middle of the length are

$$\sigma_2 - \sigma_0 = 1.34 , \quad \sigma_2 = 40.34 , \quad \sigma_1 = 38.66 \text{ daN/mm}^2 .$$

Repeating the calculation for increasing values of σ_0, we obtain

σ_0 =	40	44	45	46	47	48	daN/mm²
f =	0.103	0.200	0.235	0.273	0.455	0.730	mm
σ_1 =	38.66	41.9	42.6	43.3	42.9	41.1	daN/mm²

The stress σ_1 passes through a maximum $\sigma_{1m} = 43.3$ for $\sigma_0 = 46$; the assumption of the Figure 3.57 is then no longer satisfied.

If we proceed with the same calculations for another moment-curvature plot on the basis of the assumption of Figure 3.58, using

$$\Delta = \epsilon_2 - \epsilon_{1m} + \frac{\sigma_{1m} - \sigma_1}{E} ,$$

we obtain

σ_0 =	46	48	49	daN/mm²
f =	0.273	0.670	1	mm
σ_1 =	43.3	42.3	40.8	daN/mm² .

For $\sigma_0 = 49$ daN/mm² , the stable equilibrium deflection curve is y_1 :

x =	0	20	40	60	80	100 mm
y_1 =	0	0.32	0.59	0.81	0.95	1 mm ;

the unstable equilibrium deflection curve is y_2 :

y_2 =	0	0.61	1.12	1.54	1.8	1.9 mm .

In Figure 3.61 the variation of the deflection f in the middle of the length and that of the stresses σ_1, σ_2 are plotted as a function of σ_0 .

With values of σ_0 between 48 and 50 daN/mm², the assumption of Figure 3.57 leads to the critical buckling value $\sigma_{cr.} = 48.5$ daN/mm² , at which the stable and unstable deflection curves are identical. The assumption of Figure 3.58 results in $\sigma_{cr.} = 49.5$ daN/mm² . If we suppose $\sigma_{1m} = \sigma_0$, which is Karman's hypothesis for zero eccentricity, we have $\sigma_{cr.} = 56$ daN/mm² , i.e., 15% above the critical value in the case of eccentricity. Substituting the tangent modulus E_σ for Kármán's reduced modulus E_r , we obtain $\sigma_{cr.} = 49.4$ daN/mm² (without eccentricity).

It is seen that the introduction of the tangent modulus in buckling calculations is one way of offsetting the ignorance of eccentricity.

Let us now go into the case of zero eccentricity but with an initial deflection a_0 in the middle of the bar. To simplify computation, we shall assume initial and final deflection curves of sinusoidal form

$$a = a_0 \sin \frac{\pi x}{L} ,$$

$$y = f \sin \frac{\pi x}{L} ,$$

whence

$$y'' = -(\pi^2 f/L^2) \sin \frac{\pi x}{L} .$$

For small values of the bending moment, the differential equation of the problem with the assumption of Figure 3.57 is

$$\sigma_0(a + y) = -(h^2/4)y''E_\sigma$$

or

$$y'' + (4\sigma_0/E_\sigma h^2)y = -(4\sigma_0/Eh^2)a_0 \sin \frac{\pi x}{L} .$$

If $y = f \sin(\pi x/L)$, we have

$$f = \frac{a_0}{\sigma^*/\sigma_0 - 1} ,$$

where $\sigma^* = E_\sigma \pi^2/\lambda^2$ is the critical stress without eccentricity, calculated on the basis of the tangent modulus E_σ . Here $\sigma^* = 49.4$ daN/mm² for $\lambda = 30$. Having an approximate value of deflection, we may proceed

with a series of iterations as in the former case. We may also use the graphic-collocation method. Equations (47) and (48) are as follows for the middle of the bar:

$$\frac{\sigma_2 - \sigma_0}{2\sigma_0} - \frac{a_0}{h} = \frac{f}{h} \tag{49}$$

and

$$\Delta = \epsilon_2 - \epsilon_1 = (4\pi^2/\lambda^2)(f/h) . \tag{50}$$

On a $(\sigma_2 - \sigma_0)/2\sigma_0 = F(\sigma_0, \Delta)$ plot, the value of f/h that satisfies Equations (49) and (50) will result from the intersection of the σ_0 curve with the straight line of slope $\lambda^2/4\pi^2$ originating at point $\Delta = 0$, $(\sigma_2 - \sigma_0)/2\sigma_0 = a/h$. In Figures 3.60 ($\sigma_1$ and σ_2 increasing with σ_0) and 3.62 (σ_1 decreasing from $\sigma_{1m} = \sigma_0$, Kármán's hypothesis) examples of intersections are illustrated. The σ_0-mark on the curve which is tangent to the straight line represents the critical buckling stress. In Figure 3.60, for instance, the stable equilibrium deflection under $\sigma_0 = 42$ for $\lambda = 30$ and $a_0/h = 0.06$, here $a/L = 4/1000$, corresponds to $f_1/h = 0.09$, that is, $f_1 = 0.12$ mm ; the second intersection corresponds to an unstable equilibrium deflection, $f_2 = 0.285$ mm. The critical stress is slightly less than 43 daN/mm^2. From the same figure, the critical deflection may be determined for $\sigma_0 = 40$ daN/mm^2 and $\lambda = 30$. A tangent of appropriate slope gives $a_0/h = 0.1$, i.e., a_0 critical = 1.33 mm. The critical deflection under load equals the difference between the ordinate of the tangential point (0.25) and $a_0/h = 0.1$: $f = 0.15\ h = 2$ mm.

Calculations not reproduced here have shown that the foregoing method is applicable for an eccentricity e, provided an equivalent initial deflection is assumed:

$$e = 0.8\ a .$$

We may recall that in the elastic range near the buckling load we have

$$e = a/4 = 0.785\ a .$$

It is interesting to know the load-axial strain curve of a column. If we use the preceding data and put $e = 0.12$ mm, δ being the longitudinal displacement and δ_0 the displacement resulting from the difference between arc and chord,

$$\delta_0/L = (\pi^2/4)\frac{f^2 + 2a_0 f}{L^2}$$

for a sinus-like deflection curve, and

$$\delta_0/L = \frac{8}{3}\frac{f^2}{L^2}$$

for an eccentric parabolic deflection curve.

In the latter case, computation yields:

σ_0 =	44	46	48	49	49	48	46	44 daN/mm^2
f =	0.235	0.273	0.670	1	1.9	2.4	3.7	4.3 mm
1,000 δ_0/L =	0.004	0.005	0.030	0.067	0.24	0.39	0.90	1.23
1,000 ϵ_0 =	3	3.3	3.7	3.9	3.9	3.8	3.7	3.65
1,000 δ/L =	3.004	3.305	3.730	3.967	4.14	4.19	4.60	4.88

Figure 3.63 shows the variation of $1{,}000\ \delta/L$ with σ_0 ; if a longitudinal deformation is imposed, the stress increases up to the critical value and then decreases fairly rapidly.

On the other hand, elementary calculations for several cross-sectional bar shapes (thin tubes or concentrated flanges), using a σ–ϵ curve made up of two straight lines of slopes E and E' which intersect at $\sigma = \sigma_e$, have led us to moment-curvature plots,

$$Mh/I(\sigma_e - \sigma_0) = F(E\Delta/(\sigma_e - \sigma_0)),$$

that are identical for $\sigma_0 > \sigma_e$, and to approximately corresponding plots for $\sigma_0 < \sigma_e$, the correspondence being obtained by using a fictitious initial deflection for the tube,

$$(a/L)' = 0.7\ a/L ,$$

as well as the plots established for concentrated flanges.

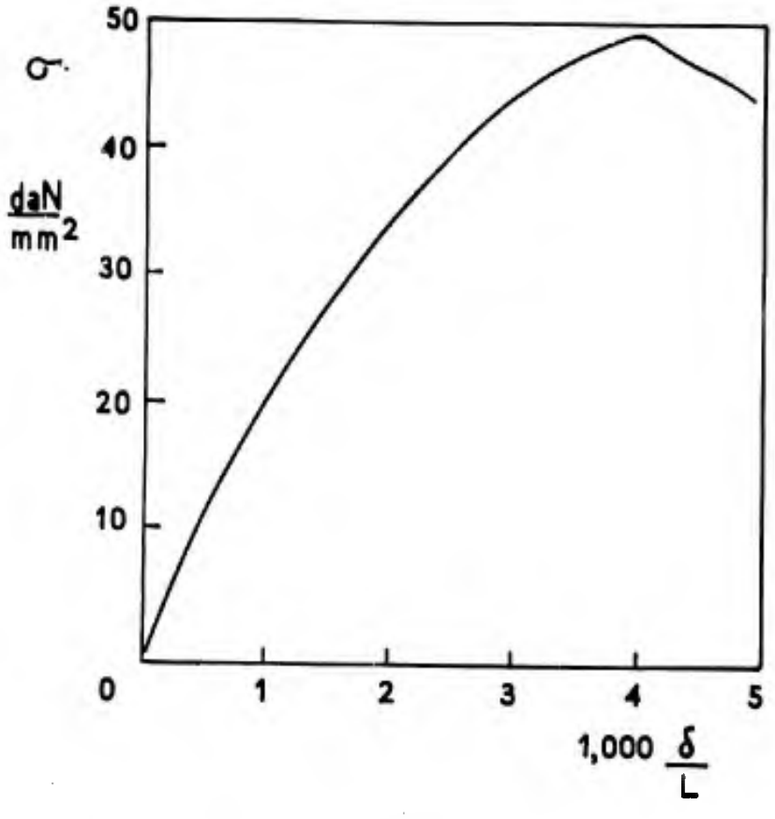

Figure 3.63

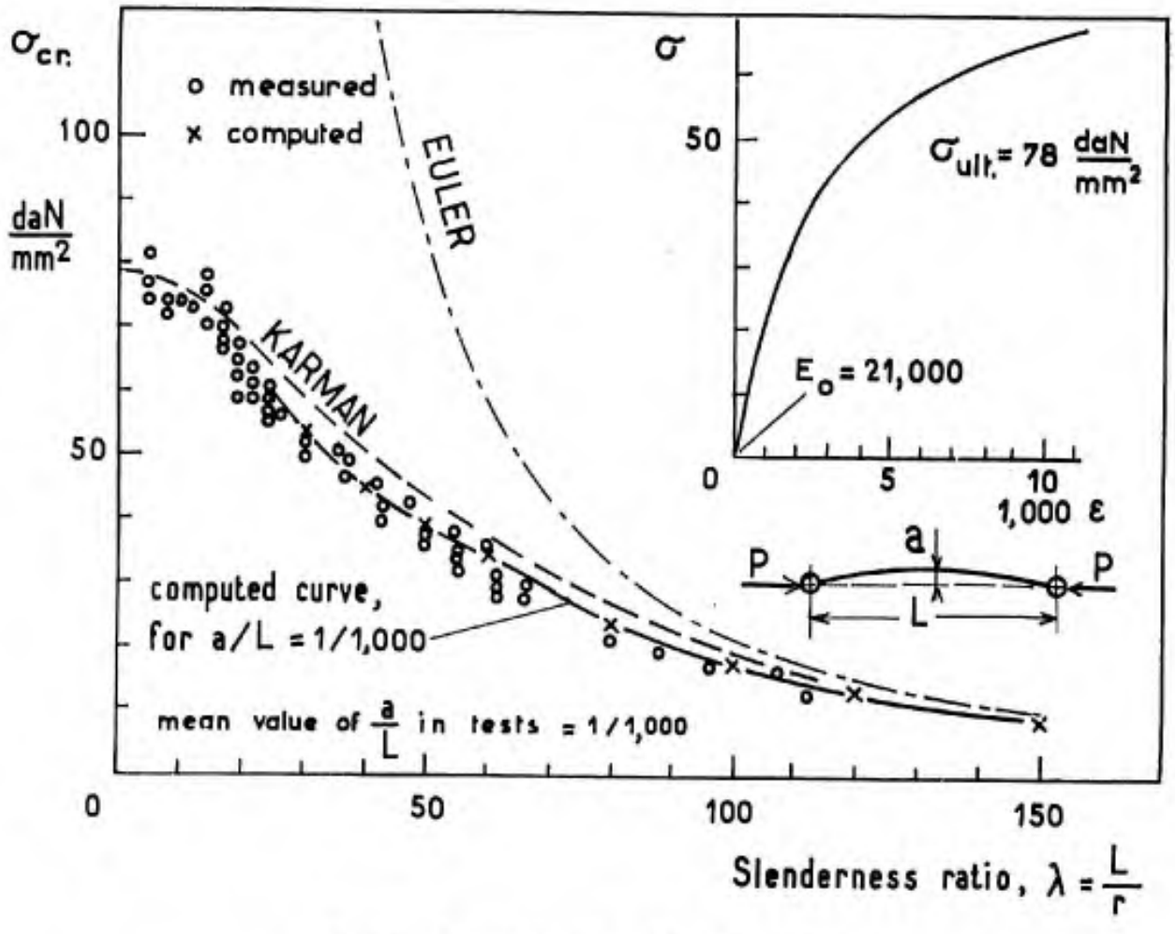

Fig. 3.64 Inelastic buckling of Cr-Mo steel tubes

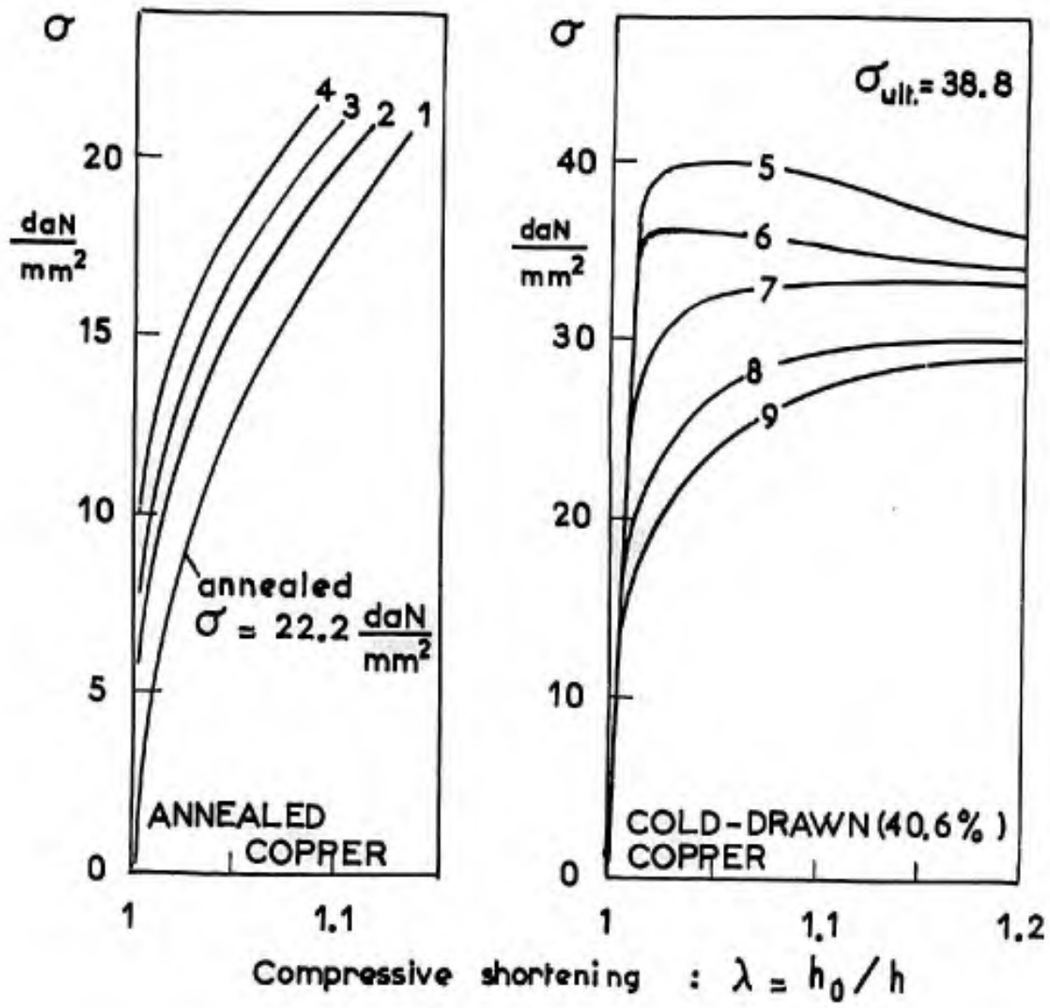

LEGEND :

1 - Annealed.
2 - After 20,000 cycles of $\sigma = \pm 5.2$ daN/mm²
3 " 25,000 " " "
4 " 28,000 " 7.2 "

5 - Cold-drawn.
6 - After 6,000 cycles of $\sigma = \pm 19.6$ "
7 " 273,000 " " "
8 " 83,000 " 20.3 "
9 " 317,000 " " "

Fig. 3.65 Effect of fatigue on the compression stress-strain curves of annealed or cold-drawn copper

Figure 3.64 contains the results from tests carried out, in 1943, by the "Etablissement Aéronautique de Toulouse" on Cr-Mo steel tubes defined by the σ–ϵ curve of Figure 3.59. For comparison, the following theoretical curves have been plotted:

(a) the Euler curve, $\sigma/E = \pi^2/\lambda^2$,

(b) the Kármán curve, $\sigma/E_r = \pi^2/\lambda^2$,

(c) the curve calculated from the plots of Figure 3.60 and $a/L = 1/1,000$, $(a/L)' = 0.7/1,000$.

On the tubes tested, $0.7/1,000 \leqslant a/L \leqslant 2/1,000$ was obtained, the mean value being 1/1,000. For $\lambda = 30$, th calculated critical stress ranged from 48.5 to 56 daN/mm^2 and the three values measured were between 49 and 53 daN/mm^2. We see that the experimental check is adequate and that the assumption of increasing stresses σ_i , although conservative, does not lead to excessively low results.

Before 1945, the British military regulations for the design of aircraft recommended the following values of eccentricity for tubes:

$$e = \frac{d}{40} + \frac{L}{600} .$$

i.e., for the above-mentioned tubes of $d = 25$ mm :

$$e/L = 4.8/1,000 .$$

3.4.2 Changes in Static σ-ϵ Curves under the Effect of Hot Soaking, Creep or Fatigue

Very few data are available concerning the changes in compressive curves under the effect of temperature, fatigue and creep.

In rapid static tension of A-U4SG (French equivalent of U.S. 2014), 1.5 mm thick sheet, hot ageing gives the following values of $\sigma_{ult.}$ and $\sigma_{0,2}$ at room temperature[93] :

	Time of soaking, hours					
	0	100	1,000	3,000	10,000	
1. T4 condition						
Soaking at 130°C, $\sigma_{ult.}$	46	46	46.5	43	39.5	daN/mm^2
$\sigma_{0,2}$	27	28	31	33.5	29	"
150°C, $\sigma_{ult.}$	46	45	40	37	37	"
$\sigma_{0,2}$	27	28	29	26.5	26.5	"
2. T6 condition						
Soaking at 120°C, $\sigma_{ult.}$	51	51		54	52.5	"
$\sigma_{0,2}$	37.5			42	40.5	"
130°C, $\sigma_{ult.}$	51		53	52	46	"
$\sigma_{0,2}$	37.5		41.5	38.5	33	"
150°C, $\sigma_{ult.}$	51	52	45	38	37	"
$\sigma_{0,2}$	37.5	42	35	34	22	"

On the more stable A-U2GN, the changes are not detectable at 130°C and remain small at 150°C. We have no indication concerning the yield strength in compression. We do not know either how hot creep or fatigue modifies the stress-strain curve in compression.

Polakowski and Palchouduri[94] have determined the variations of compression σ–ϵ curves for various metals: copper, tin bronze (95-5), copper-nickel (80-20), nickel, 99% aluminium, manganese aluminium (1.2%), steel containing 0.2% C and 0.72% Ti (not ageing). Fatigue was applied with a vibrophore in alternating tension-compression. The σ–ϵ curve was measured up to 0.1% strain. Cold-working was performed by 20 to 40% drawing, depending on the metal. Some specimens had initially been annealed for half-an-hour, at 600°C for copper and 750°C for nickel. In the cold-drawn condition, the specimens exhibited very little compression creep at room temperature and the limit strain under a given load was reached within a short time.

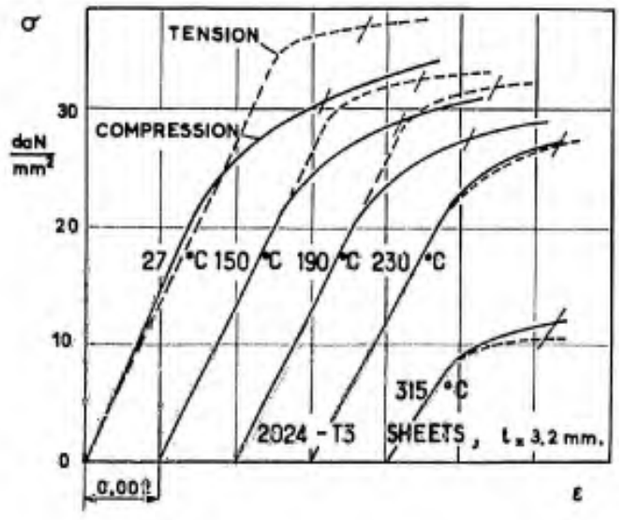

Fig. 3.66 Tensile and compressive σ–ε curves of 2024-T3 aluminium alloy sheets

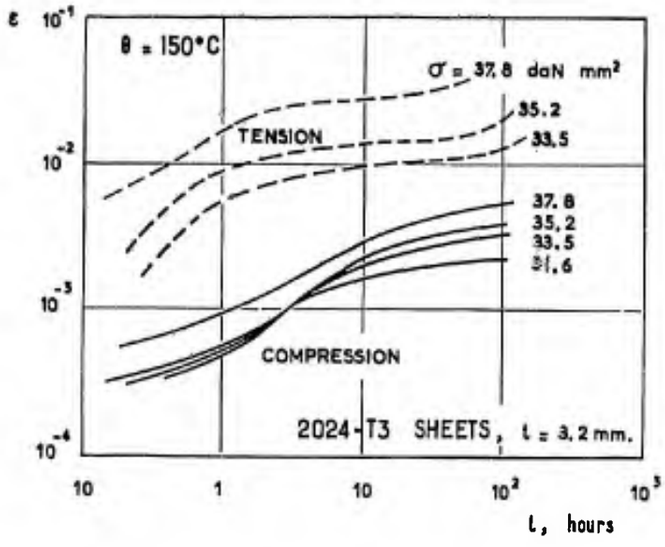

Fig. 3.67 Tensile and compressive creep of 2024-T3 aluminium alloy sheets at 150°C, from Heimerl and Farquar[95]

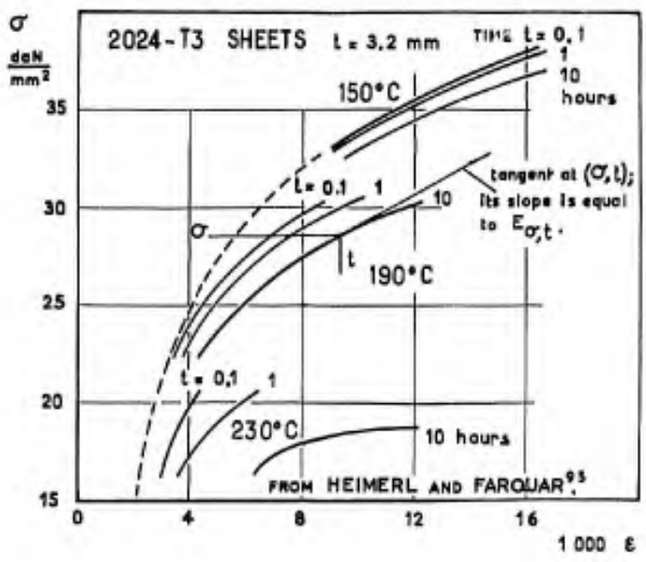

Fig. 3.68 Isochronous compression stress-strain curves of 2024-T3 sheets

After fatigue, the specimens previously cold-worked (drawn) exhibited compression creep even under small loads; this process of creep was not yet terminated after one minute of loading. Figure 3.65 shows the σ-ϵ curves of copper, for which softening or hardening by fatigue is encountered again (see Chapter II, Section 2.1.3), depending on whether the metal was initially work-hardened or annealed. Similar results were found for the other metals investigated. The absence of heating was checked during the fatigue test, except for copper-nickel and steel, for which the test was interrupted from time to time. The effect of heating after drawing was examined: it was negligible for copper-nickel (2 hours at 220°C) and steel (1 hour at 500°C) but produced hardening in nickel and tin bronze (2 hours at 220°C).

Such tests should also be performed on aeronautical engineering metals as they might explain why buckling is encountered in service or in fatigue testing under loads that are much smaller than those imposed on new structures during static tests under ultimate loads.

It is to be feared that for metals initially work-hardened by rolling, drawing or forming, fatigue or hot creep has similar implications even if the metal is presumably stable during hot soaking. In the case of aircraft structures this problem is associated with buckling under a rapidly applied load (during 0.1 to 1 sec) after an operating duration which can be equal to the required service life. This is the most significant aspect of the problems related to buckling, but it has never been studied thoroughly, possibly because of the stability of standard engineering metals at moderately elevated temperatures (between -30°C and +50°C in service). For conventional subsonic aircraft, the lowering of the critical buckling loads remains within the strength margin that corresponds to the factor of safety, unless exceptionally severe conditions are encountered.

As regards supersonic aircraft structures which are subjected to temperatures of 120°C to 150°C in the case of light alloys and to temperatures above 200°C in the case of titanium alloys, the buckling strength under manoeuvre or gust loads after creep and fatigue should be checked and compared with those of the metals employed on former cold aircraft.

3.4.3 Hot Static and Creep Properties

Heimerl and Farquar[95] have studied the creep of US 7075-T6 and 2024-T3 aluminium alloys in tension and compression over comparatively short lengths of time, ranging from 0.1 to 1,000 hours. To that end, 3.2 mm thick sheets were stressed in the direction of rolling. The results were as follows:

For 7075-T6, the σ-ϵ curves were identical in tension and compression from room temperature to 315°C. Furthermore, in creep behaviour, there were no appreciable discrepancies in the 150 to 315°C region until 1% strains occurred.

For 2024-T3, the σ-ϵ curves in the range of room temperature to 190°C exhibited a lower yield strength in compression than in tension; owing to the Bauschinger effect, the metal is softer in compression (Fig. 3.66). Conversely, at 150°C (Fig. 3.67), the metal deforms more in tension than in compression.

This may be accounted for by the elimination of some rather unstable slip barriers which result from the initial stretching of the sheets and disappear during compression loading (see Chapter II, Section 2.1.3). From 230 to 315°C, the σ-ϵ and ϵ-t curves are again identical in tension and compression, the prior mechanical history being cancelled. The conclusion is that compression creep can greatly differ from tension creep and that direct tests should be carried out for each metal.

If a three-dimensional surface diagram representing the creep relationship $\sigma = f(\epsilon, t)$ is cut by a set of planes defined by specified values of the time t, the set of the so-called *isochronous stress-strain curves*, plotted in Figure 3.68 for 2024-T3 aluminium alloy, is obtained. They may be used to calculate the deflection curves of bars in bending-compression with creep and thus to solve the problem of eccentric buckling under constant load. Moreover, the same figure shows that the metal concerned has greater plasticity at the longer times.

The above data are only given for reference purposes; the corresponding durations are too short to allow computation, unless laws of extrapolation are used, these being, however, likely to produce questionable results. Few test results are available for creep in compression.

Some information is to be found in the work of Schlechte[96] and Shanley[89]. One may also refer to the work of Jahsman and Field[97] and Hoff[98,99].

REFERENCES

1. MacGregor, C.W. — *The True Stress-Strain Test.* Journal Franklin Institute, Vol.238, 1944, p.111.

2. Templin, R.L.; Sturm, R.G. — *Some Stress-Strain Studies of Metals.* J. Roy. Aer. Soc., March 1940, p.189.

3. Roberts, C.S. et al. — *The Initiation of Plastic Strain in Plain Carbon Steel.* Trans. A.S.M., Vol.44, 1952, p.1150.

4. - — Service Technique Aeronautique, C.E.A.T. (Toulouse), Etude A 36/M, Rapport 29, P.V. essai 2565 MY, Avril 1952.

5. Tietz, T.I.; Dorn, J.E. — *The Effect of Strain Histories on the Work-Hardening of Metals* in "Cold-Working of Metals". Published by A.S.M., 1949, p.163.

6. Nadai, S.; Manjoine, M.J. — *High-Speed Tension Tests at Elevated Temperatures.* Parts II and III, Trans. A.S.M.E., Vol.63, A 77-A 91, June 1941.

7. Clark, D.S.; Wood, D.S. — *The Time Delay for the Initiation of Plastic Deformations at Rapidly Applied Constant Stress.* Proc. A.S.T.M., Vol.49, 1949, p.717.

8. Boas and Schmid — Z. Physik, Vol.71, 1931, p.703.

9. McAdam, -. et al. — *Influence of Low Temperatures on the Mechanical Properties of 18-8 Chromium Nickel Steels.* Journal Research National Bureau of Standards, Vol.40, 1948, p.375.

10. Seigle, L.; Brick, R.M. — *Mechanical Properties of Metals at Low Temperatures - A Survey.* Trans. A.S.M., Vol.40, 1948, p.813.

11. Kalish, H.S.; Dunkerley, F.Y., Jr. — *The Temperature Properties of Tin and Tin-Lead Alloys.* A.I.M.E. Metals Technology, T.P.2442, 15 Sept. 1948.

12. Swift, H.W. — *Tensional Effects of Torsional Overstrain in Mild Steel.* Journ. Iron and Steel Inst., Vol.151, 1939, p.181.

13. Ripling, E.J.; Baldwing, W.M., Jr. — *Rheotropic Brittleness: General Behaviours.* Proc. A.S.T.M., Vol.51, 1951, p.1023.

14. Ewing, -. — *Strength of Materials.* 1914, p.35.

15. Griffis, R.O. et al. — In Yearbook of American Iron and Steel Institute, Vol.23, 1933, p.142.

16. Hayes, A.; Griffis, R.O. — Metals and Alloys, Vol.5, 1934, p.110.

17. Kenyon, R.L.; Burns, R.S. — Proc. A.S.T.M., Vol.34, 1934, pp.48,58.

18. Ripling, E.J. — Trans. A.I.M.E., Vol.206, 1956, p.502.

19. Polakowski, N.H. — *Effects of Residual Stresses on Yielding and Strain-Ageing of Carbon Steel.* Journal of the Iron and Steel Institute, Dec. 1952, pp.369,376.

20. Howard, R.T.; Cohen, M. — Trans. A.I.M.M.E., Vol.172, 1947, p.413.

21. Bullen, F.P. et al. — *Structural Changes During the Fatigue of Metals.* Proc. Roy. Soc., Vol.A 216, 1953, p.332.

22. Martinod, H. — O.N.E.R.A., Etude 427 R, Paris, 1952.

23. Dixon, E.O.; Foley, E.J. — *How Forging Acts to Enhance Metal Properties.* Trans. A.S.M.E., Feb.1949, p.147.

24. Hertz, -. — Gesammelte Werke 1, Barth, Leipzig, 1895.

25. O'Neill, H. — *The Hardness of Metals and its Measurement.* The Sherwood Press, Cleveland, Ohio, 1934.

26. Meyer, E. — *Untersuchungen über Härteprüfung und Härte*. Physik Zeits, Vol.9, 1908, p.66; Z. V.D.I., Vol.52, 1908, pp. 645, 740, 835.

27. Meyer, M.A. Block, van Laer, K.J. — Nature, Vol.169, Feb. 9, 1952, p.237.

28. - — *Hardness Tests*, A.S.M. Metals Handbook, Vol.105, 1948, p.93.

29. Brinell, J.A. — Baumaterialienkunde, Vol.5, 1900, pp.276, 294,.., 412.

30. Holm, E. and R. Shobert, E.I. — Journal Applied Physics, Vol.20, April 1949, p.319.

31. Sines, G. Carlson, R. — A.S.T.M. Bulletin (TP 31), Feb. 1952, p.180.

32. Blain, P. — Journal of The Institute of Metals, Vol.44, 1930, p.241.

33. Pomey, J. et al. — Métaux-Corrosion-Industries, Vol.XXVI, Sept. 1951, p.313.

34. Hausseguy, L. Martinod, H. — La Recherche Aéronautique, No.37, Janvier-Fevrier 1954.

35. Barrois, W. — Doc-Air-Espace, No.84, Janvier 1964, p.33.

36. Crussard, C. Jaoul, B. — Revue de Métallurgie, Vol.47(8), 1950, p.469.

37. Jaoul, B. — Bulletin S.F.M., Paris, Juin 1952.

38. Gensamer, M. — *Strength and Ductility*. Metal Progress, Vol.49, 1946, p.731; quoted by Lacombe, Rev. Métallurgie, No.12, Nov-Dec. 1946, p.197.

39. Garrod, R.I. et al. — Phil. Mag., Vol.43, June 1952, p.677.

40. Lubahn, J.D. — *Creep of Metals* in "Cold-Working of Metals". A.S.M., 1949.

41. da C. Andrade, E.N. — *La Physique de la Déformation des Métaux*. Revue de Métallurgie, Vol.49(7), Juillet 1952, p.469.

42. da C. Andrade, E.N. — *On the Viscous Flow in Metal and Allied Phenomena*. Proc. Roy. Soc., Vol.A 84, 1910, pp. 1, 12.

43. Davis, E.A. — Journal Applied Mechanics, Vol.A-101, June 1943.

44. Sud-Aviation — Compte-rendu No.6, 1962, p.96. (Not published).

45. Ripley, E.L. — Meeting, International Committee on Aeronautical Fatigue (I.C.A.F.), Roma, 1963.

46. Wood, D.S. Clark, D.S. — Trans. A.S.M., Vol.44, 1952, p.726.

47. Carreker, R.P. et al. — Metals Technology, A.I.M.E., Vol.15, T.P.2477, Sept. 1948.

48. Sherby, O.D. et al. — Proc. A.S.T.M., Vol.56, 1956, p.789.

49. Shahinian, P. Achter, M.R. — Crack Propagation Symposium, Cranfield, 1961.

50. Berkovits, A. — N.A.S.A. T.N. D-799.

51. Soderberg, C.R. — Trans. A.S.M.E., Vol.58, 1936, p.733.

52. Graham, A. — Research, Vol.6, 1953, p.92.

53. Walles, K.F.A. Graham, A. — Journal Iron and Steel Institute, Vol.179, 1955, p.105.

54. Dorn, J.E. — Journal Mech. Phys. Solids, Vol.3, 1955, p.85.

55. Manson, S.S. Haferd, A.M. — N.A.C.A. TN 3195, 1954.

56. Hollomon and Jaffe — A.M.M.E., T.P. No.1831, 1945.

57. Larson, F.R. Miller, J. — Trans. A.S.M.E., Vol.74(5), 1952, p.765.

58. - — Sud-Aviation, not published.

59. Grant, N.J. — *High-Temperatures Properties of Metals.* A.S.M., 1950, p.55.

60. Hsiao, C.C. Sauer, J.A. — Journal Applied Physics, Vol 21, Nov. 1950, p.1071.

61. Stroh, A.N. — Proc. Roy. Soc., Vol.A-232, 1955, p.548.

62. Frey, D.N. et al. — N.A.C.A. TN 2472, Oct. 1951.

63. - — O.N.E.R.A., Not published, tests carried out under the sponsorship of Sud-Aviation and Service Technique Aéronautique, Juin 1967.

64. Martinod H. Calvet, J. — *Sur la Stabilité à Chaud des Alliages d'Aluminium Refractaires du Type A-U2GN.* Note Technique No.67, O.N.E.R.A., Paris, 1962.

65. Smith, C.S. van Wagner, C. — A.S.T.M., Vol.41, 1941, p.825; quoted by McLean in "Mechanical Properties of Metals", p.188.

66. Phillips, V.A. et al. — J.I.M., Vol.81, 1953, p.625; quoted by McLean, p.291.

67. - — NACA Subcommittee on Power Plant Materials, NACA Report 1288 and NACA TN 3216, 1955, 1956.

68. Guarneri, J.C. — W.A.D.C. Technical Report 53-24, Part I and II, May and Sept. 1954; Part III, Jan. 1955.

69. Padlog, J. Schnitt, A. — W.A.D.C. Technical Report 58-294, July 1958.

70. Kennedy, A.J. — Inst. Mech. Engineers, International Conference on Fatigue of Metals, Vol.401, 1956.

71. Kennedy, A.J. — *Process of Creep and Fatigue in Metals.* Oliver and Boyd, London, 1962.

72. Simmons, W.F. Cross, H.C. — Symposium on the Effect of Cyclic Heating and Stressing on Metals at Elevated Temperatures. A.S.T.M. Special Publication No.165, 1954.

73. Shinn, D.A. — *Report on Selected Properties of Materials at Elevated Temperatures.* A.G.A.R.D. Report No.104, 1957.

74. Caughey, R.H. Hoyt, W.B. — A.S.T.M. Special Publication No.165.

75. Guarneri, C.J. — A.S.T.M. Special Publication No.165, 1954.

76. Daniels, N.H.G. Dorn, J.E. — W.A.D.C., T.R. 54-104, Oct. 1954.

77. Robinson, A.J. Dorn, J.E. — W.A.D.C., T.R. 54-40, 1954.

78. - — Sud-Aviation, Marché 2149/61, 7° C.A., Tome 1, p.2. (Not published.)

79. Manjoine, M.J. — Proc. A.S.T.M., Vol.49, 1949, p.757.

80. - — Sud-Aviation, Marché 2149/61, P.V. 26712/8.

81. Shepard, L.A. et al. — *The Creep Properties of Metals under Intermittent Stressing and Heating Conditions. Parts I, II, III.* W.A.D.C., T.R.536336, May to July 1954. Quoted in Reference 69.

82. Klinger, L.J. Sachs, G. — Journal Aeronautical Sciences, Vol.15, March 1948, p.151.

83. Sachs, G. et al. — N.D.R.C., War Metallurgy Division, Report Special No. M 171, 1944.

84. Davis, H.E. Parker, E.R. — Journal Applied Mechanics, Sept. 1948, p. 201.

85. Wu, M.H.L. — N.A.C.A. TN 2217.

86. Timoshenko, S. — *Stability of Elastic Equilibrium.*

87. von Kármán, Th. — *Untersuchungen über Knickfestigkeit.* Forschungsheft auf dem Gebiet des Ingenieurwesens, V.d.I. No. 81, 1910.

88. Barrois, W. — *Le Calcul et l'Utilisation du Module Réduit de Flambage.* Technique et Sciences Aéronautique, Tome 4, Paris, 1943.

89. Shanley, F.R. — *Weight-Strength Analysis of Aircraft Structures.* US Air Force Project RAND, July 1962.

90. Fraeijs de Veubeke, B. — *Creep Buckling* in "High-Temperature Effects in Aircraft Structures (Edited by Hoff.) A.G.A.R.D., Pergamon Press, 1958.

91. Chapman, J.C. et al. — *A Theoretical and Experimental Investigation of Creep Buckling.* Int. J. Mech. Sci., Vol. 1, Pergamon Press, 1960, pp. 145, 194.

92. Barrois, W. — *Etude du Flambage Plastique des Barres Comprimées et Fléchies.* Note No. 29, S.T.Aé./EG du 4.5.1944. (Not published).

93. - — Sud-Aviation, Marché 2149/61, P.V. 26.712/8. (Not published).

94. Polakowski, N.H. Palchouduri, A. — *Softening of Certain Cold-Worked Materials under the Action of Fatigue Loads.* Proc. A.S.T.M., 1954, p. 701.

95. Heimerl, G.J. Farquar, J. — N.A.S.A. TN D-160, Dec. 1959.

96. Schlechte, F.R. — N.A.S.A. TN D-95, Sept. 1959.

97. Jahsman, W.E. Field, F.A. — *Comparison of Theoretical and Experimental Creep-Buckling Times of Initially Straight Centrally Loaded Columns.* Jour. Aerospace Sci., Vol. 29, No. 4, April 1962, pp. 431, 433.

98. Hoff, N.J. — *Mechanics Applied to Creep Testing.* Annual Meeting of the Society for Experimental Stress Analysis, 1958.

99. Hoff, N.J. — *Reversed Creep: A Remark to the Cr. p Buckling Theory of Rabotnov and Shesterikov.* Jour. Mech. Phys. Solids, Vol. 12, Pergamon Press, 1964, pp. 113, 123.

100. Hoff, N.J. — *A Survey of the Theories of Creep Buckling.* From preprint without reference.

101. Barrois, W. — *Eléments de Calcul Matriciel.* From lectures at the Ecole Nationale des Travaux Aéronautiques, Paris, 1956.

102. Coffin, L.F., Jr. — *The Flow and Fracture of a Brittle Material.* Journal Applied Mechanics, Vol. 17(3), Trans. A.S.M.E., Vol. 72, 1950, p. 233.

103. Steele, M.C. — *Partially Plastic Thick Walled Cylinder Theory.* Journ. Applied Mechanics, Vol. 19(2), June 1952, p. 133.

104. Davis, E.A. — *Increase of Stress with Permanent Strain and Stress-Strain Relations in Plastic State for Copper under Combined Stresses.* Journ. Applied Mechanics, Vol. A-187, Dec. 1942.

105. Heimerl, G.J. Manning, -. — *A High-Speed Pneumatic Testing Machine.* A.S.T.M., Materials Research and Standards, April 1962.

106. Späth, W. — *Physik und Technik der Härte und Weiche.* Springer ed., Berlin, 1940, p. 217.

107. Kurth, A. — *Uber die Beziehungen der Kugeldruckhärte zur Streckgrenze und Zerreissfestigkeit zäher Metalle.* Mitt. Forsch. Arb. V.D.I., 1909.

108. Ewing, J.F. Freeman, J.W. — *Influence of Hot-Working Conditions on High-Temperature Properties of a Heat-Resistant Alloy.* N.A.C.A., T.N. 3727, August 1956. (University of Michigan, May 1955).

CHAPTER IV

STATIC STRENGTH OF NOTCHED OR CRACKED COMPONENTS

STATIC STRENGTH OF NOTCHED OR CRACKED COMPONENTS

Although this chapter is mainly concerned with the residual static strength of simple fatigue-cracked structural components, we shall first examine the static strength of components containing various machined notches.

4.1 STATIC STRENGTH OF COMPONENTS CONTAINING MACHINED NOTCHES

Machined notches are often a necessary part of the design of a practical structure. They reduce but little, or even improve, the net static strength of standard engineering metals. However, some metals are sensitive to sharp notches and this becomes more apparent with increasing thickness.

4.1.1 V-type Circumferential Notches

V-type circumferential notches are less detrimental than side notches in thin sheets. Before 1940 the tensile strength of cylindrical specimens containing circumferential notches of constant root diameter was considered to be increasing with the outside diameter as a result of stress triaxiality and to tend toward a limiting value equal to the decohesion stress in static tension.

Since 1940 SACHS and his collaborators have published results from systematic tests. DANA, AULT and SACHS[1] have studied the static strength, the transverse contraction in area and the fracture process of round specimens having a diameter $d = 5.38$ mm at the root of a 60° V-type groove, with a variable radius of curvature r and several d/D ratios.

The results obtained show the same trend for the three light aluminium alloys investigated, 24 S-T, 24 S-T86 and 75 S-T. Figure 4.1 gives the results for 24 S-T alloy (similar to French A-U4G1) re-solution-heat-treated after machining (soaking for 1 hour at 493± 5°C, quenching in water at room temperature, natural ageing for 4 to 5 days). The tensile properties for smooth 5.38 mm-diameter specimens were as follows: $\sigma_{ult.} = 49$ daN/mm^2 (70,000 lb/in^2), * $\sigma_{ult.true} = 70$ daN/mm^2 and $\Sigma\% = 33$. The ductility was measured by the transverse contraction in area at fracture; it was found to be decreasing with decreasing notch radius r and with increasing percent notch depth. For a given value of the d/D ratio the apparent strength $\sigma_{ult.net}$ and the true strength $\sigma_{ult.net\ true}$ increase with the stress concentration factor and then decrease in the presence of sharp notches.

For large notch radii, i.e., for stress concentration factors K_T close to unity, the material is more resistant to plastic slip in the core of the specimen than near the notch root and is therefore subjected to higher tensile stresses.† Deep notches imply an increased triaxial stress state in the core and hence higher ultimate tensile stresses. If the notch depth remains constant, the stress at the root of the groove increases with decreasing radius r until a crack starts simultaneously at the root of the groove and in the core of the specimen. With sharper notches cracking no longer occurs in the centre of the specimen and the strength decreases after reaching a maximum. For a constant ratio of radius r to notch depth $t = (D-d)/2$, small notches prove more detrimental if the strength is related to the net section; however, the strength in relation to the section away from the notch is greater in the case of shallow notches and is at most equal to that of the unnotched specimen: the load sustained is never increased by the notch but the load sustained by the core may be increased or decreased by the extra material added to the core. η is the ratio $(\sigma_{ult.net})_{notch}/(\sigma_{ult.})_{unnotched}$.

In Figure 4.2, from WEISS, SESSLER, PACKMAN and SACHS[2], similar results are given for 4340 steel specimens subjected to different treatments. Figure 4.3, from the same authors, shows the quite distinct effect of diameter if the percent notch depth and the stress concentration factor K_T are constant. The effect of stress gradient is seen : the gradient decreases with increasing diameter, plastic displacement takes place less readily at the root of the notch, and the apparent strength decreases. The effect of stress gradient or the effect of size can be explained by the fact that the lengths are to be measured on the scale of the grains, whose boundaries are stable obstacles to the development of plastic slip. If treated to have ultra-high static strength, 4340 steel is sensitive to sharp notches and its strength is considerably lowered in the case of large diameters.

For a few years now, the "Etablissement Aéronautique de Toulouse"[3] have been carrying out systematic static tests on smooth and notched specimens for investigations of axial tension and tension– compression fatigue strength. The specimens used are of the following dimensions: $d = 7.98$ mm, $D = 14$ mm, $d/D = 0.57$ and radii r varying with K_T as follows:

---

* 1 daN/mm^2 = 1,450 lb/in^2, 1 daN/mm$^{3/2}$ = 288 lb/in$^{3/2}$.

† See the paper by BLUHM and MORISSEY[88] on internal cracks.

PRECEDING PAGE BLANK

BLANK PAGE

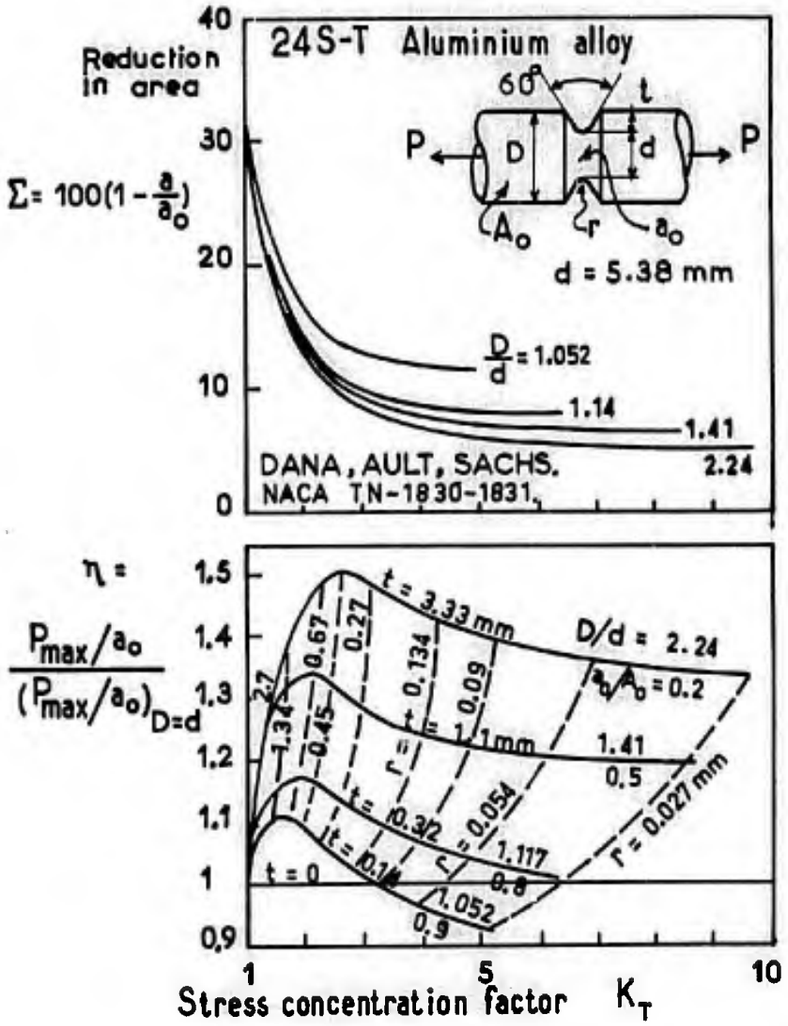

Fig.4.1 Static strength of 24 S-T aluminium alloy round notched specimens from results of Dana, Ault and Sachs[1]

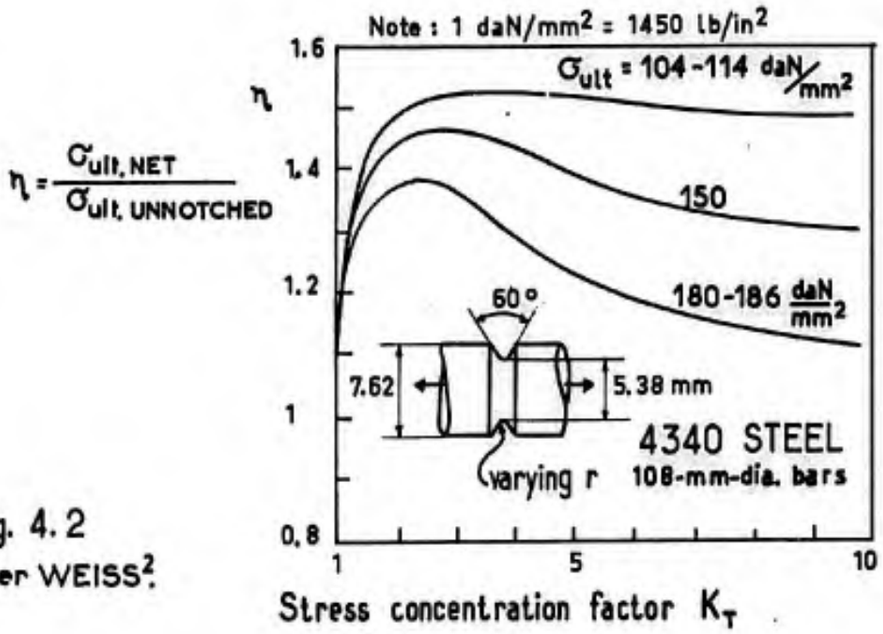

Fig. 4.2
After WEISS[2]

Fig.4.2 After Weiss[2]

K_T =	1.035	1.3	1.7	2.3	3.3	5
r =	105	5.5	2	0.85	0.35	0.14 mm.

Table 4.1 below gives some results for various materials:

TABLE 4.1

Static Strength of Notched Specimens Used in Fatigue Tests By the "Etablissement Aéronautique de Toulouse"(E.A.T.)

Light aluminium alloys (Test Report No.M3-7873 dated January 1966)

A-U4SG in bars (similar to American 2014):

$\sigma_{0.2}$ = 50 daN/mm²(72,500 lb/in², 1 daN/mm² = 1450 lb/in²),
$\sigma_{ult.}$ = 56.3, $\sigma_{ult.true}$ = 66.4 daN/mm², A % = 11.4, Σ % = 23.

K_T =	1.035	1.7	3.3
η =	1.06	1.36	1.36.

A-U4SG in thick plates:
Longitudinal direction:

$\sigma_{0.2}$ = 46 daN/mm², $\sigma_{ult.}$ = 50.6, $\sigma_{ult.true}$ = 63, A % = 9, Σ % = 20.

Large transverse direction:

$\sigma_{0.2}$ = 46 daN/mm², $\sigma_{ult.}$ = 49.7, $\sigma_{ult.true}$ = 57.2, A % = 8, Σ % = 14.

K_T =	1.035	1.7	3.3
η long. =	1.11	1.42	1.38
η transverse. =	1.04	1.37	1.21

A-U2GN in thick plates (similar to English RR 58).
Longitudinal and large transverse directions:

$\sigma_{0.2}$ = 40 daN/mm², $\sigma_{ult.}$ = 43.2, $\sigma_{ult.true}$ = 52.5, A % = 7, Σ % = 24.

K_T =	1.035	1.7	3.3
η long. =	1.02	1.46	1.32
η transverse. =	1.14	1.16	1.39

Steels 30 NCD 16 (E.A.T. Technical Note, LABORDE and DOUILLET, October 1963)

K_T =	1.035	1.7	2.3	3.3	5
η $\sigma_{ult.}$ = 120 daN/mm²	1.08	1.57	1.6	1.65	1.62
η $\sigma_{ult.}$ = 180 daN/mm²	1.05	1.48	1.5	1.5	1.33

40 CDV 20 (H-11, Vascojet 1000) in bars (Test Report 39317 dated September 1963), treated for high and very-high tensile strength:

$\sigma_{0.2}$ = 137.5 daN/mm², $\sigma_{ult.}$ = 160 daN/mm²(230,000 lb/in²), $\sigma_{ult.true}$ = 215, A % = 9, Σ % = 43,

$\sigma_{0.2}$ = 151 daN/mm², $\sigma_{ult.}$ = 200 daN/mm²(290,000 lb/in²), $\sigma_{ult.true}$ = 248 daN/mm², A % = 8, Σ % = 30.

Results:

K_T =	1.035	1.3	2.3	3.3	5
η $\sigma_{ult.}$ = 160, =	1.16	1.5	1.58	1.58	1.38
η $\sigma_{ult.}$ = 200, =	1.08	1.27	1.34	1.14	0.67

40 CDV 20, vacuum-melted, in bars (Test Report M4-7743, April 1966)

$\sigma_{0.2}$ = 170 daN/mm², $\sigma_{ult.}$ = 178(260,000 lb/in²), A % = 12.5:

K_T =	1.035	1.7	3.3
η. =	1.04	1.52	1.67

Maraging steel, Vascomax 300, in bars (Test Report No 32531, dated March 1966),

$\sigma_{0.2}$ = 180 daN/mm², $\sigma_{ult.}$ = 193(280,000 lb/in²), A % = 10, Σ % = 52:

K_T =	1.035	3.3	3.83	10
η =	1.08	1.35	1.54	1.35

(Continued on page 133)

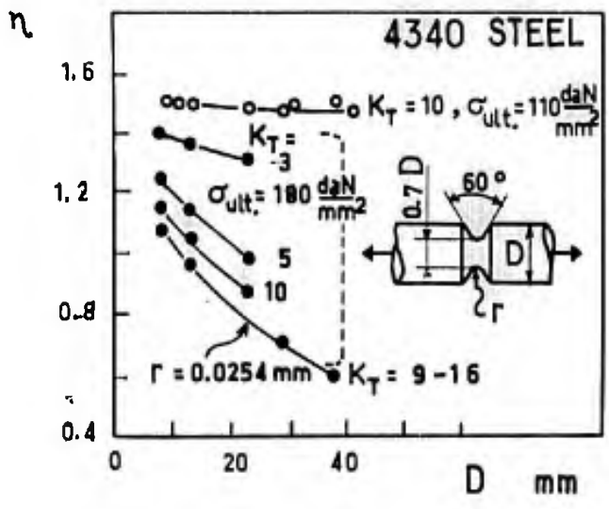

Fig. 4.3 Size effect after Weiss[2]

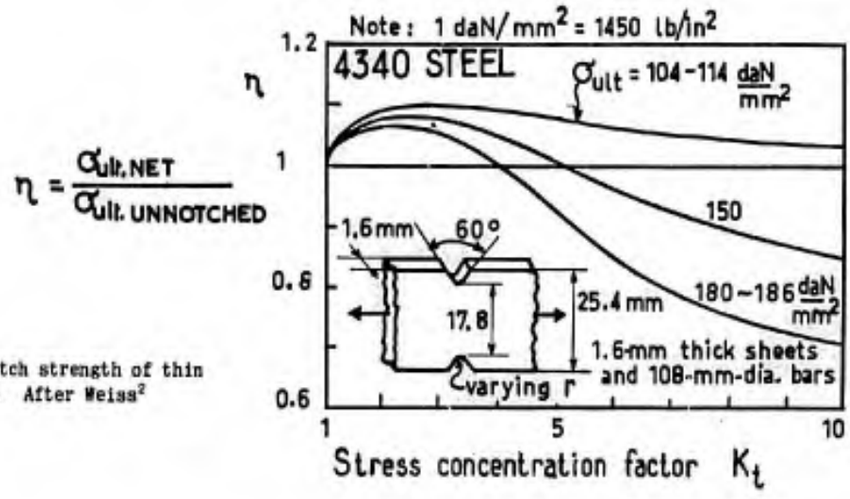

Fig. 4.4 Relative notch strength of thin steel specimens. After Weiss[2]

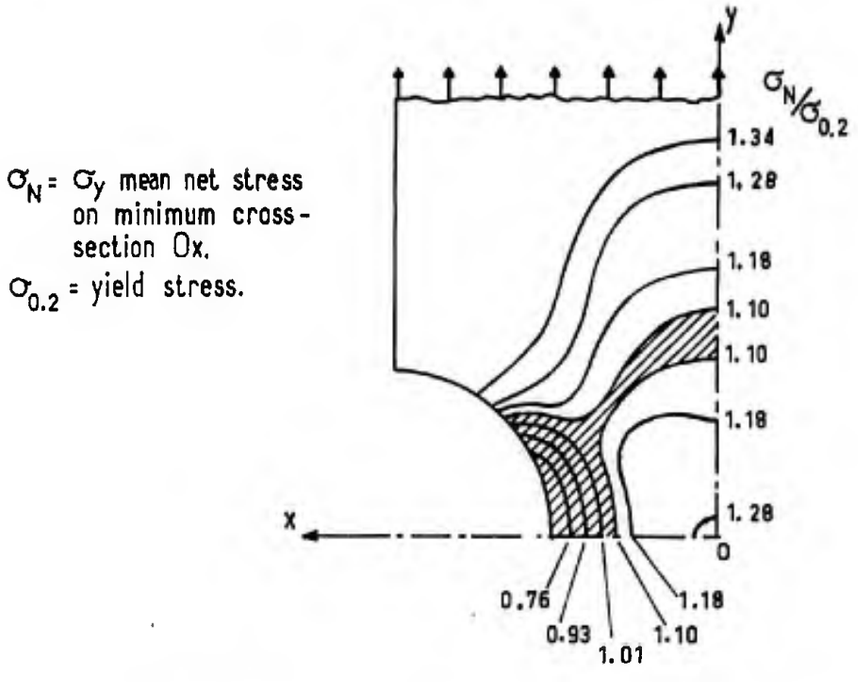

Fig. 4.5 Tensile stress distribution in a notched specimen, after Dixon[4]

TABLE 4.1 Cont'd.

Static Strength of Notched Specimens Used in Fatigue Tests
By The "Etablissement Aeronautique de Toulouse" (E.A.T.)

T-A6V titanium alloy in bars (Test Report MO-7334/2 dated August 1965)

$\sigma_{0.2}$ = 88 daN/mm², $\sigma_{ult.}$ = 91(132,000 lb/in²), A % = 14.5, Σ % = 50:

K_T =	1.035	1.3	2.3	3.3	5
η =	1.1	1.32	1.64	1.64	1.64

Among the above mentioned material for which small test pieces were used, only 40 CDV 20 air-melted and treated to 200 daN/mm²(290,000 lb/in²) proves markedly weak for d/D = 0.57 and $K_T > 3.3$. However, in view of the size effect observed on 4340 steel, the strength of severely notched thick specimens may well be substantially less than that of smooth specimens. We know of a static test in which a decrease in strength of 33% was caused by the superposition of stress concentrations due to holes on a landing gear made from 35 NCD 16 steel which was treated to 180 daN/mm²(260,000 lb/in²).

4.1.2 Thin Flat Specimens

Consider flat specimens of width D having two rounded V-type edge notches of root radius r, with a net width d between the notch roots. Figure 4.4, after, WEISS and his co-authors[2], shows a behaviour similar to that of round 4340 steel specimens. If a size effect due to stress gradient is taken into account, then the results are comparable to those given in the previous figures for round specimens, at least for $K_T < 5$. The improvement is poor for $K_T > 5$ owing to the fact that the reduction in area occurs mainly in the direction of thickness and is therefore less affected by the notch. Moreover, the beneficial effect is solely associated with stress biaxiality in the plane of the specimen, hence a greater decrease in strength is found for large values of K_T.

In Figure 4.5, from DIXON[4], the successive boundaries of the region where the yield strength is exceeded are shown in relation to increasing load. The load is measured by means of the $\sigma_N/\sigma_{0.2}$ ratio of net stress to yield strength. The strains are measured by the photoelastic-coating method. The yield strength is exceeded in the entire cross-sectional area of the specimen only if the average net stress is more than 1.28 times the yield strength.

WEISS, SESSLER, GREWAL and CHAIT[5], who measured the strains ϵ_y and ϵ_x, showed that the lateral contraction decreased from $0.5\,\epsilon_y$ (in plasticity), at the edge of the notch, to between 0 and $0.15\,\epsilon_y$, at the centre of the specimen, for ARMCO iron in which Poisson's ratio is $\nu = 0.25$. This implies stresses σ_x that are zero at the edge and may approach $0.25\,\sigma_y$ at the centre; there is a lateral tension at the centre which reduces the octahedral shear stress responsible for plastic slip as well as for the process leading to failure. Fracture begins on sharp edges at the notch root and the strength may be increased by rounding off these edges.

KAUFMAN, discussing a paper by HEYER[24], produced some results which indicated that the strength of sharply notched specimens was largely dependent on thickness. The following test results were obtained on flat specimens of width w = 76.2 mm having two 12.7 mm-deep 60° V-type edge notches, with radii equal to or less than 0.0127 mm :

		thicknesses in mm :	1.5	3.2	6.35
7075-T 651,	$\sigma_{ult.net}$	in daN/mm²	36	34	24.3
		in 1000 lb/in²	52	49	35
7079-T 651,	$\sigma_{ult.net}$	in daN/mm²	35.5	33.2	20.8
		in 1000 lb/in²	51	48	30

Consequently, for notches of this sharpness, the behaviour observed is similar to that of fatigue-cracked specimens.

4.1.3 Section Size Effect in Tension and Bending

WEISS, SCHAEFFER and FEHLING[6], using ultra-high-strength H-11 Steel (Vascojet 1000), 2014-T6 and 7075-T6 aluminium alloys and Plexiglas, made a comparative investigation of the effect of section size on the tensile and bend strength of smooth, notched and fatigue-cracked specimens. The designs of the tensile and bend specimens are illustrated in Figure 4.6. The test results for H-11 steel and Plexiglas are given in Figure 4.7.

Smooth specimens of series S exhibited no size effect in the tensile test of H-11 steel but showed a marked effect in bending for both steel and Plexiglas. This effect is attributed by the authors to plastic flow which is considerable in bending for a large stress gradient, i.e., for a small section size. In other tests – not reproduced here – performed on 2014-T6 aluminium alloy, no section size effect was found in bending for thicknesses of 10.8 to 50 mm, this being associated with the extensive plastic flow to failure that was observed in

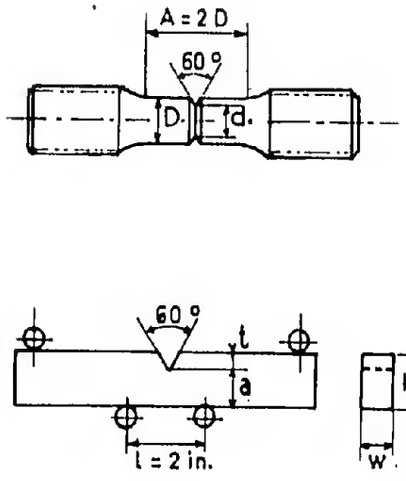

Fig. 4.6 Dimensions of the specimens used in the tests reported in Figure 4.7

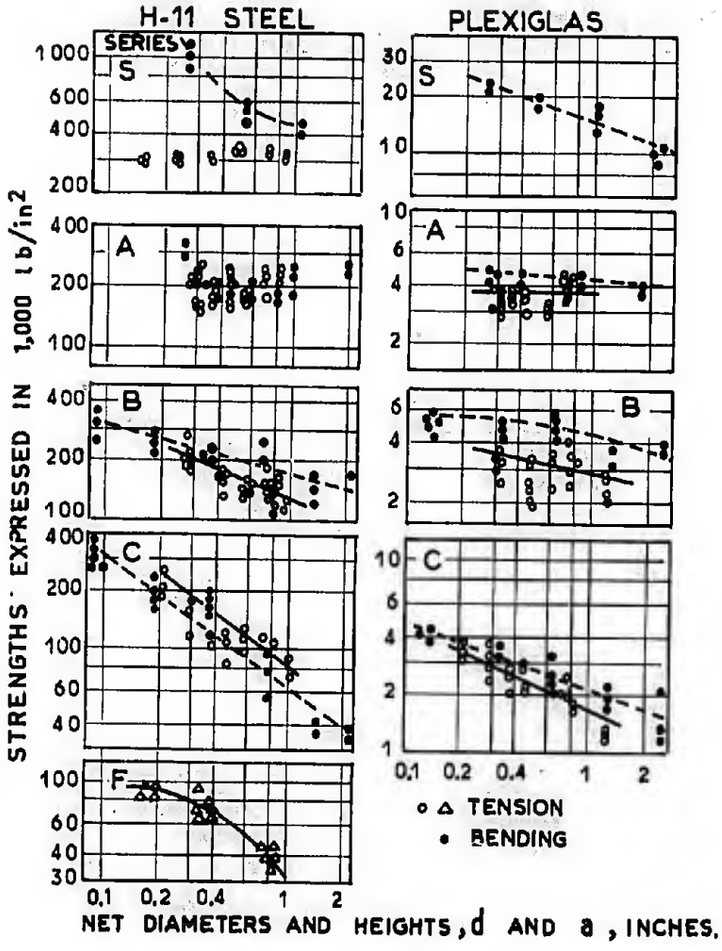

Fig. 4.7 Size effect on the notch-strength of H-11 steel and plexiglas. After Weiss et al.[6]

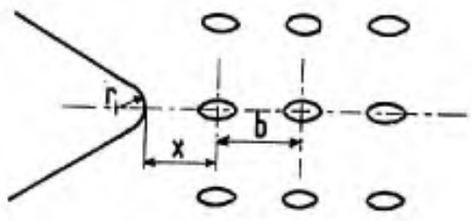

Fig. 4.8 Pattern of distributed cavities, after Weiss et al.[6]

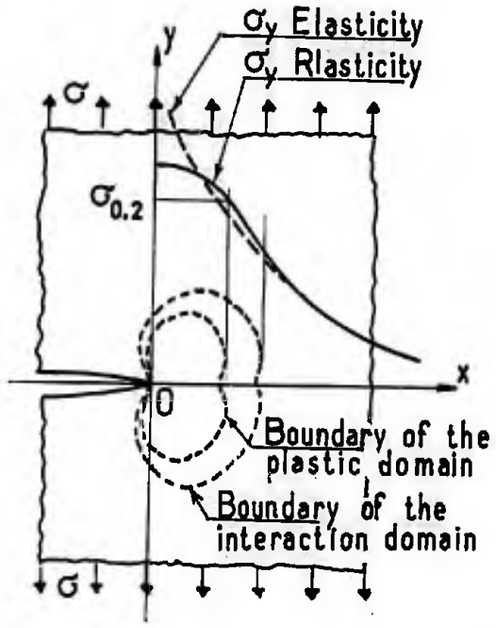

Fig. 4.9 Plasticity effect on stresses neighbouring the crack tip

all specimens. Incidentally we note that for H-11 steel and 2014-T6 alloy the largest ratio between the nominal strengths in bending and in tension is approximately 3, which implies another cause in addition to yielding and may possibly be related to some parasitic reactions of the supports resulting from large deflections in the bending tests.

Specimens of series A were designed to have a constant stress concentration factor ($K_T = 6$) and a constant relative stress gradient $\gamma_r = 120/mm$ (root radius = 0.075 to 0.100 mm). Here, H-11 steel and Plexiglas showed no size effect. For the 2014-T6 and 7075-T6 aluminium alloys, however, an asymptotic decrease in strength of 30% was observed from $d = 7.5$ mm to $d = 20$ mm., the relative notch depth being changed from 85 to 15% to permit constancy of K_T and γ_r. This is ascribed by the authors to the effect of notch depth, as shown by SACHS[1] (see Figure 4.1).

In series B, with $K_T = 6$, the percent notch depth remained constant ($d/D = 0.7$) but the stress gradient decreased with increasing diameter or thickness. The decrease in strength with diameter observed in bending and tension was comparatively large for H-11 steel, less for Plexiglas and still less for the two aluminium alloys. This unquestionable effect of stress gradient is not attributed to yielding but to the presence of inhomogeneities, such as inclusions or microcracks, as assumed by WEIBULL[7] in his statistical theory of strength, in which the strength varies as $V^{-1/m}$, V being the volume of material subjected to stress and m an empiric coefficient.

In series C the notch root radius was very small ($r \leqslant 0.025$ mm), with a constant ratio $d/D = a/h = 0.7$. Consequently, the stress concentration factor K_T increased with increasing size and relative gradient $\gamma_r = 2\ K_T/r$; despite the beneficial effect of an increasing gradient, the increase of K_T produced a fictitious size effect that was quite significant. For H-11 steel, however, it was demonstrated by the authors that the $\sigma_N \cdot K_T$ product decreased as the volume of material subjected to stress increased. This supports the view that the oxide inclusions contained in the steel exert an influence. On the contrary, for A1 7075-T6 and 2024-T6, $\sigma_N \cdot K_T$ increased with increasing size, which is a beneficial effect of the increase of the relative gradient due to the fact that the grains near the surface exhibit greater plasticity. It was also observed by the authors that the slopes of the log σ_N versus log D curves are about – 0.7 for steel and tend toward – 0.5 for both alloys when D increases, whereas the GRIFFITH-IRWIN theory would yield – 0.5 for very sharp notches (see later in this chapter). IRWIN'S stress intensity factor, K_c, was computed by the authors. If the diameter increases, K_c decreases for H-11 steel, which, added to the large scatter of the test results, represents corroborative evidence for the effect caused by inclusions. Conversely, for 2014-T6 aluminium alloy, K_c increases with increasing diameter, owing to the effect of plasticity.

It should be noted that the difference in behaviour of H-11 steel and standard 2014-T6 and 7075-T6 aluminium alloys may be reduced in practice since *forgings and parts cut from thick plates are sometimes stressed in the short transverse direction which contains a large number of flaws likely to reduce the ductility;* even in aluminium alloys, the strength $\sigma_N \cdot K_T$ can decrease with an increasing volume of material subjected to tensile stress in the short transverse direction.

4.1.4 WEIBULL's Theory

WEIBULL's statistical theory[7] met with some success when it was first applied to highly brittle materials such as glass, ceramics, etc., in which fracture initiation leads to complete failure. It may be useful to recall the reasoning of the author when he tried to determine in what way the basic assumptions were applicable to metals that appear brittle to the engineer but remain fairly ductile on a sufficiently fine scale of observation.

Consider a specimen subjected to a tensile stress σ. The probability of rupture will be $S = f(\sigma)$; for very low stresses $S = 0$ and for very high stresses $S = 1$. Let us now consider, after WEIBULL, two specimens placed beside each other and subjected to the same stress σ. The probability of each rod withstanding the load will be $S_1 = 1 - S$; the probability of both withstanding the load will be $S_{12} = (1 - S)^2$. *WEIBULL assumes that primary rupture of one specimen, which doubles the stress in the other specimen results in the immediate rupture of the other.* This assumption has been substantiated for specimens assembled in series; indeed, the failure of a chain is conditioned by the rupture of its weakest link.

In a second report, WEIBULL[7] examined the case of secondary ruptures following primary rupture; his calculations, however, remain somewhat theoretical and, so far as we know, they have not yet been substantiated by experiments.

Let us return to the preceding assumption. Consider a unit volume V_0 for which the probability of primary rupture is S_0. The probability of rupture S of a volume V composed of identical volume elements V_0 will be such that

$$\log (1 - S) = V \log (1 - S_0) .$$

For an infinitesimal volume element dv we shall have

$$d \log(1 - S) = dv \log(1 - S_0) .$$

and, S_0 being a function of σ, we may put

$$n(\sigma) = -\log(1 - S_0) ,$$

hence

$$\log(1 - S) = -\int n(\sigma)\, dV .$$

The probability of rupture will be

$$S = 1 - e^{-\int n(\sigma)\, dV} .$$

WEIBULL also puts

$$n(\sigma) = -(\sigma/\sigma_0)^m ,$$

hence, if σ is constant in the volume V,

$$S = 1 - e^{-V(\sigma/\sigma_0)^m} ,$$

where σ_0 is the stress that gives a probability of rupture of 0.63 for the unit volume.

The average strength, $\sigma_{ult.}$, is defined by

$$\sigma_{ult.} = \int_0^1 \sigma . dS .$$

Taking the extreme values of S, 1 and 0, for $\sigma = \infty$ and $\sigma = 0$, we may integrate

$$\sigma_{ult.} = \int (1 - S)\, d\sigma - \left| \sigma(1 - S) \right| \begin{matrix} S = 1, \sigma < \infty \\ S = 0, \sigma = 0 \end{matrix} .$$

It follows that

$$\sigma_{ult.} = \int_0^\infty e^{-V(\sigma/\sigma_0)^m}\, d\sigma ,$$

with a standard variance given by

$$a^2 = \int_0^\infty (\sigma - \sigma_{ult.})^2\, dS .$$

In *tension* we obtain

$$\sigma_{ult.} = \sigma_0\, I_m / V^{1/m} ,$$

and

$$a^2 = \sigma_0^2 (I_{m/2} - I_m^2)/V^{1/m} ,$$

where

$$I_m = \int e^{-z^m}\, dz ,$$

and, numerically,

m =	1	2	3	4	8	16	∞
I_m =	1	0.886	0.896	0.908	0.940	0.965	1
$a/\sigma_{ult.}$ =	1	0.52	0.36	0.28	0.16	0.09	0

In *bending* it is demonstrated by calculation that the ratio of ultimate bending strength $\sigma_{ult.b.}$ to ultimate tensile strength $\sigma_{ult.}$ is

$$\sigma_{ult.b.}/\sigma_{ult.} = (2m + 2)^{1/m} .$$

Furthermore, if we consider two geometrically similar specimens characterized by the dimensions d_1 and d_2, with ultimate strengths σ_1 and σ_2, we shall have

$$\sigma_1 = \sigma_2 (d_2/d_1)^{3/m} .$$

The fundamental assumption on which the foregoing calculations are based implies the existence of such volumes V_0 that the probability function $S_0(\sigma)$ for a localized fracture to cause complete failure is the same for all the domains. If stress σ is variable, the domain V_0 must be small enough for σ to remain substantially constant in this domain; on the other hand, V_0 must be large enough – compared to the flaws which represent potential fracture initiations – for $S_0(\sigma)$ to remain stationary in the solid. These requirements are rather contradictory. If, for example, the flaws are very small compared to the volume V_0, it is unlikely that a localized fracture will extend through the entire volume V_0 unless the flaws in the neighbourhood are substantially of the same severity, i.e., if the scatter due to the flaws is low and if the decrease in stress on the neighbouring flaws caused by plastic adjustment near the primary fracture is less than the increase in stress caused by elastic redistribution.

WEISS, SCHAEFFER and FEHLING[6] have presented a simple model to explain the effect of inhomogeneities on the strength of sharply notched H-11 steel specimens. They assumed, as shown in Figure 4.8, that the solid contains equidistant stress raisers having a spacing b and a stress concentration factor K_b. Considering only the stresses in the direction of loading and neglecting any biaxiality effects, the strength of such a model is given by

$$\sigma_N = \sigma_{max}\left(\frac{r + 4x}{r}\right)^{1/2} / K_T K_b \,.$$

where σ_{max} is the strength of a flawless and unnotched smooth specimen, r the root radius of the notch, and x the distance between the root of the notch and the nearest stress raiser. If we allow the flaw to be anywhere between $x = 0$ and $x = b$ with equal probability, the average notch strength is

$$\bar{\sigma}_N = \frac{\sigma_{max}}{K_T K_b} \cdot \frac{(1 + 4b/r)^{3/2} - 1}{6\ b/r}$$

with a relative standard deviation squared of

$$\left(\frac{a}{\bar{\sigma}_N}\right)^2 = \frac{(6\ b/r)^2(1 + 2\ b/r)}{[(1 + 4\ b/r)^{3/2} - 1]^2} - 1 \,.$$

The relative standard deviation varies from zero for $b/r = 0$ to 0.354 for $b/r = \infty$, increasing monotonically with b/r, from $\sigma_{max}/K_T K_b$ for small values of b/r to σ_{max}/K_T for large values of b/r, the expression of $\bar{\sigma}_N$ being no longer valid.

We believe that this model, although grossly oversimplified as admitted by the authors themselves, is more appropriate than WEIBULL's theory to account for the effect of inhomogeneities on the strength of notched specimens made from engineering metals which are always ductile to some extent.

4.2 STATIC STRENGTH OF CRACKED SPECIMENS – GENERAL

4.2.1 Survey of the Problem

One essential problem associated with the service behaviour of structures is that of the mechanical strength of components having sharp notches due to fatigue cracks, corrosion cracks, quench shrinkage cracks or other fabrication defects undetected during inspection, such as laps, faulty weldments, etc.

This problem has recently been encountered in aircraft engineering, first in connection with the fail-safe concept which imposes a specified residual static strength for aircraft sheet panels that have suffered fatigue damage, then more drastically with the use of ultra-high tensile steels treated to 170-200 daN/mm^2 (245,000 – 290,000 lb/in^2). Experience gained in service has shown that very small cracks undetected by standard inspection methods can reduce the static strength of vital components by 20 to 30%.

In such cases the engineer would normally be inclined to avoid the use of brittle materials. However, brittleness depends on the length of the crack and it must be remembered that high tensile metals have other properties of interest; a compromise is therefore necessary. What is required is a means for characterizing the brittleness of a material in its service condition when a crack has formed; this means should be as easy to implement as the smooth-specimen tensile test which is typical of the strength in the absence of notches. Then, the material and its service condition being specified, this would help to assess the residual static strength of a cracked component in relation to the nature and detectable size of the crack.

To meet the first need, i.e., to select a material, a set of computation results and brittle-fracture theories were evolved by specialists in elasticity calculation and by research-laboratory metallurgists, following GRIFFITH[8] and IRWIN[9]; a number of tests have also been carried out with a view to determining a physical quantity invariant with the size of the components or the cracks and characteristic of the behaviour of the material in the presence of a crack.

In the case of the highly brittle materials considered by GRIFFITH, this invariant quantity is given by the surface density of the elastic energy U which is released due to increase in the area A of the cracked section,

$$\mathcal{G} = dU/dA ;$$

fracture occurs, then, for a given decohesion work per unit area. In fact, W being the total decohesion work and $2A$ the area of the two faces of the crack, GRIFFITH introduced the "surface tension" concept

$$T = \frac{1}{2} dW/dA ,$$

so that the catastrophic crack growth corresponded to the condition

$$\mathcal{G} \geqslant 2T .$$

It is our belief that because of the inadequacy of the term "surface tension" engineers refrained for a long time from extending GRIFFITH's ideas to less brittle materials such as structural metals.

IRWIN[9], investigating metals, took account of the work due to plastic strain. Fracture occurs at a critical value $\mathcal{G}_c$ of $\mathcal{G}$. However, $\mathcal{G}_c$ is not an invariant of the metal but decreases with increasing thickness and is dependent on crack length for plane stress problems. It has been demonstrated experimentally that $\mathcal{G}_c$ approaches a lower limit $\mathcal{G}_{Ic}$ when the thickness increases; $\mathcal{G}_{Ic}$ would thus be the invariant sought; but measurements of $\mathcal{G}_{Ic}$ on specimens of different types but comparable thicknesses reveal that the values vary to a large extent. In our opinion, $\mathcal{G}_{Ic}$ is not an invariant and reliable predictions of strength cannot be made using it; moreover, the situation is complicated by the fact that $\mathcal{G}_{Ic}$, being an elastic quantity, can be computed only for certain shapes and often cannot be measured with precision. Furthermore, in practice, our interest in $\mathcal{G}$ is restricted to the case of brittle materials; now, apart from ultra-high-strength steels, most of the standard engineering metals and alloys are brittle solely under tensile stress applied in the direction of thickness, where it is difficult to cut simple specimens that are easy to calculate. An effort is being made by specialists to develop specimens that are easy to fabricate and to test, i.e., tensile specimens with machined notches of very small root radii, bend specimens with sharp notches deepened by fatigue, specimens cut from plates in the direction of the thickness and capable of being tested in tension in the short transverse direction.

We consider that this problem must be dealt with on a practical basis : if the specimens must be easy to fabricate and to test, they must also be representative of the cracks existing in service on actual components. In this sense, a centrally cracked specimen cut from a thin sheet is typical of riveted skin panels containing a crack on each side of a rivet hole. A tensile or bend specimen with a semi-elliptic surface crack is typical of the behaviour of thick components with a crack originating from a surface flaw. Similarly, we recommend the use of a square tensile or bend specimen containing a quadrant-shaped crack centred on and perpendicular to an edge for investigation of the behaviour of components with an incipient fracture starting at an edge or the behaviour of pin-loaded holes with a crack initiated from the inside contour of the bearing surface of the holes. In addition, there is a need for a specimen that would be used to test thick plates and components in the short transverse direction.

For thin sheets, IRWIN also introduced the concept of *stress intensity factor* K, such that

$$K^2 = E\mathcal{G} ,$$

which depends on the external load, the crack length and the sheet width. The stress field in the neighbourhood of the crack tip is defined by an invariant spatial distribution function multiplied by the factor K. One may wonder how an elastic stress distribution can be of assistance in explaining the fracture of plastic metals. Let us consider the case of Figure 4.9. The stresses assume very high values in the immediate neighbourhood of a very sharp notch or crack tip; the yield strength $\sigma_{0,2}$ is reached and then exceeded. If the yield strength is exceeded only in a small volume of material so that the stress field modification remains local compared to the theoretical elastic field, then a somewhat larger interaction domain exists, at the boundary of which strains, stresses and displacements are substantially equal to the corresponding theoretical elastic values.

For two different notches contained in different components the stress state will be the same if the same metal and the same metallurgical and work-hardening conditions are used and if the strains imposed at the boundaries of the domains of interaction are identical. These conditions are met in several cases of static and fatigue loading:

(1) In fatigue, prior to the development of a visible crack at the root of a notch, these conditions can be satisfied if the plastic region is small enough for the stress concentration factor, K_T, and the relative stress gradient in the direction perpendicular to the surface, $(1/K_T)\partial\sigma/\partial z$, to determine the strain conditions at the boundary of the plastic region as well as the size of this region.

(2) These conditions are also satisfied in fatigue for cracked components of same thickness with the same value of stress intensity factor, K, and under static loads if the metal is brittle enough for the mean fracture stress to be well below the elastic limit.

When these conditions are satisfied, the static strength, fatigue crack propagation rate and fatigue strength depend on the parameters that govern the elastic stress distribution. This leads to a classification of the type of notches from the point of view of the elastic stress state existing near the notch root or crack front. In each category the stress intensity is defined by one parameter, the distribution being specified but not the multiplying factor.

In the conventional smooth-specimen tensile test using a loading machine, the strain rate is imposed and the reaction of the specimen is a stress increasing with the strain up to a maximum which is higher if the strain rate is higher. This maximum, termed "ultimate stress", corresponds, in the case of ductile materials, to plastic instability of the specimen, which exhibits a localized constriction or "neck". After a certain amount of elongation, rupture occurs without previous apparent cracking. If the test is discontinued after the onset of necking and if the specimen is cut along a diametral plane, a plane crack is often observed at the centre of the specimen (see Paragraph 4.1.1). The last stage of rupture takes place on a conical surface at 45^{0} to the tension axis, thus resulting in a "cup and cone" fracture.

On a flat specimen having a circular hole at the centre, an incipient crack is sometimes found at the edge of the hole if the tensile test is carried out very slowly. This cracking is stable as long as the elongation of the specimen and the load applied do not increase. It may also be said that the stress relaxation caused by the virtual growth of the crack length under a constant overall elongation of the specimen is more significant than the increase of the stress caused by reduction of the resistant cross-sectional area. If the elongation is further increased, a crack extension and an increase in the load are observed up to a value at which fracture occurs; it may then be stated that *the crack has reached its critical length of instability for the load considered.*

The phenomenon of stable crack growth with increasing load up to a critical length of instability led to the term "static crack propagation" or "*slow crack growth*" which is only remotely connected with the concepts and needs of the engineer. Indeed, in the case of a cracked component, the engineer is anxious to know what load can be sustained without failure or what number of fatigue cycles is necessary, under a given set of loads, for the crack length to increase until the residual static strength is no longer high enough to withstand the highest random load that may be encountered in service. In fact, the engineer is mainly interested in the crack propagation rate under fatigue conditions and in the residual static strength of a component containing a crack with a fixed initial length; he is rarely concerned with the stable slow growth of a crack under static loading from the initial length to the critical length.

BROEK[78] has studied the residual strength of cracked specimens made from 2024-T3 and 7075-T6 aluminium alloy sheets and the slow crack growth; in some tests, the loadings were interrupted after intermediate slow crack growth. His conclusions were:

(a) The interruption of a residual strength test by unloading to zero stress and reloading has no influence on the residual strength. At reloading slow crack growth starts at a stress somewhat below the stress at which the test was interrupted but soon after the re-initiation of crack growth the original crack propagation curve is followed again. The critical fracture stress and the critical crack length are the same for a continuous test on specimens with the same initial crack length.

(b) The residual strength of structures containing service cracks will not be impaired by one or two high loads which cause a small amount of stable crack extension.

(c) The test results reasonably obeyed the fracture criterion

$$\sigma_c \; l_o^p = \text{constant}$$

and the criterion for slow crack growth:

$$\sigma_i \; l_o^{0,5} = \text{constant} \; ,$$

where σ_c is the critical nominal fracture stress,
σ_i the nominal stress to initiate the slow growth,
l_o the initial crack length.

This supports our point of view on the importance of the initial crack length for correlating residual strength tests; this is also KUHN's opinion[10]. It should be pointed out that in this chapter we are not considering delayed fracture under static load.

In thin sheets necking prior to fracture takes place mainly in the direction of thickness; if the ultimate stress $\sigma_{ult.}$ and the corresponding elongation $\epsilon_{ult.}$ are known from a small-smooth-specimen tensile test, an attempt can be made to predict the strength of a cracked sheet either by using the IRWIN concept or by determining the external load for which $\sigma_{ult.}$ or $\epsilon_{ult.}$ is reached in the vicinity of the notch. KUHN[11] and WELBOURNE[12] have developed prediction methods based on the second term of the alternative. These methods are inefficient for thick parts of small width because the reduction in area of tensile specimens is different from that of cracked parts. That is the reason why we are interested in IRWIN's "fracture mechanics" methods. Indeed, in practice, the engineer is more embarrassed by brittle fracture of thick parts originating in very small cracks than by brittle fracture of thin sheets where cracks of considerable length can be tolerated and crack-arresting techniques can be used to stop the growth of cracks under fatigue loading over a great length of time.

4.2.2 Stress Distribution in an Infinite Thin Sheet Having a Transverse Elliptic Hole. Limiting Case of the Slot

The problem of elastic stress distribution in an infinite thin sheet having a transverse elliptic hole was first examined by INGLIS[13] and by MUSKHELISVILI[14] for the general case of tensile and shear stresses at infinity, away from the hole.

Consider (Fig.4.10) a thin sheet subjected, away from the hole, to a stress state

$$\sigma_x = p\,, \qquad \sigma_y = q\,, \qquad \tau_{xy} = \tau$$

and initially containing an elliptical hole of semi-axes $a = \lambda(1+k)$ and $b = \lambda(1-k)$. If $k = 1$ $(a = 2\lambda\,,\ b = 0)$, we shall have the limiting case of the slot, which represents a rectilinear crack. For computation we shall first take $\lambda = 1$. With the change of complex variables

$$z = x + iy = \xi + \frac{k}{\xi}\,,$$

calculation by the MUSKHELISVILI method yields

$$\sigma_x + \sigma_y = 4 \text{ real part of } \left(\frac{d\xi}{dz}\,.\,\frac{dF}{d\xi}\right), \tag{1}$$

$$\sigma_y - \sigma_x + 2i\,\tau_{xy} = 2\,\frac{d\xi}{dz}\left[\bar{z}\,\frac{d}{d\xi}\left(\frac{d\xi}{dz}\,.\,\frac{dF}{d\xi}\right) + \frac{dH}{d\xi}\right], \tag{2}$$

where

$$F(\xi) = \frac{p+q}{4}\,\xi - \frac{1}{2\xi}\left[\frac{k}{2}(p+q) + q - p - 2i\tau\right],$$

$$H(\xi) = \frac{q-p+2i\tau}{2}\,\xi - \frac{1}{2\xi}\left[p+q+\frac{1+k\xi^2}{\xi^2-k}\left(k(p+q)+q-p-2i\tau\right)\right].$$

The radius of curvature, ρ, at $x = a$ is $\rho = b^2/a$, hence

$$\rho/a = b^2/a^2 = \left(\frac{1-k}{1+k}\right)^2, \qquad k = \frac{1-\sqrt{(\rho/a)}}{1+\sqrt{(\rho/a)}}\,.$$

The precise calculation of the stresses is a time-consuming task, therefore our analysis will be restricted to the specific case of tension: $q = \sigma$, $p = \tau = 0$; we shall solely consider the stresses on the Ox-axis, where $z = x$. Putting $u = 1/(\xi^2 - k)$, we obtain

$$\tau_{xy} = 0\,,$$

$$\sigma_y/\sigma = 1 + (1+k)u\left[\frac{1+k}{2} + (1-k^2)u(1.5 + ku)\right], \tag{3}$$

$$\sigma_x/\sigma = (1+k)u\left[2 - \frac{1+k}{2} - (1-k^2)u(1.5+ku)\right]. \tag{4}$$

σ_y/σ assumes its greater value, K_T, at the edge of the hole at $x = a$:

$$K_T = (\sigma_y/\sigma)_{max} = 1 + \frac{2a}{b} = 1 + 2\sqrt{(a/\rho)}\,.$$

Then, as x increases, σ_y/σ decreases constantly whereas σ_x/σ, which is zero at $x = a$ and $x = \infty$, reaches a maximum for

$$u = \frac{1}{2k}\left[-1 + \sqrt{\left[1 + \frac{2k(3-k)}{3(1-k)^2}\right]}\right].$$

In terms of x we have

$$\xi = \frac{1+k}{2}\left[\frac{x}{a} + \sqrt{\left[\left(\frac{x}{a}\right)^2 - \frac{4k}{(1+k)^2}\right]}\right].$$

For various values of k numerical computation gives the results of Table 4.2, which are reproduced in Figure 4.11.

TABLE 4.2

Tensile Stresses Near the Extremity of the Large Axis of an Elliptical Hole in a Tension-loaded Infinite Thin Sheet (see Figure 4.11)

x/a	1	1.01	1.02	1.05	1.1	1.2	σ maximal σ_i/σ x/a	
Circle, $\rho/a = 1$								
σ_y/σ	3	2.93	2.87	2.69	2.43	2.07	1.63	1.41
σ_x/σ	0	0.03	0.06	0.13	0.22	0.25	0.38	
Ellipse $\rho/a = 0.1$								
σ_y/σ	7.3	6.05	5.19	3.73	2.70	1.94	3.22	1.07
σ_x/σ	0	0.55	0.85	1.17	1.16	0.91	1.21	
$\rho/a = 0.01$								
σ_y/σ	21	7.9	5.5	3.41	2.45	1.82	8.5	1.01
σ_x/σ	0	3.8	3.37	2.32	1.54	0.93	3.82	
$\rho/a = 0.001$								
σ_y/σ	64	7.29	5.13	3.29	2.40	1.81	25	1.001
σ_x/σ	0	6.01	4.15	2.4	1.5	0.9	12	
Slot, $\rho/a = 0$								
σ_y/σ	∞	7.12	5.1	3.3	2.4	1.8		1
σ_x/σ	0	6.12	4.1	2.3	1.4	0.8		

For the slot ($k = 1$) we obtain at $y = 0$, $x = a$:

$\sigma_x = 0$ if we set $x = a$ and if ρ tends toward zero,

$\sigma_x = \infty$ if we set $\rho = 0$ and if x tends toward a.

This leads us to investigate the distribution of the stresses measured on the scale of $(\sigma_y)_{max.}$ by measuring the distances on the scale of the minimum radius of curvature, ρ. We take

$$v = \frac{x - a}{\rho} = \frac{R}{\rho},$$

and

$$S_y = \frac{1}{K_T}\frac{\sigma_y}{\sigma}, \qquad S_x = \frac{1}{K_T}\frac{\sigma_x}{\sigma}.$$

Numerical computation yields the results of Table 4.3, which are reproduced in Figure 4.12. Near the edge of the hole, at $x = a$, the relative stress gradient is

$$\frac{1}{\sigma}\cdot\frac{\partial\sigma_y}{\partial R} = \frac{K_T}{\rho}\cdot\frac{\partial S_y}{\partial v} = -\frac{K_T}{\rho}\frac{3 + 4\sqrt{(a/\rho)}}{1 + 2\sqrt{(a/\rho)}},$$

and

$$\frac{1}{\sigma}\frac{\partial\sigma_x}{\partial R} = \frac{K_T}{\delta}\frac{\partial S_x}{\partial v} = -K_T/\rho.$$

WEISS, SESSLER, PACKMAN and SACHS[15] have used K_T and the relative stress gradient to establish some correlation between the results of brittle-fracture tensile tests performed on notched specimens.

From Figure 4.12 it is seen that the curves $S_y(v)$ are practically identical from $v = 0$ to $v = 1$ and that at $v = 0$ the gradients dS_y/dv vary but little (-2.33 for the circle and -2 for the slot). The curves $S_x(v)$ have the same gradient, which is equal to 1 at $v = 0$, and differ little up to $v = 0.4$ if we except the circle, for which the stresses σ_x are always negligible compared to the stresses σ_y (Fig. 4.11).

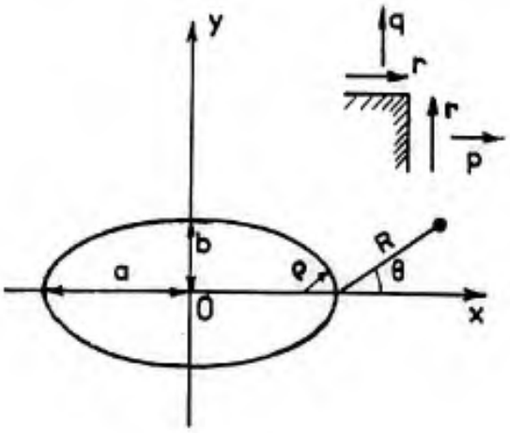

Figure 4.10

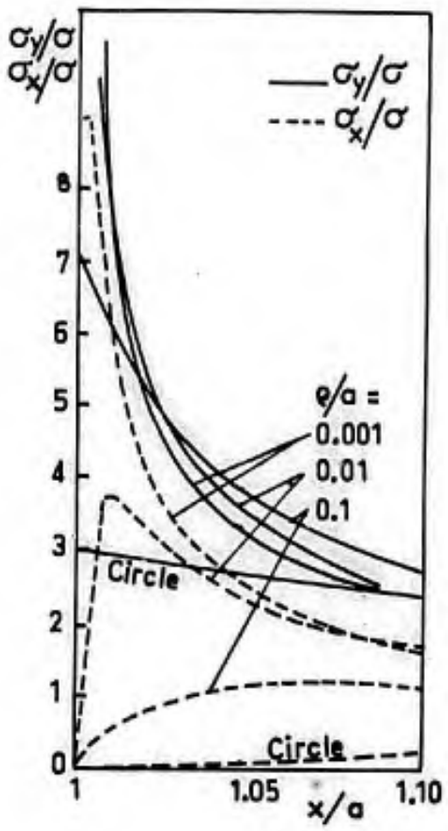

Fig. 4.11 Elliptic hole – stresses at $y = 0$; the distances x are expressed in terms of a

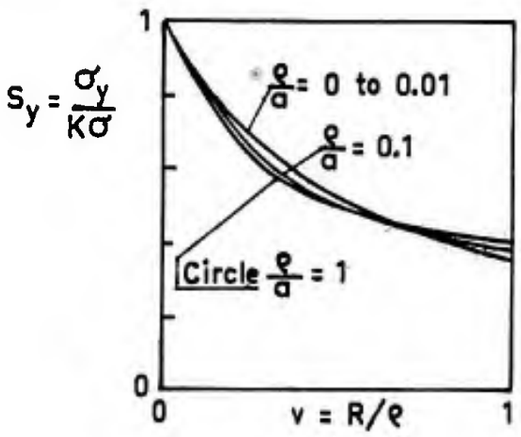

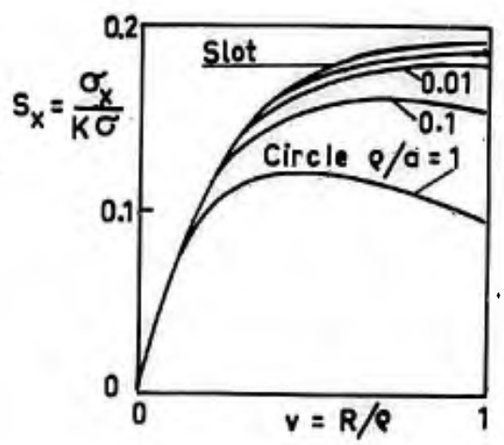

Fig. 4.12 Elliptic hole – distribution of the stresses σ/σ_{max}. For $\theta = 0$. Distances are expressed in terms of notch radius ρ (See Figure 4.10)

Consequently, we assume that for a distance R to the notch root, which is 0.4 times the notch radius ρ, the stress state σ_y, σ_x, τ_{xy} is fairly well defined by the sets of values

$$K_T, \rho \text{ and } \sigma, \text{ or } K_T, \sigma \text{ and } \frac{\partial \sigma_y}{\sigma \partial R} \simeq 2\frac{K_T}{\rho}, \text{ or } \sigma_{max} \text{ and } \frac{\partial \sigma_y}{\sigma \partial R},$$

provided the maximum stress value at the edge of the hole, σ_{max}, is low enough for the plastic zone, with $\sigma_y \geqslant \sigma_{0,2}$, to have a small radius compared to $0.4\,\rho$. The use of K_T and $\partial\sigma_y/\sigma\partial R$ as comparison parameters is thus restricted to the case of low K_T-values (3 to 7) and ρ-radii greater than the grain size of the metal, the surface grains exhibiting a low yield strength. In practice, the correlation with σ_{max} and with the gradient $\partial\sigma_y/\partial R$ will only be valid for the fatigue behaviour of moderate notches under low stresses and with a large number of cycles to failure.

TABLE 4.3

Elliptical Hole, Stresses at y = 0 Expressed in Terms of σ_{max} in Locations Whose Distances from the Root of the Notch are Expressed in Terms of the Notch Radius ρ.

											S_x MAX.	
v = R/ρ	0	0,1	0,2	0,4	0,6	0,8	1	1,2	1,4	1,6	S_x	v
Circle ρ/a = 1												
Sx	1	0,8126	0,6902	0,5485	0,4747	0,4324	0,4063	0,3891	0,3773	0,3689	0,542	0,4142
Sy	0	0,0717	0,1061	0,1249	0,1190	0,1067	0,0938	0,0820	0,0717	0,0630	0,125	
Ellipse ρ/a = 0,1												
Sx	1	0,8265	0,7085	0,5595	0,4700	0,4106	0,3685	0,3371	0,3129	0,2936	0,47	0,6
Sy	0	0,0745	0,1158	0,1523	0,1624	0,1622	0,1577	0,1514	0,1445	0,1376	0,163	
ρ/a = 0,01												
Sx	1	0,8332	0,7187	0,5721	0,4820	0,4210	0,3767	0,3430	0,3165	0,2949	0,42	0,8
Sy	0	0,0755	0,1191	0,1613	0,1769	0,1815	0,1811	0,1783	0,1744	0,1699	0,182	
ρ/a = 0,001												
Sx	1	0,8356	0,7225	0,5772	0,4875	0,4265	0,3820	0,3481	0,3212	0,2993	0,39	1
Sy	0	0,0759	0,1202	0,1642	0,1816	0,1879	0,1888	0,1872	0,1843	0,1808	0,189	
Slot ρ/a = 0												
Sx	1	0,84	0,73	0,58	0,49	0,43	0,39	0,35	0,33	0,30	0,39	
Sy	0	0,076	0,121	0,166	0,184	0,192	0,193	0,191	0,189	0,186	0,193	1

As far as sharp notches with high values of K_T ($\geqslant 60$) are concerned, the dimensions of the plastic zone, where $\sigma_y \geqslant \sigma_{0,2}$, largely encompasses the range of maximum $\sigma_x (R > \rho)$. The elastic stress distribution may be compared, then, by leaving this range out of consideration. The results in Table 4.2 and Figure 4.11 show that for $\rho/a \leqslant 0,0001$ the stress distribution is determined by σ and R/a. These stress distributions are relevant if the radius r_y of the plastic domain is small compared to R although large compared to ρ, i.e., if

$$\rho \ll r_y \ll R ;$$

this will be the case for large cracks in brittle materials.

4.2.2.1 Approximate Stress Distribution

We shall now consider the limiting case of the slot and examine the stress state near the extremity of the slot. With $\rho = 0$ and $k = 1$, the equations (1) and (2) become

$$\sigma_y + \sigma_x = p + \text{real part of } \left[q\left(\frac{\xi^2 + 3}{\xi^2 - 1}\right) - \frac{4\,i\tau}{\xi^2 - 1}\right],$$

$$\sigma_y - \sigma_x + 2\,i\tau_{xy} = -p + q\left[1 + 4\,\frac{\xi^3}{(\xi^2 - 1)^3}\left(\xi + \frac{1}{\xi} - \bar{\xi} - \frac{1}{\bar{\xi}}\right)\right] +$$

$$+ 2\,i\tau\left[\frac{\xi^3}{(\xi^2 - 1)^3}\left(\left(\xi + \frac{1}{\xi}\right)^3 - 6\left(\xi + \frac{1}{\xi}\right)\right) + 2\left(\bar{\xi} + \frac{1}{\bar{\xi}}\right)\right].$$

Near the extremity of the slot, $z = 2\left(1 + \frac{R}{a}e^{i\theta}\right)$ still equals $\xi + \frac{1}{\xi}$; hence, putting $\xi = 1 + \epsilon$, we find

$$z = 2 + \epsilon^2 \text{ and } \epsilon = \sqrt{\left(\frac{2R}{a}\right)}\, e^{i\theta/2} .$$

If the powers of ϵ up to the fourth are used in the intermediate calculations and if only the first is retained in the results, the above equations become approximately

$$\sigma_y + \sigma_x \approx p + q\left(-1 + 2\sqrt{\left(\frac{a}{2R}\right)}\cos\frac{\theta}{2}\right) + 2\tau\sqrt{\left(\frac{a}{2R}\right)}\sin\frac{\theta}{2}, \tag{5}$$

$$\sigma_y - \sigma_x + 2i\tau_{xy} \approx p + q\left(1 + \sqrt{\left(\frac{a}{2R}\right)}\sin\theta\sin\frac{3\theta}{2}\right) + \frac{\tau}{2}\sqrt{\left(\frac{a}{2R}\right)}\left(3\sin\frac{\theta}{2} + \sin\frac{5\theta}{2}\right)$$
$$+ 2i\left\{\frac{q}{2}\sqrt{\left(\frac{a}{2R}\right)}\sin\theta\cos\frac{3\theta}{2} + \frac{\tau}{4}\sqrt{\left(\frac{a}{2R}\right)}\left(3\cos\frac{\theta}{2} + \cos\frac{5\theta}{2}\right)\right\}. \tag{6}$$

The stress p at infinity, which acts parallel to the slot, is transferred unchanged. These approximate relations do not satisfy the boundary conditions at infinity or at the slot since $\theta > \pi/2$ cannot be taken into consideration if $R > 0$ is maintained. With $p = q$, these stresses correspond to a localized disturbance due to the slot, which can be superimposed on the stress state that exists in the absence of a slot.

For $p = q = \sigma$ and $\tau = 0$ the approximate disturbance is

$$\sigma_y = \sigma\sqrt{\left(\frac{a}{2R}\right)}\cos\frac{\theta}{2}\left(1 + \sin\frac{\theta}{2}\sin\frac{3\theta}{2}\right); \tag{7}$$

$$\sigma_x = \sigma\sqrt{\left(\frac{a}{2R}\right)}\cos\frac{\theta}{2}\left(1 - \sin\frac{\theta}{2}\sin\frac{3\theta}{2}\right); \tag{8}$$

$$\tau_{xy} = \frac{a}{2}\sqrt{\left(\frac{a}{2R}\right)}\sin\theta\cos\frac{3\theta}{2}. \tag{9}$$

The principal stresses are σ_1 and σ_2, such that

$$\frac{\sigma_1 + \sigma_2}{2} = \sigma\sqrt{\left(\frac{a}{2R}\right)}\cos\frac{\theta}{2},$$
$$\frac{\sigma_1 + \sigma_2}{2} = \sigma\sqrt{\left(\frac{a}{2R}\right)}\frac{\sin\theta}{2}; \tag{10}$$

these expressions allow comparisons to be made in connection with other crack problems.

Fairly good approximations are thus obtained when $\frac{R}{a} \geqslant 0.01$ is not too large. With $q = \sigma$ and $p = \tau = 0$ we have on the Ox-axis, where $\theta = 0$:

$$\sigma_y = \sigma\sqrt{\left(\frac{a}{2R}\right)} \text{ and } \sigma_x = \sigma_y - \sigma;$$

numerical computation yields

	R/a	0.01	0.02	0.05	0.10	0.20	1
σ_y/σ	approximate	7.07	5	3.16	2.24	1.58	0.71
	correct	7.12	5.08	3.28	2.40	1.81	1.15
σ_x/σ	approximate	6.07	4	2.16	1.24	0.58	-0.29
	correct	6.12	4.08	2.28	1.40	0.81	0.15 .

4.2.2.2 Displacements at the Edge of the Ellipse

In the MUSKHELISVILI method the displacements u and v along Ox and Oy are

$$u + iv = \frac{1}{E}\left\{(3 - \nu)\,F(z) + (1 + \nu)\left[z\overline{F'(z)} + \overline{H(z)}\right]\right\}.$$

On the contour of a slot with $k = 1$, $z = \xi + \frac{1}{\xi}$ and $\xi = e^{i\beta}$, we find for $q = \sigma$, $p = \tau = 0$:

$$u + iv = \frac{\sigma}{E}(-2\cos\beta + 4i\sin\beta),$$

if $a = 2$ and $x = 2\cos\beta$. With $a \neq 2$ we have

$$u/a = -\frac{x}{a}\frac{\sigma}{E}, \qquad v/a = \frac{2\sigma}{E}\sqrt{[1 - (x/a)^2]} . \tag{11}$$

4.2.2.3 Potential Elastic Energy, Analysis of $\mathcal{G} = \partial U/\partial A$.

The potential elastic energy U of a plate containing a hole is the difference between the energy U_1 of the plate without a hole and the work required to cancel out the displacements at the edge of the hole when applying to the contour of the hole the stresses of the state 1 which are considered as external loads :

$$U = U_1 - \frac{1}{2}\int \sigma v \, ds .$$

The potential elastic strain energy relaxed by an increase dA in the area cut by the slot is then

$$\mathcal{G}\, dA = \frac{\partial}{\partial A}\left(\frac{1}{2}\oint \sigma v \, ds\right) dA .$$

In the preceding case, we have $\sigma_1 = \sigma$ and $\sigma_x = 0$ on the contour, and the displacement along σ is v ; the work necessary for closure of the slot is

$$\sigma \int_{-a}^{+a} v \, dx , \qquad \text{i.e.} \quad \frac{\sigma^2}{E} a^2 \pi .$$

Putting $dA = 2\,da$, we have

$$\mathcal{G} = \frac{\partial U}{\partial A} = \frac{\sigma^2}{E} a\pi .$$

4.2.2.4 Case of Plane Strain

Computation shows that the stress distributions are identical with those obtained in the case of plane stresses but the modulus of elasticity E is replaced by $E/(1 - \nu^2)$ in the expressions for the displacements and for $\mathcal{G}$.

4.2.2.5 Case of an Orthogonally Anisotropic Plate

The elastic properties are defined by

$$\epsilon_x = \frac{\sigma_x}{E_x} - \nu_y \frac{\sigma_y}{E_y} , \qquad \epsilon_y = \frac{\sigma_y}{E_y} - \nu_x \frac{\sigma_x}{E_x} .$$

The MAXWELL principle of reciprocation implies $\nu_y/E_y = \nu_x/E_x$.

After MENDELSON and SPERO[16], we put

$$\beta^2 = E_y/E_x = \nu_y/\nu_x ,$$

$$e_x = \epsilon_x \frac{E_y}{\sigma} , \qquad e_y = \epsilon_y \frac{E_y}{\sigma} , \qquad S_x = \sigma_x/\sigma , \qquad S_y = \sigma_y/\sigma ;$$

it has been demonstrated that at $y = 0$

$$S_y(x,0)_{orth.} = S_y(x,0)_{iso.} , \qquad S_x(x,0)_{orth.} = \frac{1}{\beta} S_x(x,0)_{iso} .$$

$$x(x,0)_{orth.} = \frac{1+\beta}{2} v(x,0)_{iso.} ,$$

where there is equality of E_y , and that

$$\mathcal{G}_{orth.} = \frac{1+\beta}{2} \mathcal{G}_{iso.} .$$

4.2.3 Thin Sheet of Finite Width Having a Transverse Central Slot

There is no correct solution; WESTERGAARD[17] has studied the problem of an infinite plate having periodic slots with a distance w between the axes in the x-direction, the stress at infinity ($y = \infty$) being $\sigma_y = \sigma_x = \sigma$ (Fig. 4.13).

With the complex function $F = \sqrt{\left\{1 - \left(\frac{\sin \frac{\pi a}{w}}{\sin \frac{\pi z}{w}}\right)^2\right\}}$,

we have

$$\frac{\sigma_y + \sigma_x}{2} = \text{real part of } F ,$$

$$\frac{\sigma_y + \sigma_x}{2} = \text{y. imaginary part of } dF/dz ,$$

$$\tau_{xy} = - \text{y. real part of } dF/dz .$$

For plane stresses the displacement along Oy is v :

$$E\,v = -(1+\nu)\,y\ (\text{real part of } d^2F/dz^2) + 2\ (\text{imaginary part of } dF/dz) .$$

The foregoing function satisfies the boundary conditions :

on the slots, c being an integer, at $cw - a < x < cw + a$: $\sigma_y = \sigma_x = \tau_{xy} = 0$;

at $z = x \pm i(\infty)$: $\sigma_x = \sigma_y = \sigma$, $\tau_{xy} = 0$.

Near the extremity of the slot we again obtain the expressions (7), (8) and (9) of the stresses in an infinite plate, multiplied by the correction factor for finite width

$$c_w = \sqrt{\left(\frac{w}{\pi a} \tan \frac{\pi a}{w}\right)} . \tag{12}$$

On the slot, at $y = 0$, the displacement v is given by

$$E\,v = 2\,\frac{\sigma w}{\pi} \cosh^{-1}\left(\frac{\cos \pi x/w}{\cos \pi a/w}\right), \tag{13}$$

allowing the computation of $\mathcal{G}$, for which the value

$$\mathcal{G} = \frac{\pi}{E}\sigma^2\, a\, c_w^2 \tag{14}$$

is found.

If the plate is cut along lines such AB , we obtain sheets of finite width w with a central slot (Fig.4.14) but with variable stresses σ_x on the longitudinal edges; the latter stresses can be cancelled out by constant stresses σ which are introduced without disturbance and by a self-balanced perturbation of zero value at infinity which tends to open the slot, hence to increase $\mathcal{G}$ or c_w . On the axis the intensity of these parasitic stresses is

$$a\left(\frac{1}{\cos \pi a/w} - 1\right);$$

the unknown correction of c_w is small if a is much less than w/2 .

In the approximate expressions from Equations (7), (8) and (9) for the stresses near the crack tip, the stresses are dependent on R and on the factor $k = \sigma\sqrt{a}$, if one uses the former PARIS[18,19] notations, or on the IRWIN[9] factor

$$K = \sigma\sqrt{(\pi a)} .$$

This factor K is called *stress intensity factor* and is useful because the stress distribution around the crack front is given, for all cracks subjected to tensions perpendicular to their planes, by the expressions (7), (8) and (9), except for one variable factor. In the two preceding cases of a central slot contained in an infinite sheet and in a sheet of finite width, calculations show that K is associated with the IRWIN parameter $\mathcal{G}$ by the relation

$$K = \sqrt{(E\mathcal{G})} . \tag{15}$$

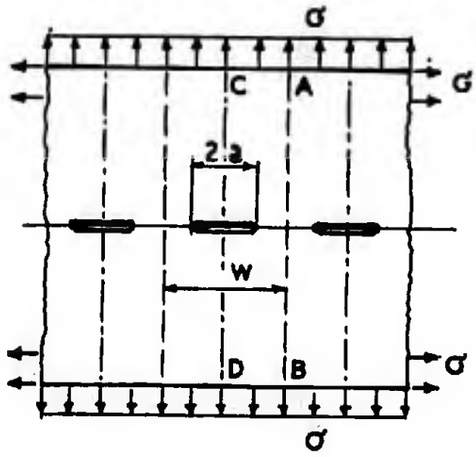

Fig.4.13 Periodic slots, after Westergaard[17]

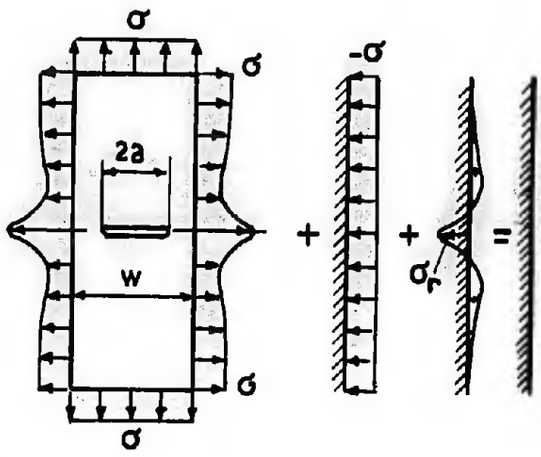

Fig.4.14 Strip of finite width cut from the infinite sheet of the Figure 4.13

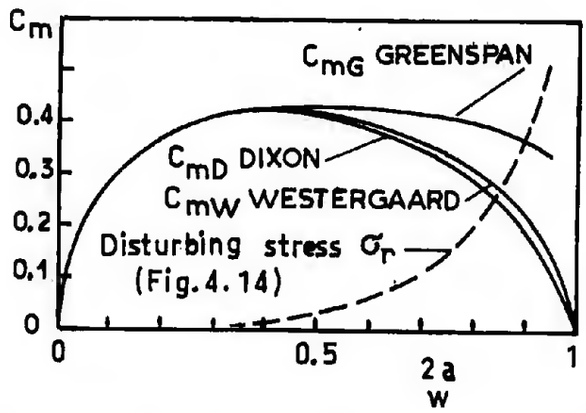

Fig.4.15 Comparison of the C_m - coefficients in the expression $K = \sigma_m \sqrt{(\pi w/2)}$. C_m ; σ_m is the net mean stress

Taking into account the SAINT-VENANT principle, we shall consider that the relation remains valid. Besides, $\mathcal{G}$ is only of interest to us because it can be assessed by measurements, as will be shown later.

For a plate of finite width, we have

$$K = \sigma\sqrt{(\pi a)} \cdot c_w \cdot \tag{16}$$

Instead of the stress σ away from the slot, we may use the mean stress in the uncracked net section

$$\sigma_m = \sigma/(1 - 2a/w)$$

and define a new coefficient for finite width, c_{mw}, such that

$$K = \sigma\sqrt{(\pi a)} \cdot c_w = \sigma_m\sqrt{\left(\frac{w}{2}\right)}\sqrt{(\pi)} \cdot c_{mw} \tag{17}$$

and

$$c_{mw} = (1 - 2a/w)\sqrt{\left(\frac{2}{\pi}\tan\frac{\pi a}{w}\right)}, \tag{18}$$

according to WESTERGAARD's results.

DIXON[20], referring to a calculation in which the stress distribution is assumed to be identical, except for one factor, in the cases of finite and infinite widths, and to photo-elastic measurements on plates containing slots with round extremities, suggested that c_w be replaced by a correction factor

$$c_D = 1/\sqrt{\left[1 - \left(\frac{2a}{w}\right)^2\right]}, \tag{19}$$

hence, if the net stress is considered, by a coefficient

$$c_{mD} = \sqrt{\left[\frac{2a}{w}\,\frac{1 - 2a/w}{1 + 2a/w}\right]}. \tag{20}$$

LACEY[75], using a calculation made by GREENSPAN[74] for a circular hole but based on questionable assumptions, proposed, for $\mathcal{G}$, the expression

$$\mathcal{G} = \frac{\pi\sigma^2}{E}\,2a\,\frac{2 + m^4}{[2 - m^2 - m^4]^2},$$

where $m = 2a/w$, the corresponding value of c_m being

$$c_{mG} = (1 - m)\,\frac{\sqrt{[2\,m(2 + m^4)]}}{2 - m^2 - m^4}. \tag{21}$$

LACEY reports test results from BRISTOL AIRCRAFT which provide experimental data for the longitudinal stiffness of aluminium alloy sheets. We have re-calculated c_m on the basis of these results and found values that were substantially constant with $m = 2a/w$ above $2a/w = 0.4$. It should be noted that all the tests were carried out without anti-buckling bars capable of preventing buckling of the crack edges in compression. This question will be examined in detail on page 170 when discussing KUHN's method of prediction.

According to PARIS and SIH[21], ISIDA[22] calculated the stress concentration factors at the round extremities of a slot of length $2a$ and radius ρ, contained in a strip of width w, and he found

$$\sigma_{max} = 2\sigma\sqrt{(a/\rho)} \cdot f(m),$$

where $m = 2a/w$. Considering the net mean stress, we may write

$$\sigma_{max} = 2\sigma_m\left(\frac{w}{2\rho}\right) \cdot (1 - m) \cdot \sqrt{(m)} \cdot f(m);$$

thus a correction factor

$$c_{mI} = (1 - m) \cdot \sqrt{(m)} \cdot f(m)$$

is obtained. ISIDA found the following results by numerical computation :

m =	0.074	0.207	0.275	0.337	0.410	0.466	0.535	0.592
$f(m)$ =	1	1.03	1.05	1.09	1.13	1.18	1.25	1.37.

With the four expressions of c_m, direct numerical calculation or interpolation yields the results reproduced in Table 4.4 and in Figure 4.15. In the case of $2a/w < 0.5$ no test is accurate enough to permit selecting one mode of determination, so we shall use c_{mD} as it is easy to calculate numerically. Our working hypothesis will be

$$c_m = \begin{cases} \sqrt{\left(m \dfrac{1-m}{1+m}\right)} & \text{for } m = 2a/w \leqslant 0.4 \\ 0.414 & \text{for } 0.4 \leqslant m < 0.8 \,. \end{cases} \qquad (22)$$

Note that in a recent paper by FICHTER[55] for a plate of infinite width and height L the ratio $(K)_L/(K)_{L=\infty}$ is shown to be increasing asymptotically toward unity with increasing L/a and with a uniform relative displacement at the grip edges :

L/a =	1	2	3	4	5
$(K)_L/(K)_\infty$ =	0.57	0.78	0.89	0.92	0.95

The test results reported by LACEY as well as ISIDA's numerical calculations may be accounted for by an effect of finite height on K that is qualitatively of the same nature. However, in the case of uniform stress, as may be obtained substantially with a whiffle-tree arrangement, FISHER's calculations indicate a ratio K_I/K_∞ greater than unity.

To substantiate ISIDA's results, FEDDERSEN[83] has proposed the formulation

$$K = \sigma\sqrt{(\pi a)}\left[\cos\frac{\pi}{2}m\right]^{-1/2} ,$$

$$c_{mF} = (1-m)\left[m/\cos\frac{\pi}{2}m\right]^{1/2} .$$

TABLE 4.4

Central Crack in a Sheet of Finite Width According to Figure 4.15. Values of c_m in $K = \sigma_m\sqrt{(\pi w/2)}$. $c_{m'}$

2a/w		0	0.1	0.2	0.3	0.4	0.5	0.6	0.7	0.8	0.9
WESTERGAARD	c_{mw}	0	0.287	0.362	0.398	0.408	0.400	0.374	0.337	0.280	0.200
DIXON	c_{mD}	0	0.286	0.365	0.402	0.414	0.408	0.387	0.360	0.300	0.220
GREENSPAN	c_{mG}	0	0.286	0.365	0.404	0.420	0.425	0.424	0.418	0.414	0.411
ISIDA	c_{mI}	0	0.284	0.366	0.410	0.43	0.43	0.415			
FEDDERSEN	c_{mF}	0	0.286	0.368	0.40	0.422	0.422	0.400	0.373	0.322	0.240

4.2.4 Plasticity Correction

For most industrial metals such as steels and light aluminium alloys the stress-strain curve flattens at $\sigma > \sigma_{0.2}$. If it is assumed that the strain distribution is given by the theory of elasticity, the highest actual stresses will be little in excess of $\sigma_{0.2}$.

Figure 4.16, relative to a central crack of length $2a_0$ contained in a sheet of finite width w, illustrates the elastic distribution of the stresses σ_y on the X-axis going through the crack. With this distribution the yield strength $\sigma_{0.2}$ will be reached at a distance r_Y from the crack front. Computation yields

$$\sigma_{0.2} = K\sqrt{\left(\frac{1}{2\pi r_Y}\right)} \text{ and } r_Y = \frac{K^2}{2\pi\sigma_{0.2}^2} = \frac{a_0}{2} c_w^2 \left(\frac{\sigma}{\sigma_{0.2}}\right)^2 .$$

In order to preserve the load balance across the width of the sheet, the stress distribution assumes the shape of the solid-line curve in Figure 4.16 and the actual plastic range corresponds to a radius $R_Y > r_Y$, the difference increasing more rapidly than 2a/w.

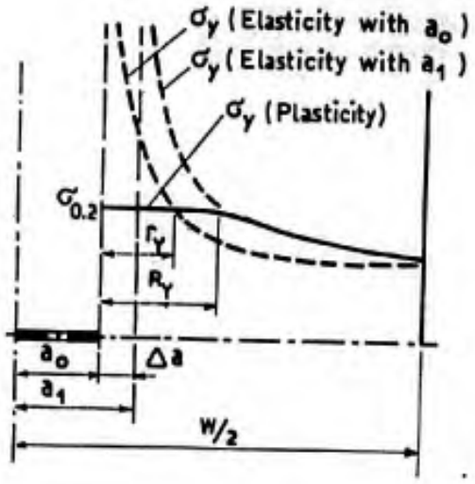

Fig. 4.16 Radii of the plastic zone

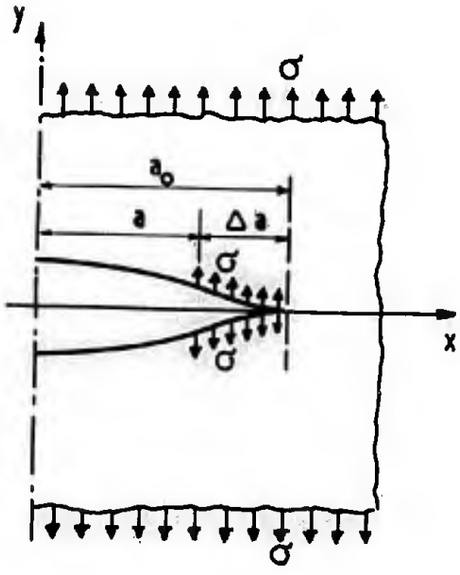

Fig. 4.17 Replacing of the plasticity effect by tensile stresses at the crack tip (after Burdekin[38])

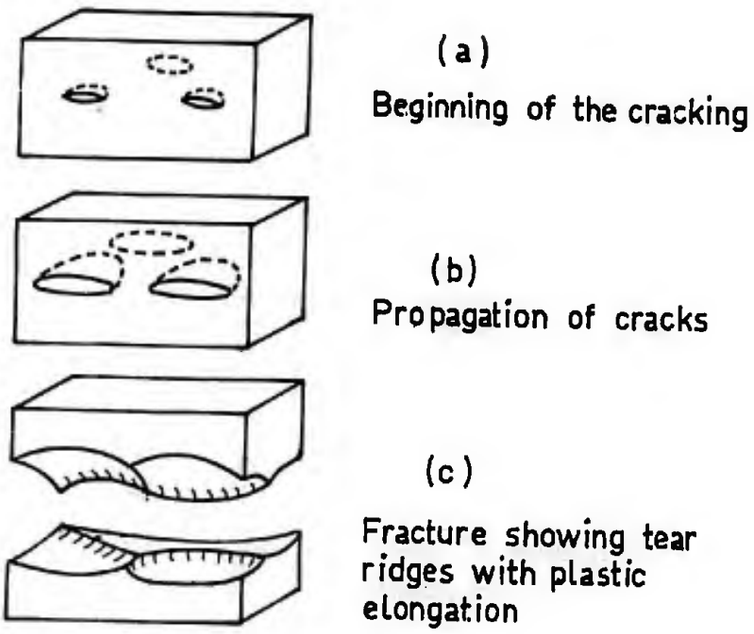

Fig. 4.18 Sketch of the development stages in "quasi-cleavage". After Beachem and Pelloux[31]

An approximation of the elastic portion of this curve can be obtained by assuming a crack of half-length $a_1 = a_0 + \Delta a$. The ASTM indicated that tests on high-strength steels were fairly well correlated by taking

$$\Delta a = r_Y \text{ or } a_1 = a_0\left[1 + \frac{c_w^2}{2}\left(\frac{\sigma}{\sigma_{0,2}}\right)^2\right]. \tag{23}$$

Discussing a paper by WEISS and YUKAWA[26], LIU[27] examined the representativeness of K for the stress distribution ahead of the crack front by comparing two cracks of different lengths a_1 and a_2 for equal K_c-values. For a crack of length 2a in an infinite sheet, subjected to tensile stress σ, if x is the distance to the centre of the crack, as measured in the direction of the crack, then the exact distribution of the tensile stresses σ_y in the crack plane is

$$\sigma_y = \sigma\frac{x}{a}\Big/\sqrt{\left[\left(\frac{x}{a}\right)^2 - 1\right]}.$$

Putting $x = a + R$ and with $K_c = \sigma_1\sqrt{(\pi a_1)} = \sigma_2\sqrt{(\pi a_2)}$, it follows that

$$\frac{\sigma_{y1}}{\sigma_{y2}} = \frac{1 + R/a_1}{1 + R/a_2}\sqrt{\left[\frac{1 + R/2a_2}{1 + R/2a_1}\right]};$$

for equal values of the stress intensity factor, the stresses away from the crack tip are such that $(\sigma_{y1}/\sigma_{y2}) > 1$ when $a_2 > a_1$. If the same stresses are to be found at the boundaries of the interaction range (see Figure 4.9), σ_2 must be increased and we shall have $K_{c1} < K_{c2}$. For a correction, K_c should be further increased for short cracks. This is done by the usual plastic-zone correction with $\Delta a = r_Y$.

In the final discussion at the ASTM-NASA Symposium in 1964[28], WELLS, BURDEKIN and STONE[29,30] pointed out that in ductile materials such as mild steel the plastic flow observed at the crack tip permits a relative displacement of the crack faces without any increase of the crack length because of an opening of the slot; they calculated the slot opening by using the theory of elasticity and supposing that, since the plastic flow is restricted to a very small domain ahead of the crack and on each side of its plane (Fig.4.17), the stresses $\sigma_{0,2}$ applied to the slot over a length $\Delta a = a_1 - a$ and superimposed on the general tension at infinity, σ, caused the stress σ_y to be finite at the extremity of the plastic zone. Their calculations led to

$$a/a_1 = \cos\left(\frac{\pi}{2}\sigma/\sigma_{0,2}\right)$$

and yielded for the slot opening

$$\delta = \frac{8\sigma_{0,2}a}{\pi E}\log_e\left[\sec\left(\frac{\pi}{2}\sigma/\sigma_{0,2}\right)\right].$$

On the other hand, they considered that $\mathcal{G} = \sigma_{0,2}\cdot\delta$, hence

$$\mathcal{G} = \frac{\pi\sigma^2 a}{E}\left\{1 + \frac{\pi^2}{24}\left(\frac{\sigma}{\sigma_{0,2}}\right)^2 + \frac{\pi^4}{360}\left(\frac{\sigma}{\sigma_{0,2}}\right)^4 + \dots\right\}.$$

This result, restricted to the first two terms, is in fairly good agreement with the ASTM recommendations.

The starting point was WELLS'[29] hypothesis of a critical crack opening displacement; this concept is in accordance with the advanced ideas concerning crack initiation by a series of microcracks ahead of the crack front, followed by a stretch of the regions between the microcracks until fracture occurs (see Figure 4.18).

4.3 INITIATION AND GROWTH OF CRACKS

Under an increasing load, pre-existing or load-induced microcracks on a submicroscopic scale join to form a visible crack which grows until the GRIFFITH-IRWIN instability occurs, that is, when the elastic energy released by the crack extension is at least equal to the decohesion work required to increase the fractured surface area. A quite significant amount of plastic deformation work is included in the decohesion work.

4.3.1 Fracture Modes on a Submicroscopic Scale

From recent studies on microfractography by means of an electronic microscope and especially from a paper by BEACHEM and PELLOUX[31] it may be stated that there are four main fracture modes on the scale of the electronic microscope:

- cleavage,
- quasi-cleavage,
- coalescence of microvoids,
- intergranular separation.

Cleavage, as illustrated fairly well by the splitting of mica into foils, corresponds, in the case of metals, to a separation along crystalline planes of high atomic density. This type of fracture is preceded by some plastic deformation and propagates along different parallel planes connected by steps.

In *quasi-cleavage*, cleavage cracks initiated at certain locations join, leaving at their junctions small ridges which are plastically deformed, as shown by the sketch in Figure 4.18.

If the metal contains a large number of hard precipitates or oxide inclusions, the differences in elastic and plastic properties between the matrix of the metal and the inclusions cause the plastic strain to generate voids at the interfaces between the particles and the matrix. These voids tend to develop into round cavities which continue to grow under further plastic strain. As in quasi-cleavage, the material between neighbouring voids becomes thinner while stretching and it finally fractures, thus achieving the *coalescence* of several cavities into one.

In both cases of quasi-cleavage and of coalescence of voids, one observes a growth of microcracks and plastic elongation followed by fracture of the regions that separate the microcracks. It is known that precipitates, inclusions and solute foreign atoms stabilize the matrix, impede plastic deformation and permit cleavage fracture; it may be assumed that fracture develops by cleavage in the first place until the residual section area between two voids becomes so small that it is no longer stabilized by precipitates, hence elongation becomes possible. If the material is very stable as, for example, in low-temperature tests or high-speed impact tests, cleavage fracture extends much further before plastic elongation occurs.

Intergranular separation is of fairly rare occurrence except in the cases of corrosion, stress-corrosion and embrittlement by hydrogen; it will not be examined further in this chapter.

For engineering metals selected with reference to their fields of application, the most frequent mode of fracture will be the coalescence of voids or microcracks. In this respect, computation shows that the stress intensity factor at the near tips of two neighbouring cracks are much greater than those at the far tips[32]. Consequently, neighbouring cracks will tend to join more rapidly than they grow outwards. If the barriers to plastic slip are very finely divided and if the material is not very heterogeneous, there will be few crack initiations and the cracks will grow by cleavage. If the density of distribution of the slip barriers exhibits weak areas, elongation of these areas will overstress the other regions, where cleavage will be initiated, and the cracks will spread to the plastic regions (quasi-cleavage). With many heterogeneous points, the number of initial cracks increases and local fracture through coalescence of voids may be obtained.

"In engineering alloys, as a result of recent work on specimens pulled under the microscope one may conclude that the first observable voids are due to fracture of large intermetallic particles. Fracture of these particles takes place at about 6% strain. Later voids are a result of decohesion of the interface of smaller particles. From electron fractography, it is clear that voids generally do not grow by cleavage but by slip plane decohesion" (after BROEK[79]).

4.3.2 The Stability Concept

IRWIN and KIES[33] have adopted GRIFFITH's point of view, taking into consideration the plastic strain work. Let an elastic specimen be subjected to a force F which causes a displacement f of its point of application, such that

$$f = F/M ,$$

where M measures the stiffness of the specimen. The potential elastic energy is

$$U = \frac{1}{2}\frac{F^2}{M} .$$

Consider a variation A of the fractured area A while assuming that the deflection f remains constant. If $\delta W = (\partial M/\partial A)\delta A$ is the work done by the decohesion and plastic deformation forces, the conservation of the energy implies

$$\frac{\partial W}{\partial A}\delta A + \left(\frac{\partial U}{\partial A}\right)_{f=\text{constant}} \delta A = 0 .$$

Now $(\partial U/\partial A)_{f=\text{constant}} = -\mathcal{G}$, by definition of $\mathcal{G}$, hence

$$\mathcal{G} = -\frac{1}{2}\left(\frac{F}{M}\right)^2 \frac{\partial M}{\partial A} = \frac{1}{2}F^2 \frac{\partial(1/M)}{\partial A} .$$

Equilibrium implies that

$$\frac{\partial W}{\partial A} \geq \mathcal{G} .$$

Let us now suppose a constant force F. The variation of the work done by the external forces is $\delta C = F.\delta f$ and the variation of the potential energy is $\delta U = (\partial U/\partial A)_{F=\text{constant}}.\delta A$; it follows that

$$\delta C = F^2 \frac{\partial(1/M)}{\partial A} \delta A = 2\,\mathcal{G}\,\delta A , \qquad \delta U = \frac{1}{2} F^2 \frac{\partial(1/M)}{\partial A} \delta A = \mathcal{G}\,\delta A .$$

Equilibrium implies that

$$\delta C \leq \frac{\partial W}{\partial A} \delta A + \delta U$$

or

$$\frac{\partial W}{\partial A} \geq \mathcal{G} = \frac{1}{2} F^2 \frac{\partial(1/M)}{\partial A} .$$

In the first case, the loading is carried out in a very rigid machine which imposes a displacement, whereas in the second case the loading is by means of weights or by a quite flexible machine. Therefore, irrespective of the type of loading, the equilibrium will be stable if

$$R = \frac{\partial W}{\partial A} \geq \mathcal{G} = \frac{1}{2} F^2 \frac{\partial(1/M)}{\partial A} . \tag{24}$$

$\mathcal{G}$ is the elastic energy released under deflection for a unit increase of the fractured area A. It is a quantity that depends on the applied load and on the shape and size of the specimens; it characterizes the imposed elastic strains.

R defines the fracture work required to increase the area A of the fractured section and is a measure of the *fracture toughness;* it is a physical quantity dependent on the state of the material and on the local state of stress. For very brittle materials such as those investigated by GRIFFITH, R is a constant independent of the crack length and rupture occurs at a critical value R_c of $\mathcal{G}$:

$$\mathcal{G}_c = R_c .$$

It may also be noted that $\mathcal{G}$ and R are expressed in $\text{daN.mm/mm}^2 = \text{daN/mm}$ or $\text{lb.in/in}^2 = \text{lb/in}$, that is, in the same units as the surface tension of a liquid; GRIFFITH's use of the term "surface tension" for $T = R/2$ puzzled the engineers for a long time as they did not see what hidden stress was covered by this designation.

4.3.3 Experimental Measurement of $\mathcal{G}$

During the loading of a cracked specimen, a small volume of material near the crack front lies in the plastic range and, consequently, the curve $f - F$ is not a straight line; however, the material hardens under the load and becomes elastic under lower loads.

$\mathcal{G}$ can be calculated from measurements of the relation $f/F = 1/M$ carried out during unloading on the *same* specimen for various apparent dimensions of the crack, if $\mathcal{G}$ is supposed to be dependent only on these dimensions, or on several specimens, which will then be fractured for determination of the crack dimensions.

In the bending test on two supports of a square bar represented in Figure 4.19 (20-20-150 mm-bar with supports that are 120 mm apart, and a semi-elliptical crack initiated in fatigue from an electrical scriber mark), DOUILLET, SERTOUR and AUVINET[34] measured the rigidity $M = P/f$, which is the ratio of the load P, applied at mid-length, to the deflection f measured during unloading. If M_o is the value of M for an uncracked bar, we may write

$$\mathcal{G} = \frac{1}{2M_o} P^2 \frac{\partial(M_o/M)}{\partial A} .$$

Figure 4.20 contains a curve $M_o/M = f(A)$, which applies to all the metals tested and is drawn at best through very scattered test results; according to the authors, the curve holds true only for $40\ \text{mm}^2 \leq A \leq 80\ \text{mm}^2$. In order to effect a derivation, and taking into account that $\mathcal{G}$ is always proportional to a linear dimension, we put

$$\frac{\partial(M_o/M)}{\partial A} = \frac{3}{2} k\sqrt{A} ,$$

hence

$$M_o/M = 1 + k\,A^{3/2} .$$

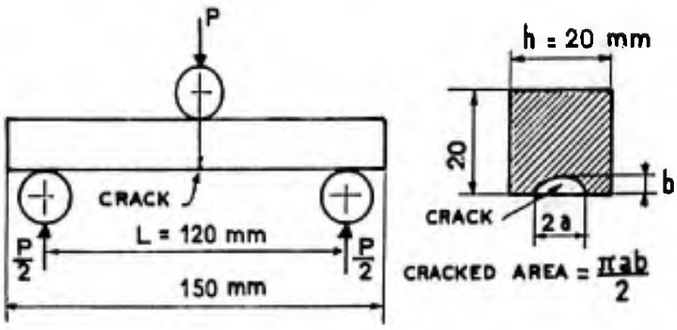

Fig. 4.19 Bending of cracked square bars. Tests by Douillet et al.[34]

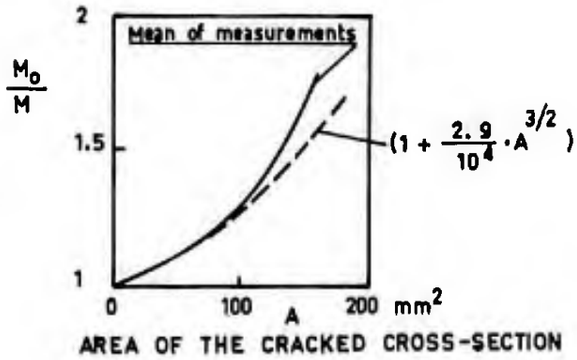

Fig. 4.20 Bending elastic properties of the square bars. M P/f where P is the load and f is the deflection (See Figure 4.19)

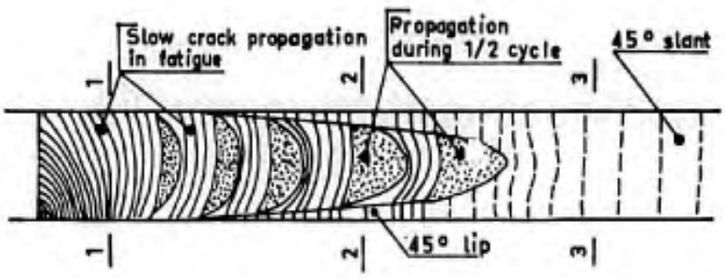

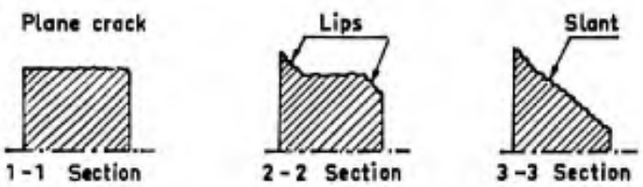

Fig. 4.21 Crack propagation in fatigue

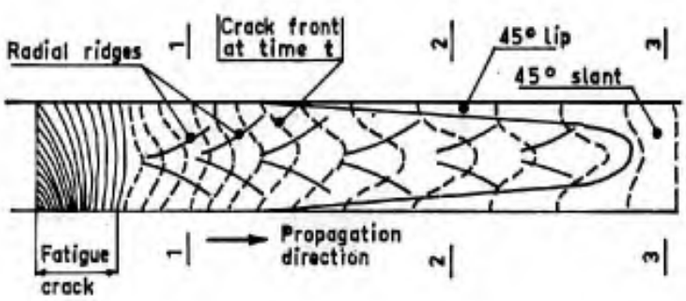

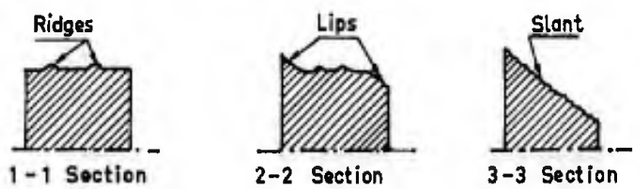

Fig. 4.22 Static brittle crack propagation

With $k = 2.9\ 10^{-4}$, the dotted curve in Figure 4.20 is identical with the solid curve for $A < 80\ mm^2$. Further, we have

$$M_o = P/f = 48\ EI/L^3 = E/2.7$$

and

$$G_f = (P^2/2M_o)\ .\ 4.35\ 10^{-4}\ \sqrt{A} = 5.85\ 10^{-4}\ P^2\ \sqrt{A}\ /E\ .$$

For the bars investigated, the semi-elliptical cracks of length $2a$ at the surface and of depth b showed a mean ratio $a/b = 1.2$, hence

$$A = \pi a^2/2.4$$

and

$$G_f = 6.7\ 10^{-4}\ P^2 a/E\ . \qquad (25)$$

Thus, we obtain

$$K = \sqrt{(E G_f)} = 0.0259\ P\ \sqrt{A}\ . \qquad (25\ bis)$$

Although subsequent approximate calculations confirm this value of K , no correct solution is available, so direct measurements, despite the large number of sources of errors they include, prove very helpful. The difficulty is that measurements are inaccurate for small cracks and that the crack shape becomes rather erratic for large cracks.

4.3.4 Behaviour of Cracked Plates in Fatigue and Static Failure

We shall first examine the *propagation of fatigue cracks* since fracture observations are facilitated by the existence of striations or "tide marks" whereby the successive positions of the crack front are identified for each load cycle. The finest lines are visible only in the electron microscope but irregularities of the load or of the material and possible test interruptions produce groups of striations that are visible to the naked eye. Apart from these striations, in some specific cases dark areas are created by rapid propagation of the crack, as in a static fracture.

In Figure 4.21, the propagation of a fatigue crack from a geometrical notch in a plate is shown schematically[35]. At the beginning, the crack starts at a point A and remains plane; it spreads in the direction of the arrow, leaving visible marks due to the successive positions of the crack front. For a constant stress σ applied to the sections far above and below the crack plane, the mean stress in the still uncracked section and the stress concentration near the crack front increase with the crack length, which explains why the distance between the successive stop lines and the propagation rate increase with the crack length.

From a given crack length, intermittent crack propagation by big leaps is sometimes found in plates, each leap corresponding to a partial static fracture. The front of this quick static growth of the crack develops more rapidly in the core of the plate than at the surface. As with the central fracture of static-tension specimens, this seems to result from the greater ease of plastic elongation near the faces, which reduces locally the applied load. Static fracture is limited because its development lowers the stress concentration at the tip, the uncracked edges continuing to sustain an increasing amount of the load. The edges are, then, subject to quite considerable alternating strains inducing a slow propagation of the fatigue crack which, being more rapid at the edges, leads to a change of the crack front in such a manner that the conditions of a new static-fracture phase are created.

Final static fracture under fatigue loading occurs when the supporting effect of the edges is no longer sufficient to balance the increase of the mean stress.

The large plastic deformations near the faces generate high local tensile stress concentrations and vacancy concentrations on slip planes close to the shear plane; they cause a slant 45°-cracking which produces *ductile lips* or *borders*. The width of the lips increases slowly with the mean stress and extents through the thickness unless final rupture occurs before.

Let us now consider the *static fracture of a part fatigue-cracked* under a much smaller load or containing a very sharp notch which results in a stress concentration similar to that of a fatigue crack. In Figure 4.22 the crack propagation is illustrated for thin sheets or plates.

At the onset of crack extension, a plane fracture substantially normal to the sheet plane is often observed, with slightly marked undulations which appear as ribs radiating from mid-thickness to the faces of the plate. These *"herring-bone" lines* are characteristic of the "brittle"-type fracture, the apexes being oriented toward the origin of the crack. The successive positions of the crack front sweep across the fracture surface without leaving visible traces. They are shown in Figure 4.22 as dotted lines for constant time intervals. If, because of instability, the rate of cracking is very high, then the shape of the successive positions can be revealed by a dye-staining technique using ink which is sucked into the crack, as has been observed for example by KRAFFT,

SULLIVAN and BOYLE[16]. This shape exhibits the same relative progress at mid-thickness (*tunnelling*) as in the discontinuous static fractures encountered in fatigue, and can be explained in the same manner. As in fatigue, the ductile slant-fracture lips develop gradually and result, on thin sheets, in a slant through-thickness fracture. In thick plates of small width, only lips of very small width are obtained.

For bars containing a semi-elliptical surface crack and subjected to tension or bending, the fracture illustrated in Figure 4.23 shows similar ductile lips originating from the crack surface edges and radiating ribs.

4.3.5 Effect of Sheet Thickness

In Paragraph 4.2.2.1 we examined the state of *plane stress* around a crack tip subjected to tension. This analysis holds for thin sheets. Consider now a thick plate having a central crack of length 2a and a rectilinear crack front of length AB equal to the plate thickness. Figure 4.24a is a plot of the variations of the stresses σ_y and σ_x near the crack tip.

The lateral contraction, which is quite significant near the crack front AB, reduces the latter from AB to A'B'. This variable contraction induces shear stresses τ_{xz} which tends to impede it. The supporting effect of the material far away from the crack border produces stresses σ_z (Fig.4.24b) which reach a maximum on the crack border. At C, where the median plane of the plate intersects the crack front, the state of stress is more triaxial if the thickness is larger or if, for the same thickness, the decrease of the stresses σ_x along Ox is faster. There is a tendency toward the *state of plane strain*, in which σ_x, σ_y and τ_{xz} assume the values given by expressions (7), (8) and (9) in Paragraph 4.2.2.1, relating to the plane stress case. Away from the crack, the mean lateral contraction is, with $\sigma_z = \sigma_x = 0$,

$$-\epsilon_z = \frac{\nu}{E}\sigma .$$

On the median plane, the lateral contraction at C would be, if it were unimpeded, equal to

$$\frac{\nu}{E}(\sigma_x + \sigma_y) .$$

The stiffness effect can only alter the lateral contraction to

$$\frac{\nu}{E}(\sigma_x + \sigma_y - \sigma) ;$$

σ is small compared to σ_x and σ_y; consequently, if the plate is very thick, the stress σ_z at C will be

$$\sigma_z = \nu(\sigma_x + \sigma_y) .$$

Near the crack front it may be considered that $\sigma_x = \sigma_y$ and $\sigma_z = 2\nu\sigma_x$. Now $\nu \approx 1/3$ in the elastic range and $\nu = 0.5$ in the plastic range.

It is seen that the state of stress is very close to triaxiality in the elastic range and that the onset of plastic flow tends to produce a hydrostatic stress state in tension without shear. Thus, the conditions are met for fracture initiation, the only significant plastic strains occurring on the crack border itself and on the edges of internal microcracks. Furthermore, plastic elongation on the crack border causes a transfer of the load to the neighbouring microcracks.

From the remark made in Paragraph 4.2.2.4 there result the following values of K and $\mathcal{G}$:

$$K^2 = \pi\sigma^2 a , \qquad \mathcal{G} = \frac{1-\nu^2}{E}K^2 . \tag{26}$$

In view of the possibilities of plastic displacements near the faces of the plate, it is to be expected that the crack will extend more rapidly at mid-thickness.

To investigate the effect of thickness, tests are usually conducted on plates of same widths. It may be assumed that the effect of thickness is due to departure from the geometrical similarity caused by the existence of grains whose sizes are independent of the thickness.

Let us first suppose a complete geometrical similarity between two specimens, including the grains, subgrains and the entire fine structure of the metal. The distance between an internal point and the faces of the specimen will be measured on the scale of the grains, so the behaviour of two geometrically similar plates will be identical from the points of view of stress distribution, plastic flow and fracture.

Returning to the case where the absolute sizes of the grains and of the fine metal structure do not vary with thickness, it may be considered that the proximity of the faces will be effective at the same absolute distance and that the ductile lips will be of the same absolute width for the same length of crack propagation $(a - a_o)$. If this applies, then the relative width of the ductile lips will be smaller for the thickest plate

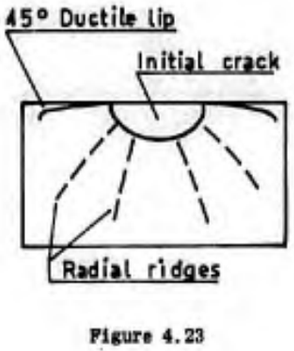

Figure 4.23

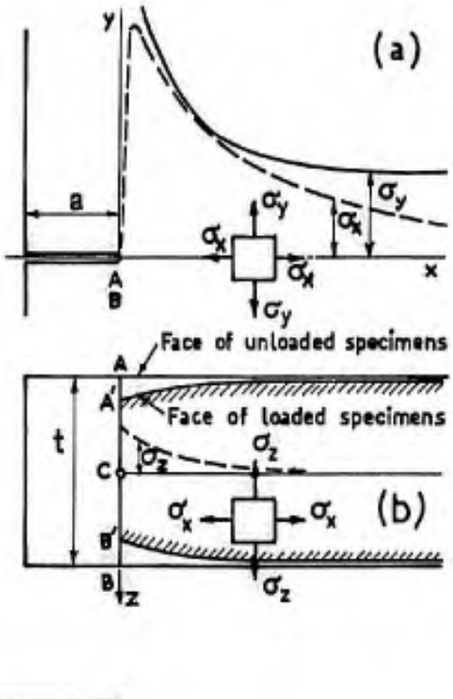

Figure 4.24

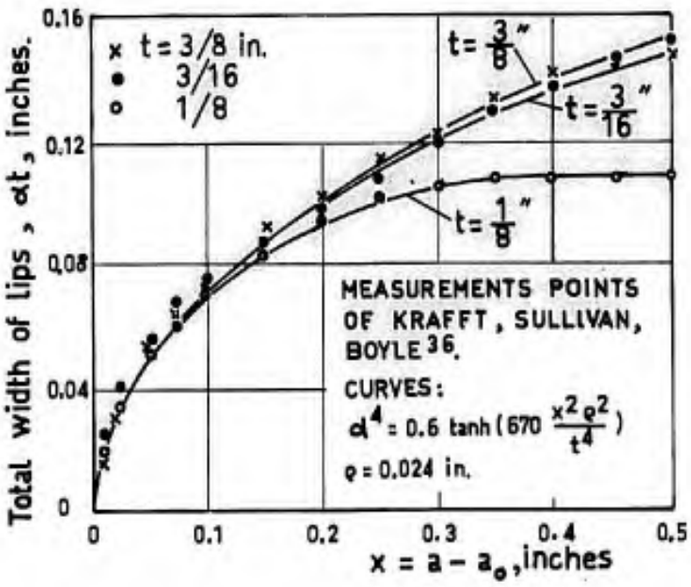

Figure 4.25

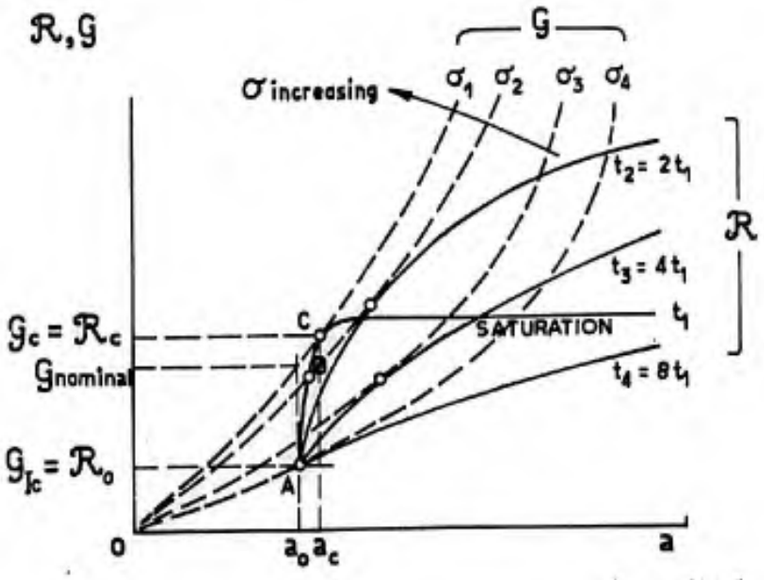

Fig. 4.26 Variation of $\mathcal{R}$ against $a - a_0$ and the thickness – variation of $\mathcal{G}$ with σ ; failure condition

and the value of a corresponding to the full slant fracture implies more plastic strain work and hence a greater levelling of the stresses. As a result, thick parts will prove less resistant for the same absolute length of the initial cracks.

For 7075-T6 aluminium alloy sheets 1/8, 3/16 and 3/8 inches thick, KRAFFT, SULLIVAN and BOYLE[36] measured the absolute values, αt , of the ductile lips (Fig. 4.25). At first, the curves are identical; the absolute lip width does not depend on thickness but merely on crack extension. Then, the curve corresponding to the smallest width becomes distinct from the others, the absolute lip width being restricted to the thickness. The authors found some correlation between

$$R = \frac{1}{2t} \cdot \frac{dW}{da} \text{ and } \alpha^2 t \ ;$$

for 7075-T6 we have

$$R = 1.25 + 0.287\,\alpha^2 t \quad \text{daN/mm} \ ,$$

with t expressed in mm. Most tests were carried out with $w = 76$ mm and the largest cracks were observed for $2a/w = 0.33$; the maximum value of R was not reached.

If we assume that, for $\alpha t \ll t$, αt depends only on $a - a_o$, there results

$$R - R_o = \frac{1}{t} f(a - a_o) \ ,$$

whereas at "saturation", with $\alpha = 1$, $R - R_o = 0.287\ t$.

Taking into consideration this qualitative effect of thickness, we obtain the curves $R(a - a_o, t)$ reproduced in Figure 4.26. In fact, there is only one way to determine R . The initial half-length, a_o , of the crack prior to loading is known and at the time of rupture the critical half-length, a_c , can be assessed, for example from ink staining of the surface. G_c is calculated from a_c and from the fracture stress σ_c . At C , the curve $R(a - a_o)$ is tangent to the curve $G(a - a_o)$. If the calculations are made for several values of a_o and of the width w , then R can be determined by means of the successive tangents, as was done by KRAFFT and his co-authors.

Let us see how a test is conducted. For low values of σ , the curve $G(\sigma, a)$ passes below the point $A(R_o, a_o)$ and the initial crack is not modified. For high values of σ , such as σ_2 , the curve $G(\sigma_2, a)$ intersects the curve $R(a - a_o, t_1)$ at point B . Assuming a crack length smaller than $2\,a_B$, we have $G > R$ and the equilibrium is unstable, as the crack extends from a_o to a_B ; if $a > a_B$, we have $G < R$ and the equilibrium will again be stable.

It is seen that there are cases where the application of a load causes an extension of the initial crack until a stable value is attained.

If the applied stress increases again, the crack continues to grow until the curves G and R are tangent; the equilibrium is, then, no longer stable and the crack develops abruptly until final fracture occurs. The corresponding crack length is called "critical length" and the corresponding critical value of G is denoted G_c . This type of crack growth and instability has been described by the ASTM[25].

The minimum value of G_c , $G_{Ic} = R_o$, characterizes the material, irrespective of the thickness. If the thickness increases, the "saturation" value of R for the full slant is increased but is reached for higher values of $a - a_o$, as is shown qualitatively by the curves R in Figure 4.26; with a thickness t_4 , instability appears for $a = a_o$ and $G_c = G_{Ic} = R_o$. For greater thicknesses, the same critical value G_{Ic} of G is obtained.

The G_c -values also depend on the sheet width w . For $2a/w \geqslant 0.4$, the expression

$$G = (0.414)^2\ (\pi w/2)\ \sigma^2/(1 - 2a/w)^2$$

is a function of $\sigma^2 w$ and $2a/w$. On the other hand, if the thickness is constant, $R = f(a - a_o)$ increases with $a - a_o$ and hence with w for the same value of $2a/w$. Figure 4.27 shows that G_o is substantially constant for large-size specimens and approaches $G_{Ic} = R_o$ for narrow specimens.

For each thickness there is a lower limiting value of width below which fracture is brittle and is defined by $G_{Ic} = R_o$, and an upper limiting value above which $G_c = R_c$ is fairly constant.

From the point of view of fracture, metals are not intrinsically ductile or brittle. They are more brittle for thick and narrow parts, and more ductile for thin and wide parts.

However, in the case of specimens of small width, the net fracture stress must be less than the yield strength of the material: fracture is of the brittle-type only if $2a/w$ assumes large values. This explains why G_c or K_c are unreliable quantities for the strength prediction of thin parts containing notches of moderate lengths. On the other hand, although the behaviour of thin and wide parts is ductile, their strengths are low because of the effect of width on the stress intensity factor.

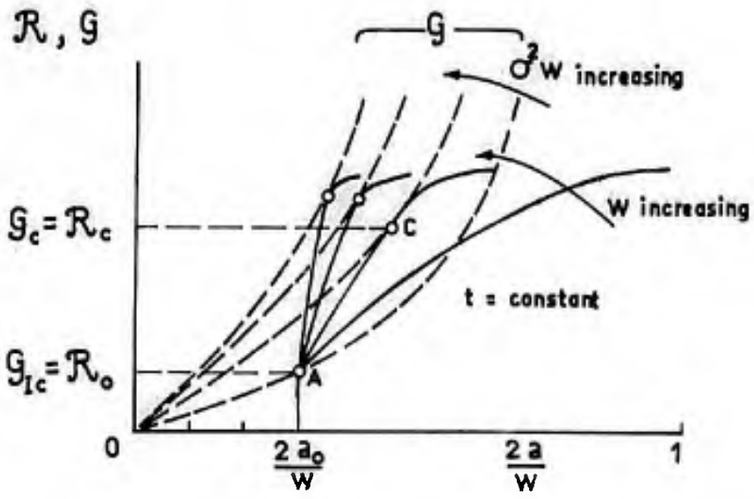

Fig.4.27 Variation of $\mathcal{R}$ and $\mathcal{G}$ with the width w

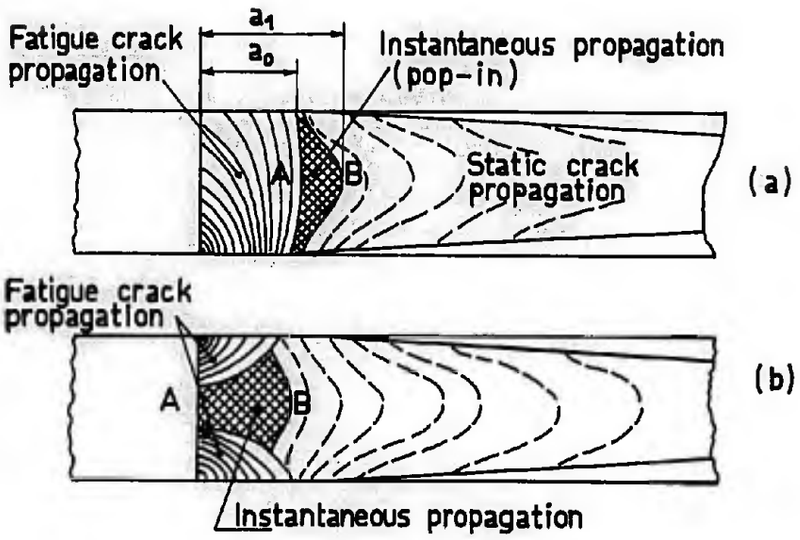

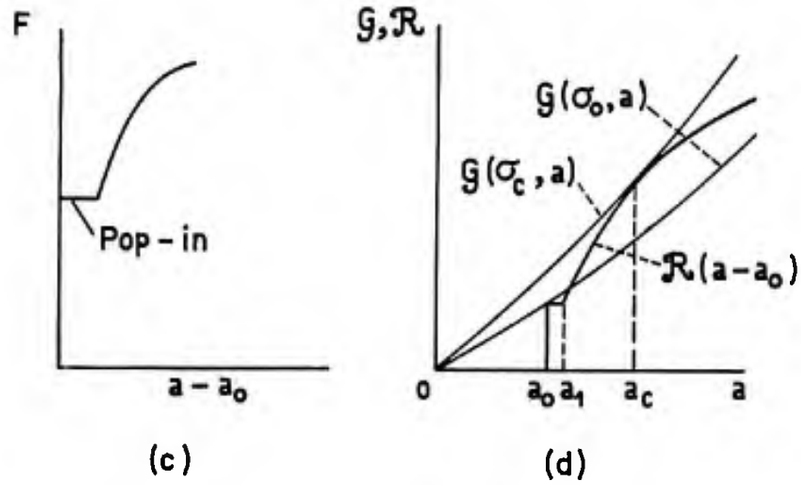

Fig.4.28 Discontinuous crack propagation under static load

Shape of $R(a - a_0)$ *curves; measurement of* $R_0 = G_{Ic}$.

The first data published on $R(a - a_0)$ curves were obtained by KRAFFT et al.[36] on thin 7075-T6 aluminium alloy sheet. More $R(a - a_0)$ data have since been published by BROEK[80], and by CARMAN, ARMIENTO and MARKUS[81] for aluminium alloy sheets. These curves are, of course, smooth, being envelopes of families of tangential $G(a)$ curves. Moreover, a large number of tests are required to establish them. Besides, engineers are much more interested in the minimum value of R , i.e., $R_0 = G_{Ic}$, which is typical of the strengths of thick parts containing small cracks, than in the G_c-values applicable to large cracks in thin sheets. Therefore, in order to characterize the material, the metallurgists have tried to obtain the value of $R_0 = G_{Ic}$ from single-specimen tests.

Consider Figure 4.28a which illustrates the fracture of a specimen with a crack initiated in fatigue by a pulsed tensile load. Under much higher static tension entailing crack extension, the weak point will be located at A , i.e., at mid-thickness, whilst the material near the faces can elongate further without breaking. As in the case of discontinuous static crack growth under fatigue loading (Fig.4.21), a quasi-instantaneous extension can be observed from a_0 to a_1 up to a position B of the crack front, where the material close to the faces causes a reduction of the stress intensity factor at mid-thickness. If the instability which determines G_c through tangency of the curves R and G is not yet encountered, then the crack extends further with increasing load, as illustrated in Figure 4.28d.

Sometimes, in order to obtain sharper machined notches, incipient fatigue cracks are created at the intersection of the sheet faces with the notch root by alternating bending, as shown in Figure 4.28b. In this case, the metal at A , i.e., at mid-thickness, has less support and the quasi-instantaneous extension from A to B occurs more frequently than in the preceding case.

In both cases the initial crack boundary is unstable; for a given crack surface area there is a shape of crack front that provides maximum resistance.

The quasi-instantaneous crack extension is called *"pop-in"*. It produces an audible noise and can be detected by several means. SRAWLEY and BROWN[37] have undertaken a very comprehensive study of the measurements used in practice:

(1) Measurement of the electrical potential change between two points spanning the crack;

(2) Measurement of the elastic displacement per unit load between two points spanning the crack at its half-length (so-called compliance method); this method is also used to obtain experimental G -values[38];

(3) Acoustic measurement with a microphone.

The elastic-displacement method consists in an experimental determination of the critical length from an analysis of the load-displacement record. The critical displacement would correspond to the "pop-in" phenomenon, i.e., to the passage of the load through a maximum value with an increasing displacement. Then, an experimental curve relating the dimensionless quantity, $vE/w\sigma$, to the ratio of crack length to specimen width, $2a/w$, permits to determine the critical length, a_c , associated to the critical displacement, v_c . Finally, the critical stress intensity factor K_{Ic} is computed by means of such theoretical or empirical expressions as have been considered in Paragraph 4.2.3, pages 145 and 146. To measure the displacements, FISHER et al.[84] have developed a double cantilever beam gauge consisting of two flexible arms made from solution-treated beta titanium; these two arms have a high ratio of yield strength to modulus and support four epoxy-resin bonded foil resistance strain gauges fixed to either side of each arm and connected together in an electrical resistance bridge.

In Figure 4.29, the effect of sheet thickness on toughness is shown for several materials. Note the rapid decrease in K_c with increasing thickness for H-11 and AM 355 steels as well as for the titanium alloy; the same tendency exists in the 2024-T3 clad aluminium alloy for thicknesses greater than 3 mm.

4.4 DATA FOR COMPUTATION OF K AND G

We have, in the foregoing, discussed the values of the stress intensity factor K and of IRWIN's parameter G for thin sheets containing a central slot. We shall now examine the solutions suggested by the theory of elasticity for other problems that may have some technical connection with cracked components.

4.4.1 Crack-tip Stress Field

For a central slot, the method of analysis consists in solving exactly an elliptical-hole problem, in investigating the limiting case of the slot, and finally in searching approximate solutions in the neighbourhood of the slot extremity. This analysis indicates the form of the stress field in the vicinity of the crack point, its intensity K and IRWIN's parameter G . For a plate of finite width, K is different while the distribution of stress remains the same. In the following, when extending NEUBER's calculations to other notches, we shall verify that the distribution depends only upon the local mode of loading, except for the factor K .

As regards the stress distribution at a crack point, WILLIAMS[42] proposed series expansions whose first term, in $1/\sqrt{(R)}$, is identical to those which we have seen previously. More recently, PARIS and SIH[21], using WESTERGAARD's method of computation, analysed the loading modes illustrated in Figure 4.30 and found the following approximate results in the case of plane strain (thick plates and parts):

Mode I – Tension normal to the crack plane.

$$\sigma_x = (K_I/\sqrt{(2\pi R)}) \cdot \cos\frac{\theta}{2}\left[1 - \sin\frac{\theta}{2}\sin\frac{3\theta}{2}\right],$$

$$\sigma_y = (K_I/\sqrt{(2\pi R)}) \cdot \cos\frac{\theta}{2}\left[1 + \sin\frac{\theta}{2}\sin\frac{3\theta}{2}\right], \qquad (27)$$

$$\tau_{xy} = (K_I/\sqrt{(2\pi R)}) \cdot \cos\frac{\theta}{2} \cdot \sin\frac{\theta}{2} \cdot \cos\frac{3\theta}{2},$$

$$\sigma_z = \nu(\sigma_x + \sigma_y), \qquad \tau_{xy} = \tau_{yz} = 0 .$$

The displacements, namely, u along Ox , v along Oy and w along Oz , are

$$u = \frac{2(1+\nu)}{E} \cdot K_I\sqrt{\left(\frac{R}{2\pi}\right)} \cdot \sin\frac{\theta}{2}\left[1 - 2\nu + \sin^2\left(\frac{\theta}{2}\right)\right],$$

$$v = \frac{2(1+\nu)}{E} \cdot K_I\sqrt{\left(\frac{R}{2\pi}\right)} \cdot \sin\frac{\theta}{2}\left[2 - 2\nu - \cos^2\left(\frac{\theta}{2}\right)\right], \qquad (27\text{ bis})$$

$$w = 0 .$$

IRWIN's parameter is defined by

$$\mathcal{G}_I = K_I^2 \cdot (1-\nu^2)/E . \qquad (28)$$

In the case of plane stress, we have $\sigma_z = 0$, the other stresses are the same as above; in the expression for the displacements and for $\mathcal{G}$, $E/(1-\nu^2)$ must be replaced by E .

For a central slot of length $2a$ in a plate subjected to a normal tensile stress σ away from the slot, we have

$$K_I = \sigma\sqrt{(\pi a)} .$$

Mode II – Shear in a plane normal to the crack front.

With a stress τ away from the slot, we have

$$\sigma_x = -(K_{II}/\sqrt{(2\pi R)}) \cdot \sin\frac{\theta}{2} \cdot \left(2 + \cos\frac{\theta}{2} \cdot \cos\frac{3\theta}{2}\right),$$

$$\sigma_y = (K_{II}/\sqrt{(2\pi R)}) \cdot \sin\frac{\theta}{2} \cdot \cos\frac{\theta}{2} \cdot \cos\frac{3\theta}{2}, \qquad (29)$$

$$\tau_{xy} = (K_{II}/\sqrt{(2\pi R)}) \cdot \cos\frac{\theta}{2} \cdot \left(1 - \sin\frac{\theta}{2} \cdot \sin\frac{3\theta}{2}\right).$$

These expressions are identical to those of Equations (6) in Paragraph 4.2.2.1, taking account of the identities

$$\sin\frac{5\theta}{2} = \sin\frac{\theta}{2} + 2\sin\theta \cdot \cos\frac{3\theta}{2},$$

$$\cos\frac{5\theta}{2} = \cos\frac{\theta}{2} - 2\cos\theta \cdot \sin\frac{3\theta}{2}$$

and of $K_{II} = \tau\sqrt{(\pi a)}$ for a central slot in an infinite sheet. For the case of plane strain, the displacements and IRWIN's parameter are given by

$$u = (K_{II}/E) \cdot 2(1+\nu) \cdot \sqrt{\left(\frac{R}{2\pi}\right)} \cdot \sin\frac{\theta}{2}\left[2 - 2\nu + \cos^2\left(\frac{\theta}{2}\right)\right],$$

$$v = (K_{II}/E) \cdot 2(1+\nu) \cdot \sqrt{\left(\frac{R}{2\pi}\right)} \cdot \cos\frac{\theta}{2}\left[-1 + 2\nu + \sin^2\left(\frac{\theta}{2}\right)\right],$$

$$w = 0 .$$

$$\mathcal{G}_{II} = K_{II} \cdot (1-\nu^2)/E .$$

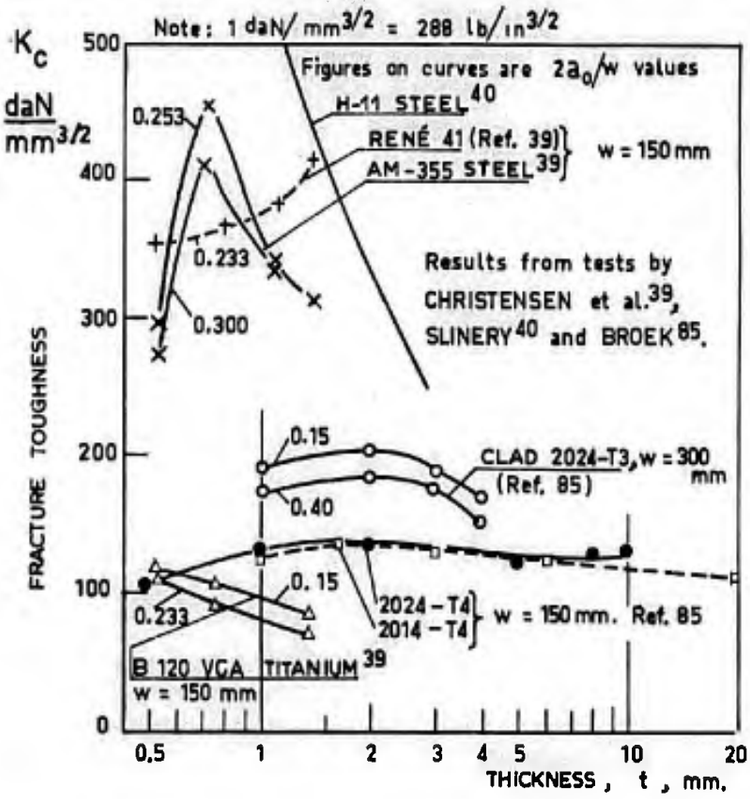

Fig. 4-29 Variation of K_c against thickness

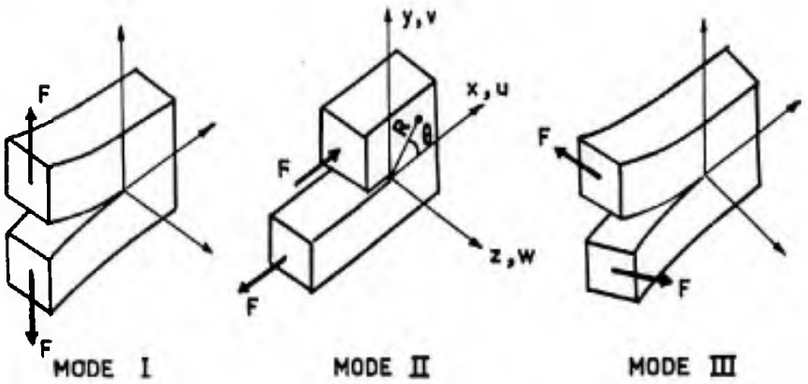

Fig. 4-30 Basic displacement modes in crack opening after Paris and Sih[21]

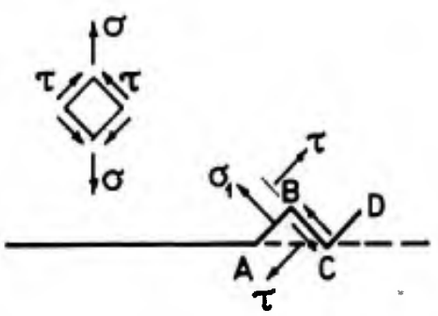

Fig. 4.31(a) Tension-loaded crack – Mode I

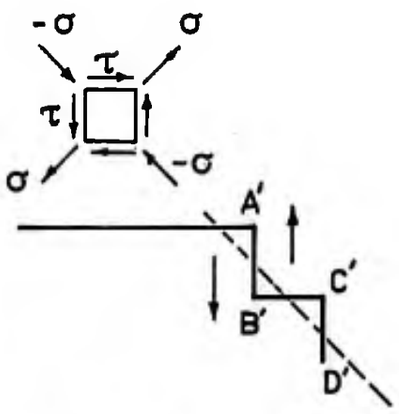

Fig. 4.31(b) Shear-loaded crack – Mode II

Fig. 4.31 Stability of the mean direction or change in the crack propagation direction

Mode III - Shear in a plane normal to the slot and passing through the crack front

The expressions for the stresses and displacements are:

$$\tau_{xz} = -(K_{III}/\sqrt{2R}) \cdot \sin\frac{\theta}{2},$$

$$\tau_{yz} = (K_{III}/\sqrt{2R}) \cdot \cos\frac{\theta}{2},$$

$$\sigma_x = \sigma_y = \sigma_z = \tau_{xy} = 0,$$

$$w = (K_{III}/E) \cdot 2(1+\nu)\sqrt{\left(\frac{2R}{\pi}\right)} \cdot \sin\frac{\theta}{2},$$

$$u = v = 0.$$

For a crack of depth a located on the edge of a semi-infinite body we have, after SIH (referred to in Reference 21),

$$K_{III} = \tau\sqrt{(\pi a)}.$$

4.4.2 Directional Stability of Crack Extension

Although this is not always absolutely correct, in particular for plane stress problems where the crack is under 45^0 with the sheet surface, we assume that crack extension is such that its mean surface is perpendicular to the maximum tensile stress.

Let us consider the tip of the crack for Mode I loading as analysed in the previous section. The principal stresses are

$$\sigma_1 = (K_I/\sqrt{(2\pi R)}) \cdot \cos\frac{\theta}{2}\left(1+\sin\frac{\theta}{2}\right),$$

$$\sigma_2 = (K_I/\sqrt{(2\pi R)}) \cdot \cos\frac{\theta}{2}\left(1-\sin\frac{\theta}{2}\right). \qquad (31)$$

The angle α of σ_1 to the Oy-axis is given by

$$\tan 2\alpha = 2\tau_{xy}/(\sigma_x - \sigma_y) = \cot\frac{3\theta}{2}.$$

σ_1 has a maximum on the axis of the slot ($\theta = 0$) and is inclined by $\pi/4$ to Oy, as indicated in Figure 4.31a; the crack tends to propagate along the perpendicular facet AB. At the extremity B, the overall loading σ tends to generate the stress distribution of Mode II in the direction of the arrow τ.

For Mode II, the principal stress σ_1 and σ_2, with $\sigma_1 > \sigma_2$, are such that

$$\sigma_1 + \sigma_2 = -(K_{II}/\sqrt{(2\pi R)}) \cdot 2\sin\frac{\theta}{2},$$

$$\sigma_1 - \sigma_2 = (K_{II}/\sqrt{(2\pi R)}) \cdot 2\sqrt{(1-\frac{1}{2}\sin\theta)}, \qquad (32)$$

and

$$\sigma_1 = (K_{II}/\sqrt{(2\pi R)})\left(\sqrt{(1-\frac{1}{2}\sin\theta)} - \sin\frac{\theta}{2}\right).$$

The stress σ_1 reaches a very flat maximum with $\sigma_1 \approx 2K_{II}/\sqrt{(2\pi R)}$ for $-\pi < \theta < -\pi/2$ and is substantially identical to σ_x since the facet concerned is almost perpendicular to the slot; the crack will tend to grow along the line A'B' in Figure 4.31b. At the new extremity B', shear acts in the direction of the arrows and tends to direct the crack path along B'C'; finally, the crack tends to become normal to the tensile stress $\sigma = \tau$ at infinity.

Returning to Mode I and supposing that the crack is stopped at point B in Figure 4.31a, it can be observed that the local loading is equi-axial tension and shear which tends to direct the crack path along BC.

4.4.3 Crack at the Edge of a Circular Hole

In 1956, BOWIE[43] treated the case of cracks at the edge of a circular hole in an infinite plate, as illustrated in Figure 4.32. Using the preceding notations of k, K and $\mathcal{G}$, we have

$$K = \sqrt{(E\,\mathcal{G})} = k\sqrt{(\pi)} ,$$

$$K = \sigma\sqrt{(\pi L)} \cdot F(L/R) , \qquad (33)$$

where R is the radius of the hole, L the length of a radial crack, and where $F(L/R)$ assumes the values summarized in Table 4.5 for the four cases under study: one or two radial cracks and one axial ($\sigma_2 = 0$) or bi-axial ($\sigma_1 = \sigma_2 = \sigma$) load.

Consider the case of uni-axial tension and of two symmetrical cracks for which $F(L/R)$ is given by the third line in Table 4.5, and let us compare it with the case of a single crack of length $2a = 2(R + L)$ for which

$$K = \sigma\sqrt{(\pi a)} = \sigma\sqrt{(\pi L)} \cdot \sqrt{(1 + R/L)} ;$$

the factor $\sqrt{(1 + R/L)}$, quoted in the fifth line of Table 4.5, differs from $F(L/R)$ by less than 5% if $L/R > 0.2$ and approaches $F(L/R)$ with increasing L/R. Our conclusion is as follows:

The shape of the boundary of a hole having two opposite cracks does not change the stress distribution near the tips of the cracks if the latter exhibit a length greater than one tenth of the largest dimension of the hole. The presence of the hole eliminates the compressive stresses on the edges of the slot; consequently, buckling of the edges in a thin sheet does not affect significantly the stresses at the crack tips in the median plane, although it may induce secondary bending stresses capable of modifying the static strength (see page 169).

TABLE 4.5

Cracks at the Edge of a Hole (Figure 4.32).
Values of F(L/R) in Equation (33).

	L/R	*0.02*	*0.05*	*0.1*	*0.2*	*0.3*	*0.4*	*0.5*	*0.6*	*0.8*	*1*	*1.5*	*2*	*3*	*5*
	one crack														
1	$\sigma_1 = \sigma$, $\sigma_2 = 0$			2.73	2.30	2.04	1.86	1.73	1.64	1.47	1.37	1.18	1.06	0.94	0.8
2	$\sigma_1 = \sigma_2 = \sigma$	2.74	2.21	1.98	1.82	1.67	1.58	1.49	1.42	1.32	1.22	1.06	1.01	0.93	0.81
	two cracks														
3	$\sigma_1 = \sigma$, $\sigma_2 = 0$			2.73	2.41	2.15	1.96	1.83	1.71	1.58	1.45	1.29	1.21	1.14	1.07
4	$\sigma_1 = \sigma_2 = \sigma$	2.74	2.21	1.98	1.83	1.70	1.61	1.57	1.52	1.43	1.38	1.26	1.20	1.13	1.06
5	$\sqrt{\left(1 + \frac{R}{L}\right)}$	7.12	4.58	3.32	2.45	2.08	1.87	1.73	1.63	1.5	1.41	1.29	1.22	1.15	1.09

For small values of L/R, the case $\sigma_1 = \sigma_2 = \sigma$ corresponds to cracks in an annular disk subjected to the centrifugal force. WINNE and WUNDT[44] have applied BOWIE's results to the strength analysis of turbine wheel disks, in which case the components are of large thicknesses and the state of stress is similar to that of the plane stress state, so that E must be replaced by $E/(1 - \nu^2)$.

The effect of the hole remains negligible if the hole assumes any shape and this explains why *an initial crack originating from any defect or notch grows toward a surface normal to the highest tensile stress*, as stated in the previous paragraph for shear-loaded cracks (Mode II).

4.4.4 Edge Cracks in Plates

4.4.4.1 Edge Notches in a Semi-infinite Sheet Subjected to Tension

NEUBER[45] has investigated the case of a shallow edge notch in an infinite half-plane. This notch, represented in Figure 4.33, is defined by a curve which satisfies the equations

$$x = v - v/(u^2 + v^2) , \qquad y = u + u/(u^2 + v^2) ,$$

with $u = u_0$. The notch root radius is

$$\rho = (u_0^2 - 1)/2u_0 .$$

If $u_0 = 1$, ρ is equal to zero and the sharp notch is bounded by a curve bitangential to the Oy-axis, as a dotted line in Figure 4.33. Linearization of NEUBER's results in the vicinity of the notch tip yields the following expressions for the principal stresses σ_1 and σ_2 :

$$\frac{\sigma_1 + \sigma_2}{2} = \frac{3}{2\sqrt{(2)}}\,\sigma\sqrt{(a/2R)}\,.\,\cos\frac{\theta}{2}\,, \qquad \frac{\sigma_1 - \sigma_2}{2} = \frac{3}{2\sqrt{(2)}}\,\sigma\sqrt{(a/2R)}\,.\,\sin\frac{\theta}{2}\,. \tag{34}$$

i.e., the general expressions of Mode I, from Equations (31), with

$$K_I^2 = (9/8)\,\pi\sigma^2 a\,, \tag{35}$$

where a is the depth of the sharp notch.

It is relevant to note that the notch is not a slot and that the missing material with regard to the slot causes a decrease of the K-value, which would be higher in the case of a slot.

4.4.4.2 Symmetrical Edge Notches in a Sheet of Finite Width Subjected to Tension

Figure 4.34 shows a specimen of width w containing two edge notches of depth a . WESTERGAARD's solution is the same as for the central crack: the sheet is cut by lines such as CD (Fig.4.14); however, the non-zero stresses on the edges of the specimen are different. Cancellation of these parasitic stresses will cause an opening of the crack, which will be significant if the crack is deep, and an increase of the coefficient c_m .

For very small edge cracks, expression (35) obtained from NEUBER's calculations yields an approximate K-value. The ASTM[25] proposes the value

$$K_I^2 = 1.2\,\pi\sigma^2 a\,, \tag{36}$$

i.e., 20% more than WESTERGAARD's theoretical value. We may recall that WESTERGAARD's solution for finite width is

$$K = \sigma\sqrt{(\pi a)}\,.\sqrt{\left(\frac{w}{\pi a}\tan\frac{\pi a}{w}\right)}. \tag{37}$$

For this case the ASTM proposes

$$K^2 = \sigma^2 w\,.\,\tan\frac{\pi a}{w}\,.\left[1 + 0.2\left(\cos\frac{\pi a}{w}\right)^2\right], \tag{38}$$

hence

$$c_m = (1 - 2a/w)\sqrt{\left\{\frac{2}{\pi}\tan\frac{\pi a}{w}\,.\left[1 + 0.2\left(\cos\frac{\pi a}{w}\right)^2\right]\right\}},$$

and, numerically,

$2a/w$ =	0	0.1	0.2	0.3	0.4	0.5	0.6	0.7	0.8
c_m =	0	0.312	0.394	0.430	0.435	0.420	0.388	0.342	0.282 .

BOWIE[46] made computations reproduced by PARIS and SIH in the form

$$K = \sigma\sqrt{(\pi a)}\,\sqrt{\left(\frac{w}{\pi a}\tan\frac{\pi a}{w}\right)}\,.\,h(2a/w)\,. \tag{39}$$

In Table 4.6, the values of $h(2a/w)$ are listed for two ratios $2L/w$, where L is the specimen height.

TABLE 4.6

Values of the Correction Factor h(2a/w) in Expression (39), from BOWIE[46].

$2a/w$		0.1	0.2	0.3	0.4	0.5	0.6	0.7	0.8	0.9
$h(2a/w)$	$2L/w = 1$	1.13	1.13	1.14	1.16	1.14	1.10	1.02	1.01	1
	$2L/w = 3$	1.12	1.11	1.09	1.06	1.02	1.01	1	1	1
$K/\sigma\sqrt{(\pi a)}$: $\left(\frac{2L}{w} = \infty\right)$		1.12	1.12	1.13	1.14	1.15	1.22	1.34	1.57	2.09

The last line of Table 4.6 corresponds, with an accuracy of 1%, to the values proposed by the ASTM (Equation 38).

4.4.4.3 NEUBER's Deep Symmetrical Notches in Tension and Bending

NEUBER[45] has studied the deep hyperbolic notch (Fig.4.35) under tensile and bending loads. The boundary of the notch is defined by the equations

$$y = \sinh u . \cos v , \qquad x = \cosh u . \sin v ,$$

with

$$c = \sin v_o , \qquad \rho = c / \tan^2 v_o .$$

In *tension* the mean stress is

$$\sigma_m = P/2cd ,$$

where d is the thickness.

According to NEUBER's Equation (61), the stresses are

$$\sigma_u = (A/h^2)\cosh u.\cos v. \frac{2 + \cos^2 v_o - \cos^2 v}{h^2} ,$$

$$\sigma_v = (A/h^4)\cosh u.\cos v. (\cos^2 v - \cos^2 v_o) ,$$

$$\tau_{uv} = (A/h^4)\sinh u.\sin v. (\cos^2 v_o - \cos^2 v) ,$$

with

$$h^2 = \cos^2 v + \sinh^2 u \text{ and } A = \sigma_m \frac{\sin v_o}{v_o + \sin v_o . \cos v_o} .$$

In the case of a slot, we have $v_o = \pi/2$, $c = 1$ and $A = (2/\pi)\sigma_m$; if we linearize and then compute the principal stresses, we obtain, near the crack tip,

$$\begin{aligned} (\sigma_1 + \sigma_2)/2 &= (2/\pi)\sigma_m\sqrt{(c/2R)}.\cos \theta/2 , \\ (\sigma_1 - \sigma_2)/2 &= (1/\pi)\sigma_m\sqrt{(c/2R)}.\sin \theta , \end{aligned} \tag{39}$$

which, in comparison to the value of Mode I, yields

$$K_I = (2/\sqrt{\pi})\,\sigma_m\sqrt{c} . \tag{40}$$

With $\sigma_m = \sigma w/2c$ and $c = w/2 - a$, WESTERGAARD's expression (37) tends toward expression (40) when $2a/w$ tends toward unity, whereby WESTERGAARD's expression is verified for the limiting case $a = w/2$.

In *pure bending* the same stress distribution is found near the crack front, but the stress intensity factor is different; the half-sum of the principal stresses is

$$(\sigma_1 + \sigma_2)/2 = \frac{4}{3\pi}\sigma_n \sqrt{(c/2R)} . \cos \frac{\theta}{2} , \tag{41}$$

where $\sigma_n = M/(I/c)$ is the maximum nominal stress, I the moment of inertia in bending, and c the distance from the axis.

In the two preceding cases of tension and bending, the stress distributions on the Ox-axis ($y = 0$, $\sigma_y = \sigma_v$) are:

$$\text{in tension, } \sigma_y = A/\cos v, \text{ where } A = (2/\pi)\,\sigma_m ,$$

$$\text{in bending, } \sigma_y = A'\tan v, \text{ where } A = (4/3\pi)\,\sigma_n .$$

Furthermore, we have $x = \sin v$ on the Ox-axis.

The two cases may be combined to obtain an approximate solution for the bending problem of a bar of unit thickness with a deep single notch (Fig.4.36). If we set

$$(\sigma_1 + \sigma_2)/2 = (B + B')\sqrt{(c/2R)} . \cos \frac{\theta}{2} ,$$

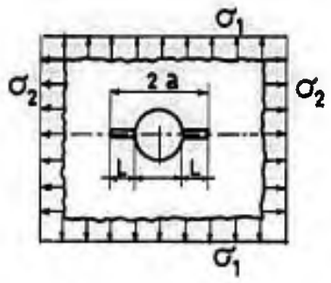

Fig.4.32 Bowie's slot[43]

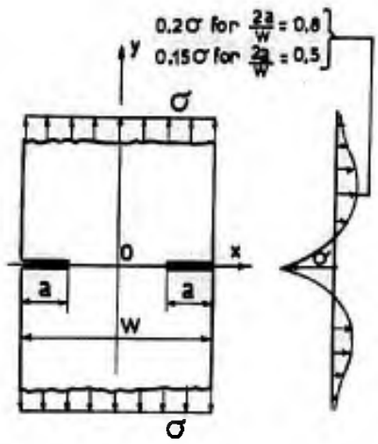

Fig.4.34 Edge slots in a finite-width sheet – case of Westergaard

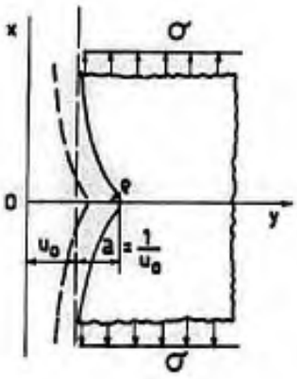

Fig.4.33 One-sided edge notch of Neuber in a semi-infinite sheet

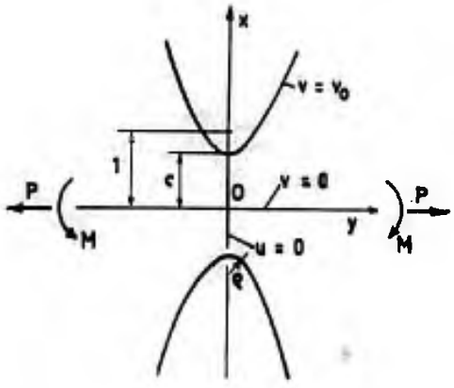

Fig.4.35 Neuber's deep hyperbolic notches[45]

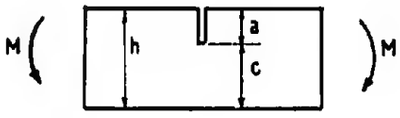

Figu4.36 Bending of a one-sided cracked bar

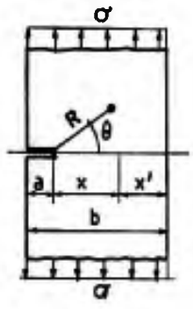

Fig.4.37 Tension of a one-sided edge slotted strip

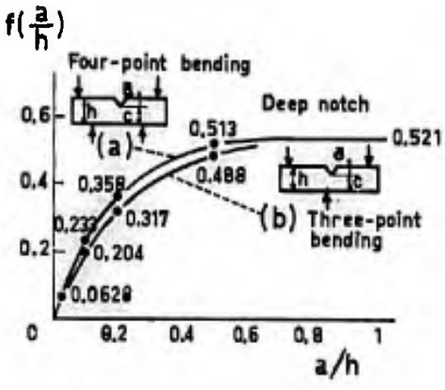

Fig.4.38 Bending a one-sided cracked bar, after Wundt[51]

and

$$\sigma_y = B/\cos v + B' \tan v ,$$

equilibrium implies

$$0 = \int_0^{\pi/2} (B/\cos v + B' \tan v) \cos v . dv = B\pi/2 + B' ,$$

$$M = c^2 \int_0^{\pi/2} (B/\cos v + B' \tan v) \sin v . \cos v . dv = c^2(B + B'\pi/4) ,$$

and hence

$$B' = - B\pi/2 , \qquad M = c^2 B(1 - \pi^2/8) , \qquad B + B' = B(1 - \pi/2) .$$

Finally, it follows that

$$(\sigma_1 + \sigma_2)/2 = \frac{\sigma_n}{6} \frac{4 - 2\pi}{8 - \pi^2} \sqrt{(c/2R)} . \cos \frac{\theta}{2} ,$$

then

$$K = \frac{2\pi - 4}{\pi^2 - 8} \frac{\sigma_n}{6} \sqrt{(\pi c)} ,$$

and

$$K^2 = 0.521 \, \sigma_n^2 \, c , \tag{42}$$

where $\sigma_n = 6M/c^2$, M being the bending moment.

4.4.4.4 Single-edge Notch in a Plate Strip Subjected to Tension

In Figure 4.37, the single-edge-notch specimen investigated by GROSS, SRAWLEY and BROWN[47] is represented. The authors carried out a numerical computation using the WILLIAMS[42] stress function $\chi(R, \theta)$ and satisfying the boundary conditions on the slot and at a finite number of points on the edges of the plate.

For Mode I this function is

$$\chi(R, \theta) = \sum_{n=1,2,\ldots}^{\infty} \left\{ (-1)^{n-1} . d_{2n-1} . R^{n+1/2} \left[- \cos (n - 3/2) \theta + \frac{2n - 3}{2n + 1} \cos (n + \frac{1}{2}) \theta \right] + \right.$$

$$\left. + (-1)^n d_{2n} R^{n+1} \left[- \cos (n - 1) \theta + \cos (n + 1) \theta \right] \right. . \tag{43}$$

In the vicinity of the crack point, the dominant terms of the series give a stress field which has already been obtained previously with

$$K^2 = E \mathcal{G} = \sigma^2 b \alpha = \sigma^2 \pi a k^2(a/b) , \tag{44}$$

where α and $k(a/b)$ have the following numerical values:

a/b =	0.05	0.10	0.15	0.20	0.25	0.30	0.40	0.50
α =	0.204	0.445	0.758	1.18	1.77	2.60	5.60	12.40
k(a/b) =	1.14	1.19	1.27	1.37	1.50	1.66	2.12	2.82

The average values of several specimen measurements are:

α meas.	0.314	0.56	0.82	1.18	1.74	2.57	5.44	10.48 .

GROSS' s calculations are in agreement with BOWIE's[46].

4.4.4.5 Single-edge Notch in a Bar Subjected to Bending

If the crack depth, a , of a bar (Fig.4.38) is very small compared to the height, h , we have, as in the case of tension,

$$K^2 = \pi\sigma^2 a = \pi\sigma_n^2 c(a/b) (1 - a/h)^3 ,$$

where $\sigma_n = 6\,M/h^2$,

corresponds to a bar of unit thickness.

WUNDT[51], referring to BUECKNER's results, proposes the expression

$$K^2 = \sigma_n^2 \cdot c \cdot f(a/h) \ , \tag{45}$$

where $f(a/h)$ is the function shown in Figure 4.38 by the curve (a) for pure four-point bending and by the curve (b) for three-point bending. In pure bending, the curve (a) may be approximated by the empirical expression

$$f(a/h) = \pi \frac{(a/b)(1 - 0.28\ a/h)}{1 + 3.4\ a/h} \ . \tag{46}$$

More recently, the case of pure four-point bending has been examined by GROSS and SRAWLEY[48], who employed the method of numerical analysis described for tension in Paragraph 4.4.4.4. With M/t equal to the bending moment per unit thickness, they obtained

$$K^2 = (M/t)^2\ Y^2/\ h^3 \ , \tag{47}$$

where Y^2 is a function of a/h . In Table 4.7, the results are compared with BUECKNER's[50] calculations and with LUBAHN's[49] measurements. For comparison with expression (45), from WUNDT, $f(a/h)$ is computed as follows:

$$f(a/h) = (Y^2/36)(1 - a/h)^3 \ .$$

Because of LUBAHN's experimental confirmations, we would prefer the values of GROSS to the limiting values derived by an approximate calculation from NEUBER's results (Equ.42), and to the empirical expression (46) gained from BUECKNER's results; however, with $a/h < 0.3$, the discrepancies are not significant in practice, especially as, for $a/h > 0.3$, interpretation of the test data is made difficult by the presence of plastic strains.

TABLE 4.7

Bending of a Cracked Bar

(a) Values of Y^2 *in Equation (47)*									
a/h =	0.10	0.15	0.20	0.25	0.30	0.35	0.40	0.45	0.50
GROSS	12.4	18.5	25.3	33.2	42.8	55.2	71.4	92.7	123
BUECKNER	12.2		25.2						151.2
LUBAHN	11.8	17.4	24.2	32.15	41.9	53.9	68.6	88.9	118
(b) Values of f(a/h) *in Equation (45)*									
GROSS	0.250	0.32	0.36	0.39	0.41	0.422	0.425	0.425	0.425
BUECKNER	0.233		0.358						0.513
Equa. (46)	0.248	0.300	0.353	0.395	0.427		0.473		0.50

4.4.5 Cracks Subjected at Their Boundaries to Concentrated Forces

The problem of an elliptical hole subjected at its boundary to a force F has been examined by MUSKHELISVILI[14]. For a central crack of length $2a$, as illustrated in Figure 4.39, PARIS and SIH give the expressions of K_I and K_{II}:

$$K_I = \frac{P}{2\sqrt{(\pi a)}} \sqrt{\left(\frac{a+b}{a-b}\right)} + \frac{Q}{2\sqrt{(\pi a)}} \left(\frac{k-1}{k+1}\right) ,$$

$$K_{II} = -\frac{P}{2\sqrt{(\pi a)}} \left(\frac{k-1}{k+1}\right) + \frac{Q}{2\sqrt{(\pi a)}} \sqrt{\left(\frac{a+b}{a-b}\right)} , \tag{48}$$

where P and Q are the components of F along Ox- and Oy-axis, and

$$k = 3.4\nu \approx 1 \ .$$

With these expressions, the problem of a crack contained in any stress field can be solved by subjecting the crack to the stresses that exist in the absence of the crack, as long as the stresses at the boundaries of the skin panel considered are not disturbed by the presence of the crack. If, for simplification, we introduce

$k = 1$ in the expressions (48) and if $\sigma_y(x, 0)$, which is normal to the crack, and $\tau_{xy}(x, 0)$, which is parallel to the crack, are the stresses existing in the absence of the crack, then we have

$$K_I = \frac{1}{\sqrt{(\pi a)}} \int_{-a}^{+a} \sigma_y(x, 0) \left(\frac{a + x}{a - x}\right) dx ,$$

$$K_{II} = \frac{1}{\sqrt{(\pi a)}} \int_{-a}^{+a} \tau_{xy}(x, 0) \left(\frac{a + x}{a - x}\right) dx . \qquad (49)$$

Let us take $c = (a - b)$ and analyze the influence of P when b is very close to a, that is, for a finite value of c and a very large value of a. It follows that

$$K_I = \frac{2P}{\sqrt{(2\pi c)}} , \qquad (50)$$

which corresponds to the loading illustrated in Figure 4.40.

Other results are quoted in a paper by PARIS and SIH[21] as well as in papers by BARENBLATT[32] and GILMAN[52]. FICHTER[55] has studied the case of plate strips of infinite width and restricted height under concentrated forces or distributed forces normal or tangential to the longitudinal crack.

4.4.6 Internal and Surface Cracks

An internal crack may assume a circular shape at its tip or border and be the boundary of an infinitesimally thin disk. It may also be elliptical and thus represent the boundary of an infinitesimally thin ellipsoid. Finally, there are cracks extending from the outer surface of components with a semi-elliptical crack-boundary shape. Surface cracks are mainly encountered in thick mechanical components, which are therefore more brittle; the technical problems involved are more difficult to solve than those concerning through-thickness cracks in thin components. Unfortunately, as we shall see, no exact theoretical solution has yet been found for the elasticity problem of surface cracks.

4.4.6.1 Circular Internal Crack

For a flat disk-shaped crack inside an infinite volume subject to tension perpendicular to the crack plane (Fig.4.41), SNEDDON[53] has calculated the stresses near the crack border. If Oy is the axis of revolution, Ox a radial axis, and if Oz is normal to the Oxy-plane, the stresses are given by the expressions (27) of Mode 1, where the stress intensity factor is

$$K_I = \frac{2}{\pi} \sigma \sqrt{(\pi a)} . \qquad (51)$$

IRWIN's parameter is found to be

$$G_I = \frac{4}{\pi} \frac{1 - 2\nu^2}{E} \sigma^2 a , \qquad (52)$$

ν being Poisson's coefficient.

Although no direct application is given, one may study the influence exerted by the finite diameter, D, of round bars having a central crack with a circular boundary. With NEUBER's[45] results for the normal stress σ_y, we have, in the crack plane and at a distance $x > a$ from the centre,

$$\sigma_y = \sigma \left[1 + \frac{2}{\pi} \left(\frac{1}{\sinh u} - \arctan \frac{1}{\sinh u}\right)\right] , \qquad (53)$$

where

$$\cosh u = x/a .$$

Numerical calculations yield the following distribution:

x/a =	1.01	1.02	1.05	1.1
σ_y/σ_x =	4.59	3.31	2.30	1.48
$(\pi/2)\ \sigma_y/\sigma_x$ =	7.2	5.2	3.62	2.32 ,

which is comparable to that of centrally notched plates (Table 4.2).

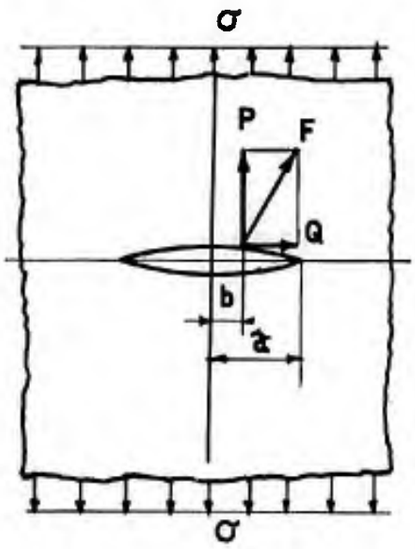

Fig. 4.39 Concentrated force acting on the surface of the crack

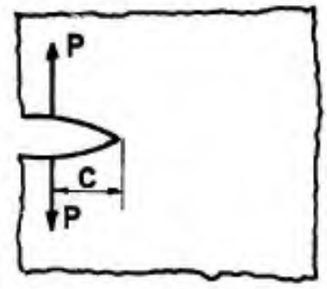

Figure 4.40

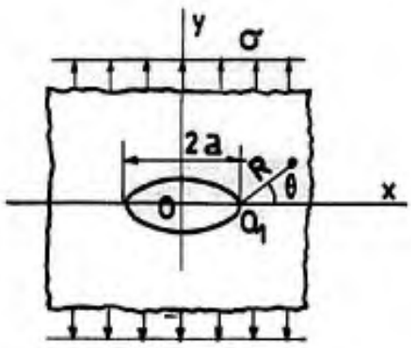

Figure 4.41

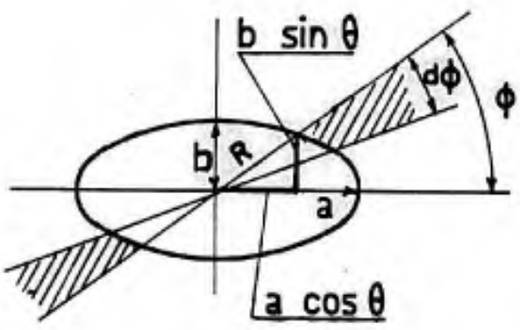

Fig. 4.42 Internal crack

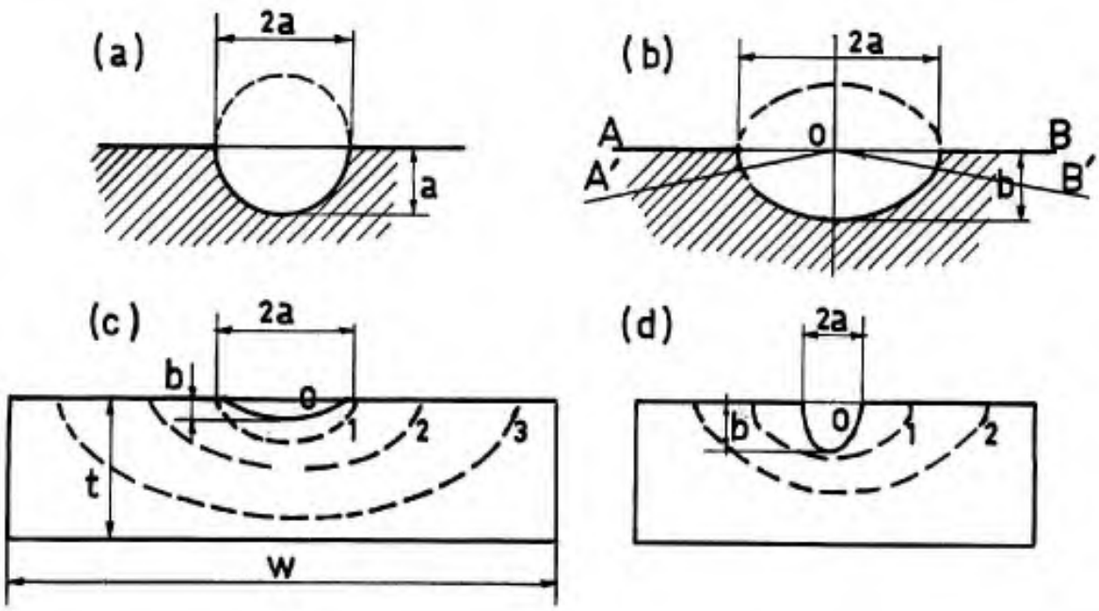

Fig. 4.43 Surface cracks

Like DIXON[20] for central notches contained in sheets, we assume that the stress distribution remains the same for a finite diameter D, its intensity being multiplied by a factor k. From computation we obtain

$$1/k = 1 + \frac{2}{\pi}\left[\eta\sqrt{(1-\eta^2)} - \arctan\frac{\eta}{\sqrt{(1-\eta^2)}}\right], \tag{54}$$

where $\eta = 2a/D$. Numerical calculations yield the approximate expression

$$k = 1 / \sqrt{(1 - 0.95\ \eta^3)} > 1 . \tag{55}$$

We then have

$$K = \frac{2}{\sqrt{\pi}}\sigma\sqrt{a}.\ k , \tag{56}$$

and, for the IRWIN parameter,

$$\mathcal{G} = \frac{1-\nu^2}{E}K^2 = \frac{4}{\pi}\frac{1-\nu^2}{E}\sigma^2\ a\ k^2 . \tag{57}$$

Supposing that the distribution of the perpendicular crack-surface displacements remains elliptical, as in the case of an infinite solid, we may write

$$v = v_0\sqrt{[1 - (x/a)^2]} ,$$

with

$$v_0 = \left(\frac{4}{\pi}\frac{1-\nu^2}{E}\sigma\ a\right) C ,$$

where the quantity in parentheses represents the value of v for $D = \infty$. The volume of the crack is

$$V = \frac{4}{3}\pi v_0 a^2 = \frac{16}{3}\frac{1-\nu^2}{E}\sigma\ a^3\ C .$$

If we consider that C varies very little with a, it follows by differentiation that

$$\frac{\partial V}{\partial A} = \frac{1}{2\pi a}\frac{\partial V}{\partial a} = \frac{8}{\pi}\sigma\ a\ C\ \frac{1-\nu^2}{E} .$$

However, $d\mathcal{G} = \sigma\ (\partial V/\partial A)\ .\ \delta A$ is the product of the change in volume and the normal stress at infinity:

$$\mathcal{G} = \sigma\frac{\partial V}{\partial A} = \frac{8}{\pi}\sigma^2\ a\ C = \frac{4}{\pi}\frac{1-\nu^2}{E}\sigma^2\ a\ k^2 ,$$

hence

$$C = k^2/2 ,$$

and

$$v_0 = \frac{2}{\pi}\frac{1-\nu^2}{E}\sigma\ a\ k^2 = \frac{1}{\sqrt{\pi}}\frac{1-\nu^2}{E}K\sqrt{a}\ .\ k . \tag{58}$$

4.4.6.2 Elliptical Internal Crack

This problem has been treated by IRWIN[53] using the GREEN-SNEDDON[54] result concerning the relative displacements of the two crack surfaces. Consider a plane crack of elliptical boundary shape and of dimensions $2a$ along Ox and $2b$ along Oy. If the displacements of the surface along Oz are denoted by v, the GREEN-SNEDDON results give

$$v = v_0\left(1 - \frac{x^2}{a^2} - \frac{y^2}{b^2}\right)^{1/2} . \tag{59}$$

With $x = a\cos\theta$ and $y = b\sin\theta$, the crack-border-length segment is

$$ds = (a^2\sin^2\theta + b^2\cos^2\theta)^{1/2}\ d\theta .$$

Inside the border of the crack and at a small distance ϵ on the normal to this border, Equation (59) becomes

$$v^2 = v_o^2 \frac{2\epsilon}{ab} (a^2 \sin^2\theta + b^2 \cos^2\theta)^{1/2} . \tag{60}$$

For the slot-opening Mode I, the second Equation (27 bis) from Paragraph 4.4.1 yields, with $\theta = +\pi$,

$$v = \frac{2}{\sqrt{\pi}} \frac{1 - \nu^2}{E} \sqrt{(2\epsilon)} . K_I . \tag{61}$$

By equating the two values of v, IRWIN found

$$K_I^2 = \frac{\pi}{4} \left(\frac{E}{1 - \nu^2}\right)^2 \frac{v_o^2}{ab} \sqrt{(a^2 \sin^2\theta + b^2 \cos^2\theta)} . \tag{62}$$

At this point, the calculation is unquestionable. It is, then, necessary to evaluate v_o. Note, after IRWIN, that K_I reaches a maximum for $\theta = \pi/2$ at the ends of the shortest diameter of the ellipse. Consequently, crack extension will be faster at these points and the elliptical boundary shape will tend to become circular. Notwithstanding this remark, IRWIN assumes, for the computation of v_o, that the crack grows along geometrical similar boundaries, that is, less rapidly along the shortest diameter. He determines v_o by calculating the potential energy change

$$dU = \mathcal{G} dA = \left(\frac{1 - \nu^2}{E}\right) \oint K^2 r \, ds ,$$

where r is a normal outward displacement and ds a border-length segment. If a becomes $a + \epsilon a$ and b becomes $b + \epsilon b$, one has

$$r = \frac{ab\epsilon}{(a^2 \sin^2\theta + b^2 \cos^2\theta)^{1/2}} ,$$

$$dU = \pi v_0^2 \epsilon \, \mathcal{E}(k) \frac{E}{1 - \nu^2} a ,$$

where $\mathcal{E}(k)$ is the elliptic integral,

$$\mathcal{E}(k) = \int_0^{\pi/2} \sqrt{(1 - k^2 \sin^2\phi)} \, d\phi ,$$

with $k^2 = 1 - b^2/a^2$.

On the other hand, if one assumes, as for a circular crack, that v_o is proportional to the size of the crack, v_o becomes $v_o + \epsilon v_o$ and the change in crack volume is equal to $4\pi ab v_o \epsilon$. The energy change then is

$$dU = 2\pi ab v_o \epsilon \, \sigma ,$$

and, by equating the two equations of dU, one obtains

$$v_o = 2 \frac{b/\sigma}{\mathcal{E}(k)} \frac{1 - \nu^2}{E} ,$$

hence

$$K_I^2 = \pi\sigma^2 \frac{b/a}{\mathcal{E}^2(k)} \sqrt{(a^2 \sin^2\theta + b^2 \cos^2\theta)} , \tag{63}$$

thus, for $x = a$, $y = 0$,

$$K_{Ia} = \frac{\sigma}{\mathcal{E}(k)} b \sqrt{(\pi/a)} , \tag{64}$$

and, for $y = b$, $x = 0$,

$$K_{Ib} = \frac{\sigma}{\mathcal{E}(k)} \sqrt{(\pi b)} .$$

Although IRWIN's hypothesis of a similar crack-border growth is erroneous, the K_{Ia} - and K_{Ib} - values are correct.

Indeed, with $\tan \Phi = y/x$, KASSIR and SIH[56] found

$$K_I^2 = \frac{\sigma^2 b}{\mathcal{E}^2 a} \sqrt{(a^2 \sin^2 \Phi + b^2 \cos^2 \Phi)} ,$$

where $\tan \Phi = (b/a) . \tan \theta$ and $\theta = \Phi$ for $\theta = 0 , \pi/2 , \pi , 3\pi/2 , 2\pi$. It should be noted that, if the angle θ is introduced, the preceding equation becomes

$$K_I^2 = \pi \frac{\sigma^2}{\mathcal{E}^2} \frac{b^2}{\sqrt{(a^2 \cos^2 \theta + b^2 \sin^2 \theta)}} ,$$

or, with $R^2 = x^2 + y^2$,

$$K_I^2 = \pi \frac{\sigma^2}{\mathcal{E}^2} \frac{b^2}{R} . \qquad (65)$$

At the ends of the axes of the ellipse IRWIN's values are again found.

Expression (65) can also be obtained by an approximate computation. Consider the elliptical crack in an infinite solid shown in Figure 4.42. Through the intersection of two neighbouring diametral planes forming an angle $d\Phi$, we isolate a sector with a crack of radius R subjected to a tensile stress σ_R at infinity along Oz. For a circular crack of radius R , the displacement of the centre is

$$v_o = \frac{4}{\pi} R \sigma_R \frac{1 - \nu^2}{E} .$$

If all the sectors are to exhibit the same displacement v_o at the centre, the stresses σ_R at infinity must be variable:

$$\sigma_R = \frac{\pi E v_o}{4(1-\nu^2)} \frac{1}{R} .$$

If we suppose that these variations diminish at some distance from the crack plane, the actual stress at infinity would be the average stress

$$\sigma = \frac{1}{\pi} \int_0^{\pi} \sigma_R \, d\Phi .$$

With $d\Phi = (ab/R^2) \, d\theta$, $R = a\sqrt{(1 - k^2 \sin^2 \theta)}$ and $k^2 = 1 - (b^2/a^2)$, it follows that

$$\sigma = \frac{v_o E}{4(1 - \nu^2)} \frac{b}{a^2} \int_0^{\pi} \frac{d\theta}{(1 - k^2 \sin^2 \theta)^{3/2}} .$$

The elliptic integral equals $2 (a^2/b^2) \mathcal{E}$, hence

$$\frac{E v_o}{4(1 - \nu^2)} = \frac{\sigma b}{2 \mathcal{E}} ,$$

and

$$\sigma_R = \frac{\pi}{2} \sigma b / \mathcal{E} R .$$

Finally, there results

$$K_R{}^2 = \frac{4}{\pi} \sigma_R \sqrt{R} = \pi \frac{\sigma^2}{\mathcal{E}^2} \frac{b^2}{R} ,$$

i.e., the "exact" value. Therefore, the stresses σ_R becomes uniform far away from the crack so that the local stresses are not affected.

4.4.6.3 Semi-elliptical Surface Cracks

In the case of a surface crack with a semi-circular boundary, as illustrated in Figure 4.43a, or with a semi-elliptical boundary, as illustrated in Figure 4.43b, it may be conjectured, after IRWIN, that the stress distribution near the crack border is the same as for an internal crack, provided the intersection of the infinite solid by a diametral symmetry plane does not disturb the distribution. This is not entirely exact; SMITH, EMERY and KOBAYASHI[77] have studied, by theoretical and numerical analysis, the case of a semicircular crack in the surface of a half space in simple tension. The local stress intensity factor on the cracking front at the extremity of a radius, a , is expressed by

$$K_{I\theta} = \frac{2}{\sqrt{\pi}} \sigma \sqrt{a} \, . \, k(\theta) , \qquad (66)$$

where θ is the angle of the radius, a, measured from the surface and $k(\theta)$ has the following values:

$\frac{2}{\pi}\theta$	0	0.2	0.4	0.6	0.8	1
$k(\theta)$	1.21	1.12	1.07	1.04	1.03	1.02

Let a semi-elliptical crack originate from one surface of a bar of width w and thickness t (Figure 4.43c and d). IRWIN, assuming that the stress distribution is not disturbed with respect to that of an internal crack and supposing a constant a/b ratio during crack extension, recommends, after estimating a plastic-zone correction, the expression

$$K_{Ic}^2 = 1.2\,\pi\sigma^2\, b \,/\, \mathcal{E}^2(k) \,.\, \left[1 - 0.212\,\frac{\sigma^2}{\sigma_{0.2}^2}\right], \qquad (67)$$

where the factor 1.2 is empirical to take account of the edge effect already mentioned for the part-through crack on the edge of a thin sheet. This expression holds for $2a/w \leqslant 0.5$ and $b \leqslant t/2$.

After SMITH et al.[77], a factor equal to 1.4 should be used instead of the previous value of 1.2 to take account of the edge effect; the stable shape of the crack front would approximately correspond to values of a/b ranging from 1.3 to 1.6. However, the surface grains of the material are more ductile and can undergo more strain before failure; this is why the actual practical value of the edge factor is less than 1.4. This explains why the stable shape is, in practice, closer to a semi-circular shape than is shown by SMITH's calculations.

Consider next a shallow crack (Fig.4.43c). If the load is increased, the crack first tends to propagate in the direction of thickness due to the higher stresses which exist at the end of the minor axis of the ellipse. Then, the crack border attains an equilibrium shape, designated as "1", such that the stress state and the strength of the material result in simultaneous propagation all along the crack border. Accordingly, the crack has a stable shape if it is still far away from the boundaries of the bar. This stable crack shape is close to a semi-circle. In the case of a very deep initial crack, as represented in Figure 4.43d, the stresses are highest at the surface; the crack will widen without growing deeper and again a stable crack shape is obtained during crack extension.

Initial crack machined by means of a milling saw or by a chemical attack always correspond to the first case. Those which are deepened by fatigue exhibit a shape approaching the stable condition. For this reason, we shall suppose that the static strength of a cracked component is governed only by the surface width of the crack. This applies especially when the crack depth is far from being negligible with respect to the thickness, since the bending stiffness of a thin bar is low compared to the tension rigidity and since the resistance to crack-opening mainly comes from the sectors located in the neighbourhood of the crack surface area.

From the foregoing we may consider that the surface sectors, denoted AOA′ and BOB′ in Figure 4.43b, are parts of a cylinder of outside diameter w with a circular internal crack of radius a. According to Paragraph 4.4.2.1, we shall have

$$K = \frac{2}{\sqrt{\pi}}\sigma\sqrt{a}\,.\,k \qquad (67\text{ bis})$$

with

$$k = 1 \,/\, \sqrt{[1 - 0.95(2a/w)^3]} > 1\,.$$

Furthermore, we shall assume that fracture occurs under loads not much higher than those which cause crack extension from the stable condition; this suggests that a good correlation of the test results will be obtained using a computed nominal K_c-value based on the initial crack surface width and on expression (67 bis).

For low-alloy carbon steel (0.47 C – 0.77 Mn – 1.6 Si – 2 Cr – 0.47 Mo – 0.08 Va) quenched in a salt bath and tempered for 30 min. at 425° C from 960° C, SRAWLEY and BEACHEM[57], using IRWIN's expression (67), obtained a better correlation of the test results with the initial crack dimensions than they did with the dimensions for the unstable fast extension of the crack. The ratio of crack depth to crack length was between 0.13 and 0.55. The nominal values of K_c resulting from the initial crack dimensions were independent of this ratio. The crack dimensions were identified only by the crack areas, so that our expression (67) cannot be verified.

Tests conducted by CORN and NIXON[58] on maraging steel (aged martensite hardened by tempering after quenching) containing 18% Ni – 9 Co – 5 Mo and treated to $\sigma_{ult.} = 214$ daN/mm^2 and $\sigma_{0.2} = 210$ daN/mm^2 were fitted fairly accurately by the expression

$$\sigma_{critical} \cdot (2a)^{0.63} = \text{constant}\,,$$

where $\sigma_{cr.}$ is the stress away from the crack corresponding to the maximum breaking load. The specimens of width $w = 25.4$ mm were divided into three series of different thicknesses (t), with $w/t = 4$, 10 and 14.3.

In the first series artificial cracks were extended in fatigue to obtain various values of the a/b ratio. From a rough analysis of the data it appears that σ_{cr} does not depend on the a/b ratio. For this series, we have used expression (67) to calculate K_c and obtained an average value of 244 daN/mm$^{3/2}$(70,200 lb/in$^{3/2}$)* , with a relative scatter of 4% over 17 results.

For the second test series, with w/t = 10 , an average value of 250 daN/mm$^{3/2}$(72,000 lb/in$^{3/2}$) was found on the basis of seven results.

The values of K_{Ic} in the first series were computed by the authors with IRWIN's expression (66); the average value was 250 daN/mm$^{3/2}$, but the relative scatter was equal to 8%. In addition, for the largest crack of smallest per-cent depth, with 2a = 0.48 in , a/b = 3.2 , the nominal fracture stress was 82.3 daN/mm$^{3/2}$(119,500 lb/in$^{3/2}$), which gives K_{Ic} = 204 daN/mm$^{3/2}$(58,500 lb/in$^{3/2}$) according to IRWIN's expression, and K_c = 243 daN/mm$^{3/2}$(70,000 lb/in$^{3/2}$) according to expression (67 bis), which is substantially the average value. This test confirms the tendency of cracks to grow toward a stable shape; here, the crack, which is too flat at the onset, deepens until the edges of the crack at the surface and the root exhibit the same relative strength, and it then propagates along the entire front.

In the case of *pure bending*, SMITH et al.[77] have shown that for a semi-circular crack that is sufficiently small with respect to the cross-section of the bar the stress intensity factor at the end of a radius defined by an angle θ to the surface is expressed by

$$K_{I\theta} = \frac{2}{\sqrt{\pi}} \sigma \sqrt{a} \ . \ k(\theta, a/c)$$

where σ is the surface nominal tensile stress at the origin of the crack in the uncracked bar,

c the distance between the origin and the neutral axis,

a the half-length of the crack at the surface,

$k(\theta, a/c)$ a factor having the following values:

$2\theta/\pi$ a/c	0	0.2	0.4	0.6	0.8	1
0	1.21	1.12	1.07	1.04	1.03	1.02
0.2	1.18	1.02	0.96	0.92	0.90	0.88
0.4	1.14	0.96	0.86	0.80	0.66	0.64
0.6	1.10	0.90	0.77	0.67	0.62	0.60
0.8	1.07	0.82	0.66	0.55	0.48	0.44
1	1.03	0.77	0.59	0.41	0.34	0.30 .

Tests carried out by DOUILLET et al.[34], which have already been mentioned in Paragraph 4.3.3, page 153, and will be examined further in Paragraph 4.5.5, page 186, exhibited a mean value of the a/b ratio equal to 1.2. This value changed but little during crack growth even when the crack length at the surface was almost equal to the bar width and the crack root was close to the neutral axis. This suggests that SMITH's theoretical results are not valid in practice for actual fatigue cracks, probably because the plasticity of the material is higher near the surface and reduces the surface stresses, thus causing a delay in the propagation of the crack at the surface.

4.5 METHODS OF PREDICTION AND TEST DATA

Prediction of the residual static strength of cracked components is performed on a somewhat empirical basis. One method is to compute the value of the IRWIN parameter, $\mathcal{G}$ or K , which is associated with the design and loading of the component, and then to assume that fracture occurs at a critical value of this parameter; this value is assumed to be an invariant typical of the material in its final service condition. The known cases of cracking and loading for which a solution has been found by analytical or numerical computation are reviewed. As in the case of classical elasticity, solutions have been obtained for problems that are easy to solve, but it is unlikely that the problems of actual mechanical parts with complex shapes can be solved as easily. Furthermore, K_{Ic} is not a real invariant: even if it was, the engineer would not gain from using the K_{Ic}-values as allowable values for K , as they correspond to lower strength limits. In the following, some physical methods applicable to thin sheet material are analyzed.

4.5.1 Correlation parameter $K_N S_{Net}$ of McEVILY and ILLG[59].

To investigate the rate of propagation of fatigue cracks, DONALDSON and ANDERSON[60] use the stress intensity factor $k_w = \sigma \sqrt{(a) c_w}$ (see Paragraph 4.2.3).

---

* 1 daN = 1.02 kg-weight, 1 daN/mm^2 = 1450 lb/in^2, 1,000 lb/in^2 = 0.69 daN/mm^2, 1 lb = 0.445 daN, 1 daN/mm$^{3/2}$ = 288 lb/in$^{3/2}$, 1,000 lb/in$^{3/2}$ = 3.47 daN/mm$^{3/2}$.

McEVILY and ILLG follow NEUBER's reasoning and propose a correlation factor based on the stress concentration factors of the ellipse. Their studies concern thin sheet containing a central crack of length $2a$. At the extremities of the major axis of the ellipse which simulate the crack, we have $(\sigma_{max})_E = \sigma[1 + 2\sqrt{(a/\rho)}]$, ρ being the smallest radius of the ellipse; for the circle, we have

$$(\sigma_{max})_C = 3\sigma = \sigma[(1+2\sqrt{(a/a)}] ,$$

and hence, for a plate of infinite width, with $\sigma = \sigma_m$,

$$\sqrt{(a/\rho)} = \left[\left(\frac{\sigma_{max}}{\sigma_m}\right)_E - 1\right] \Big/ \left[\left(\frac{\sigma_{max}}{\sigma_m}\right)_C - 1\right] . \tag{68}$$

For the circular hole contained in a sheet of finite width, w, HOWLAND has calculated numerically a coefficient D_H such that

$$\left(\frac{\sigma_{max}}{\sigma_m}\right)_{C,w} = D_H \left(\frac{\sigma_{max}}{\sigma_m}\right)_{C,w=\infty} , \tag{69}$$

for which HEYWOOD[61] has suggested an approximate expression,

$$D_H = 1 - \frac{2a}{w} + \left(\frac{2a}{w}\right)^2 - \frac{1}{3}\left(\frac{2a}{w}\right)^3 .$$

If expression (68) is applied to a plate of finite width, w, it follows, with

$$\left(\frac{\sigma_{max}}{\sigma_m}\right)_{C,w} = 3\, D_H ,$$

that

$$\left(\frac{\sigma_{max}}{\sigma_m}\right)_{E,w} = 1 + [3\, D_H - 1]\sqrt{(a/\rho)} .$$

If we write $\sigma_m = S_{Net}$ for the average stress on the uncracked cross-sectional area and if K_N is the stress concentration factor, there results

$$(\sigma_{max})_{E,w} = K_N\, S_{Net} \quad \text{and} \quad K_N = 1 + (3\, D_H - 1)\sqrt{(a/\rho)} . \tag{70}$$

The effective radius, ρ, of a crack depends upon the material; with $\rho = 0.05$ mm for aluminium alloys and $a > 5$ mm, unity is negligible with respect to K_N and one has

$$K_N\, S_{Net} \approx 2\sigma\sqrt{(a/\rho)} \,.\, c_1 ,$$

with

$$c_1 = \frac{1 - 3a/w + 1.5(2a/w)^2 - 0.5(2a/w)^3}{1 - 2a/w} . \tag{71}$$

This expression may be compared with $k_D = \sigma\sqrt{a} \,.\, c_D$. Numerical computation of c_1 and c_D yields

$2a/w =$	0	0.1	0.2	0.3	0.4	0.5	0.6	0.7	0.8
$c_1 =$	1	0.96	0.94	0.98	1.01	1.12	1.33	1.71	2.52
$C_D =$	1	1.005	1.02	1.05	1.09	1.15	1.25	1.4	1.67 .

Comparison shows that, for $0 < 2a/w < 0.6$, the discrepancies are less than 8%, so that the test results should be correlated equally well either with the parameter $K_N\, S_{Net}$, or with the stress intensity factor K_I and the IRWIN parameter $\mathcal{G}$.

4.5.2 Kuhn's[62] Method

In order to use the considerable amount of test data available on the strength of sharply notched specimens, KUHN undertook to develop methods of prediction that cover both cracks and geometrical notches, namely, the method of "notch-strength-analysis" (NSA) and the method of "crack-strength-analysis" (CSA). The usefulness of this proposal is that certain parameters can be evaluated by application of one of the methods to some test results and then be employed for the approximate strength prediction of a specimen to which the other method is applicable.

4.5.2.1 The Notch-Strength-Analysis (NSA) Method

If σ_N is the net stress on the cross-sectional area passing through the notch and K_T the theoretical concentration factor, and if the specimen remains in the elastic range, the maximum stress at the notch root is

$$\sigma_{max} = \sigma_N K_T . \tag{72}$$

NEUBER assumed that the material consists of "building blocks" suggested by, but not identifiable with, the grains, and postulated that each block reacts only to the average stress across its face; he considered that this property can be represented by introducing a quantity ρ', called the "effective" sharp-notch radius, which characterizes the material and implies a "practical" stress concentration factor,

$$K_N = 1 + \frac{K_T - 1}{1 + \frac{\pi}{\pi - w_0}\sqrt{(\rho'/\rho)}} , \tag{73}$$

where ρ is the geometrical notch radius and w_0 the "effective" notch flank angle, defined as being equal to half the real angle w if $w > 0.7\pi$. For fatigue, NEUBER has used the formula

$$\text{"effective" } \sigma_{max} = \sigma_N K_N = \text{Endurance limit} .$$

Some curves showing the variation of the constant ρ' as a funtion of $\sigma_{ult.}$ have been plotted by KUHN[11] for aluminium and titanium alloys.

For static strength, the failure criterion is $\sigma_{max} = \sigma_{ult.}$. In order to take due account of plasticity, KUHN introduced the "ultimate" stress concentration factor,

$$K_u = 1 + (K_N - 1)(E_u/E) , \tag{74}$$

which is applicable if $\sigma_N < \sigma_{0,2}$; $E_u = \sigma_{ult.}/\epsilon_u$ is the secant modulus corresponding to the related strain ϵ_u prior to necking. As this information is very rarely published, E_u is evaluated from the total elongation after necking and failure, A %, such that

$$(E_u/E) = 1 / (1 + 0.8\ AE/100\ \sigma_{ult.}) , \tag{75}$$

where the factor 0.8 is intended to subtract the elongation due to necking from the total elongation ($\epsilon_u = \sigma_{ult.}/E + 0.8\ A/100$).

For $\sigma_N > \sigma_{0,2}$, the few test data available have been fitted best by using the expression

$$K_u = 1 + (K_N - 1)\ E_u/\sqrt{(E.E_N)} ,$$

where $E_N = \sigma_N/\epsilon_N$ is the secant modulus pertaining to σ_N.

At the beginning of this chapter we have seen that a number of materials are strengthened by moderate notches and exhibit $\sigma_{Nu} > \sigma_{ult.}$, σ_{Nu} being the net stress to failure of a notched specimen and $\sigma_{ult.}$ being that of the standard unotched specimen. In that case, the above mentioned method is not valid since $K_u < 1$. Furthermore, this method is applicable only if $\sigma_{ult.}$ and ϵ_u are measured on a specimen having the same thickness and made by the same fabrication procedure as notched components, so that the tensile properties of the material and the fracture mode - ductile or brittle - are the same for the specimen and the notched components.

4.5.2.2 The Crack-Strength Analysis (CSA) Method

In connection with the method used for notches, KUHN idealizes the central crack contained in an infinite sheet into a central elliptic hole of minimum radius ρ. The stress concentration factor is

$$K_T = 1 + 2\sqrt{(a/\rho)} .$$

For a sheet of finite width, DIXON[20] has proposed

$$\sigma_{max} = K_T \sigma_N , \qquad K_T = [1 + 2\sqrt{(a/\rho)}]\ k_w , \tag{76}$$

with

$$k_w = \sqrt{\left(\frac{1 - m}{1 + m}\right)} ,$$

where

$$m = 2a/w ,$$

w being the sheet width and a the major half-axis of the ellipse.

In order to avoid the absurdity of obtaining $K_T < 1$ for large m-values, KUHN suggests the following:

$$K_T = 1 + 2\, k_w \sqrt{(a/\rho)} \ . \tag{77}$$

This expression is sufficiently accurate for cracks, slots with round extremities as studied by DIXON, notches of large radii and even circular holes. To KUHN's proposals we shall, however, add our hypothesis (22) described in Paragraph 4.2.3, i.e.,

$$k_w = \sqrt{\left(\frac{1-m}{1+m}\right)} \text{ if } m < 0.4 \text{ and, } k_w = 0.414/\sqrt{m} \text{ if } m > 0.4 \ . \tag{78}$$

Moreover, for symmetrical edge notches in a sheet of finite width, KUHN has proposed

$$k_w = 1 - m \ . \tag{79}$$

Referring to Paragraph 4.4.4.2, we propose

$$k_w = 1.1 \sqrt{\left(\frac{1-m}{1+m}\right)} \ . \tag{80}$$

With $w = 0$ for the slot, NEUBER's expression (73) becomes

$$K_N = 1 + \frac{K_T - 1}{1 + \sqrt{(\rho'/\rho)}} \ ,$$

that is, with expression (77) for K_T and if ρ tends toward zero,

$$K_N = 1 + 2\, k_w \sqrt{(a/\rho')} \ . \tag{81}$$

To allow for plasticity, KUHN further suggests

$$\sigma_N = \sigma_{ult.}/K_u \ ,$$

where

$$K_u = 1 + 2\, k_w \sqrt{(a/\rho')} \ . \ E_u/E \ , \tag{82}$$

$$(\sigma_N < \sigma_{0,2}) \ .$$

Here ρ' should have, in principle, the same values as in the case of sharp notches. If only a correlation of the crack strength tests is to be established, the ρ' and E_u/E may be replaced by a single constant

$$C_m = \frac{2}{\sqrt{\rho'}} \ . \ E_u/E \ ,$$

with

$$K_u = 1 + C_m\, k_w \sqrt{a} \ , \qquad (\sigma_N < \sigma_{0,2}) \ . \tag{83}$$

Note that the width effect may be written in the form

$$K_u = 1 + c_D \sqrt{(w/2)} \ . \ C_m \ ,$$

with

$$c_D = \sqrt{\left[m\, \frac{1-m}{1+m}\right]} \text{ if } m = 2a/w \leqslant 0.4, \text{ and } c_D = 0.414 \text{ if } m > 0.4 \ . \tag{84}$$

Although no direct evidence of notch strengthening was found by KUHN in the very large amount of test data available, the assumption of an "ultimate" strength greater that the standard strength $\sigma_{ult.}$ has led to an improved correlation in some cases for which KUHN proposes

$$K'_u = 1 + C'_m\, k_w \sqrt{a} \ , \qquad (\sigma_N < \sigma_{0,2}) \ ,$$

$$\sigma_N = \sigma'_u/K'_u \ ,$$

C'_m and σ'_u being so determined that they provide a better correlation. The above expression constitutes the "modified" form of the CSA method. This modified CSA method yields an excellent correlation of BROEK's[86] test results (Figures 7 and 9 of the author) on clad 2024-T3 and 7075-T6 aluminium alloy sheets. In Figure 4.44a and b, test data from the Boeing Company correlated by KUHN by means of the "basic" and the "modified" CSA methods are reproduced. In both cases, if $m = 2a/w > 0.4$, the correlations are further improved by expression (84); the new expression is represented in the Figure by dashed straight lines after $2a/w = 0.4$.

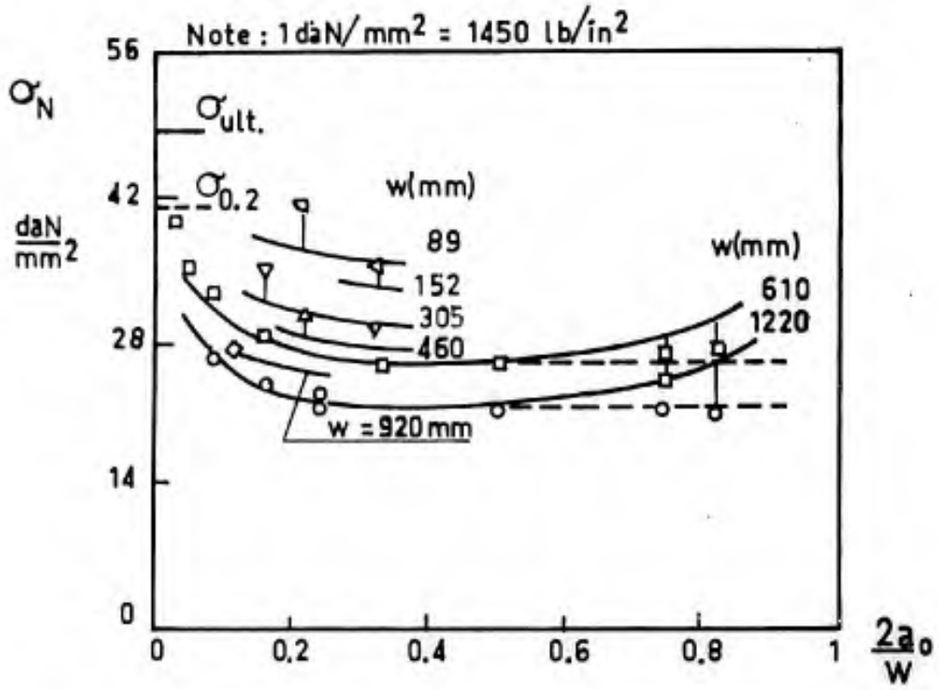

(a) The curves are calculated with $\sigma_{ult.}$ = 48 daN/mm² ; $C_m = 0.126/\sqrt{m}m$.

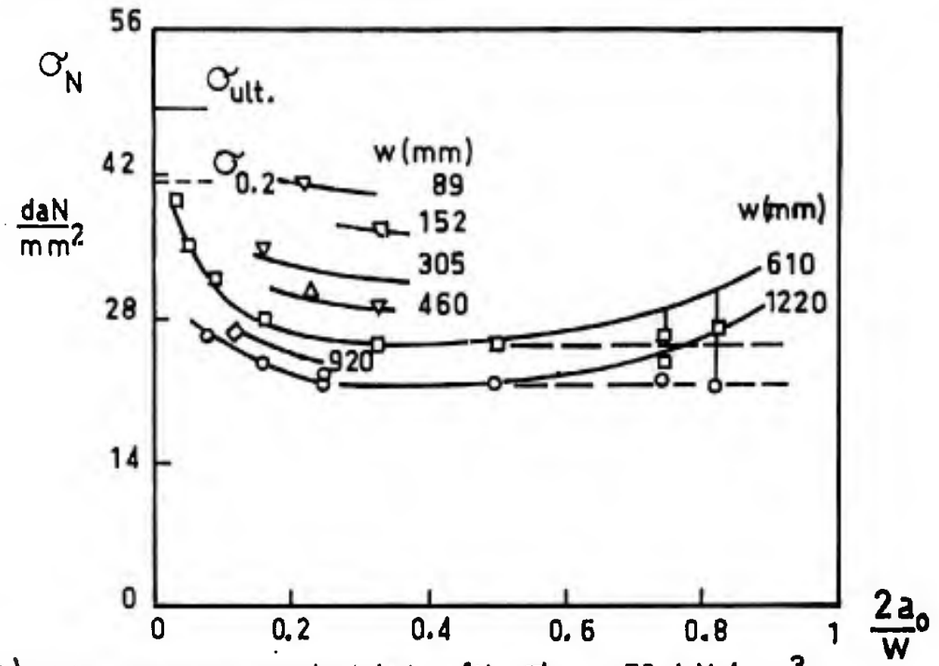

(b) The curves are calculated with $\sigma_{ult.}$ = 59 daN/mm²; $C_m = 0.182/\sqrt{m}m$.

Fig. 4.44 Static net residual strength of 2.54 mm thickness 2219-T87 aluminium alloy sheets. Tests carried out by Boeing with anti-buckling bars, after Kuhn[62]

If a new material is to be evaluated, a minimum of two tests should be made, with the two widths w as different as possible. If both tests give about the same value of C_m, the use of the "basic" method is appropriate. If not, the modified method should be used. To avoid undue test sensitivity, w and $2a/w$ should be chosen large enough to make $K_u > 1.1$, at least.

Crack-lip buckling effect

We have seen, in Paragraph 4.4.3, that buckling of the crack lips has little influence on the stress distribution at the tips of a crack, at least in the median plane of the sheet. It is likely that the faces of the sheet are subject to secondary bending stresses at the crack tips. Experience shows that the strength reduction can be as much as 30% with respect to cases where the buckling is prevented by "anti-buckling guides". For sheets of aluminium alloys, KUHN and FIGGE[63] have proposed the empirical reduction factor

$$(1 - 0.001\ 2a/t) \ . \qquad (86)$$

Remarks on the two methods

KUHN reports some test results. The proposed correlations seem to hold good for ductile materials but appear doubtful in the case of brittle materials and very-high-strength steels because no test series covering a reasonable range of w and $2a/w$ are available for such materials. In the following, we quote remarks made by KUHN:

"In the CSA method, the material constants (C_m, or C_m' and the ratio $\sigma_u'/\sigma_{ult.}$) must be determined for each material from crack strength tests. A strength calculation for an untested configuration thus is not a true prediction, but simply an interpolation between, or extrapolation from, tests of the same type".

"The NSA method, on the other hand, has been developed for aluminium alloys (and, to a lesser extent, for titanium alloys) to the point where only conventional stress-strain data are needed as basis for making crack strength calculations. These calculations, then, may be classified as "predictions", at least from the engineering view point. The elimination of the relatively cumbersome crack strength tests is a substantial practical gain, particularly considering tests at other than room temperature. Moreover, the possibility of making direct comparisons between crack strength tests and notch strength tests permits exacting new information from a vast body of published tests and correlating hitherto uncorrelated data".

The accuracy of prediction of all methods, including the Fracture Mechanics one, is good to fair in the majority of cases, and thus definitely useful, but with no guaranty against a significant percentage of very poor predictions.

Concerning this last point, we may refer to the existence of rare and severe statistical families mentioned by TAYLOR[76] for aircraft service loads; no method of analysis can take into consideration the unknown scatter of extremely rare occurrences in order to provide a basis for statistical calculations. Of course, tests on actual parts are always necessary. In Table 4.8 below, from KUHN, some orders of magnitude of the constant C_m are given for various aircraft engineering materials.

TABLE 4.8

Test values of crack sensitivity, C_m, at room temperature (For orientation purposes only).

Material	*Thickness, mm*	C_m, $mm^{-1/2}$	*Notes*
2014-T6	1.52	0.238	
X2020-T6	1,52	0.6	
2024-T3	1 - 2.54	0.10	
2024-T86	1.52	0.36	
2219-T87	2.54	0.12	
7075-T6	1 - 2.54	0.28	
4330M	2	0.10	$\sigma_{ult.}$ = 155 daN/mm^2
4330M	3.55	0.18	$\sigma_{ult.}$ = 154 daN/mm^2
AM350(SCT950)	1.27	0.08	
17-7PH(RH1050)	1	0.18	
PH15-7Mo(TH1050)	0.63	0.14	
PH15-7Mo(RH950)	1.27	1.4	
H-11	1.52	3.75	Aged 540°C(1 + 1 + 1 hr)
Vascojet 1000	1.52	4.75	Aged 540°C(2 + 2 + 2 hr)
Ti 2.5Al-16V	2	7.1	Aged 4 hrs at 372°C to obtain maximum brittleness
Glass		20.5	Griffith tests

The simulation of cracks by saw cuts, from KUHN

"The shape of the end of a saw cut, particularly in thin sheets, is rather indefinite. The calculation of the stress concentration factor can therefore only produce two limits. The upper limit is obtained on the assumption that the ends of the saw cut are ideally square; the cut then acts like a crack. The lower limit is obtained by assuming that the end of the saw cut is semi-circular with a radius equal to one-half the thickness of the saw."

"The data shown suggest that the difference between "saw-cut strength" and crack strength can be estimated fairly well if the necessary materials data are available. Together with other scattered data, they suggest that the direct simulation of cracks by saw cuts (with maximum errors less than, say, 10%) is probably possible in materials which give no concern about service behavior (2024-T3). However, when the service behavior is considered as marginal, the useability of saw cuts becomes very marginal also. Finally, it should be noted that the ratio of saw-cut strength is size-dependent. For instance, for the PH15-7Mo steel, and a fixed value of $2a/w = 0.2$, the ratio is calculated as 1.46 for $w = 1$ inch (25.4 mm), 1.68 for $w = 4$ inches (101.6 mm), and 2.00 for 50 inches (1270 mm)".

From an experimental investigation of the residual strength of 300-mm wide and 2-mm thick 2024-T3 and 7075-T6 specimens, BROEK[67] has drawn the following conclusions:

"a. In specimens for residual strength tests the initial fatigue crack may be simulated by a fine saw cut. This may give slightly unconservative results for the stress at the onset of slow crack growth, but reliable results are obtained for the critical crack length and the residual strength (critical gross stress at fracture).

b. The fatigue loads at which cracks were formed do not affect the results of the residual strength tests.

c. *Stop holes at the crack tips increase the stress for the initiation of slow crack growth, but have no favourable effect on the residual strength,* unless they are so large that the onset of crack growth is postponed to a stress higher than the fracture stress for the case without stop holes. In the latter case immediate fracture occurs as soon as the crack starts to extend. In other words: if slow crack growth precedes fracture, the critical stress is not affected by the acuteness of the initial crack and there always is slow crack growth, provided that crack extension starts at a stress below the critical stress of a specimen with a fatigue crack of the same initial length".

4.5.3 Welbourne's[12] Method

The method of WELBOURNE is the basis of the Royal Aeronautical Society Data Sheets. WELBOURNE assumes that failure occurs when the maximum strain at the root of a very sharp notch or crack of "effective" radius ρ' attains the maximum total strain corresponding to the ultimate tensile strength, $\sigma_{ult.}$; he also supposes that the stress or strain concentration factor, K_T, of the theory of elasticity is valid in the plastic range for strains only:

$$\epsilon_{max} = K_T \, \epsilon_N \, . \tag{87}$$

At failure, it follows that

$$K_T . \epsilon_N = \sigma_{ult.}/E + \epsilon_{max} = \epsilon_u \, , \tag{88}$$

where ϵ_N = total strain associated with σ_N,

ϵ_{max} = plastic strain at $\sigma_{ult.}$,

ϵ_u = total strain at $\sigma_{ult.}$.

WELBOURNE uses the strain concentration factor

$$K_T = [1 + 2\sqrt{(a/\rho')}] \, k_w \, , \tag{89}$$

where ρ' is the "effective" radius, equal to 0.063 mm for aluminium alloys, a the half-length of a central crack in a thin sheet, and k_w the width-effect coefficient of expression (78) quoted in the previous Paragraph, since he assumes constancy of the $k_w/\sqrt{m}$-value after $m = 2a/w = 0.4$ in order to fit his test data.

For computation purposes, the curve σ–ϵ of the material is given in the form

$$\epsilon_N = \sigma_N/E + \epsilon_{max} \, (\sigma_N/\sigma_{ult.})^n \, ,$$

where the exponent n is calculated as follows:

$$n = \log_{10}\left(\frac{\epsilon_{max}}{0.002}\right) \Big/ \log_{10}\left(\frac{\sigma_{ult.}}{\sigma_{0.2}}\right) \, .$$

One then obtains

$$\frac{\sigma_n}{\sigma_{ult.}} + \frac{\epsilon_{max} \cdot E}{\sigma_{ult.}} \left(\frac{\sigma_n}{\sigma_{ult.}} \right)^n = \frac{1}{K_T} \left(1 + \frac{\epsilon_{max} \cdot E}{\sigma_{ult.}} \right),$$

which permits the computation of σ_N .

If the proportional limit stress is designated as σ_p and $\sigma_N < \sigma_p$, there results

$$\epsilon_N = \sigma_N / E$$

and

$$\epsilon_u = \sigma_{ult.} / E_u = (\sigma_N / E) \left[1 + 2 \sqrt{(a/\rho')} \right] k_w ,$$

hence

$$K_u = \sigma_{ult.} / \sigma_N = \left[1 + 2 \sqrt{(a/\rho')} \right] k_w \, E_u / E , \qquad (90)$$

which may be compared with expression (82), from KUHN:

$$K_u = 1 + 2 \sqrt{(a/\rho')} \, k_w \, E_u / E .$$

The two methods give different results for K_T and k_w (if $m = 2a/w > 0.4$). With $w = 25$ mm , $2a = 10$ mm and $\rho' = 0.06$ mm , the values of K_T are 12.6 for WELBOURNE and 12.9 for KUHN. Consequently, there is no significant difference in cracked-sheet applications, except that k_w must be corrected in KUHN's expressions for $2a/w > 0.4$.

It may, however, be remarked that the more general value of K_T used by KUHN could also be utilized in the WELBOURNE method if some experimental knowledge of ϵ_{max} was available. In the absence of such information, we believe, after KUHN, that it is preferable to resort to a correlation formula, such as expression (83), for interpolating direct test results.

4.5.4 Test Data on Sheet Material

A vast body of test data exists for centre-cracked sheets. It may serve to provide orders of magnitude, but engineers should always refer to direct tests; nevertheless, even direct test results must be used with great caution if correct service behavior predictions are to be derived for actual structures.

In the application to sheet material, the two methods described above give better results than the method of IRWIN. We have applied them to tests conducted by McEVILY, ILLG and HARDRATH[64] on 2-mm-thick sheets:

2024-T3 ($\sigma_{ult.}$ = 50.2 daN/mm^2, $\sigma_{0.2}$ = 37, E = 7,500 daN/mm^2, A % = 19.5) ,

7075-T6 ($\sigma_{ult.}$ = 57 daN/mm^2, $\sigma_{0.2}$ = 52, E = 7,200 daN/mm^2, A % = 12.8) .

The computation results are compared to measurements for $2a/w = 0.4$; in addition, we have calculated the value of the IRWIN parameter with respect to the initial crack length. In the last column of Table 4.9, it is shown that the strength depends on the elongation at failure, A %.

TABLE 4.9

Strength of centre-cracked sheets, from test results reported by McEvily, Illg and Hardrath[64].

Alloys	*w, mm*	*Measurements* $\sigma_N/\sigma_{0.2}$	*Measurements* $\sigma_N/\sigma_{ult.}$	*Calculated* $\sigma_N/\sigma_{ult.}$ *KUHN*	*Calculated* $\sigma_N/\sigma_{ult.}$ *WELBOURNE*	G_c *daN/mm*	$\sigma_N / A \, \sigma_{ult.}$
				$\rho' = 0.05$	$\rho' = 0.063$		
2024-T3	57	1.15	0.8	0.71	0.79	3.2	0.041
	305	0.81	0.6	0.51	0.66	9.7	0.031
	890	0.47	0.35	0.38	0.42	9.7	0.018
				$\rho' = 0.06$	$\rho' = 0.063$		
7075-T6	57	0.77	0.7	0.61	0.86	3.4	0.056
	305	0.44	0.4	0.4	0.33	5.8	0.032
	890	0.27	0.25	0.28	0.23	5.7	0.018

The two methods, that is, KUHN's and WELBOURNE's, give fairly accurate orders of magnitude for the strength. On the other hand, it cannot be considered that the IRWIN parameter, $\mathcal{G}_c$, calculated on the basis of the initial crack length, is an invariant. For narrow specimens, $\mathcal{G}_c$ approaches its minimum value, $\mathcal{G}_{Ic}$; however, IRWIN's theory is hardly applicable since the entire specimen section is in the plastic range.

Residual strength tests by BROEK[80] and 2024-T3 aluminium alloy sheet yield K_c-values (which we have computed on the basis of the initial crack length) ranging from 135 daN/mm$^{3/2}$, for $w = 150$ mm and $2a/w = 0.133$, to 312 daN/mm$^{3/2}$; for $w = 600$ mm and $2a_o/w = 0.2$; the corresponding values of $\mathcal{G}_c$ vary from 2.6 to 14 daN/mm.

The relative success of KUHN's and WELBOURNE's methods of analysis and correlation for wide and thin sheet is due to the fact that crack extension before final fracture is such that the ductile lips are as fully developed as in the comparative tensile test on unnotched specimens cut from the same sheet material.

The beneficial effect of a large elongation at fracture, A%, is not always established. Thus, FIGGE[65] has verified the method of KUHN fairly well, apart from a few anomalies, for 203-mm wide and 1-mm thick titanium-alloy sheet specimens, and 0.6-mm thick stainless-steel and superalloy specimens. For instance, in the case of cold-rolled AM-350 stainless steel with a thickness reduction of 20%, ρ' must be equal to 1,000 mm to fit the hot-test results (290°C), which means that $\sigma_N/\sigma_{ult.}$ is close to unity and that the notch sensitivity is zero although the elongation at fracture is small, i.e., A % = 2.7 at 290°C; under these circumstances, it may be surmised that prior fatigue and initiation of plastic strain during the rupture test cause a softening of the material and induce residual compressive stresses on the crack border (some signs of martensitic transformation were observed).

In order to insist on the need for proceeding with caution, we shall examine some test data from LOCKHEED and BOEING reported by CRICHLOW[66] and relating to 2024-T3 aluminium-alloy sheets 1 to 2.34-mm thick, 190 to 890-mm wide, and with heights equal to twice the corresponding widths. These specimens contained central cracks of initial lengths $2a_o$ and of measured critical lengths $2a$. We have computed the values of the IRWIN parameter K_c without plastic-zone correction for $E = 7{,}500$ daN/mm^2 and

$$K_c^* = \sqrt{(\pi w/2)} \cdot \sigma_c \cdot c ,$$

with

$$c = \sqrt{[m/(1 - m^2)]} \text{ if } m = 2a/w \leqslant 0.4 , \text{ and } c = 0.414/(1 - m) \text{ if } m > 0.4 .$$

The asterisk indicates that rough results have been used without correction of the critical strength σ_c for the crack-lip buckling. The nominal value of K_c^*, i.e., $\bar{K}_c^*$, is obtained by a calculation based on the initial crack length $2a_o$. The $\bar{K}_c$-values that correspond to absence of lip buckling were estimated by dividing σ_c by the KUHN's lip-buckling correction factor, hence

$$\bar{K}_c = \bar{K}_c^* / (1 - 2\, a_o/1{,}000\, t) . \qquad (91)$$

C_m^* is expressed by the formula

$$C_m^* = (\sigma_{ult.}/\sigma_N - 1) \,/\, c_D \sqrt{(w/2)} ,$$

with

$$c_D = \sqrt{\left(m \frac{1 - m}{1 + m}\right)} \text{ if } m = 2\, a_o/w \leqslant 0.4, \text{ and } c_D = 0.414 \text{ if } m > 0.4 .$$

C_m is computed by dividing σ_N by KUHN's correction factor. The variation of K_c^* and of $\bar{K}_c$ in relation to $m = 2a_o/w$ does not exhibit a clear crack-lip length effect. Conversely, C_m increases regularly with $2a_o/w$. Taking into consideration the preceding NASA buckling correction (published in 1962) and calculating C_m with the corrected value of σ_N, we find substantially constant values as listed in Table 4.10.

In this table, the relative dispersion, V %, is computed from the interquartile range for 1.02-mm-thick sheet, as though departures from the median values were simply due to chance; the buckling correction allows adequate fits, the best being obtained for KUHN's constant C_m. A large amount of published data, however, relate to tests carried out with no particular precaution against buckling and C_m should be calculated if the variation and scatter of C_m with respect to the material, heat treatment, hardening state, etc., are to be determined. This operation is probably useless if we consider that the test considerations of unstiffened plane sheets differ from the stressing of sheets used as parts of structural components.

TABLE 4.10

Tests on fatigue-cracked 2024-T3 sheet specimens, from Crichlow[66].
Width w = 508 mm, height L = 1016 mm.

(1) Thickness $t = 1.02$ mm , $\sigma_{ult.} = 44$ daN/mm^2

	Measured quantities					Calculated quantities						
$2a_o$ mm	$2a$ mm	$2a_o/w$	σ_c daN/mm^2	σ_N daN/mm^2	$\sigma_N/\sigma_{ult.}$	K_c^* daN/mm$^{3/2}$	$\bar{K}_c^*$ daN/mm$^{3/2}$	$\bar{K}_c$ daN/mm$^{3/2}$	C_m^*	C_m	$\sigma_c^*\sqrt{(2a_o)}$ daN/mm$^{3/2}$	$\sigma_c\sqrt{(2a_o)}$ daN/mm$^{3/2}$
45.7	75.4	0.09	28.6	31.5	0.71	314	245	257	0.09	0.08	194	202
45.7	74.5	0.09	28.8	31.6	0.715	312	244	256	0.09	0.08	196	204
56.5	84	0.111	27.4	30.8	0.695	316	256	272	0.09	0.07	205	217
57	82.7	0.112	27.4	30.8	0.695	316	259	269	0.09	0.07	207	220
92	134.5	0.181	21.4	26.2	0.59	320	259	285	0.12	0.09	205	230
92	122	0.181	21	25.7	0.58	298	255	281	0.13	0.09	202	227
137.5	191	0.272	16.8	22.4	0.505	344	270	313	0.16	0.116	198	228
137.5	224	0.272	17.1	23.4	0.526	356	251	290	0.14	0.100	200	232
178	238	0.352	13.6	21	0.475	299	228	278	0.17	0.13	182	222
180	222	0.354	14.1	21.8	0.49	292	236	288	0.16	0.12	188	230
256	288	0.505	10.2	20.7	0.467	274	204	275	0.17	0.09	162	215
255	328	0.501	10.1	20.3	0.455	332	201	270	0.18	0.08	162	215
	Relative dispersion, V % = ...					5.2	7.5	4.6		2.3	6.9	4.8

(2) Thickness $t = 2.34$ mm ; $\sigma_{ult.} = 46.5$ daN/mm^2

45.5	85.5	0.089	31.6	34.3	0.74	364	266	275	0.08	0.066	212	220
45.5	80	0.089	31.4	34.3	0.735	382	294	310	0.08	0.066	212	220
91.5	126	0.18	23.9	29.2	0.63	340	289	317	0.10	0.075	228	250
91	122	0.18	25.6	31.2	0.67	362	310	340	0.09	0.066	244	267
137	173	0.27	18.9	25.9	0.56	328	285	330	0.12	0.083	221	257
137	178	0.27	19.3	26.4	0.57	340	292	338	0.12	0.082	226	262
179	216	0.35	16.6	25.5	0.55	338	294	357	0.12	0.072	222	270
178	215	0.35	16.7	25.7	0.535	338	295	358	0.13	0.080	223	272
254	290	0.50	11.7	23.4	0.505	321	274	366	0.15	0.074	186	250
255	300	0.50	11.8	23.6	0.51	338	288	385	0.15	0.07	189	254

Note: K_c is calculated with $2a/w$; K_c and $\bar{K}_c$ are nominal values calculated with $2a_o/w$; the asterisk indicates that no crack-lip buckling correction has been made.

1 daN/mm^2 = 1450 lb/in^2 , 1 daN/mm$^{3/2}$ = 288 lb/in$^{3/2}$

The following recommendations may be formulated for designers:

(a) For a rough prediction of the magnitudes, the methods of KUHN and of WELBOURNE should be utilized with reference to the static tensile properties of the materials.

(b) For a more accurate prediction of the residual strength of cracked plane sheets, interpolation on published test data should be effected on the basis of the most appropriate of the the above mentioned quantities.

(c) For an adequate strength prediction of actual structures, the only correct means consists in using previous tests performed on similar structures or in carrying out partial tests for which the sheet elements are assembled so as to be representative of the structure and that the local conditions are represented adequately.

As an example for evaluating orders of magnitude, let us consider a tension-loaded 7075-T6 sheet in a section containing 4-mm-diameter rivets, 20 mm apart, and 0.75-mm-long fatigue cracks on each edge of the rivet holes, all along the rivet line. In expression (83) we have $C_m = 0.28$ according to Table 4.8, $w = 20$ mm , $2a = 5.5$ mm according to the remark made in Paragraph 4.4.3, $k_w = 0.755$ and $K_u = 1.35$. The load withstood will only be 3/4 of that of the uncracked component; this case corresponds roughly to a localized failure that occurred in flight on a military aircraft designed and substantiated for an ultimate load of 10 g and subjected to a load of about 7 g. A subsequent inspection check revealed that there were cracks all along the rivet line but that these were hidden by the rivet heads.

4.5.5 Test Data for Bars with Surface Cracks Subjected to Bending

For thick bars with surface cracks, even more than for thin sheets with through-thickness cracks, it would be unwise to recommend a method for predicting the residual static strength. At best, systematic tests can be run to characterize the various engineering materials by quantities that are valid only for comparison purposes. Even then, the type and size of the test piece must be selected carefully so that the resultant classification

proves adequate for the actual behaviour of the structures. The present trend of the Service Technique Aéronautique (French Army) is to conduct residual-static-strength tests on square bars of section 20 x 20 mm as part of a systematic test programme designed to furnish a classification of the materials and to serve as a basis for more complete investigations before these materials are used in service. The test specimens and test procedures have been described in Paragraph 4.3.3. It is relevant to recall that the semi-elliptical cracks are initiated from electric-scriber marks by subjecting the specimens to bending fatigue; final static failure in bending is obtained with the same test set-up (see Figure 4.19 for the specimen).

The tests under review were carried out at the Centre d'Essais Aéronautiques de Toulouse (CEAT, formerly EAT). In some cases, IRWIN's experimental method of test data analysis for the determination of $\mathcal{G}_c$ was employed, but we have proposed elsewhere[67] an approximate method for which it is only necessary to know the breaking load P and the apparent surface crack length, 2a , prior to the static failure test.

The notation used is:

P = ultimate static load to failure of the fatigue-cracked bar,

P_u = ultimate static load to failure of an uncracked bar,

$P_T = 44.4(\sigma_{ult.})$ = ultimate theoretical value of P_u , calculated assuming that the bar is perfectly elastic and that the maximum stress is equal to $\sigma_{ult.}$; P_T is expressed in daN if $\sigma_{ult.}$ is expressed in daN/mm^2.

The effect of plasticity in bending and the friction on the supports give

$$P_u \geqslant 1.5\, P_T .$$

With the ratio P/P_T plotted on the y-axis and $1/\sqrt{(2a/h)}$ plotted on the x-axis, where h is the width of the square bar, Figure 4.45 illustrates the relation

$$\eta = \frac{P}{P_T}\sqrt{(2a/h)} ,$$

which is represented by a straight line originating at point o $(2a/h = \infty)$ and passing through the experimental points. In practice, the correlation holds for $P/P_T \leqslant 1$ and $2a/h \leqslant 0.8$. The value of $E\mathcal{G}_c$ is calculated from expression (25) quoted in Paragraph 4.3.3:

$$E\,\mathcal{G}_c = \left(\frac{\sigma_{ult}}{0.854}\right)^2 \eta^2 ,$$

where $\sigma_{ult.}$ is the ultimate tensile strength of a standard specimen. K_c is obtained from $\sqrt{(E\,\mathcal{G}_c)}$ or

$$K_c,\ \text{daN/mm}^{3/2} = \frac{P\ \text{daN}\sqrt{(a\ \text{mm})}}{38.5} .$$

We also have

$$(K_c/\sigma_{ult.})\ \text{mm}^{-1} = 3.65\,\eta\ \text{mm}^{-1} . \qquad (92)$$

K_c is proportional to the absolute residual static strength, while η and except, for one factor, $K_c/\sigma_{ult.} = 3.65\eta$ represent the relative strength, i.e., the ratio of the measured strength to the theoretical nominal strength of uncracked specimens, calculated by neglecting the plasticity in the elementary expressions. In Figure 4.45, the correlation is very good for high-strength steels that have been air-melted and are brittle owing to oxide inclusions; it is still acceptable for 35 NCD 16 steel treated to the usual strength of 140 daN/mm^2(203,000 lb/in^2) as well as for T-A6-V titanium alloy, although most points are in the plastic range. In the last case, it would be interesting to have some test data available for specimens of greater cross-sectional area so as to avoid unexpected difficulties in the plastic range.

One could try and summarize the test data published on the strength of components with surface cracks. It is our belief that this would be a vain effort because of the large variations due to shape of the specimens. Thus, DOUILLET[67] demonstrated that K_c lies between 135 and 180 daN/mm$^{3/2}$ for the same cast of 40-CDV20 steel treated to $\sigma_{ult.}$ = 170 daN/mm^2(246,000 lb/in^2) , by carrying out tests on flat specimens with semi-elliptical cracks (method of SRAWLEY) as well as on the above mentioned bars subjected to bending. For several casts of the same material the extreme values ranged from 135 to 290 daN/mm$^{3/2}$(1 daN/mm$^{3/2}$ = 288 lb/in$^{3/2}$).

The discussion about the true value of K_{Ic} remains academic. Nevertheless, it is important to have reference values for classification of the various materials that are used in the engineering field. To this end, the Service Technique Aéronautique conducts, in the laboratories of the Centre d'Essais Aéronautiques de Toulouse (CEAT), systematic tests on fatigue-cracked bars subjected to bending in order to qualify the various states of alloys and to investigate components that have suffered damage in service.

In Table 4.11, the compositions together with the mechanical and fracture properties of 20 x 20 x 150 mm bars, loaded in bending, are listed for several high-strength aluminium alloys used in aircraft engineering.

In Table 4.12, the same results are given for high-strength low-alloy steels, for steels with structural hardening by precipitation and for maraging steels with martensitic hardening by ageing.

First, a few general remarks can be made. Some metallurgists still assume that the ratio $\sigma_{ult.}/\sigma_{0.2}$, which is close to unity, is correlated with brittleness. No such correlation appears in Tables 4.11 and 4.12. Similarly, for 35-NCD16 steel, no direct correlation is found in Table 4.12 between K_c, on the one hand, and the notch impact strength K_{UF}, the elongation at failure A % and the reduction in area Σ %, on the other hand; this shows the need for rupture tests on fatigue-cracked specimens with a view to characterizing the brittleness of the materials.

The high values of $K_c/\sigma_{ult.}$ obtained for conventional steels, such as 3.5 for 25-CD4-S treated to 107 daN/mm^2 and 15-CDV6 treated to 110 daN/mm^2, 3.45 for 40-CDV20 treated to 130 daN/mm^2, give evidence of the excellent service behaviour of medium and high-strength steels. Lower values are found on ultra-high-strength steels (180 to 200 daN/mm^2); it should be noted, however, that, of the air-melted low-alloy steels, 35-NCD16 is better than 40-CDV20. Vacuum re-melting improves slightly the 35-NCD16 steel treated to 180 daN/mm^2 (+10 %) and to 195 daN/mm^2 (+20 %), whereas refrigeration before tempering causes no change. If treated adequately, maraging steels behave very well.

TABLE 4.11

Aluminium alloys – Bending tests on fatigue-cracked 20 x 20 mm bars

(a) Compositions and treatments

No	*Alloy*	*Form*	*Composition %*							*Treatment*
			Cu	*Si*	*Mg*	*Mn*	*Fe*	*Ti*	*Ni*	
1	2014	Spar Cap	4.6	0.82	0.28	0.81	0.64	0.03		Unknown
2	A-U4SG	Spar Cap	4.2	1.18	0.49	0.87	0.35	0.03		Unknown
3	A-U4SG	Bar	4.3	0.83	0.39	0.84	0.39	0.09		T6, 16 h, 160°C
4	A-U4SG	Thick Plate	4.25	0.80	0.63	0.85	0.44	0.12		T 651
5	A-U2GN	Thick Plate	2.5	0.20	1.65		0.98	0.08	1.20	T 651, 20 h, 190°C

(b) Tensile properties

No	*Alloy*	σ_p	$\sigma_{0.05}$	$\sigma_{0.1}$	$\sigma_{0.2}$	σ_{ult}	$\sigma_{ult}^{\bullet}$	*E*	*A %*	Σ %
		Values in daN/mm^2								
1	2014	41.4	56.4	57.2	57.6	60.6	71.4	6,900	10.2	17
2	A-U4SG	33.6	42.1	43.4	44.4	49.5	58.1	7,300	9.8	18.2
3	A-U4SG bars	40	49	50	51	56	67.5	7,230	11.3	26
4a	A-U4SG plate, long	36.6	44.6	45.8	46.4	50.4	60.5	7,260	8.5	20.6
4b	A-U4SG plate, transverse	34.7	42.6	44.2	45.2	49.6	56.3	7,350	7.6	13.4
5a	A-U2GN, long	31.3	38.1	39	39.6	43.2	50.7	7,020	7.8	24.1
5b	A-U2GN, transverse	27.9	35.2	36.9	38.3	43.2	50.1	7,340	6.2	19.4

TABLE 4.11 (Cont'd)

Aluminium alloys – Bending tests on fatigue-cracked 20 x 20 mm bars

(c) Impact strength and static toughness.

No	K_{UF} J/cm²	G_{c} meas. daN/mm	η	V	K_c daN/mm$^{3/2}$	G_c daN/mm	P_u/P_T	$K_c/\sigma_{ult.}$	$\sigma_{ult.}/\sigma_{0.2}$
1	6.5		0.58	0.09	130	2.44	1.67	2.13	1.05
2	8		0.73	0.02	135	2.5	1.5	2.74	1.12
3	13.2	4	0.84	0.05	175	4.2	1.7	3.13	1.10
4a	8.7	2	0.71	0.05	132	2.4	1.6	2.6	1.09
4b	3.9	1.4	0.58	0.07	106	1.54	1.5	2.14	1.10
5a	6	1.9	0.78	0.03	122	2.1	1.7	2.84	1.09
5b	5	1.3	0.68	0.05	109	1.6	1.6	2.5	1.12

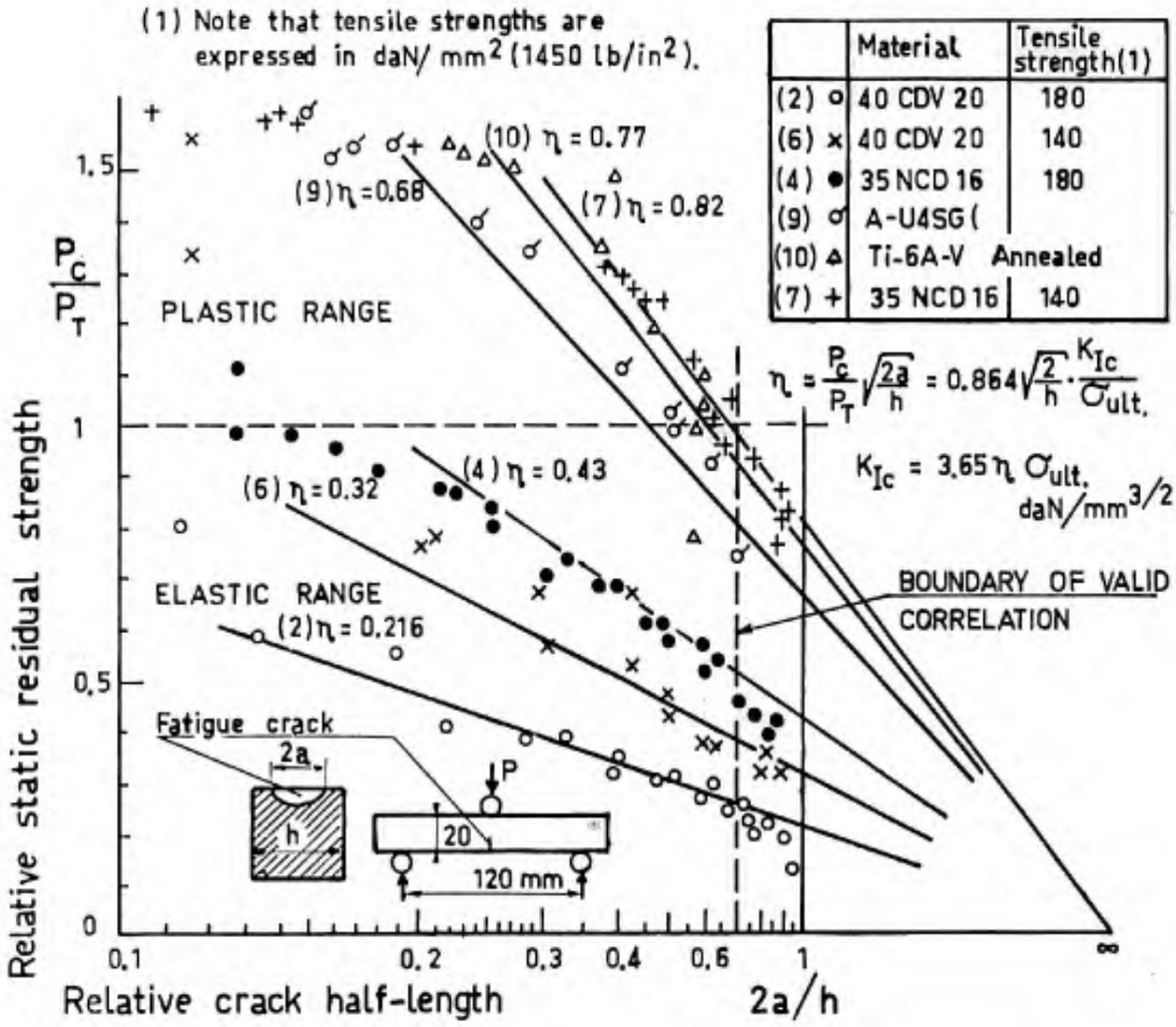

Fig.4.45 Relative static residual strength of bars containing a fatigue surface crack. Three-point bending tests by the Centre d'Essais Aeronautique de Toulouse

TABLE 4.12

Steels – Bending tests on fatigue-cracked 20 x 20 mm bars

(a) Compositions

No	*Designation*	*Form*	*Reference Origin*	*Second Melting*	*Composition, per cent:*											
					C	*Cr*	*Co*	*Ni*	*Mo*	*Mn*	*V*	*Al*	*Si*	*Ti*	*S*	*P*
1	25-CD4-S	30 mm-dia. bar	5C, France	Air	0.20	0.99		0.11	0.20	0.61			0.05			
2	15-CDV6	30 mm-dia. bar	5D, U.S., Vascojet 90	Air	0.16	1.28			0.84	0.74	0.22		0.10			
3	4340	30 mm-dia. bar	4E, U.S.,	Air	0.41	0.82		1.67	0.24	0.66			0.28			
4	35-NCD16	30 mm-dia. bar	4K, France	Air	0.39	1.56		3.80	0.45	0.35			0.23			
5	35-NCD16	30 mm-dia. bar	5E, France	Vacuum	0.40	1.85		4.02	0.45	0.47			0.28			
6a	35-NCD16	Thick plate	19298, Fr.	Air	0.39	1.96		4.17	0.47	0.60			0.36		<0.004	0.009
6b	35-NCD16	Thick plate	19298, Fr.	Vacuum	0.40	1.95		4.12	0.45	0.43			0.30		<0.002	0.004
7	40-CDV20	30 mm-dia. bar	9E, U.S., Vascojet 1000	Air	0.40	5		0.24	1.21	0.36	0.40		0.84		0.004	
8	40-CDV20	30 mm-dia. bar	3C, France	Air	0.44	5.3			1.3	0.26	0.51		0.92			
9	40-NDV18	35 mm-dia.	4M, France	Air	0.51	0.52		4.8	1.26	0.23	0.48		0.37			
10a		50 mm square bar	4P, France	Air	0.06		9.8	18.8	4.8	0.08		0.12	0.05	0.96		
10b		50 mm square bar	4Q, France	Vacuum	0.06		9.8	18.8	4.8	0.08		0.12	0.05	0.96		
11	YNC18	30 mm-dia. bar	4J, France	Air	0.06		8.4	18.5	4.4	0.04		0.30	0.07	0.72		
12	Vascomax 300 M	30 mm-dia. bar	2B, U.S.,	Air	0.03		9.1	18.3	4.7	0.06		0.06	0.09	0.57		0.006
13	Vascomax 300 M	30 mm-dia. bar	4H, U.S.,	Air	0.07		9.1	18.7	4.4	0.05		0.11	0.05	0.74		0.004

TABLE 4.12 (Cont'd)

Steels - Bending tests on fatigue-cracked bars

(b) Heat treatments

No	Designation	CEAT Reference	Pre-treatment	Austenite conditioning	Quenching	Refrigerating	Tempering	Cooling
1	25-CD4-S	5C		Air, 40', 870°C	Oil	No	1h, 525°C	Oil
2	15-CDV6	5D		Air, 1h, 970°C	Oil	No	1h15', 650°C	Oil
3	4340	4E	Yes	Salt, 40', 840°C	Oil	No	2h, 280°C	Oil
4	35-NCD16	4K, 2D	Yes	Salt, 30', 875°C	Air	No	1h, 220°C	Air
	35-NCD16	4K, F2D	Yes	Salt, 30', 875°C	Air	4h, -76°C	1h, 220°C	Air
5	35-NCD16	5E	Yes	Salt, 30', 875°C	Air	-10°C, 4h at -76°C	1h, 220°C	Air
6a	35-NCD16	19298	Yes	Air, 1h30', 875°C	Air	4h at -80°C	8h, 220°C	Air
6b	35-NCD16	19298, Z187	Yes	Air, 1h30', 875°C	Air	4h at -80°C	8h, 220°C	Air
7a	40-CDV20	9E	Yes	Salt, 15', 1010°C	Air	No	1h, 625°C	Air
7b	40-CDV20	9E, 14	Yes	Salt, 15', 1010°C	Air	No	1h + 1h, 610°C	Air
7c	40-CDV20	9E, 18	Yes	Salt, 15', 1010°C	Air	No	1h, 575°C	Air
7d	40-CDV20	9E, 18	Yes	Salt, 15', 1010°C	Air	No	1h + 1h, 580°C	Air
7e	40-CDV20	9E, 20	Yes	Salt, 15', 1010°C	Air	No	1h + 1h, 550°C	Air
8a	40-CDV20	3C	Yes	Salt, 15', 1010°C	Air	No	1h + 1h, 640°C	Air
8b	40-CDV20	3C	Yes	Salt, 15', 1010°C	Air	No	1h + 1h, 590°C	Air
9	40-NDV18	4M	No	Air, 30', 875°C	Air	No	1h, 350°C	Air
			Solution Treatment					
10a		4P	1h at 820°C		Air		3h at 435°C	
10b		4Q	1h at 820°C		Air		3h at 435°C	
11	YN 18C	4J	1h30' at 870°C		Air		4h at 480°C	
12	Vascomax 300 M	2B	1h at 820°C		Air		3h at 480°C	
13	Vascomax 300 M	4H	1h30' at 870°C		Air		4h at 480°C	

(Continued)

TABLE 4.12 (Cont'd)

Steels – Bending tests on fatigue-cracked bars

(c) Tensile properties, impact- and bending-toughness strengths

No	*Steel*	*CEAT Reference*	*Values in* daN/mm²							A %	Σ %	K_{UF} J/cm²	K_c daN/mm$^{3/2}$	$K_c/\sigma_{ult.}$	V	P_u/P_T	$\sigma_{ult.}/\sigma_{0.2}$
			σ_p	$\sigma_{0.05}$	$\sigma_{0.1}$	$\sigma_{0.2}$	$\sigma_{ult.}$	$\sigma^*_{ult.}$	E								
1	25-CD4-S	5C	80	90	95	97	107	175	19,500	14	62	114	380	3.5	0.09	1.8	1.10
2	15-CDVG	5D	78.5	97.5	101	104	110	200	20,500	17	67.5	107.5	390	3.5		2	1.06
3	4340	4E	134	142	144	146	178	235	19,500	11.2	42.5	17	145	0.82	0.03	1.85	1.21
4a	35-NCD16	4K, 2D	94.5	119	125	140	178	280	19,600	12	50	50	272	1.52	0.05	1.86	1.28
4b	35-NCD16	4K, F2D	89.4	119	130	141	181	248	18,500	10.7	41.5	49.5	272	1.5	0.05	1.88	1.28
5	35-NCD16	5E	100	124	132	144	182	256		12	45	50	306	1.68	0.10	1.88	1.27
6a	35-NCD16	19298				160	196			9	34	36	320	1.63	0.06		1.23
6b	35-NCD16	19298, Z187				161	194			12.3	40	70	395	2.04	0.06		1.21
7a	40-CDV20	9E, 140					140		18,100				257	1.84	0.12	1.8	
7b	40-CDV20	9E, 14				124	144		18,100	11	44		152	1.05	0.30		
7c	40-CDV20	9E, 18					180		18,100				113	0.63	0.07	1.9	
7d	40-CDV20	9E, 18	92	120	136	151	190	241	18,100	10	35		148	0.78	0.07		1.25
7e	40-CDV20	9E, 20	92	120	136	153	203	244	18,100	7.5	24.5		120	0.59	0.04		1.34
8a	40-CDV20	3C, 140	117				130		20,000	14		56	450	3.45	0.05		
8b	40-CDV20	3C, 180	127				179		20,000	11		43	144	0.8	0.06		
9	40-NDV18	4M, 180	130	150	157	162	181	200	20,000	7	26	34	258	1.44	0.06	1.82	1.12
10a		4P	137	162	167	175	182	295	16,600	8.7	41	30.5	175	0.96	0.30	1.83	1.04
10b		4Q	148	165	174	180	188	300	17,700	10.2	60	39.2	280	1.49	0.25	1.85	1.05
11	YN18C	4J	116	146	160	167	175	232	17,100	11.2	56	45	562	3.2	0.08	1.84	1.05
12	Vascomax 300 M	2B	127	160	168	175	184	254	16,500	9.5	54	46	500	2.72	0.05	1.8	1.05
13	Vascomax 300 M	4H	141	160	167	173	184	237	16,000	8.8	47	38	410	2.22	0.08	1.8	1.05

4.6 CONCLUSION

We have pointed out in Paragraph 4.3.4 for flat specimens with through-thickness cracks and in Paragraph 4.4.2 for semi-elliptical surface cracks that the values of K_{Ic} depend to a large extent on the critical crack length and on the possible difference between the initial shape and the equilibrium shape during crack propagation under a load leading to failure; this difference is affected by the method used to achieve the initial crack, by the specimen thickness, the general crack shape (part-through crack or surface crack), etc.

It may be interesting to compare the cracks in standard specimens with those frequently observed in service. Figure 4.46 shows a thin specimen with a central crack enlarged in fatigue by repeated tension; it is typical of the process in thin sheets loaded in tension and assembled by rivets or bolts. The central crack in Figure 4.46b grown from a slot that was increased by fatigue in bending and fractured in tension, does not correspond, in practice, to a frequent case and is therefore of little significance. As for the semi-elliptical crack in the tension specimen illustrated in Figure 4.46c, it involves parasitic bending loads which change with the crack dimensions and specimen thickness; it is representative only of a few cases among many others. The cracked bar loaded in bending mentioned previously and shown in Figure 4.46d has the advantage of containing a crack that develops while retaining the similarity of its shape in most engineering alloys; provided the thickness is sufficient, this specimen is fairly representative of cracks originating from surface defects such as that shown at section A-A of a cracked shaft in Figure 4.46f.

To simulate cracks contained in lugs as illustrated in Figure 4.46g, we suggest the use of the bar shown in Figure 4.46e with a crack starting at an edge; this type of crack is, in practice, often found on sharp edges that have not been blunted during fabrication. Finally, to represent cracks in shafts as shown in Figure 4.46b at section B-B near the shoulder, we can see no other possibility than the use of a specimen of similar design.

As regards thin sheet, we have already underlined the interest of the methods of KUHN or WELBOURNE, which require only elementary calculations based on the $\sigma - \epsilon$ curves of the materials.

In the case of thick parts with brittle behaviour, we have made no plasticity correction of the rough results. We believe that such a correction is not justified. First, the stress state tends toward triaxiality, which gives a yield stress greater than that of unnotched specimens. Secondly, WEISS, SESSLER, GREWAL and CHAIT[5], discussing the photo-stress measurements made by SPETNAK[68] and DIXON[4] on thin sheets with round V-notches, demonstrated that yielding occurs at the notch root only if the average net stress is quite close to the yield stress of the material, irrespective of the magnitude of the theoretical stress concentration factor. This result is attributed by the authors to the transverse retention of plastic flow which yields a surface slip concentration factor $K_{\epsilon,p}$ substantially equal to the elastic value until the plastic zone extends over the entire cross-section:

$$K_{\epsilon,p} = \frac{(\epsilon_p - \epsilon_q)_{max}}{(\epsilon_p - \epsilon_q)_{mean}} \qquad (93)$$

where ϵ_p and ϵ_q are the principal elongations.

The CHARPY or IZOD impact specimens have often been utilized by metallurgists in their studies on the effect of composition, heat treatment and fabrication methods on brittleness. The notch-impact strength is, now-a-days, no longer used as a significant physical quantity by engineers. In order to obtain a more selective quantity for the classification of materials from the point of view of brittleness and yet retain the impact specimen, since its small size permits easy sampling, the metallurgists deepen the V-groove in the CHARPY specimen by subjecting it to fatigue. A small-size crack specimen is thus obtained, as shown in Figure 4.47a. In three-point bending, this specimen can be broken slowly by a static load or, dynamically, by a ram impact, as in the conventional notched-bar impact test. In the latter case, the energy absorbed by fracture or the maximum load sustained during the test can be measured.

Figure 4.47b shows the size of another specimen used by FORD, RADON and TURNER[69] to investigate the effect of temperature, specimen size and loading rate on fracture. In Figure 4.47c, the related test data are plotted. The critical value of K_c of IRWIN's parameter was calculated by means of the SRAWLEY-BROWN[37] expression

$$K_c^2 = \frac{1}{1-\nu^2}\left(\frac{P}{B}\right)^2 \frac{L^2}{w^3}\left[31.7\left(\frac{a}{w}\right) - 64.8\left(\frac{a}{w}\right)^2 + 211\left(\frac{a}{w}\right)^3\right], \qquad (94)$$

where the crack depth, a, is equal to

$$a_0 + \frac{1-\nu^2}{6}\left(\frac{K}{\sigma_{0.2}}\right)^2,$$

i.e., the initial length, a_0, increased by a plasticity correction, w being the total specimen height, B the specimen thickness, L the half-length between the supports, P the breaking load, and ν POISSON's ratio (about 0.3). At low temperature, between $-200^{\circ}C$ and $-120^{\circ}C$, the steel investigated (1.6% Mn - 0.5 Ni - 0.30 Cr - 0.30 Mo - 0.30 Cu - 0.19 C ; $\sigma_{0.2} = 57$ daN/mm^2 , $\sigma_{ult.} = 69.5$ daN/mm^2 , A% = 23 , Z% = 53) exhibited a brittle behaviour such that the three tests yielded comparable results. With increasing test temperature, slow static fracture and fast impact fracture still give comparable results which vary little for small-size CHARPY

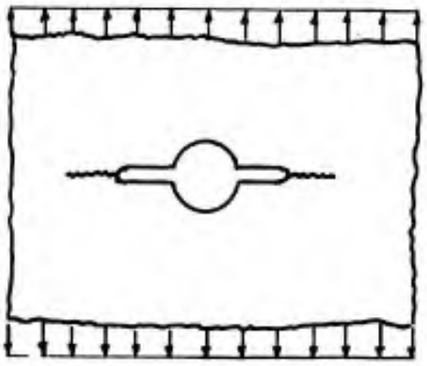

(a) A.S.T.M. THIN SPECIMEN CENTRE NOTCH LENGTHENED IN FATIGUE - TENSION.

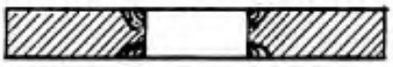

(b) CENTRE SLOT SHARPENED IN BENDING FATIGUE.

(c) TENSION SPECIMEN SEMI-ELLIPTICAL CRACK.

(d) BEND SQUARE BAR - SURFACE CRACK.

(e) BEND SQUARE BAR - EDGE CRACK (proposal).

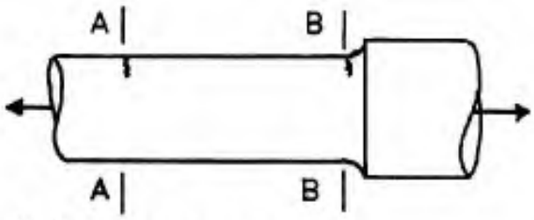

(f) CRACKED SHAFT.

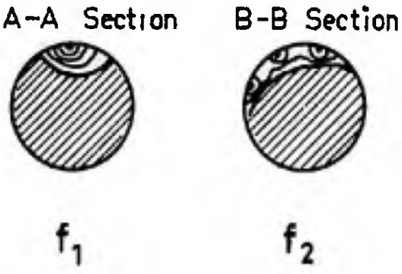

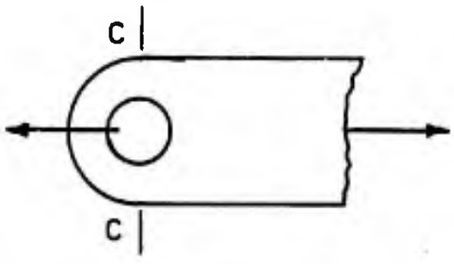

(g) CRACKED LUG

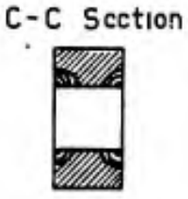

Fig. 4.46 Crack types

specimens; the apparent K_c value of the large-size specimens is, however, considerably influenced by an increase in the test temperature. In fact, the material exhibits plastic behaviour and the load increases whilst the crack grows. As with thin sheets, we consider that the minimum value K_{Ic} of K_c is more easily attained on small-size specimens, provided the material is brittle enough for the nominal stress to remain below the conventional yield strength.

As in the case of geometrical notches, the strength can be changed by residual stresses due to pre-loading. For instance, the aforementioned authors report the case of a specimen, with a notch on the compression side, that was first subjected to inverse bending at – 75°C for determination of the nominal yield strength, and then tested under normal conditions at the same temperature. The K_c-value thus obtained was approximately a quarter of that found in a direct test. *The detrimental effect of the residual tensile stresses induced by previous compression is again apparent.*

We shall bear in mind that *the various methods proposed for the experimental determination of* K_{Ic} *may be considered as valid for a first classification of the materials with regard to their brittleness in the presence of fatigue cracks, provided the specimens and test conditions are the same for all tests.* In all cases, the numerical results obtained should be used with caution for strength predictions of actual cracked components.

Furthermore, it is noteworthy that in practice *brittle failures of cracked parts are often caused by tensile loads applied in the short transverse direction,* that is, perpendicular to the rolling, forging or dye-forging plane. In this direction, ductility is often very low and can be further reduced if the material is *sensitive to stress-corrosion.*

The advanced methods for milling aircraft wing box panels from thick plates may involve tensile stresses in the direction of the thickness to be generated by secondary loads, and, consequently require a high degree of ductility in this direction. With thick plates of A-U4SG (similar to American 2014), tension tests on micro-specimens cut from plates in the direction of the thickness resulted in unmeasurable elongations at failure; improvement of the forging process by previous "kneading" in the three directions before final rolling to thickness has given A% = 3, compared to about 10% in the direction of the rolling.

In thick plates, there are six different orientations for crack specimen sampling. In Figure 4.48, from PAYNE[70], these orientations are identified by the direction of the specimen length and the direction of crack propagation. Results of PELLISSIER[71] relating to maraging steel (250) are reported by PAYNE:

G_{Ic} =	5.55	4.35	4.10	2.67	daN/mm
Specimen direction	Length	Length	Width	Thickness	
Crack propagation	Thickness	Width	Length	Width	

To study the brittleness in any of the directions, KAUFMAN and HUNSICKER[72]; from ALCOA, devised the specimen illustrated in Figure 4.49 and having a V-notch of very small radius. In the plot of the load-elongation curve, fracture toughness is characterized by the nominal bend-tension stress corresponding to the maximum stress before failure,

$$P/A + Mv/I = P/bt + 3P/bt = 4P/bt ,$$

and by the *unit energy of crack propagation,* defined as the quotient of the work of the load – from the attainment of the maximum value to failure – by the net cross-sectional area to be fractured:

$$(\int P.\Delta l)/bt .$$

One may hope that investigations of this sort will allow the development of a test that is simple enough to provide comparative data on the strength of engineering metals for the three principal directions involved in the service behaviour of actual parts.

KIES, SMITH, ROMINE and BERSTEIN[73] have studied the brittleness of weldments in maraging steel (250) containing 18.4 % Ni – 4.7 % Mo – 8.5 % Co – 0.4 % Ti – 0.13 % Al with $\sigma_{ult.}$ = 186 daN/mm² (270,000 lb/in²), $\sigma_{0.2}$ = 172 daN/mm², A % = 4 and Σ % = 30. With ν = 0.3 and E = 18,000 daN/mm², G_{Ic} and K_{Ic} had the following values:

Unwelded plates	G_{Ic}, daN/mm	K_{Ic}, daN/mm$^{3/2}$	$\nu(K_{Ic})$
Longitudinal direction	4.25	295	0.041
Transverse direction	3.55	270	0.06

The strength was little affected by the weldments.

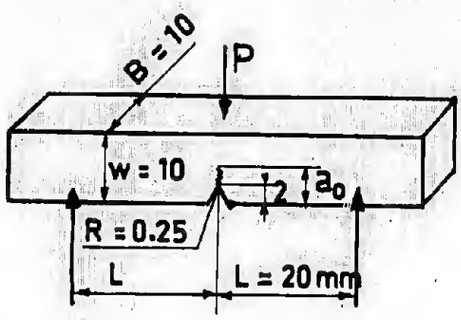

(a) Cracked Charpy specimen

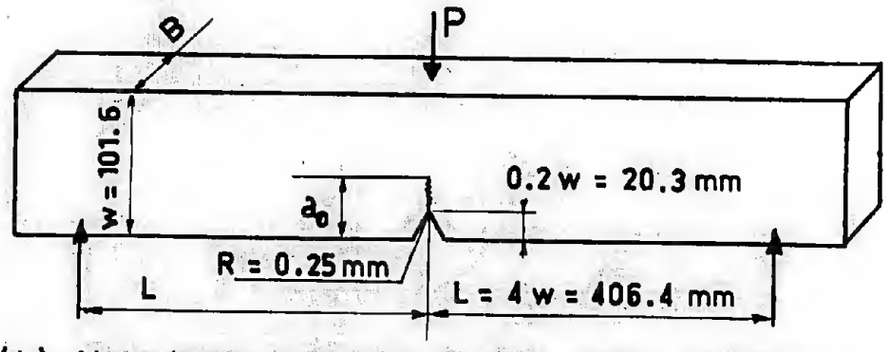

(b) Very large specimen on the gross thickness B of the plate, $2 < \frac{w}{B} < 8$.

(c) Values of K_c

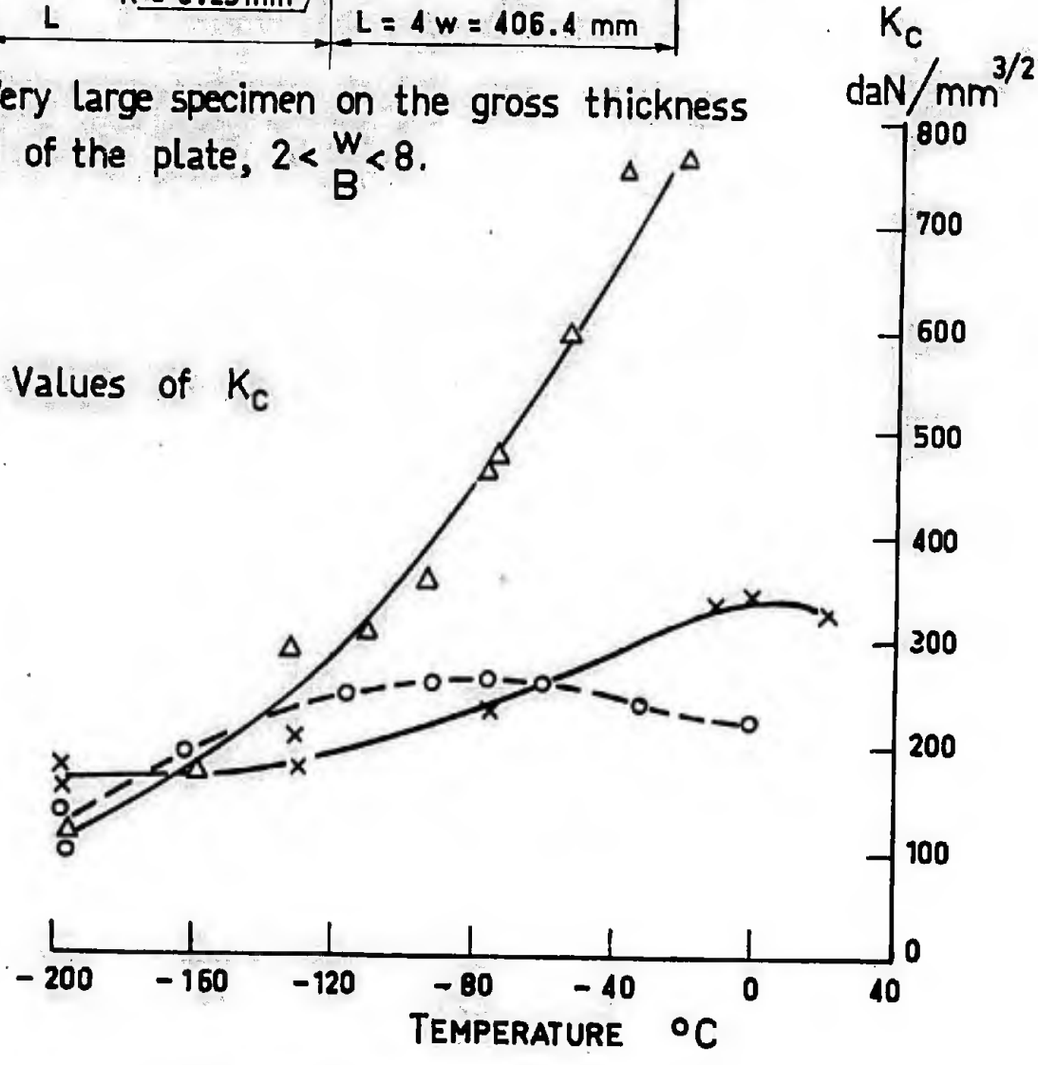

Fig. 4.47 Measured K-values, after Ford, Radon and Turner[42]

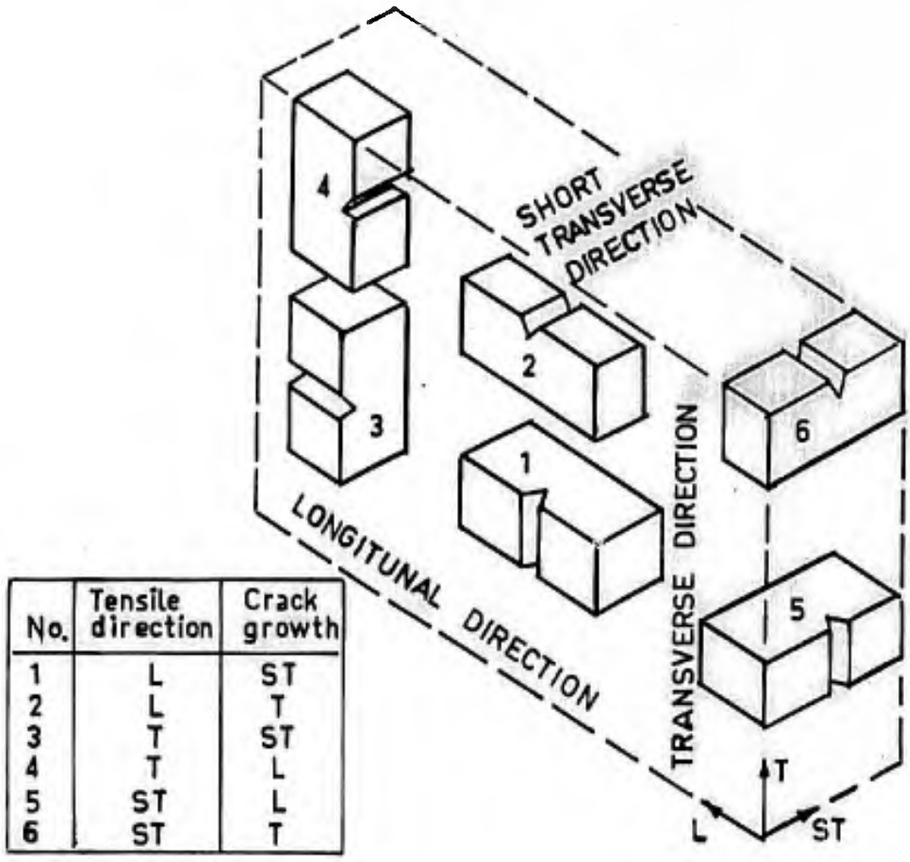

No.	Tensile direction	Crack growth
1	L	ST
2	L	T
3	T	ST
4	T	L
5	ST	L
6	ST	T

Fig.4.48 Various positions of specimens in a thin plate

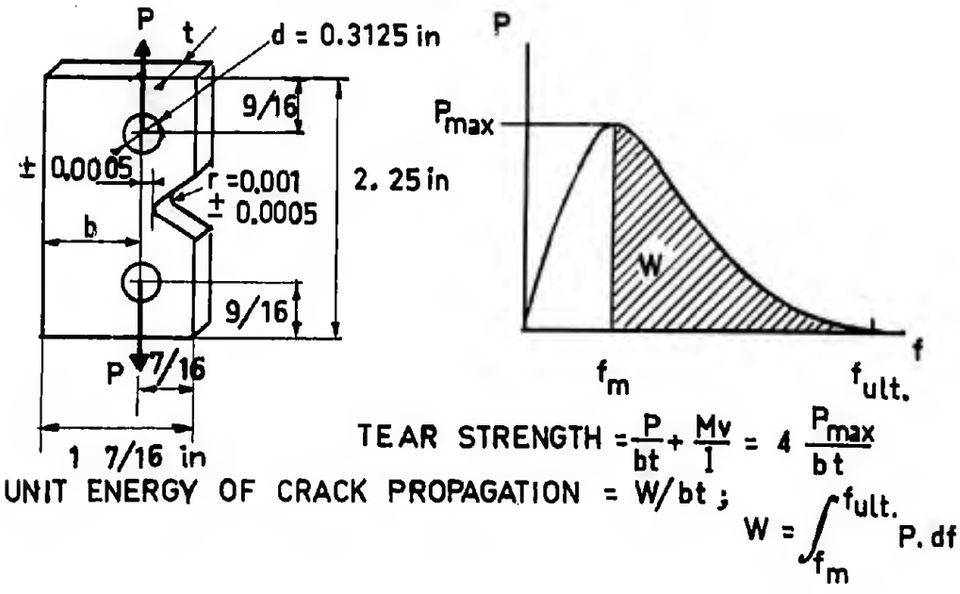

$$\text{TEAR STRENGTH} = \frac{P}{bt} + \frac{Mv}{I} = 4\,\frac{P_{max}}{bt}$$

$$\text{UNIT ENERGY OF CRACK PROPAGATION} = W/bt\,; \qquad W = \int_{f_m}^{f_{ult.}} P.\,df$$

Fig.4.49 Tear energy specimen

REFERENCES

4.1 Dana, A.W. et al. — NACA TN 1830, 1831, March 1949.

4.2 Weiss, V. et al. — WADD Technical Report 60-310, Wright Air Development Division, September 1960.

4.3 — Etablissement Aéronautique de Toulouse; PV M3-7873 (January 1966), PV 39317 (September 1963), PV M4 7743 (April 1966), PV 32531 (March 1966), PV MO 7334/2 (August 1965).

4.4 Dixon, J.R. — *Elastic-plastic Strain Distribution in Flat Bars Containing Holes or Notches.* Journal of the Mechanics and Physics of Solids, Vol.10, 253, 1962.

4.5 Weiss, W. et al. — *The Effect of Stress Concentration on the Fracture and Deformation Characteristics of Ceramics and Metals.* Techn. Documentary Report No ASD-TDR-63-380, Syracuse University, April 1963.

4.6 Weiss, V. et al. — *Effect of Section Size on Notch Strength.* Journal of Basic Engineering, Trans. of the ASME, 675-681, September 1966.

4.7 Weibull, W. — *A Statistical Theory of the Strength of Materials.* Proceedings, Royal Swedish Instr. Engr. Research, No.151, 1939. *The Phenomenon of Rupture in Solids.* No.153, 1939.

4.8 Griffith, A.A. — *The Phenomena of Rupture and Flow in Solids.* Philosophical Transactions, Roy. Soc. (London), Series A, Vol.221, 163-198, 1920.

4.9 Irwin, G.R. — *Fracture.* Encyclopedia of Physics, Vol.6, 551-590, Springer, 1958.

4.10 Kuhn, P. — *Fracture Toughness Testing and its Applications.* Panel Discussion, p.389, 1964. ASTM Special Technical Publication No.381, 1965.

4.11 Kuhn, P. — *Notch Effects on Fatigue and Static Strength.* Symposium ICAF – AGARD on Aeronautical Fatigue, Roma, 1963.

4.12 Welbourne, E.R. — *The Correlation of Unstable Crack Length Data for Sheet Materials.* The Aeronautical Quarterly, Vol.12, November 1961.

4.13 Inglis, C.E. — *Stresses in a Plate due to the Presence of Cracks and Sharp Corners.* Proceedings, Inst. Naval Architects, Vol.60, 1913.

4.14 Muskhelishvili, N.I. — ZAMM (in Germany), 264-282, 1933; English translation, P.Noordhoff and Co., 1953.

4.15 Weiss, V. et al. — WADD Technical Report 60-310, September 1960.

4.16 Mendelson, A. Spero, S.W. — NASA TN D-2260, 1964.

4.17 Westergaard, H.M. — *Bearing Pressures and Cracks.* Transactions ASME, Journal of Applied Mechanics, Vol.6, No.2, 1939.

4.18 Paris, P.C. — *The Trend in Engineering.* Vol.13, No.1, 9, University of Washington, Seattle, January 1961.

4.19 Anderson, W.E. Paris, P.C. — Engineering Quarterly, Vol.1, No.2, ASM, May 1961.

4.20 Dixon, J.R. — Journal Royal Aeronautical Society, March 1960.

4.21 Paris, P.C. Sih, G.C. — *Stress Analysis of Cracks.* P.30-38 in the same publication as Reference 4.10.

4.22 Isida, M. — *On the Tension of a Semi-Infinite Plate with an Elliptic Hole.* Trans. Japan Soc. Mechanical Engineers. Vol.22, 1956. *The Effect of Longitudinal Stiffener in a Cracked Plate Under Tension.* Proceedings fourth US Congress of Applied Mechanics, 1962.

4.23 Kaufman, J.G. — Discussion of the HEYER's paper, Reference 4.24.

4.24 Heyer, R.H. — *Evaluation of Proposed Recommended Practice for Sharp-Notch Tension Testing.* In ASTM Special Publication 381, 199-209, 1965.

4.25 — *Fracture Testing of High-Strength Sheet Materials.* Report of a special ASTM committee, January 1960.

4.26 Weiss, V. Yukawa, S. — *Critical Appraisal of Fracture Mechanics.* In ASTM, STP No.381, 1-29, 1965.

4.27 Liu, H.N. — Discussion of the Reference 4.26.

4.28 — *Fracture Toughness Testing and its Applications.* ASTM, Special Publication No.381, p.406.

4.29 Wells, A.A. — *Notched Bar Tests, Fracture Mechanics and Strength of Welded Structures.* British Welding Journal, Vol.12, No.1, January 1965.

4.30 Burdekin, F.M. Stone, D.E.W. — Fracture Mechanics Progress Report C 140/1, 1964. British Welding Research Assn. 1965.

4.31 Beachem, C.D. Pelloux, R.M.N. — *Electron Fractography - A Tool for the Study of Micromechanisms of Fracturing Processes.* 210-245 in Reference 4.28.

4.32 Barenblatt, G.I. — *Mathematical Theory of Equilibrium of Cracks in Brittle Fracture.* Advances in Applied Mechanics, Vol.7, Academic Press, New York, 1962.

4.33 Irwin, G.R. Kies, J.A. — Welding Journal, Supp. Vol.31(2), 95-S, February 1952.

4.34 Douillet, D. et al. — Revue de Métallurgie, Vol.61, No.10, 877-883, October 1964.

4.35 Barrois, W. — *Résistance Statique des Eprouvettes et des Eléments Fissurés.* Second part, DOC-AIR-ESPACE No.92, 13-32, May 1965.

4.36 Krafft, J.M. et al. — *Effect of Dimensions on Fast Fracture Instability of Notched Sheets.* Crack Propagation Symposium, Cranfield, 1961.

4.37 Srawley, J.E. Brown, W.F. Jr — *Fracture Toughness Testing.* p.133-198 in Reference 4.28.

4.38 Lubahn, J.D. — *Experimental Determination of Energy Release Rates for Notch Bending and Notch Tension.* Proceedings ASTM, Vol.59, 885-915, 1959.

4.39 Christensen, R.H. Denke, P.H. — *Crack Strength and Crack Propagation Characteristics of High Strength Metals.* Techn. Doc. ASD.TR-61-207, January 1962.

4.40 Slinery, J.L.Jr — *Notch Properties of Five per cent Chromium-Molybdenum-Vanadium Steel Sheet as Affected by Heat Treatment, Test Temperature and Thickness.* Preprint 72, ASTM, 1962.

4.41 Repko, A.J. et al. — *Influence of Sheet Thickness on Sharp-Edge-Notch Properties of a Titanium Alloy at Room and Low Temperatures.* ASTM, STP No.302, 213, 1962.

4.42 Williams, M.L. — *Some Observations Regarding the Stress Field Near the Point of a Crack.* Symposium on Crack Propagation, Cranfield, Proceedings, 1961.

4.43 Bowie, O.L. — Journal of Mathematics and Physics, Vol.25, 60, April 1960.

4.44 Winne, D.H. Wundt, B.M. — *Application of the GRIFFITH-IRWIN Theory of Crack Propagation to the Bursting Behaviour of Disks, Including Analytical and Experimental Studies.* Trans. ASME, Vol.80, No.8, November 1958.

4.45 Neuber, H. — *Kerbspannungslehre.* Springer, 1948.

4.46 Bowie, O.L. — *Rectangular Tensile Sheet with Symmetric Edge Cracks.* Trans. ASME, Journal Applied Mechanics, Vol.31, Ser. E, No.2, 208-212, June 1964.

4.47 Gross, B. et al. — NASA, TN D-2395, 1964.

Srawley, J.E. et al. — NASA TN D-2396, 1964.

4.48 Gross, B. Srawley, J.R. — NASA TN D-2603, 1965.

4.49 Lubahn, J.D. — Proc. ASTM, Vol.59, 885-913, 1949.

4.50 Bueckner, H.F. — *Boundary Problems in Differential Equations*. Langer ed.; Univ. of Wisconsin Press, 215, 230, 1960.

4.51 Wundt, B.M. — *An Unified Interpretation of Room-Temperature Strength of Notched Specimens as Influenced by their Size*. ASTM Publication, Paper No.59, Met-9, February 1959.

4.52 Gilman, J.J. — *Fracture*. John Wiley and Sons, Inc., New York, 1964.

4.53 Irwin, G.R. — *Crack Extension Force for a Part-Through Crack in a Plate*. Trans. ASME, Journal of Applied Mechanics, 651-654, December 1962.

4.54 Green, A.E. Sneddon, I.N. — *The Distribution of Stress in the Neighbourhood of a Flat Elliptical Crack in an Elastic Solid*. Proc. of Cambridge Philosophical Society, Vol.46, 159-164, 1950.

4.55 Fichter, W.B. — *Stresses at the Tip of a Longitudinal Crack in a Plate Strip*. NASA TR-265, April 1967.

4.56 Kassir, M.K. Sih, G.C. — *Three-Dimensional Stress Distribution Around an Elliptical Crack Under Arbitrary Loadings*. Journal Applied Mechanics, 601-609, September 1966.

4.57 Srawley, J.E. Beachem, C.D. — *Fracture of High-Strength Sheet Steel Specimens Containing Small Cracks*. ASTM Special Publication No.302, 1961.

4.58 Corn, D.L. Mixon, W.V. — Douglas Aircraft paper, September 1965.

4.59 McEvily, A.I. Illg, W. — NASA TN 4394, 1958. NASA TN D-52, 1959.

4.60 Donaldson, D.R. Anderson, W.E. — *Crack Propagation Behaviour of Some Airframe Materials*. Crack Propagation Symposium, Cranfield, 1961.

4.61 Heywood, R.B. — *Designing by Photo-Elasticity*. Chapman and Hall, London, 1952.

4.62 Kuhn, P. — *Residual Strength in the Presence of Fatigue Cracks*. (Part I), AGARD Structures and Materials Panel, Meeting of TORINO, April 17, 1967.
Residual Strength in the Presence of Fatigue Cracks. (Part II), Meeting of OTTAWA, September 25, 1967.

4.63 Kuhn, P. Figge, I.E. — *Unified Notch-Strength Analysis for Wrought Aluminium Alloys*. NASA TN D-1259, 1962.

4.64 McEvily, A.J. Jr et al. — *Static Strength of Aluminium-Alloy Specimens Containing Fatigue Cracks*. NASA (NACA) TN 3816, October 1958.

4.65 Figge, I.E. — *Residual Strength of Alloys Potentially Useful in Supersonic Aircraft*. NASA TN D-2613, 1965.

4.66 Crichlow, W.J. — *Ultimate Strength of Damaged Structures*. Proc. ICAF-AGARD Symposium, Amsterdam, Pergamon Press, 1959.

4.67 Douillet, D. — Revue de Métallurgie, No.9, p.725-730, Paris, September 1966.

4.68 Spretnak, J.W. Ault, R.T. — *Initial Yielding and Fracture in Notched Sheet Molybdenum*. ASD-TDR-62-223, 1962.

4.69 Ford, G. et al. — *Fracture Toughness of a Medium Strength Steel*. Imperial College of Science and Technology, Department of Mechanical Engineering, London, 1967.

4.70 Payne, W.F. — *Incorporation of Fracture Information in Specifications*. ASTM Special Publication No.381, p.357-372, 1965.

4.71 Pellissier, G.E. — *Some Microstructural Aspects of Maraging (250) Steel in Relation to Strength and Toughness*. Third Maraging Steel Review Conference, RTD-TDR-63-4048, p.407-428, Wadd, Dayton, Ohio, 1963.

4.72 Kaufman, J.G. Hunsicker, H.Y. — *Fracture Toughness Testing at ALCOA Research Laboratories*. ASTM, STP, No.381, p.290-308, 1965.

4.73 Kies, J.A. et al. — *Fracture Testing on Weldments*, ASTM, STP, No.381, p.328-356, 1965.

4.74 Greenspan, M. — *Axial Rigidity of Perforated Structural Members.* Journal Research Nat. Bureau of Standards, Vol.31, No.27/57, December 1957.

4.75 Lacey G.C. — *The Residual Static Strength of Structures Containing Cracks.* Aeronautical Research Laboratories, S and M Report 288, April 1962.

4.76 Taylor, J. — *Manual of Aircraft Loads.* AGARD, Pergamon Press, 1965.

4.77 Smith, F.W. et al. — *Stress Intensity Factors for Semicircular Cracks, Part 2 – Semi-infinite Solid.* Journal of Applied Mechanics, p.953, December, 1967.

4.78 Broek, D. — *The Residual Strength of Cracked Sheet. Tests Interrupted After Intermediate Slow Crack Growth.* NLR – TR M.2145, Amsterdam, July 1965.

4.79 Broek, D. — Private Communication, 1968.

4.80 Broek, D. — *The Effect of Finite Specimen Width on the Residual Strength of Light Alloy Sheet.* NLR – TR M.2152, Amsterdam, September 1965.

4.81 Carman, C.M. et al. — First Int. Conf. on Fracture, (Sendai, 1965), Vol.2, p.995.

4.82 Brown, W.F. Jr Srawley, J.E. — *Plane Strain Crack Toughness Testing of High Strength Metallic Materials.* ASTM Special Technical Publication No.410, 1966.

4.83 Feddersen, C.E. — In discussion of the Reference 82, p.79.

4.84 Fisher, D.M. et al. — *Design and Use of Displacement Gage for Crack Extension Measurements.* NASA TN D-3724, November 1966.

4.85 Broek, D. — *The Effect of the Sheet Thickness on the Fracture Toughness of Cracked Sheet.* NLR – TR M.2160, Amsterdam, January 1966.

4.86 Broek, D. — *The Residual Strength of Cracked Sheet and Structures.* NLR – TM.2135, Amsterdam, August 1964.

4.87 Broek, D. — *The Residual Strength of Aluminium Alloy Sheet Specimens Containing Fatigue Cracks or Saw Cuts.* NLR – Report M.2143, Amsterdam, February 1965.

4.88 Bluhm, J.I. Morissey, R.J. — *Fracture in a Tensile Specimen.* Proc. First International Conference on Fracture, Vol.3, 1739-1780, 1965.

CHAPTER V

PHYSICAL CHANGES AND DAMAGE DURING FATIGUE

W.Barrois: Fatigue of Structures, Vol.I,
"Fundamental and Physical Aspects", AGARD, 1970

PHYSICAL CHANGES AND DAMAGE DURING FATIGUE

5.1 PLASTIC PROCESS PRIOR TO THE APPEARANCE OF VISIBLE CRACKS

We have seen in Chapter II, Paragraph 2.2.2, that plastic, static, creep or fatigue straining causes simultaneous softening and hardening of the material and, consequently, an increased local diversification of the latter; some domains become plastically more rigid than the bulk of the material and hence carry a larger portion of the applied load. However, this increase in stiffness remains limited; indeed, it may be concomitant with a general softening of the material. Thus, the most stable obstacles to plastic slip are overstressed and surrounded by a high-stress field. In addition, some dislocations are stopped by these obstacles and pile up against them, while vacancies are created in the crystalline lattice and the overstressed region exhibits less strength in cleavage under normal tensile stresses.

We have also pointed out that the plastic changes of the bulk of the material are governed by the following law:

> Static or alternating loads tend to modify the previous strain-hardened state associated with the mechanical and thermal history of the material by substituting a new state independent of the former and consistent with the new load applied (see Paragraph 2.1.3). In particular, initially annealed materials tend to harden and initially cold-worked tend to soften under fatigue.

5.1.1 Adjustments and Creep during Fatigue

As stated in Paragraph 2.1.3, the reversed stress-strain loop of an initially cold-worked material widens during fatigue toward a stable shape. If the straining occurs under a reversed stress of constant amplitude, $2\sigma_0$, the amplitude of the reversed strain in the stable condition, $2\epsilon_2$, is greater than its original value, $2\epsilon_0$ (Fig. 5.1). If a reversed strain, $2\epsilon_0$, is imposed on the specimen, the corresponding value of the stress, σ_1, is smaller than the original, σ_0.

These conditions would be inverse for an initially annealed material stressed above its yield strength; thus, the reversed strain in a constant-stress-range test with σ_0 tends to decrease whilst the stress in a constant-strain-range test with ϵ_0 tends to increase.

This process is of paramount importance for a clear understanding of the fatigue behaviour of notched and cracked specimens. A small volume of material at the notch root or at the crack tip is subject to very high stresses which cause rapid plastic changes during fatigue. The strains at the boundary of this region remain elastic owing to the elastic behaviour of the remainder of the material. The small plastic domain is therefore subjected on a gross basis to constant-strain-amplitude fatigue which result in a decrease of the local stresses if the material has been initially cold-worked. Now we have seen that the plastic flow process depends mainly on shear strains while crack propagation is also influenced by tensile stresses. Crack propagation will be delayed by plastic adjustments if the material is subjected to a strain cycle of constant amplitude and softens. In the case of a material hardened by fatigue, no assertion can be made because the plastic process, which increases the normal tensile stress, also causes a decrease in plasticity and hence reduces the subsequent changes.

Again, this phenomenon accounts for the different shapes of the fatigue-life curves obtained with the two types of loading, i.e., *constant-stress-range tests* and *constant-strain-range tests*.

Since Wöhler, almost all the engineering fatigue tests have been carried out under constant nominal-stress amplitude. Actually, constant-load-range bending tests[2] and tension-compression tests on mildly notched specimens are intermediate cases since the stress and strain values vary at the surface during the tests. The same difficulty is encountered in interpreting the data from constant-strain-range tests.

5.1.1.1 Static and Cyclic σ-ϵ Curves after Fatigue

If stabilized σ-ϵ loops from constant-stress-amplitude or constant-strain-amplitude tests are considered (Fig. 5.2), the set of points $(\Delta\sigma/2, \Delta\epsilon/2)$ describes a cyclic σ-ϵ loop. For materials such as annealed or severely cold-worked copper in which no crystalline phase change is caused by fatigue, tests by Tuler[3] showed that after fatigue the static σ-ϵ curves are very similar to those obtained on the same specimen by incrementally increasing the stress and by measuring the strain after each increment as soon as the loop has become stable. As in the case of static curves, if we consider the true stress P/A, where P is the load and A the cross-sectional area, and the true strain $\epsilon^* = \int dl/l$, we find that the cyclic σ-ϵ curves satisfy the relation

PRECEDING PAGE BLANK

BLANK PAGE

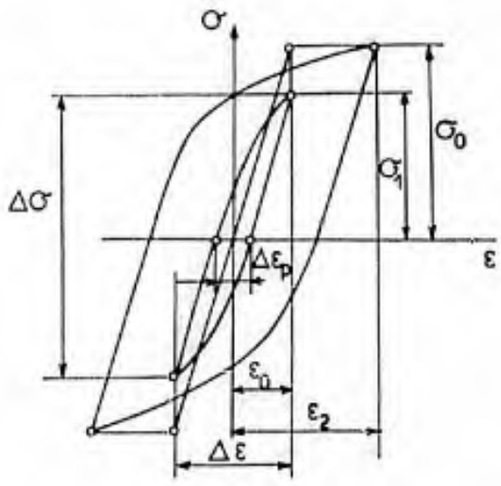

Fig.5.1 Changes in stress-strain loop during fatigue

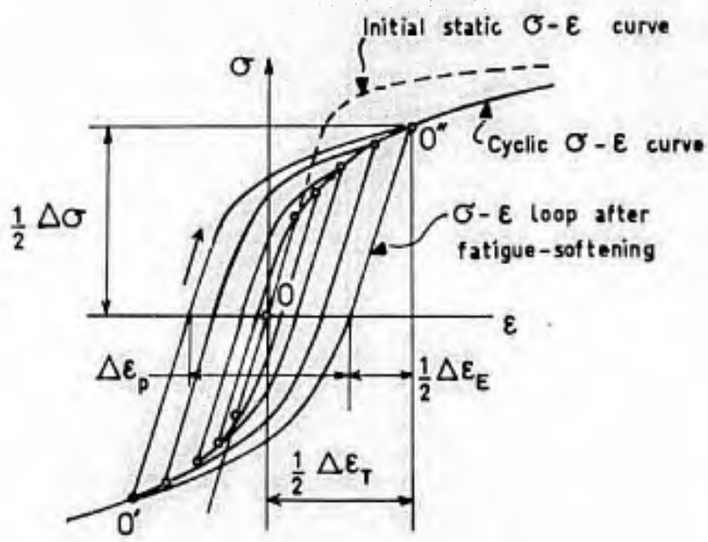

Fig.5.2 Stress-strain loops and stress-strain static and cyclic curves

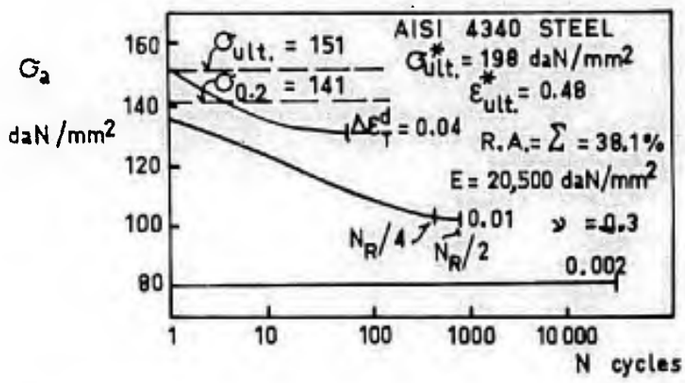

Fig. 5.3 Changes in alternating stress during fatigue tests under fixed alternating strain, after Smith, Hirschberg and Manson[5]

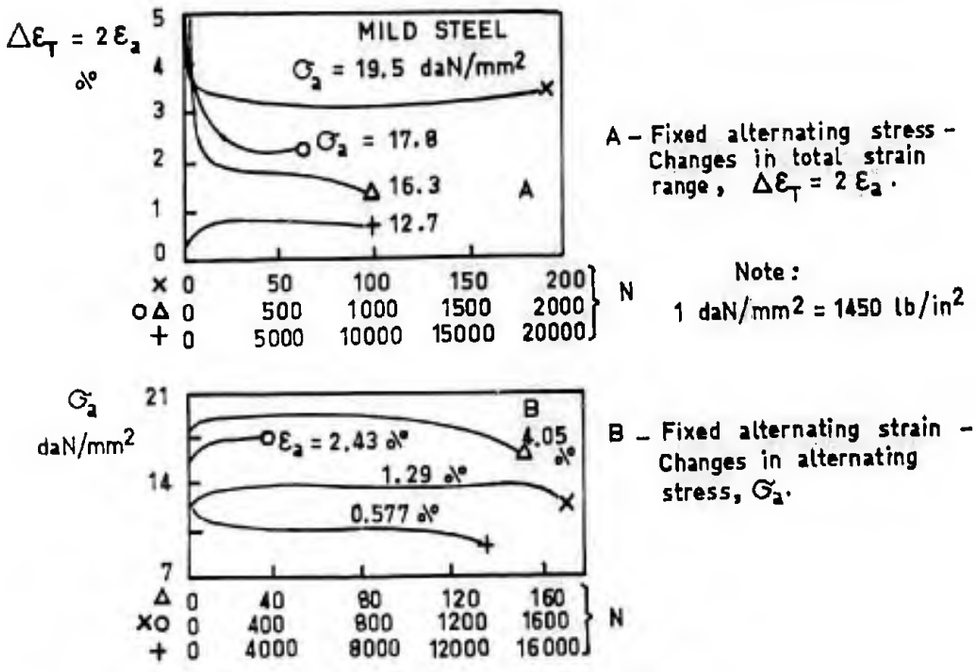

Fig. 5.4 After Benham and Ford[6]

$$\epsilon^{\bullet} = \sigma/E + \epsilon^{\bullet}_{ult.}\,(\sigma/\sigma^{\bullet}_{ult.})^{1/n}\,, \qquad (1)$$

where $\epsilon^{\bullet}_{ult.}$ = true elongation at static failure: $\epsilon^{\bullet}_{ult.} = \log_e\left(\frac{1}{1-\Sigma}\right)$,

Σ = reduction in area = $(A_o - A_{ult.})/A_o$,

A = cross-sectional area, initial (A_o) or at failure $(A_{ult.})$,

$\sigma^{\bullet}_{ult.}$ = true ultimate stress = $F_{ult.}/A_{ult.}$,

n = *strain-hardening exponent.*

For initially cold-worked materials or quenched and tempered carbon steels, n is smaller on the cyclic curve than on the static curve. Considering two half-loops originating respectively at point 0′ and point 0″, Halford[4] observed that each half-loop could be obtained approximately from the cyclic σ–ϵ curve 0′ 0″ by multiplying the ordinates and the abscisses by a factor 2.

Instead of measuring the axial strain $\Delta\epsilon/2$ of the tension-compression test, Smith, Hirschberg and Manson[5] measured the diametrical contraction on the specimen, which is easier to perform in practice and permits the use of specimens with an hour-glass shape (waisted specimens). The amplitude, $\Delta\epsilon^{d}_{T}$, of the diametrical total cyclic contraction is measured and the amplitude, $\Delta\epsilon^{l}_{T}$, of the axial total cyclic strain is calculated as follows:

$$\Delta\epsilon^{l}_{T} = 2\Delta\epsilon^{d}_{T} + (1 - 2\nu)\frac{\Delta\sigma}{E}\,. \qquad (2)$$

Figure 5.3, relating to an American ultra-high-strength steel (AISI 4340), shows that the change in the σ–ϵ loop under an imposed $\Delta\epsilon^{d}_{T}$ is slow for hard metals as used in the manufacture of structures; our opinion is that obstacles to plastic slip are very stable in that case. However, in most materials investigated, the process is practically complete after one-quarter of the fatigue life.

In mild steel the hardness does not result from a metallurgical transformation but from strain-hardening which implies a much faster plastic process, as illustrated in Figure 5.4, from Benham and Ford[6]. In a constant-strain-range test (Fig. 5.4(b)) the process is complete after one-tenth of the life; on the contrary, in a constant-stress-range test the process is both more significant and slower. This can be explained by the fact that the stress assumes a constant amplitude in the latter case whereas it decreases in the former case and thus restrains the plastic process.

5.1.1.2 Physical Changes in Constant-Stress-Range or Constant-Strain-Range Tests

Figures 5.5.(a) and 5.5(b), concerning an initially cold-worked material which softens in fatigue, show the variation of the σ–ϵ curve under repeated strain or stress of constant amplitude. In a constant-strain-range test the loop tends toward a stable shape under a stress varying between a positive and a negative value which become increasingly similar in magnitude. In a constant-stress-range test the specimen length is gradually increased by *fatigue creep*. This leads us to the second law examined in Chapter II, Paragraph 2.1.3:

> A reversed strain superimposed on a steady static stress partly destroys the previous cold-work and is likely to cause plastic flow or creep in the direction of the static stress. This accounts for the changes occurring in the residual stresses which tend to disappear during fatigue.

Two examples have already been given, namely Figure 2.22 in Paragraph 2.1.3, from Bairstow, for steel, and Figure 3.52, from Kennedy, for the creep of lead. The same phenomenon was observed by Coffin[7] for the cyclic tension of annealed copper and the static torsion of American 2S aluminium subjected to reversed axial tension. Feltner[8] studied the effect of reversed stress on the creep of copper, aluminium and cadmium at -195°C and +27°C. In Figure 5.6, it is seen that for aluminium at +27°C, the elongation under constant maximum stress is at first less rapid with increasing minimum stress, the test duration at high stress being shorter; the yield passes through a minimum for $\sigma_{min}/\sigma_{max} = 0.25$ and the increases, assuming such values that failure occurs under a repeated load with $\sigma_{min} = 0$. Recently, Plenard and Plessier[9] have reported a case of fatigue creep in cast iron.

5.1.1.3 Development and Variation of Residual Stresses in Constant-Strain-Range Tests

Let us return to Figure 5.5(a): the change in the loop can be associated with a compressive residual stress under zero strain. Now suppose a first strain of very high value due to overloading and followed by a repeated strain test. Figure 5.7 shows how the static residual stress due to overloading under ϵ_1 varies and decreases through a change in the loop for a strain range included between 0 and $\epsilon_2 < \epsilon_1$: the residual stress approaches the value corresponding to the fatigue load. However, as will be explained later, fatigue exerts a more complex effect owing to variations in the density of the material caused by the dislocations or, in the case of some alloys, by phase changes similar to those which take place in the austenite-martensite transformation of steels.

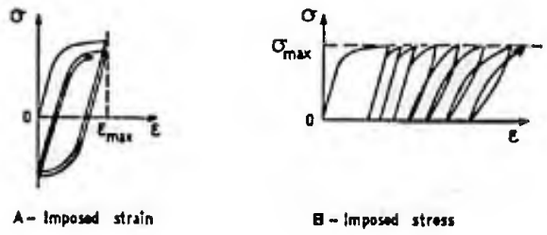

Fig. 5.5 Changes in stress-strain loop under repeated fatigue loading

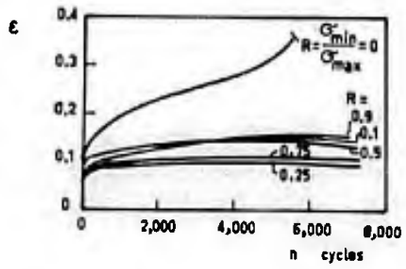

Fig. 5.6 Creep of aluminium at room temperature, after Feltner[5]. The creep is favoured by the unloading

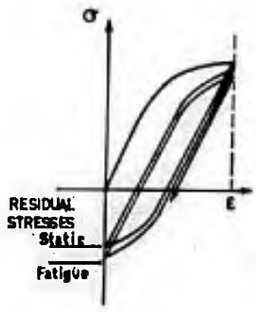

Figure 5.7

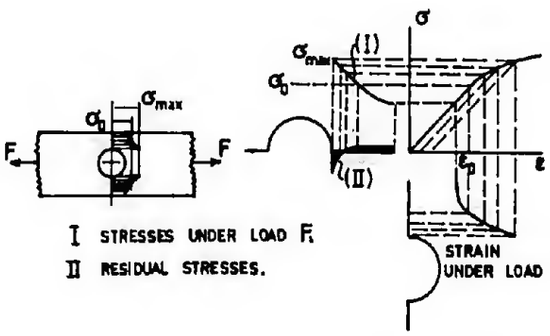

Figure 5.8

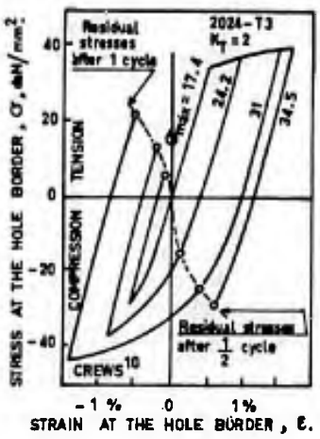

Figure 5.9

Nevertheless, fatigue under constant-amplitude stress also involves a decrease of high initial residual stresses as a result of yielding.

All the processes described above are of great significance in the behaviour of notched parts or specimens since, as mentioned previously, the material at the root of a notch is subject to substantial changes under constant-amplitude strain.

Figure 5.8 illustrates the development of residual stresses after application and removal of a static load on a bar containing a circular hole.

The changes in stress-strain cycle at the roots of notches were measured by Crews[10] on flat 4.1 mm thick and 302.4 mm wide 2024-T3 aluminium alloy specimens which contained two edge notches having a depth of 51.6 mm and a radius of 42.5 mm. Resistance type strain gauges were used for the strain measurements. The same strain histories were reproduced in unnotched companion specimens to determine the corresponding stresses on the basis of the applied load. However, we note that the strain histories were not exactly simulated since the strain gradients were different. In Figure 5.9, the first alternating stress-strain cycle measured at the root of the notch is plotted against the nominal stresses $\pm\sigma_{max}$

Under *repeated tensile loading* (R = 0) the residual stresses were as follows, expressed in daN/mm^2 (1450 lb/in^2):

σ_{max} *nominal*	σ_{max} *at the notch root*		σ *residual*	
	1st cycle	*Stabilized*	*1st cycle*	*Stabilized*
17.4	35.5	35	- 1.2	- 1.4
20.8	36.5	35	- 8	- 9
24.2	37	36	-13.6	-15
27.5	37	36	-19.2	-20.6
31	38.8	38	-24.2	-25.5
34.6	39.5	38.5	-28	-30

Under *reversed tension-compression loading* (R = -1) with a first half-cycle in tension the residual stresses were as follows, expressed in daN/mm^2:

Nominal stresses	*Stresses at the notch root*							
	Maximum stress		*Residual at 1/2 cycle*		*Minimum stress*		*Residual at 1 cycle*	
	Initial	*Stabil.*	*Initial*	*Stabil.*	*Initial*	*Stabil.*	*Initial*	*Stabil.*
17.4	36.3	37	- 1	0	-31	-31.5	7	6.4
20.8	35.5	38.5	- 9	-5.2	-34.4	-37.7	10.8	6.9
24.2	36.5	42	-15	-8.7	-37.2	-41.4	14.4	10.4
27.5	37		-19		-38.6		18.6	
31	39		-22.7		-43.5		22.7	
34.6	40		-26.3		-46.5		25	

It may be observed that

(a) under repeated loading the maximum and residual stresses after the first cycle assume values that are close to the stable values obtained after a large number of cycles;

(b) under reversed loading the stress-strain loop becomes narrower after the first cycle, the material hardens and the stresses increase, this behaviour being typical of a stress greater than the proportional limit of the material.

By fitting these test results to the notched and unnotched specimen fatigue data from previous NACA investigations (TN 2928 and 3866), Crews managed to establish a fairly accurate life estimate for notched specimens (K_T = 2) :

$$\frac{N_{calculated}}{N_{measured}} = 1.95 \text{ (maximum)}, \quad 1.4 \text{ (mean)}, \quad 0.97 \text{ (minimum)}.$$

Note that fatigue produces residual stresses after a short length of time but it must be kept in mind that fatigue loading in the opposite direction eliminates prior residual stresses as rapidly.

However, residual stresses are more stable if they are due to a system of cold-straining of a different type with respect to the new loading, e.g., torsion for tension in fatigue, cold-worked by machining, quenching, cold-rolling, shot-peening, etc. Moore[11] studied the effect of fatigue on residual stresses induced by shot-

peening and demonstrated that they decreased rapidly under high reversed stresses; these results were obtained by measuring the curvature of a flat specimen which was shot-peened on one surface and subjected to a reversed bending load. For SAE-1035 steel the variation under a reversed stress of ± 17 daN/mm^2 (24,700 lb/in^2) was:

N	0	10^4	10^5	10^6
percent residual stress	100	90	80	60 .

Recently, Moretti, Abel, Cohen-Hadria and Royez[36], investigating steels hardened by cementation and quenching, nitriding or induction-hardening, have shown that surface residual stresses change little below the fatigue limit and decrease considerably on specimens fractured under slightly higher stresses.

5.1.2 Fatigue Curves under Constant-Amplitude Strain Loading, ϵ–N

Assuming that the apparent complexities of the constant-load-range fatigue data were due to stress-strain loop changes in fatigue, it could be hoped that carrying out constant-strain-range tests would simplify the problem. However, in view of the difficulties involved, specialists were long dissuaded from undertaking such tests; moreover, the S-shape of the σ–N curves, which are usually horizontal up to 1,000 cycles, suggested that the elementary mechanism is different for small numbers of cycles in the finite-life range and for very large numbers of cycles (10^6 to 10^8) in the fatigue-limit range.

Since Coffin[12], in 1954, proposed and performed constant-strain-range fatigue tests, this method of testing has been employed by other investigators. The first fatigue machines used were operated at slow speed and the results obtained were thus mainly for *low-cycle fatigue* (small numbers of cycles). The need for such tests arose when attempts were made to solve the engineering problem of thermal stresses in conjunction with tubes used in chemical installation of nuclear power plants. Thus, a new field of fatigue research, previously ignored by laboratory specialists, was opened to investigations. In fact, the low-cycle fatigue field is that of military aircraft structures and has been known by structural aircraft engineers since an early date.

Using the notations of Figure 5.1, Coffin showed that fatigue failure in various annealed metals obeyed the relation

$$N^{\frac{1}{2}} \cdot \Delta\epsilon_p = C , \tag{3}$$

which also holds for static failure under $N = \frac{1}{4}$, so that

$$C = \epsilon^*_{ult.}/2 ,$$

where $\epsilon^*_{ult.}$ is the true elongation at the maximum true stress in static failure.

According to a review by Tavernelli and Coffin[13], the exponent $\frac{1}{2}$ would be valid but the straight lines sometimes pass above the point $\epsilon^*_{ult.}$, $N = \frac{1}{4}$, which would then be on the conservative side.

In alternating-tension tests conducted by Smith, Hirschberg and Manson[5], the preceding relation was verified fairly well for low-alloy steels, aluminium and 2014-T6 aluminium alloy, with exponents k in

$$N^k \cdot \Delta\epsilon_p = C \tag{4}$$

ranging from 0.52 to 0.66 and values of C greater than, or equal to, $\epsilon^*_{ult.}/2$. However, the agreement was poor for the stainless steel 18-8 AISI 304 ELC (annealed) and for the AM-350 steel (16.5 Cr - 4.25 Ni - 2.75 Mo). The exponent reaches a value of 0.73 in T-A6V titanium alloy and was reduced to 0.34 in beryllium.

In Figures 5.10, 5.11 and 5.13, the variations of $\Delta\epsilon_p$, $\Delta\sigma/E = \Delta\epsilon_e$ and of the total strain amplitude $\Delta\epsilon_T = \Delta\epsilon_p + \Delta\epsilon_e$ are plotted as a function of the number of cycles. When the relationship is verified fairly well, Figures 5.10 and 5.11 prove to be representative since the plastic strain $\Delta\epsilon_p$ and the elastic strain $\Delta\epsilon_e$ corresponding to the total strain range $\Delta\epsilon_T$ vary regularly with the number of cycles to failure. If apparent axial stresses were used instead of true strains, σ–N curves with shapes similar to those of the usual Wöhler curves would be obtained since the apparent nominal stress is constant between $\Delta\sigma/2 = \sigma_{ult.}$ and $\Delta\sigma/2 = \sigma^*_{ult.}$. Plastic strains are negligible with large numbers of cycles above 10^5; as a result, the constant-strain-range test does not differ from the constant-stress-range test in the range $N > 10^5$.

A comparison of various $\Delta\epsilon_T - N$ curves is given in Figure 5.12, after Smith and others[5]. In the short-life region ($N \leqslant 10^3$), the low-alloy carbon steels AISI 4130 and 4340 (annealed or treated) exhibit a similar behaviour, whereas very different results would be found with a $\Delta\sigma - N$ representation. In the long-life region, however, the data are divided into two sets, i.e., annealed steels and treated steels. The 52100 steel (0.02 C - 0.35 Mn - 0.28 Si - 1.45 Cr), treated with final tempering at 415°C, has a behaviour quite different from that of the two preceding materials, as it is an ultra-high-strength steel ($\sigma_{ult.} = 200$ daN/mm^2, $\sigma^*_{ult.} = 227$ daN/mm^2, $\sigma_{0.2} = 196$ daN/mm^2 = 275,000 lb/in^2, $\Sigma\% = 11.2$, $\epsilon^*_{ult.} = 0.12$) with low plastic strains at fatigue failure. On the contrary, the T-6A-V titanium alloy ($\sigma_{ult.} = 126$ daN/mm^2 = 182,000 lb/in^2, $\sigma^*_{ult.} = 176$ daN/mm^2, $\sigma_{0.2} = 122$, $\Sigma\% = 41$, $\epsilon^*_{ult.} = 0.53$) ranks as a better strain-resisting material. High-strength aluminium alloy (2014-T6) and annealed AM 350 steel (16.5 Cr - 4.25 Ni - 2.75 Mo) show intermediate curves.

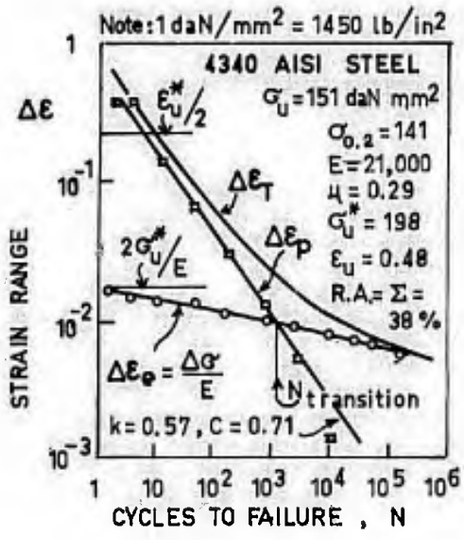

Fig. 5.10 After Smith, Hirschberg and Manson[5]

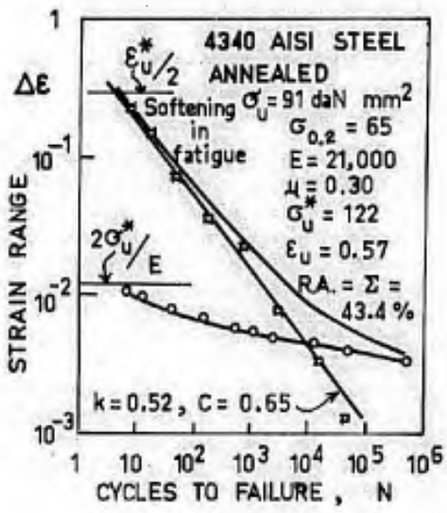

Fig. 5.11 From Reference 5

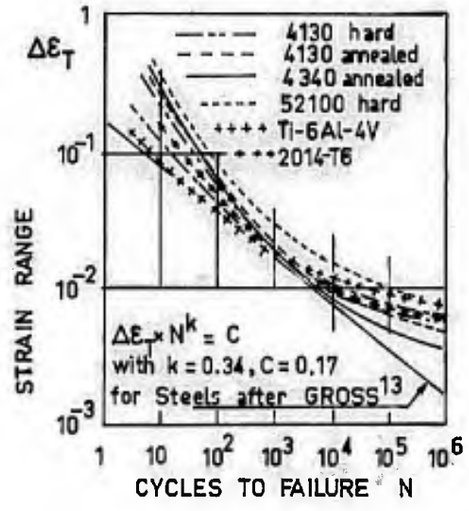

Fig. 5.12 After Smith et al.[5]

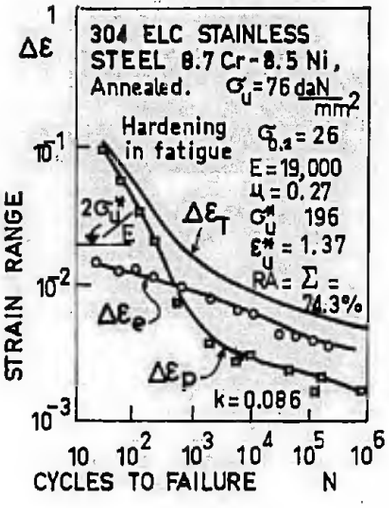

Fig. 5.13 From Reference 5

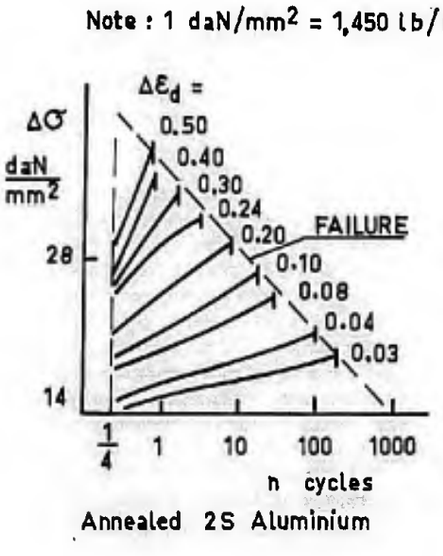

Fig. 5.14 After Coffin[7]

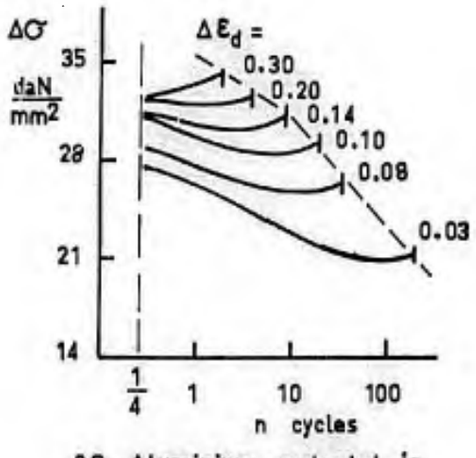

Figure 5.15

Although the differences between the various metals investigated are smaller than in constant-stress-range tests, there is no $\Delta\epsilon_T - N$ *curve applicable to the various engineering materials.*

Figure 5.13 contains an example where the relationship of expression (4) is not verified.

5.1.2.1 Stability of the Cold-Worked State

When studying the effect of preloading and overloading during fatigue, it is helpful to know how stable the cold-worked and the fatigue strain-hardened states are. In Figures 5.14 and 5.15, after Coffin[7], the stress amplitude $\Delta\sigma$ is plotted against the number of cycles for alternating-tension tests on 2S aluminium with a diametral total strain range $\Delta\epsilon_d$. Annealed 2 S-O aluminium (see Figure 5.14) hardens through fatigue and the stress amplitude $\Delta\sigma$ gradually increases under constant $\Delta\epsilon_d$. The 2S aluminium is initially hardened by a compression prestrain $\epsilon_0 = -0.20$ and softens under alternating strains of different amplitude in tension. It is seen that the effect of static prestraining disappears very slowly although the fatigue life is only slightly modified. The effect of tensile and compressive preloading is illustrated in Figure 5.16.

In Figure 5.17, after Dugdale[14], the plastic changes in copper are shown by the variation in stress amplitude, i.e., $\Delta\sigma$ versus cumulative plastic strain $\Sigma_n\Delta\epsilon_p$. The return to steady conditions takes place fairly rapidly after each drop in the load level. Tuler[3] found similar results: the return to normal conditions is fast in terms of number of cycles, and the previous strain history seems to be cancelled out rapidly if the plastic strains are moderately high.

5.1.2.2 Torsion Tests

Halford and Morrow[15] carried out constant-strain-amplitude torsional fatigue tests in the life range of ½ to 20,000 cycles. Tubular specimens were used for brass and SAE-4340 steel (D = 14.3 mm and thickness t = 1.6 mm for the brass; D = 9.05 mm and t = 0.51 mm for the steel).

The tensile properties of the cold-rolled 19 mm diameter brass bars were as follows:

	$\sigma_{0.2}$	$\sigma_{ult.}$	$\sigma^*_{ult.}$	E	$\Sigma\%$	$\epsilon^*_{ult.}$
daN/mm²	30				47	0.675
lb/in²	43,500	57,300	107,000	$13.3\ 10^6$		

with $\sigma = 69\ \epsilon_p^{0.21}$ daN/mm².

In static torsion, $\tau_{ult.} = 36$ daN/mm² and $\gamma_{ult.} = 0.879$ were obtained for $N = \frac{1}{4}$ cycle.

In fatigue under alternating torsional straining, if $\Delta\gamma_p$ represents the τ-γ loop width which is kept substantially constant during the test, the points $\log\Delta\gamma_p - \log N$ are plotted on a straight line of slope 0.52 which passes through the static test point: $\Delta\gamma_p(2N)^{0.52} = \gamma_{ult.}$.

The SAE-4340 steel, containing 0.40 C - 0.81 Mn - 0.85 Cr - 0.24 Mo - 0.25 Si, autenized at 830°C, quenched in oil and tempered for 1 hour at 205°C, machined and then stress-relief treated for 1 hour at 205°C, had the following properties:

	$\sigma_{0.2}$	$\sigma_{ult.}$	$\sigma^*_{ult.}$	E	$\Sigma\%$	$\epsilon^*_{ult.}$
daN/mm²	172	192	265	21,300		
					41	0.524
lb/in²	250,000	280,000	384,000	31×10^6		

with $\sigma = 255\ \epsilon_p^{0.057}$ daN/mm². In static torsion $\tau_{ult.} = 120$ daN/mm² and $\gamma_{ult.} = 0.29$ were obtained for $N = \frac{1}{4}$ cycle. In fatigue, $\Delta\gamma_p \cdot (2N)^{0.60} = \gamma_{ult.}$ was found.

5.1.2.3 Bending Tests

Gross[16] carried out constant-deflection alternating-bending tests on slightly notched specimens ($K_T = 1.03$). The strains, which were measured with strain gauges bonded to the test section, and the bending moments, which were measured with strain gauges bonded on the loading bar, were fed into a recorder and moment-strain loops were obtained. Thus, the total strain $\Delta\epsilon_T$ could be determined with accuracy and the plastic strain was defined by the loop width. The range of numbers of cycles to failure was comparatively small: between 10^2 and 10^4 for HY-100 steel, between $6 \cdot 10^2$ and 10^4 for most of the other cases. In this low-cycle region, the regression lines $\log\Delta\epsilon - \log N$ which fit best to the test results were determined by the author. If we define a transition life N_t for which $\Delta\epsilon_e = \Delta\epsilon_p$ (see Figure 5.10), most of the results obtained by the author correspond to $N \geqslant N_t$, whilst previous test data often implied $N \leqslant N_t$. It is therefore normal that the author should find values for the exponent k in $\Delta\epsilon_p \cdot N^k = C$ that are smaller than those indicated by the preceding investigators. For comparison of the results with those of NASA[5], we have plotted the expression $\Delta\epsilon_p \cdot N^{0.34} = 0.17$, proposed by Gross for steels, in Figure 5.12, which gives some NASA results. This curve and the data for 4130 and 4340 steels are very similar in the range of $600 < N < 2 \cdot 10^4$. Thus, the results of Gross are apparently valid but his interpretation is questionable for $N < 100$ and $N > 10^4$. An equally good agreement is found between the

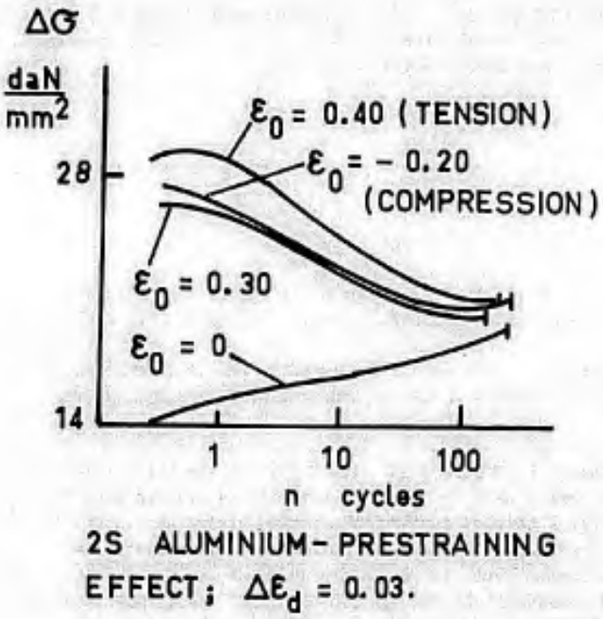

2S ALUMINIUM – PRESTRAINING EFFECT; $\Delta\varepsilon_d = 0.03$.

Fig. 5.16 After Coffin[7]

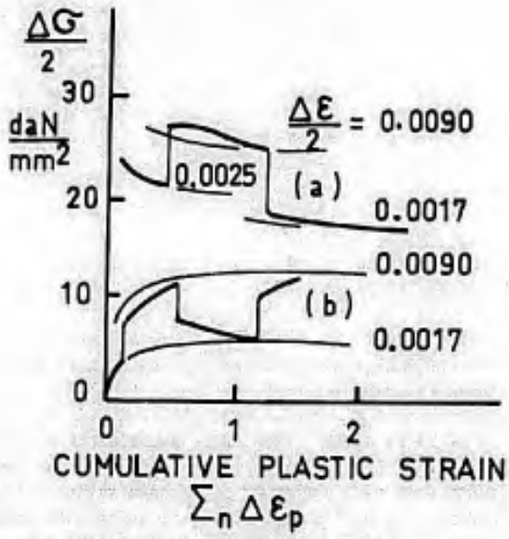

COPPER: (a) hardened, (b) annealed.

Fig. 5.17 After Dugdale[11]

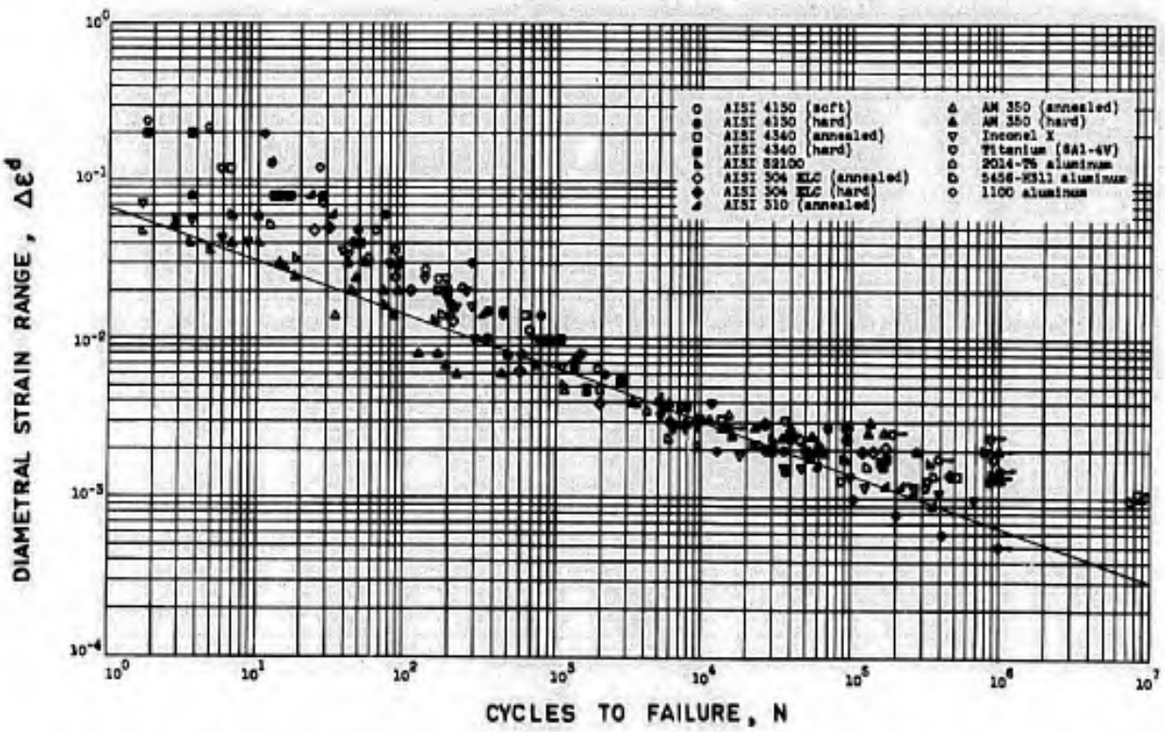

Fig. 5.18 Effect of diametral strain range on fatigue life, from Smith, Hirschberg and Manson[5]

Gross's results and the NASA's results for 5456-H 311 aluminium alloy containing 5% Mg and 0.73% Mn, for which the relationship $\Delta\epsilon_T \cdot N^{0.22} = 0.07$ is verified by the NASA results in the region of $10^3 < N < 10^4$ whereas it appears too conservative outside this range.

If we consider the NASA results in terms of total diametral strain, $\Delta\epsilon^d$, it is seen from Figure 5.18 that all the materials investigated exhibit similar $\Delta\epsilon_T^d - N$ curves in the region $10^3 < N < 10^4$. Gross proposed to take the following average expression for all the steels and alloys which he studied:

$$\Delta\epsilon_T \cdot N^{0.34} = 0.17 . \qquad (5)$$

In the plastic range we have $\nu = 0.5$ and in the elastic range roughly $\nu = 0.3$. By using an intermediate value, $\nu = 0.4$, it follows that

$$\Delta\epsilon_T^d = 0.4\,\Delta\epsilon_T \quad \text{and} \quad \Delta\epsilon_T^d \cdot N^{0.34} = 0.068 .$$

This expression is illustrated in Figure 5.18 by a line which is slightly conservative with respect to the NASA results in the region $10^3 < N < 10^4$; it is highly conservative for some materials outside this region.

We recognize that flexural tests are useful for constant-strain-range fatigue studies but it is our belief that the whole range included between static failure and 10^6 cycles should be explored since extrapolations always yield questionable results.

Let us return to the plastic and elastic strain indicated in Figure 5.10. If $N > 10^6$, the mean plastic strain will be negligible, which does not mean that the damage will no longer be governed by plastic strain but simply that the latter, of small mean value, will be greater in some favourably oriented grains and in small domains with stress concentrations inside the grains. Therefore, ϵ_T appears to be a better parameter than ϵ_p in the high-cycle region. With $\Delta\epsilon_p \cdot N^k = C$, Gross showed that, if $10^3 < N < 10^4$, k varies from 0.42 to 2.40 depending on the material and does not have the constancy obtained for $N < 10^3$ by other experimentators. Note that, as regards stainless steels, Figure 5.13 indicates $k = 0.82$ for $N < 10^3$ and $k = 0.086$ for $10^3 < N < 10^6$.

For these reasons, fatigue life calculations based on the plastic strain energy release during fatigue, as proposed by Feltner and Morrow[14], Morrow and Tulor[15] and other authors, are restricted to the $10 < N < 10^3$ range, except for some materials.

5.1.3 Changes in Stiffness and in Damping During Fatigue

Much work has been devoted to the changes that occur in the physical properties of materials during fatigue: σ–ϵ loop adjustment (see Paragraph 5.1.1), elongation (see Paragraphs 2.1.3, 3.2.6 and 5.1.1.2), crystal lattice disorientation, electrical resistivity, thermoelectrical coefficient, magnetic permeability, modulus of elasticity, damping, etc. We shall first examine the *changes in the modulus of elasticity and in damping as measured under low-amplitude vibration.*

In his thesis Karius[19] investigated the changes in the modulus of elasticity and internal damping of standard engineering materials subjected to rotating-bending fatigue. Measurements of the modulus of elasticity and of damping were carried by the Forster method on the basis of the response of the specimen to 500 Hz vibration excitation in bending under very low stresses of about 10 daN/cm^2. The damping was caused by the thermoelastic or magnetoelastic effects which have been studied by Zener[20] and was influenced by the heterogeneous material structure and the internal stresses. Figure 5.19 shows the changes in the modulus of elasticity, E, and Figure 5.20 the changes in damping in German St.37 mild steel. Karius concludes as follows:

1. Changes due to reversed loading are of the same nature and develop in the same manner under fatigue conditions for all polycrystalline materials.
2. The increase in damping and the decrease in the modulus of elasticity are due to plastic strain and to changes in the internal stresses; the significant final changes indicate macroscopic cracks.
3. Notched-specimen tests have demonstrated that the changes are dependent on the volume of stressed material. The initial changes take place in the entire volume whereas the large changes prior to failure are observed only in the fracture area. In severely notched specimens where the stressed volume is very small, some visible cracks which do not propagate are formed prematurely.
4. In the initial stage, the changes in the modulus and in damping can be partially restored at room temperature and completely restored above 150°C. From this we may conclude that the crystal lattice distortions are responsible for the changes.
5. Heating of the specimens is responsible for certain anomalies under high stresses.

We believe that the changes in the modulus of elasticity correspond to changes in the mean value of the lattice parameter of the crystal unit cell, owing to lattice distortions and to nonlinear relationship between the interatomic forces and the atomic spacings, as was seen in Paragraph 2.1.1. In Figure 5.21, let d_0 be the size of the unit cell in the absence of strain, and f_c, f_t, the interatomic compressive and tensile forces. If we assume an average equilibrium in the material and compare the compressive and tensile strains d_c and d_t with the condition $f_c = f_t$, then the unit cell d_c subject to compression and the unit cell d_t subject to

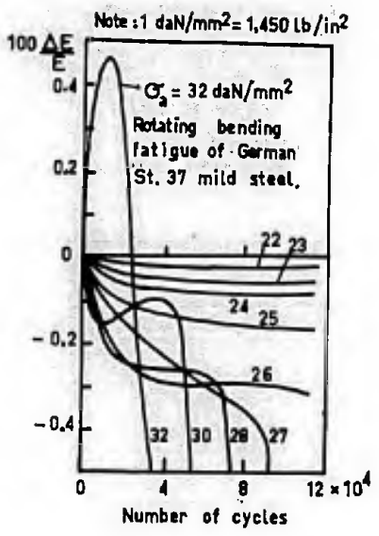

Fig. 5.19 Changes in modulus E during fatigue, after Karius[19]

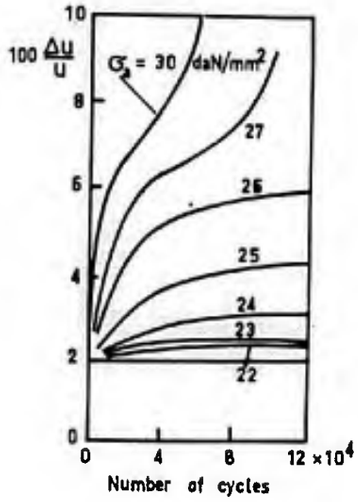

Fig. 5.20 Changes in damping[19]

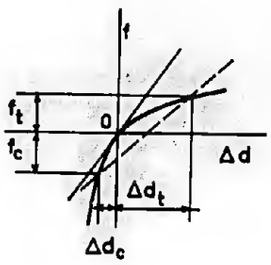

Figure 5.21

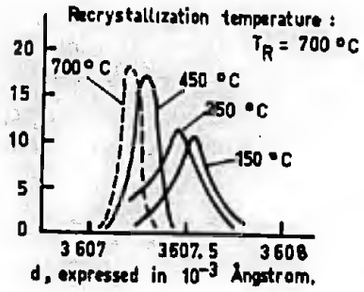

Fig. 5.22 Size of the lattice unit cell of copper, after Crussard and Aubertin[21]

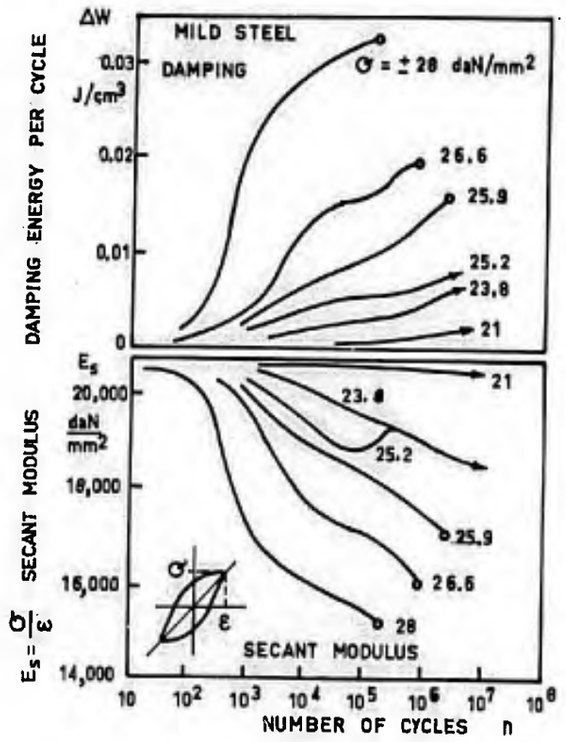

Fig. 5.23 Rotating bending fatigue of mild steel changes in damping and in secant modulus, after Lazan[22]

tension are such that $(d_0 - d_c) < (d_t - d_0)$. The mean unit cell d_m increases if there are internal stresses or lattice distortions, and the modulus of elasticity decreases since the changes in the atomic spacings are greater in tension than in compression. The change in density with strain-hardening has been investigated by many authors. Crussard and Aubertin[21] have found that, in the case of copper, strain-hardening increases the mean value of the unit cell size while maintaining the minimum value; in Figure 5.22, the reverse effect of recrystallization on the statistical unit cell distribution between the newly formed grains is illustrated for very pure copper. The unit cell of the perfect material is $(3607 \pm 0.05) \cdot 10^{-3}$ A ; through recrystallization, grains with a small unit cell develop at the expense of the others.

We may consider that in Figure 5.19 the decrease in the modulus of elasticity implies an increase of the crystalline lattice distortions and of the dislocation or vacancy density.

Lazan[22] studied the changes of the secant modulus of elasticity, $E_s = \sigma/\epsilon$, and of the energy release per cycle during rotating-bending fatigue tests. If h is the deflection in the direction of the load and l the deflection in the perpendicular direction at the end of a cantilever specimen, the secant modulus is measured by $K\sigma/h$ and the energy dissipation by $k\sigma l$. Figure 5.23 reproduces some of Lazan's results for mild steel.

Under stresses below the fatigue limit, the secant modulus and the damping tend to assume steady values; however, these latter values are not constant as they depend on frequency. Thus, for mild steel SAE 1020 subjected to $3 \cdot 10^7$ fatigue cycles at $\sigma = \pm 23.2$ daN/mm^2 and then cooled and tested at various frequencies, the damping value reaches a maximum at 1 c/m ($\Delta W = 24.5$ J/cm^3) and then decreases ($\Delta W = 9.8$ J/cm^3) at 1,000 c/m.

Furthermore, plastic damping varies with the duration of the period of rest: it first increases by recovery and then decreases after the solute carbon atoms have returned to their ordered locations[23]. Karius observed the same cause of decrease with damping at very low vibration amplitudes.

After the period of rest, subsequent fatigue reduces the stabilized plastic damping to a value smaller than that observed before rest[24]. From this we can conclude that *in the case of mild steel the changes in damping and in the modulus of elasticity cannot be used as a reference for fatigue damage.*

Indeed, rotating-bending tests conducted by Lazan and Wu[23] on 14.8 mm and 13.2 mm diameter mild steel tubes showed that the damping became again stable even in specimens that later failed under the same alternating stress (Fig. 5.24), and that the same damping value, for example 0.01, corresponded to a relative duration of N/10 for $\sigma = \pm 26.2$ daN/mm^2 and of N/500 for $\sigma = \pm 29.6$ daN/mm^2.

Apart from plastic damping, Zener[26] describes other forms of damping:

- Considerable damping is caused in ferromagnetic materials by the magnetic hysteresis and eddy currents.
- In carbon steels, the solute carbon atoms, after settling in the dislocations, move along with these dislocations, which involves greater resistance and a dephasing between the load and the deflection[26].
- The thermoelastic coupling investigated by Zener[20,27] results from cooling during adiabatic elongation and from thermal expansion under constant pressure. If the stress is not uniform, then the temperature will not be uniform either; thus, the stress gradients, and hence the temperature gradients, will produce heat fluxes which will cause an increase of the entropy and an irreversible transformation into heat of a certain amount of the mechanical energy.

  In the case of elastic materials subjected to slow loading, the *isothermal modulus of elasticity* is Young's conventional modulus; on the other hand, with rapid loading, no heat release can take place, thermal agitation diminishes the compressibility, and the adiabatic modulus obtained is higher than the isothermal modulus. The heat transfer from highly stressed regions to regions subject to lower stresses produces a damping loop. This loop exists even with stresses that are homogeneous on the geometric scale, owing to the crystalline anisotropy on the scale of the grains.

  At very low frequencies, loading and unloading are isothermal and the damping is negligible. At very high frequencies, both conditions are adiabatic and the damping is still very low. At intermediate frequencies, the damping goes through two maximums, the first being associated with the stress gradients on the geometrical scale and the second with the stress gradients on the scale of the grains.

In assemblies, *dry friction* between the various components covers all other forms of damping. It increases during fatigue because of the increased play due to wear or fretting. On structures of fairly simple design, a change in damping may indicate an incipient damage, as was the case with the fan blades of the large ONERA wind tunnel at Modane (France), when damping measurements under resonant vibration conditions were followed by a check which showed the need for further tightening of the blade attachment nuts.

On complex structures, localized changes in the damping of a particular assembly cannot be distinguished from the overall damping and are therefore undetectable. It follows that, while measurement of a large change in damping may indicate an overall increase of the plays in the assemblies, the absence of any detectable change does not allow the statement that the structure concerned is not severely damaged.

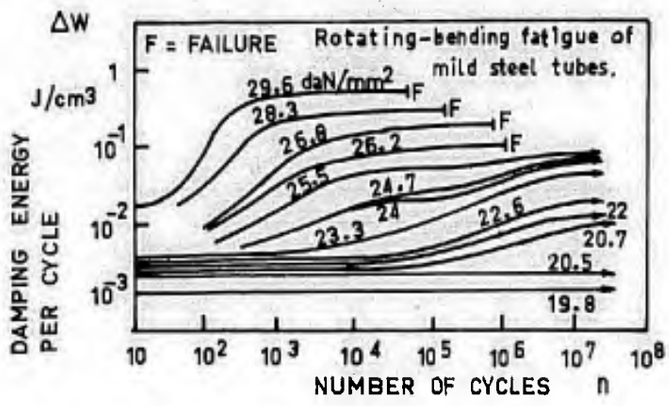

Fig. 5.24 After Lazan and Wu[23]

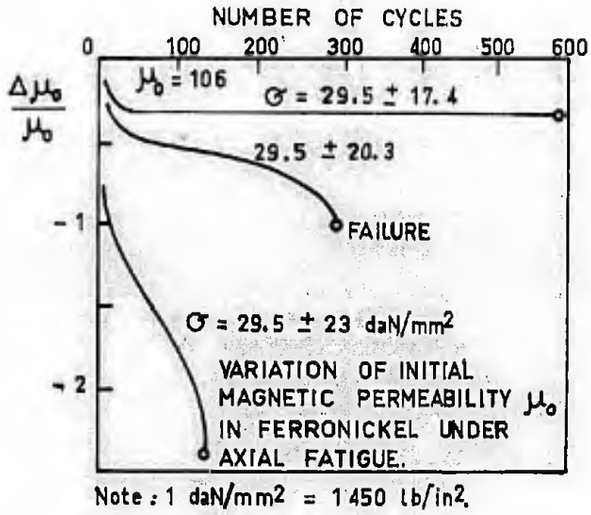

Fig. 5.25 After Schweizerhof[32]

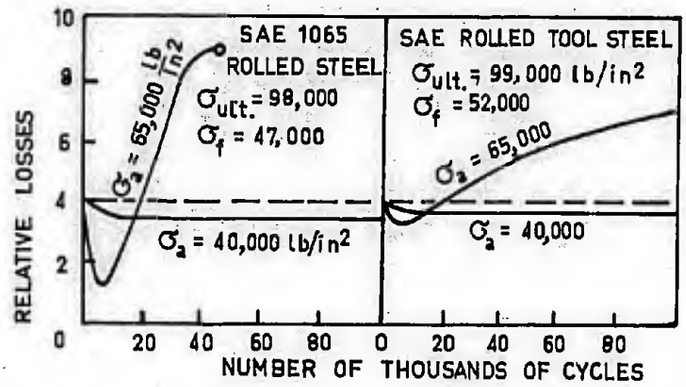

Fig. 5.26 Magnetic tests of fatigued specimens after Cavanagh[35]

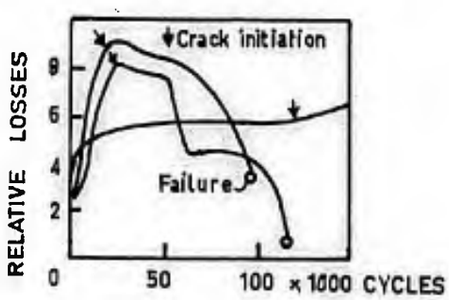

Fig. 5.27 Fatigue test on a rail with measurement of the losses in several sections by means of the cyclograph at a field magnetic strength of 1 Oe under 5,000 Hz, after Cavanagh[35]

5.1.4 Changes in the Magnetic Quantities during Fatigue

Some investigators have attempted to analyze the fatigue phenomena in materials by means of magnetic measurements so as to determine the fatigue limit of magnetic materials by a nondestructive method. Mönch[28], for example, studied the changes in reverse magnetostriction during torsional fatigue. Fink and Hempel[29] studied the induction changes at constant magnetic field during rotating-bending fatigue. Langevin and his co-workers[30,31] examined the variation of magnetic permeability with the loads applied during a tension test. Thus, they showed the existence of a function, the discontinuity of which is associated by them with the fatigue limit.

In Chapter II, Paragraphs 2.2.2 and 2.2.3, we have made the assumption, well supported by known facts, that plastic changes leading to fatigue failure correspond to the distribution of external forces over a decreasing number of regions which would thus be subjected to local overloads. If, by some method, a quantity varying with the local stresses during loading and with the local residual stresses after loading could be measured, there would be hope that fatigue failure might be predicted from the changes of this quantity.

In this connection we invited Schweizerhof[32] to investigate the potential uses of magnetic measurements. The subsequent experimental study, continued by Guyot[33], was concerned with pure nickel and 48% Ni ferronickel wires subjected to static tension and to fluctuating fatigue with a static component. However, this study was brought to an end before actual measurements could be carried out under loading conditions, so that only data on the changes in the magnetic quantities as affected by residual stresses are available.

According to Schweizerhof, the initial magnetic permeability at low magnetic field, μ_0, is associated with Kersten's average stress[34],

$$\bar{\sigma}_1 = \text{average of } [|\sigma_1 - \sigma_2| + |\sigma_1 - \sigma_3|] ,$$

through the relation

$$\mu_0 = \frac{C}{\sigma_1} ,$$

σ_1 being the highest tensile stress and $|\sigma_1 - \sigma_2|$, $|\sigma_1 - \sigma_3|$ the absolute shear values on the planes at 45° with the direction of σ_1. Consequently, in the tests conducted on the unloaded specimen, μ_0 was associated with an average of the absolute residual shear values.

Figure 5.25 shows the variation of the initial permeability, μ_0, in ferronickel wires under axial fatigue. It is seen that the curve is similar to that of damping as studied by Lazan for mild steel (Fig. 5.24), and that *time to failure cannot be predicted on the basis of this quantity*.

For completeness we must also mention Cavanagh's work[35]. He performed rotating-bending fatigue tests on hourglass-shaped Avery specimens having a minimum diameter of 12.7 mm. Using a detection coil which was placed around the specimen and a Du Mont cyclograph which produced a magnetic field strength of 1 Oe at a frequency of 5,000 Hz and was still active over a depth of 0.6 mm in SAE 1025 steel, he measured the sum of the losses due to eddy currents, to resistivity and to magnetic permeability, as well as the variation of these losses during fatigue.

For 60-40 brass, aluminium and several steels, the changes observed exhibited the same form, as illustrated in Figure 5.26. Under alternating stresses below the fatigue limit, the relative losses in naturally work-hardened engineering metals decrease and asymptotically approach steady values. Under alternating stresses above the fatigue limit, the initial decrease in relative losses is more pronounced but, after reaching a minimum, these losses again increase until fracture occurs. We may compare this to the hardness changes measured by Polakowski and examined in Chapter II, Paragraph 2.1.3, Figure 5.27, after Cavanagh[35] contains similar measurements performed on a rail section during fatigue tests under a rolling load. *No correlation was found between the measured losses and the fatigue damage*.

5.1.5 Electrical Resistivity Changes with Plastic Strain, Annealing and Fatigue

The *electrical conductivity* is very high at very low temperatures near the absolute zero (superconductivity), whereas the thermal conductivity is very low under the same conditions. A good correlation was found by Powell, Hickman and Tye[37] between the thermal conductivity, λ, and electrictrial resistivity, ρ, of magnesium and thirty magnesium alloys over the temperature range 293-523°K:

$$\lambda = 2.206\ 10^{-8}\ T\rho^{-1} + 0.096 ,$$

the maximum difference between the measured values and the values of this expression being about 5%. Accordingly, the resistivity of a material that is stabilized by annealing does not seem to be dependent on thermal agitation.

The present opinion of physicists is that electrical conductivity consists in the passage of an electron from the outer shell of an atom to that of a neighbouring atom through covalent bonds (electrons circulating around two atoms). Thermal agitation causes the electrons to move in a disorderly manner which delays the electron flow and favours collisions between electrons and positive ions.

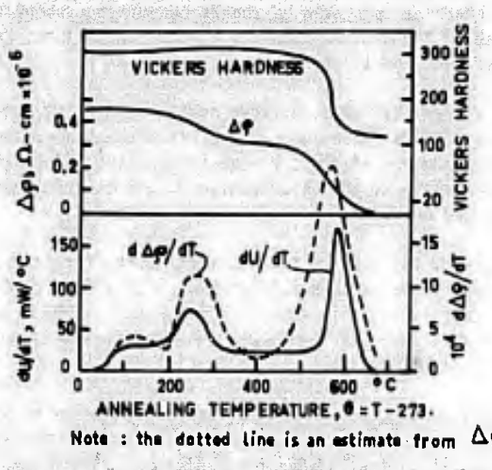

Fig. 5.28 Comparison of the rate of release of stored energy upon annealing, (dU/dT), with the decrease in resistivity ($\Delta\rho$) and the Vickers hardness number for various annealing temperatures (after Boas[42] who reports results obtained by Clarebrough, Hargreaves and West on specimens deformed in torsion to $nd/l = 2.34$)

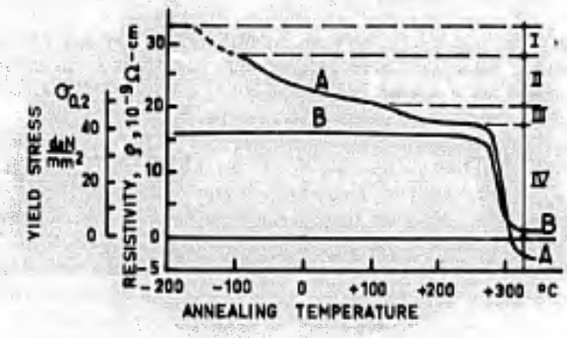

Fig. 5.29 Electrical resistivity (A) and yield stress (B) of copper strain-hardened in tension at 4.2 °K after annealing to various temperatures (after Berghout; Figure taken from Reference 40)

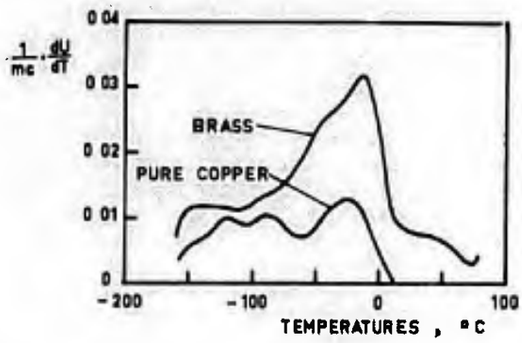

Fig. 5.30 The energy release spectrum for brass and pure copper compressed at liquid-nitrogen temperature (after Henderson and Koehler[43])

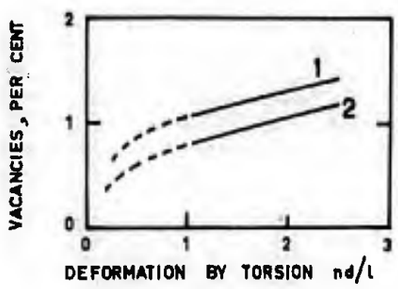

Fig. 5.31 Vacancy concentration in nickel as a function of deformation by torsion. Curve 1: from density measurements. Curve 2: from measurements of electrical resistivity (after Boas[42])

Vacancies, stacking faults and dislocations introduce local disturbances in the orderly crystal arrangement, so that the electrons in the outer shell of each atom no longer occupy interchangeable relative positions; this causes the electron flow to decrease in the same way as with thermal agitation. Feltham[38] assumes that vacancies correspond to a missing positive ion and tend to repel free electrons.

Basinski, Dugdale and Howie[39] consider that elastic shear strain in crystal lattice unit cells is more efficient than expansion for the resistivity increase, and that it accounts more adequately for the action of the dislocations. Furthermore, in the course of their movement resulting in plastic deformation by slip, the dislocations generate vacancies, especially at the intersection of two dislocations, on two different slip planes, whereby a step (jog) is created on the path of one of the dislocations.

Some correlation has been established between the resistivity and the strain energy liberated upon annealing. The changes in Vickers hardness, resistivity and rate of release, dU/dT, of stored energy (expressed in mW/degree) are plotted in Figure 5.28 for nickel specimens, after Boas[42]. For comparison, a dotted line is drawn to indicate a rough estimate of $d\Delta\rho/dT$; the rate of change in resistivity varies with the annealing temperature in accordance with the rate of energy release.

In Figure 5.29, from the work of Berghout quoted in a review of the matter by Koehler, Henderson and Bredt[40], the changes in resistivity (curve A) and in yield stress (curve B) are shown for copper work-hardened at a very low temperature, 4°K, after annealing at various higher temperatures. Four stages of rapid decrease in resistivity can be observed. In Figure 5.30, from Henderson and Koehler[43], the rate of change $(1/mc)(dU/dT)$ of the energy liberated on annealing at a temperature T is illustrated for brass and polycrystalline copper by a spectrum containing one or more maximums which may be compared with the maximum resistivity slopes of Figure 5.29. The copper was compressed at liquid-nitrogen temperature. In the expression $1/mc$, m is the mass of the electron, i.e. $9.01 \cdot 10^{-28}$ g, and c the velocity of light, i.e. $2.998 \cdot 10^{10}$ cm/sec.

Stages I and II of rapid change in resistivity with annealing temperature are mainly found in specimens irradiated at low temperature with nuclear particles. Stage I is ascribed to the motion of interstitial atoms in an ideal lattice. It is assumed that Stage II results from interstitial "crowdions" which have been trapped at lattice vacancies in the manner suggested by Lomer and Cottrell[44]. Stage III is believed to result from the motion of di-vacancies, and Stage IV from that of single vacancies[40]. The multiple peaks in the energy release may arise from the effect of residual internal stresses on the migration energy of the vacancies. Stage V appears in cold-worked specimens for an annealing temperature range 130-230°C; it does not affect the yield stress. Stage VI, which occurs at about 300°C for annealed copper, seems to be associated with recrystallization.

The assignment of every peak in the energy release to a particular cause within a given temperature range results from a comparison of theoretical and experimental activation energy values (see Section 2.5 and Paragraph 5.2.4); it is, to a large extent, associated with vacancies, probably because the theoretical values are then more readily calculated.

We shall simply bear in mind that the variation of resistivity with work-hardening is dependent on the lattice distortions induced by plastic strain, and that its reverse variation with annealing temperature reflects the distribution of stability of these distortions with regard to thermal agitation. If the damage suffered by a material under static, creep or fatigue loadings is, as we believe it to be, related to a constant increase of the portion of external loads that is sustained by domains which decrease in number and size and thus form more stable obstacles to plastic deformation, then the changes in resistivity will, at best, be a rough reference for damage. If the crystal lattice distortions increase homogeneously in number while causing the stiffness of all slip barriers to be raised proportionally, then the resistivity increase will not correspond to damage. On the contrary, as we have seen in Paragraphs 2.1.3 and 3.4.2, static or fatigue deformation first involves a decrease in the previous work-hardening, hence probably in resistivity, although this process leads to subsequent damaging. *We shall therefore assume that resistivity does not provide a measure of damage but that it is one of the best possible references for it.*

In the case of the pure metals investigated, i.e. 99.999% copper studied by Blewitt, Coltman and Redman[45], and silver studied by Kovacs, Nagy and Feltham[46], the resistivity change due to plastic slip was found to be in direct ratio to the square of the applied stress and to increase with the shear strain energy. Inasmuch as the plastic strain energy used in the successive fatigue cycles reaches a given value at fatigue failure, the same reasoning might be applied to the resistivity. However, the resistivity, like the energy release per cycle varies no longer after a large number of cycles at stresses below the fatigue limit, whereas the total energy release is constantly increased.

By ascribing to vacancies the total changes in density and resistivity which occur in nickel deformed by torsion (see Figure 5.28) in the temperature range of 200-300°C, Boas[42] calculated the vacancy concentration, in atomic %, from density measurements - the increase in volume associated with the formation of a vacancy being 0.9 of an atomic volume - and from resistivity changes - an increase of 1 at. % vacancies corresponding to $4\ \mu\Omega$ cm. Figure 5.31 contains the results of these calculations. We shall find similar curves for the changes in resistance in fatigue life gauges.

5.1.6 Fatigue Gauges

Since World War II, "stresses", or - to use a more correct language - strains at the surface of parts have been measured by means of *strain gauges* bonded to the test pieces. Initially, these gauges, which were developed by De Forrest, consisted in very thin folded and heavily work-hardened constantan or ferronickel wire. More recently, foil gauges, made from thin work-hardened foils by cutting or chemical machining, have been used.

In 1959, the Boeing Flight Test Organization reported an anomalous increase in resistance in some of these gauges and the same changes were observed during fatigue tests in gauges bonded to specimens. After various investigations, Harting[47] attributed these resistance changes to modifications in the gauge material under the effect of plastic strain and fatigue. He then proceeded to a study of the use of specially designed gauges, highly sensitive to the fatigue of structures. The -S/N-Fatigue Life Gage[48], which has been developed and patented by the Micro-Measurements Inc., is a small bondable resistance sensor similar in appearance to a foil strain gauge. The sensing metal element is made from very thin rolled and annealed aluminium foil and is encapsulated with a soft material backing which can be bonded to metals.

In January of 1967, Horne[49] examined the above mentioned gauges and some others in a feasibility study of their use as fatigue damage indicators. More recently, Matlock[50] undertook a supplementary study on the same subject. Various similar investigations are now being conducted by NASA at Langley Field, Sud-Aviation at Marignane, Fiat in Torino, and others.

Owing to their high degree of work-hardening, strain gauges, whether extruded or rolled, proved to be stable enough in fatigue to prevent any plastic change from being detected during dynamic measurements; they were moderately responsive to temperature changes since most of their resistivity resulted from crystal lattice distortions due to work-hardening and residual stresses. An additional mean tensile stress would cause a cross-sectional area reduction of the foil or grid, whereby the resistance would be increased with no significant change in resistivity. After removal of the load, the resistance would again assume its initial value.

On the other hand, measurements published in connection with fatigue damage gauges have all been carried out upon unloading. These measurements are relating to the resistivity changes under the effect of plastic deformation in the gauge material subjected to strains by the basic structure. As the gauge material has initially been annealed, the greatest portion of the initial resistance results from thermal agitation, hence the coefficient of thermal variation is much greater than for strain gauges. During fatigue, the amount of resistivity due to stable lattice distortions which are produced by strain-hardening in fatigue is constantly raised and the gauge becomes less and less temperature-sensitive[49].

As long as no microcracks appear in the gauge material, the resistivity reflects the crystal lattice distortions created by plastic slip, i.e., by shear; consequently, the changes in resistivity should be the same, whether the basic structure is subjected to compression or to tension. This was observed by Horne with static loading and by Matlock with repeated tensile or compressive straining.

The gauge experiences the straining of the basic structure only through the largest shear strain to which the structure has been subjected previously and through the whole shear strain history; the response of the gauge consists in a particular summation which is not necessarily a measure of its own fatigue damage and certainly not a measure of the damage suffered by the structure since it does not distinguish between tensile and compressive stresses.

It should be remembered that a fatigue gauge is also a strain gauge under load, the gauge factor, i.e. the ratio of change in resistance, $\Delta R/R$, to change in elongation, $\Delta L/L$, being substantially equal to 2; if the proper weight of the structure has an effect on the gauge, then the measurements must be carried out under the same loading conditions.

Methods of Testing

Since fatigue damage gauges are sensitive to strains imposed upon them by the basic structure, test data analysis would prove easier if the specimens were subjected to known strains. It is difficult to control tests with conventional strain gauges as the scatter in fabrication and errors due to thermal compensation do not permit absolute measurements to be made within more than 10^{-5} of relative elongation. Horne performed most of his tests on coupons subjected to known axial stresses; however, some tests conducted on bending beams under constant-amplitude surface stresses were in good agreement with the axial tests. Hence bending specimens can be used for the evaluation of fatigue sensors and the test will be a constant-amplitude strain test if the load applied results from the deflection imposed by an eccentric, at least as long as the stiffness of the specimen is not modified by cracks.

Shape and Representation of ΔR–n Curves

Figures 5.32 and 5.33 show the results of two tests carried out by Sud-Aviation[51] to investigate the changes in resistance in NA-01 fatigue gauges. The gauges were placed on flat specimens subjected to repeated bending. The data are represented on logarithmic and linear scales, respectively. On the $\log \Delta R$–$\log n$ diagram, the two triangles indicate a shift in slope in the curves, which, according to the gauge manufacturer, is the sign of crack initiation. This may be possible; however, in the course of the same test series, some gauges, with a shift in slope for ΔR-values included between 4 and 7, remained uncracked after the fatigue tests were continued up to considerable values of ΔR, ranging from 19 to 95. In our opinion, the shift in slope was an indication of fatigue within the gauge but not of fatigue within the structure. It would be of interest to study the gauge independently of the structure. The only way of doing this would be to use a structure capable of sustaining a very high "endurance limit" strain; during the fatigue under axial tension, a check would have to be made to establish that the σ–ϵ curve of the structure does not vary in the cyclic strain range under review.

Threshold Sensibility

Figure 5.34 contains calibration curves for NA-01 fatigue sensors based on information from the manufacturer. For moderately high strains and small numbers of cycles, the rectilinear portions of the curves satisfy the expression

$$\Delta R = 6.63 \cdot 10^{-5} (\epsilon_a - \epsilon_0) \cdot n^k ,$$

where ΔR = change of resistance from the initial value of 100 ohms,
n = number of applied cycles,
ϵ_a = alternating strain,
ϵ_0 = gauge "endurance limit" strain (about $\pm 1400 \cdot 10^{-6}$),
k = exponent ranging from 0.4 for low strain values to 1 for the highest strain values.

For values of ϵ_a smaller than ϵ_0, the change in resistance is negligible in practice, except for very high numbers of cycles ($> 10^6$) in which case the resistance approaches a saturation limit; the orders of magnitude of these values range from 0.03 ohm at $\pm 900 \cdot 10^{-6}$ to 1 ohm at $\pm 1400 \cdot 10^{-6}$. Like the conventional fatigue limit, the "endurance limit" under reversed strain decreases if a steady simultaneous tensile or compressive strain is applied. Since no cracking is involved, the maximum shear strain is predominant for the overcoming of the obstacles to plastic slip. Consequently, steady tensile strains and steady compressive strains play the same role in the process.

Effect of Changes in Load Amplitude

The solid curve in Figure 5.35 represents the changes in resistance in a NA-01 fatigue gauge bonded to a bend specimen which was subjected to the following sequence of fatigue loads:

$10^6 \epsilon =$	± 1480;	1500 ± 1500;	2500 ± 1500;	± 1500;	± 2000;	± 1000
$n =$	300	600	3100	6000	30,000	30,000

and finally 30,000 cycles with $10^6 \epsilon = \pm 2000$.

First, after 10,000 cycles at $10^6 \epsilon = \pm 1500$ the curve $\Delta R = f(n)$ approaches fairly rapidly the dotted calibration curve which corresponds to a constant strain amplitude of $\pm 2000 \cdot 10^{-6}$; 10,000 cycles at ± 1500 and 20,000 cycles at ± 2000 yield a result similar to that of 30,000 at ± 2000. If the calibration curve is shifted so as to pass through point A, it is found that the first loading at ± 1500 increases the rate of strain-hardening, $d\Delta R/dn$, at the onset of the second loading; apparently, the crystal lattice distortions of the gauge are greater in number although less intense than those generated over 1800 cycles at ± 2000 (point A'). Under further loading at ± 2000, these distortions promote the initiation of further more severe distortions which are greater in number at the beginning. The additional strain-hardening is measured by calculating the difference of the ordinates between the curve AB and the calibration curve which is shifted toward the n-axis and passes through point A.

After a high enough number of cycles, here at point B, the additional strain-hardening becomes constant and the curve approaches the dotted calibration curve for ± 2000.

Secondly, subsequent loading under $10^6 \epsilon = \pm 1000$ below the gauge threshold sensitivity has a similar but very small effect on the strain-hardening caused by restoration of the load at ± 2000 (curve CD).

Let us go back to Figure 5.16, which concerns the effect of pre-straining on the stress-strain cycle of aluminium. The effect of high tensile or compressive pre-straining disappears after a few hundred cycles. It may be assumed that the same phenomenon occurs in fatigue gauges and that the steady mean strain produces merely the resistivity increment that is caused by its first application, as was observed by Micro-Measurements[48].

Although the variation of the stress-strain curve of 7075-T6 aluminium alloy sheets is certainly subject to some scatter - since the strains in work-hardened materials tend to increase in constant-strain tests as a result of fatigue - and although there is no indication that the gauges as such showed no scatter, the tests conducted by Horne and plotted in Figure 5.36 exhibited a slight effect of mean strain on resistance change during fatigue, at least as long as the slope of the curve $\Delta R = f(n)$ was not modified.

Scatter and Interpretation of the Test Results

The test results in Table 5.1 were obtained by Sud-Aviation[51] in an attempt to assess the capabilities of fatigue gauges. The shape of the bend specimen used and the locations of the fatigue and strain gauges are illustrated in Figure 5.37. The test was performed by applying a repeated deflection to the free end of a cantilever specimen by means of an eccentric.

For 35 tests run at various stresses, the value of ΔR at the change in slope was included between 3.5 and 8.4 ohm the average being 5.9; the ratios of the number of cycles prior to the appearance of a visible crack to the number of cycles prior to the change in slope was included between 1.2 and 3.2. No definite correlation was observed between the slope change and the appearance of a visible damage in the specimen; perhaps the shift in slope indicates the existence of invisible damage in the specimen or in the gauge.

TABLE 5.1

Increase in Resistance in NA-01 Fatigue Damage Gauges on Aluminium Alloy Specimens Subjected to Repeated Bending

Specimen No.	*Stress, in daN/mm²* *	*Conditions when the change in slope occurred*		*Conditions when the test was stopped*		*Remarks*
		ΔR ohms	n/10⁶	ΔR ohms	n/10⁶	
14	13.3 ± 13.3	7.2	0.28	64	0.71	Fractured 5.11 · 10⁶
15	13 ± 13	5.4	0.30	19.4	0.71	Uncracked
16	13.3 ± 13.3	7.6	0.21	165	0.71	Cracked at R = 11.03
17	13.2 ± 13.2	5.1	0.24	7	0.35	Cracked near attachment
19.1	13 ± 13	4.9	0.23	5.7	0.30	Uncracked
20.1	13 ± 13	5.6	0.26	10	0.45	Cracked near attachment
21.1	13.3 ± 13.3	5.1	0.21	6.3	0.33	Cracked near gauge
22.1	13 ± 13	4.7	0.24	7.9	0.40	Uncracked
23.1	13.2 ± 13.2	4.8	0.21	6.7	0.30	Uncracked
24.1	13.3 ± 13.3	5.8	0.15	8.9	0.22	Uncracked
25.1	13 – 13	5.7	0.26	6.8	0.32	Uncracked

* Note: 1 daN/mm² = 1450 lb/in².

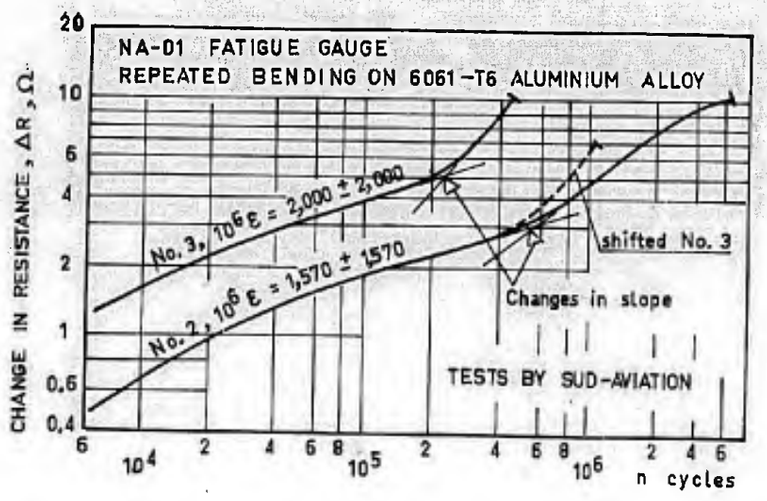

Fig. 5.32 Changes in resistance in fatigue gauges, log ΔR - log n diagram

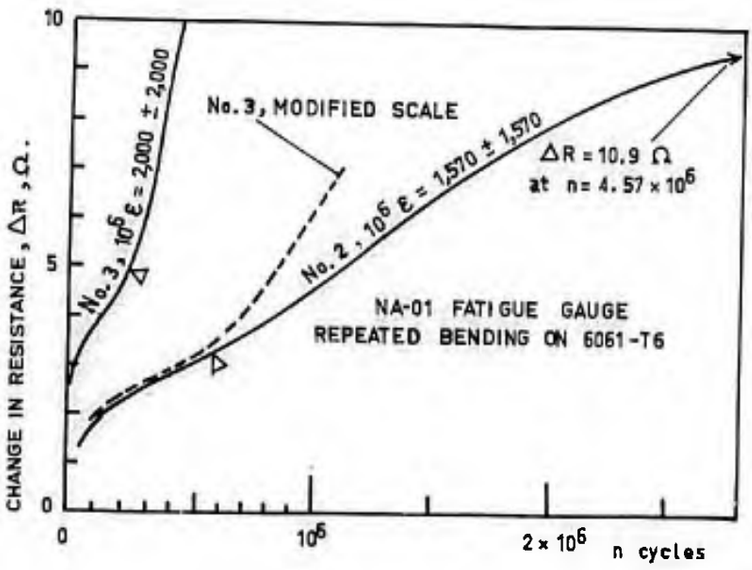

Fig. 5.33 ΔR-n representation of the results from Figure 5.32

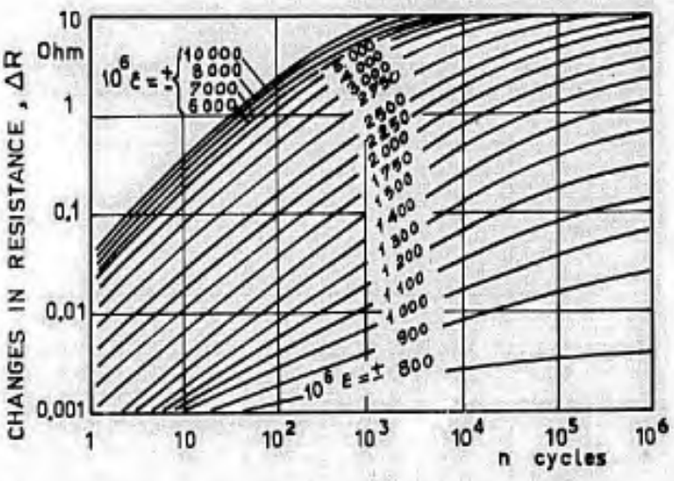

Fig. 5.34 Constant-amplitude calibration curves of NA-01 fatigue gauges

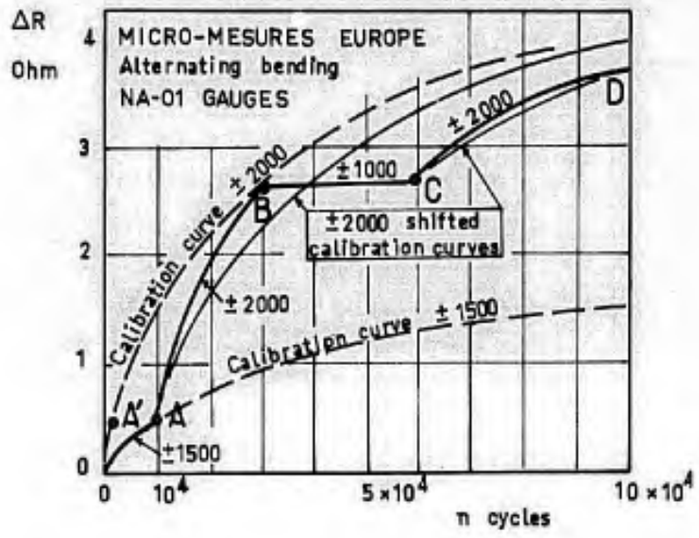

Fig. 5.35 Effect of change in fatigue strain amplitude[52]

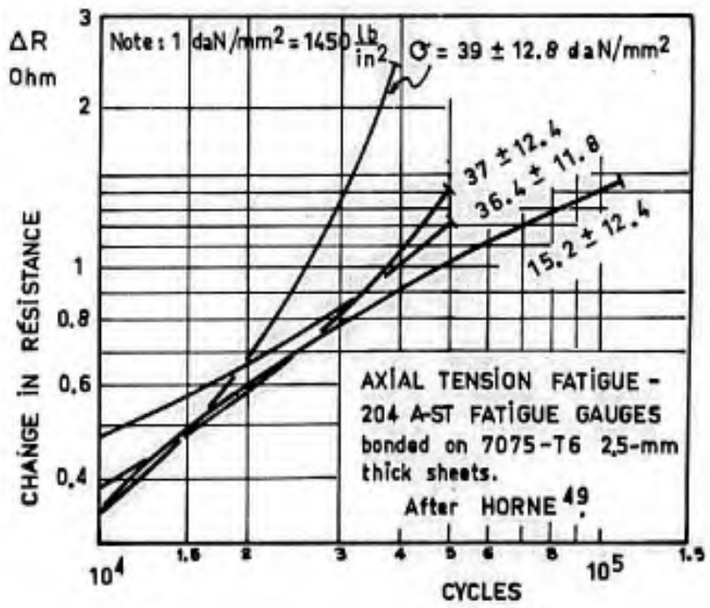

Fig. 5.36 Effect of the mean stress

Three types of fatigue gauge utilization can be considered:

1. Fatigue gauges may be used to *obtain some indication on the damage or pre-crack state of mechanical components*. We have seen that the change in resistance is not a reliable quantity in this respect.

2. Fatigue gauges may be used to assess the *severity of fatigue loads on specific structures* as compared with similar structures placed in a different environment.

3. Fatigue gauges may be used to detect hidden cracks in assemblies through the effect of an increase in stress in gauges located nearby and of a change in slope of the curve $\Delta R = f(n)$.

Before we conclude, some points ought to be emphasized:

(a) *The fatigue gauge does not reflect the state of the structure; it is only affected by the successive straining to which it is subjected.* In particular, it is usable to determine whether the material of the structure is tough or not, whether it includes crack-promoting or crack-impeding residual stresses, whether it has experienced corrosion or not, etc.

(b) *The increase in resistivity of a gauge is not a measure of its own damage experience.* Although there is no certainty about this, we shall assume that the fatigue of materials in general and that of gauges in particular are caused by the overstressing of some domains which are more rigid than the neighbouring domains, and by the creation of submicroscopic voids and microcracks accompanied by a continuous increase of the local stresses which favours the growth and joining of microcracks (see Chapter II, Sections 2.1.3, 2.2.1 and 2.5.3). The increase in resistivity of the gauge is due to the increasing number of dislocations, vacancies and microcracks, as well as to residual elastic shear stresses; however, each phenomenon does not necessarily play the same part in the probability of failure and in the increase in resistivity.

(c) *The material of the gauge is not the same as that of the inspected structure and behaves differently.* Indeed, the engineering metal used is often a work-hardened material which contains residual stresses, irrespective of its structure and its metallurgical texture.

(d) *The design of the gauge is different from that of the structure.* In stress concentration, the softening process of a work-hardened material and - in an opposite sense - the fretting phenomenon have a prevailing effect on the fatigue of the structure which is not detected by a gauge even if this gauge is located in the immediate neighbourhood of the maximum stress point.

We may now return to the possible gauge utilizations. From the above four points it follows that no prediction of structure pre-crack damage can be derived from the electrical-resistance measurements of a number of fatigue gauges.

Fatigue gauges may prove useful in assessing the relative severity of unknown service loads. To this end, counting accelerometers or extensometers, which provide a statistical summation of the number of times a given acceleration or stress is attained or exceeded, should be replaced by less complex instruments which can be interpreted without requiring the elaborate calculations and extensive knowledge of fatigue specialists for each type of structure. The gauge-structure assembly could thus be used as in the case of strain-gauges, where the structure is considered as a dynamometer for the determination of the loads after calibration. In such a case the fatigue gauges would have to be positioned away from stress concentrations, on components subject to high but homogeneous stresses. A conventional strain gauge, acting as the sensor of a counting extensometer, could be mounted at the same location for checking the quality of the overall information given by the fatigue gauge.

If we extend an idea of Christensen[54] which was later developed by Hooson[55], we may also suggest the installation of one or more fatigue gauges on specimens of variable cross-sectional area which would act as strain amplifiers if attached to the structure at both ends (this idea was independently developed by Harting[90]). Except for one factor, the various gauges would be subjected to the same strain history. By adequate calibration during a fatigue test on the basis of load spectra substantiated in service, it would be possible to select the best gauge location for appropriate overall information with respect to the structural damage state at weak points revealed by the fatigue test and located away from the gauges; these weak points being sensitive to the same load spectra.

Finally, after detection through service experience of possible crack initiations at some hidden locations, the use of fatigue gauges in the immediate neighbourhood of such locations would yield valuable information as regards the extension of cracks which are undetectable by any other method, thanks to the shift in slope of the curve $\Delta R = f(n)$, n being the number of turns of a machine, or the number of flights of an aircraft structure, or the number of service hours of a structure subjected to constant-amplitude vibrations, etc.

Such applications will be more convenient as soon as a better knowledge is gained concerning the properties of gauges under individual or block load sequences of same or opposite sign and of different magnitude. On the other hand, it is recommended that statistical data should be gathered on the constancy of gauges and on the restrictions required to prevent the gauges themselves from cracking (supersensitivity).

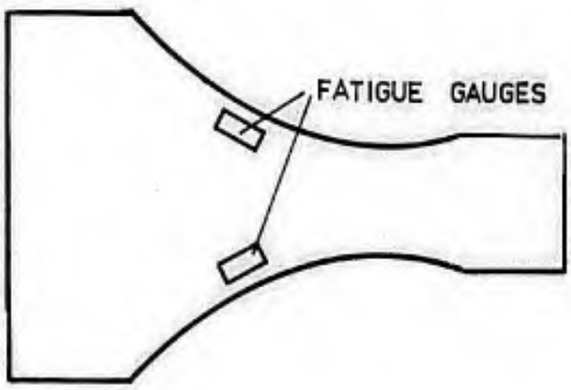

Fig. 5.37 Bending fatigue specimen

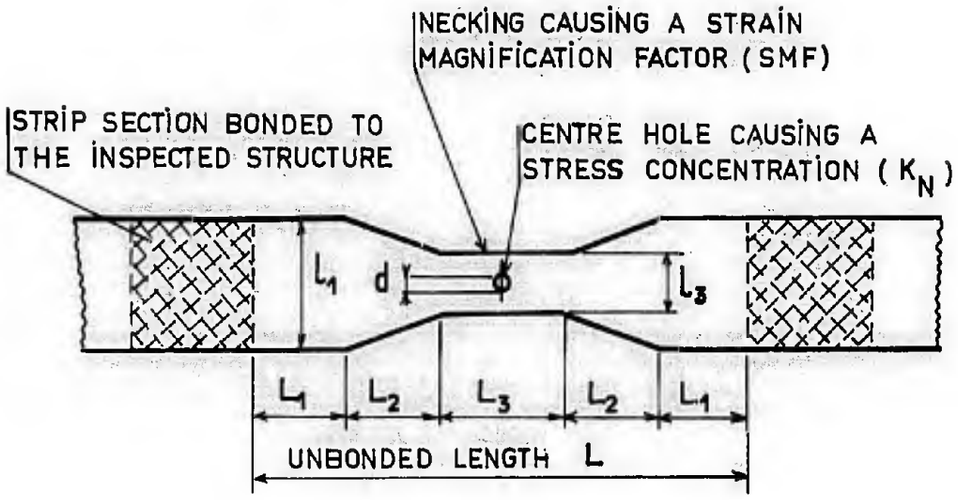

Fig. 5.38 Sketch of a fatigue monitor

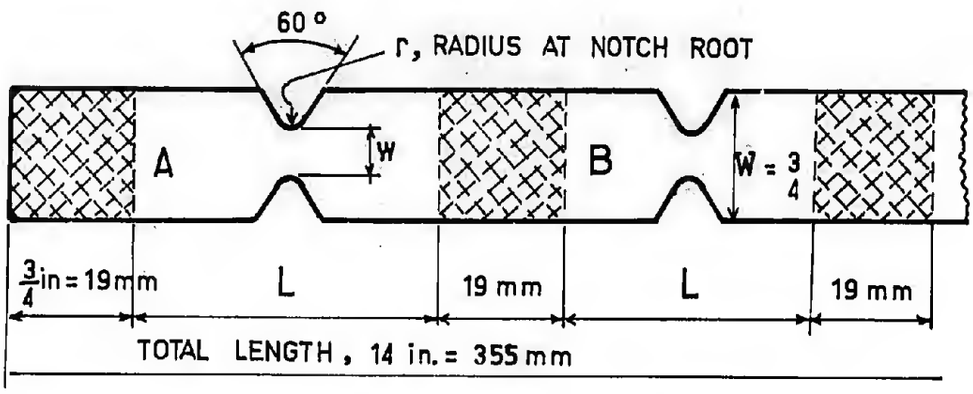

SIZES AND CHARACTERISTICS OF STRIP MONITORS (A TO F)

REFERENCE	A	B	C	D	E	F
L	2 3/4 in. = 70 mm	1 5/8 in.	3/8 in.	1 in.	5/8 in.	1 3/8 in.
W	0.125 in = 3 18 mm	0.085 in.	0.085 in.	0.085 in.	0.085 in.	0.085 in
r	0.033 in = 0.85 mm	0.033 in.	0.033 in.	0.033 in	0.033 in	0.007
SMF, theoretical	4.7	5.3	5	4.3	3.3	4.4
K_N, NEUBER	1.46	1,32	1.32	1.32	1,32	1.80
$K_N \times SMF$	6.8	7	6.6	5.7	4.4	7.9

Fig. 5.39 Fatigue monitor strips used in a full-scale test by Hobson[55]

5.1.7 Fatigue Monitors

The purpose of a study by Hooson[55], taking up an idea of Christensen[54] was to develop a device which would indicate visually the accumulation of fatigue damage in a given airplane structure. The device, called a "monitor", should provide information for estimating the time after which the structure under investigation should undergo a detailed inspection for fatigue damage. It should indicate at various intervals during service lifetime the proportion of safe life that an aircraft has used up. Being installed on every structure, it should help to determine whether a particular structure has been subjected to loads either more or less severe than the fatigue test loading; thus the varying degree of load severity from one aircraft to another could be taken into account in service life prediction.

Furthermore, an indication of the local severity of a load should be given by the behaviour of the monitor and it is unnecessary to convert measured accelerations into local stresses by means of calculations using transfer functions which are often ill-known. Note that, in principle, counting extensometers and fatigue gauges offer the same advantage.

The monitor consists of a metal strip bonded to the airplane structure; it includes unbonded areas with machined notches which are severe enough for the strip to fail before the structure suffers service damage. Higher stresses are obtained in the notches by increasing the lengths of the unbonded areas. In the case of a strip such as that depicted in Figure 5.38, if we neglect the centre hole and ignore the stress concentration factor inside the notch, the nominal strain magnification factor, S M F , will be defined as the ratio of the mean strain of the centre section, L_3 , to the mean strain of the structure within the inner boundaries of the bonded monitor areas. This factor is approximately

$$\epsilon_3/\epsilon = L \Big/ \left[2L_1 l_3/l_1 + L_3 + 4.6\, L_2 \frac{l_3}{l_1 - l_2} \log_{10}(l_1/l_3) \right] .$$

Measurements on strips containing no drilled hole with $L_2 = 0$ indicate a strain magnification factor of about 60% of the calculated values.

The use of round V-type side notches instead of a drilled hole offers better reliability. Figure 5.39 shows the monitor that was considered best after successful tests performed on a full-scale aircraft wing structure. However, if the stresses in the basic structure are low, it may be adequate to use monitors with a drilled hole in the necked-down centre section. Our opinion is that the notches should be representative of the weak points in the inspected structure, while the strain magnification should offset the low stresses in the basic structure and add an overall increment resulting in a more or less premature fracture, depending on the unbonded lengths.

The SMF was included between 3.3 and 5.3, the Neuber notch factor K_N (see expression 73 in Chapter IV) between 1.32 and 1.8, and the product (SMF) K_N between 4.4 and 7.9. A loop of fine wire was bonded to each monitor for easy detection of the failure. The monitors were machined from 7075-T6 aluminium alloy sheet, 0.7 mm (0.028 in.) thick, having the following tensile properties: $\sigma_{ult.}$ = 57 daN/mm^2 (83,300 lb/in^2), $\sigma_{0,2}$ = 51.5 daN/mm^2, E = 7,000 daN/mm^2, and A% = 8.8.

Cold bonding is not yet fully efficient and curing of the adhesive at high temperature (104°C, i.e. 220°F) causes the fatigue life to be reduced by 35 to 40% owing to the tensile residual stresses which are induced after cooling since the average temperature of the structure is below that of the monitor.

In the present state of the art, it appears to us that monitors are as difficult to use as fatigue gauges. If the sole objective is to obtain information on the relative severity of service and fatigue test loadings, then we consider that fatigue gauges can be combined with the strain magnification principle. However, we think it is important to use notches that are representative of the "equivalent" notches of the structure with a magnification factor giving a stress level slightly higher than that existing in the weak points of the structure. The failure of the monitor will thus give some "fail-safe" help to prevent a possible failure of the fatigue gauge.

5.2 FATIGUE CRACK PROPAGATION

Very little information is available regarding the fatigue crack propagation in thick components, so our study will be mainly concerned with sheet materials and thin components typical of the behaviour of conventional airframe and rocket structures.

In fatigue, final fracture takes place statically when the size of the crack is such that the applied load just equals the residual static strength of the cracked component (see Chapter IV). Consideration of the crack growth rate under fatigue loading is therefore essential in fatigue life investigations. It is also of paramount importance for determining the time between maintenance inspections in conjunction with the fail-safe concept, i.e., the service life from the time when a crack reaches a length large enough for it to be safely detected during routine inspections, to the time when the crack length is such that the margin between the residual static strength and the maximum service load expected during this time interval is considered to be just sufficient.

Finally, although it is common practice to distinguish between the crack initiation period and the crack propagation period before final fracture, it should be emphasized that this distinction is arbitrary. First, the crack initiation period can be very short if efficient crack detection methods are used; in fact, it is doubtful that there is any period of time without cracking. Second, the plastic and metallurgical transformation prior to the appearance of a crack continues ahead of the crack tip during the entire crack growth period. Consequently, it is of great interest to know how the crack extension is influenced by the various factors which are usually taken into account in fatigue surveys, such as mean stress, frequency, temperature, load level sequences, static overloads, etc.

5.2.1 Physical Process of Cracking

In general, fatigue cracks originate at the surface of components in high stress concentrations due to scores, corrosive attacks, fabrication defects resulting in slots, sharp notches, inhomogeneities such as local decarburization in steels, inclusions of constituent particles harder than the basic materials, e.g. metallic oxide inclusions (for this reason some ultra-high-strength steels are vacuum-remelted). In cases where the surface is protected by compressive residual stresses which delay the onset of cracking, it is sometimes found that cracks start from large internal flaws in the core of the component.

With perfect surface conditions, cracks appear as a result of shear strains following the plastic changes described in Chapter II, Paragraph 2.5.3. Crevices and extrusions (as observed by Forsyth[53]) and, subsequently, microcracks will thus form on those planes most closely aligned with the maximum shear stress planes. These cracks will join and extend on the slip planes from the surface grains to the depth of the component (Forsyth's Stage I). This mode of crack growth is favoured by shear stresses and by the existence of a favourably oriented single set of slip planes. Corrosion-fatigue conditions at low stresses may cause complete failure on a slip plane in single crystals.

In engineering metals, a crack initiated by the above described process deviates very quickly and follows a median path along a plane perpendicular to the maximum tensile stress or containing the maximum shear stress, depending on the relative importance of the direct tensile stresses due to applied external loads or of the shear-induced local tensile stresses near the slip barriers. This second mode of crack propagation (Forsyth's Stage II) is governed by the normal tensile stress near the crack tip. The fracture surface has a smooth and bright appearance and exhibits plateaux deepened by grooves which delineate the successive positions of the crack tip at the various stress cycles. It is assumed that these tide-marks are the result of local plastic deformations at the crack tip with a periodic deviation of the crack path (Chapter IV, Paragraph 4.4.2); they are most clearly revealed in ductile materials. Under a tensile mean stress the striations are flatter at the top, which means that the fracture contains a larger cleavage component, the striation side corresponding to a greater contribution of shear. The length of the cleavage crack of each cycle is a function of the stress level. The local variations in striation spacing will depend on the stress concentrations due to local inhomogeneities in the material which will cause irregularities in the crack front.

The striations studied by Forsyth have spacings that may identify the crack growth during a bloc test programme with different load levels. Investigation of these striations may sometimes aid in determining whether a component fractured in service was subjected to high load and low load cycles.

The cleavage region of each striation and the striation spacing are greater in low-frequency tests (20 c/m) than in high-frequency tests (180 c/m), although there is no such marked *effect of frequency* on the total lifetime. In the case of brittle materials, the striations contain less plastic deformation and a greater cleavage component, and are less apparent.

Stage I crack propagation along the slip planes is comparatively very slow and occurs only in a small depth near the surface of the material. Stage II crack propagation is more rapid and continues in thick parts until final fracture takes place. In thin sheet materials, Stage II develops into the formation of ductile lips inclined at 45° to the plane of the sheet.

Let us consider a point on the crack path far ahead of the crack tip. The alternating stress amplitude remains constant at that point as long as the crack size is very small, whereas in the course of crack extension the stress increases as the crack front comes closer. The material undergoes a plastic transformation and the stress loop changes in shape during the fatigue process. At the beginning, the material, if it is an initially work-hardened engineering metal, softens and the loop opens. Plastic deformation increases as the crack tip comes nearer to the point considered; at the same time, the mean static stress component produces a mean elongation which causes it to decrease in the region of the crack front. In other words, the mean stress concentration tends to decrease as the corresponding mean stress distribution tends to become uniform because of *fatigue creep* (see Paragraph 5.1.1.2). The stress-strain cycle tends to become an alternating cycle but it cannot be predicted whether the loop will continue to open (softening) or to close (hardening). Some authors believe that the material hardens, which would involve a stress increase likely to account for the failure. However, failure without hardening can be easily conceived, if it is recognized that the strength can be lowered either by the development of a large number of microcracks or by the overstressing of small hardened domains within a softer assembly or by a combination of these two processes. From the work of Forsyth, it may be concluded that the crack front is the seat of considerable plastic strains.

We may summarize as follows:

1. At a point far ahead of the crack tip, the plastic changes which are at first fairly rapid, become steady before it increases again for two reasons: (a) as a result of the increase in net stress due to crack

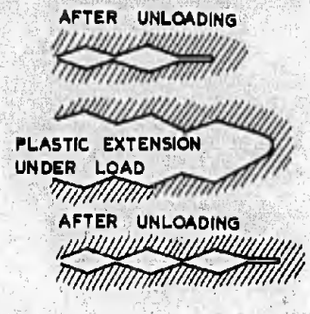

Fig. 5.40 Ductile fatigue crack propagation (after McMillan, Pelloux and Schijve)

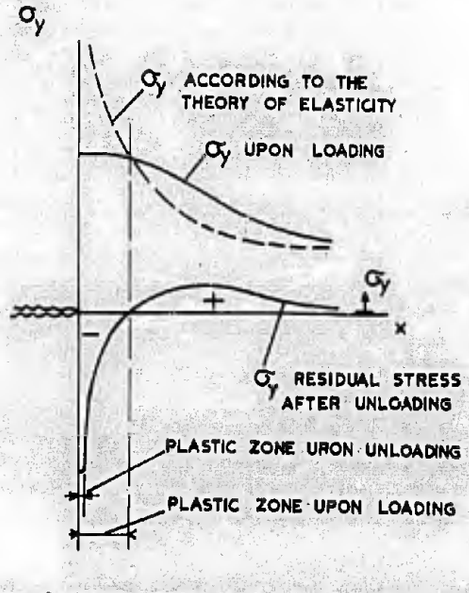

Fig. 5.41 Distribution of stresses under load and of residual stresses ahead of a crack, as modified by the plastic displacements

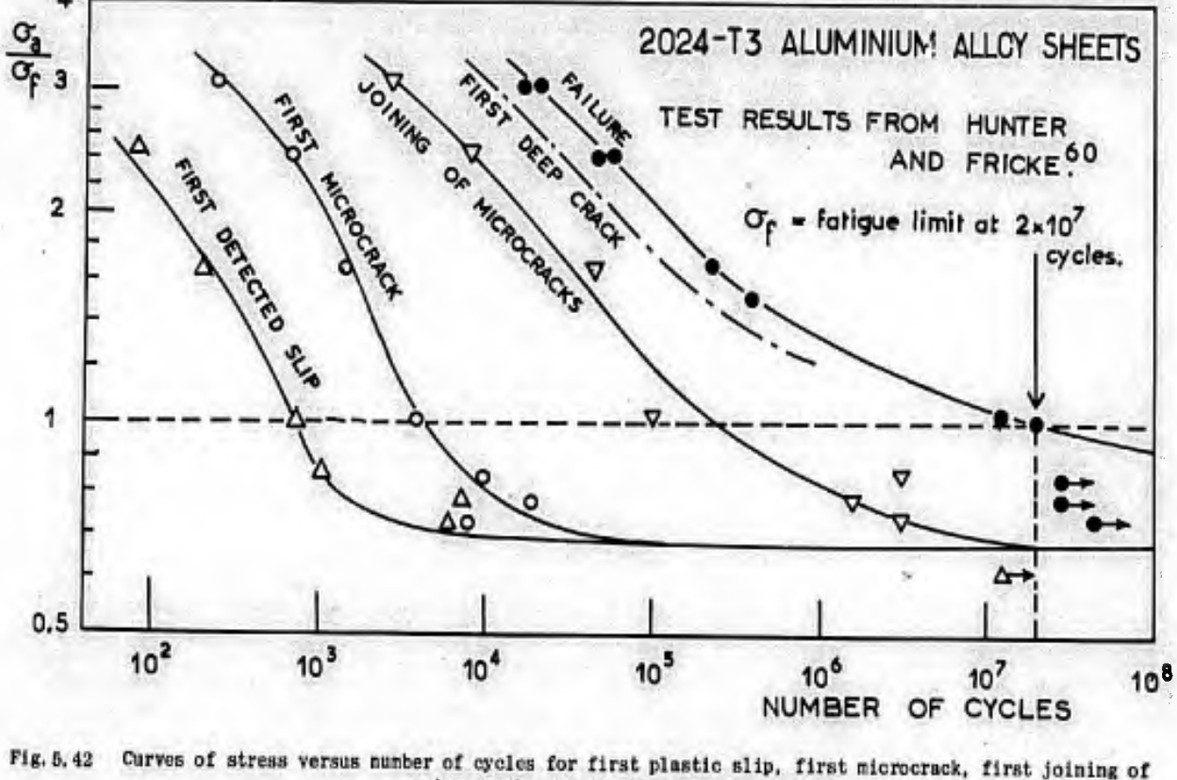

Fig. 5.42 Curves of stress versus number of cycles for first plastic slip, first microcrack, first joining of microcracks, first deep crack and failure

propagation in tests with constant external loading, (b) because of the stress concentration that occurs near the crack tip.

2. In the region of the crack tip, the plastic changes are dependent on the strains that are introduced into a small volume of the material subject to rapid transformation by the remaining bulk of the material in which the transformation is much slower. The strains applied to the boundaries of the small volume can be represented fairly well by those obtained with the theory of elasticity, provided the outer volume remains practically in the elastic range.

3. Accordingly, the most significant criterion for the stress and strain state at the boundaries of a small domain subject to rapid plastic changes is Irwin's stress intensity factor K, as defined in the preceding Chapter IV, Paragraphs 4.2.3 and 4.4.

The creation of crevices and extrusions described by Forsyth was also observed by Wilkow and Shield[56] on materials of face-centered cubic structure, i.e., aluminium, silver, copper, nickel and gold. From their observations it appears that some concentrations of vacancies or of foreign interstitials, which are in excess of the average equilibrium density, occur during cyclic straining and are then shifted through plastic slip toward the surface, where they accumulate into stable crevices or extrusions. There is no qualitative difference in the effect of fatigue at temperatures of 4°K, 77°K or 300°K; however, a decrease in temperature increases the striation spacing and reduces the rate of coalescence as well as the size of the depressions which form at the surface.

Striation Formation

It seems well established that under constant-amplitude stress the crack front progresses at each cycle during the load rise sequence.

In ductile materials, the extension of the crack tip results in crack propagation with a round-off. Upon unloading - which has a compressive effect owing to the residual stresses - the crack closes as shown in Figure 5.40, or in a more complex manner as suggested by Laird[57], in which case two subsidiary notches appear under 45° at the extremity of the closed crack.

According to Broek and Van der Vet[85], the striated fracture surface is sometimes deformed by folds due to plastic slip which occurs after the passage of the crack front. Comparison of the crack propagation rate and of the striation pitch on 2 mm thick 2024-T3 and 7075-T6 sheets shows that the pitch is greater with slow crack propagation rates - the advance is irregular and may halt locally - and smaller with fast crack propagation rates owing to the rapid advances through successive static fractures.

In brittle materials, the crack propagation during the load rise sequence is caused by cleavage, that is, by the joining of microcracks; the crack tip is rounded off as it spreads into a less damaged area. During unloading, two subsidiary notches form at an angle of 45°, one of which will be the origin of further crack extension by cleavage during the next loading sequence.

In both cases it must be assumed that the crack growth comes to a stop when reaching a less damaged area of the material, and that shear during the compression sequence causes damage to the still uncracked material, which favours further crack propagation. The damaged area is large if the alternating stress is high and the crack propagation in a given damage area increases with maximum stress.

Figure 5.41 shows the stress distribution ahead of the crack as modified by plastic elongation. One may distinguish three zones: an elastic zone with a mean stress distribution that is in good agreement with the theoretical elastic distribution in spite of the existence of plastic displacements on the smaller scales of the grains, subgrains and precipitates; a plastic zone upon loading in which the stress is limited by plastic shear flow; finally, a plastic zone upon unloading in which the compressive residual stress is limited by plastic shear flow of reverse direction with respect to the previous shear.

Starting from the tip of a crack, the above zones account for the changes in striation spacing and perhaps define the boundaries of zones that allow prediction of such changes:

Zone I of subsequent crack propagation, located in the immediate neighbourhood of the crack front. If brittle, the material contains a large number of microcracks; if ductile, it has become quite soft. In both cases the material which is still uncracked during loading is about to crack and the unloading sequence which results into compression with shear produces the additional damage conducive to further extension of the crack. The existence of this zone is quite logical. The damage will be significant if the last maximum load and the last alternating load applied are high.

Zone II with moderate damage and compressive residual stresses. Microcracks are less in number and severity and compressive residual stresses are observed on the geometrical scale. These residual stresses, which lower the damaging effect, are found in an area which increases in size with the last application of maximum load.

Zone III of understressing. The fatigue, being moderately severe, has as yet developed but a small number of microcracks while the yield due to stress variations on the scale of the grains and subgrains or precipitates has caused a decrease in the pre-existing residual stresses and thus reduced the tendency of microcracks to appear (understressing).

The existence of these zones - unquestionable as regards Zone I and Zone II - helps explain the changes in crack propagation rate whenever the material is subjected to successive loadings of different levels.

If at constant maximum load the alternating load is reduced, the spacing of striations decreases and crack growth may even be stopped for a while before it continues, because the additional damage of Zone I upon the first unloading is not sufficiently severe for continued crack extension, so that additional cycling is necessary (see tests by McMillan and Pelloux[58]).

If at constant alternating load the maximum load is reduced, it is found (Hertzberg[59]) that the first cycle under the lower maximum load results in a striation spacing that is somewhat wider than under the subsequent cycles, the reason being that Zone I as damaged by the last cycle of the higher maximum load is slightly larger than it will be under the next cycle.

Although fractographic analysis of replicas with the electron microscope reveals a regular striation spacing in small regions inside the grains, the crack propagation rate varies from grain to grain owing to scatter in the properties of the material, to the specific orientation of each grain, and to the corresponding variation of the residual stresses. On the geometrical scale a certain irregularity is also found but it is not permanent: if for some reason the crack propagation rate was above the normal, the material of Zone I will not remain as long in damage Zone II and the crack propagation rate will decrease. However, the material of the present Zone II will, in turn, not stay as long in Zone III of understressing and will thus be improved to a lesser degree; consequently, a further increase in crack propagation rate will ensue. Toward the end of crack propagation the damaged zone ahead of the crack enlarges considerably and the irregularity disappears, together with its self-regulating process.

5.2.2 Relative Durations of Crack Initiation and Crack Propagation Stages

In view of the complexity of the fatigue failure process it is difficult to define what is called crack initiation. In Figure 5.42, after Hunter and Fricke[60], curves of stress versus number of cycles are shown for thin 2024-T3 aluminium alloy sheet for the following phenomena: first plastic slip, detection of the first microcrack through analysis of a replica with the electron microscope, joining of microcracks, first deep crack, fracture. The number of cycles from the appearance of the first microcrack to failure may be quite high; there may even be non-propagating microcracks.

Bennett[61] has developed a method of separating the damaging effect of crack initiation from that of crack propagation. He showed that fatigue crack propagation in certain metals resulted in the evolution of dissolved hydrogen. If the evolved gas is trapped under transparent pressure-sensitive tape, it forms bubbles which provide a convenient and sensitive means for detecting small cracks and for determining if a crack is propagating. Fatigue bend specimens made from bar stock of 2024-T4 aluminium alloy were subjected to a fatigue load defined by $\sigma_{a1} = 40{,}000$ lb/in^2 with $\sigma_m = 0.25\,\sigma_a$ until bubbles were observed. Some specimens were stressed under the same conditions up to failure or $N = 5 \times 10^6$; others were stressed at lower stress amplitudes. The purpose was to determine the fatigue limit of specimens exhibiting no bubbles during the initial stressing and that of specimens after crack initiation. Some test results are plotted in Figure 5.43; the round points represent specimens without bubbles; the open circles indicate that the specimens did not fail, the closed circles that crack propagation was observed, and the half-open point that the specimen failed. From this it may be concluded that the fatigue limit is about 30,000 lb/in^2 for specimens without incipient cracks. On the contrary, triangular points are used for specimens that exhibited incipient cracks detected by the presence of bubbles; the open triangles indicate that no crack propagation took place, and the solid triangle that crack propagation was observed. The fatigue limit of cracked specimens is thus of the order of 10,000 lb/in^2.

Bennett's conclusions were:

1. The fatigue strength of 2024-T4 specimens containing a small fatigue crack was 50 to 60% less than that of specimens subjected to nearly the same number of damaging stress cycles without developing a detectable crack.
2. The decrease in fatigue strength was only 10 to 20% if a detectable crack had not developed.
3. In attempts to evaluate cumulative damage, it is essential to consider the crack initiation and crack propagation stages separately.

The absolute duration of the crack propagation stage is not dependent on the surface condition which, on the contrary, plays a prevailing part in the duration of the fatigue process prior to the development of a visible crack. De Forrest and Magnuson[62] investigated the crack propagation in rotating-bending tests on 5/8 in. diameter specimens made from mild SAE-1020 steel. The cracks were semi-circular at their initiation and then semi-elliptical. On some specimens the shape of the cracks was determined by dipping the cracked specimens into liquid air, after which they were broken with a hammer. Small cracks were detected by means of a magnetoscope. Four test series were performed with the following specimen conditions:

(a) Bars in the as-delivered, cold-rolled condition,

(b) Annealed bars with coarse circumferential scores obtained with a bastard file,

(c) Annealed bars with fine circumferential scores obtained with emery paper No. 0,

(d) Annealed bars with coarse circumferential scores obtained with coarse emery paper No. 73.

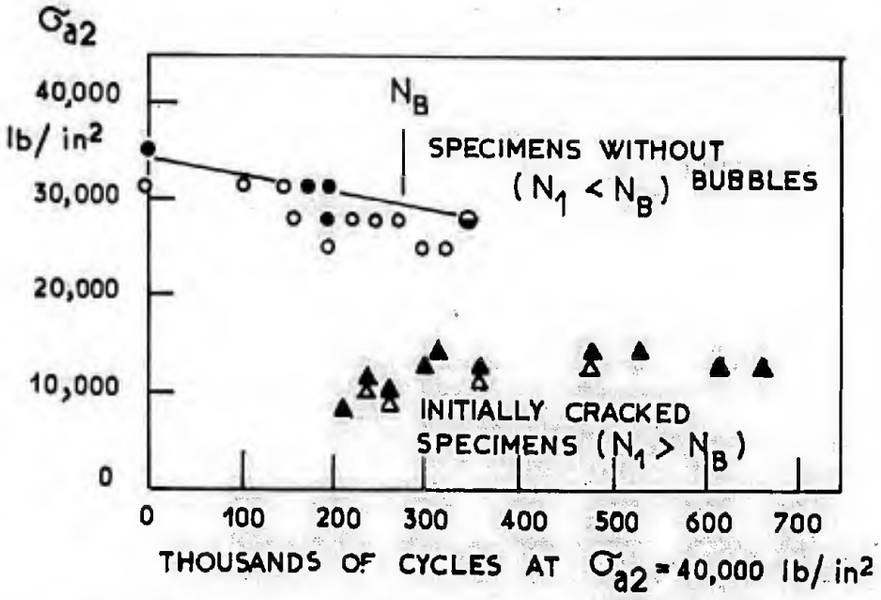

Fig. 5.43 Results of tests to determine the fatigue strength of specimens that had been stressed for N_1 cycles at σ_{a1} = 40,000 lb/in^2 (after Bennett[61])

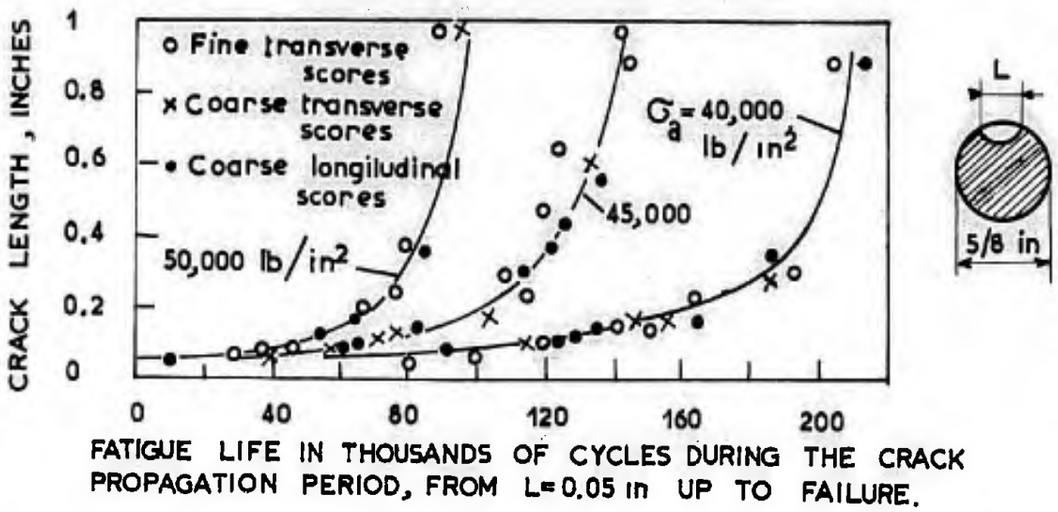

Fig. 5.44 Crack propagation under rotating-bending in mild SAE-1020 steel, annealed and machined (after De Forrest and Magnuson[62])

TABLE 5.2

Effect of Surface Condition on Crack Nucleation and Crack Propagation Periods

Mild SAE-1020 steel bars subjected to rotating-bending (after De Forrest[62]); number of 1,000 cycles required to obtain:

σ_a 1,000 lb/in^2	*Crack propagation from 0.08 to 0.1 in.*				*Crack propagation from 0.1in. to failure*				*Crack initiation from nucleation to 0.1 in.*			
	a	b	c	d	a	b	c	d	a	tb	c	d
65								19				40
55								27				130
50	7		8	20	41	48	51	88	90	217	288	690
45	12		15	50	61	75	71	353	166	482	748	1430
40	20	17	22		105	100	100		436	1600	2720	

Figure 5.44 contains the crack growth data of the annealed bars from a surface length of 0.05 in. up to failure; the crack propagation stage is not dependent on the surface condition. Table 5.2 shows the effect of surface condition on the crack nucleation period. It is seen that the surface condition is a determining factor of the fatigue duration required for crack initiation in annealed specimens, but it has no effect on the crack propagation rate.

As a rule, all methods of surface hardening which create compressive residual stresses at the surface involve crack initiation delays but do not modify the time period between the appearance of a crack and failure.

Crack initiation is relatively shorter in notched specimens than in unnotched specimens; with equal stress and strain states at the tip of a crack, the stresses and strains responsible for the fatigue process prior to crack initiation appear to be greater in unnotched specimens than in notched specimens. From this the following important practical implication may be derived, after Christensen and Harmon[63]:

Adequately designed components or components with an improved surface condition can sustain higher service stresses prior to crack initiation but the crack propagation period may be comparatively so short that the crack will prove catastrophic before it can be detected at all through service inspection. Conversely, poorly designed components or components with an inappropriate surface condition, for example arc-welded parts, withstand lower service stresses but crack propagation is so slow that it can often be detected before it becomes too hazardous.

As shown by the tests of Schijve and Jacob[64] on 2 mm thick 2024-T3 aluminium alloy sheets, the greatest scatter in fatigue life before a crack is detected is mainly found under low stresses. The same result was obtained in tests run by Jaillon and Lachenaud[65] on A5-clad A-U4G1 (2024-T351) aluminium alloy sheets. Using these results and taking $\sigma_{ult.} = 46.8$ daN/mm^2 (68,000 lb/in^2), $R = \sigma_{min}/\sigma_{max} = 0.1$, we have computed the mean values and scatters listed below for ten tests in each series on 100 mm wide and 1.5 mm thick specimens containing a 2 mm diameter hole at their centres:

$\sigma_{max}/\sigma_{ult.}$ =	0.5		0.4		0.3	
	log N	s(log N)	log N	s(log N)	log N	s(log N)
Crack initiation	4.338	0.033	4.637	0.048	5.088	0.100
Total fatigue life	4.495	0.030	4.874	0.048	5.381	0.046

It may be assumed that the degree of initial work-hardening exhibits more scatter in actual structures than in small test pieces, and that this has a direct impact on the crack nucleation period whereas the regulating effect of fatigue on the degree of work-hardening introduces less scatter in the crack propagation period to failure.

5.2.3 Fatigue Crack Growth Rate

If l is the length of a fatigue crack in thin sheet and n the number of cycles, we have a ratio dl/dn called growth rate or "propagation" rate. The term "propagation", however, causes confusion with the slow crack propagation which takes place under static load until rapid unstable propagation occurs (see Chapter IV, Paragraph 4.3.2).

Most of the experimental studies have been made with thin specimens having a centre crack initiated at the contour of a hole, and sometimes containing two sharp, diametrically opposed side cuts. Specimens were usually subjected to repeated or fluctuating tension, and more rarely to reversed tension-compression.

Some tests, like Weibull's[66,67,68,69], were performed with a net stress in the uncracked cross-sectional area, σ_N, kept constant in amplitude by reducing the load whenever the crack length tended to increase. Most of the other tests were run under a constant-amplitude load defined by the nominal stress, σ, of a section away from the crack. In all cases, however, if we consider the actual stress state at a given point of the material before the crack extends to this point, we find that the local stress is constantly raised as the crack tip draws nearer. This increase occurs less rapidly if the load is periodically reduced to maintain a substantially constant net mean stress.

We are thus led to first investigate the possible effects of prior fatigue or static loads, peak loads, and load level variations during fatigue.

O'Neill[70], using 2 mm (0.08 in.) thick 2024-T3 aluminium alloy sheets, studied the effect of fatigue loading prior to notching on the growth rate of a crack obtained under fatigue loading after notching. In Figure 5.45, each curve is the average of two tests. The effect is quite significant although it can be masked by scatter, especially by that of batches of material of various origins.

The rate of growth is slower in material that has been fatigued prior to the starting of a crack; the more severe the previous loading, the slower is the rate of growth.

This is a particular case of the general improving effect of plastic changes in fatigue observed prior to the development of microcracks. As in the case of notched specimens, we would suggest that the improvement is essentially a decrease of the tensile residual stresses and an increase of the compressive residual stresses in micro-ranges in which the loading sequence causes tensile stress concentrations.

Hudson and Hardrath[71] conducted fatigue crack propagation tests at two successive load levels, σ_1 and σ_2, as well as tests at a single level, σ_c. When the first stress level, σ_1, is lower than the second, σ_2, the rate of growth at comparable crack lengths is substantially the same as in the single-level test if $\sigma_c = \sigma_2$.

On the other hand, if σ_2 is lower than σ_1, and if we compare the rate of growth with what it would be in the absence of preload σ_1 for the same length of the crack, then prior loading has two effects:

1. No further crack growth takes place during a number of cycles at level σ_2 which is large if σ_1 is high.

2. The crack growth then continues at an increased rate if the delay of growth has been considerable.

These tests were carried out on thin 2024-T3 and 7075-T6 aluminium alloy sheets. The same results were found on the same alloys by Hartman et al[72].

There are two explanations for these results. First, if we compare them with the results of the two-level creep tests performed by Carreker et al[73] on lead, copper and 61-ST aluminium alloy, we may suggest the explanation given previously (Chapter III, Paragraph 3.2.2) by replacing the creep-induced plastic transformation by that due to fatigue loading. After n_1 cycles at σ_1, the plastic changes due to fatigue ahead of the crack front reach a steady state with a strain-hardened condition defined by a statistical distribution of the stability of the crystal lattice distortions. When the stress is reduced to a value σ_2, most of the lattice distortions are very stable and plastic transformation ceases almost completely. With repeated cycling, the less stable distortions are progressively released while the others are overstressed, which weakens the relative stability. As a result of the missing distortions, plastic transformation is then more rapid than in the absence of previous loading.

Secondly, the process investigated can be explained by the compressive residual stresses that are created by the peak load ahead of the crack front. The residual stresses induced by the second loading are lower and the crack growth retardation would correspond to the plastic transformation of the residual stresses from the higher value of the first loading to the lower value of the second loading. The faster crack growth rate following the halt could then be accounted for by the greater number of fatigue cycles of the material ahead of the crack front. While the residual stresses decrease slowly, they are, however, increased by the first application of the peak load, which explains the regular behaviour observed when the first load level is the lowest.

The two explanations are complementary and are both applicable to all plastic metals; hence, the phenomenon under review is not restricted to aluminium alloys and appears to have a general significance. The more rapid transformation after a delay probably occurs in all cases of improvement produced by compressive residual stresses and should incite the engineer to use this technique with caution: while the total life is increased, the crack propagation period is shortened to a relatively large extent.

If a small number of preloads is applied (1 to 3 cycles), tests by Weibull (Figure 10 from Reference 69) show that the retardation of crack growth is then quite considerable although the subsequent growth rate is not modified significantly, but the relative crack propagation period becomes very short.

Schijve[74] states that, if overloads are applied in the course of crack propagation, each group of these loads (1 to 3 cycles) will at first cause a delay of crack growth, after which crack extension tends to continue at the rate it would assume in the absence of peak loads. Figures 5.46 and 5.47, after Schijve, show the effect of overloads on crack growth in clad 2024 aluminium alloy sheets; the effect of a tensile overload is much greater than that of a reversed overload with compression. From Figure 5.47 it is seen that the beneficial effect of a tensile overload is significantly lessened by the immediate application of a compressive overload, even if the latter is very small. From this we may conclude that *in simulating service fatigue loads by a test one should not forget the drop of loads to zero or slightly negative values which correspond to rests or operational interruptions.* The third overload causes a slight extension of the crack. The compressive residual stress ahead of the crack tip due to the tensile overload is corresponding to a local slot opening at crack tip, whereby the compressive overload can reduce the residual stress.

Though we have seen (Fig. 5.45) that there is an effect of prior fatigue loading on crack growth rate, this effect is found only at the beginning of crack growth and disappears at great crack lengths. Provided the stress intensity factor, K, varies slowly, the rate of growth is dependent on K alone if the application of the preload or peak load has not been effected recently.

Swanson, Cicci and Hoppe[75] have carried out a comprehensive study of the rate of crack growth in thin clad 7079-T6 aluminium alloy sheets which were cold-rolled after being treated (0.080 in. and 0.125 in. thick) or left unprocessed after treatment (0.16 in. and 0.25 in. thick). Four specimen widths were chosen (5 - 7.5 - 10 - 12.5 in.) with each specimen containing a centre notch. The modes of testing, for which a special electronically controlled fatigue machine was used, were as follows:

Constant load amplitude - no load shedding (CA-NLS). This is a most popular method of testing in published work. The crack surface, at first perpendicular to the sheet surfaces, exhibits an onset of shear lip activity at 45° (see Figure 4.21 in Chapter IV) for a value K_1 of the stress intensity factor that is independent of thickness. The shear lips are fully developed across the thickness at a total crack length L_2, the corresponding value of the stress intensity factor being K_2. The angle of shear lip development from L_1 to L_2 varies in a manner similar to the crack growth rate, da/dn, where a is the half-crack length.

Random load amplitude. When excited by filtered white noise, the resonance test machine produces a load amplitude following a *Rayleigh distribution for the cumulative frequency* F (probability of attaining or exceeding level L):

$$F = e^{-(L/L_e)^2},$$

where $L_e^2 = \int_1^0 L^2 dF$ is the squared r.m.s. of the random load. In such tests, the arrest lines associated with the higher load values assume a regular curvature instead of the irregular alternating growth from midthickness to the sheet surfaces ("tunnelling") that is often found in constant load amplitude tests.

Constant K amplitude. The load is constantly reduced during the test in order to maintain a constant stress intensity factor, K, the value of which is defined by Westergaard's finite-width correction or by Isida's more accurate correction (see Chapter IV, Paragraph 4.2.3). From the discussion of the results it follows that *the crack growth rate is constant when K is constant.*

Random K amplitude. A constant growth rate is also observed when the r.m.s. value of K is constant. The crack growth rate that will be found in random tests can be predicted from the rates obtained in constant amplitude tests by means of the expression

$$da/dn = \int_1^0 f(K)dF,$$

where $f(K) = AK^m$ refers to constant-amplitude tests.

Constant amplitude of the net stress in the uncracked area. Tests of this type were performed with a view to checking the validity of Weibull's assumption - based on his test results - that the rate of crack growth is constant after a period of transition and proportional to the specimen width. Tests by Swanson show a point of inflection on the curve a-f(n) that corresponds to the fairly flat maximum of the stress intensity factor as calculated by Isida's method. Transition from the tensile fracture surface perpendicular to the sheet surfaces to the fracture surface with ductile lips at 45° occurs before the maximum of K is reached; it actually takes place at a value of K comparable to that of the inverse transition after the maximum value of K has been exceeded.

5.2.4 Representation and Mathematical Expression of the Crack Growth Rates

As with many other problems, the mathematical expressions proposed by various authors for convenient formulation of their test results reflect their desire to eliminate scatter by using a rectilinear plot on a diagram with abscissas and ordinates to suit specific functional scales. If the initial phase of a test is inconsistent with the empirical rule suggested afterwards, then it is considered to be a period of transition between crack initiation and normal crack propagation. Similarly, there is admittedly another transition before final static failure occurs between fatigue crack propagation and static crack propagation to failure.

For formulation of their results obtained on mild steel and on the British 4% copper-aluminium alloy B.S. L71, Frost and Dugdale[76] used the expression

$$da/dn = A\sigma_a^3 a, \qquad (6)$$

where A is a coefficient dependent on mean stress, σ_m, a the half-crack length of a centre crack in thin sheet, and σ_a the alternating stress. Frost and Denton[77] found the same result for commercially pure titanium, a 5% aluminium-titanium alloy and a 15% molybdenum-titanium alloy. The specimen were 10 in. wide and 10 in. long in the test section, beyond which they enlarged with 10 in. radii. The thicknesses were about 0.13 in. (3.3 mm). Some results are given in Table 5.3 for the materials investigated.

The table shows that the propagation rate increases with mean stress in sheets made from B.S. L71 aluminium alloy (similar to 2024-T3), and that it is independent of it in mild steel, in titanium and in the two titanium alloys. The crack plane remained at 90° to the sheet surfaces until complete failure occurred in both the titanium and the 5% aluminium-titanium alloy, while there was a change from 90° to 45° prior to final failure in the 15% molybdenum-titanium alloy. Complete failure of the commercially pure titanium occurred through yielding of the uncracked cross-sectional area, which led to a ductile-type tensile failure. Complete failure of the two titanium alloys occurred in a brittle manner, but at different crack lengths - at great crack lengths with the 5% aluminium-titanium alloy and at very small crack lengths with the 15% molybdenum-titanium alloy. For the latter alloy the authors indicate the crack lengths that were obtained at the beginning of the change from the 90° growth to the 45° growth, as well as those obtained at final fast failure, but from this we could derive no simple correlation in terms of alternating or maximum stress intensity factor.

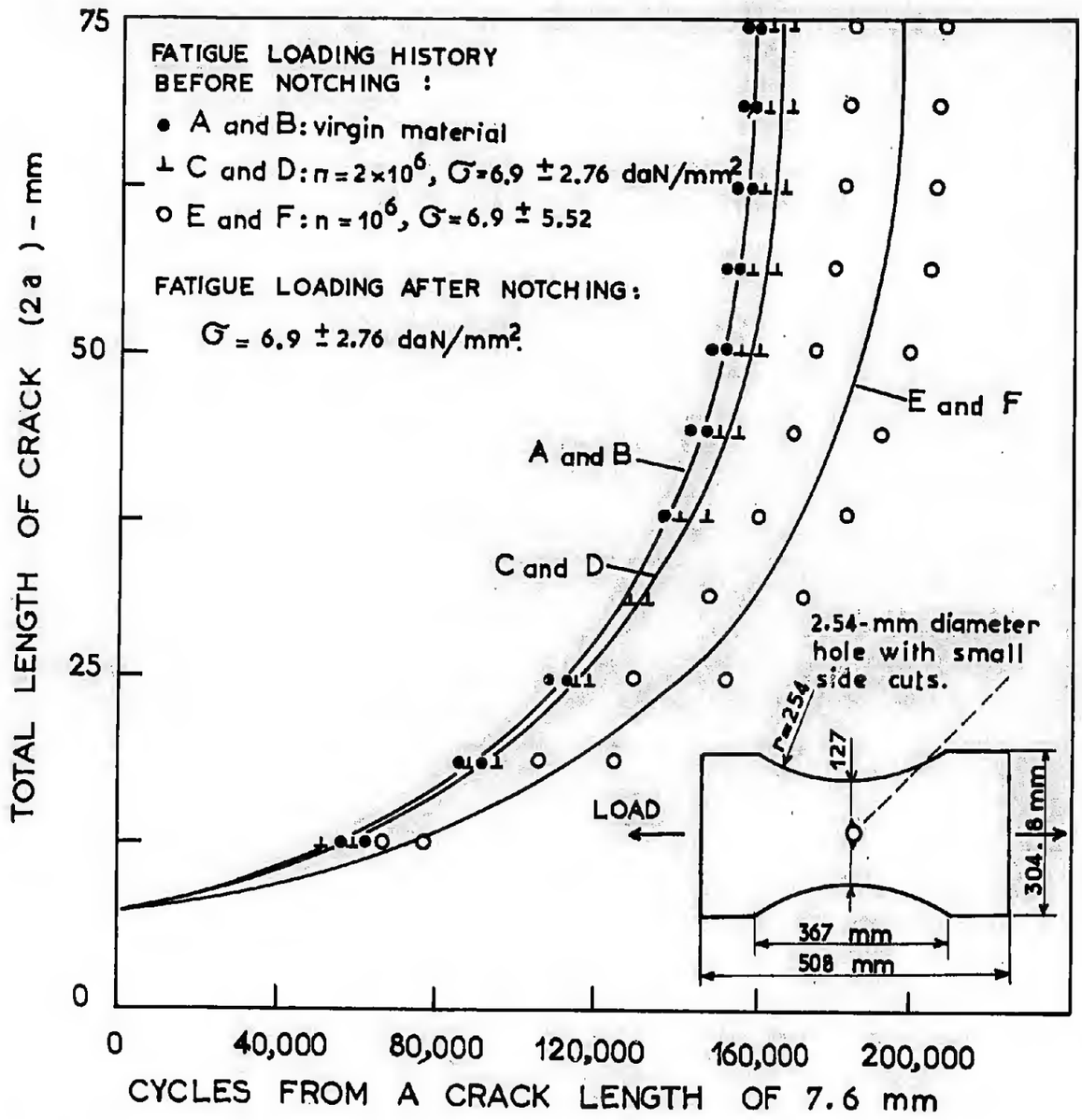

Fig. 5.45 Effect of fatigue loading prior to crack initiation on the subsequent crack growth rate (after O'Neill[70])

TABLE 5.3

Values of A in Tests by Frost

Material	*Tensile mean stress (expressed in daN/mm²)*	10^6 *A*
Commercially pure titanium	5.1 to 34	0.34
5% Al - titanium alloy	12 to 42.5	0.217
15% Mo - titanium alloy	12 to 34	0.36
"	42.5	0.60
Mild steel	3.08 to 18.5	0.0246
4% Cu - aluminium alloy	3.08	0.35
" (B.S. L 71)	4.6 to 6.2	0.75
"	23	3.15
"	35.5	4.95

Note: The values of A are for da/dn expressed in mm/cycle, a in mm, and σ_a in daN/mm².

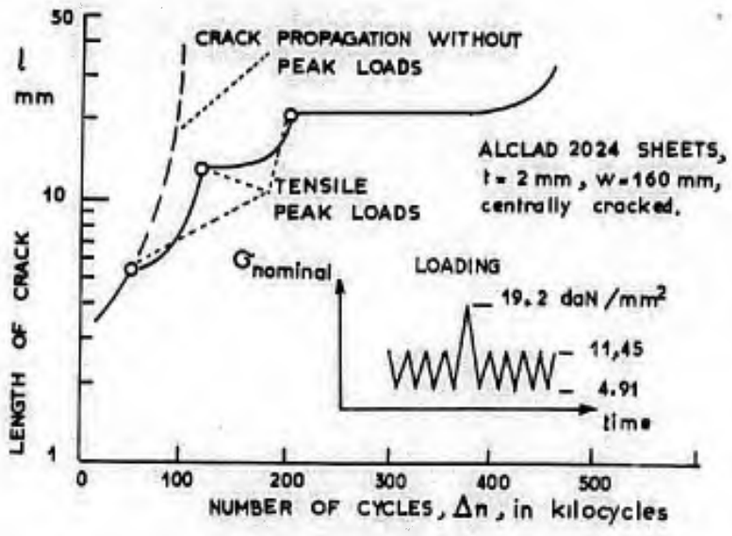

Fig. 5.46 Delaying effect on crack propagation as caused by tensile peak loads (after Schijve[74])

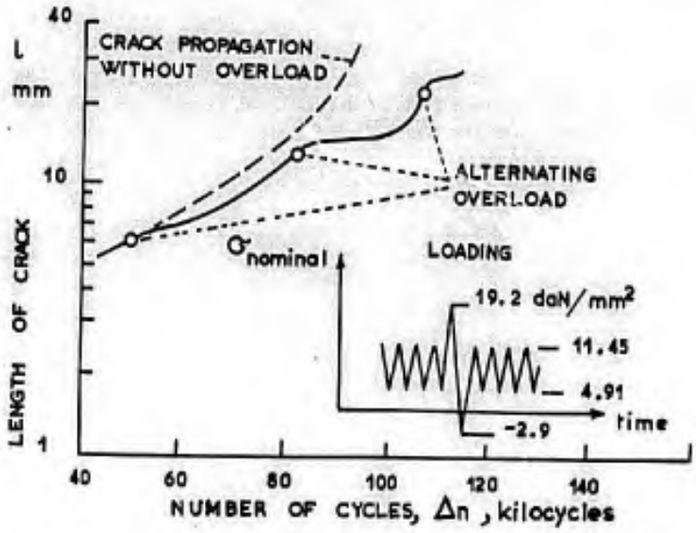

Fig. 5.47 Delaying effect on crack propagation as caused by alternating overload (after Schijve[74])

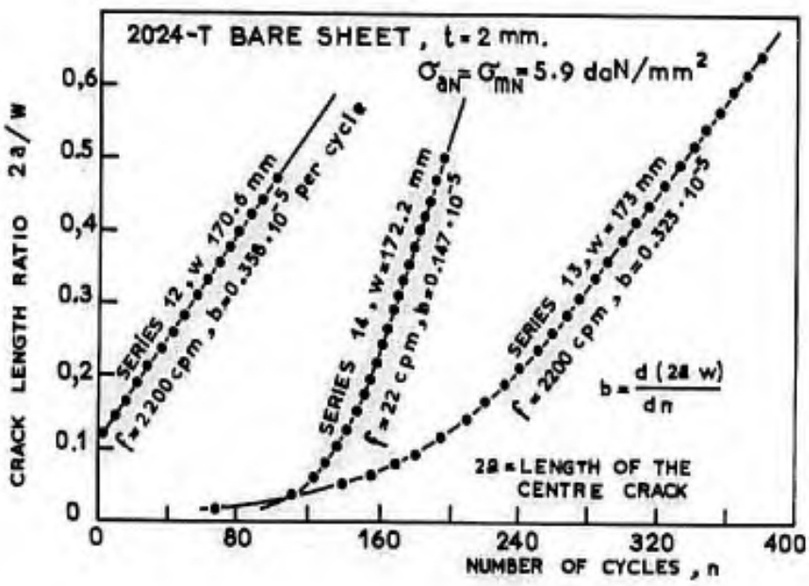

Fig. 5.48 Fatigue crack propagation in constant net-stress amplitude tests (after Weibull[68])

According to the authors, the expression (6) for the rate of growth is applicable to cracks with a relative length $2a/w$ of less than 0.125, but the values found for greater relative crack lengths are too small. The alternating stress intensity factor may be introduced into the expression by putting $K_a = \sigma_a\sqrt{(\pi a)}$; it follows that

$$da/dn = \frac{A}{\pi}\sigma_a K_a^2 . \qquad (6b)$$

This law is not met by test data from other sources, even with respect to the beginning of crack propagation. For lack of cross-experiments with different methods of testing and with specimens assuming different shapes and made from identical materials, it is difficult to decide what, in the presentation of test results, is proceeding from the unconscious desire to use linear plots on appropriate functional scales and what is an implication of experimental techniques.

Weibull's test at constant mean net stress*, σ_N , is fairly similar to the constant K test in the range of relative crack lengths 0.3 to 0.6. We have seen from recent tests by Swanson[75] that the crack propagation rate depends on K alone when K is constant or regularly increasing. As indicated in Chapter IV, Paragraphs 4.2.4 and 4.5.2.2, the stress intensity factor in thin sheet of width w subjected to a constant-amplitude net stress, σ_N , and containing a through centre-crack of length $2a$ is given by the expression

$$K = \sigma_N\sqrt{\left(\frac{w}{2}\pi\right)}\, c_m , \qquad (7)$$

with

$$c_m = \sqrt{\left[\frac{m(1-m)}{1+m}\right]} ;$$

c_m is substantially constant with a value of 0.414 for values of $m = 2a/w$ between 0.4 and 0.6. Weibull considers that after a transition period at crack initiation the crack growth rate, da/dn , *remains constant and exhibits a size effect* in accordance with the law

$$da/dn = C.w.f(\sigma_N) . \qquad (8)$$

Figure 5.48 shows some of Weibull's results for 2024 aluminium alloy. After a period of transition the growth rate becomes stable and remains constant. In the case of Series 13 and 14 which contain an initial slot of relative length $2a_0/w = 0.014$, the change in crack propagation rate can be accounted for by the increase of the coefficient c_m , hence of the stress intensity factor K . In the case of Series 12 which contains a bigger initial slot of relative length $2a_0/w = 0.12$, the absence of transition is not explained by the coefficient c_m , which is stable only at $2a/w = 0.3$. It should be noted that scatter in the crack initiation period may be responsible for the absence of apparent effect of c_m on crack propagation rate. Figure 5.49 gives the results of three tests conducted by Weibull under identical conditions on specimens made from the same sheet as those used in the preceding tests.

The size effect indicated by Weibull can be reconciled with the law

$$da/dn = f(K) , \qquad (9)$$

where K is the stress intensity factor, if we write

$$da/dn = BK^2 = C\sigma_N^2\frac{\pi}{2}w .$$

This expression allows a fairly adequate formulation of Weibull's tests if it is recognized that C is an increasing function of σ_N .

More recently, Broek et al[78] carried out crack propagation tests under constant net-stress amplitude with 160 mm wide and 2 mm thick specimens made from clad 2024-T3 aluminium alloy sheet, the properties of which were as follows: $\sigma_{ult.} = 47.5$ daN/mm^2, $\sigma_{0.2} = 36.2$ and $A\% = 16$. In Figure 5.50, the results are on the whole correctly represented by the expression

$$da/dn = 1.35 \times 10^{-7} \times K_a^{2.67} . \qquad (10)$$

Transition between a plane crack perpendicular to the sheet surfaces and that inclined at 45° to these surfaces is designated by the letter T . No obvious correlation is found for the change in fracture surface and the correlation of da/dn and of K_a is not affected by this change. From the detailed results (Figures 1 to 5 of the authors) it can be seen that the rate of growth is substantially constant from $2a/w = 0.3$ to 0.55 . On the whole, these results give support to the assumption that the stress intensity factor plays a major role.

---

* We use σ_N instead of the notation σ_m used in Chapter IV in order to reserve the index m for the mean static component of the fatigue loading.

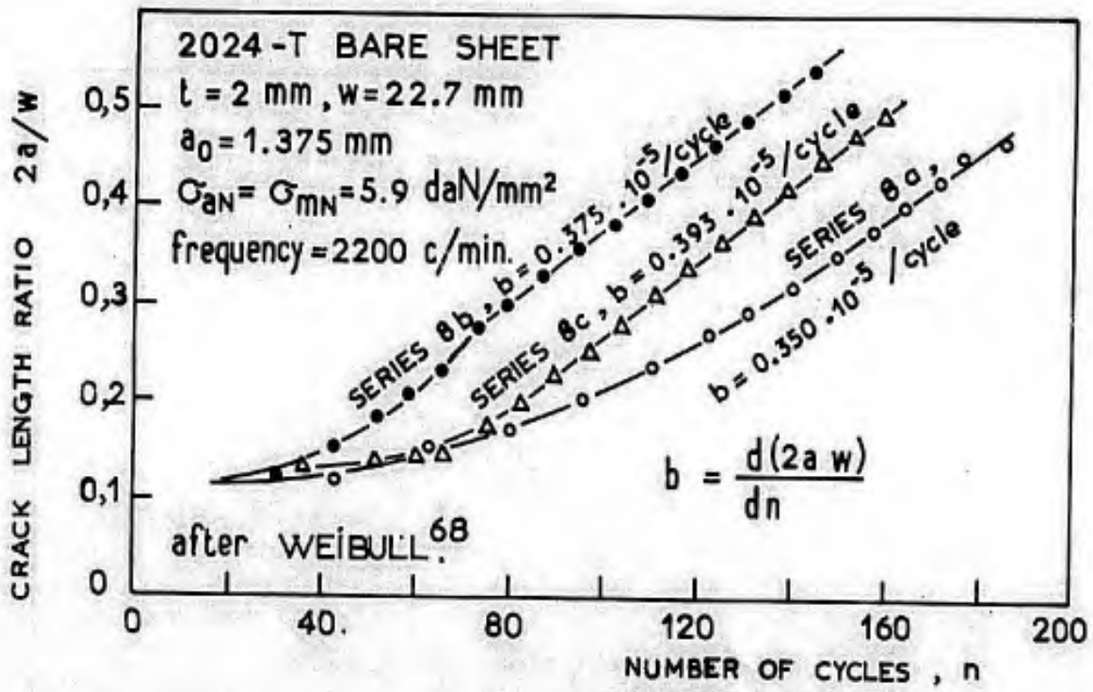

Fig. 5.49 Scatter in crack propagation rate in constant net-stress amplitude tests (after Weibull[68])

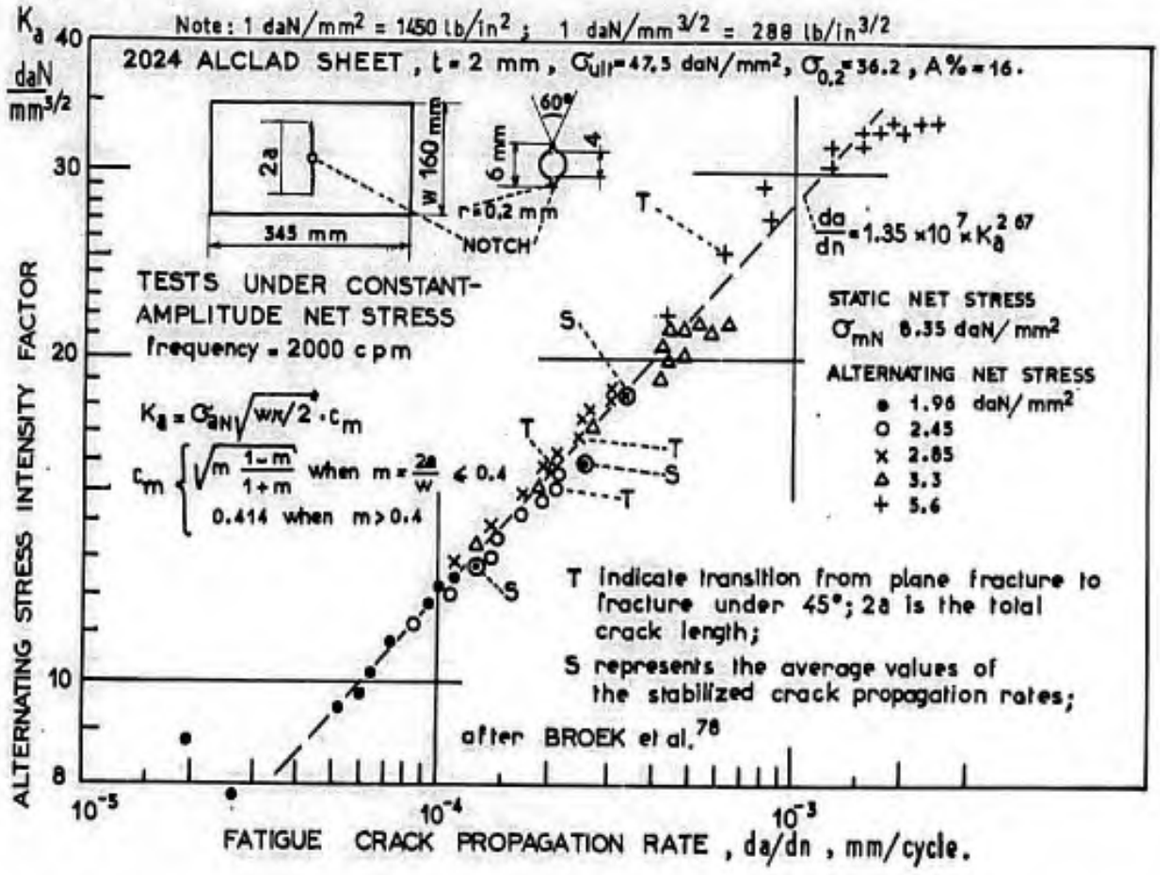

Fig. 5.50 Correlation between the crack propagation rate, da/dn, and the alternating-stress intensity factor (from constant net-stress amplitude tests carried out by Broek et al.[72])

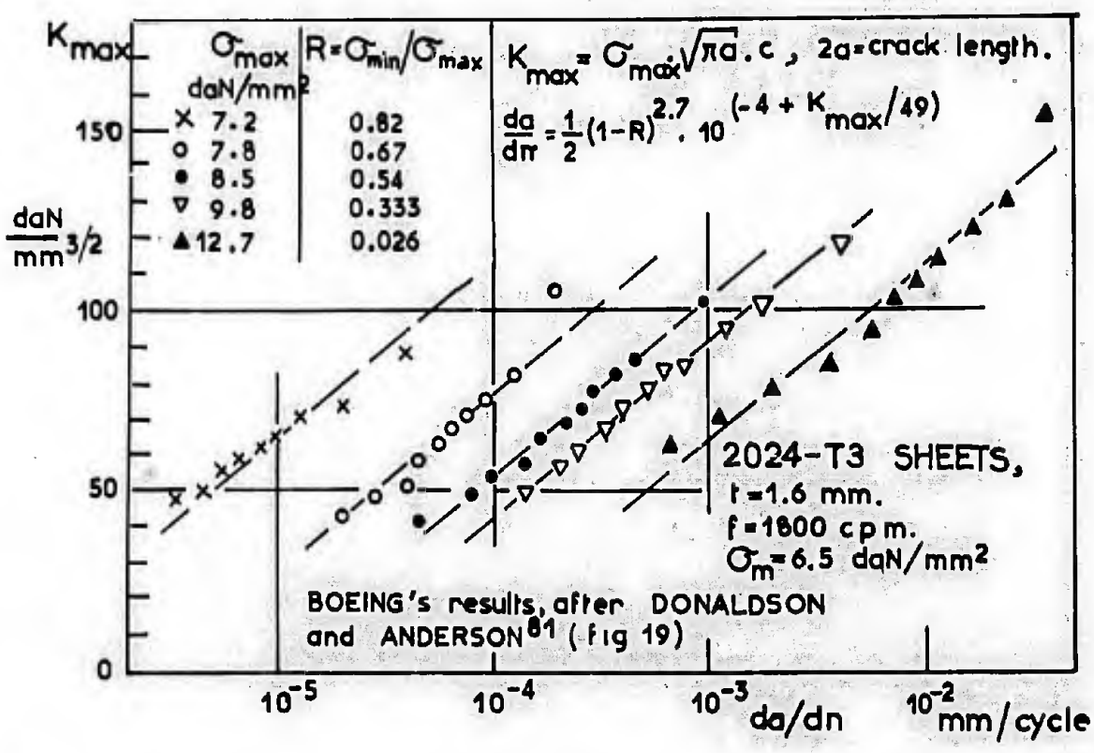

Fig. 5.51 Effect of variation range R

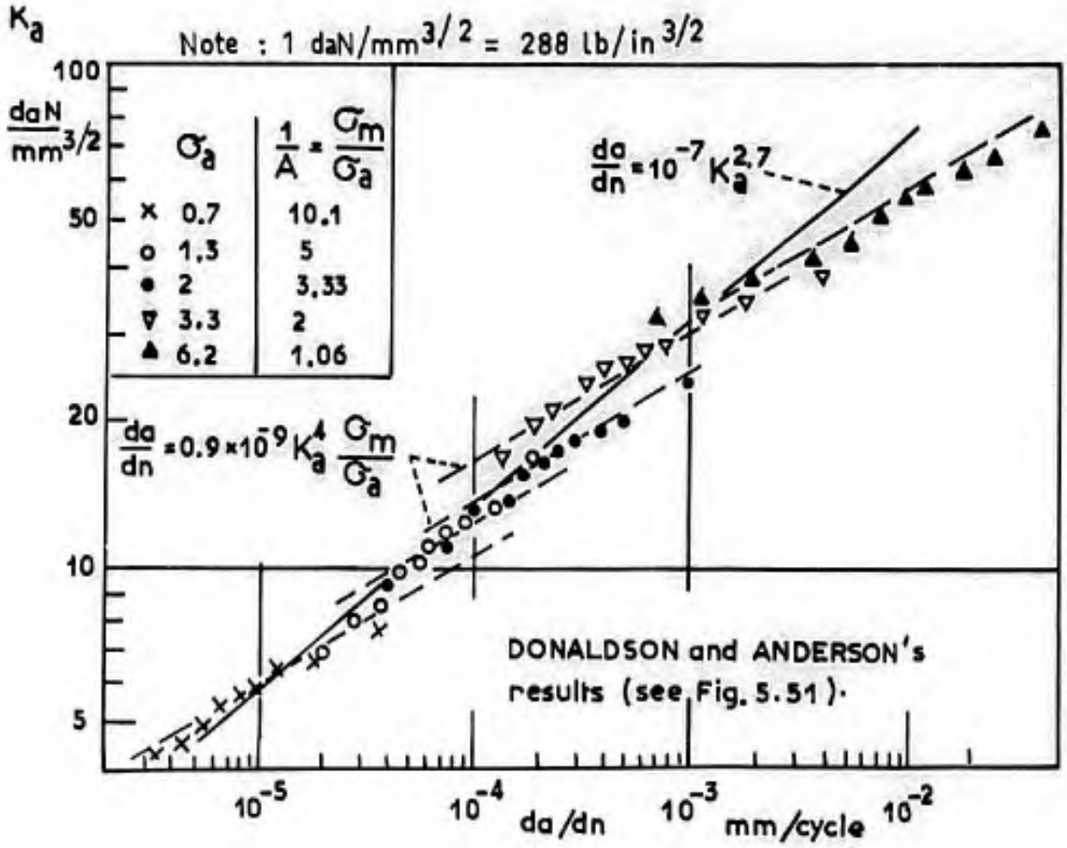

Fig. 5.52 Effect of mean stress

Apparently, the *size effect* is merely the result of the relation between crack propagation rate and stress intensity factor, provided the sheet thickness is constant and only the width, w, is subject to changes. It has been demonstrated by Schijve et al[79] on clad 2024-T3 sheet material and by Rooke et al[80] on British sheet material meeting the specification 5070A (RR 58 or A-U2GN) that the effect of the absolute value of width is included in the effect of K.

5.2.5 Effect of Mean Stress

In the presence of a load with mean and alternating components, the stress intensity factor may be defined by a complex form

$$K = K_m \pm K_a ,$$

which may also be expressed by K_a and $K_{max} = K_m + K_a$. Most published data are represented by means of K_{max} and $R = K_{min}/K_{max}$. This is the case with the Boeing results reported by Donaldson and Anderson[81] (Figure 19 of the authors) and plotted on a K_{max} – log da/dn diagram. These results suggest the relation

$$da/dn = \tfrac{1}{2}(1 - R)^{2,7} \times 10^{(-4+K_{max}/49)} \qquad (11)$$

and are reproduced in Figure 5.51.

If a diagram with log K_a – log da/dn scales is used as in Figure 5.52, the same results appear to be more concentrated, thereby emphasizing the predominant effect of the alternating component of the stress intensity factor. The results may be represented by the expression

$$da/dn = 0.9\ 10^{-9} \cdot \frac{\sigma_m}{\sigma_a} \cdot K_a^4 , \qquad (12)$$

If the ratio of mean stress to alternating stress is left out, an approximate expression of the results for mean stress of 6,5 daN/mm^2 would be

$$da/dn = 10^{-7} \cdot K_a^{2,7} . \qquad (13)$$

If enough test data are available for several mean stress values, it would be more rational to use a $K_a - K_m$ plot with level curves corresponding to given values of the crack growth rate, da/dn. In Figure 5.53, some results from tests performed by Broek and Schijve[82] on centrally-cracked 2024-T3 aluminium alloy specimens with a cross-sectional area of 160 mm by 2 mm are plotted in this way. The effect of the mean component is clearly visible and has a regular form; the results may be represented by

$$K_a + K_m/6 = 4(6.4 + \log_{10} da/dn)^2 . \qquad (14)$$

For 7075-T6 aluminium alloy sheets characterized by $\sigma_{ult.} = 52$ daN/mm^2, $\sigma_{0,2} = 46.5$ daN/mm^2 and A% = 9.4, the same authors obtained results which are represented in Figure 5.54 and may be expressed by

$$K_a + K_m/4 = 3.05(7.3 + \log_{10} da/dn)^2 . \qquad (15)$$

These test results can be plotted on log K_a – log da/dn diagrams by parallel curves with the following expressions: for 2024-T3, $\sigma_m \leqslant 11.8$ daN/mm^2, $\sigma_a \leqslant 6.4$ daN/mm^2, $10^{-5} \leqslant da/dn \leqslant 10^{-3}$:

$$da/dn = 10^{-8} \frac{\sigma_m}{\sigma_a} K_a^3 ; \qquad (16)$$

for 7075-T6, $\sigma_m \leqslant 12$ daN/mm^2, $\sigma_a \leqslant 6.8$ daN/mm^2, $10^{-4} \leqslant da/dn \leqslant 10^{-3}$:

$$da/dn = 1.6 \times 10^{-8}(\sigma_m/\sigma_a)^{1,32} \cdot K_a^{3,3} . \qquad (17)$$

On K_a – log da/dn diagrams the same results will be represented by converging straight lines:

for 2024-T3, $10^{-4} \leqslant da/dn \leqslant 10^{-2}$:

$$K_a = 24.6(\sigma_a/\sigma_m)^{0,375}(4.8 + \log_{10} da/dn) ; \qquad (18)$$

for 7075-T6, $5\ 10^{-4} \leqslant da/dn \leqslant 10^{-2}$:

$$K_a = 19.6(\sigma_a/\sigma_m)^{0,4}(4.5 + \log_{10} da/dn) . \qquad (19)$$

All these formulations are substantially equivalent in the range $10^{-4} \leqslant da/dn \leqslant 10^{-3}$. The mathematical form of the expressions is implied by the functional scales of the diagrams. When using such empirical relations, one should always specify their range of application. The crack propagation values resulting from expressions (16) and (17) are too small for large values of K_a - it would seem that the crack propagation rate rises considerably as final static failure is about to occur. Conversely, the crack growth rate values given by expressions (18) and (19) are too high for small values of K_a at crack initiation - one might say that this is the "transition" phase prior to the establishment of a permanent regime.

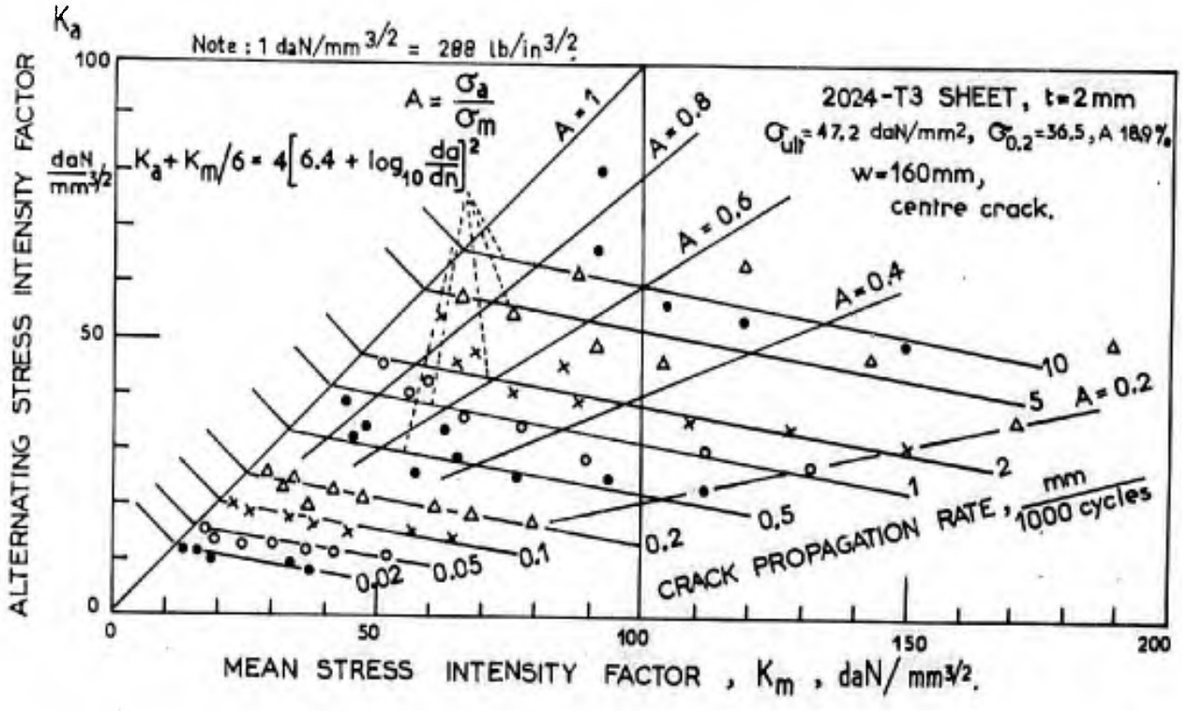

Fig. 5.53 Effect of mean stress intensity factor on crack propagation rate under alternating loads defined by the alternating stress intensity factor (tests conducted by Broek and Schijve[82] on thin 2024-T3 aluminium alloy sheets)

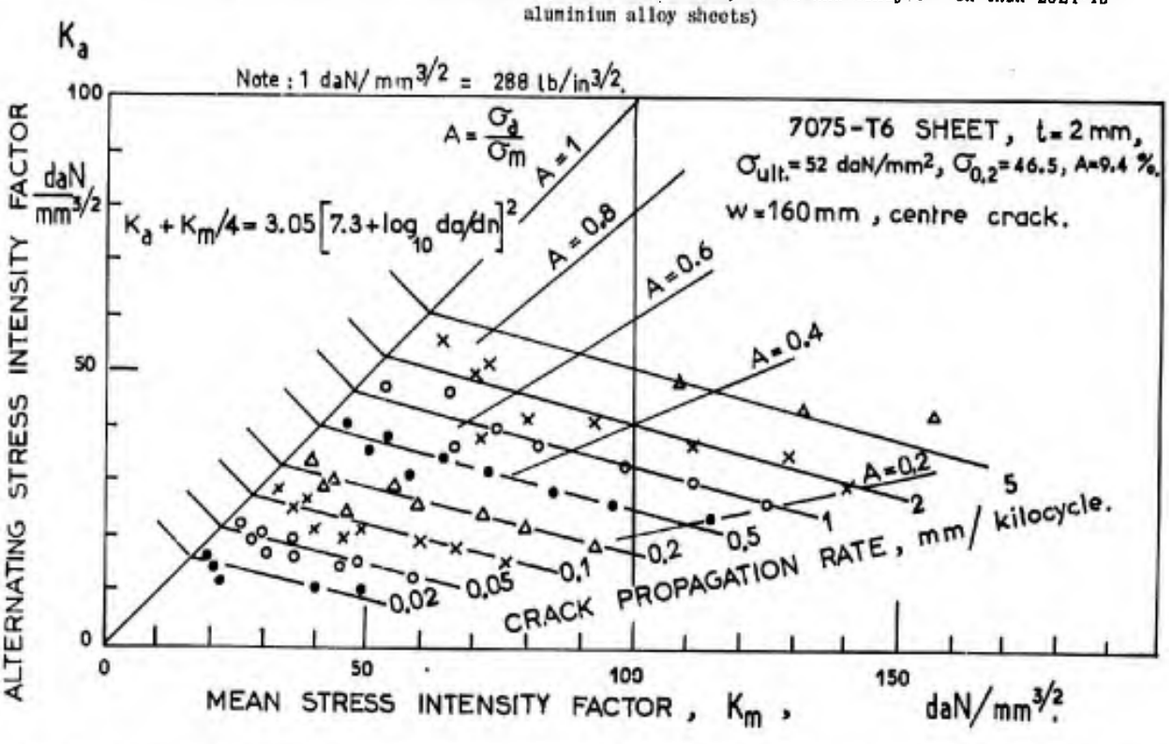

Fig. 5.54 Diagram of interaction of alternating stress and mean stress intensity factors on crack propagation rates (tests by Broek and Schijve[82] on thin 7075-T6 aluminium alloy sheets)

Furthermore, the above expressions are no longer valid when the minimum stress is changed into compression, that is, when $\sigma_m > \sigma_a$. If we take into account a possible scatter coefficient, it is seen that tests performed by McEvily and Illg[83,84] indicate the same crack propagation rates for the same values of K_{max} in thin 2024-T3 and 7075-T6 aluminium alloy sheets (w = 305 mm, t = 2 mm) subjected to repeated tension from 0 to σ_{max} and alternating tension-compression from $-\sigma_{max}$ to $+\sigma_{max}$. This may be explained by assuming that compressive stresses cause the two crack borders to draw closer to each other and that they create negligible stress concentrations.

5.2.6 Effects of Frequency, Temperature and Humidity

In the work of Illg and McEvily[84], the crack propagation rate at 1200 c/m is compared with that at 13 c/m. It appears that the rate of growth is approximately 40% greater at 13 c/m than at 1200 c/m. Similarly, Schijve et al[86] have found a clear but small effect of frequency on crack growth rate at room temperature: The rate is about 30% greater at 14 c/m than at 1200 c/m.

Some results of Schijve and De Rijk[87] are illustrated in Figure 5.55. Temperature, low test frequencies and high mean stresses cause an increase in crack propagation rate. Since with increase in temperature, test durations over hours and high mean stresses favour fatigue yielding and possibly add a certain amount of creep, it may be considered that this complex creep process plays a predominating part. Generally, the increase in crack propagation rate is much faster toward the end of the test with great crack lengths, the unfracturated cross-sectional area being almost completely subjected to stresses in the plastic range. In such cases the test results show a negligible effect of frequency and of temperature and most of the yield seems to be governed by the number of cycles and not to be attributable to creep dependent on time and on temperature. The authors ascribe the effect of temperature on the 2024-T3 alloy to a change in the precipitation state associated with a decrease in ductility. We believe that ductility, as in numerous metallurgical transformations, increases during the transformation under the effect of fatigue and temperature, thereby promoting plastic changes far ahead of the crack, and that it decreases on completion of the transformation in the immediate neighbourhood of the crack tip. This assumption is supported by Curve 2 in Figure 5.55. Before point A is reached, transformation occurs only in the plastic range ahead of the crack and is in progress when the region concerned is swept by high stresses. Beyond point A, the transformation is completed before the crack extends to the region concerned and temperature no longer favours plastic elongation at the crack tip. Under lower alternating stresses this behaviour is no longer apparent, but comparison of curves 7 (20°C) and 8 (150°C) shows that the rates of growth are the same at very small crack lengths when the transformation has not yet started and at great crack lengths when the transformation is completed.

Figures 5.56 to 5.58 contain results from Hardrath et al[72] with respect to the fatigue crack propagation rates in 1 mm thick and 70 mm wide clad 2024-T3 alloy sheet specimens with a centre crack, tested at various frequencies in dry air, wet air (100% R.H.) and distilled water (PH 6-8). We have used the K_a – log da/dn representation, where K_a again designates the alternating component of the stress intensity factor with Irwin's notation ($K_a = \sigma_a\sqrt{(\pi a)}$ for a sheet of infinite width). At high frequencies (3,400 c/m), the crack propagation rate is slower in dry air (2 p.p.m.) than in water and wet air (100% saturated), as shown in Figures 5.56 and 5.57.

The difference is attenuated with fast propagation rates at high stresses and low frequencies. From Figure 5.58 it is seen that in dry air, at rates of $10^{-4} < da/dn < 10^{-3}$ mm/cycle, the effect of frequency becomes apparent at less than 30 c/m. At 24 c/m the results obtained in dry air are similar to those obtained in distilled water at 3,400 c/m.

Figure 5.57 shows that crack propagation rates are somewhat slower in air saturated with water vapour than in distilled water. In previous tests on 1 mm thick clad 2024-T3 aluminium alloy sheets, Hartman[88] investigated the rates in dry or wet air, in dry or wet argon, and in dry or wet oxygen. His conclusion was that, of the three components of air, i.e., oxygen, nitrogen and water vapour, the latter exerted the most significant effect on fatigue crack initiation. The water vapour content of the three gases - oxygen, argon and air - was the overwhelming factor with respect to the fatigue life. The effect of water vapour was more pronounced under low stresses and at small crack lengths. In normal air the relative humidity ranges from 30 to 100% and within this range crack growth rates are associated with the formation of hydrogen which creates high pressures in the cavities of the deformed region ahead of the crack.

Maurin and Barrois[89] have presented results from systematic tests conducted by Sud-Aviation on clad A-U2GN sheets with the following composition:

	Cu	Mg	Si	Fe	Mn	Ni	Ti	Zn	Pb	Sn	Al
At the core, minimum	1.8	1.2	0.15	0.9							
maximum	2.7	1.8	0.25	1.4	0.2	1.4	0.2	0.1	0.05	0.05	the remainder
Cladding, minimum								0.8			
maximum								1.2			the remainder

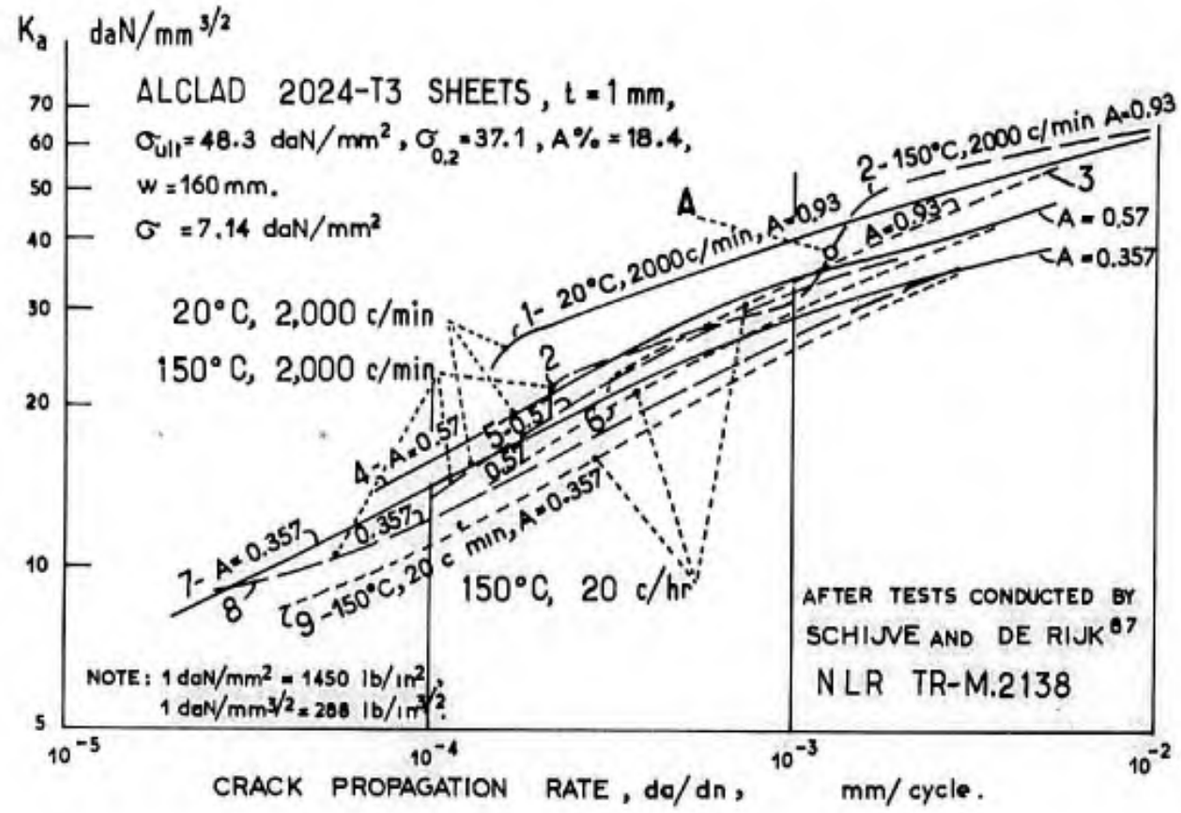

Figure 5.55

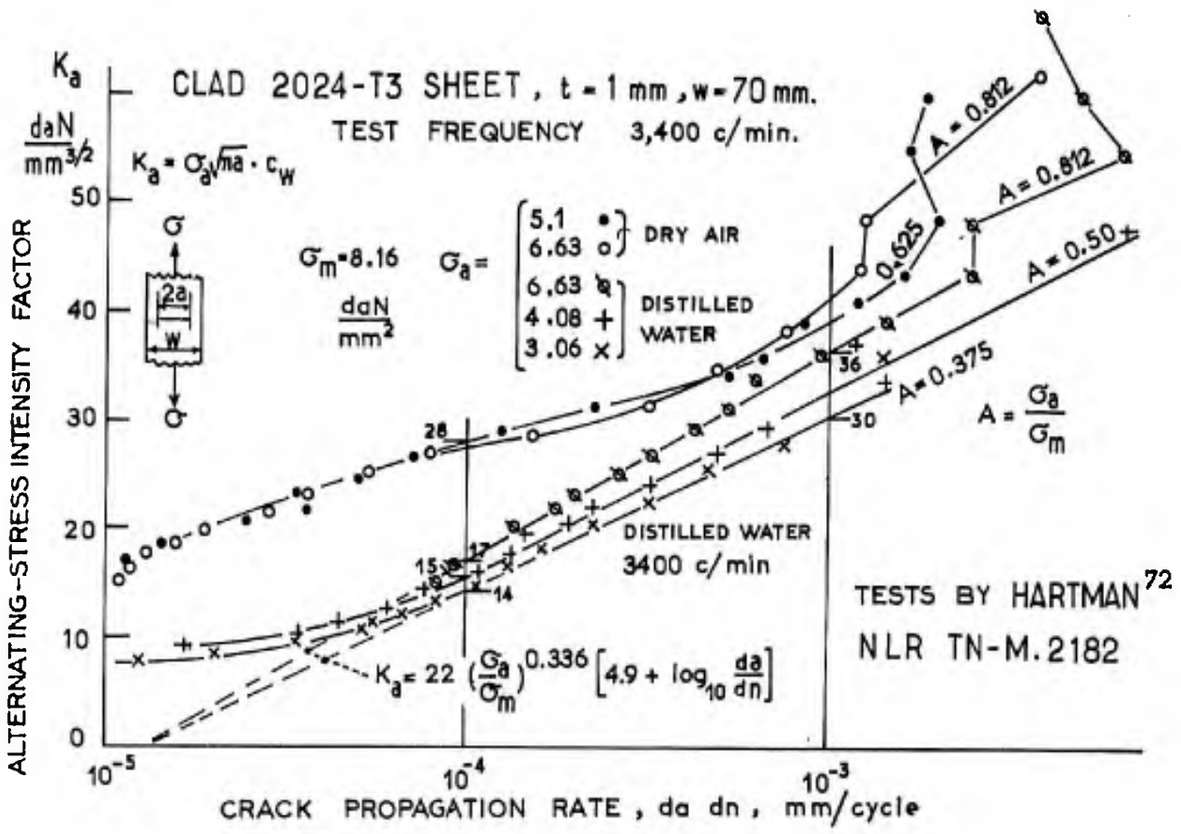

Fig. 5.56 Effect of environment on fatigue crack propagation in clad 2024-T3 sheets

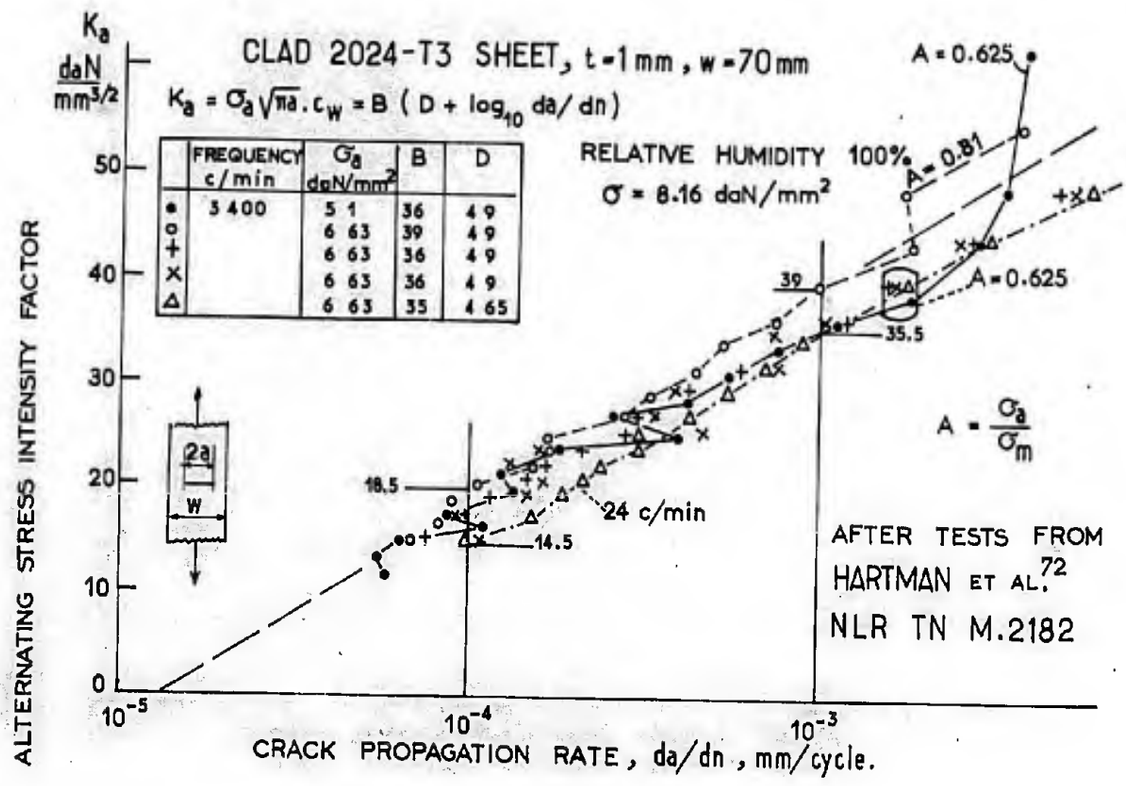

Fig. 5.57 Effect of frequency on crack propagation rate in clad 2024-T3 sheets in saturated wet air

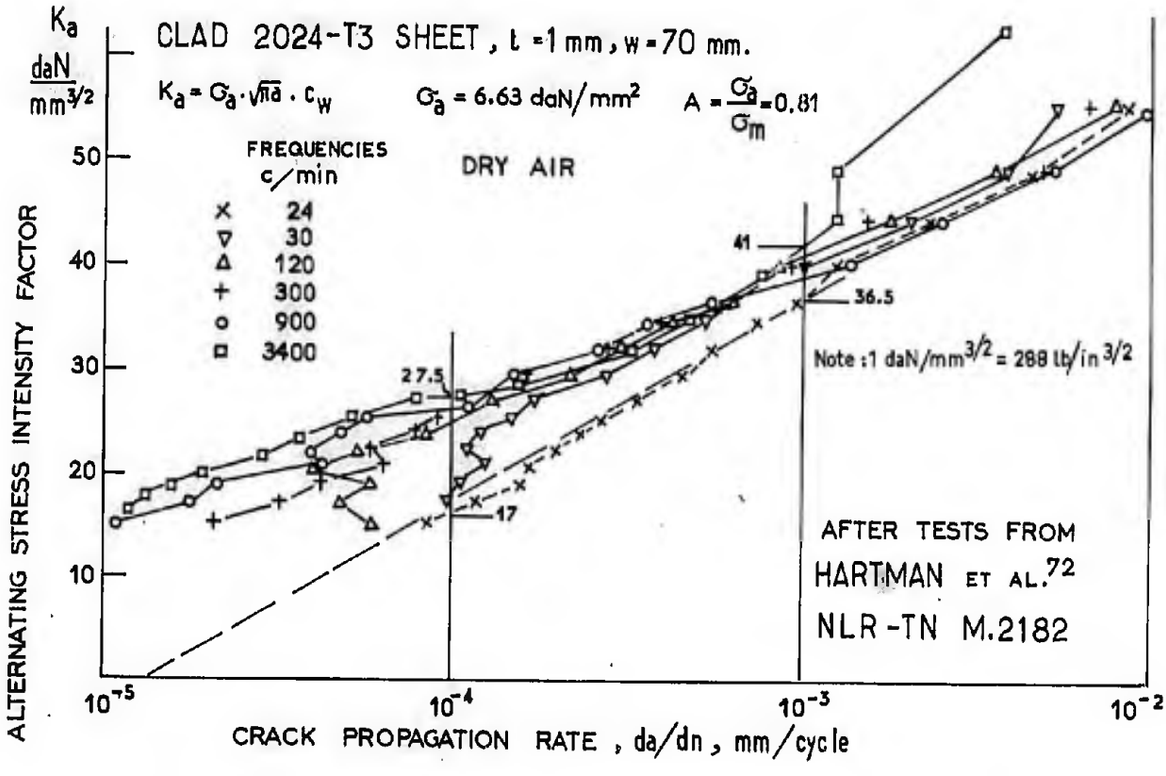

Fig. 5.58 Effect of frequency on crack propagation rate in clad 2024-T3 sheets in dry air

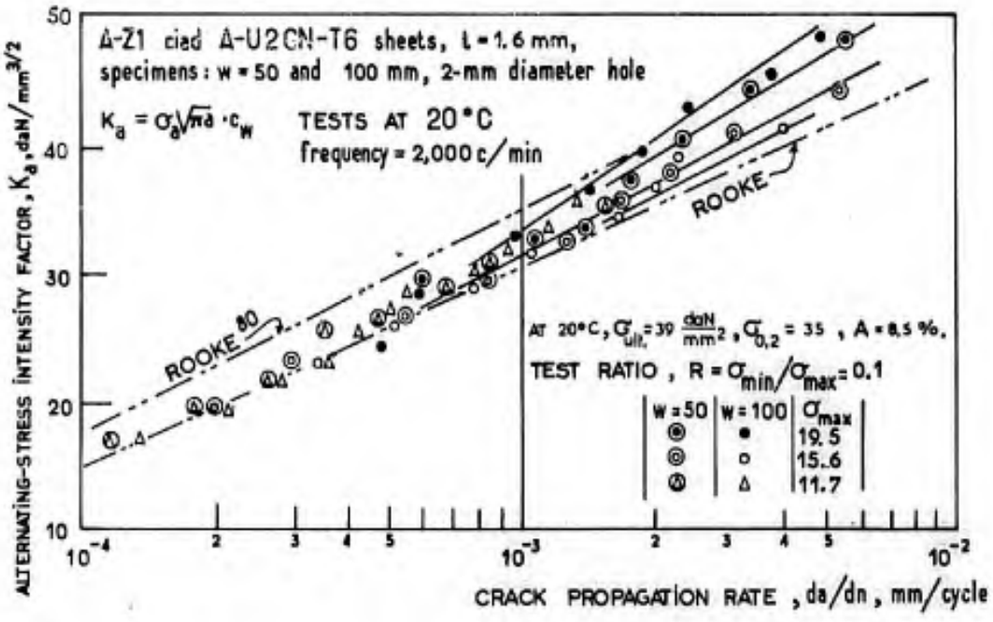

Fig. 5.59 Fatigue crack propagation rates in thin A-U2GN-T6 sheets at 20°C, after Maurin and Barrois[89]

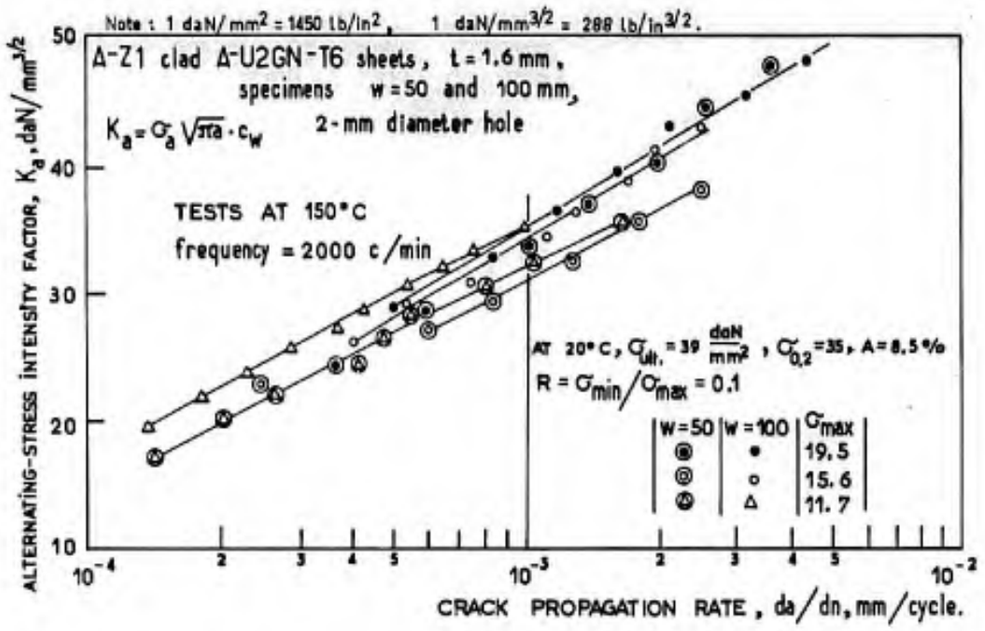

Fig. 5.60 Fatigue crack propagation rates in thin A-U2GN-T6 sheets at 150°C, after Maurin and Barrois[89]

TABLE 5.4

Low-frequency Fatigue of Type-F Specimens made from A-Z1 clad A-U2GN-T6 Sheet Material (Ref. 89)

Items	*N*	*log N*	*s(log N)*	*Test number*	*Time under load* per cycle	total	*Time of resting* per cycle	total	*f* c/hr
65	13700	4.136	0.027	10	75"	286 hr	15"	56 hr	40
66	14600	4.164	0.028	10	15"	61 hr	75"	304 hr	40
67	10350	4.015	0.019	5	75"	216 hr	165"	475 hr	15
68	4770	3.678	0.005	5	15"	20 hr	1185"	1570 hr	3
69	2630	3.420	0.039	5	1185"	865 hr	15"	12 hr	3
70	121	2.083	0.055	5	37135"	1248 hr	65"	2.2 hr	0.095
72	1770	2.471			3540"	1740 hr	60"	29.5 hr	1

The T6 treatment was effected under the following conditions: 40 minutes at 530 ± 5°C, water quenching below 40°C, ageing at 190 ± 5°C for 19½ ± ½ hours. The sheet material used had the following properties: $\sigma_{ult.}$ = 42.5 daN/mm², $\sigma_{0.2}$ = 37.5, A% = 10. The specimens, of widths w = 50 and 68 mm and thicknesses t = 1.5 mm and 2 mm, contained a centre hole of 2 mm in diameter. The effect of frequency on total life was very small at 20°C; the life at 10 c/hr was approximately 1.5 times less than at 4,800 c/m. The effect of frequency being insignificant, the rate of growth at 20°C was studied only at a frequency of 2000 c/m on specimens of widths w = 50 and 100 mm (Fig. 5.59). A stress ratio $A = \sigma_a/\sigma_m = 0.81$ and three alternating stress values, σ_a = 5.27, 7.02 and 8.8 daN/mm², were considered.

Figure 5.60 shows but a small effect of temperature at 150°C and 2000 c/m. However, the crack propagation rate at 150°C and 20 c/hr is greater by half. In all cases, the effect of specimen width is included in the stress intensity factor K_a .

In order to investigate the effect of creep on the fatigue of a supersonic aircraft structure having an average external skin temperature of 120°C and subjected to very-low-frequency flight manoeuvres and ground-air-ground loads, a comprehensive study of the effect of frequency in the range of 4,800 c/m (288,000 c/hr) to 1 c/hr was carried out on drilled specimens and small riveted assemblies made from A-Z1 clad A-U2GN-T6 sheet, identical with the British RR 58 alloy sheet material conforming to DTD 5070A. The specimen sizes are given in Figure 5.61. At 20°C, frequency has little influence on fatigue life, expressed in cycles, as shown in Figure 5.62. At 150°C it is seen from Figure 5.63 that there is a significant and almost regular effect of the total test time - expressed in hours - on the number of cycles to failure. As long as this effect remains small, the law of Wade and Grootenhuis $N = N_1(f/f_1)^n$, which we express by

$$N = N_1(t/t_1)^{(1-n)/n}$$

in order to introduce the total test time, t , can be verified fairly well. Here n varies from 0.10 to 0.13. The values of n are given in the table below for the specimens investigated.

	D					F		Al
σ_{max} =	10.5	14.7	16.5	19.3	22.5	20	22.5	15.7
n, 20°C	0.07	0.07		0.04			0.05	0.07
120°C			0.09	0.10	0.13		0.10	0.07
150°C			0.10	0.20		0.12		0.12

The test results exhibit some scatter although the average values of five tests were taken; the preceding values of n are therefore only indications. However, the effect of frequency at 20°C seems to be independent of the stress value. For the type-D specimen with σ_{max} = 19.3 and N = 20,000 , the life would be 1,000 hours at 20°C, 20 hours at 120°C, and 0.7 hour at 150°C. If we assume that time and temperature are equivalent on the basis of parameter $t.e^{-Q/RT}$, we obtain activation energies, Q , of 8,900 cal-g/deg/mole in the range 20°C to 120°C, and of 37,000 cal-g/deg/mole in the range 120°C to 150°C. From creep tests on the same sheets reported in Chapter IV, Paragraph 3.2.3, we have activation energies, Q , of 31,000 cal-g/deg/mole between 150°C and 175°C, and of 42,000 cal-g/deg/mole between 130°C and 150°C with σ = 20 daN/mm² and ϵ = 0.02% . If a regular decrease of the activation energy between 120°C and 20°C is assumed in order to obtain the above mentioned average of 8,900 cal-g/deg/mole, it must be recognized that the value is very low at 20°C, which implies that the effect of time may include a small amount of corrosion.

It is of interest to consider the behaviour of the specimens at 150°C and at very low frequencies since creep plays a most important part under these conditions. Elongation measurements away from the hole on F-type specimens (Fig. 5.61) subjected to σ_{max} = 20 daN/mm² with R = 0.1 at 150°C showed that the elongations were not dependent on the number of cycles but on the total time at the maximum stress of the tooth-shaped loading, and that they assumed values comparable to the elongations measured in creep without fatigue. Results of the fatigue tests are given in Table 5.4.

Statistical tests reveal that the results vary significantly, the significance level being 95% for the couple 65-66 and much more than 99% for couple 68-69. Inversion of the magnitudes of the loading and resting times per cycle results in a slight decrease in endurance through an increase in the time under load as regards the pair 65-66, and in a considerable decrease in endurance as regards the pair 68-69 in which the total time under load, expressed in hours, is multiplied by more than 40, while the endurance, expressed in cycles, is divided by 1.8. Therefore, a *damaging effect of the time under load is observed,* as with pure creep.

We have seen at the beginning of this chapter how the fatigue of work-hardened metals under constant-amplitude strain may cause a change in the stress-strain loop (Fig. 5.2) and a transformation which tends toward an alternating-stress state through the creation of residual stresses of opposite sign with respect to the initial mean strain (see Figures 5.5 and 5.7). This behaviour is of paramount importance for the understanding of fatigue test results from notched components, unnotched bend specimens and cracked specimens, all containing a maximum-stress point or region at the surface of the material and a negative stress gradient depthwise. *A small volume of material at the root of the notch or at the extremity of the crack is subjected to very high stresses, hence*

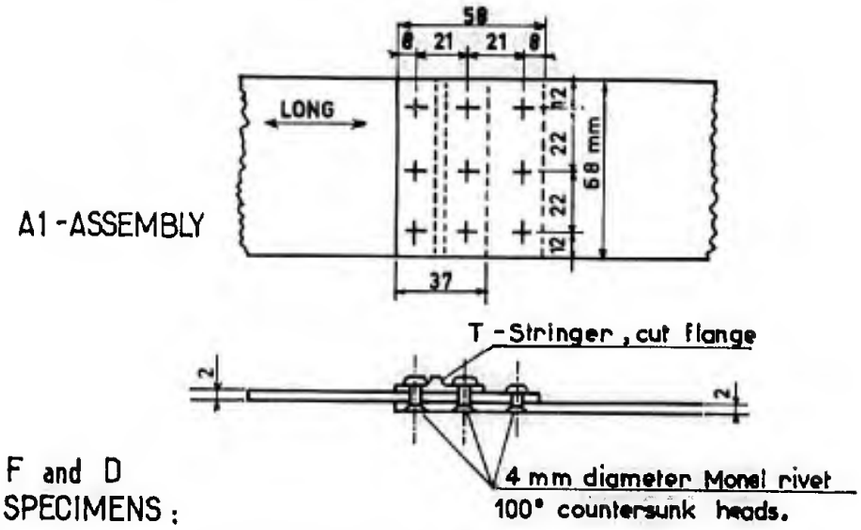

Drilled thin specimens of 1.6-mm thickness containing a centre 2-mm diameter hole ; 50-mm wide for the type F and 68-mm wide for the type D.

Fig. 5.61 Thin A-U2GN aluminium alloy sheet specimens. Tests related in Figures 5.62 and 5.63 after Maurin and Barrois[89]

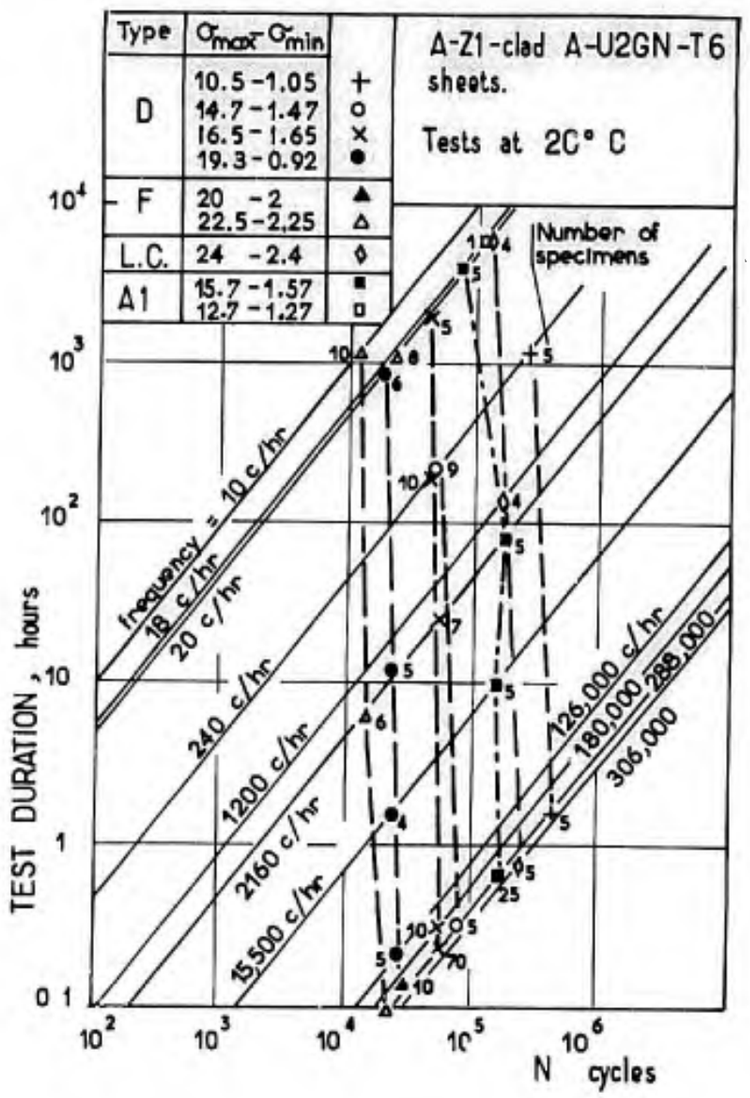

Fig. 5.62 Frequency effect on fatigue at 20°C of A-U2GN-T6 sheets (after Maurin and Barrois[89])

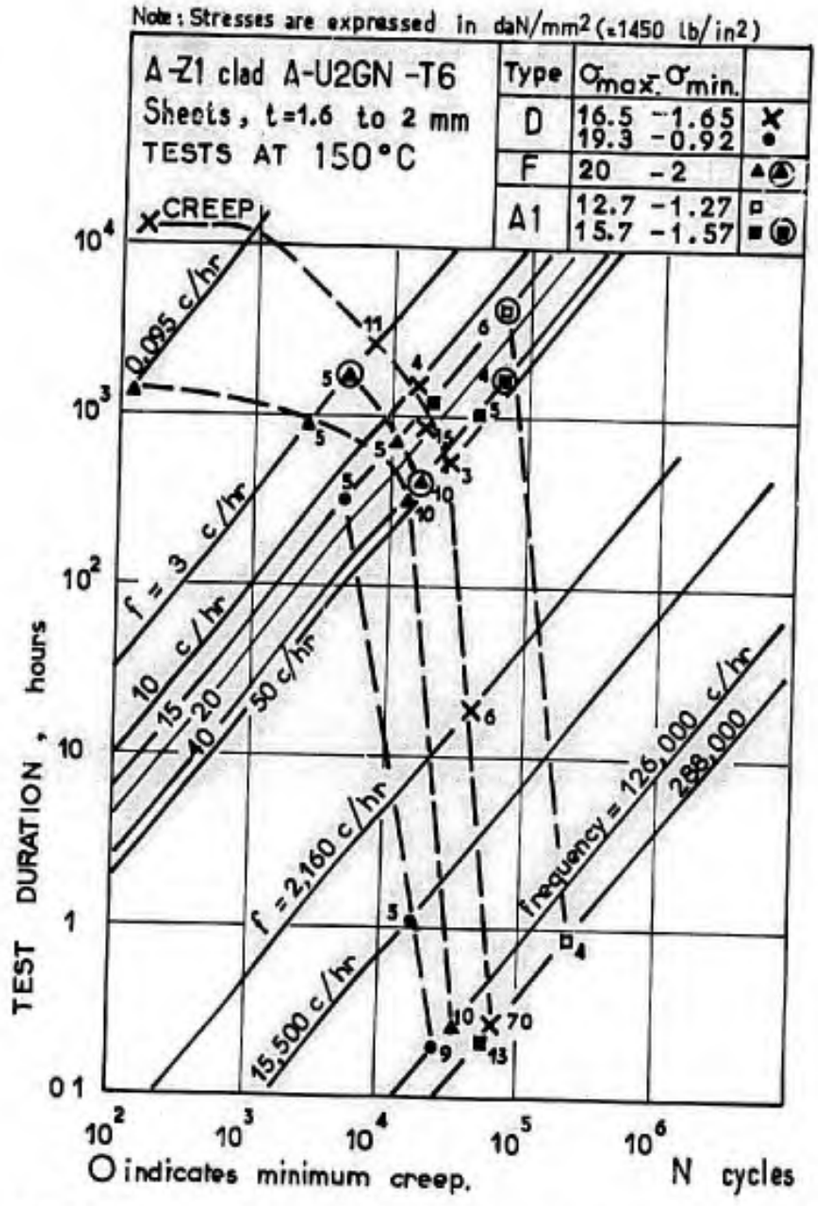

Fig. 5.63 Frequency effect on fatigue at 150°C of A-Z1 clad A-U2GN-T6 thin sheets

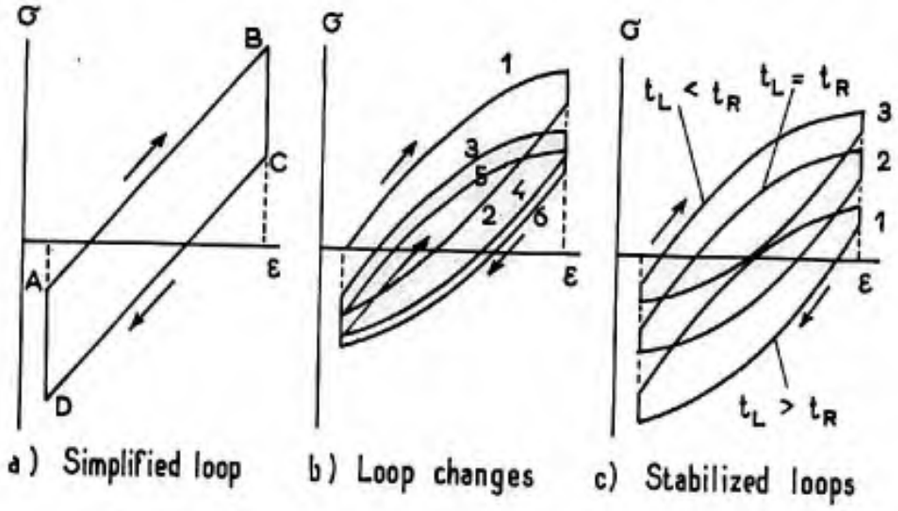

Fig. 5.64 Adjustment through relaxation of stress-strain loops under constant amplitude strain. Effect of the loading and resting times of the cycle

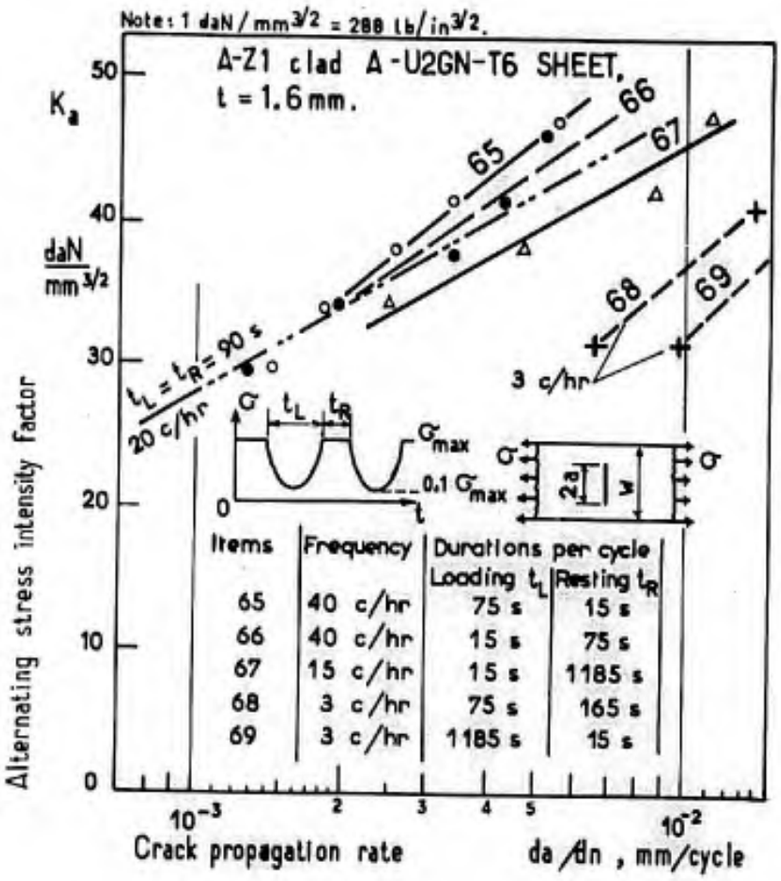

Fig. 5.65 Crack propagation rates in thin A-Z1 clad A-U2GN-T6 sheet specimens at very low frequencies. Effect of unequal loading and resting periods. After Maurin and Barrois[89]

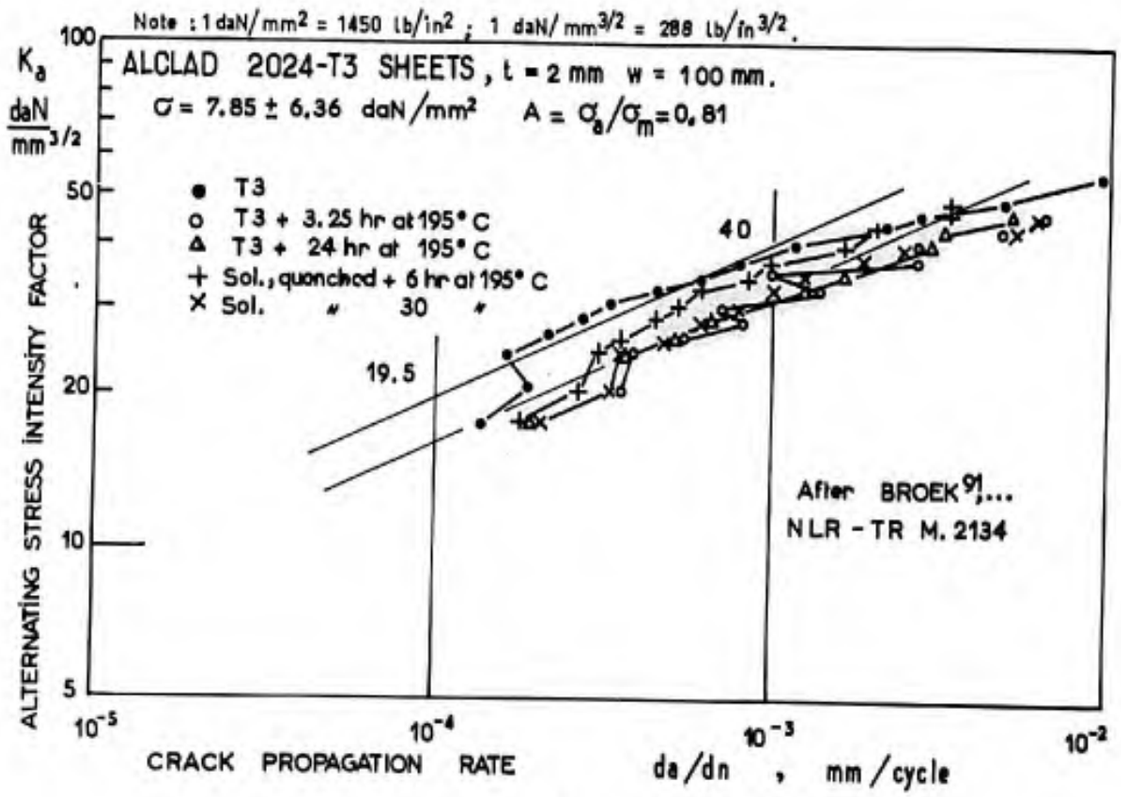

Figure 5.66

to rapid plastic transformation during fatigue. The strains at the boundaries of this domain are substantially elastic and keep substantially the same values as those imposed by the elastic behaviour of the remainder of the specimen.

Let us return to the above mentioned tests. To simplify the reasoning, we shall first assume that the loading and unloading sequences are fast enough for the material at the root of the notch to behave elastically during these two very short periods. On the other hand, the time periods for loading and resting in each cycle will be supposed sufficiently long for the applied or residual stresses to be relaxed. In Figure 5.64(a), a simplified cycle is represented in the form of a parallelogram ABCD. Owing to the elasticity, the segments AB and CD have the same lengths, and the stress variations by relaxation must be identical during the application of load and after removal of the load. If the periods of loading and resting are equal, the preceding equality implies equal absolute values of the maximum and minimum stresses of opposite sign (Figures 5.64(a) and 5.64(c), curve 1).

When the period of loading is greater than the period of resting, the absolute value of the maximum stress is necessarily less than that of the minimum stress if the relaxation strains are to be equal; hence the loop tends to be shifted toward the lower stresses. A longer period of time under load, however, involves greater activity in the creation of microcracks, whereby the improving effect of compressive residual stresses is offset or exceeded (Figure 5.64(c), curve 2).

If the period of resting is greater than the period of loading, the maximum stress tends to be increased and the loop moves toward the maximum stresses, which implies damage caused by plastic transformation generating microcracks, and by a decrease of the favourable compressive residual stresses (Figure 5.64(c), curve 3).

These considerations explain why a *damaging effect of resting is* found for equal periods of loading. This effect is observed in the crack propagation rates of the previously mentioned specimens (Fig. 5.65). The crack propagation rates of specimens 65 and 66 are comparable, the rate being slightly faster for specimen 66 although the total life is greater, probably the crack initiation period is longer. Comparison of items 65 and 67 for the same time of loading per cycle shows a detrimental effect of resting on crack propagation rate, which is similar to the effect of resting on total life as mentioned above. The dotted line indicates the crack propagation rate at 20 c/hr for equal durations of the loading and resting sequences. Similar results are found at 120°C.

In tests performed recently, Hartman and Schijve[95] made a further study of the effect of frequency and environment on crack propagation rates in thin 2024-T3 and 7075-T6 aluminium alloy sheets. To correlate the results, they used an expression proposed by Forman[96]:

$$da/dn = C(K_{max} - K_{min})^p \Big/ \left[1 - \frac{K_{min}}{K_{max}} K_c - (K_{max} - K_{min}) \right] \qquad (20)$$

where K_c is the critical stress intensity factor for complete static failure of the cracked specimen. This relation gives an infinite growth rate for $K_{max} = K_c$. Previous test results of the NLR reported in Reference 88 have been analyzed using the preceding expression for K_c-values derived from tests by Schijve and De Rijk[97], that is, with $K_c = \sigma\sqrt{(\pi a)}$ for an infinite sheet, $K = 253$ daN/mm$^{3/2}$ (72,800 lb/in$^{3/2}$)* for the 2024-T3 alloy and $K_c = 259$ daN/mm$^{3/2}$ (74,500 lb/in$^{3/2}$) for the 7075-T6 alloy. An excellent correlation is obtained through a straight line on a logarithmic diagram with $\log \Delta K$ on the x-axis and $\log(da/dn)[(1 - R)K_c - \Delta K]$ on the y-axis for clad sheets of 7075-T6 material placed in very dry air and 2024-T3 material placed in dry argon. In other instances the correlation proves less good, as with all mathematical expressions used for crack propagation rates.

However, since final failure in any fatigue test is a static failure, it is useful to discuss this point, which is dealt with in Chapter IV. Broek[98] investigated the residual static strength of thin clad 2024-T3 sheets from five different manufacturers and indicated the stresses σ_i for enlargement of the crack beyond the initial crack length $2a_0$, the critical stresses σ_c for the instability leading to failure, and the corresponding lengths $2a_c$. Three values of K may be derived from these data: $K_i = \sigma_i\sqrt{(\pi a_0)}$ for enlargement of the crack, $K_c = \sigma_c\sqrt{\pi a_c}$ for the instability, and the nominal value $K_0 = \sigma_c\sqrt{(\pi a_0)}$ which is of interest to the engineer. Table 5.5 contains the values of K computed with Irwin's definition and Dixon's finite-width correction.

K_i varies from 166 to 197, i.e., by 19%, K_0 from 168 to 222, i.e., by 32%, K_c from 208 to 284, i.e., by 36%. K_c is therefore less invariant than K_i and it is not surprising that attempts to correlate da/dn using K_c are not always successful. The foregoing values of K are expressed in daN/mm$^{3/2}$ and have been computed for

$$K = \sigma\sqrt{\left(\frac{a}{1 - (2a/w)^2}\right)}.$$

---

* 1 daN = 1.02 kg-weight, 1 daN/mm^2 = 1450 lb/in^2, 1000 lb/in^2 = 0.69 daN/mm^2, 1 lb = 0.445 daN, 1 daN/mm$^{3/2}$ = 288 lb/in$^{3/2}$, 1000 lb/in$^{3/2}$ = 3.47 daN/mm$^{3/2}$.

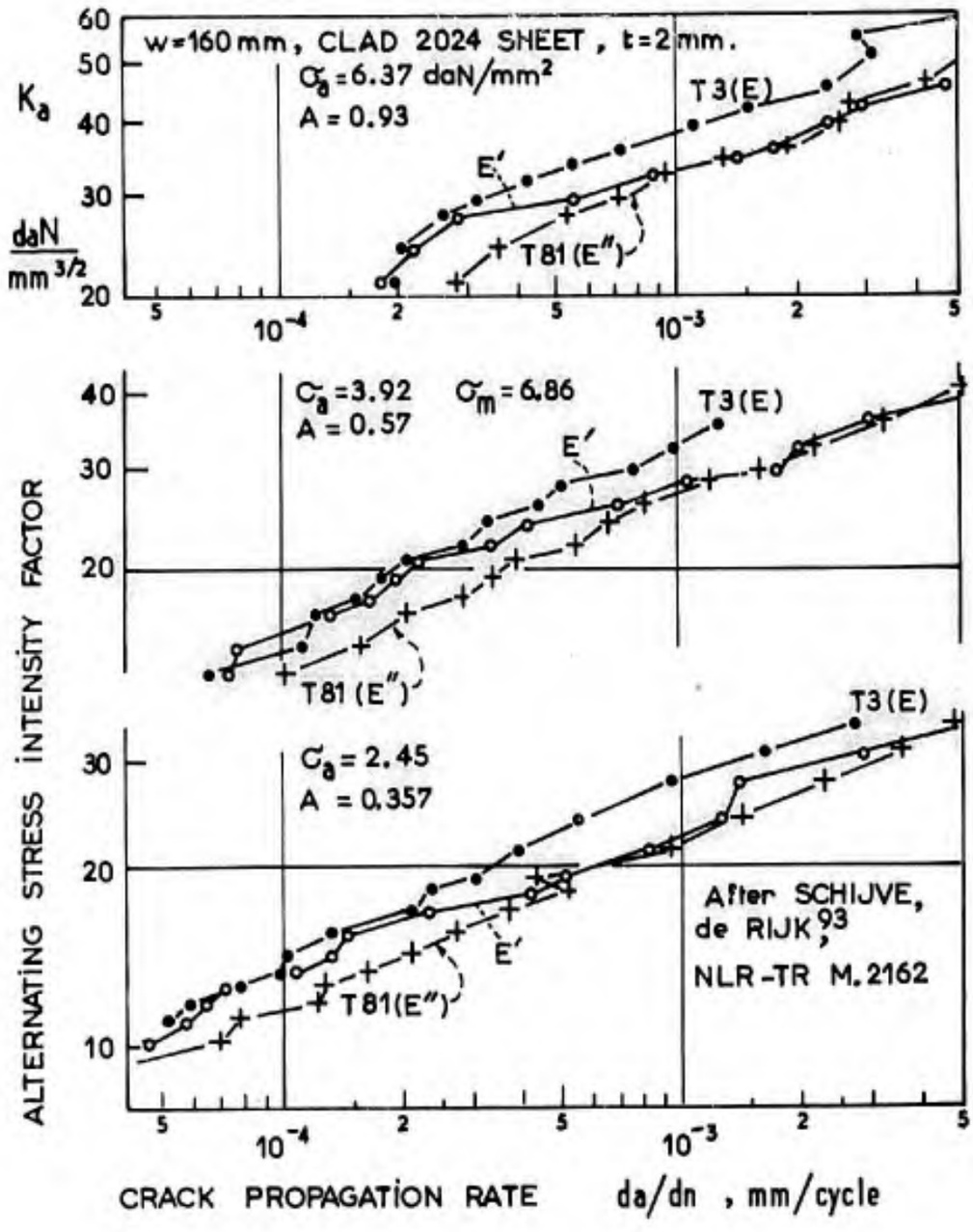

Figure 5.67

TABLE 5.5

Residual Static Strength of Thin Clad 2024-T3 Sheets of w = 150 mm and t = 2 mm Except for Manufacturer B (t = 2.4 mm). Values of K Expressed in daN/mm$^{3/2}$

	Manufacturers														
	B			*D*			*E*			*F*			*G*		
	$\sigma_{0,2}$ 38,6	σ_R 45,5	A% 19	$\sigma_{0,2}$ 34,7	σ_R 47	A% 22,5	$\sigma_{0,2}$ 36,4	σ_R 46,7	A% 21	$\sigma_{0,2}$ 34,5	σ_R 45,3	A% 22	$\sigma_{0,2}$ 35,7	σ_R 46,6	A% 18
n_0	K_I	K_0	K_c	K_I	K_0	K_c	K_I	K_0	K_c	K_I	K_0	K_c	K_I	K_0	K_c
10	180	185	226	155	168	208		175	213	166	178	206	176	179	216
15	191	208	239	182	192	221	182	196	230	172	198	216	166	197	229
20	161	216	283	184	206	218	172	206	242	186	213	247	179	210	245
40	197	222	284	156	200	232		200	239	174	210	245	188	196	236

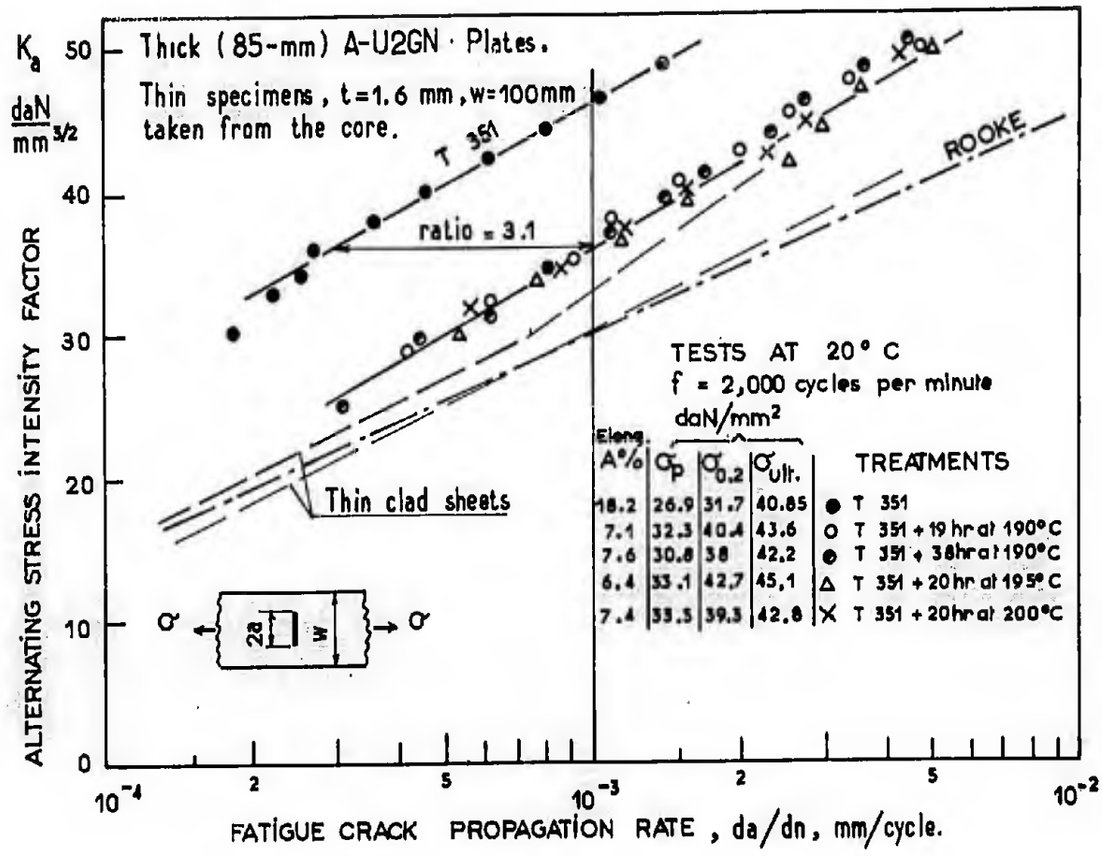

Figure 5.68

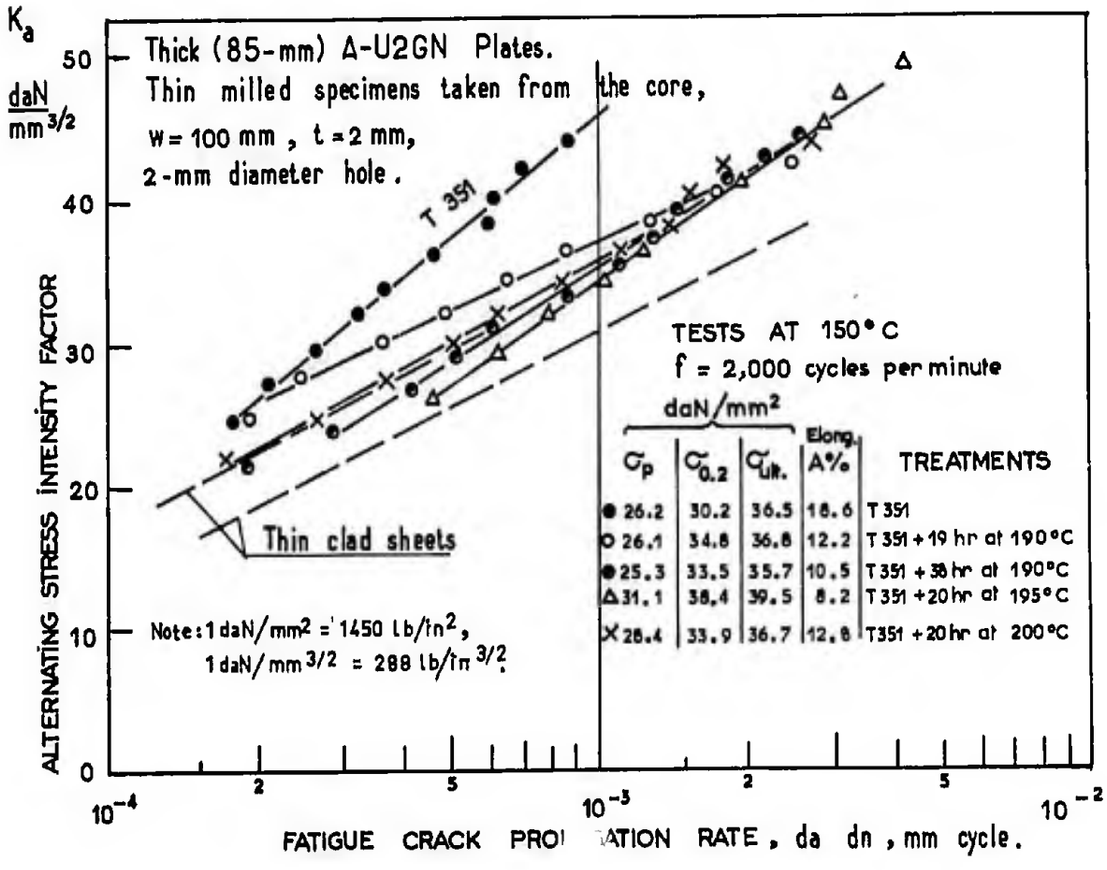

Figure 5.69

5.2.7 Effect of Heat Treatment

Generally, crack propagation is slower in aluminium alloys having the T3 condition, that is subjected first to natural ageing after quenching and then to moderate work-hardening, Brock et al[91] investigated the effect of heat treatment on crack propagation rates in 2 mm thick 2024 clad aluminium alloy sheets in the following conditions:

	σ_{ult}	$\sigma_{0.2}$	A%	*Vickers hardness*	
As-delivered condition T/3	47.5	36.8	18.5	154	
T3 + 3 hr at 195°C	49.2	46.5	7.5	156	Critical ageing
T3 + 24 hr at 195°C	46.6	41.2	7	149	Overageing
Solution heat treatment for 50 hr at 495°C, quenching, and 6 hr at 195°C	46	39.2	9	151	Critical ageing
Solution heat treatment for 50 hr at 495°C, quenching, and 30 hr at 195°C	38.7	30.6	8	118	Overageing
	daN/mm²				

Overageing corresponds to the attainment of maximum hardness. In Figure 5.66, the rate of crack growth versus alternating stress intensity factor is given for centrally cracked specimens of width $w = 100$ mm. It is less for the as-delivered condition T3, this being probably due, to some extent, to the fabrication work-hardening. Any additional artificial ageing involves an increase of the crack propagation rate, which may be caused by the disappearance of the work-hardened state since metallurgical transformations favour plastic deformation, hence the relaxation of residual stresses. For the T3 condition, test results with $\sigma_m = 7.85$ daN/mm² and $\sigma_a = 2.45 - 3.92 - 6.36$ daN/mm² may be expressed by the following formulation, assuming that $\sigma_m \geqslant \sigma_a$:

$$da/dn = 10^{-3}(\sigma_m/\sigma_a)^{1.305} \cdot (K_a/43.5)^{3.23} . \qquad (21)$$

Brock[92] also studied bare 3 mm thick 2024-T8 aluminium alloy sheet material, the treatment of which included ageing for 9 hours at 190°C after quenching. The tensile properties were as follows:

	$\sigma_{ult.}$ (daN/mm²)	$\sigma_{0,2}$	Elongation, A%
T3 condition	46.7	36.4	21
T8 condition	47.7	45.4	6.5

The fatigue specimens, which contained a centre hole, had a width $w = 160$ mm. The test frequency - not indicated - was probably of the order of 1,000 to 2,000 c/m. The test results may be represented by the following expression, where $\sigma_m \geqslant \sigma_a$:

$$da/dn = 10^{-3}(\sigma_m/\sigma_a)^{1.27} \cdot (K_a/30.5)^{3.7} . \qquad (22)$$

In Figure 5.67, the results of Schijve and De Rijk[93] are plotted for clad 2024 aluminium alloy sheets in the following conditions: T3 condition denoted by E; E′ = T3 condition followed by ageing for 6 hours at 190°C; E″ = T3 condition followed by ageing for 9 hours at 190°C (T81). With three different values of the alternating stress, the crack propagation rates computed from the average of measurements on three specimens exhibit the same trend: fatigue induces additional ageing in E′ specimens, which is detectable because of the change in crack propagation rate from the values corresponding to the T3 condition at small crack lengths to those obtained in the T81 condition at great crack lengths.

The A-U2GN aluminium alloy is more stable at room temperature and Figure 5.68 indicates that equivalent results[89] were obtained with different heat treatments on thick sheet materials used in the manufacturing of the Concorde prototype aircraft, although the crack growth is considerably faster than in the as-delivered T351 condition; the latter cannot be used owing to the static properties at low temperature. Instability in fatigue is again found in tests at 150°C. Figure 5.69 shows that in specimens subjected to an additional ageing treatment for 19 hours at 190°C the rates of crack growth vary from the values corresponding to the T351 condition at small crack lengths to those found with more complete ageing processes at great crack lengths. As in the above described case of the 2024 alloy, we ascribe this effect to a progressive increase of the fatigue net stress during crack propagation. In Figures 5.68 and 5.69, the points are averages computed from the curves $a = f(n)$ which have been plotted through the experimental points of ten test specimens.

5.2.8 Variations with the Batch, the Manufacturer and the Rolling Direction

Like other mechanical properties, the fatigue crack propagation rates depend upon the mechanical and thermal history of the material which exerts an influence on the stability of crystal lattice distortions and on brittleness. Different growth rates can be observed even with identical static tensile properties.

TABLE 5.6

Crack Propagation Rate Variations in 2 mm Thick 2024-T3 Clad Aluminium Alloy Sheet Materials from Several Manufacturers. Effect of Rolling Direction. (After Schijve and de Rijk[93])

Values of the alternating stress intensity factor, K_a, for a mean stress σ_m = 6.86 daN/mm^2, expressed in daN/mm$^{3/2}$ (288 lb/in$^{3/2}$)								
σ_a	σ_a/σ_m	*da/dn* mm/cycle	*Manufacturers* F	C	D	G	E	A
2.45	0.357	10^{-4}	15.5	13	14	13	13	13.5
		10^{-3}	31	27	28	26.5	27	26
3.92	0.57	10^{-4}	20	14	16	14	14	16
		10^{-3}	36	31	32	31	31	30
		10^{-2}	58	49	52	51	51	48
6.37	0.93	10^{-4}	25	19.	22	19	19	19
		10^{-3}	44	38	38	38	38	35
		10^{-2}	60	55	55	55	53	53

Values of K_a on longitudinally loaded (L) and transversely loaded (T) specimens as overall averages for all the manufacturers				
σ_a	*da/dn* =	10^{-4}	10^{-3}	10^{-2}
2.45	Longitudinal L	14	29	46
	Transverse T	12.5	26	40
3.92	L	16.5	33	52
	T	12.5	30	50
6.37	L	20	40	63
	T	17.5	35	64

TABLE 5.7

Gust Load Occurrences in the 10 Different Types of Flights for Crack Propagation Tests (after Schijve, Jacobs and Tromp[101])

Flight type	*Number of flights*	*Number of gust cycles with amplitude σ_a, expressed in daN/mm^2* 11.75	10.8	9.7	8.62	7.55	6.47	5.4	4.32	3.24	2.16	1.08	*Total number of cycles per flight*
A	1	1	0	1	1	2	3	5	9	15	27	43	107
B	2		1	1	1	1	2	4	8	14	26	43	101
C	2			1	1	1	2	3	7	12	25	43	95
D	10				1	1	1	3	5	11	24	43	89
E	27					1	1	2	3	9	22	43	81
F	91						1	1	3	7	18	43	73
G	301							1	2	4	15	42	64
H	858								1	3	11	38	53
J	3165									1	7	28	36
K	543										1	19	20
Total number of cycles in 5,000 flights		1	2	5	15	43	139	495	1903	8000	39252	149902	
Number of exceedings		1	3	8	23	66	205	700	2603	10603	49855	199757	

Using clad 2024-T3 aluminium alloy sheet materials from two different manufacturers and from two different batches of each manufacturer, Schijve and De Rijk[93] obtained crack propagation rate variations that were as high as the ratio 1:3, the slower crack propagation corresponding to the higher ductility as indicated by a large elongation to tensile failure, A%, and a low yield stress value $\sigma_{0,2}$; this is an illustration of the part played by brittleness in the crack propagation. However, the rates of growth for batches of both manufacturers with very similar tensile properties were significantly different. The same phenomenon is reported by Piper et al[94] for the 7178 aluminium alloy. These discrepancies can only be explained by differences in the manufacturing and rolling procedures at low and high temperatures.

For the same batch, *crack propagation is faster in the transverse direction than in the rolling direction;* Rooke[80] found a life shorter by 20% for the DTD 5070A (A-U2GN in France) aluminium alloy. Table 5.6 gives some indications on the test results obtained by Schijve and De Rijk[93] on 2024-T3 sheet materials from seven different manufacturers. Including previous test results, the test data show a variation in growth rate with a ratio of 1:3 for the manufacturers considered as a whole. The variation would be lower in programmed tests. However, *to cover the scatter, the authors recommended a factor of 3 in relation to the crack propagation rate measured in a test on a complete structure. The crack* propagation rate is 30 to 60% slower in the transverse direction than in the longitudinal direction; the above mentioned authors also recommended *that in a pressurized aircraft fuselage the rolling direction be parallel to the hoop stresses* in order to obtain a low crack propagation rate with high hoop stresses.

5.2.9 Effect of Load Sequences

During the flight of aircraft, the bending moment of the wing varies continuously. On the ground, before take-off takes place, the lower wing is subjected to compression due to the dead weight of the wing and to the fuel weight contained therein. During taxiing at low speed, the surface irregularities of the taxiways cause the wing to be excited in bending vibrations. In flight, the lower wing surface is subjected to tension due to the permanent equilibrium loads which vary slowly with the fuel consumption. The manoeuvre loads and the response of the aircraft to gusts in turbulent air produce random loads above or below the preceding mean value. Subsequently, the wing is subjected to vibrations as a result of more or less severe impact loads. Finally, taxiing again generates a mean compressive load with superimposed vibrations induced by braking and by runway or clearway irregularities.

Naumann[99] evaluated the influence on fatigue life of random flight loads and of ground-air-ground cycles, i.e., of the periodical return to taxiing loads. Tests were carried out with edge notched specimens ($K_T = 4$) cut from 2.3 mm thick 2024-T3 and 7075-T6 aluminium alloy sheets. The test loads were derived from gust velocity statistics of commercial aircraft. The conclusions were as follows:

"1. The insertion of ground-air-ground cycles produced a large decrease in the number of simulated flights when compared with similar tests without the ground-air-ground cycle. The number of flights simulated was found to be influenced as indicated by the following conditions: (a) ground-air-ground cycle range - number of flights decreased as ground-air-ground range increased (the change is much greater than anticipated by $\Sigma n/N$, and (b) degree of load randomization - the decrease in number of flights was greater in random tests than in block tests having ground-air-ground cycles with the same range.

2. Ground-air-ground cycle spacing has a definite influence on the fatigue life as measured by the number of flights simulated, whereas no effect was noted on the basis of summation of cycle ratios $\Sigma n/N$.

3. In tests using random-load sequences, the degree of load randomization influences the fatigue life; the latter increases as the degree of randomization increases.

4. The omission of the lowest load level did not significantly affect the number of flights simulated for tests in which the ground-air-ground cycle was introduced.

5. All the trends noted herein can be explained qualitatively by using the concepts of residual stresses and residual-static strength."

In a preliminary study, Schijve and De Rijk[100] investigated the effect of ground-to-air cycles on the fatigue crack propagation in centre-notched specimens (w = 100 m, t = 2 mm) cut from 2024-T3 clad sheet material. Their conclusions were as follows:

"In two test series constant-amplitude loading at $\sigma = 8.83 \pm 2.94$ daN/mm^2 was periodically interspersed with down loads to $\sigma_{min} = 0.49$ daN/mm^2 after each 10 or 50 cycles respectively. This load sequence implied a simplified flight simulation as applied in older prototype testing of aircraft structures, i.e., gust cycles with a constant amplitude and ground-to-air cycles."

The results reported in Figure 5.70 show that with 10 gust cycles between two ground-air-ground loads the crack propagation rates that were measured and those which were calculated from constant-amplitude tests by means of the expression

$$da/dn = \frac{\Sigma n_i (da/dn)_i}{\Sigma n_i}$$

proved to be very similar, except for great crack lengths. With 50 gust cycles no significant effect of the ground-air-ground cycles was found.

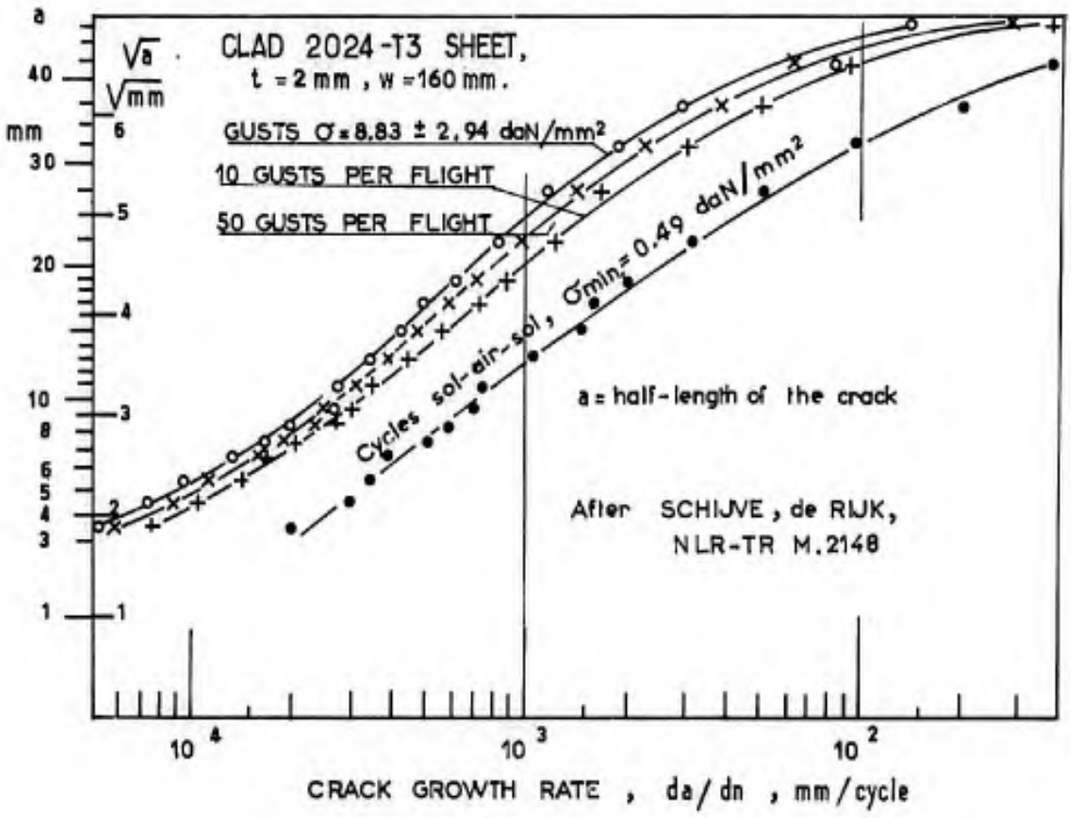

Fig. 5.70 Effect of ground-to-air cycles on the fatigue crack propagation

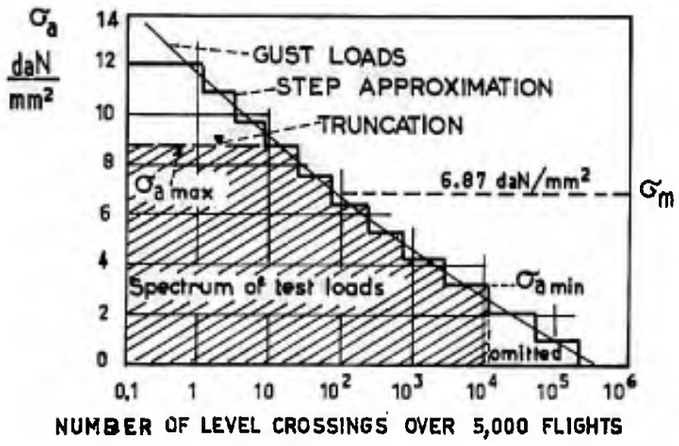

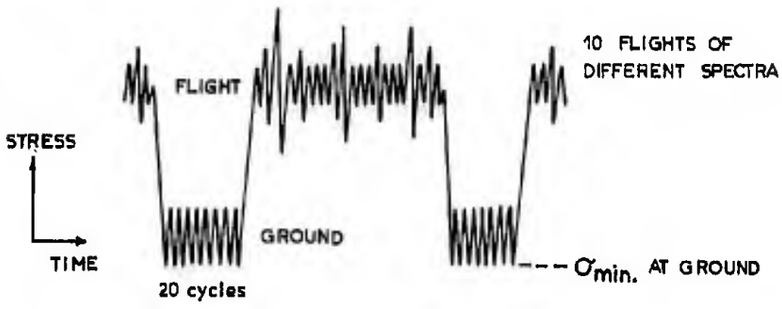

LOAD SPECTRUM AND LOAD DIAGRAM

Fig. 5.71 Loading in crack propagation test on clad 2024-T3 sheet specimens subjected to various load sequences. Figure after Schijve[101]

A more comprehensive study by Schijve, Jacobs and Tromp[101] brought this result again in question. The authors, adopting the principle of fatigue testing on a flight-by-flight basis, posed the following questions:

"1. Should the sequence of loads within each flight be a random sequence or could a programmed sequence be allowed? A truly randomized sequence and a programmed sequence are thought to be the most extreme possibilities.

2. What is the maximum load to be applied in the test (truncation of load spectrum)?

3. Could small load fluctuations be omitted from the test in view of time saving?"

To answer these questions, the authors proceeded to systematic fatigue crack propagation tests on 160 mm wide specimens cut from 2 mm thick 2024-T3 and 7075-T6 aluminium alloy sheet materials. The specimens contained a small incipient central fatigue crack which was initiated under $\sigma = 4.9 \pm 4.9$ daN/mm^2 at 100 Hz from two short saw cuts at both sides of a hole. In order to prevent buckling of the crack lips, the specimens were placed between guide plates to which felt was bonded; they were loaded in an MTS fatigue machine of type 901.55 having a maximum dynamic capacity of 25 tons - this fatigue machine is fitted with an integrated computer and is capable of any loading program. The load frequency was 10 Hz for small loads (σ_a = 1.08 - 4.3 daN/mm^2) and varied from 9 to 3.6 Hz for σ_a included between 5.39 and 11.85 daN/mm^2.

The gust loads were derived from flight data obtained on civil aircraft; they are represented by an overall spectrum in Table 5.7 which also gives partial spectra for different types of flights of decreasing severity, each characterized by statistical distributions of same shape. In order to prevent perturbation of the crack propagation tests, the most severe flights were uniformly distributed over the total sequence. In the tests, such a block of 5,000 flights was repeated periodically. The random sequence of moderately high loads was distributed over 4,958 flights which were divided into 42 groups. These groups were separated by special flights for simulation of the more severe load statistics. The main random sequence included 91 flights of type F, 301 flights of type G, 858 flights of type H, 3165 flights of type J and 543 flights of type K. The interspersed flights were introduced in the following sequence: E, D, E, B, E, D, E, E, C, E, E, D, E, E, D, E, E, A, E, E, C, E, E, D, E, E, B, E, D, E, E, D, E, E, C, E, E, D, E.

The maximum gust load corresponded to what is encountered at least 10 times in the predicted life time of the aircraft, following the French practice of full-scale fatigue testing[102]. The ground load was simulated by two values of the mean stress, i.e., $\sigma_m = 0$ and $\sigma_m = -1.96$ daN/mm^2, the vibrations due to taxiing being simulated by an alternating stress $\sigma_a = \pm 1.37$ daN/mm^2.

The test results show that omission of the alternating ground loads does not affect the crack propagation. This has been confirmed by tests conducted by Gassner and Jacoby[103] for the total life to failure. Let us return to the preceding tests; the minimum negative ground stress assumed values of -1.37 and -3.34 daN/mm^2 in some tests; its effect was negligible for the 7075-T6 alloy and small for the 2024-T3 alloy. Together with the authors, we believe that this is due to the closing of the crack lips in compression.

Omission of the smallest gust loads may reduce the test duration considerably; however, the crack propagation rate decreases and the crack propagation life, expressed in flights, increases. Omitting the lowest level, i.e., $\sigma_a = \pm 1.08$ daN/mm^2, increases the life by 20% for the 2024 material and by 40% for the 7075-T6 material; omitting also the level $\sigma_a = \pm 2.16$ daN/mm^2 nearly doubles the life of the two truncation levels (σ_{max} = 6.47 and 7.55 daN/mm^2) in tests with random or programmed loads.

Figure 5.71 gives a cumulative spectrum of the number of level-crossings over 5,000 flights. Truncating at a specified value of $\sigma_{a\,max}$ implies that the amplitude of the more severe loads should be reduced to a corresponding value. The effect of truncation is shown in Figure 5.72 for the 2024-T3 material. *Under the highest load levels the crack propagation rate in the case of small cracks tends to decrease with further crack extension; even after it has again increased, the crack propagation rate is still less than that obtained for the same crack length if the highest load levels are omitted.* This effect is attributed by the authors to interactions between successive loads of different levels. Tests performed by the authors show that the influence on the period prior to crack propagation exhibits the same trend although it is smaller; in the case of the 2024-T3 material, the ratios of durations are as follows for a 160 mm wide specimen with a 20 mm diameter hole at its centre:

σ_a of truncation daN/mm^2	Duration prior to crack propagation		Duration of crack propagation	
	Number of flights	Relative duration	Number of flights	Relative duration
4.32	12,600	1	5,200	1
6.47	13,900	1.1	11,600	2.2
7.55	18,200	1.45	20,500	3.9

In our opinion, these results correspond to a specific case of a *quite general law on the behaviour of notched specimens, according to which any fatigue first improves the fatigr life under subsequent loads of lower level by creating beneficial compressive residual stresses at the notch roots subjected to tension.* Cracks are particularly severe notches and it is quite normal that the general phenomenon should be observed.

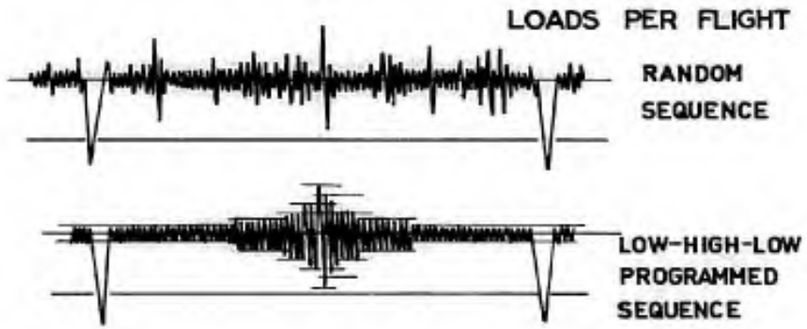

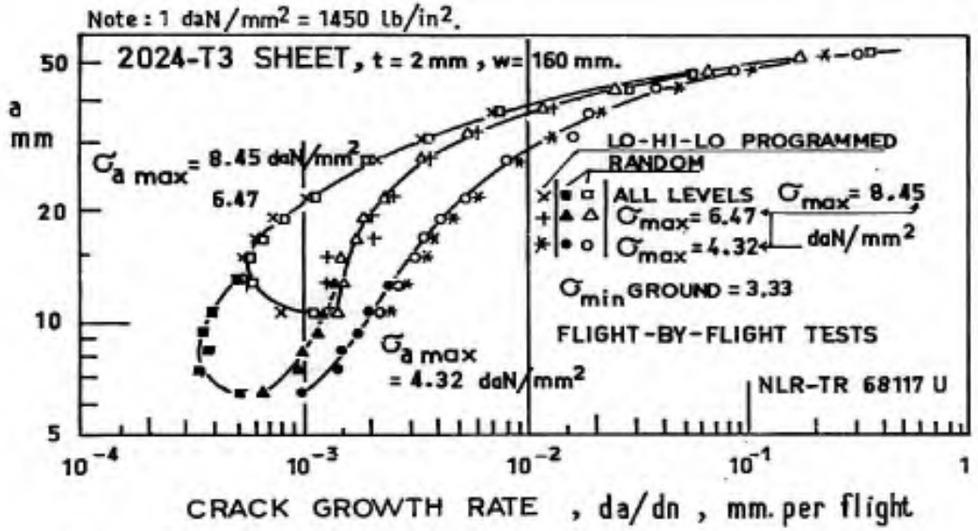

Fig.5.72 Crack propagation in 2024-T3 aluminium alloy sheet specimens subjected to random or programmed loads. After Schijve, Jacobs and Tromp[101]

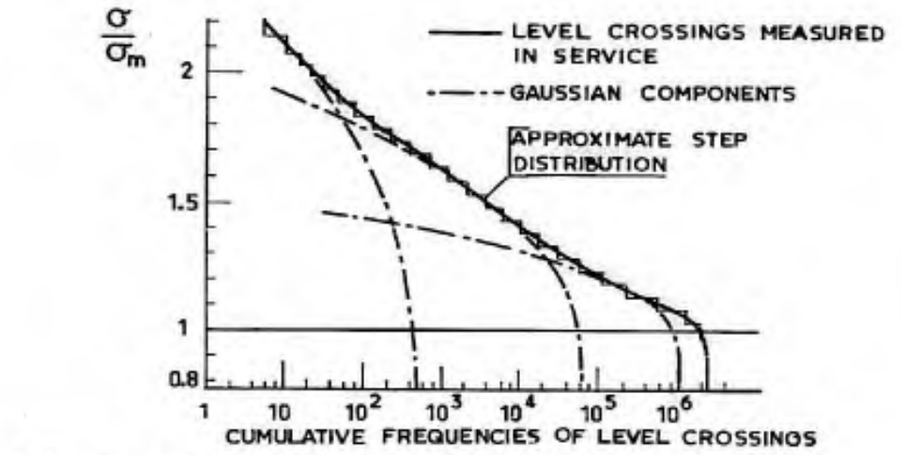

(a) STATISTICAL DISTRIBUTION OF LOADS

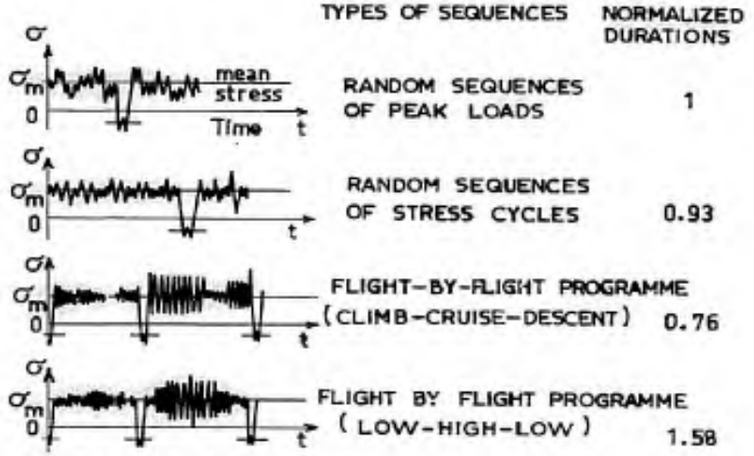

(b) SEQUENCES OF TEST LOADS

Fig.5.73 Influence of loading sequences on the fatigue life of notched 2024-T3 specimens under simulated aircraft flight loads. (After Jacoby[104])

It should be noted that during crack propagation there is always a more or less stable improving effect due to the application of high tensile loads; indeed, high tensile loads produce favourable compressive residual stresses whereas high compressive loads cause the crack to close, and thus have very little effect. From this it follows that the crack propagation rate given by a load spectrum should be less than that predicted by a computation of the average

$$(da/dn)_{average} = \sum \frac{n_i}{n} (da/dn)_i ,$$

where n_i/n is the ratio of the number of cycles under the i^{th} load level to the total number of cycles and, $(da/dn)_i$ is the crack propagation rate measured in a constant-amplitude test under the i^{th} load level for a given crack length, a. From test results obtained by Schijve et al[101] for 2024-T3 alloy (a = 15 mm, $\sigma_{a\,max}$ = 6.47 daN/mm^2, $\sigma_{a\,min}$ = 1.08, no return to ground condition), the computed average crack propagation rate is about eight times the really measured value. In the same test, the Miner's cumulative damage ratio, $\Sigma n_i/N_i$, where N_i is the number of cycles at failure under the i^{th} load level in a constant-amplitude test, was equal to 3.4 for the entire life before failure. This shows that the improving effect of high loads is higher during crack propagation than during the crack initiation period.

Effect of load sequencing in a flight. The differences obtained by the previously mentioned authors in tests with random or programmed load sequences applied in the order low-high-low loads are not significant. This is again observed in the case of gust reversals, beginning with a positive or negative half-cycle in random tests; *the gust load sequence would be of no practical significance for the crack propagation rate.*

The application of one load per flight simulating the highest upward gust increases the crack propagation period by a factor of 3 and is unacceptable in a crack propagation investigation.

The omission of the return to ground condition increases the crack propagation period by 50% for the 7075-T6 material and by 80% for the 2024-T3 material.

The importance of crack propagation tests in a study of the effects of load sequencing and of the effects of other test or environment parameters that govern the fatigue damage lies in the fact that the crack propagation rate is one of the rare physical quantities that can be measured and directly related to the fatigue life. Anything that affects crack propagation also affects the total life at failure.

Figure 5.73(a) contains the load spectrum used by Jacoby[104] to define the loads on 2024-T3 sheet specimens having a centre hole with a stress concentration factor K_T = 3.1. The initial spectrum was established by counting the number of lond level crossings. Actually, service peak loads are not necessarily followed by a passage through the mean flight load. Consequently, the ratio N_0/N_1 of number of passages through the mean value to number of positive peaks characterizes the irregularity of the load curve (Kowalewski[105]). With a Gaussian process, the distribution of peaks is related to the level crossings. Using the graphical method described by Press[106], Jacoby broke the level cross spectrum down into three Gaussian components and took a value N_0/N_1 = 0.8 to calculate the total distribution of peak loads. The test sequences and the relative durations, expressed in number of flights, are shown on Figure 5.73(b); all of the tests satisfied the same total statistical distribution. With this same distribution, the Miner rule gave a relative duration of 2.73 while block tests including ground-air-ground loads yielded values of 4.12 or 6.84 depending on whether the vibrations due to taxiing were simulated or not; a relative duration of 18.3 was obtained in a test including one flight load varying between the highest and the lowest level that are attained approximately once per flight.

Whatever the interest of "randomized" loads, that is, of sequences determined by means of a table of random numbers, we consider that the load distributions between "severe" flights and "moderate" flights should be based on statistical load spectra measured during individual flights and on *distributions of the intensity of the load spectra between flights.* Statistics of the *extreme load values per flight* could perhaps provide a basis for such distributions. In a test, the individual flight load spectra could be introduced into a sequence defined at random for moderately severe load spectra; flights of exceptionally high severity should not be simulated at the beginning of a test in order to prevent the structure from being prematurely improved compared with the aircraft which might encounter the corresponding high loads only after a longer period of time. In this regard, we recommend separate investigations of the period prior to crack initiation and of crack propagation. During the plastic changes that precede crack propagation, the only physical quantity that can be measured is the variation in stress amplitude in a test with controlled strain sequences. The purpose would be to highlight the effect of various sequences on residual stresses inside a notch where the material is subjected to an elastically controlled deformation which causes straining of the material in the plastic range near the notch root. Finally, the severe loads should be taken into consideration for final fracture after crack propagation.

5.2.10 Measurement and Evaluation of the Stress Intensity Factor in Thin Sheet Structures

In the foregoing paragraphs it has been demonstrated that the fatigue crack propagation in thin sheets is governed by the intensity factor of mean and alternating stresses, $K = K_m \pm K_a$, the second term being predominating. The application of this to the prediction of crack propagation rates in actual structures involves two difficulties: first, the stress state in the absence of crack is not homogeneous in the direction of the sheet width; second, the problem is complicated by the presence of stiffeners.

Considering a homogeneous stress field without cracks and using digital calculations, Isida[107] treated the case of sheets stiffened by stringers with a regular spacing, whose direction was parallel to that of the tensile stress. A first calculation for an unstiffened sheet of finite width yielded the following expression as regards the stress concentration at the tip of a centre slot of length 2a contained in a sheet of width w:

$$K_T = \frac{\sigma_{max}}{\sigma_0} = 2\sqrt{\left(\frac{a}{\rho}\right)}(1 + 0.5948\ m^2 + 0.4812\ m^4 + 0.3963\ m^6 + 0.3367\ m^8 + 0.2972\ m^{10} + 0.2713\ m^{12} + 0.2535\ m^{14})$$

$$+ 1 + 1.389\ m^2 + 1.8128\ m^4 + 1.7466\ m^6 + 1.6753\ m^8 , \qquad (23)$$

where σ_0 is the tensile stress in the absence of a crack,
ρ the radius of curvature at the tip of the slot,
$m = 2a/w$.

When the radius of curvature at the tip of the slot is very small, the second term of expression (23) can be neglected and the *stress intensity factor* will be

$$(K)_t = \sigma_0\sqrt{(\pi a)} \cdot (1 + 0.5948\ m^2 + 0.4812\ m^4 + 0.3963\ m^6 + 0.3367\ m^8$$

$$+ 0.2972\ m^{10} + 0.2713\ m^{12} + 0.2535\ m^{14}) , \qquad (24)$$

where the factor in parentheses indicates the *effect of the finite sheet width.*

Another problem treated by Isida for sheets of finite width concerned the *plane bending of an infinite strip* with a central transverse crack. The stress concentration factor is given by the expression

$$(K_T)_b = \frac{\sigma_{max}}{\sigma_b} = 2\sqrt{\left(\frac{a}{\rho}\right)}(1 + 0.4079\ m^4 + 0.1456\ m^6) + 1 + 0.8218\ m^4 + 0.3411\ m^6 , \qquad (25)$$

where σ_b denotes the bending stress at the tip of the slot in the absence of a slot.

This expression is no longer valid for a very small slot radius since the slot lips are mutually supported in compression. However, it is applicable in conjunction with the preceding expression in combined cases of tension and bending if the slot is nowhere subjected to compression. The *stress intensity factor in bending* is

$$(K)_b = \sigma_b\sqrt{(\pi a)}\,[1 + 0.4079\ m^4 + 0.1456\ m^6] . \qquad (26)$$

In combined tension and bending, with a stress varying linearly in the absence of a crack from σ_0 at the centre to $\sigma_0 + \sigma_b$ at the subsequent location of the crack tip, the resulting stress intensity factor will be

$$K = (K)_t + (K)_b .$$

The stress intensity factor may thus be calculated for a stress field that varies little in the absence of a crack.

An approximation of the problem of a centre crack located between two stringers in a stiffened plane panel was carried out by Isida for a plane panel with an infinite row of parallel stringers and with identical round-tip slots at every two stringer spacings, as shown in Figure 5.74. The numerical treatment yielded values for the function $F(m,\alpha,k)$ which is used in the following expression of *stress concentration.*

$$\frac{\sigma_{max}}{\sigma_0} = 2\sqrt{\left(\frac{a}{\rho}\right)} \cdot F(m,\alpha,k) , \qquad (27)$$

where ρ denotes the radius at the tips of the slot,
$k = 2A/wt$ the ratio of the cross-sectional stringer area A to the half-cross-sectional sheet area between two stringers,
$\alpha = I_{zz}/t(w/2)^3$, I_{zz} being the moment of inertia of the cross-sectional stringer area in relation to an axis perpendicular to the sheet,
w the width of a stringer spacing between the axes of two stringers,
t the sheet thickness,
σ_0 the tensile stress in the absence of slots.

With ρ tending toward zero, the *stress intensity factor* may be defined by

$$K = \sigma_0\sqrt{(\pi a)} \cdot F(m,\alpha,k) , \qquad (28)$$

The curves in Figure 5.74, which summarize the calculations by Isida, show that the function $F(m,\alpha,k)$ always decreases with increasing relative cross-sectional stringer area, k, m and α being fixed. However, the variation of F becomes progressively smaller with increasing k and α, and F approaches certain limiting values as k and α tend toward infinity. In practice, k is included between 0.4 and 2, while α ranges between 0.05 and 5.

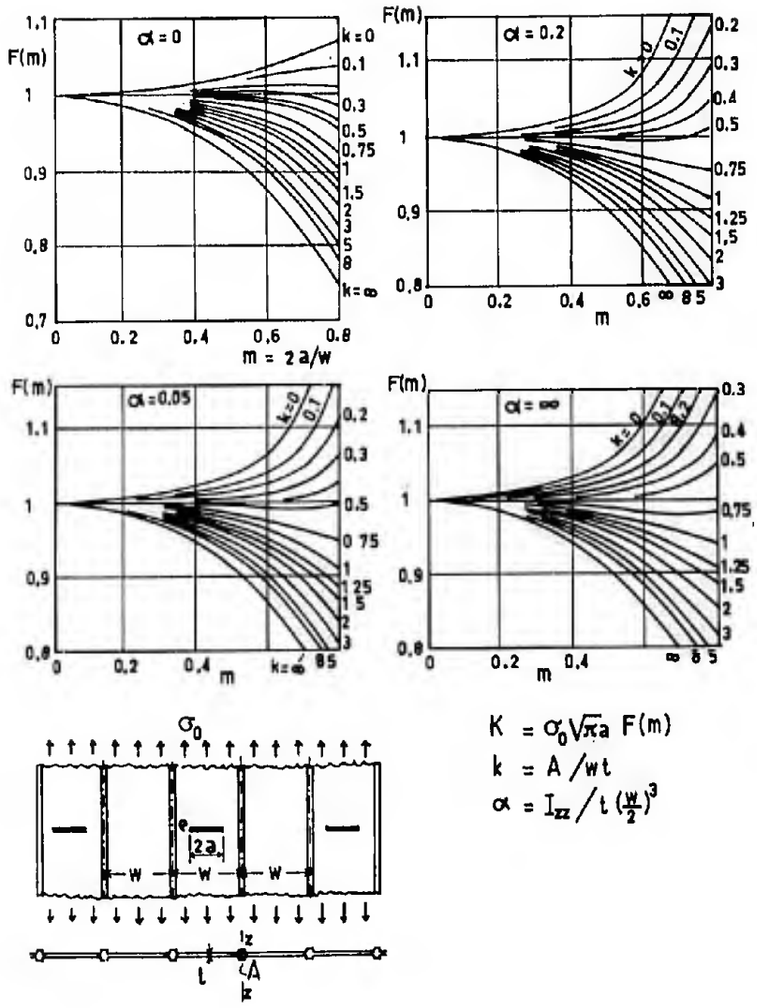

Fig. 5.74 Influence of stiffeners on the stress intensity factor. After Isida[107]

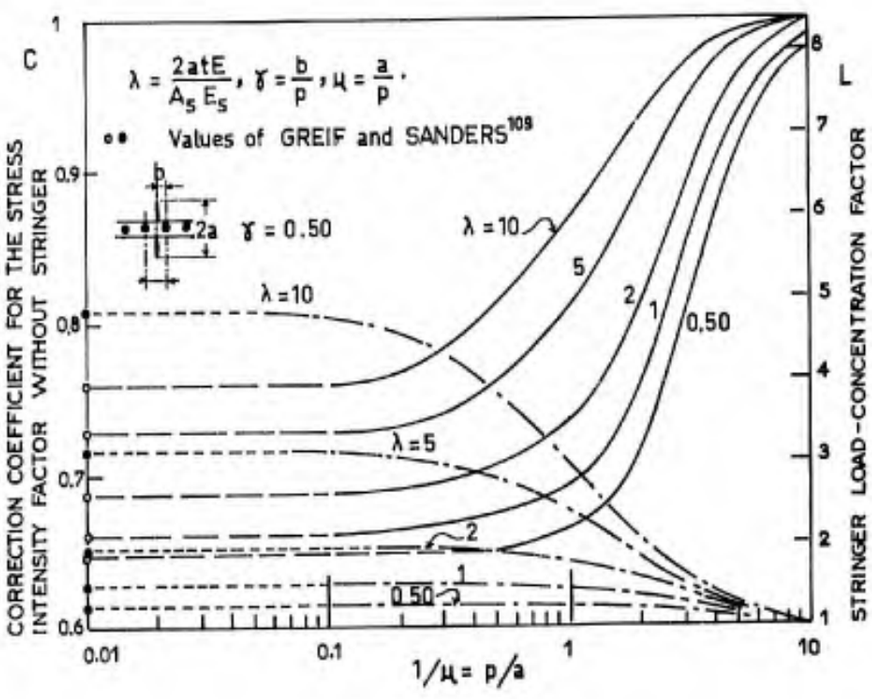

Figure 5.75

Several searchers have studied the effect of riveted stringers on stress at the tip of a crack located near the stringer. Sanders[108], and later Greif and Sanders[109], considering the case of a stringer attached to a sheet along a continuous line, investigated the effect on the stress field at the tip of a crack symmetric or non-symmetric with the stringer axis. Bloom[110] analyzed the same problem, taking into account the spacing of the rivets used for attaching the stringer to the sheet. In all these calculations, an infinite sheet with a single stringer was taken into consideration and subjected to a stress σ_0 at infinity, parallel to the direction of the stringer.

For cracks symmetric with the stringer axis, the parameters of the problem were as follows:

- the ratio of rigidities, $\lambda = 2\pi tE/A_s E_s$,
- the ratio, $1/\mu = p/a$, of rivet spacing to half-crack length,
- the ratio, $\gamma = b/p$, of the distance b from crack to nearest rivet and the spacing p .

The other quantities were as follows:

$2a$, the crack length,

t, the sheet thickness,

A_s, the cross-sectional stringer area,

E and E_s, the moduli of elasticity of sheet and stringer, respectively.

If a correction factor C is defined as the ratio between the stress intensity factor of a sheet with a stringer and that of a sheet without a stringer, we shall have for the stiffened sheet

$$K = \sigma_0\sqrt{(\pi a)} \cdot C \,. \tag{29}$$

Let us consider both cases, i.e., the uncracked stringer and the fractured stringer. In the first case, crack extension causes the stringer to be overstressed and a *stringer-load-concentration factor*, L , is defined such that the stress in the stringer becomes $L\sigma_0$. For a stringer attached along a continuous line to a sheet which contains a symmetric crack, calculations by Greif and Sanders give the following values of C and L:

	λ =	0.50	1	2	5	10
Uncracked stringer	C =	0.65	0.66	0.69	0.73	0.76
	L =	1.30	1.60	1.94	3.18	4.88
Fractured stringer	C =	1.79	1.42	1.16	1.10	1.05 .

The uncracked stringer reduces the stress intensity factor at the crack tip but it is heavily overstressed; in practice, if the stringer is made of the same material as the sheet, fatigue crack propagation will start quite early and it can be assumed that fracture will occur within a short time. The fractured stringer should therefore be taken into consideration for prediction of the subsequent crack growth. We thus see the advantage of using crack-stoppers with a high fatigue strength as obtained by bonding, by techniques for local improvement (such as coining), or by the selection of a material of higher strength or with a greater modulus.

Figure 5.75, after Bloom[110], shows the effect of relative rivet spacing, p/a , on the correction coefficient for stress intensity and on the stringer-load-concentration factor; the stringer is less efficient if the rivet spacing is greater. In practice, we shall always have $a/p < 10$, so that there will be some effect of rivet spacing. The case of integral stringers - obtained by milling - is not to be considered for symmetric cracks, except when assuming that the stringer is fractured and when applying the corresponding solution proposed by Greif and Sanders.

Considering the problem of an eccentric crack approaching and then traversing the stringer, Bloom demonstrated that the stress intensity factor passes through a minimum when the crack extends beneath the stringer, which explains why a stringer can be a "crack-stopper" provided, as indicated previously, it is not itself about to crack. For integral stringers, that is, in the case of zero rivet spacing, calculations made by Greif and Sanders show that the stress intensity factor becomes very small at the tip of the crack when the latter reaches the stringer; this implies, theoretically, a considerable crack-growth retardation in the sheet but at the same time an increased overstressing of the stringer which then constitutes a notched component likely to crack. The crack will extend further in the sheet only if it has developed to a sufficient height on the stringer. Indications on the comparative efficiency of riveted and integral stringers with regard to crack propagation in sheets can only be obtained from tests.

No calculation data for evaluation of the stress intensity factor are available for the more general cases of structures consisting of stiffened thin sheets. In our view, it is sometimes useful to measure this factor during a structure fatigue test in order to decide whether the test can be continued without the hazard of excessive subsequent crack propagation and brittle failure. We suggest one *measure the stress intensity factor by means of strain-gauges mounted ahead of the crack tip*. The problem may be put as follows[111]:

Determine the stress intensity factor of a centre crack in a thin sheet of infinite extent which would have the same distribution of the strain ϵ_y perpendicular to the crack plane and ahead of the crack as the actual component under investigation.

In an infinite sheet containing a centre crack of length $2a$ along the Ox-axis and subjected to a tensile stress σ_0 along the Oy-axis, the stress distribution at the points located on the Ox-axis in prolongation of the crack is given by

$$\sigma_y = \sigma_0/\sqrt{(1 - a^2/x^2)}, \qquad \sigma_x = \sigma_y - \sigma_0 , \tag{30}$$

where a is the half-crack length, x the distance from the point considered to the axis of symmetry, and σ_0 the stress applied remote from the crack plane in the Oy-direction. Using the relation $E\epsilon_y = \sigma_y - \nu\sigma_x$, we obtain

$$E\epsilon_y = \left[\frac{1 - \nu}{\sqrt{(1 - a^2/x^2)}} + \nu\right]\sigma_0 ; \tag{31}$$

with

$$\sigma_0 = K/\sqrt{(\pi a)} ,$$

it follows

$$E\epsilon_y = \frac{K}{\sqrt{(\pi a)}}\left[\frac{1 - \nu}{\sqrt{(1 - a^2/x^2)}} + \nu\right] . \tag{32}$$

This expression allows the stress intensity factor, K, to be calculated from one measurement of strain ϵ_y if the crack is located in a homogeneous stress field prior to crack propagation and if the symmetry axis of the crack is known.

In an actual structure, although the total apparent length is known, lack of symmetry due to loading and the influence of unfractured stringers require that an equivalent half-crack length, $\bar{a}$, be defined. Moreover, the exact location of the crack tip is uncertain because of the oblique direction and the curvature of the crack front and owing to the fact that the damaged material ahead of the crack front may include microcracks which reduce the stiffness of the material, all conditions being equivalent to a crack of greater length. Accordingly, the distances of the points for elongation measurements, $R_i = x_i - a$, to the crack tip must be reduced by an unknown quantity, b. We may then write the equation (32):

$$E\epsilon_y = \frac{K}{\sqrt{(\pi a)}}\left[\frac{1 - \nu}{\sqrt{1 - \dfrac{1}{\left(1 + \dfrac{R - b}{\bar{a}}\right)^2}}} + \nu\right] , \tag{33}$$

hence

$$K = E\epsilon_y\sqrt{(\pi a)}\Bigg/\left(\frac{1 - \nu}{\sqrt{1 - \dfrac{1}{\left(1 + \dfrac{R - b}{\bar{a}}\right)^2}}} + \nu\right) \tag{34}$$

In the most general case we have three unknowns, K, b and $\bar{a}$; theoretically, the problem can be solved by three measurements of ϵ_y. We may eliminate K by dividing the measurements of ϵ_{yi}:

$$A_{ij} = \frac{\epsilon_{y_i}}{\epsilon_{y_j}} = \left[\frac{1 - \nu}{\sqrt{(1 - 1/\eta_i^2)}} + \nu\right]\Bigg/\left[\frac{1 - \nu}{\sqrt{(1 - 1/\eta_j^2)}} + \nu\right] , \tag{35}$$

where

$$\eta_i = 1 + \frac{R - b}{\bar{a}} .$$

Suppose successive values of b, beginning with $b = 0$. For each value of b, try successive values of $\bar{a}$; we shall retain, if it exists for the supposed value of b, the value of $\bar{a}$ that yields the measured values of the ratios A_{12} and A_{13}. To aid the numerical computation, we may use a table of the values of

$$z = \frac{1 - \nu}{\sqrt{(1 - 1/\eta^2)}} + \nu$$

as functions of

$$\eta - 1 = \frac{R - b}{\bar{a}} = \sqrt{\frac{1}{1 - \left(\dfrac{1 - \nu}{z - \nu}\right)^2}} - 1 .$$

If the problem implies symmetric conditions, we may put $\bar{a} = a + b$; K can be calculated on the basis of two measurements of $E\epsilon_y$ if the distribution of ϵ_y is not too different from the theoretical distribution. We may also use the method of Bhandari[112]: with $b = 0$, calculate the successive values of K_i corresponding to each value of $E\epsilon_{yi}$ and then extrapolate to obtain the value of K at the crack tip. If the experimental

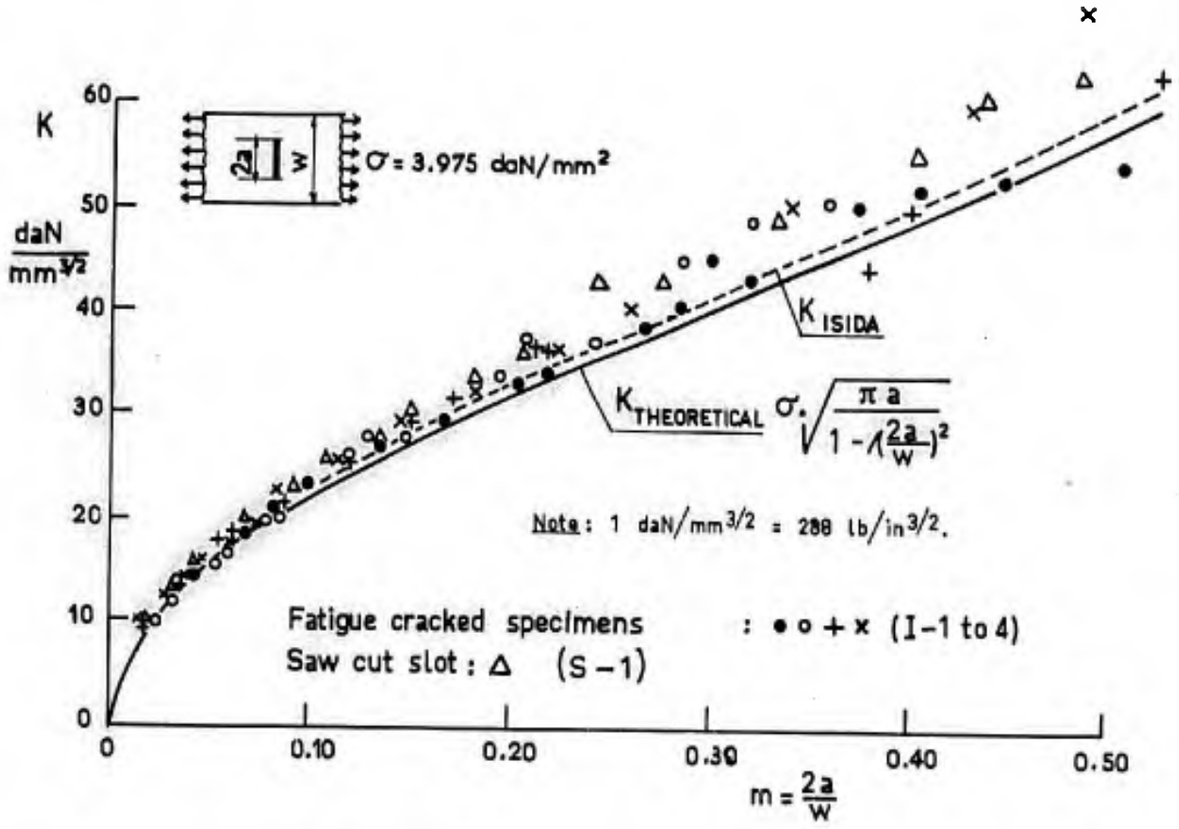

Fig. 5.76 Comparison of measured and theoretical values of the stress intensity factor in thin sheet specimens containing a centre crack (after Bhandari[112])

TABLE 5.8

Measured Values and Theoretical Values of the Stress Intensity Factor in a Centre-Cracked Sheet of Finite Width Subjected to σ_0 = 3.91 daN/mm²

2a/w	0.052	0.056	0.076	0.097	0.117	0.149	0.197	0.212	0.242	0.282
K_M	16	16.3	20	22.1	26.1	27.7	33.7	37.2	37	45
K'_M	16.7	16.7	20.2	22.8	26	26	32.7	36.2	37.8	42.2
K_{Tw}	15.7	16	19.1	21.5	23.9	27.4	32	33.3	36.2	40

distribution approaches the theoretical distribution of an infinite plate, the successive values of K_i will be close to each other and it will be sufficient to take the average of these values.

When treating the problem of elasticity, we should avoid any plastic deformation in the measurements. The latter should therefore be carried out while unloading the specimen between two values of the load; the smaller load value must be high enough for a linear relationship to be maintained between the load and the measurement and no plastic deformation due to residual stresses should occur.

Tests were performed by Bhandari on 200 mm wide and 1.6 mm thick sheet specimens made from clad A-U4G1-T3 aluminium alloy (similar to the 2024-T3 Al clad material). Figure 5.76 gives the results of extrapolations carried out by Bhandari, using elongation measurements which were made at at least six locations ahead of the crack tip; on four specimens the cracks were obtained by fatigue whereas the slot of the fifth specimen was made by a saw cut. Table 5.8 summarizes the results of our calculations for one of these tests which was carried out on a centre-cracked specimen; K_M is the measured value obtained by extrapolation, K'_M was determined on the basis of three measurements by neglecting the test symmetry and by not taking into consideration the crack length, and K_{Tw} is the theoretical value which takes into account Dixon's finite-width correction. (See Table 5.8). The results are expressed in $daN/mm^{3/2}$ (288 $lb/in^{3/2}$).

The validity of these measurements was confirmed by further tests on specimens fitted with centre or edge stringers. The theoretical trends of the effect of stringers were again observed and for equal measured values of the alternating stress intensity factor the same fatigue crack propagation rate was found, except for the scatter.

Strain-gauge measurements are not easy to carry out in the case of very small cracks. We would suggest one measure the elastic variation of the crack opening upon unloading by means of a method similar to that used by Srawley (See Chapter 4, Page 4.53 and Reference 4.84). In an infinite sheet the slot opening assumes an elliptic shape (see Chapter 4, Paragraph 4.2.2.2) given by the expression

$$\delta = 4a \frac{\sigma_0}{E} \sqrt{(1 - x^2/a^2)}, \tag{36}$$

where a denotes the half-crack length, and x the distance of the point of measurement to the crack axis. With $K = \sigma_0 \sqrt{(\pi a)}$, it follows

$$\delta = \frac{4K}{\sqrt{(\pi \cdot E)}} \sqrt{(1 - x^2/a^2)}. \tag{37}$$

If the problem implies a symmetry axis, K can be determined from the measurement of the elastic crack opening at the centre, δ_0 :

$$K = \frac{\delta_0 E}{\sqrt{a}} \cdot \frac{\sqrt{\pi}}{4}.$$

If the problem does not imply symmetric conditions, we need two measurements, δ_1 and δ_2, at points located at R_1 and R_2 from the considered crack tip. If we put $R = \bar{a} - x$, we have

$$\delta = \frac{4K}{E\sqrt{\pi}} \sqrt{[R(2\bar{a} - R)]},$$

hence

$$A_{12} = \frac{\delta_1}{\delta_2} = \sqrt{\left[\frac{R_1(2\bar{a} - R_1)}{R_2(2\bar{a} - R_2)}\right]}.$$

With this ratio we may determine the equivalent length, $2\bar{a}$, of the symmetric crack that exhibits the same relative lip displacements at the measurement locations. The same expressions are valid for surface cracks if E is replaced by $E/(1 - \nu^2)$, where ν is the Poisson ratio.

5.3 CONCLUSION ON THE FATIGUE BEHAVIOUR OF STRUCTURES

The considerable amount of experimental work performed on assemblies, mechanical parts, notched and smooth specimens in connection with the fatigue problem of structures has revealed the most significant elementary aspects of fatigue behaviour, the combination of which is a great help for understanding the actual phenomena from a qualitative point of view and for predicting the required action in each particular case. Although few of the practising engineers are fully aware of the fatigue phenomena, specialists have at present no great difficulty in understanding these phenomena but their advice often holds only on a qualitative basis since a quantitative interpretation of laboratory tests in terms of structural fatigue life under actual environmental conditions is sometimes quite difficult to achieve.

Before we study, in a second volume, the technological problems of the strength of structures, it seems relevant to make a survey of what we consider to be established facts concerning the average qualitative laws that govern the behaviour of materials and of structures in fatigue.

5.3.1 General Technical Aspect of Fatigue

The first point of a qualitative theory of fatigue was put forward by research in the physics of metals. It thus appeared that the first physical changes caused by fatigue are associated with the plastic straining of crystals which takes place through relative slip along certain crystalline planes. This slip involves the motion from one atom to the next of a linear singularity, called *dislocation* (see Chapter II, Paragraph 2.1.1). Technically speaking, it may be concluded from this that *plastic shear strains condition the physical process prior to crack initiation and during crack propagation in fatigue.*

Successive changes result in the modification of the relative stabilities under load of distortions and crystal lattice defects which are obstacles to dislocation propagation and hence lead to plastic deformation. Consequently, some barriers disappear while others are overstressed; vacancies - due to the lack of atoms in the crystal lattice - cluster together, and microcracks are created (see Paragraph 2.5.3). *Fracture Mechanics* explains why these vacancies and microcracks may extend under the effect of local tensile stresses just ahead of a crack tip where they exist in large numbers as a result of great plastic strains and high stresses (see Paragraphs 4.3.1 and 5.2.3). *The detrimental effect of tensile static stresses superimposed on alternating fatigue stresses was confirmed by all the tests performed.*

For the time being, no further conclusion can be drawn from the work carried out on the physics of metals, although this work is being continued with the aim of evolving a quantitative theory.

We may try to show some other aspects of the fatigue behaviour of structures considered fundamental from the engineering viewpoint. First, the *notch effect* may be characterized by the behaviour of a small volume of material subjected to strains in the plastic range by the surrounding material which remains substantially in the elastic strain range. After much time had been wasted, Coffin undertook to study the fatigue under constant-amplitude strain (see Paragraph 5.1.2) in connection with the fatigue failure of pipes in radioactive isotope splitting-plants under thermal stresses due to cyclic temperature variations.

Other technical investigations underlined the great practical significance of *compressive residual stresses* at the surface of components. Such stresses are in metastable equilibrium and rapidly decrease in magnitude as a result of fatigue. Some effect, however, remains since compressive residual stresses are produced by work-hardening which implies plastic strains along sets of crystalline planes other than those involved in the cyclic plastic strains of the fatigue process. This raises the more general problem of the *stability under load of a set of crystal lattice distortions due to a given type of loading when the same crystal lattice is subsequently subjected to another type of loading.*

The subject of the *mechanical stability of strain-hardening* may be first dealt with by examining another fundamental technical problem associated with fatigue and even with creep. This concerns the changes that occur in the stability of a strain-hardened state - due to loadings at a given level - as a result of subsequent continuous or discrete loadings at a different level. *In fatigue any repeated load first increases the life that will later be obtained under a smaller load* (Ref. 113); If the number of applications of the high load is raised, the fatigue life under the smaller second load will be shortened; this phenomenon is referred to as the *damaging effect* of the first load. If the first load level is below the fatigue limit - assuming that the latter exists - , it will cause an improvement which can be evidenced by a second loading at a level slightly above the fatigue limit of virgin specimens. This phenomenon is called *"understressing"*; as it occurs but rarely, it is considered to be questionable or odd. The more general phenomenon of improvement caused by *overstressing* is not well known to experimentalists who work with smooth specimens in the constant-amplitude stress range. This effect is fundamental in the behaviour of notched specimens and is easily accounted for by the creation of compressive residual stresses at the root of a notch. It may be studied on smooth specimens by means of constant-amplitude strain range tests with axial-load cycling (see Paragraphs 5.1.1 and 5.1.2). The changes in the stress-strain cycle are the only physical quantities associated with fatigue that can be measured during the process prior to crack initiation (see Paragraphs 5.1.3, 5.1.4 and 5.1.5 for measurable quantities that are not as well correlated with fatigue).

The improving effect of high loads during crack propagation appears even more distinctly, as was shown by Dutch tests reported in Paragraph 5.2.3, Figure 5.47, and in Paragraph 5.2.9, Figure 5.72. In service, with the exception of a few cases, structures are subject to load sequences of quite different levels and occurring in a complex order; in defining test loads and in interpreting test data from a single structure tested under a particular load sequence, it is very important to know what destructive and improving effects are likely to be encountered.

On the more fundamental level of research work, one should endeavour to study the stability under mechanical loads with the same care as the stability under thermal agitation. The two problems involve different concepts. The effect of heat has been treated by Statistical Mechanics which postulates *statistical independence* for elementary phenomena of the same nature; this method consists in taking averages which are then explained by the activation energy of the transformation investigated. For the phenomena associated with instability under loads or strains the equilibrium theorems of Statics are used as a primary means of reasoning. The pattern applied is the behaviour of *chains loaded in parallel* and not that of the weakest link of chains loaded in series. During the stressing of crystals under plastic deformations, the large number of barriers which impede the occurrence of slip are stressed in parallel, all the slip planes being "pinned" together by point defects, inclusions or grain and subgrain boundaries in heavily worked metals. The stresses which counterbalance the loads are irregular in their profile. When the stability of a barrier is overcome by a high enough shear stress, slip passes across the obstacle and the relieved local load is distributed over the neighbouring

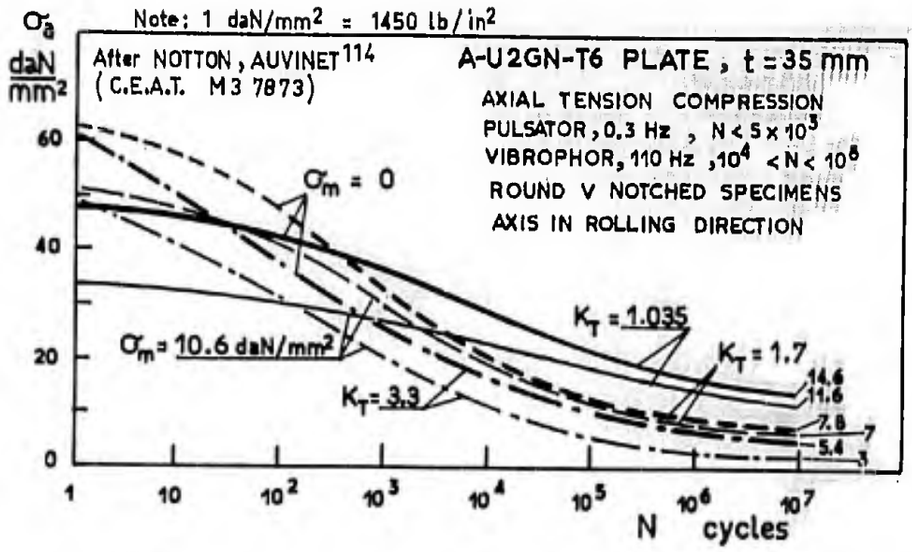

Figure 5.77

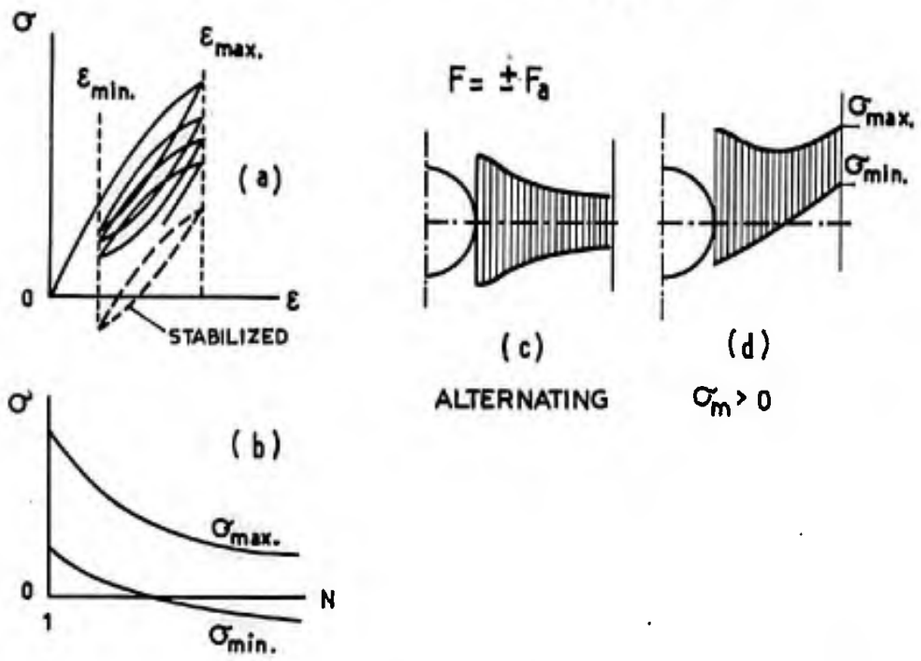

Fig. 5.78 Changes in stress-strain loops at notch root

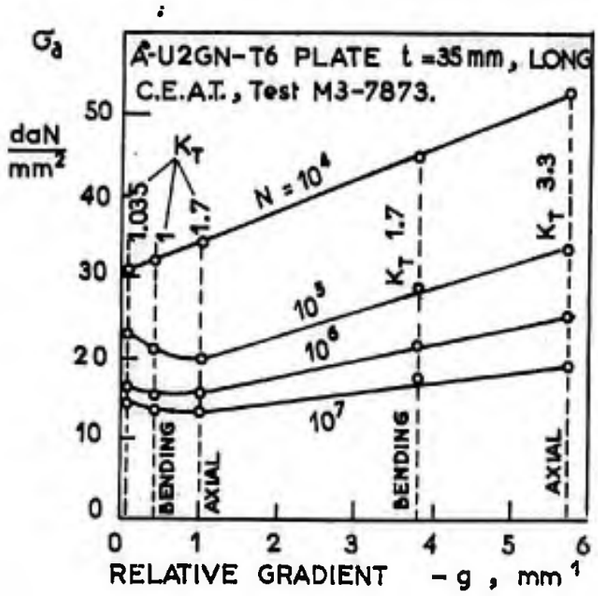

Figure 5.79

obstacles, which sometimes causes avalanche equilibrium failures (see Paragraph 2.3, Page II.38, Kaiser and Rusch, for avalanches). The probability of failure at a given point depends statistically on what has occurred on the neighbouring points.

The same pattern of chains loaded in parallel may be applied to the case of *plastics* although the latter contain no crystals and exhibit no plastic slip. Being of molecular structure, plastics have only one feature in common with metals, of crystalline structure, that is, the existence of metastable configurations which become unstable under the effect of temperature or of loads applied long enough or often enough. Here, plasticity is replaced by viscosity, and slip by the unrolling of molecular chains embedded in the viscous material. There is also a mode of brittle fracture which is governed by the parameter K of Fracture Mechanics and by the rate of loading. The above mentioned concepts are sufficient for a qualitative explanation of the fatigue phenomena that are common to metals and to plastics; besides, this was our starting point (see the beginning of Chapter II). A general theory of the strength of materials should first cover all the materials showing a similar behaviour in actual components and then include a number of particular theories to account for the differences.

As to the technical problem of the notch effect, we believe that this is the primary subject of investigation that might prove useful to the engineer; the slow progress achieved in the field of basic research over the last thirty years is obviously due to the fact that scientific experimentalists often used smooth specimens to separate the effects of parameters and to study the fatigue phenomenon *per se*. In our opinion, *notches are the most important factor*; they can be defined by a value of the surface stress and by a stress gradient in depth. As the process of plastic adjustment in notched specimens is found to be amplified in relation to unnotched specimens which are subjected to a more uniform stress state on the scale of the design but to a quite disturbed stress state on the scale of the metal structure, *the study of notches is the first step in an investigation of the fatigue behaviour of materials* and the final step in an investigation of the fatigue behaviour of structures.

5.3.2 Effect of Stress Gradient - Size Effect

Although there is also a size effect in crack propagation, the following discussion on the effect of stress gradient relates principally to crack initiation.

In Figure 5.77 the σ_a-N curves of the fatigue lives of round A-U2GN aluminium alloy specimens[114] are plotted for three values of the geometric notch factor under reversed loading with a mean tensile stress $\sigma_m = 10.6$ daN/mm^2 (15,300 lb/in^2). Over a small number of cycles the strength of the notched specimen is greater than that of the smooth specimen, this being the usual case with the static strength (see Paragraph 4.1.1); the mean tensile stress reduces considerably the allowable value of the alternating stress. With large number of cycles, however, the effect of mean stress, which is significant on unnotched specimens ($K_T = 1.035$), becomes very small on severely notched specimens ($K_T = 3.3$) under high mean-stress values, as shown by the following values of the fatigue limit at 3×10^7 cycles (the results for $\sigma_m = 21.2$ daN/mm^2 are not plotted in the figure).

	σ_m =	0	10.6	21.2	
K_T = 1.035		14.6	11.6	9	expressed in
K_T = 1.7	σ_a =	7.8	7	5.4	daN/mm^2
K_T = 3.3		5.4	3	3	(1450 lb/in^2)

This condition, which is quite frequently observed, seems to be due to fatigue "creep" (see Paragraph 5.1.1.2) at the root of the notch, whereby local stresses of substantially constant amplitude are found for the same overall strain around the small, plastically deformed region in spite of increasing geometric concentration factors; this is explained by the fact that yielding causes a shift of the stress-strain loop toward the low stress range with a fairly constant location, as illustrated in Figure 5.78.

The adjustment of the stress-strain loop depends on the plastic slip, hence on the octahedral stress examined in Chapter III, Paragraph 3.3.2, which is a shear stress, and on the relative gradient in depth. Sometimes Von Mises' "equivalent" stress

$$\sigma_{eq.} = \sqrt{(\sigma_1^2 + \sigma_2^2 - \sigma_1\sigma_2)}$$

and the equivalent relative gradient

$$g_{eq.} = \frac{1}{\sigma_{eq.}} \cdot \frac{\partial \sigma_{eq.}}{\partial z}$$

are used as references; in pure tension, the equivalent stress is reduced to the usual tensile stress but in all cases it is proportional to the octahedral stress. To simplify, one uses

$$\sigma_S = \sigma_{surface} = K_T \cdot \sigma_a ,$$

$$\text{relative gradient} \quad g = \frac{1}{\sigma_S} \cdot \frac{\partial \sigma_S}{\partial z}$$

in practical cases where the second principal stress, σ_2, is low compared with the highest principal stress σ_1. For a circumferential V-type notch with a round root of radius r and of groove diameter d we have

$$\text{in tension} \quad g = -2/r ,$$
$$\text{in bending} \quad g = -2(1/r + 1/d) .$$

For thick A-U2GN sheet material tested in the direction of rolling we find the following alternating surface stresses (expressed in daN/mm²) at fatigue failure in notched and smooth specimens subjected to axial tension-compression loads or to bending:

	K_T	$-g$	$N \rightarrow$	10^4	10^5	10^6	10^7	
Reversed tension-compression, $\sigma_m = 0$	1.035	0.037		31	23	16	15	
	1.7	1		34	19.5	15.2	13.2	
	3.3	5.7	$\sigma_a =$	53	33	24	17.8	daN/mm²
Rotating-bending	1	0.43		32	21	15.7	13.7	
	1.7	3.84		44	29	21	18	

These results are plotted in Figure 5.79 which shows that the values in rotating-bending are comparable to those obtained in reversed tension-compression with the same surface stresses and the same relative gradients. In Figure 5.80, from the tests by Esquerre[115], the ratio

$$\frac{\sigma_S}{(\sigma_a)_{K_T=1}} = \frac{K_T}{K_f}$$

is given as a function of the relative gradient $-g$ for a 35 NCD16 steel treated to a tensile strength of 126 daN/mm² (183,000 lb/in²).

One conclusion is that *the results of fatigue bending tests cannot be compared with those of axial tension-compression tests performed on smooth specimens, but only with those of axial tension-compression tests performed on notched specimens with the same alternating surface stress and the same stress gradient in the direction perpendicular to the surface.*

Since the existence of a stress gradient increases the allowable value of the alternating surface stress, the conservative approach will be to calculate the applied stress by the theory of elasticity and to take the stress sustained by the axially-loaded smooth specimen as the allowable value.

Furthermore, there is a size effect related to the stress gradient during the crack initiation period and to the stress intensity factor during the crack propagation period. In geometrically similar specimens the stress gradient decreases with increasing absolute size. Using bars of Italian PAZ 5.8 aluminium alloy containing zinc (similar to 7075), Massa[116] carried out rotating-bending tests on three geometrically similar sets of smooth and notched specimens, the small specimens having been cut from those areas of the large specimens which were little stressed in fatigue. The specimen sizes were as follows:

	Hourglass-shaped specimens, $K_T = 1.04$				*Notched specimens*, $K_T = 3.7$			
	d	D	r	$-g$	d	D	r	$-g$
		(mm)		(mm^{-1})		(mm)		(mm^{-1})
A	2.5	4	10.5	0.99	2.5	4	0.05	40.8
B	8	13	33	0.31	8	13	0.16	12.8
C	25	40	105	0.099	25	40	0.50	4.08

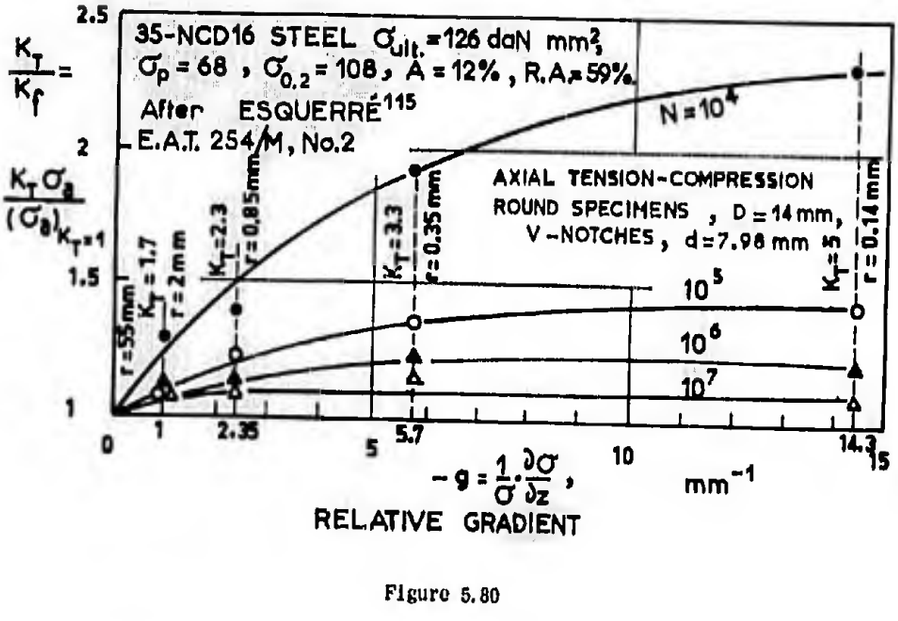

Figure 5.80

FATIGUE LIVES IN PROGRAMME TESTS

Type of programme	Distribution of load levels in programme tests				Mean life cycles
I	σ/σult. = 0.3	0.4	0.5	0.6	220,000
	N = 65,000	20,550	6,500	2,055	(2.5 blocks)
II	σ/σult. = 0.3	0.4	0.5	0.6	7,270,000
	N = 80,000	800	8	1	(90 blocks)
III	σ/σult = 0.2	0.267	0.333	0.4	1,440,000
	N = 65,000	20,550	6,500	2,055	(15.3 blocks)

FATIGUE LIVES IN SINGLE LEVEL TESTS

σ/σult =	0.3	0.4	0.5	0.6
N =	170,000	63,000	26,000	15,000

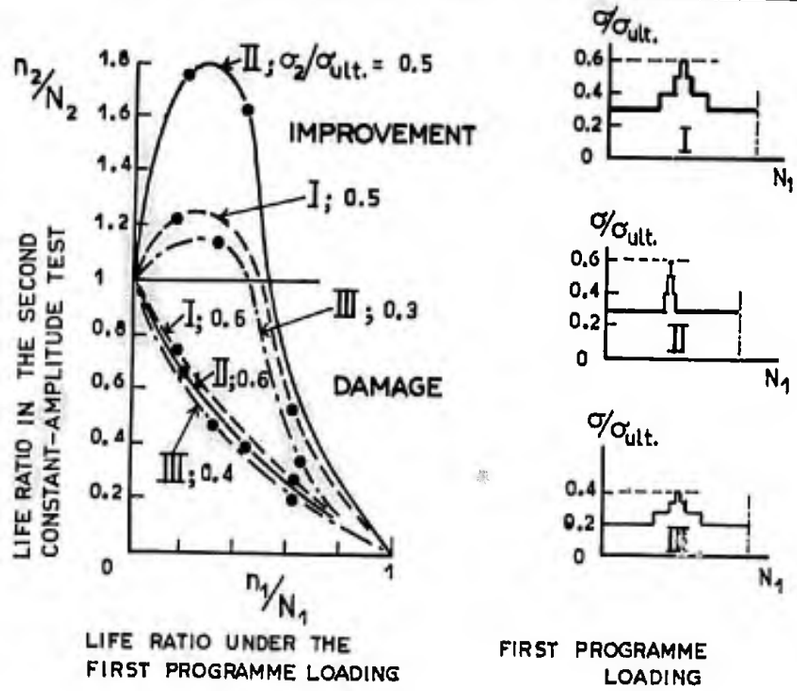

Fig. 5.81 Damage or improvement under first programme loads applied to drilled specimens made of Russian D-16T (about 2024-T6) aluminium alloy sheet as measured by the residual life under constant-amplitude loads. After Galkin, Gringaouz and Pestof[119]

The following results were obtained:

Type	Small diameter, d(mm)	Alternating stress, σ_a, for the failure after N cycles, expressed in daN/mm²(1450 lb/in²)				$\sigma_a \cdot K_T$ (daN/mm²)	$-\chi$ (mm^{-1})
		N = 10^4	10^5	10^6	10^7		
Notched specimens	2.5	18.5	13	8.5	6.7	25	40.8
	8	17.5	11.8	7.6	6	22.4	12.8
	25	15.5	9.6	6	4.75	17.7	4.1
Smooth specimens	2.5	40	30	22	18.5	10.3	0.99
	8	39.5	29.3	21.3	18.1	18.7	0.31
	25	38	26	18	15	15.6	0.099

The strength ratios of the largest specimens to the smallest specimens were as follows:

N =	10^4	10^5	10^6	10^7
Notched specimens	0.84	0.73	0.71	0.71
Smooth specimens	0.95	0.87	0.82	0.81 .

Like the static strength of notched specimens (see Paragraph 4.1.1), *the fatigue strength decreases with increasing absolute component size.* This has already been stated with regard to the residual static strength of cracked components (see Paragraph 4.3) and with respect to the fatigue crack propagation rate (see Paragraph 5.2), these two phenomena being governed by the stress intensity factor in which the square root of the absolute crack size is an important factor. In all cases the size effect is mainly dependent on the stress gradient.

The second parameter that determines the size effect is the absolute size of a surface element with physical properties differing from those of elements in depth. It may be, for example, the average size of grains since surface grains, being less supported by their neighbours, are more subject to deformation and yield under load without breaking. It may also be the thickness of a work-hardened surface layer containing compressive residual stresses which delay failure and crack initiation.

It appears that great caution is needed when using the results of small-specimen fatigue tests for prediction of the strength of large-size components.

If test data from specimens made of the same material and subjected to the same machining and surface-treatment processes as the component under investigation are available, then the experimental values K_T *corresponding to a stress gradient value smaller than that of the component investigated can be used as a first approximation.*

5.3.3 Damaging and Improving Changes During the Fatigue Process

When a notched part is subjected to an increasing static load, the elastic stress distribution near the notch root is modified and the maximum surface stress ceases to increase as soon as the yield point of the material is reached. During the load increase the plastic range extends progressively over the cross-sectional area before fracture occurs. This phenomenon is known as plastic adjustment.

At the beginning of this chapter (Paragraph 5.1.1) we examined the changes during fatigue in the stress-strain loop of the material located near the maximum stress point at the root of the notch. If the material has initially been annealed, fatigue exerts a hardening effect and the stress-strain loop, which is at first quite wide, tends to narrow. In an initially cold-worked engineering metal fatigue tends to reduce the previous work-hardened state, and the stress-strain loop, which is at first narrow, tends to widen, which implies that *under alternating strains the material softens while the stress decreases.* Now the small volume of material near the notch root is subjected to cyclic strains imposed by the surrounding material which remains substantially in the elastic range; as a result, the decrease in stress entails crack growth retardation in that area. On the other hand, if the loading includes a static component, the reduction caused by the alternating component in the previous work-hardened state induces permanent fatigue "creep" (see Paragraph 5.1.1.2) whereby the stress-strain loop is shifted toward the permanent component of the applied load; *the loop tends to assume the shape of a symmetric tension-compression loop.* All this phenomenon constitutes what is called the *fatigue accommodation.* It involves the creation of compressive residual stresses at the root of the notch and provides a full explanation of the improving processes in fatigue due to the effect of overloads when applied a small number of times as well as to the effect of understressing.

The statements on qualitative laws which we have examined previously and which are derived from the bulk of the test data published in the international technical literature may be summarized as follows:

I - Static or alternating loads tend to change the work-hardened state which depends on the mechanical and thermal history of the material; it also tends to substitute a new state independent of the former and associated with the new load applied. Fatigue hardens initially soft materials and softens initially cold-worked materials (see tests by Bairstow and by Polakowski in Paragraph 2.1.3).

II - Under constant-range stress the alternating component superimposed on a static component destroys in part a pre-existent work-hardened state or a strain-hardened state produced by a first load application, and it may favour fatigue "creep" or classical creep (see Paragraphs 2.1.3, 3.2.6, 3.4.2 and 5.1.1.2). Under constant-range strain the alternating component superimposed on a static component softens the initially cold-worked material, causes the stress to decrease by relaxation, and leads to a shift of the loop toward an alternating tension-compression loading condition with a simultaneous decrease in the alternating stress amplitude.

III - In a material cold-worked prior to fatigue and subjected to alternating tension-compression, fatigue continuously lowers the proportional limit and the yield point of the material at the notch root. The region near the maximum stress point is practically subjected to fatigue under strains imposed by the surrounding material which remains in the elastic range. The stress at the notch root decreases asymptotically and approaches a limiting value with increasing number of cycles as long as no crack is initiated (see Paragraphs 2.1.3 and 3.4.2 for the changes in the static stress-strain curves).

IV - In the presence of a static component of the load, for example in the case of a repeated load ranging from zero to maximum value, there is more fatigue "creep" at the root of the notch. The permanent elongation increases with the number of cycles and generates compressive residual stresses at the notch root which are offset by small tensile residual stresses in the more remote areas (see Paragraph 5.1.1.3).

V - The application of a static preload producing tension in the stress concentration region induces compressive residual stresses which result in a higher fatigue strength under subsequent loading, provided the preload does not introduce microcracks.

VI - Through the creation of favourable residual stresses any fatigue loading first causes an improvement which is detectable by the greater fatigue life under subsequent loading at a lower level, but after a number of cycles corresponding to the maximum improvement increasing damage is observed up to failure.

Point V is a well-known fact which has been recognized since the comprehensive tests performed by Kepert and Payne[117] on 91 "Mustang" wing structures from World War II surplus stocks. It has been the subject matter of numerous studies which we shall examine in connection with the structures in a second volume of the present work. Point VI was raised at a relatively recent date and will be discussed in the next paragraph.

Although they help to explain some of the aspects of the behaviour of smooth specimens, the preceding qualitative laws are actually verified only in the case of notched specimens, or in the case of smooth specimens during the crack propagation period since cracks are equivalent to very sharp notches. In smooth specimens there may be a prevailing effect of understressing on the scale of the grains, subgrains or precipitates where stress concentration microregions exist with tensile and compressive residual stresses which are first reduced by fatigue to a level such as would be reached in the absence of the first load if the process were not halted by microcracks. The first loading produces an improvement only within a rather narrow stress range below and above the fatigue limit; moreover, since the initial residual stresses in the microregions are created by cooling following the heat treatment, they remain very stable under an external load that involves other slip planes of the crystal lattice; the first fatigue loading must therefore be applied over a very large number of cycles if its possible improving effect is to appear. This is the origin of all the discussions between fatigue test specialists on the influence of load sequences on smooth or slightly notched specimens.

5.3.4 Improving Effect of Overloads. Tests on Components Removed After Service Operation

Tests conducted by Schijve, Jacobs and Tromp[101], and referred to in Paragraph 5.2.9, showed the improving effect of high loads on crack propagation (see Figure 5.72). This phenomenon is quite frequently observed in laboratory tests performed on components which are removed after a given operational time. In order to investigate the residual fatigue life of components after various service periods, Galkin, Gringaouz and Pestof[119] proceeded to carry out tests on notched specimens, on assemblies of aluminium alloy sheets and extrusions, and on assemblies of welded steel tubes and end pieces. These components were subjected to a first fatigue loading as defined by a programme of successive loads of different levels. The second fatigue loading carried out until fracture under a load of constant amplitude then showed an improvement or a damage depending on whether the level of the second loading was lower than, or equal to, the highest level of the first loading. Figure 5.81 contains a set of results from drilled 80 mm wide and 4 mm thick sheet specimens which were made from Russian D-16T aluminium alloy quenched and artificially aged ($\sigma_{ult.} = 50$ daN/mm^2, $\sigma_{0,2} = 34$, $A\% = 8$). No improvement is found if the level of the second test load is equal to the highest level of the first load. In the opposite case, i.e. with a higher first load, the second test shows an improvement which turns into damage if the first fatigue loading is continued up to 50% of the specimen fatigue life in one single test.

Tests carried out by Schijve[118] on riveted 2024-T3 and 7075-T6 aluminium alloy assemblies with programme loading blocks illustrate the effect of high positive loads, of negative loads and of the corresponding sequences of application. Using σ_i for each load level of the loading programme, n_i for the number of

FATIGUE ENDURANCE OF VIRGIN RODS IN CONSTANT-AMPLITUDE TESTS

$P_{max.}$	8,200	9,000	6,200	8,000	5,800	6,000	6,000	5,000	4,400	8,000	kg-weight
$P_{min.}$	-3,200	0	0	1,500	0	500	3,200	0	0	4,000	kg-weight
N	70,000	70,000	200,000		300,000		500,000		1,000,000		cycles

LANDING LOAD BLOCK simulating 500 landings on the basis of service load statistics; this loading was applied to virgin specimens of series IV prior to the tests under repeated constant-amplitude loads.

$P_{max.}$	9,000	10,000	8,000	6,500	6,500
$P_{min.}$	6,000	-2,000	0	2,500	3,500
n cycles	24,400	5	900	66,400	17,200.

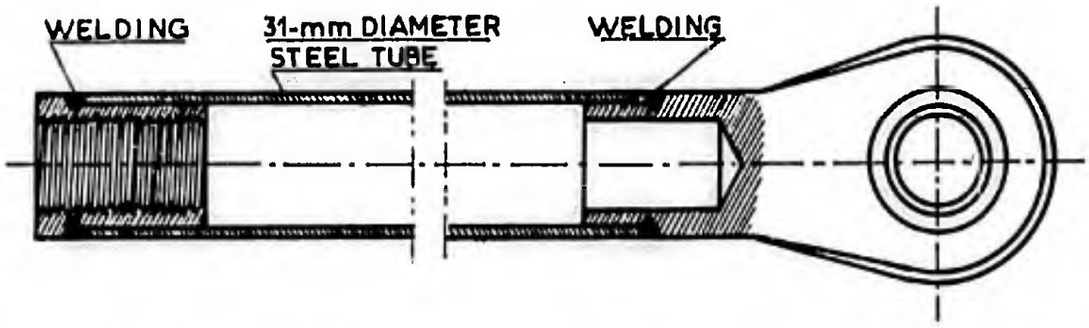

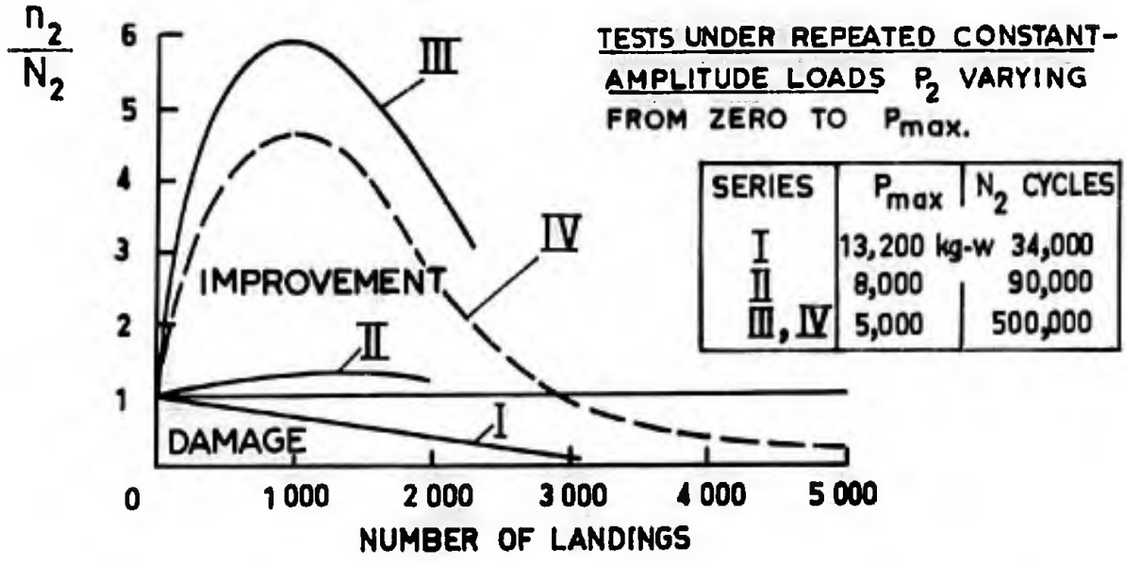

Fig. 5.82 Welded steel rods - effect of service duration on fatigue endurance after removal from the aircraft. After Galkin, Gringauoz and Pestof[119]

cycles at this level, and N_i for the number of cycles to failure at this level, Miner and Palmgren defined the cumulative damage by $D = \Sigma_i (n_i/N_i)$ and assumed that under successive loads of different levels failure would occur when $D = 1$. In tests by Schijve the loading blocks each corresponded to $D = 0.1$, that is, failure would theoretically occur after 10 blocks. In the case of the 7075-T6 aluminium alloy one single overload equal to 75% of the static ultimate load $P_{ult.}$ caused the value of the cumulative damage to failure, $D_{ult.}$, to increase from 1.08 to 1.42; the application of a positive load of 0.39 $P_{ult.}$ at the end of each block yielded $D_{ult.} = 9.9$; when this load was removed after the 50th block ($D = 4.65$), only $D_{ult.} = 5.51$ could be obtained; the application of the same load every two blocks resulted in $D_{ult.} = 3.68$. With a negative load such as $P_a = -0.39\ P_{ult.}$ at the end of each block, $D_{ult.} = 0.51$ was found. With $P_a = +0.39\ P_{ult.}$ and then $P_a = -0.39\ P_{ult.}$ at the end of each block, one had $D_{ult.} = 0.70$, and with $P_a = -0.39\ P_{ult.}$ followed by $P_a = +0.39\ P_{ult.}$ at the end of each block, $D_{ult.} = 3.11$. Analogous results were obtained on the 2024-T3 alloy. Apparently, the last load applied at the end of each block creates compressive residual stresses in the case of positive loads (improving effect) or tensile residual stresses in the case of negative loads (damaging effect), and the residual stresses slowly return to stable values which depend upon the loading levels of each block.

The improving effect of overloads during fatigue is not peculiar to aluminium alloys. In the above quoted work of Galkin et al. some test results are reported with respect to tubular rods made from Russian 30 XGSA steel and consisting of tubes with welded end pieces. From Figure 5.82 it is seen that the application on new rods of two loading blocks which simulate 1,000 landings of an aircraft equipped with such rods resulted in considerable improvement (dotted curve IV) in relation to the fatigue life of rods not subjected to previous loading; here, the test load, which was equal to 5,000 daN, was substantially smaller than the highest load of the preloading programme (10,000 daN). On curves I, II and III the test results are plotted for repeated loads of 13,200, 8,000 and 5,000 daN which were applied to rods removed from service after 1,000, 2,000 and 3,000 landings. In Series I the test load is greater than the highest loads applied in service and the test shows that damage increases with the number of landings. In Series II, with a test load of 5,000 daN, a slight improvement is observed with increasing number of landings. In Series III, which is comparable to Series IV, a considerable improvement passing through a maximum for removal after 1,000 landings is again found under a repeated load of 5,000 daN. As a rule, the qualitative law set forth under point V in Paragraph 5.3.3 is verified fairly well; previous fatigue under a high load increases the fatigue life obtained under a subsequent smaller load up to a number of cycles at which the high load begins to exert a damaging effect.

From the foregoing results we may draw some practical conclusions:

(a) Prior loads increase the fatigue strength of structures. Consequently, one should avoid distorting the meaning of a fatigue test by using - for reasons of economy - a specimen that was first subjected to static testing under high loads. Some improvement could be expected from the systematic application of high static loads generating compressive residual stresses in the notches. However, owing to the risk of obtaining microcracks and even undetectable cracks in cases that are too scarce to be revealed by destructive testing and too frequent to be acceptable from the point of view of the probabilities of accident, this procedure may be resorted to only in full production of mechanical parts where continuous checks can be effected by statistical quality control methods requiring a certain percentage of samples for destructive testing.

(b) Tensile overloads significantly increase the fatigue strength provided they do not first introduce damage and provided the structure has not been damaged by the other loads. Hence, premature introduction of such overloads in a single structural fatigue test may give an illusive guarantee as to the service behaviour of structures that would perhaps not be subject to these loads before the latter have a damaging effect.

(c) There is no point in fixing the residual fatigue life of a component removed after a given operational time by carrying out an additional fatigue test and by comparing the result with the life of a new component. Indeed, if the test loads are smaller than those sustained in service, the component investigated will last longer if it has been removed after a longer period of time, unless the removal takes place so late that failure may occur in service; if the test loads are more severe than those encountered in service, the results will prove less erroneous but again one runs the risk of assuming that service has no damaging effect.

(d) Fatigue cracks constitute quite severe notches and the effect of loading sequences on crack propagation is even more distinct than that on the total times to failure. The application of an overload may halt the crack propagation which will subsequently continue under a smaller load - very slowly at first and then at an increasingly faster rate. As a result, observation of the propagation rate of a crack on a structure used in service may lead to imprudent conclusions as to the operational life that can be reached before the crack becomes too hazardous. No crack occurrence can be tolerated in service if complete failure of the cracked component endangers the structure and if the failure cannot be detected before other components are also damaged.

REFERENCES

1. Barrois, W. — ONERA, Memo technique No. 27, Note dated 1952, distributed in 1963.

2. Blatherwick, A.A. Lazan, B.J. — *Effect of Changing Cyclic Modulus on Bending Fatigue Strength.* WADC Technical Report 56-127, Part II, University of Minnesota, May 1959.

3. Tuler, F.R. — *Cyclic Stress-Strain Behavior of OFHC Copper.* MS Thesis, University of Illinois, Urbana, 1962.

4. Halford, G.R. Morrow, JoDean — *Low Cycle Fatigue in Torsion.* TAM Report No. 203, University of Illinois, Urbana, Oct. 1961.

5. Smith, R.W et al. — *Fatigue Behaviour of Materials under Strain Cycling in Low and Intermediate Life Range.* NASA, TN D-1574, April 1963.

6. Benham, P.P. Ford, H. — *Low Endurance Fatigue of a Mild Steel and an Aluminium Alloy.* Journ. Mechanical Engineering Science, Vol. 3, No. 2, 1961.

7. Coffin, L.F., Jr. — *Low Fatigue: A Review.* Applied Materials Research, Vol. 1, No. 3 Oct. 1962, pp. 129-140.

8. Feltner, C.E. — *Cycle Dependent Deformation Behavior of Close-Packed Metals.* USAF Contract, Report TDR-63-4149, University of Illinois, Nov. 1963.

9. Plenard, E. Plessier, J. — C.R. Acad. Sciences, Paris, t. 261, 1965, p. 732.

   Plenard, E. Boutault, J. — C.R. Acad. Sciences, Paris, t. 264, 1967, p. 487.

10. Crews, J.H., Jr. — NASA TN D-3152, Dec. 1965.

11. Moore, H.F. — *A Study of Residual Stresses and Size Effect and a Study of the Effect of Repeated Stresses on Residual Stresses Due to Shot Peening of Two Steels.* Experimental Stress Analysis, Vol. II, No. 1, 1944, p. 170.

12. Coffin, L.F., Jr. — Trans. ASME, Vol. 76, 1954, p. 923.

13. Tavernelli, J.F. Coffin, L.F., Jr. — Trans. ASME, Vol. 51, 1959, p. 438.

14. Dugdale, D.S. — *Stress-Strain Cycles of Large Amplitude.* Jour. Mech. Phys. Solids, Pergamon Press, London, Vol. 7, 1959, p. 135.

15. Halford, J.R. Morrow, JoDean — *Low Cycle Fatigue in Torsion.* ASTM Preprint No. 63, 1962.

16. Gross, M.R. — *Low Cycle Fatigue of Materials for Submarine Construction.* National Aeronautical Meeting, Washington, SAE Preprint No. 690 B, April 1963.

17. Feltner, C.E. Morrow, JoDean — *Micro-Plastic Strain Hysteresis Energy as a Criterion for Fatigue Fracture.* ASTM Publication 60 Met-2, Los Angeles, April 1960.

18. Morrow, JoDean Tuler, F.R. — *Low Cycle Fatigue Evaluation of Inconel 713C and Waspaloy.* Trans. ASME, Publication 64-Met-15, Detroit, May 1964.

19. Karius, -. — *Beitrag zur Frage der Werkstoffveränderungen bei Dauerbeanspruchung.* Thesis at the Polytechnic University of Braunschweig, 1943.

20. Zener, C. — *Internal Friction in Solids.* Phys. Soc. Vol. 52(I), 1940, p. 152.

21. Crussard, C. Aubertin, F. — Revue de Métallurgie, June 1949, p. 354.

22. Lazan, B.J. — Trans. ASM, Vol. 42, 1950, p. 499.

23. Lazan, B.J. Wu, T. — *Damping Fatigue and Dynamic Stress-Strain Properties of Mild Steel.* Proc. ASM, Vol. 51, 1951, p. 649.

24. Wu, T. — *A Theoretical Study of the Fatigue and Related Problems.* Syracuse University, N.Y., T.R. 50.1, Part II, 1950, p. 20.

25. Lazan, B.J., Demer, L.J. — *Damping, Elasticity and Fatigue Properties of Temperature-Resistant Materials.* Proc. ASTM, Vol.51, 1951, p.611.

26. Zener, C. — *Anelasticity of Metals.* Metals Technology, Aug. 1946.

27. Zener, C. — Physical Review, Vol.52, 1937, p.230; Vol.53, 1938, p.90; Vol.53, 1938, p.582; Vol.53, 1938, p.100.

28. Mönch, E. — Forschung auf dem Gebiete des Ingenieurwesens, Vol.II, 1940, p.324.

29. Fink, K., Hempel, M. — Archiv. f. Eisenhüttenwesen, Vol.20, 1940, p.75.

30. Langevin, A. et al. — Journal de Physique et Le Radium, Vol.11, 1950, p.596.

31. Langevin, A. — Journal de Physique et Le Radium, Vol.12, 1951, p.476.

32. Schweizerhof, S. — *Analyse Magnétique de l'Etat des Contraintes Résiduelles dans les Métaux Etirés ou Fatigués en Traction Ondulée.* ONERA, Paris. Problème 1499 MR, Note Technique No.1, Jan. 1953.

33. Guyot, H. — *Evolution après Ecrouissage de la Perméabilité Initiale et du Coefficient de Rayleigh.* ONERA, Paris. Problème 1499 M , Note Technique No.2, June 1953.

34. Kersten, M., Becker, R., Kersten, M. — Z. Physik, Vol.76, 1932, p.505; Elektrot. Z.S., Vol.60, 1939. Z. Physik, Vol.64, 1930, p.660.

Kersten, M. — Z. Physik: (a) Vol.71, 1931, p.553; (b) Vol.76, 1932, p.505; (c) Vol.82, 1933, p.723; (d) Vol.85, 1933, p.708; (e) Z. Techn. Physik, Vol.12, 1931, p.665.

35. Cavanagh, P.E. — *The Progress of Failure in Metals as Traced by Changes in Magnetic and Electrical Properties.* Proc. ASTM, Vol.47, 1947, p.639.

36. Abel, L. et al. — *Méthode de Mesure des Contraintes Résiduelles dans les Métaux durs - Répartition Spatiale - Conséquences sur le Comportement en Fatigue.* Régie Nationale des Usines Renault, Compte-rendu final 64.00.231.00.212.75.01, Recherche avec le concours des Laboratoires et de l'Ecole de l'Armement, Boulogne-Billancourt, Dec. 1966.

37. Powell, R.W. et al. — *The Thermal and Electrical Conductivity of Magnesium and Some Magnesium Alloys.* Metallurgia, Oct. 1964, p.159.

38. Feltham, P. — *The Electrical Resistivity of Metals Due to Plastic Deformation.* Metallurgia, August 1964, p.55.

39. Basinski, Z.S. et al. — Phil. Mag., Vol.8, 1963, p.989.

40. Koehler, J.S. et al. — *The Thermal Annealing of Imperfections in the Noble Metals.* In Reference 41, 1957, pp.587-600.

41. Fisher, J.C. et al. — *Dislocations and Mechanical Properties of Crystals.* John Wiley & Sons, N.Y., 1967.

42. Boas, W. — *Lattice Defects in Plastically Deformed Metals.* In Reference 41, 1957, p.334.

43. Henderson, J.W., Koehler, J.S. — Phys. Review, Vol.91, 1953, p.1115.

44. Lomer, W.M., Cottrell, A.H. — Phil. Mag., Vol.46, 1955, p.711.

45. Blewitt, T.H. et al. — Phys. Review, Vol.91, 1953, p.448.

46. Kovacs, I. et al. — Phil. Mag., Vol.9, 1964, p.797.

47. Harting, D.R. — *The -S/N- Fatigue Life Gage: A Direct Means of Measuring Cumulative Fatigue Damage.* Experimental Mechanics, Vol.6, No.2, 19A-24A, Feb. 1966.

48. Micro-Measurements Inc. — *Applications Manual, the -S/N- Fatigue Life Gage,* August 1966.

49. Horne, R.S. — *A Feasibility Study for the Development of a Fatigue Damage Indicator.* Lockheed Georgia Co. Technical Report AFFDL-TR-66-113, August 1966.

50. Matlock, R.W. — *An Evaluation of Fatigue Damage Gages.* AIAA 4th Annual Meeting and Technical Display, Anaheim, Cal., Oct. 1967.

51. Sud-Aviation — Essais non publiés, P.V. 29801 du 6. 10. 66, Courbevoie, unpublished test results, Marignane, 1967.

52. Micro-Mesures Europe — Test results, Private communication, Paris, Dec. 1967.

53. Forsyth, P.J.E. — *A Two-Stage Process of Fatigue Crack Growth.* Crack Propagation Symposium, Cranfield, 1961.

54. Christensen, R.H. — *Fatigue Cracking, Fatigue Damage, and Their Detection.* Metal Fatigue, Chapter 17, McGraw-Hill Book, 1959.

55. Hooson, R.E. — *An Aircraft Fatigue Monitoring System.* Grumman Aircraft Engineering Corp., Report AD 612 727, 1st Feb. 1965.

56. Wilkow, M.A.
Shield, P. — *Crack Initiation Fatigue in Metals.* AFOSR Final Scientific Report 66-0856, University of Texas, Austin, May 1966.

57. Laird, C. — *The Influence of Metallurgical Structure on the Mechanisms of Fatigue Crack Propagation.* STP 415, ASTM, 1967.

58. McMillan, J.C.
Pelloux, R.M.N. — *Fatigue Crack Propagation under Program and Random Loads.* ASTM, STP 415, 1967.

59. Hertzberg, R.W. — *Fatigue Crack Surface Appearance.* ASTM, STP 415, 1967.

60. Hunter, M.S.
Fricke, W.G., Jr. — *Metallographic Aspects of Fatigue Behavior of Aluminum.* Proc. ASTM, 1954.

61. Bennett, J.A. — *The Effect of a Fatigue Crack on the Fatigue Strength of an Aluminum Alloy.* Materials Research and Standard, Vol. 5, No. 5, May 1965.

62. De Forrest, A.V.
Magnuson, F.W. — *The Rate of Growth of Fatigue Cracks.* Journal Applied Mechanics, Vol. 3, A-23, 1936.

63. Crichlow, W.J.
Wells, R.H. — *Crack Propagation and Residual Static Strength of Fatigue-Cracked Titanium and Steel Cylinders.* ASTM, STP 415, 1967.

64. Schijve, J.
Jacobs, F.A. — *Fatigue Crack Propagation in Unnotched and Notched Alumnium Alloy Specimens.* NLR, TR M. 2128; Amsterdam, May 1964.

65. Jaillon, P.
Lachenaud, R. — *Influence de la Fréquence et de la Température sur la Vitesse de Propagation des Griques en Fatigue.* Sud-Aviation, P.V. 26712/4, Courbevoie, Sept. 1964.

66. Weibull, W. — *Basic Aspects of Fatigue.* Colloquium of Fatigue, Stockholm, May 1955.

67. Weibull, W. — *Effect of Crack Length and Stress Amplitude on Growth of Fatigue Cracks.* FFA Report 65, Stockholm, 1957.

68. Weibull, W. — *Size Effect on Fatigue Crack Initiation.* FFA Report 86, Stockholm, 1960.

69. Weibull, W. — *The Effect of Size and Stress History on Fatigue Crack Propagation.* Crack Propagation Symposium, Cranfield, 1961.

70. O'Neill, P.H. — *Effect of Prior Fatigue Loading on Crack Propagation Rates in 2024-T3 Sheets.* Royal Aircraft Establishment, Technical Report No. 66100, March 1966.

71. Hudson, C.M.
Hardrath, H.F. — *Effects of Changing Stress Amplitude on the Rate of Fatigue-Crack Propagation in Two Aluminum Alloys.* NASA TN D-960, Sept. 1961.

72. Hartman, A.
et al. — *Some Tests on the Effect of the Environment on the Propagation of Fatigue Cracks in Aluminium Alloys.* NLR TN M. 2182, May 1967.

73. Carreker, R.P.
et al. — AIME, Vol. 15, TP 2477, Sept. 1948.

74. Schijve, J. — *Fatigue Crack Propagation in Light Alloy Sheet Material and Structures.* NLL, Report MP 195, Amsterdam, Aug. 1960.

75. Swanson, S.R. et al. — *Crack Propagation in Clad 7079-T6 Aluminum Alloy Sheet Under Constant and Random Amplitude Fatigue Loading.* ASTM, STP 415, 1967.

76. Frost, N.E. Dugdale, D.S. — *Fatigue Tests on Notched Mild Steel Plates with Measurements of Fatigue Cracks.* Journal Mechanical Physical Solids, Vol. 5, No. 3, 1957, pp. 182-192.

77. Frost, N.E. Denton, K. — *The Fatigue Crack Propagation Characteristics of Titanium and Two Titanium Alloys.* Metallurgia, Sept. 1964, pp. 113-120.

78. Broek, D. et al. — *The Transition of Fatigue Cracks in Alclad Sheet.* NLR, TR M. 2100, Amsterdam, Nov. 1962.

79. Schijve, J. et al. — *The Effect of the Sheet Width on the Fatigue Crack Propagation in 2024-T3 Alclad Material.* NLR, TR M. 2142, Amsterdam, March 1965.

80. Rooke, D.P. et al. — *Crack Propagation in Fatigue. Some Experiment with DTD 5070A Aluminium Alloy Sheet.* Royal Aircraft Establishment, TR No. 64025, Oct. 1964.

81. Donaldson, D.R. Anderson, W.A. — *Crack Propagation Behavior of Some Airframe Materials.* Crack Propagation Symposium, Cranfield, Sept. 1961.

82. Broek, D. Schijve, J. — *The Influence of the Mean Stress on the Propagation of Fatigue Cracks in Aluminium Alloy Sheet.* NLR, TN M. 2111, Amsterdam, Jan. 1963.

83. McEvily, A.J. Illg, W. — NASA TN 4394, 1958.

84. Illg, W. McEvily, A.J. — NASA TN D-52, 1959.

85. Broek, D. van der Vet, W.J. — *Systematic Electron Fractography of Fatigue in Aluminium Alloys.* NLR, TR 68002 U, Amsterdam, Nov. 1967.

86. Schijve, J. et al. — *The Effect of the Frequency of an Alternating Load on Crack Rate in a Light Alloy Sheet.* NLR, TN M. 2092, Amsterdam, Sept. 1961.

87. Schijve, J. De Rijk, P. — *The Effect of Temperature and Frequency on the Fatigue Crack Propagation in 2024-T3 Alclad Sheet Material.* NLR, TR M. 2138, Jan. 1965.

88. Hartman, A. — *On the Effect of Oxygen and Water Vapor on the Propagation of Fatigue Cracks in 2024-T3 Alclad Sheet.* International Journal of Fracture Mechanics, Vol. 1, No. 3, 1965, p. 167.

89. Maurin, E. Barrois, W. — *Influence de la Fréquence et de la Température d'Essai sur la Durée en Fatigue d'Eprouvettes et d'Assemblages en Tôle A-U2GN-T6. Interaction Fatigue - Fluage.* L'Aéronautique et l'Astronautique, No. 9, Paris, 1969. English version in ICAF Proceedings, Stockholm, 1969.

90. Harting, D.R. — *Comportement des Indicateurs de Fatigue S/N en Régime Aléatoire.* INSA, Lyon, Conférences sur la Fatigue des Métaux et des Structures, 3rd-7th Feb. 1969.

91. Broek, D. et al. — *The Effect of Heat Treatment on the Propagation of Fatigue Cracks in Light Alloy Sheet Material.* Report NLR-TR M. 2134, Amsterdam, May 1963.

92. Broek, D. — *Crack Propagation Properties of 2024-T8 Sheet Under Static and Dynamic Loads.* Report NLR-TM M. 2161, March 1966.

93. Schijve, J. de Rijk, P. — *The Fatigue Crack Propagation in 2024-T3 Alclad Sheet Materials from Seven Different Manufacturers.* NLR-TR M. 2162, Amsterdam, May 1966.

94. Piper, D.E. et al. — *The Effect of Composition on the Fracture Properties of 7178-T6 Aluminium Alloy Sheet.* Fall Meeting of the Metallurgical Society of AIME, Oct. 1964.

95. Hartman, A. Schijve, J. — *The Effects of Environment and Load Frequency on the Crack Propagation Law for Macro Fatigue Crack Growth in Aluminium Alloys.* NLR MP 68001 U, Amsterdam, April 1968.

96. Forman, R.C. et al. — *Numerical Analysis of Crack Propagation in Cyclic-Loaded Structures.* ASTM Annual Meeting, Paper No. 66 WA/Met. 4, 1966.

97. Broek, D. — *The Effect of Finite Specimen Width on the Residual Strength of Light Alloy Sheet.* NLR-TR M. 2152, Amsterdam, Sept. 1965.

98. Broek, D. — *Static Tests on Cracked Panels of 2024-T3 Alclad Sheet Materials from Different Manufacturers.* NLR-TN M.2164, Amsterdam, Aug. 1966.

99. Naumann, E.C. — *Evaluation of the Influence of Load Randomization and of Ground-Air-Ground Cycles on Fatigue Life.* NASA TN D-1584, Oct. 1964.

100. Schijve, J. de Rijk, P. — *The Effect of "Ground-to-Air Cycles" on the Fatigue Crack Propagation in 2024-T3 Alclad Sheet Material.* NLR, TR M.2148, Amsterdam, July 1966.

101. Schijve, J. et al. — *Crack Propagation in Aluminium Alloy Sheet Materials Under Flight Simulation Loading.* NLR, TR 68117 U, Amsterdam, Dec. 1968.

102. Barrois, W. — *Les Essais Statiques et de Fatigue des Structures d'Avions en France et à l'Etranger.* Doc-Air-Espace No. 110, Paris, May 1968, p. 16.

103. Gassner, E. Jacoby, G. — *Experimentelle und Rechnerische Beurteilung von Bauteilen mit Start-Lande-Lastwechsel.* Luftfahrttechnik-Raumfahrttechnik, Vol. 11, 1965, pp. 138-148.

104. Jacoby, G. — *Comparison of Fatigue Life Estimation Processes for Irregularly Varying Loads.* Proc. 3rd Conference on Dimensioning, Budapest, 1968.

See also:

Gassner, E. Jacoby, G. — *Betriebsfestigkeits Versuche zur Ermittlung zulässiger Entwurfsspannungen für die Flügelunterseite eines Transportflugzeuges.* Luftfahrttechnik-Raumfahrttechnik, Vol. 10, 1964, pp. 6-20.

105. Kowalewski, J. — *On the Relation Between Fatigue Lives under Random Loading and under Corresponding Program Loading.* In: Full Scale Fatigue Testing of Aircraft Structures, ICAF Symposium, Amsterdam, 1959; Edited by F.J. Plantema and J. Schijve, Pergamon Press, 1961. See also: *Uber die Beziehung zwischen der Lebensdauer von Bauteilen bei unregelmässig schwankenden und geordneten Belastungsfolgen.* DVL-Bericht 249, 1963.

106. Press, H. et al. — *A Re-Evaluation of Data on Atmospheric Turbulence and Airplane Gust Loads for Application in Spectral Calculations.* NACA Report 1272, 1956.

107. Isida, M. Itagaki, Y. — *Stress Concentration at the Tip of a Central Transverse Crack in a Stiffened Plate Subjected to Tension.* Proc. 4th US National Congress of Applied Mechanics, ASME, Berkeley, Ca., Vol. II, June 1962.

108. Sanders, J.L., Jr. — *Effect of a Stringer on the Stress Concentration Due to a Crack in a Thin Sheet.* NASA TR R-13, 1959.

109. Greif, R. Sanders, J.L., Jr. — *The Effect of a Stringer on the Stress in a Cracked Sheet.* ONR Technical Report No. 17, Harvard University, June 1963.

110. Bloom, J.M. — *The Effect of a Riveted Stringer on the Stress in a Sheet with a Crack or a Cut-Out.* ONR Technical Report No. 20, Harvard University, June 1964.

111. Barrois, W. Bhandari, S.K. — *Mesures Extensométriques du Facteur d'Intensité des Contraintes.* Unpublished, Paris, 1969.

112. Bhandari, S.K. — Thèse, Ecole Nationale Supérieure de l'Aéronautique, Paris, 1969.

113. Barrois, W. — *Influence des Concentrations de Contrainte et des Entailles sur la Résistance en Fatigue.* Centre d'Actualisation Scientifique et Technique, INSA, Lyon; Semaine d'étude de la Fatigue des Métaux, Villeurbane, 3rd-5th Feb. 1969.

114. Notton, Auvinet, J. — Essais M3-7873, CEAT, Toulouse, May 1965.

115. Esquerre, R. — Etude 254/M, Rapport Technique No. 2, EAT, Toulouse, July 1958.

116. Massa, A. — *L'Influenza Della Dimensione Sulla Resistanza Alla Flexione Rotante Della Lega PAZ 5.* FIAT, April 1965.

117. Kepert, J.L. Payne, A.O. — *Interim Report on Fatigue Characteristics of a Typical Metal Wing.* Report ARL/SM. 207, Melbourne, Australia, Jan. 1955; NACA TM 1397, March 1956.

118. Schijve, J. — *The Endurance under Program-Fatigue Testing.* Report MP 178, NLL, Amsterdam, May 1959.

119. Galkin, S.I. et al. — *Investigations on the Fatigue Strength of Assemblies* (in Russian). Symposium on the Fatigue of Civil Aircraft, Moscow, Nov. 1968.

SUBJECT INDEX

A

B

C

D

E

F

G

H

M

N

O

P

Q

R

S

T

U

V

W

Y